NI

CR-166160

LEAR SIEGLER, INC.
ASTRONICS DIVISION

DEVELOPMENT AND EVALUATION OF AUTOMATIC LANDING CONTROL LAWS FOR LIGHT WING LOADING STOL AIRCRAFT

NASA CR-166160

JULY, 1981

(D. Watson)

3171 SOUTH BUNDY DRIVE
SANTA MONICA, CA. 90406
AREA CODE 213 391-7211

NASA CR-166160

DEVELOPMENT AND EVALUATION OF AUTOMATIC LANDING CONTROL LAWS FOR LIGHT WING LOADING STOL AIRCRAFT

JULY, 1981

BY

B. Feinreich

O. Degani

G. Gevaert

Prepared under Contract No. NAS2-9410 by

LEAR SIEGLER, INC., ASTRONICS DIVISION,

Santa Monica, California 90406

for

AMES RESEARCH CENTER

NATIONAL AERONAUTICS AND SPACE ADMINISTRATION

ABSTRACT

Automatic flare and decrab control laws were developed for NASA's experimental Twin Otter. This light wing loading STOL aircraft was equipped with direct lift control wing spoilers to enhance flight path control. Automatic landing control laws that made use of the spoilers were developed, evaluated in a simulation and the results compared with these obtained for configurations that did not use DLC. The spoilers produced a significant improvement in performance. A simulation that could be operated faster than real time in order to provide statistical landing data for a large number of landings over a wide spectrum of disturbances in a short time was constructed and used in the evaluation and refinement of control law configurations. A longitudinal control law that had been previously developed and evaluated in flight was also simulated and its performance compared with that of the control laws developed in this study. Runway alignment control laws were also defined, evaluated and refined to result in a final recommended configuration. Good landing performance, compatible with Category III operation into STOL runways, was obtained.

TABLE OF CONTENTS

TABLE OF CONTENTS (Continued)

LIST OF FIGURES

LIST OF FIGURES (Continued)

LIST OF TABLES

LIST OF TABLES (Continued)

REFERENCES

1. Feinreich, B. and Gevaert, G., "Development and Evaluation of Automatic Landing Control Laws for Powered Lift STOL Aircraft", NASA CR-152399, January, 1981.

2. Feinreich, B., Gevaert, G., Hardy, G. H., Watson, D. M., "Development of Automatic Landing Control Laws for Powered Lift Short Haul Aircraft", AIAA Paper No. 80-1759, August, 1980.

3. Gevaert, G., Feinreich, B., "The Development of Advanced Automatic Flare and Decrab for Powered Lift Short Haul Aircraft Using A Microwave Landing System", NASA CR-151948, April, 1977.

4. Shah, N. M., Gevaert, G., Lykken, L. O., "The Effect of Aircraft Environment on Category III Autoland Performance and Safety", AIAA 4th Aircraft Design, Flight Test, and Operations Meeting, August, 1972.

5. Gevaert, G., Lykken, L. O., and Shah, N., "A Simulation Program for Category III Autoland Certification", Summer Computer Simulation Conference, June, 1972.

6. Mineck, D. W., Derr, R. E., Lykken, L. O., Hall, J. C., "Avionic Flight Control System for the Lockheed L-1011 Tristar", SAE Aerospace Control and Guidance Systems Committee Meeting No. 30, September, 1972.

7. Anon., "Automatic Landing Systems", FAA, AC 20-57A, 12 January, 1971.

8. Neuman, F., Watson, D. M., Bradbury, P., "Operational Description of an Experimental Digital Avionics System for STOL Airplanes", NASA TM X-62, 448, 1975.

9. Anon., "Planning and Design Criteria for Metropolitan STOL Ports", FAA Advisory Circular 150/5300-8, November, 1970.

A-1. "Microwave Landing System Study - Area Navigation Impact on Autopilots", LSI ADR-765, 4 March, 1974.

LIST OF SYMBOLS

a_n	normal acceleration (positive up)
a_{nwo}	washed out normal acceleration
a_x	longitudinal acceleration
a_y	lateral acceleration
a_z	normal acceleration (positive down)
b	wing span
$\bar{c}$	mean aerodynamic chord
g	gravity acceleration
H	height
h	height
$\dot{h}$	rate of climb
$\hat{\dot{h}}$	filtered rate of climb
$\ddot{h}$	vertical acceleration
h_{ALN}	height at which runway alignment begins
h_{CG}	center of gravity height
$\dot{h}_e$	sink rate error
h_F	flare height
h_{FL}	flare height
h_{FO}	constant component of flare height
H_G	main landing gear height
h_G	main landing gear height
h_{GE}	ground effect height
h_{GS}	height at which glide slope error starts fading out
h_I	height at which flare gain starts increasing
h_o	radio altitude at which flare starts
h_o	altitude at which the alignment heading model reaches its minimum value

$\dot{h}_o$	pre flare rate of climb
h_{RA}	radio altitude
$\hat{h}_{RA}$	filtered radio altitude
$\dot{\hat{h}}_{RA}$	filtered radio altimeter derived rate of climb
h_{REC}	glide slope receiver antenna height
h_{ref}	reference altitude for wind shears
h_{TCF}	altitude at which throttle crossfeed is switched in
$\dot{h}_{TD}$	touchdown sink rate
$\dot{h}^c_{TD}$	touchdown sink rate command
h_{TFL}	throttle flare height
$\ddot{h}_{wo}$	washed out vertical acceleration
$h_{\theta FL}$	pitch flare altitude
I_x	moment of inertia about the x axis
I_y	moment of inertia about the y axis
I_z	moment of inertia about the z axis
I_{xz}	the x-z product of inertia
k_{ay}	gain of lateral acceleration to rudder
k_{DDS}	gain of vertical acceleration to spoilers (LOC TRK)
k_{DS}	gain of sink rate to spoilers (LOC TRK)
$k_{DD\theta}$	gain of vertical acceleration to pitch (FLR)
K_{ep}	elevator predict gain
k_{ev}	gain of airspeed to elevator predict
k_{evo}	gain of pre flare speed deviation to elevator predict
$k_{F\dot{h}}$	gain of sink rate to flare height

LIST OF SYMBOLS (CONTINUED)

k_{FV}	gain of speed ratio to flare height
$k_{G\theta}$	gain of closed loop pitch command to pitch predict altitude dependent gain
k_{h}	gain of glide slope error to sink rate error
$k_{\dot{h}}$	gain of sink rate error to pitch
$k_{\dot{h}DF}$	gain of sink rate to pitch (FLR)
$k_{\dot{h}DT}$	gain of sink rate to pitch (TRK)
k_{hep}	gain of altitude dependent elevator predict term
k_{hI}	glide slope integrator gain
$k_{hI\theta}$	gain of sink rate error to pitch integrator
$k_{\dot{h}o}$	zero height value of flare scheduler
$k_{\ddot{h}s}$	gain of vertical acceleration to spoilers (FLR)
$k_{\dot{h}T}$	gain of sink rate to throttle
$k_{h\theta}$	gain of glide slope error to pitch (TRK)
$k_{\ddot{h}\theta}$	gain of vertical acceleration to pitch
$k_{h\theta P}$	altitude dependent pitch predict gain
k_{Ih}	altitude dependent pitch flare gain
k_{IV}	speed dependent pitch flare gain
k_{LIM}	frequency of roll command limiter
k_{m}	conversion constant to metric units
k_{p}	pitch predict gain
k_{ps}	gain of glide slope error to spoilers (TRK)
k_{q}	gain of pitch rate to elevator
k_{qF}	incremental pitch rate to elevator flare gain
k_{R}	yaw rate gain to rudder (TRK)
k_{rCF}	yaw rate to wheel crossfeed gain
k_{rL}	yaw rate to rudder gain (ALN)

k_{SFL}	spoiler flare gain
k_{SP}	spoiler gain
k_{STR}	spoiler TRK gain
k_{u}	airspeed to throttle gain
k_{uI}	gain of airspeed integrator to throttle
k_{VI}	airspeed integrator to throttle gain (TRK)
k_{VT}	airspeed to throttle gain (TRK)
k_{VTF}	speed dependent throttle flare predict gain
$k_{\ddot{X}T}$	gain of longitudinal acceleration to throttle
$k_{\ddot{y}A}$	gain of lateral acceleration to bank angle (ALN)
k_{yI}	gain of localizer integrator to bank angle (TRK)
k_{yL}	gain of localizer deviation to bank angle
$k_{\dot{y}L}$	gain of lateral rate to bank angle
$k_{\ddot{y}L}$	gain of lateral acceleration to bank angle
$k_{\ddot{y}L\Delta}$	incremental ALN acceleration to bank angle gain
$k_{\beta CF}$	sideslip angle to wheel crossfeed gain
$k_{\delta CF}$	rudder to wheel crossfeed gain
k_{θ}	pitch to elevator gain
$k_{\theta F}$	incremental flare pitch gain
$k_{\theta I}$	elevator integrator gain
k_{ϕ}	gain of roll error to wheel
$k_{\dot{\phi}}$	roll rate gain
$k_{\phi I}$	roll integrator gain
$k_{\psi L}$	heading error gain at ALN
$k_{\psi IL}$	heading error integral gain
L	rolling moment
L_{acc}	distance of accelerometer from C.G.

L_u	longitudinal turbulence scale length
L_v	lateral turbulence scale length
L_w	vertical turbulence scale length
M	pitching moment
N	yawing moment
p	roll rate
p_{gust}	roll rate gust
q	pitch rate
$\bar{q}$	dynamic pressure
q_{REF}	reference dynamic pressure
r	yaw rate
r_{gust}	yaw rate gust
R_{LIM}	yaw rate command limit during ALN
S	Laplace operator
S_{WING}	wing reference area
U	longitudinal wind (along the runway)
U_o	approach airspeed
u	longitudinal speed perturbation
$\dot{u}$	longitudinal acceleration
u_A	airspeed perturbation
U_{WIND}	longitudinal wind in airplane axes
V	lateral speed
v	lateral speed perturbation
V_c	calibrated airspeed
$\dot{V}_c$	filtered calibrated airspeed
V_{REF}	reference airspeed

V_{co}	preflare calibrated airspeed
V_{co}^{*}	limited preflare calibrated airspeed signal
$\hat{V}_G$	filtered ground speed
V_{GO}	preflare ground speed
V_{MIN}	the lower limit on V_{co}^{*}
V_{NOM}	reference airspeed for ΔV_o
V_{WIND}	lateral wind in airplane axes
W	normal speed
w	normal speed perturbation
w_A	normal aerodynamic speed perturbation
W_{WIND}	normal wind in airplane axes
X	longitudinal force
x	longitudinal distance along the runway (measured from the GPIP)
$\ddot{x}$	longitudinal acceleration
X_{ANT}	longitudinal distance of localizer receiver antenna ahead of the C.G.
X_G	longitudinal distance of the main landing gear ahead of the C.G.
X_{REC}	longitudinal distance of glide slope receiver antenna ahead of the C.G.
X_{TD}	touchdown distance along the runway, measured from the GPIP
y	lateral deviation from the runway centerline (positive right)
y_{ANT}	deviation of the localizer receiver antenna from the runway centerline
y_{CG}	deviation of the CG from the runway centerline
y_F	filtered localizer lateral deviation signal
$\dot{y}_F$	filtered lateral rate
$\ddot{y}_{LIM}$	limiting value on $\ddot{y}$ washout
y_{NOISE}	localizer noise
$\ddot{y}_R$	lateral acceleration in runway axes

y_{RAW}	unfiltered localizer based lateral deviation signal
y_{TD}	touchdown lateral deviation
$\dot{y}_{TD}$	touchdown lateral velocity
Z	normal force (positive down)
Z_G	distance of the main landing gear from the CG along the Z axis
Z_{REC}	distance of the glide slope receiver antenna from the CG along the Z axis
α	angle of attack
α_o	trim angle of attack
β	sideslip angle
γ	flight path angle
γ_o	nominal approach flight path angle
Δh	deviation from the glide slope
$\dot{\Delta h}$	filtered glide slope derived sink rate
Δh_B	deviation from the glide slope
$\hat{\Delta h}_B$	filtered glide slope deviation
Δh_{WINDOW}	glide slope deviation at a gear height of 30.5 m (100 ft)
Δh_{100}	glide slope deviation at a gear height of 30.5 m (100 ft)
ΔV_F^c	speed reduction command at flare
ΔV_o	preflare airspeed deviation
$\Delta\theta$	incremental pitch attitude
$\Delta\theta^c$	incremental pitch attitude command
$\Delta\theta_{LIM}$	pitch command limit
$\Delta\psi$	difference between airplane and runway heading
$\Delta\psi_i$	heading difference prior to the initiation of the alignment maneuver

δ_A	aileron deflection
δ_e	elevator deflection
δ_e^c	elevator command
δ_{ep}	elevator predict term
δ_R	rudder deflection
δ_R^c	rudder command
δ_{sp}	spoiler deflection
δ_{sp}^c	spoiler command
$\delta_{sp\ NOM}$	nominal approach spoiler bias
δ_T	throttle deflection (including throttle servo dynamics)
δ_T^c	throttle command (input to throttle servo)
δ_{th}	throttle deflection (including engine dynamics)
δ_{th}^c	throttle command (input to engine)
δ_{th}^ϵ	throttle position error
δ_w	control wheel deflection
δ_w^c	wheel command
ζ	damping ratio
ζ_{DR}	Dutch Roll damping ratio
ζ_{ph}	Phugoid damping ratio
ζ_{sp}	Short Period damping ratio
θ	pitch attitude
θ_c'	pitch command due to sink rate error
θ^c	pitch command
θ_{CB}'	pitch command bias
θ_e	pitch error

θ_{FL}	pitch flare (start of flare rotation)
θ^{c}_{FLR}	pitch command at flare
θ_{o}	preflare pitch attitude
θ_{p}	pitch attitude predict term
θ_{s}	pitch attitude referenced to stability axes
θ_{T}	pitch attitude referenced to body axes
θ_{TD}	touchdown pitch attitude
θ^{c}_{TD}	touchdown pitch attitude command
θ^{c}_{TRK}	attitude command during glide slope track
μ	mean value
σ	standard deviation
τ	time constant
τ_{awo}	acceleration washout time constant
τ_{AZ}	time constant of azimuth noise model
τ_{EL}	time constant of elevation noise model
τ_{ep}	elevator predict time constant
$\tau_{\ddot{h}}$	time constant of vertical acceleration filter
τ_{R}	airframe roll mode time constant
τ_{s}	spiral mode time constant
τ_{sp}	spoiler time constant
τ_{swo}	spoiler washout time constant
$\tau_{\theta p}$	pitch predict time constant
$\tau_{\theta s}$	pitch flare command fade-in time constant
ϕ	roll attitude
$\dot{\phi}$	roll rate

ϕ_{ALIM}	wing down compensation limit
ϕ^c	bank attitude command
ϕ_{CLIM}	localizer track roll command limit
$\dot{\phi}_{CLIM}$	localizer track roll rate limit
$\dot{\phi}_e$	roll rate error
ϕ_{TD}	touchdown bank angle
ψ	heading angle
$\dot{\psi}$	heading rate
ψ_i	heading prior to initiation of runway alignment maneuver
ψ_M	heading model
ψ_o	minimum value of alignment model
ψ_{TD}	touchdown heading (referenced to runway heading)
ω	natural frequency
ω_{DR}	Dutch Roll frequency
ω_{ph}	Phugoid frequency

ACRONYMS AND ABBREVIATIONS

ALIGN	runway alignment mode
ALN	runway alignment mode
AZ	azimuth
BN	beam noise
CAT III	category III (weather minima)
CG	center of gravity
CTOL	conventional takeoff and landing
CW	crosswind
deg	degrees
DLC	direct lift control
DME	distance measuring equipment
EL	elevation
FAA	Federal Aviation Administration
FLR	flare mode
FSCG	fuselage station of the center of gravity
ft	feet
GE	ground effect
GPIP	glide path intercept point
HGT	height
HW	headwind
IC	initial conditions
ILIM	integrator limit
kt	knot
LOC	localizer
LOG	logarithmic
m	meter

ACRONYMS AND ABBREVIATIONS (CONTINUED)

MLS	microwave landing system
MODILS	modular instrument landing system
NALF	Naval Auxiliary Landing Field
NASA	National Aeronautics and Space Administration
PLA	power lever position
psf	pounds per square foot
RMS	root mean squared
RPM	revolutions per minute
rps	radians per second
RSS	root summed squared
sec	second
SHR	shear
SOW	statement of work
std	standard
STOL	short takeoff and landing
TD	touchdown
TRK	track mode
TW	tailwind
WLCG	water line of center of gravity

1.0 INTRODUCTION AND SUMMARY

1.1 INTRODUCTION

The Ames research center of NASA conducted a series of investigations to generate and verify through ground based simulation and flight research a data base to aid in the design and certification of advanced short takeoff and landing (STOL) aircraft. A modified de Havilland Canada DHC-6, Twin Otter, with direct lift wing spoilers was evaluated as a representative light wing loading STOL aircraft. The Augmentor Wing Jet STOL research airplane and the Quiet Short-Haul Research Aircraft (QSRA) are representatives of the propulsive lift technology. One portion of this program is concerned with obtaining technical information on automatic landing systems for STOL aircraft including flight path control performance and touchdown state dispersion in the presence of environmental disturbances. As part of this program, Lear Siegler's Astronics Division developed automatic landing control laws for these experimental aircraft. The results of Lear Siegler's Twin Otter work are presented in this report and previous studies are documented as References 1, 2 and 3.

The technology for the development and certification of Category III automatic landing systems for conventional takeoff and landing (CTOL) jet transports is well developed and documented, as noted in References 4 to 6 for one commercial aircraft and Reference 7 for the FAA requirements. No comparable technology exists for automatic landing systems for STOL airplanes.

The objective of the automatic landing work reported here is to gain understanding of the problems impacting the design of light wing loading short-haul airplanes that are to be landed automatically on STOL runways in adverse weather conditions. This understanding was attained by a limited coverage of important elements that are normally included in the certification process of a CAT III automatic landing system for CTOL airplanes with major emphasis on fault-free performance. The control law development concentrated on the final approach to touchdown phase of the landing.

Several longitudinal automatic landing control laws, with and without the use of the DLC spoilers, were developed as part of this study and their performance with atmospheric disturbances and landing aid noise was evaluated deterministically and statistically in a simulation. Another longitudinal control

law that had been defined independently of this study and evaluated in flight was evaluated in the simulation for comparison against the newly developed control laws. Lateral and directional control laws were also defined during this study and evaluated in the simulation.

1.2 SUMMARY

This report describes the development of a family of automatic landing system control laws and shows that this type of control law is capable of meeting requirements like those applied by the FAA to CTOL automatic landing systems. The results presented in this report are derived from simulation.

The report contains seven sections describing the development and evaluation of the automatic landing control laws. Section 2 is a brief description of the Twin Otter Airplane, the STOL approach conditions, the airplane's controls and its avionic system. Section 3 describes the design and evaluation process employed in this program. Section 4 contains a detailed description of the final longitudinal and lateral control laws that emerged from this program. Section 5 describes the longitudinal landing performance results that were obtained in the simulation. It provides data for the deterministic and stochastic performance of the control laws that were evaluated. Section 6 describes the simulation landing performance results for the lateral/directional axis. The impact of various error sources is analyzed and tradeoff studies leading to the final recommended control law are described. The conclusions derived from this work are presented in Section 7. Appendix A is a summary of airframe, controllers, sensors and disturbance mathematical models that were used in the simulation. Appendix B contains backup data for the longitudinal simulation results that are presented in Section 5 and Appendix C contains backup data for the lateral/directional results of Section 6.

2.0 THE RESEARCH AIRPLANE AND THE APPROACH CONDITION

A three view drawing of the experimental DHC-6, Twin Otter, is shown as Figure 2-1. The airplane had been originally designed as a light wing loading STOL airplane and therefore the only major airframe modification in the experimental version was the incorporation of the wing spoilers that are shown in Figure 2-1.

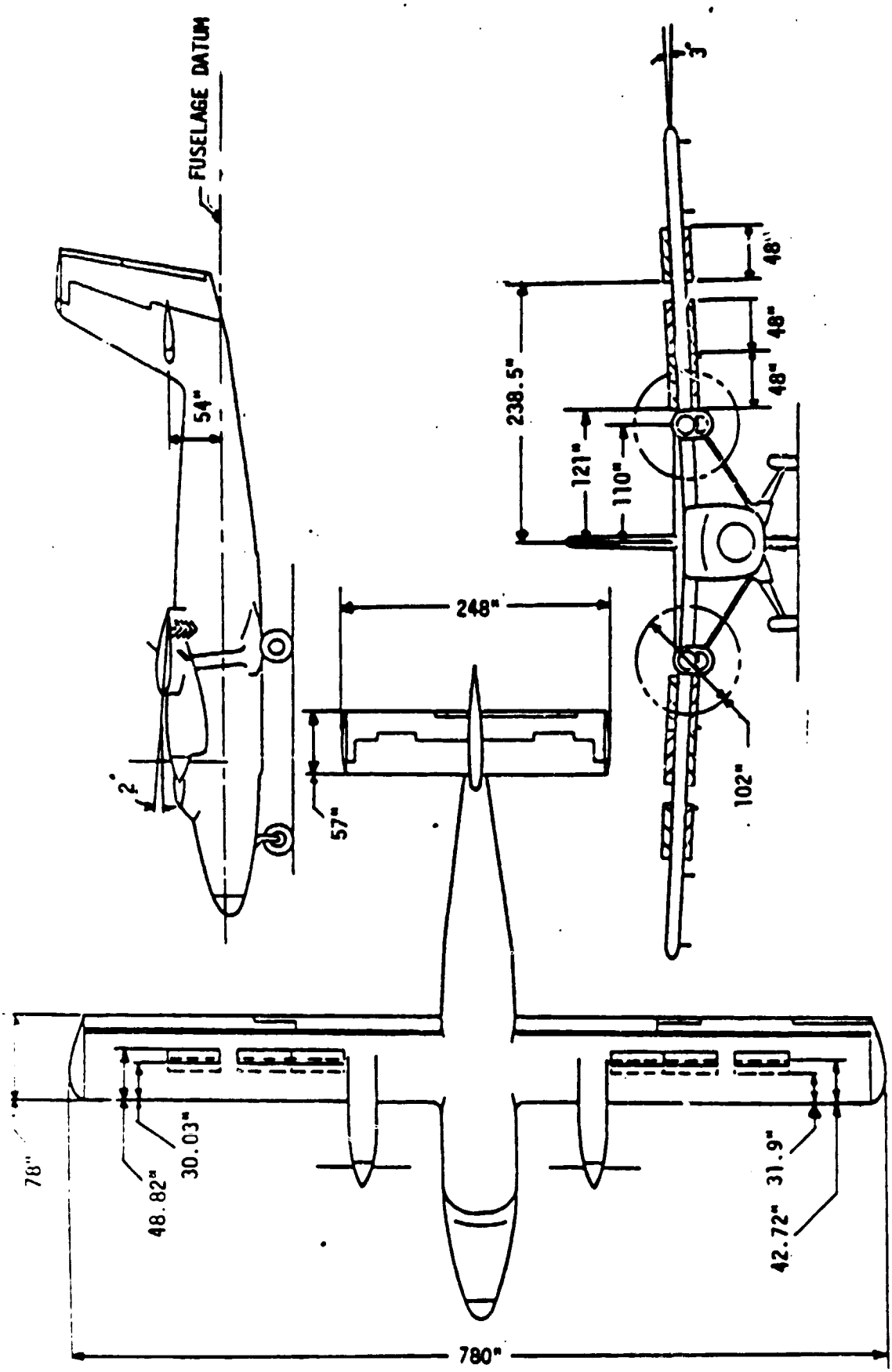

Figure 2-1. Three View Drawing of DHC-6

The nominal landing approach condition of the Twin Otter is compared in Table 2-I with that of the Augmentor Wing Research Aircraft which is a powered lift STOL airplane and the Lockheed L-1011 which is a typical example of a CTOL transport airplane.

TABLE 2-I STOL VERSUS CTOL LANDING APPROACH CONDITIONS

	AUG WING	TWIN OTTER	L-1011
Airspeed, kt	70	70	135
Glide Slope Angle, deg	7.5	6.0	2.75
Thrust Inclination, deg	90	50	0
Wing Loading N/m^2 (psf)	2378 (49.7)	1254 (26.2)	4359 (91.1)
Approach Lift Coefficient	3.0	1.5	1.5
Approach/Full Thrust, percent	85	10	25
Lift, Aerodynamic, percent	40	100	100
Cold Flow, percent	40	0	0
Hot Thrust, percent	20	0	0

NOTE: These numbers are representative and approximate; they are given in order to highlight the differences between the three aircraft rather than to provide exact data for each one.

The slow and steep approach is common to both STOL aircraft and it is in contrast with the fast and shallow approach of the CTOL airplane. The light wing loading Twin Otter, like the L-1011, derives essentially all its lift from aerodynamic sources, flies at a conventional lift coefficient value and with a low power setting. The relatively high thrust inclination of the Twin Otter is a result of the propeller flow acting on the wing and flap. Unlike the Augmentor Wing, the Twin Otter operates on the front side of the power curve at 1.3 times the stall speed and therefore the conventional control technique of using the elevator for flight path control and throttle for speed is effective for this airplane.

The spoilers shown in Figure 2-1 are the only non standard control on the Twin Otter. Each wing has a total of six panels, three on the upper surface and three on the lower one. The four inboard panels modulate lift and drag and the two outboard spoilers enhance roll control but were not used in this study. Of the four lift/drag spoilers, only the outboard upper panel was used since it was the most effective one. Flight tests show that the inner upper panel interacts with the horizontal tail and causes excessive buffetting and the lower panels have little aerodynamic effect. When used, the spoilers are biased at 20° and the airspeed is increased by four knots (to 75 knots at nominal weight) to compensate for the attendant increase in stall speed. The spoilers can be modulated between zero and 40° in the glide slope track phase, providing a direct lift control (DLC) authority of ±0.13 g. A buffetting tendency is associated with spoiler deflections of more than 40° but during the flare, deflections up to 50° are allowed.

Lateral/directional control is conventional with ailerons for roll and rudder for yaw.

The airplane is equipped with the STOLAND digital avionics system (Reference 8) providing versatile navigation, guidance, control and display functions.

During the first test period, two successive microwave landing systems were used for approach guidance, providing azimuth, elevation and distance information. The first of these was an experimental system called MODILS which had narrow azimuth coverage and a relatively granular azimuth signal. The second was a prototype of the microwave landing system that has been adapted by the Federal Aviation Administration.

3.0 DESIGN AND EVALUATION METHODS

3.1 SIMULATION

The development of a simulation allowing the collection of automatic landing performance with deterministic and stochastic disturbances is an important part of the certification process of a Category III automatic landing system for a CTOL aircraft, as described in References 1 through 6. Such a simulation of the Twin Otter was developed for this study as a major design and evaluation tool for

the control laws that were developed as part of this study. This simulation was also used for the evaluation of longitudinal control laws that were developed independently of this study. The best available airframe data were used in the simulation but a rigorous correlation between the simulation and flight test results was not included in this study. Also, the control laws that were developed during this study were not evaluated in flight as a result of flight time constraints. Thus, all landing performance results that are given in this report were obtained from the simulation.

The simulation that was used as the major tool for synthesizing and evaluating the automatic landing control laws was designed to operate ten times faster than real time in order to allow the collection of statistical data. Mathematical models of the airframe, controllers, sensors and the environment were assembled and used in the simulation. The normal set of uncoupled, linearized, small perturbation equations of motion were used in separate longitudinal and lateral simulations. Longitudinal dynamics were included in the lateral simulation to the extent necessary to account for the ground speeds associated with different headwinds. Lift, pitching moment, and drag variation due to ground effects were also included. Controller dynamics were modeled, including rate and position limits. Sensor dynamics and error models which contribute to landing dispersions were also included, such as radar altimeter dynamics and offsets, and dynamic and static vertical gyro and accelerometer errors. MLS noise was modeled and included in the simulation. Winds, shears and turbulence consistent with the definitions in the FAA Advisory Circular 20-57A (Reference 7) were used.

For statistical data collection, the simulation was run in fast time repetitive operation mode, starting at 152.4 m (500 ft) above the runway with the airplane stabilized on the glide slope or localizer, and terminating at touchdown. The 30.5 meters (100 foot) approach window states were recorded, as were the touchdown states: vertical and lateral velocity, touchdown point on the runway, and pitch, roll and heading angles. Data were taken for various levels of environmental disturbances, and system errors, covering a wider range than possible in flight. Probability distributions were generated for all touchdown state variables.

Appendix A contains a detailed description of the models used in the simulation.

3.2 THE STOL RUNWAY

The Twin Otter was flown by NASA Ames Research Center at Crows Landing Naval Auxiliary Landing Field (NALF) in California. The flight test landings were made on a simulated 518.3 by 30.5 meters (1700 by 100 feet) STOL runway with boundaries painted, in accordance with Reference 9, on a longer and wider runway. The runway geometry is shown in Figure 3-1. The 6° Glide Path Intercept Point is 71.6 meters (235 ft) beyond the threshold. All landing distance results in this report are referenced to the GPIP.

The marked touchdown zone extends from 19.8 m (65 ft) to 80.8 m (265 ft) beyond the GPIP.

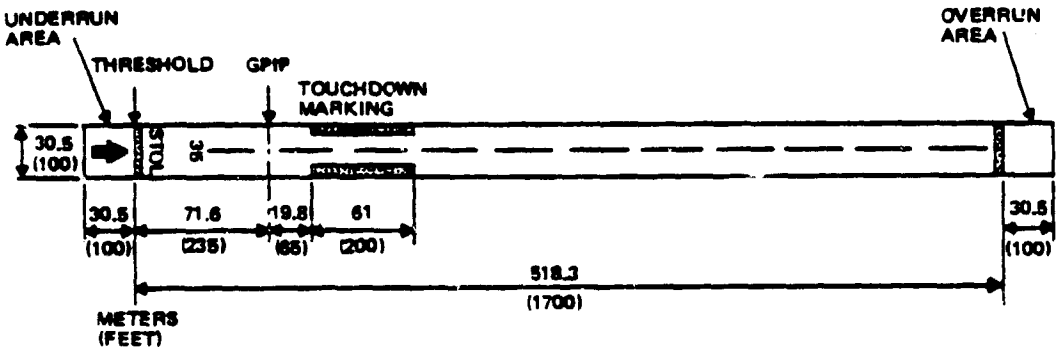

Figure 3-1. STOL Runway Geometry

3.3 LANDING PERFORMANCE OVERVIEW

A one sigma landing dispersion summary, comparing results obtained from simulation with limiting shear winds, moderate turbulence and beam noise for the Twin Otter with comparable Augmentor Wing results, is given in Table 3-I. The two aircraft differ significantly in their method of control in the longitudinal plane but are similarly controlled in the lateral/directional axis. The landing performance results are quite similar, however, in both axes.

Limiting winds refer to the limit values considered in the atmospheric disturbance model described in Appendix A; i.e., 25 kt headwinds and 10 kt tailwinds together with corresponding values of turbulence and shear. These levels should result in rather conservative estimates of aircraft dispersion due to this source but they provide a useful basis of comparison of performance between different aircraft and/or control systems.

TABLE 3-I ONE SIGMA LANDING DISPERSION SUMMARY

	TWIN OTTER		AUG WING	
	DLC	NO DLC	DLC	NO DLC
$\dot{h}$ m/sec (fps)	0.213 (0.70)	0.320 (1.05)	0.229 (0.75)	0.381 (1.25)
X m (ft)	30.5 (100)	36.6 (120)	32.0 (105)	47.2 (155)
θ deg	0.45	0.42	0.37	0.45
y m (ft)	1.49 (4.9)		1.28 (4.2)	
$\dot{y}$ m/sec (fps)	0.26 (0.85)		0.15 (0.50)	
$\Delta\psi$ deg	0.75		1.05	
ϕ deg	1.0		1.3	

NOTES:

1) The results shown are the dispersion between the mean and the one sigma point.

2) Simulation data with 70% limiting shearing headwind, 30% limiting shearing tailwind, the corresponding moderate turbulence, and beam noise.

3) Twin Otter longitudinal results are for the constant flare height low gain configuration, as defined in Section 5. Three and Two Control Augmentor wing results are given, as described in Reference 1.

Sink rate and range control for both aircraft benefit from the use of direct lift control. The Augmentor Wing no DLC longitudinal performance is 20% to 30% worse than the comparable Twin Otter results. Without DLC, flight path angle is controlled with thrust for the high wing loading Augmentor Wing airplane, and with attitude for the light wing loading Twin Otter. The results suggest that the latter is more effective for sink rate and range control. With DLC, both aircraft have similar performance as their control bandwidths are equalized. Pitch attitude dispersion is, somewhat surprisingly, similar for the two airplanes. Lateral results are also similar, with the Augmentor Wing being somewhat better in lateral displacement and velocity whereas the Twin Otter is aligned more accurately with the runway heading with somewhat less roll activity.

The Twin Otter landing performance results are described in detail in Section 5 for the longitudinal axis and in Section 6 for the lateral. Augmentor Wing results are given in Reference 1.

4.0 DESCRIPTION OF CONTROL LAWS

Two sets of control laws for automatic glide slope track and flare were evaluated in this study. One set was defined as part of the work reported here and it utilizes a constant flare initiation height and closed loop path control about a predetermined pitch trajectory command. The other set had been defined prior to this study and it uses a variable flare height and predictive pitch and elevator commands in addition to the closed loop control. The variable flare height control laws were evaluated in flight and in simulation whereas the constant flare height mechanization was evaluated in simulation only. Both sets of control laws were evaluated with and without the use of the DLC spoilers. Both control laws are described in Section 4.1. Evaluation results are given in Section 5.

Control laws for automatic localizer track and runway alignment were also defined and evaluated in simulation as part of this study. The final configuration that emerged from tradeoff studies is described here in Section 4.2. Tradeoff studies and evaluation results are presented in Section 6.

4.1 GLIDE SLOPE TRACK AND FLARE

4.1.1 CONSTANT FLARE HEIGHT

The constant flare height longitudinal control laws that have been developed for the Twin Otter as part of this study are shown in the block diagram of Figure 4-1 and the numerical values of gains an constants are defined in Table 4-I. A conventional, front side of the power curve, control technique is used on this light wing loading STOL airplane. The elevator is used for the control of flight path angle as well as attitude stabilization and control. The throttles are used for speed control. The DLC spoilers, when used, assist in the control of flight path angle.

Four filters are used to smooth inputs into the control law in order to reduce noise induced control activity. The block diagrams of the filters are given in Figure 4-2. Raw airspeed is blended with longitudinal acceleration in a complementary filter to produce a smoothed estimate of airspeed which is used to drive the throttles. Raw glide slope error, computed from elevation and range

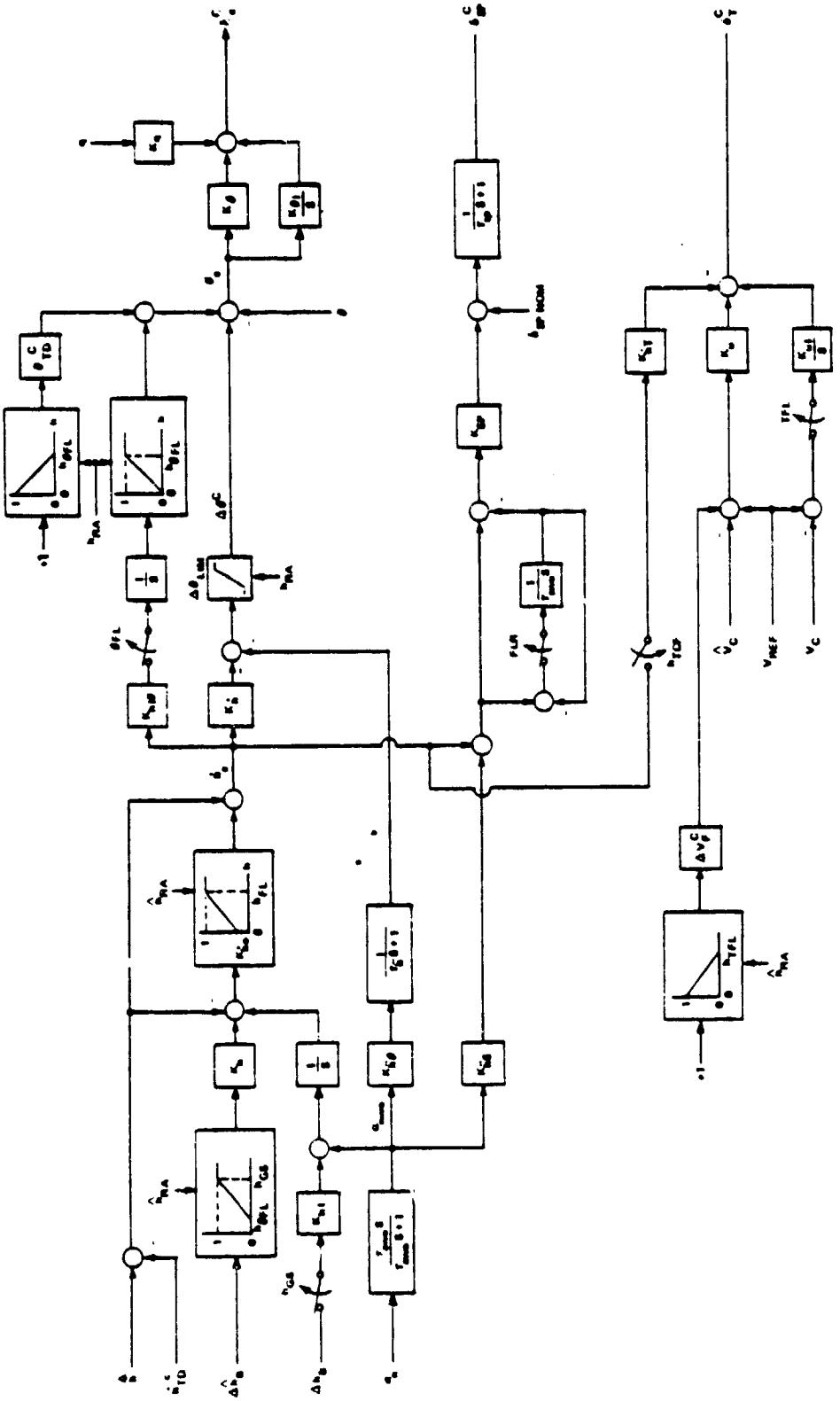

Figure 4-1. Glide Slope Track and Flare Block Diagram-Constant Flare Height

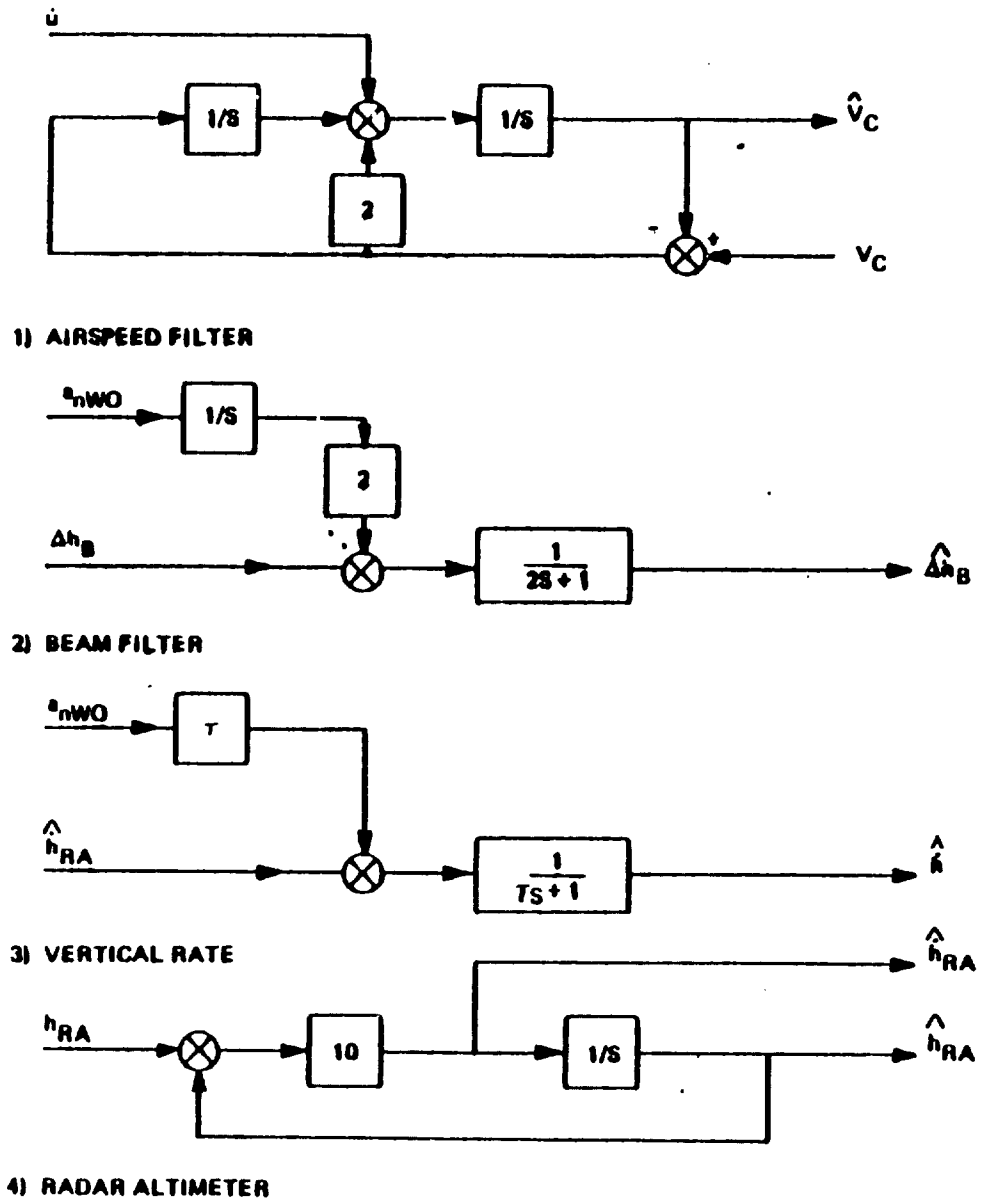

Figure 4-2. Longitudinal Filter Block Diagrams

TABLE 4-I LONGITUDINAL GAINS AND CONSTANTS
CONSTANT FLARE HEIGHT

GAINS		WITH SPOILERS	WITHOUT SPOILERS
K_q	deg/deg/sec	1.0	1.0
K_θ	deg/deg	2.0	2.0
$K_{\theta I}$	deg/sec/deg	0.50	0.50
$K_{\dot{h}}$	deg/m/sec (deg/fps)	3.28 (1.0)	3.28 (1.0)
$K_{\ddot{h}\theta}$	deg/m/sec^2 (deg/fps^2)	0.656 (0.2)	0.656 (0.2)
$K_{hI\theta}$	$\frac{\text{deg/sec}}{\text{m/sec}}$ ($\frac{\text{deg/sec}}{\text{fps}}$)	0.656 (0.2)	0.656 (0.2)
K_h	m/sec/m (fps/ft)	0.50	0.50
K_{hI}	m/sec^2/m (fps^2/ft)	0.050	0.050
K_u	cm/kt (in/kt)	0.323 (0.127)	0.323 (0.127)
K_{uI}	cm/sec/kt (in/sec/kt)	0.0323 (0.0127)	0.0323 (0.0127)
$K_{\dot{h}T}$	cm/m/sec (in/fps)	2.50 (0.30)	2.50 (0.30)
K_{SP}	deg/m/sec (deg/fps)	22.97 (7.0)	0
$K_{\ddot{h}S}$	$\frac{\text{m/sec}}{\text{m/sec}^2}$ (fps/fps^2)	0.50	-
$K_{\dot{h}0}$	-	0.20	0

CONSTANTS			
h_{GS}	m (ft)	30.48 (100)	30.48 (100)
h_{TFL}	m (ft)	12.19 (40)	18.29 (60)
$h_{\theta FL}$	m (ft)	15.24 (50)	15.24 (50)
h_{FL}	m (ft)	12.19 (40)	12.19 (40)
h_{TCF}	m (ft)	12.19 (40)	9.14 (30)
$\dot{h}_{TD}^c$	m/sec (fps)	0.853 (2.8)	1.219 (4.0)
θ_{TD}^c	deg	4.5	3.5
ΔV_F^c	kt	-14.8	-14.8

TIME CONSTANTS			
τ_{awo}	sec	15.0	15.0
$\tau_{\ddot{h}}$	sec	0.10	0.10
τ_{swo}	sec	5.0	-
τ_{SP}	sec	0.5	-

$$\Delta\theta_{LIM} = \pm 10^\circ \text{ @ } h \geq h_{\theta FL}$$
$$+10^\circ \text{ or } -10\frac{h}{h_{\theta FL}} \text{ @ } h < h_{\theta FL}$$

information, is combined with washed out normal acceleration in another complementary filter to produce an estimate of deviation from the glide-slope. A simple 0.1 second first order lag is used to filter the output of the radio altimeter and to derive sink rate. The derived sink rate is blended with washed out normal acceleration and the resultant sink rate signal is used in the flare.

Pitch attitude and rate feedbacks to the elevator are used for attitude stabilization and control (Figure 4-1). A pitch error integrator is used to maintain elevator trim. Smoothed glide-slope error is summed with the output of the glide-slope integrator to produce a sink rate error which is summed with washed out and lagged normal acceleration and commands attitude corrections. Washed out normal acceleration and raw glide slope error are used as inputs to the glide slope integrator such that it provides glide slope damping and helps to null the steady state error. While in the glide slope track mode, the radio altimeter based sink rate signal is subtracted ahead of the flare scheduler and added past it. Since this scheduler is at unity gain prior to flare the net result is that this path has no effect on the system. Attitude reference is generated by the sink rate error integrator while in the glide slope track mode. A transition from the glide slope track to the flare mode occurs between a gear height of h_{GS} (30.48 m or 100 ft) and $h_{\theta FL}$ (15.24 m or 50 ft). The glide slope error signal is faded out and the airplane maintains the glide slope sink rate. At $h_{\theta FL}$ an attitude change is commanded linearly with decreasing altitude from the approach to the touchdown value, as shown in Figure 4-3. The rotation arrests the sink rate and puts the airplane in a proper touchdown attitude. Through the flare, derived sink-rate is transitioned linearly with decreasing altitude from glide slope to radar altimeter based information, minimizing the impact of terrain irregularities. A straight line $h/\dot{h}$ profile from the existing pre-flare sink-rate to the desired touchdown value is commanded in the flare as shown in Figure 4-3. This results in an exponential flare, the time constant of which is proportional to the slope of the $h/\dot{h}$ line. The flare height is constant at 12.19 m (40 ft). The pre-flare sink-rate varies with the wind conditions, resulting in a flare time that is shorter with tailwind than with headwind. This variation in flare time tends to compensate for wind induced touchdown position dispersion. Without spoilers, a constant touchdown sink rate command of 1.219 m/sec (4.0 fps) is used. With spoilers, however,

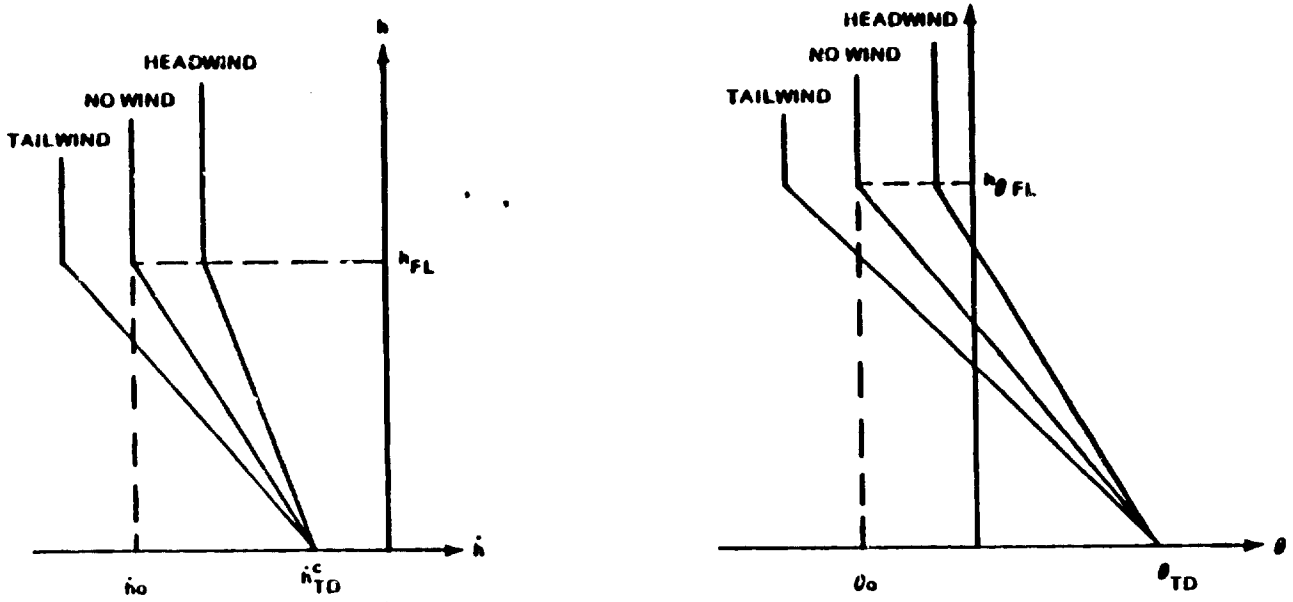

Figure 4-3. Flare Sink Rate and Attitude Trajectories

the flare scheduler gain at touchdown is non zero ($k_{\dot{h}_0}$ is 0.2, as shown in Table 4-I) and consequently an incremented touchdown sink rate command, that is a function of pre-flare sink rate, is introduced. The sink rate error is used to modulate the linear pitch attitude command that is shown in Figure 4-3. The allowed nose down command is reduced from -10° at pitch flare height to zero at touchdown, as indicated by $\Delta\theta_{LIM}$ in Figure 4-1 and Table 4-I.

The throttles are used to maintain the approach airspeed while tracking the glideslope. A speed reduction command is applied during the flare, increasing linearly with decreasing height. Sink rate error is cross fed to the throttles during the flare in order to enhance vertical control and compensate for the limited ability to use nose down commands close to the ground.

When the DLC spoilers are used they are driven with a blend of sink rate error and washed out and lagged normal acceleration. The spoilers are used for short term flight path angle corrections both in glide slope track and flare. The spoilers allow a faster modulation of normal acceleration than pitch changes do and therefore they allow an increase of system bandwidth and improve the rejection of disturbances. In glide slope track, the spoiler command is being washed out with a five second time constant in order to preserve their full dynamic range to counter rapid disturbances while handling slow trim changes with pitch attitude. In the flare, the spoiler washout is eliminated such that the full available spoiler lift modulation capability can be used and held if needed.

4.1.2 VARIABLE FLARE HEIGHT

The variable flare height control law had been designed prior to this study, excluding the spoiler control. It has been tested and refined in flight. One task of this study called for simulating this control law in order to evaluate its performance in comparison with the constant flare height control law. Also, the spoiler control law that had been developed in this study for the constant flare height mechanization was adapted and tested in flight with the variable flare height system. Elevator and throttle control of the variable flare height law are defined by the block diagram of Figure 4-4. The spoiler control for this system is shown in Figure 4-5 and the numerical values of the associated gains and constants are defined in Table 4-II.

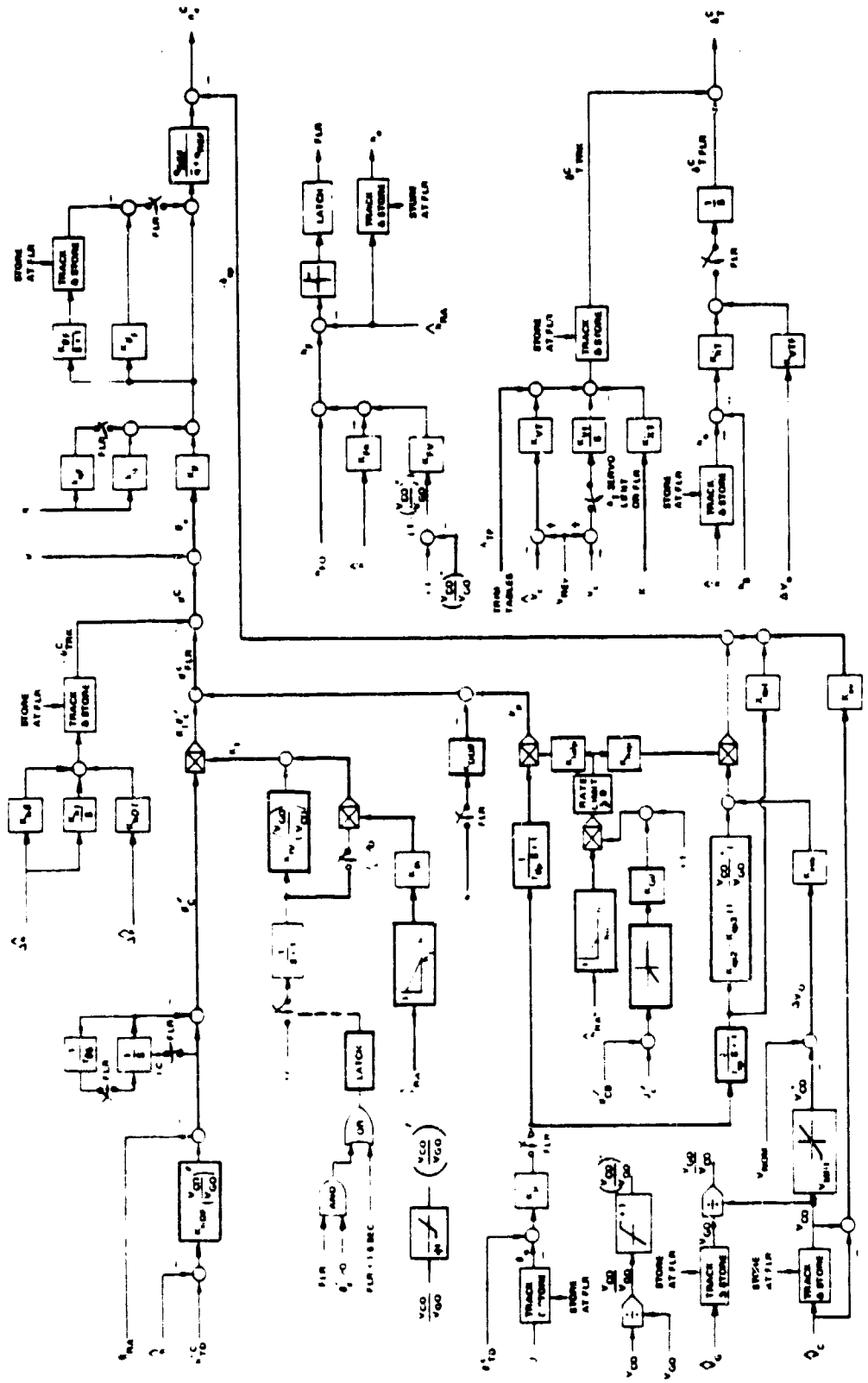

Figure 4-4. Glide Slope Track and Flare Block Diagram-Variable Flare Height

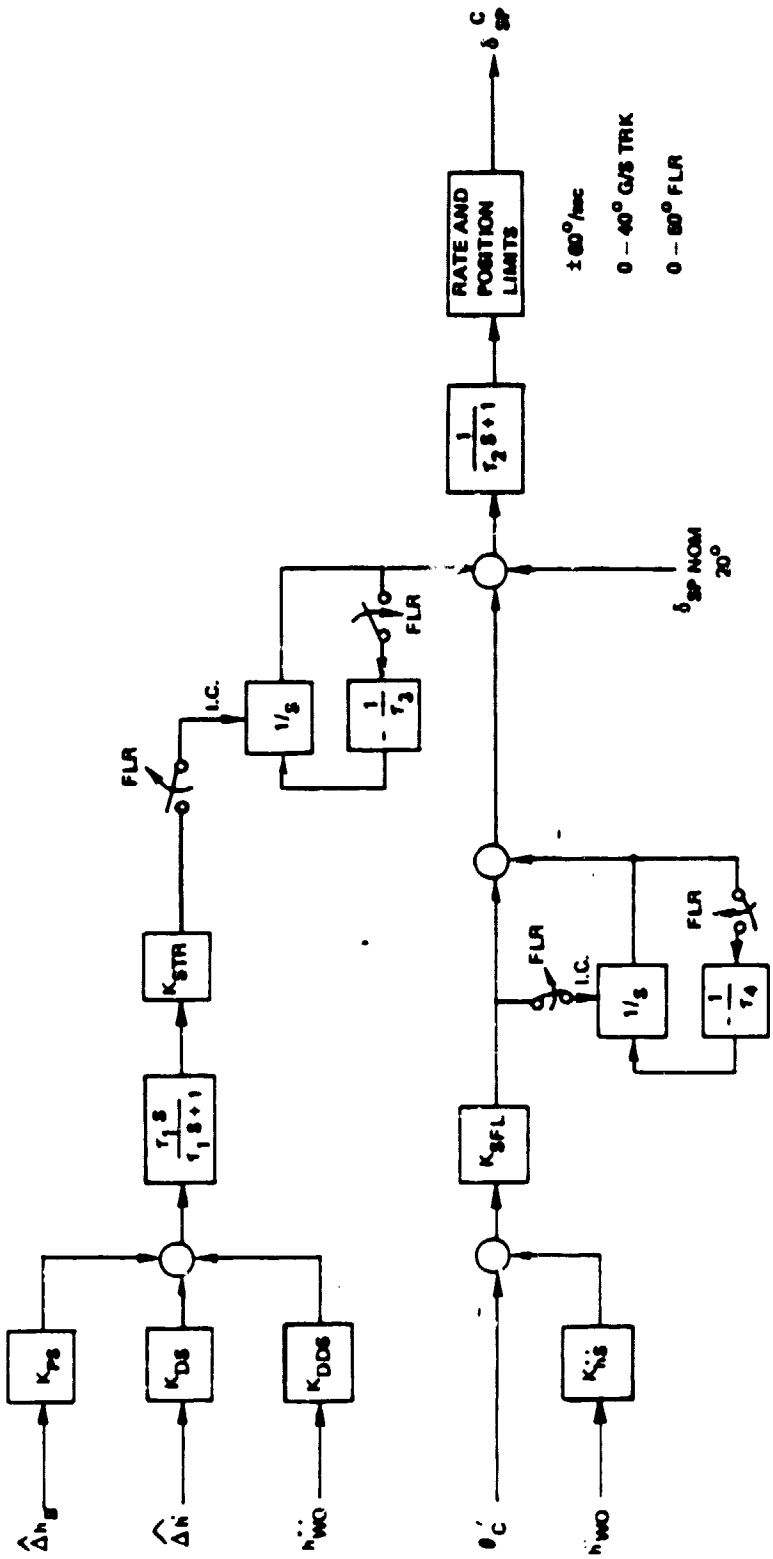

Figure 4-5. Spoiler Control Block Diagram – Variable Flare Height

TABLE 4-II LONGITUDINAL GAINS AND CONSTANTS - VARIABLE FLARE HEIGHT

PITCH SAS

K_{θ}	deg/deg	1.2
K_{θ_F}	deg/deg	1.0
K_q	deg/deg/sec	0.9
K_{qF}	deg/deg/sec	0.29
q_{REF}	N/m^2 (psf)	1532 (32.0)

θ PREDICT

θ_{TD}^{C}	deg	3.6
K_p	deg/deg	0.1818
$\tau_{\theta p}$	sec	2.0
$K_{h\theta P}$	-	5.365
θ_{CB}	deg	3.25
$K_{G\theta}$	1/deg	0.05

THROTTLE CONTROL

K_{VI}	cm/sec/kt	(in/sec/kt)	0.2032	(0.008)
K_{VT}	cm/kt	(in/kt)	0.3302	(0.13)
$K_{\ddot{X}T}$	$cm/m/sec^2$	(in/fps^2)	1.583	(0.19)
$K_{\dot{h}T}$	$\frac{cm/sec}{m/sec}$	(in/sec/fps)	0.104	(0.0125)
K_{VTF}	cm/sec/kt	(in/sec/kt)	0.127	(0.05)

G/S TRACK

K_{hI}	deg/sec/m	(deg/sec/ft)	0.0909	(0.0277)
$K_{h\theta}$	deg/m	(deg/ft)	1.093	(0.333)
K_{hDT}	deg/m/sec (deg/fps)		3.645 (1.111),	1.348* (0.411*)

CLOSED LOOP FLARE

$\dot{h}_{TD}^{C}$	m/sec (fps)	-0.686 (-2.25)	
K_{hDF}	deg/m/sec (deg/fps)	9.908, (3.02),	7.94* (2.42*)
$\tau_{\theta S}$	sec	0.65,	1.33*
K_{IV}	-	0.44	
K_{Ih}	-	0.721	
h_I	m (ft)	3.81 (12.5)	
$K_{DD\theta}$	$deg/m/sec^2$, (deg/fps^2)	0.623, (0.19)	

ELEVATOR PREDICT

K_{hep}	-	4.025
K_{ep1}	deg/deg	1.3
K_{ep2}	deg/deg	0.524
K_{ep3}	deg/deg	1.225
V_{MIN}	kt	68.0
V_{NOM}	kt	66.0
K_{evo}	deg/kt	0.04
K_{ev}	deg/kt	0.40
τ_{ep}	sec	0.33

FLARE HEIGHT

h_{FO}	m (ft)	5.27 (17.3)	
$K_{Fh}^{\cdot}$	m/m/sec (ft/fps)	2.5	(2.5)
K_{FV}	m (ft)	8.26 (27.1)	

SPOILER CONTROL

K_{ps}	deg/m	(deg/ft)	1.093	(0.333)
K_{DS}	deg/m/sec	(deg/fps)	2.005	(0.611)
K_{DDS}	$deg/m/sec^2$	(deg/fps^2)	0.984	(0.300)
K_{STR}	deg/deg		11.0	
$K_{\ddot{h}S}$	$deg/m/sec^2$	(deg/fps^2)	1.312	(0.4)
K_{SFL}	deg/deg		4.0	
τ_1	sec		3.0	
τ_2	sec		0.5	
τ_3	sec		2.5	
τ_4	sec		1.0	

* WITH SPOILERS

The allocation of controllers is the same as in the previously described constant flare height control law. The elevator is used for attitude stabilization and control and for flight path angle control. The throttles are used to maintain airspeed while tracking the glide slope. The spoilers assist in controlling flight path angle when used. Pitch attitude and rate are used as feedbacks to the elevator for pitch stabilization. The elevator gain is scheduled with dynamic pressure and the elevator and pitch rate gains are higher in the flare than in glide slope track, as can be seen in Figure 4-4. Smoothed glide slope error, its integral and estimated glide slope rate generate pitch attitude commands to track the glide slope. At flare, the last glide slope track pitch command is held and retained. Flare attitude commands come from two sources. A closed loop command, θ'_c, controlling sink rate as a function of gear height and a predictive command, θ_p, that is proportional to the difference between the commanded touchdown attitude and the approach attitude and is increased linearly with decreasing altitude. A direct predictive elevator command, δ_{ep}, is also computed based on the difference between the commanded touchdown attitude and the pre-flare attitude, pre-flare airspeed and ground speed, as shown in Figure 4-4.

Flare height is computed as a function of sink rate as shown in Figure 4-4. An increase in flare height with tailwind is computed using the ratio of airspeed to groundspeed. Flare height as a function of sink rate is given in Figure 4-6. One line is shown for headwind or zero wind and another one for a 10 knot steady tailwind. The closed loop commanded flare trajectories for a 25 knot steady headwind, zero headwind, and a 10 knot steady tailwind are also shown in Figure 4-6. These trajectories are the loci of $\theta'_c = 0$. Above the trajectory a nose down command is computed and below the trajectory nose up is commanded. The commanded touchdown sink rate is constant at 0.686 m/sec (2.25 fps). The nominal pre-flare sink rate for an approach speed of 71 knots and a glide slope of 6° is also shown in Figure 4-6 for a 25 knot steady headwind, zero headwind and 10 knots steady tailwind. In all cases flare height is above the commanded closed loop trajectory. This is done in order to allow time to "turn the corner" and minimize the undershoot of the sink rate trajectory. The initial rotation is provided by the pitch and elevator predict terms while θ'_c is inhibited during the initial 1.5 seconds of the flare if nose down is being commanded, as shown in Figure 4-4. A transition from the flare height line to the closed loop control line is computed through use of the "flare switch" circuit shown in Figure 4-4. θ'_c is faded in at flare initiation. The gain from θ'_c to pitch attitude is proportional to

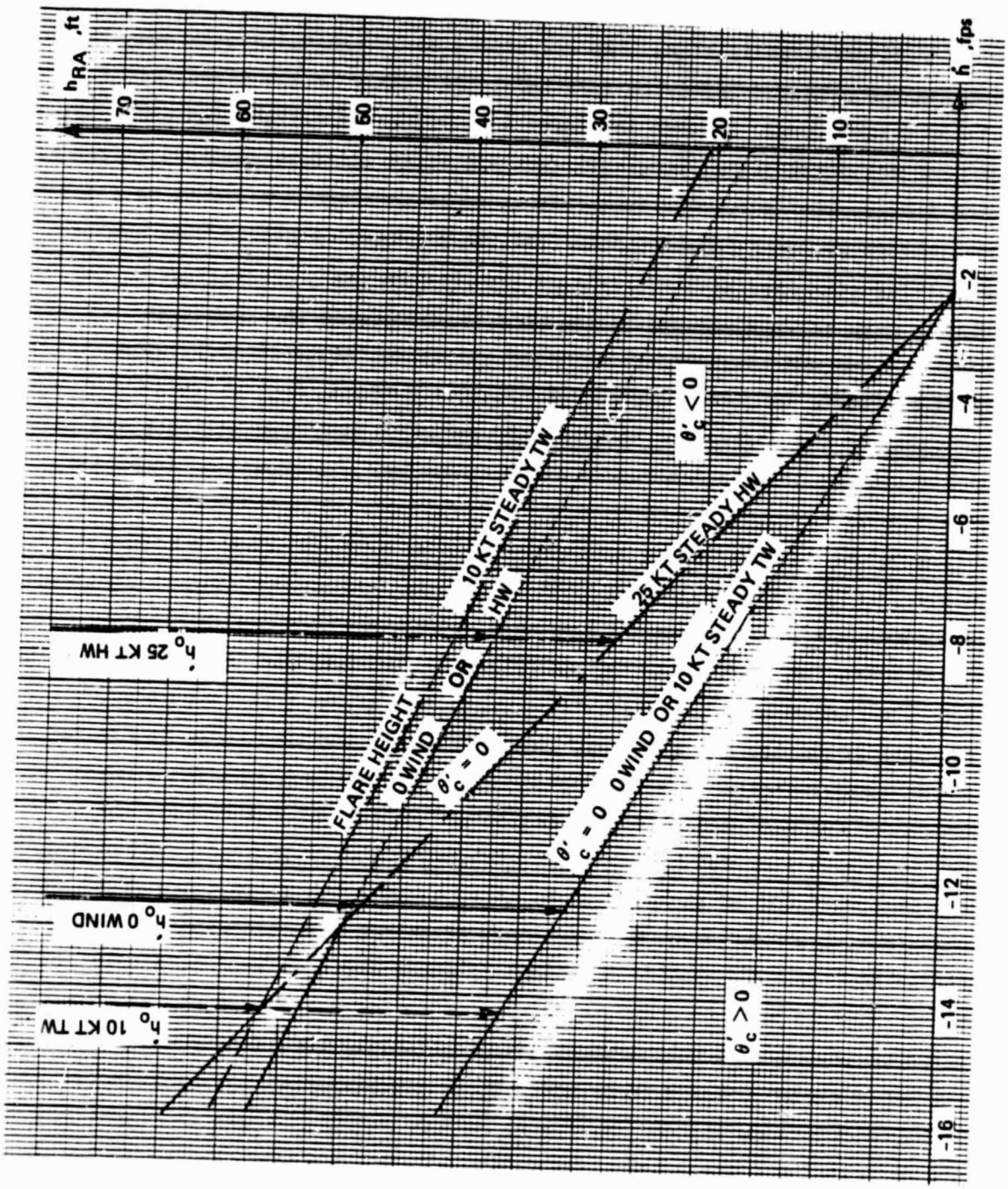

Figure 4-6. Flare Trajectories – Variable Flare Height

ORIGINAL PAGE IS
OF POOR QUALITY

the ratio between pre-flare ground speed to airspeed. Below 3.81 m (12.5 ft) higher gain is used for nose up commands than for nose down. Vertical acceleration feedback is added to the pitch command during flare to improve damping.

During glide slope track the throttles are used to control airspeed. An open loop throttle trim position is supplied from trim tables. Filtered airspeed error, the integral of raw airspeed error and longitudinal acceleration are summed to provide a closed loop throttle command. At flare, this command is held constant and a constant rate retard is computed from pre-flare sink rate and airspeed. The fact that the throttles are not used actively through the flare is considered as a disadvantage of this mechanization in comparison with the constant flare height control law.

When the spoilers are used they are biased to 20°. As in the constant flare height control law, they are used to provide rapid short term flight path angle corrections. While tracking the glide slope, filtered glide slope error, estimated glide slope deviation rate and washed out vertical acceleration are summed with the appropriate gains to generate the spoiler command (Figure 4-5). This command is washed out with a 3 second time constant in order to maintain the full steady state lift modulation capability. At flare, the glide slope command is faded out and the flare command, made of θ'_c, and washed out vertical acceleration, is faded in. The flare command to the spoilers is not washed out.

4.2 LOCALIZER TRACK AND RUNWAY ALIGNMENT

The sensitivity to external disturbances and large crab angles typical of STOL aircraft places stringent demands on the design of the automatic landing system. The accurate control of aircraft position and heading required just prior to touchdown makes the runway alignment the most critical phase of the lateral landing control problem. Several candidate control laws were developed as part of this study and evaluated by simulation. All the control laws developed in this study used toward slip for runway alignment because this technique was determined to be superior in a study that had been done for the Augmentor Wing Aircraft (Reference 3). Tradeoffs were made in other areas and the results are presented in Section 6. The control law that produced the best results is described in this

section. Figure 4-7 is a block diagram of the localizer track and runway alignment control law. The numerical values of the associated gains and constants are defined in Table 4-III. Roll control on the Twin Otter airplane is conventional with the control wheel mechanically linked to the ailerons. The lateral control law output commands a wheel position for roll control. Raw localizer lateral displacement computed from azimuth angle deviation and range, is blended with cross track acceleration in a complementary filter. The estimated localizer deviation and its rate are used to command bank angle. Additional pseudo rate is provided by filtering cross track acceleration with a 20 second first order lag. This helps reduce MLS beam noise induced control activity. The yaw rate, lateral acceleration and bank angle command signals are fed through gains and summed to drive the rudder for yaw stability augmentation and turn coordination. Yaw rate and rudder position command cross fed to the wheel are used to minimize the degradation of localizer tracking accuracy due to the airplane's pronounced dihedral effect.

A forward slip maneuver is used for runway alignment. Beginning at an altitude of 45.7 m (150 ft), an align command is switched into the yaw axis. This reference heading command is reduced from the heading error existing at alignment initiation to zero at 15.2 m (50 ft), yielding an alignment rate which is a function of both initial heading error and aircraft sink-rate. The error from the commanded heading trajectory is integrated to maintain the steady rudder required during alignment. In the roll axis, the beam computations are maintained to guide the vehicle along the desired horizontal path, with increased pseudo cross track rate gain for better control. Wing down compensation is provided by inserting cross track acceleration and bank angle through a one second lag and a $\pm 5^{\circ}$ limit. This results in a one second washout on the roll attitude feedback within the $\pm 5^{\circ}$ bank limit which allows roll attitude to reach the value needed to null the cross track acceleration. The 5° alignment limit is ample for steady crosswind levels higher than the 15 knot specifed by the FAA as the limiting case (Reference 7), and minimizes the potential for large touchdown bank angles. If the limit is exceeded, the vehicle will maintain a small crab angle.

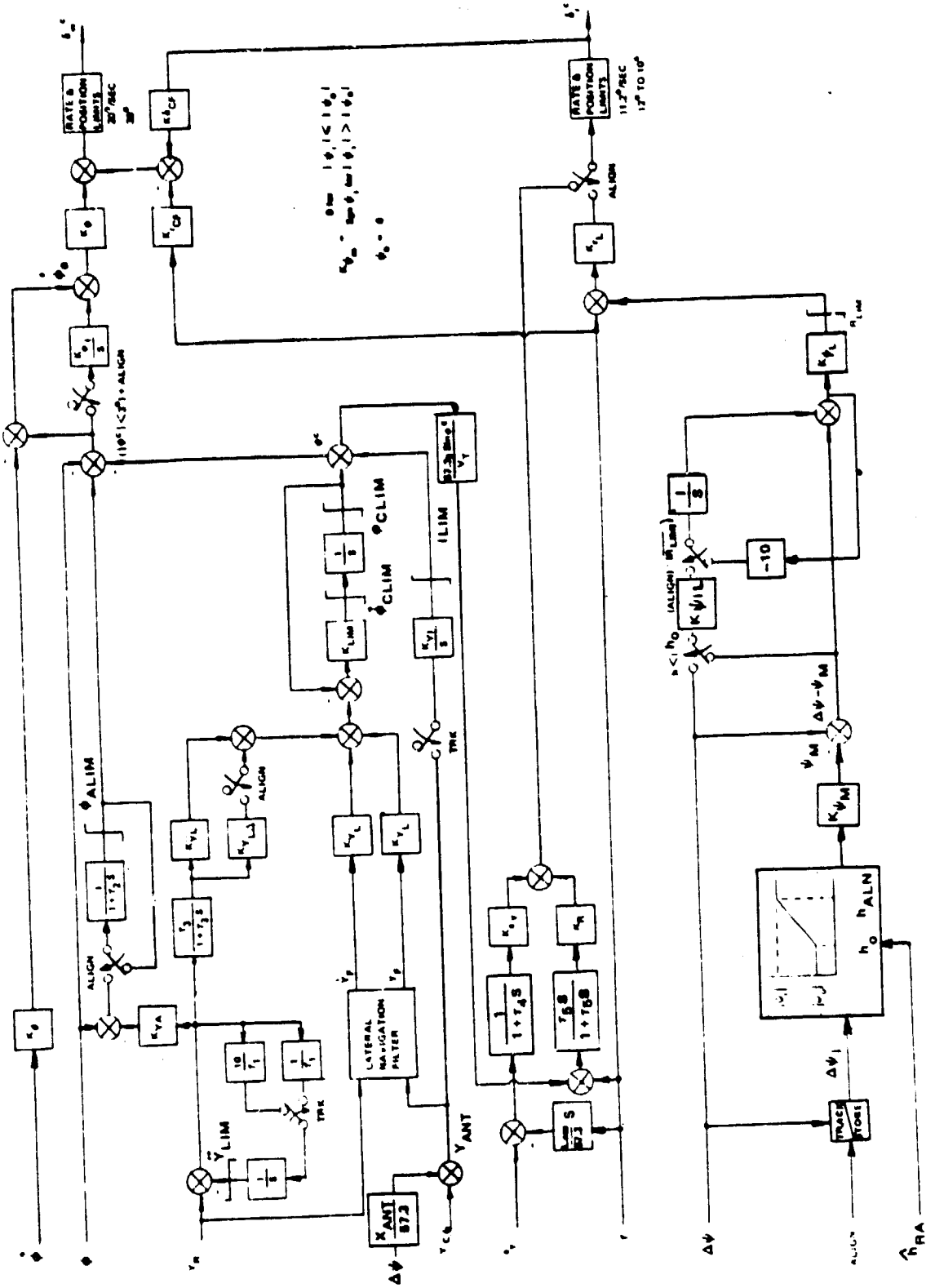

Figure 4-7. Localizer Track and Runway Alignment Block Diagram

TABLE 4-III LATERAL GAINS AND CONSTANTS

GAINS

$K_{\dot{\phi}}$	deg/deg/sec		0.25	
K_{ϕ}	deg/deg		4.0	
$K_{\phi I}$	deg/sec/deg		0.1	
$K_{\ddot{Y}A}$	deg/m/sec^2	(deg/fps^2)	5.84	(1.78)
$K_{\ddot{Y}L}$	deg/m/sec^2	(deg/fps^2)	1.23	(0.375)
$K_{\ddot{Y}L\Delta}$	deg/m/sec^2	(deg/fps^2)	1.23	(0.375)
$K_{\dot{Y}L}$	deg/m/sec	(deg/fps)	0.820	(0.25)
K_{YL}	deg/m	(deg/ft)	0.197	(0.06)
K_{LIM}	deg/sec/deg		10.0	
K_{YI}	deg/sec/m	(deg/sec/ft)	0.0033	(0.001)
K_{rCF}	deg/deg/sec		4.0	
$K_{\delta CF}$	deg/deg		0.5	
K_{ay}	deg/m/sec^2	(deg/fps^2)	5.38	(1.64)
K_{R}	deg/deg/sec		2.14	
K_{rL}	deg/deg/sec		4.0	
$K_{\psi L}$	deg/deg		0.75	
$K_{\psi IL}$	deg/sec/deg		0.10	

CONSTANTS

h_{ALN}	m (ft)	45.72	(150)
h_{o}	m (ft)	15.24	(50)
ϕ_{ALIM}	deg	±5.0	
Y_{LIM}	m/sec^2 fps^2	±0.975	(±3.2)
$\dot{\phi}_{CLIM}$	deg/sec	±3.0	
ϕ_{CLIM}	deg	±5.0	
I_{LIM}	deg	±2.0	
R_{LIM}	deg/sec	±4.0	
X_{ANT}	m (ft)	(5.97)	(19.6)
L_{acc}	m (ft)	0.706	(2.31)

TIME CONSTANTS

τ_1	sec	50.0
τ_2	sec	1.0
τ_3	sec	20.0
τ_4	sec	0.10
τ_5	sec	5.0

5.0 LONGITUDINAL PERFORMANCE

The major thrust of this study was to develop automatic landing control laws for the Twin Otter STOL airplane and to evaluate the performance of these control laws in a fast time simulation that allows the collection of statistical data based on a large number of landings. The performance results of the simulation were used to refine the control laws in order to optimize their performance. This section describes the results obtained from this fast time simulation.

The constant flare height control law, described in Section 4.1.1 was developed and evaluated as part of this study with and without the use of DLC spoilers. The variable flare height control law, described in Section 4.1.2 had been developed independently of the work reported here and it has been tested in flight and refined by NASA. This control law has been implemented in the fast time simulation and its performance was evaluated and compared with that of the constant flare height law. The results of the simulation evaluation are described in the following sections.

5.1 EVALUATED CONFIGURATIONS

A total of six glide slope track and flare control law configurations have been implemented in the simulation and evaluated during this study as shown in Table 5-I.

TABLE 5-I EVALUATED CONFIGURATIONS

FLARE HEIGHT	GAINS	SPOILERS	FLOWN
1) Variable	Low	No	Yes
2) Variable	Low	Yes	Yes
3) Constant	High	No	No
4) Constant	High	Yes	No
5) Constant	Low	No	No
6) Constant	Low	Yes	No

Initially, only two constant flare height configurations were developed (items 3, 4 in the Table). The variable flare height configurations, however, used lower gains in some paths and therefore the low gain constant flare height configurations (items 5 and 6 in the Table) were defined and evaluated in order to allow to differentiate between performance benefits that result from control law structure and these that are derived from higher gains. The high gain constant flare height system may be somewhat unrealistic since it has not been flown and the simulation math models are probably more benign than the real airplane. The low gain constant flare height configuration, however, uses gains that are equal or lower than these used in the variable flare height configuration (which was tested in flight) and therefore it is very likely to be realizable. The high gain constant flare height configuration is defined in Section 4.1.1. It's block diagrams are given in Figures 4-1 and 4-2. Table 5-II defines the numerical values of the gains and constants of the high gain and the low gain constant flare height control laws. The time constants, as given in Table 4-I, are common to both variants. The high gain constant flare height system uses the same gains for glide slope track and for flare. The variable flare height system uses higher gains for flare in some paths. Therefore, in the low gain constant flare height configuration gains are switched in order to match the variable flare height values. Table 5-III compares gains of all six configurations in all the paths. The gain of pitch rate to elevator in the high gain variant of the constant flare height control law is higher than the gain used by the variable flare height law in glide slope track but lower in the flare. In the low gain variant, pitch rate to elevator gains are adjusted to match these of the variable flare height system. Pitch attitude to elevator gain in the high gain variant is higher than used by the variable flare height law in glide slope track or flare. Again, the gains were adjusted in the low gain variant to match these of the variable flare height configuration, as can be seen from Table 5-III. The high gain constant flare height system includes a path of integrated pitch error to the elevator. The variable flare height configuration does not have such a path. Thus, this path has been eliminated from the glide slope track mode of the low gain variant. However, it has been retained in flare as it is needed to compensate for ground effect induced trim changes, a function that is handled by the elevator predict terms in the variable flare height configuration. Vertical acceleration feedback to attitude command is used by the variable flare height control law only in the flare.

TABLE 5-IIA LIST OF GAINS AND CONSTANTS - CONSTANT FLARE HEIGHT (METRIC UNITS)

			HIGH GAINS		LOW GAINS	
		SPOILERS	YES	NO	YES	NO
K_q	(TRK)	deg/deg/sec	1.0		0.585	
K_q	(FLR)	deg/deg/sec	1.0		1.55	
K_θ	(TRK)	deg/deg	2.0		0.780	
K_θ	(FLR)	deg/deg	2.0		1.56	
$K_{\theta I}$	(TRK)	deg/sec/deg	0.50		0	
$K_{\theta I}$	(FLR)	deg/sec/deg	0.50		0.50	
$K_{\dot{h}}$	(TRK)	deg/m/sec	3.28		1.35	3.28
$K_{\dot{h}}$	(FLR)	deg/m/sec	3.28		3.28	
$K_{\ddot{h}\theta}$	(TRK)	deg/m/sec^2	0.656		0	
$K_{\ddot{h}_\theta}$	(FLR)	deg/m/sec^2	0.656		0.656	
$K_{hI\theta}$		deg/sec/m/sec	0.656		0.656	
K_h		m/sec/m	0.50		0.50	0.333
K_{hI}		m/sec^2/m	0.050		0.050	0.0277
K_u		cm/kt	0.323		0.323	
K_{uI}		cm/sec/kt	0.0323		0.0198	
$K_{\dot{h}T}$		cm/m/sec	2.50		2.50	
K_{sp}		deg/m/sec	22.97	-	22.97	-
$K_{\ddot{h}s}$		m/sec/m/sec^2	0.50		0.50	
$K_{\dot{h}o}$		-	0.20	0	0	
h_{GS}		m	30.48		30.48	
h_{TFL}		m	12.19	18.29	12.19	18.29
$h_{\theta FL}$		m	15.24		15.24	

TABLE 5-IIA LIST OF GAINS AND CONSTANTS - CONSTANT FLARE HEIGHT (METRIC UNITS)

(CONTINUED)

			HIGH GAINS		LOW GAINS	
		SPOILERS	YES	NO	YES	NO
h_{FL}	m		12.19		12.19	
h_{TCF}	m		12.19	9.14	12.19	9.14
$\dot{h}^{C}_{TD}$	m/sec		0.853	1.219	1.280	1.067
θ^{C}_{TD}	deg		4.5	3.5	4.5	3.5
ΔV^{C}_{F}	kt		-14.8		-14.8	

TABLE 5-IIB LIST OF GAINS AND CONSTANTS - CONSTANT FLARE HEIGHT (ENGLISH UNITS)

			HIGH GAINS		LOW GAINS	
		SPOILERS	YES	NO	YES	NO
K_q	(TRK)	deg/deg/sec	1.0		0.585	
K_q	(FLR)	deg/deg/sec	1.0		1.56	
K_θ	(TRK)	deg/deg	2.0		0.780	
K_θ	(FLR)	deg/deg	2.0		1.56	
K_{θ_I}	(TRK)	deg/sec/deg	0.50		0	
K_{θ_I}	(FLR)	deg/sec/deg	0.50		0.50	
$K_{\dot{h}}$	(TRK)	deg/fps	1.0		0.411	1.0
$K_{\dot{h}}$	(FLR)	deg/fps	1.0		1.0	
$K_{\ddot{h}\theta}$	(TRK)	deg/fps^2	0.20		0	
$K_{\ddot{h}\theta}$	(FLR)	deg/fps^2	0.20		0.20	
$K_{h_I\theta}$		deg/sec/fps	0.20		0.20	
K_h		fps/ft	0.50		0.60	0.333
K_{h_I}		fps^2/ft	0.060		0.060	0.0277
K_u		in/kt	0.127		0.127	
K_{u_I}		in/sec/kt	0.0127		0.0078	
$K_{\dot{h}_T}$		in/fps	0.30		0.30	
K_{sp}		deg/fps	7.0	–	7.0	–
$K_{\ddot{h}_s}$		fps/fps^2	0.50		0.50	
$K_{\dot{h}_o}$		–	0.20	0	0	
h_{GS}		ft	100		100	
h_{TFL}		ft	40	60	40	60
$h_{\theta FL}$		ft	60		60	
h_{FL}		ft	40		40	
h_{TCF}		ft	40	30	40	30
$\dot{h}^C_{TD}$		fps	2.8	4.0	4.2	3.5
θ^C_{TD}		deg	4.5	3.5	4.5	3.5
ΔV^C_F		kt	-14.8		-14.8	

TABLE 5-IIIA GAIN COMPARISON (METRIC UNITS)

			VAR FLR HT		CONST FLR HT HIGH GAINS		CONST FLR HT LOW GAINS	
			TRK	FLR	TRK	FLR	TRK	FLR
$q \rightarrow \delta_e$		deg/deg/sec	0.585[1]	1.55[1]	1.0		0.585	1.55
$\theta \rightarrow \delta_e$		deg/deg	0.780[1]	1.56[1]	2.0		0.780	1.56
$\int\theta \rightarrow \delta_e$		deg/sec/deg	-	-	0.5		0	0.5
$\ddot{h} \rightarrow \theta$		deg/m/sec^2	-	0.623	0.656		0	0.656
$\dot{h} \rightarrow \theta$	NO SPOILERS	deg/m/sec	3.645	4.36[2] 11.52[3]	3.28		3.28	
$\dot{h} \rightarrow \theta$	WITH SPOILERS	deg/m/sec	1.348	3.48[2] 9.19[3]	3.28		1.348	3.28
$\int\dot{h}_e \rightarrow \theta$		deg/sec/m/sec	-	-	0.656	0	0.656	0
$\Delta h \rightarrow \theta$	NO SPOILERS	deg/m	1.09	-	1.64	-	1.09	-
$\Delta h \rightarrow \theta$	WITH SPOILERS	deg/m	1.09	-	1.64	-	0.676	-
$\int\Delta h \rightarrow \theta$	NO SPOILERS	deg/sec/m	0.0909	-	0.164	-	0.0909	-
$\int\Delta h \rightarrow \theta$	WITH SPOILERS	deg/sec/m	0.0909	-	0.164	-	0.0676	-
$\ddot{x} \rightarrow \delta_{th}$		cm/m/sec^2	1.08	-	-		-	
$U \rightarrow \delta_{th}$		cm/kt	0.33	-	0.323		0.323	
$\int U \rightarrow \delta_{th}$		cm/sec/kt	0.008	-	0.0323	-	0.0203	-
$\dot{h} \rightarrow \delta_{th}$		cm/sec/m/sec	-		-	2.5	-	2.5
τ_{th}		sec	1.0		0		1.0	
$\ddot{h} \rightarrow \delta_{sp}$		deg/m/sec^2	10.83	5.25	11.48		11.48	
$\dot{h} \rightarrow \delta_{sp}$		deg/m/sec	22.05	13.98[2] 36.88[3]	22.96		22.96	
$\Delta h \rightarrow \delta_{sp}$		deg/m	12.0	-	11.48	-	11.48	-

NOTES:) AT 71 kt 2) WITH O HW AND h <3.72m 3) WITH O HW AND $\theta_c' > 0$ AT h = 0

TABLE 5-IIIB GAIN COMPARISON (ENGLISH UNITS)

			VAR FLR HT		CONST FLR HT HIGH GAINS		CONST FLR HT LOW GAINS	
			TRK	FLR	TRK	FLR	TRK	FLR
$q \rightarrow \delta_e$		deg/deg/sec	0.586[1]	1.55[1]	1.0		0.586	1.55
$\theta \rightarrow \delta_e$		deg/deg	0.780[1]	1.56[1]	2.0		0.780	1.56
$\int\theta \rightarrow \delta_e$		deg/sec/deg	–	–	0.5		0	0.5
$\ddot{h} \rightarrow \theta$		deg/fps^2	–	0.19	0.20		0	0.20
$\dot{h} \rightarrow \theta$	NO SPOILERS	deg/fps	1.111	1.33[2] 3.51[3]	1.0		1.0	
$\dot{h} \rightarrow \theta$	WITH SPOILERS	deg/fps	0.411	1.06[2] 2.80[3]	1.0		0.411	1.0
$\int\dot{h}_e \rightarrow \theta$		deg/sec/fps	–	–	0.20	0	0.20	0
$\Delta h \rightarrow \theta$	NO SPOILERS	deg/ft	0.333	–	0.50	–	0.333	–
$\Delta h \rightarrow \theta$	WITH SPOILERS	deg/ft	0.333	–	0.50	–	0.208	–
$\int\Delta h \rightarrow \theta$	NO SPOILERS	deg/sec/ft	0.0277	–	0.060	–	0.0277	–
$\int\Delta h \rightarrow \theta$	WITH SPOILERS	deg/sec/ft	0.0277	–	0.060	–	0.0208	–
$\ddot{X} \rightarrow \delta_{th}$		m/fps^2	0.19	–	–		–	
$U \rightarrow \delta_{th}$		m/kt	0.13	–	0.127		0.127	
$\int U \rightarrow \delta_{th}$		m/sec/kt	0.008	–	0.0127	–	0.008	–
$\dot{h} \rightarrow \delta_{th}$		m/sec/fps	–		–	0.3	–	0.3
τ_{th}		sec	1.0		0		1.0	
$\ddot{h} \rightarrow \delta_{sp}$		deg/fps^2	3.3	1.8	3.5		3.5	
$\dot{h} \rightarrow \delta_{sp}$		deg/fps	6.72	4.28[2] 11.24[3]	7.0		7.0	
$\Delta h \rightarrow \delta_{sp}$		deg/ft	3.66	–	3.5	–	3.50	–

NOTES: 1) AT 71 kt 2) WITH O HW AND h < 12.5 ft 3) WITH O HW AND θ_C > O AT h = 0

The high gain variant of the constant flare height configuration uses it both in glide slope track and flare. This feedback has been eliminated from the glide slope track mode of the low gain variant in order to match the variable flare height implementation. The sink rate error to pitch command gain in the high gain variant is slightly lower than any of the equivalent gains used by the variable flare height system without spoilers and it was therefore retained in the low gain variant. With spoilers, the variable flare height control law uses significantly reduced sink rate error to pitch gain and the low gain constant flare height mechanization was modified accordingly, as shown in Table 5-III. The constant flare height system has a path of integrated sink rate error to pitch whereas the variable flare height control law does not. This path was retained in the low gain version of the constant flare height system because this integrator is used to store the pre-flare pitch trim value. Gains of glide slope error and it's integral to pitch were reduced in the low gain constant flare height system to match variable flare height gains. With spoilers, however, the gains used by the low gain configuration in these paths are somewhat lower because the same paths are used to drive the spoilers and matching the variable flare height spoiler gains resulted in lower glide slope and its integral to pitch gains. Longitudinal acceleration feedback to the throttles is used in the variable flare height control law but not in the constant flare height configuration because simulation results indicated a degradation in performance if this feedback was included in this configuration. Airspeed to throttles gain in the constant flare height system was slightly lower than in the variable flare height configuration to begin with and there was therefore no need to reduce it. The gain of the integral of airspeed to the throttles was reduced in the low gain configuration. A cross feed of sink rate error to the throttles is used by both variants of the constant flare height control law but not by the variable flare height system. The system that was actually tested in flight included software gains in the throttle servo loop that produced a one second lag from throttle command to actual position. This lag was intended to be compatible with engine loop dynamics. The high gain constant flare height control law assumed a high bandwidth throttle servo (cascaded with the engine response as defined in Appendix A). The one second lag in the throttle servo was incorporated with the low gain configuration. The gain of vertical acceleration to the spoilers is reduced for the flare in the variable flare height system but the constant flare height configuration retains the glide slope track value in the flare. Sink rate and glide slope error gains to the spoilers in the constant flare height control law were close to these used by the variable flare height system and there was therefore no need to reduce them.

TABLE 5-IV MAJOR CONTROL LAW FEATURES

	VARIABLE FLARE HEIGHT	CONSTANT FLARE HEIGHT
• ELEVATOR CONTROL IN THE FLARE	ELABORATE PITCH AND ELEVATOR PREDICT COMPUTATIONS ADDED TO CLOSED LOOP CONTROL	CLOSED LOOP WITH FLARE INTEGRATOR AND ROTATION COMMAND
• THROTTLE CONTROL IN THE FLARE	CONSTANT RATE RETARD PREDETERMINED AT FLARE INITIATION	CLOSED LOOP SPEED CONTROL WITH DECELERATION COMMAND
• THROTTLE CONTROL IN GLS TRK	THROTTLE SERVO WITH 1 RPS BANDWIDTH	*HIGH BANDWIDTH THROTTLE SERVO
	LONGITUDINAL ACCELERATION FEEDBACK TO THROTTLE	NO LONGITUDINAL ACCELERATION FEEDBACK
• PITCH CONTROL IN GLS TRK	REDUCED SINK RATE TO PITCH GAIN WITH SPOILERS	*SINK RATE TO PITCH GAIN UNCHANGED WITH SPOILERS
	LOW PITCH ATTITUDE AND RATE GAINS	*HIGH PITCH ATTITUDE AND RATE GAINS
• SPOILER CONTROL IN GLS TRK	3 SEC WASHOUT	5 SEC WASHOUT

* High Gain Version Only

Table 5-IV summarizes the major differences between the variable flare height and the constant flare height control laws. All these differences were explained in detail in the preceding paragraphs and in Section 4.

The block diagrams of Figures 4-4, 4-5 and the gain list of Table 4-II define the variable flare height system as tested in flight on the Twin Otter. An unsymmetrical wind gain function $K_{hDF}\left(\frac{V_{CO}}{V_{GO}}\right)'$ is shown in the upper left hand corner of Figure 4-4. This gain multiplies the closed loop sink rate and hence determines the closed loop flare time constant and the slope of the closed loop line shown in Figure 4-6. In the fast time simulation used for obtaining the evaluation results given in the following sections, $K_{hDF}\left(\frac{V_{CO}}{V_{GO}}\right)^*$ was implemented instead as a result of an error in the transmission of information from NASA to the contractor describing this control law. The asterisk denotes an upper limit of unity for $\frac{V_{CO}}{V_{GO}}$ whereas the prime signifies a lower limit. Hence the gain with the asterisk limits to a maximum of unity with headwinds rather than a minimum of unity in tailwinds as intended. The implementation change reduces the closed loop time constant (slopes of the closed loop lines shown in Figure 4-6) by 35 percent for maximum 25 kt headwinds and 12 percent for maximum 10 kt tailwinds. The reduced slope results in a signal to the control that the aircraft is too high at the flare entry. Note that the deterioration in landing performance will be greater for the spoiler cases, because for the spoiler control, there is no inhibiting time delay if the aircraft is initially measured to be above the closed loop line as is the case for the pitch command (OR logic for FLR + 1.5 sec in Figure 4-4).

5.2 DETERMINISTIC PERFORMANCE

Simulation was used to obtain deterministic landing data for all six longitudinal control law configurations that were described in Section 5.1. Steady and shear winds were included as disturbances. Two types of shearing winds were considered, one is linear and patterned according to FAA models (Reference 7) and the other is the sum of a logarithmic and a linear term. Both are described in Appendix A. The effect of headwinds up to 25 knots and tailwinds up to 10 knots were evaluated. (In the case of shear winds, these are the values at the reference height of 7.62 m, or 25 ft. above the ground whereas the wind magnitude at altitude is higher).

Landing time histories of the variable flare height control law with spoilers are given in Figures 5-1A and 5-1B. Three landings are shown - one with a standard FAA 25 knot shearing headwind, one with zero headwind and one with a standard FAA 10 knot shearing tailwind. The last 30.5 m (100 ft) of each of the three approaches are shown. Rotation from the approach to the touchdown attitude is performed through the flare. The approach attitude is about -9° for zero headwind (6° glide slope is used), higher with the headwind and slightly lower with the tailwind. The touchdown attitude is slightly positive for the headwind and zero wind cases and slightly negative with tailwind. (Touchdown attitude greater than -1° is required for landing on the main gear first). Glide slope error is less than 1 meter (3 ft) prior to the flare and during the flare the airplane deviates above the glide slope, as expected. Approach airspeed is 75 knots for the zero headwind case (A nominal approach speed of 71 knots is used when the spoilers are not deployed). Pre-flare airspeed is 73 knots for the headwind case and 76.5 knots for the tailwind as a result of the shears. The approach sink rate is 4.15 m/sec (13.5 fps) with zero headwind, about 2.13 m/sec (7 fps) with the headwind and 4.73 m/sec (15.5 fps) with the tailwind. Sink rate is reduced through the flare to 0.76 - 0.91 m/sec 2.5 - 3 fps) at touchdown. The spoiler time histories indicate a reduction of lift at the beginning of the flare, followed by an increase of lift later on. The initial lift reduction is a result of the pitch flare height being higher than the commanded sink rate trajectory, (as shown if Figure 4-6) causing an initially negative θ'_c, as seen in Figure 5-1B. The lift reduction with wind, particularly headwind, is more pronounced in the simulated system than in the system that was actually flown because of the difference that was explained in Section 5.1. The spoilers, throttles and elevator time histories here are given as deviations from their respective zero wind approach trim positions. The throttles are retarded to their flight idle stops in all three cases shown. An up elevator deflection of 12°-13° occurs through the flare to counter ground effect moments and provide the commanded rotation. Time histories of the major pitch command terms of the vairable flare height control law for the same three wind cases are given in Figure 5-1B. The block diagram of Figure 4-4 should be referred to in order to identify the location of each of the variables shown. The initial nose down command of θ'_c does not propagate to $K_1\theta'_c$ because of the time delayed flare switch shown in Figure 4-4. The peak normal acceleration in the flare is 0.1 g for the zero wind case and 0.16 g for the tailwind case. Additional landing time histories with the variable flare height control law are given in Appendix B. These time histories are for the no-spoiler configuration and for landings with log linear shears with or without spoilers.

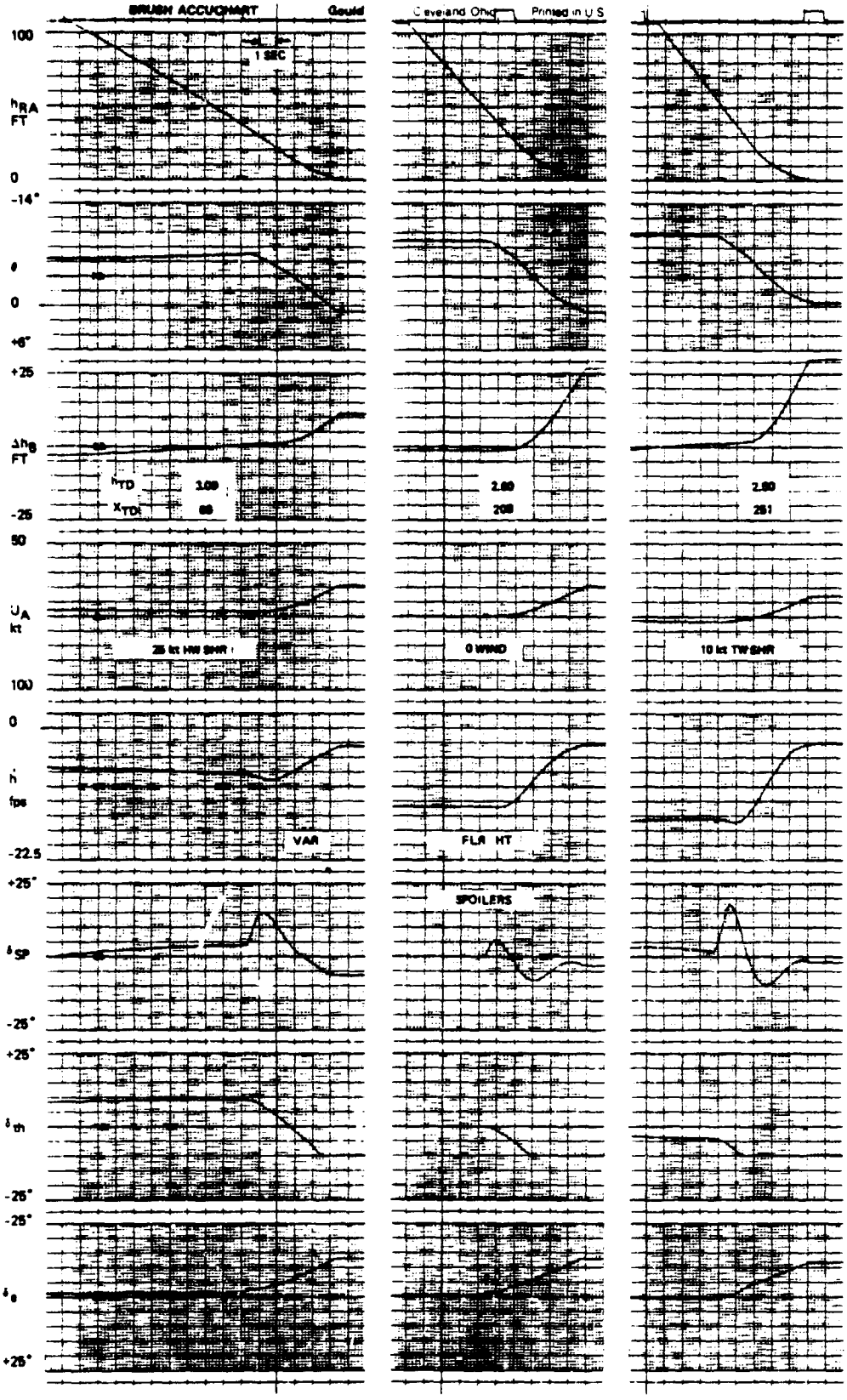

Figure 5-1A. Landing Time Histories; Variable Flare Height with Spoilers

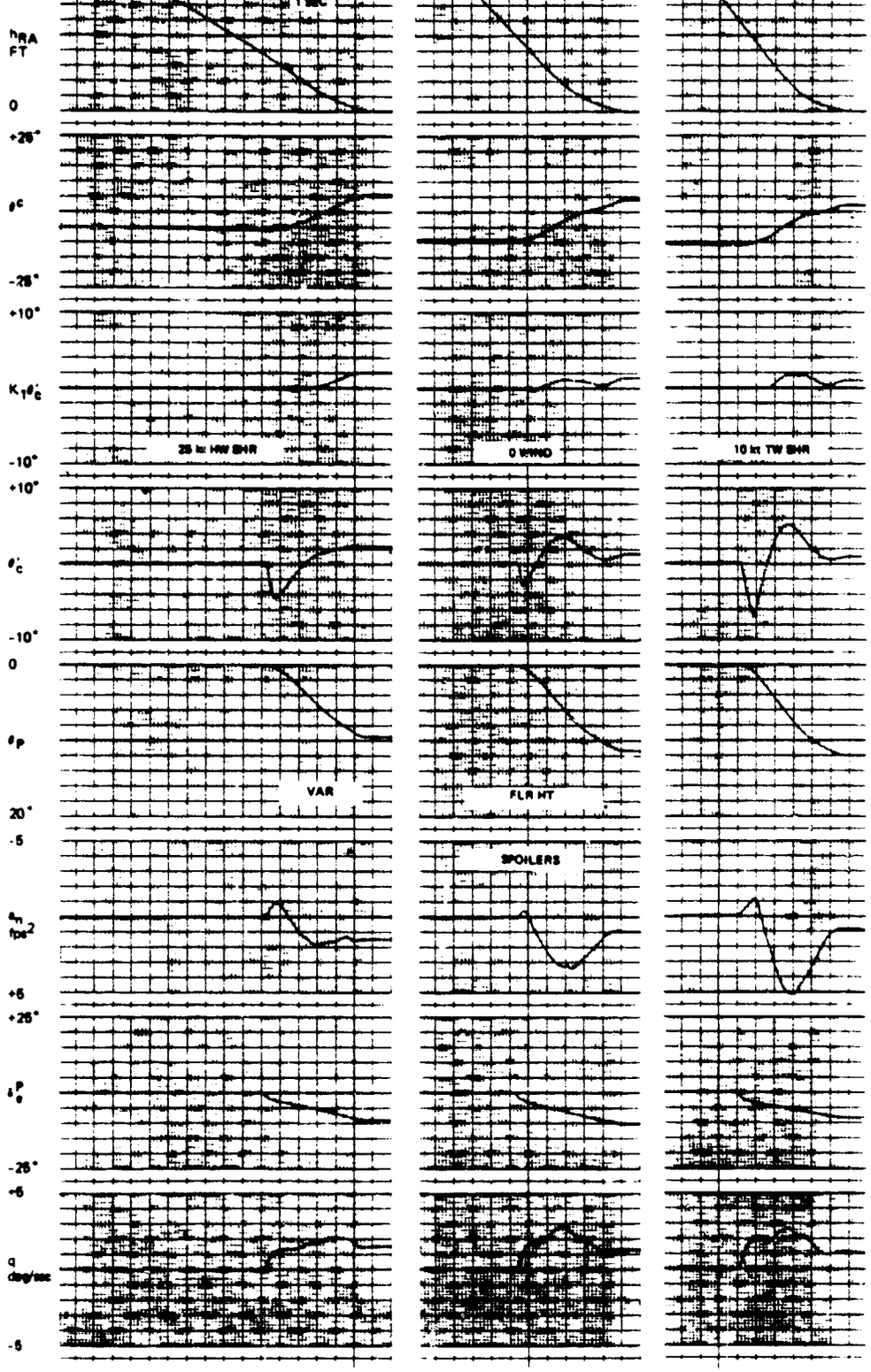

Figure 5-1B. Landing Time Histories; Variable Flare Height with Spoilers

Landing time histories of the low gain constant flare height configuration with spoilers are given in Figure 5-2 for the same wind shear cases as in Figure 5-1. Rotation from the approach attitude to a slightly positive angle is accomplished through the flare for all wind cases. Airspeed is reduced through the flare from about 75 knots during the approach to 62 knots with headwind, 64 knots with zero wind and 66 knots with tailwind. The targeted touchdown airspeed is 65 knots with the spoilers deployed (60 knots with the spoilers retracted). Sink rate is reduced from the approach value to 0.91 - 1.22 m/sec (3-4 fps) at touchdown. The spoilers reduce lift throughout the flare (because the required rotation results in excessive lift). With zero wind, and with tailwind the throttles are being retarded all the way but in the headwind case the throttles are retarded only partially because airspeed is being actively controlled and more speed is being bled off in this case in comparison with the other wind cases, producing a speed error that prevents the throttles from retarding all the way. Landing time histories of the other variants of the constant flare height system with the FAA and log-linear wind shears are given in Appendix B.

Sink rate versus altitude trajectories are given in Figure 5-3 for the variable flare height control law without spoilers and in Figure 5-4 for the low gain constant flare height configuration without spoilers. As in the time histories, the last 30.5 m (100 ft) of the approach are shown. Each figure includes three trajectories, each of which was obtained with one of the following wind conditions: 25 knots log-linear headwind shear (as defined in Appendix A), zero headwind and 10 knots log linear tailwind shear. The variable flare height characteristic is evident in Figure 5-3 with sink rate reduction starting at about 15.2 m (50 ft) for the tailwind case and at 9.1 m (30 ft) for the headwind case. With the constant flare height control law, Figure 5-4, rotation starts at 15.2 m (50 ft) for all wind cases but actual sink rate reduction starts at a slightly lower height for the tailwind case because of the higher initial sink rate involved. The touchdown sink rate dispersions are 0.67 - 1.43 m/sec (2.2-4.7 fps) for the variable flare height system and 0.66 - 1.26 m/sec (2.15 - 4.15 fps) for the constant flare height control law. Additional flare sink-rate

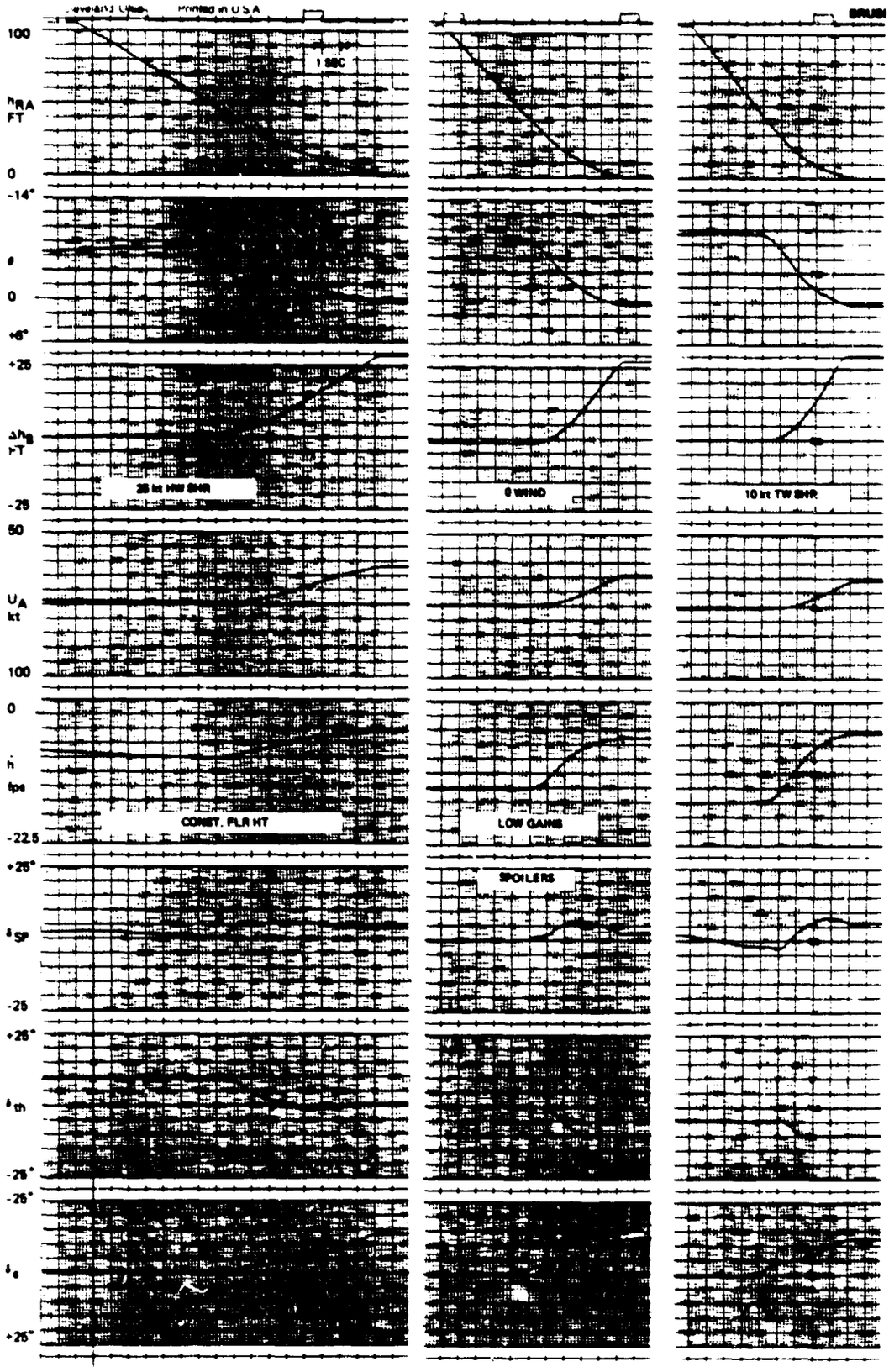

Figure 5-2. Landing Time Histories, Constant Flare Height, Low Gains, with Spoilers

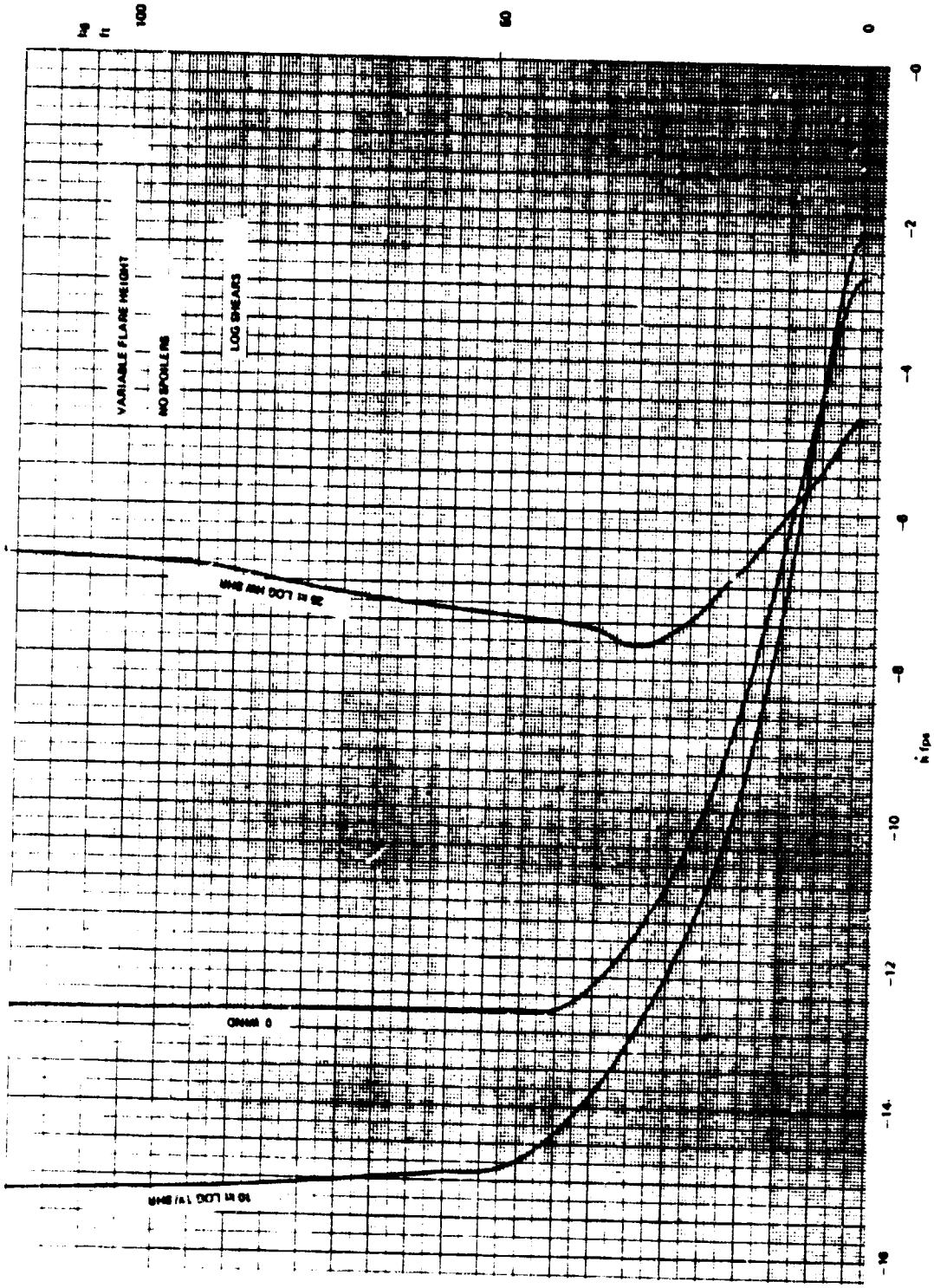

Figure 5-3. Flare h/ḣ Trajectories

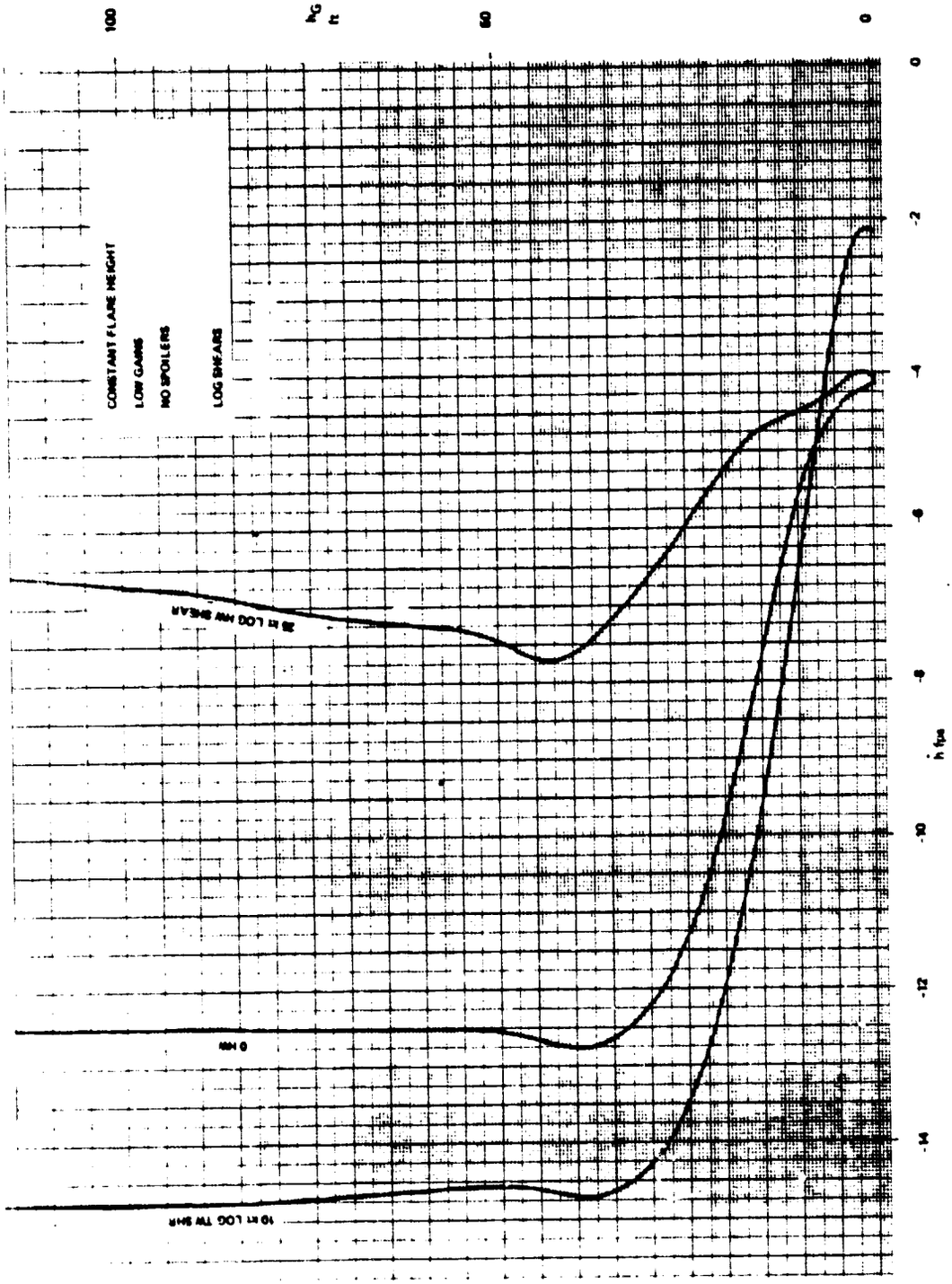

Figure 5-4. Flare h/ḣ Trajectories

trajectories, for the various control laws and deterministic wind conditions that were evaluated, are given in Appendix B.

The variation of touchdown sink rate, range and pitch attitude with wind magnitude is shown in Figure 5-5 through 5-10. Each one of the six figures is for one of the six control law configurations that have been evaluated. There are three curves in each plot - one for steady wind, one for the linear FAA shears and one for the log-linear shears (all wind models are defined in Appendix A). Wind magnitudes vary from 25 knots headwind to 10 knots tailwind. No stochastic disturbances, i.e., turbulence, were included. Deterministic touchdown results for the variable flare height control law without spoilers are given in Figure 5-5. The log-linear shears cause the largest dispersions on all three touchdown variables. This is due to the fact that with this type of shear the variation of wind close to the ground is more rapid than with the FAA linear shears. The hardest touchdown sink rate is 1.40 m/sec (4.6 fps) with 25 knots of log linear headwind shear and the softest is 0.67 m/sec (2.2 fps) with 10 knots of log linear tailwind shear. Sink rate variation with the FAA shears and steady winds is very small. Touchdown range is measured down the runway referenced to the Glide Path Intercept Point (GPIP). The shortest touchdown distance for the variable flare height configuration without spoilers is 6.1 m (20 ft) beyond the GPIP with 25 knots log linear headwind shear, as seen in Figure 5-5. The 10 knots log linear tailwind shear produces the longest landing for this configuration at 88.4 m (290 ft) beyond the GPIP. Pitch attitude varies between -0.4° and 1.9°. The equivalent results for the variable flare height configuration with spoilers are given in Figure 5-6. Sink rate dispersion is about the same as without the spoilers, range dispersion is slightly improved and touchdown attitude with spoilers varies from -0.7° to 1.4°. The tendency towards lower attitude with spoilers seems to be associated with the spoiler's tendency to increase lift at the end of the flare (see Figure 5-1A) and it could also be related to higher airspeed used with the spoilers. Deterministic touchdown results for the low gain constant flare height control law without spoilers are given in Figure 5-7 and with spoilers in Figure 5-8. Here again, the log-linear shears result in the largest dispersions. Sink rate with no wind is significantly harder, at 1.22 m/sec (4.0 fps), for the constant flare height configuration in comparison to 0.85 m/sec (2.8 fps) for the variable flare height control law. (Note that a harder touchdown sink rate will tend to reduce touchdown dispersions). Sink rate with the constant flare height does not increase significantly with headwinds. Sink rate dispersion is slightly

better with the constant flare height. Range has the same general tendency of being short with headwind and long with tailwind. Range dispersion is slightly improved with the constant flare height configuration in comparison to the variable flare height. The variation of touchdown pitch attitude with constant flare height is much smaller than with the variable flare height. The use of spoilers with the low gains constant flare height configuration results in an almost insignificant improvement of sink rate control, but range dispersion is reduced from 80.8 m (265 ft) without spoilers to 57.9 m (190 ft) with spoilers. The use of spoilers also result, with this configuration, in a slightly higher touchdown attitude. This is because with this configuration the spoilers reduce lift throughout the flare. The determinisitic touchdown results for the high gain constant flare height configuration, without and with spoilers, are given in Figures 5-9 and 5-10, respectively. Sink rate control with high gains and no spoilers is improved in comparison to the low gain configuration but with spoilers it is about the same. Range dispersion is reduced for the high gain configuration. It is 65.5 m (215 ft) without spoilers and 27.4 m (90 ft) with spoilers. Touchdown pitch attitude with the high gains is similar to that obtained with the low gains.

Table 5-V summarizes the results given in Figures 5-5 through 5-10 (Touchdown airspeed is an additional variable included in the table). The numbers given in the table are the extreme values of each variable for all wind conditions that were evaluated. The hardest sink rate values are 1.40 m/sec (4.6 fps) with the variable flare height control law and 1.25 m/sec (4.1 fps) with the constant flare height configurations. The low gain constant flare height configuration with spoilers and the high gain constant flare height configuration without spoilers provide less sink rate dispersion than the other configurations. The use of spoilers has no significant affect on sink rate control with the variable flare height control law. The use of spoilers reduces sink rate dispersion for the low gain constant flare height control law but not for the high gain version. Touchdown range dispersion is not improved by any significant amount by the use of spoilers with the variable flare height control law. Range control of the low gains constant flare height system without spoilers is about the same as with the variable flare height control law. With spoilers, however, the low gain constant flare height system obtains a 30 percent improvement in range control for these deterministic disturbances. Range control with the high gain constant flare height system is

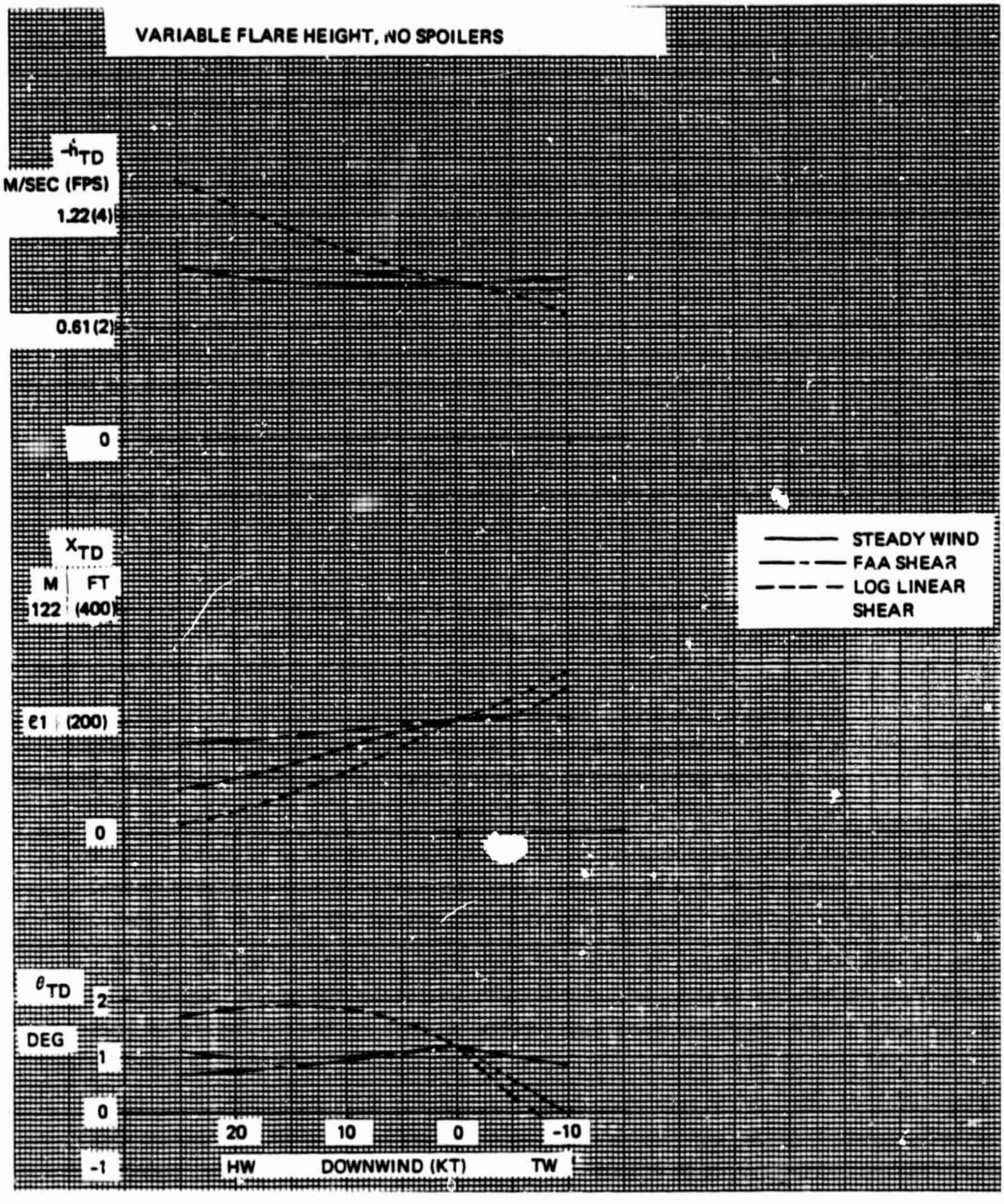

Figure 5-5. Effect of Deterministic Wind on Touchdown, Variable Flare Height, No Spoilers

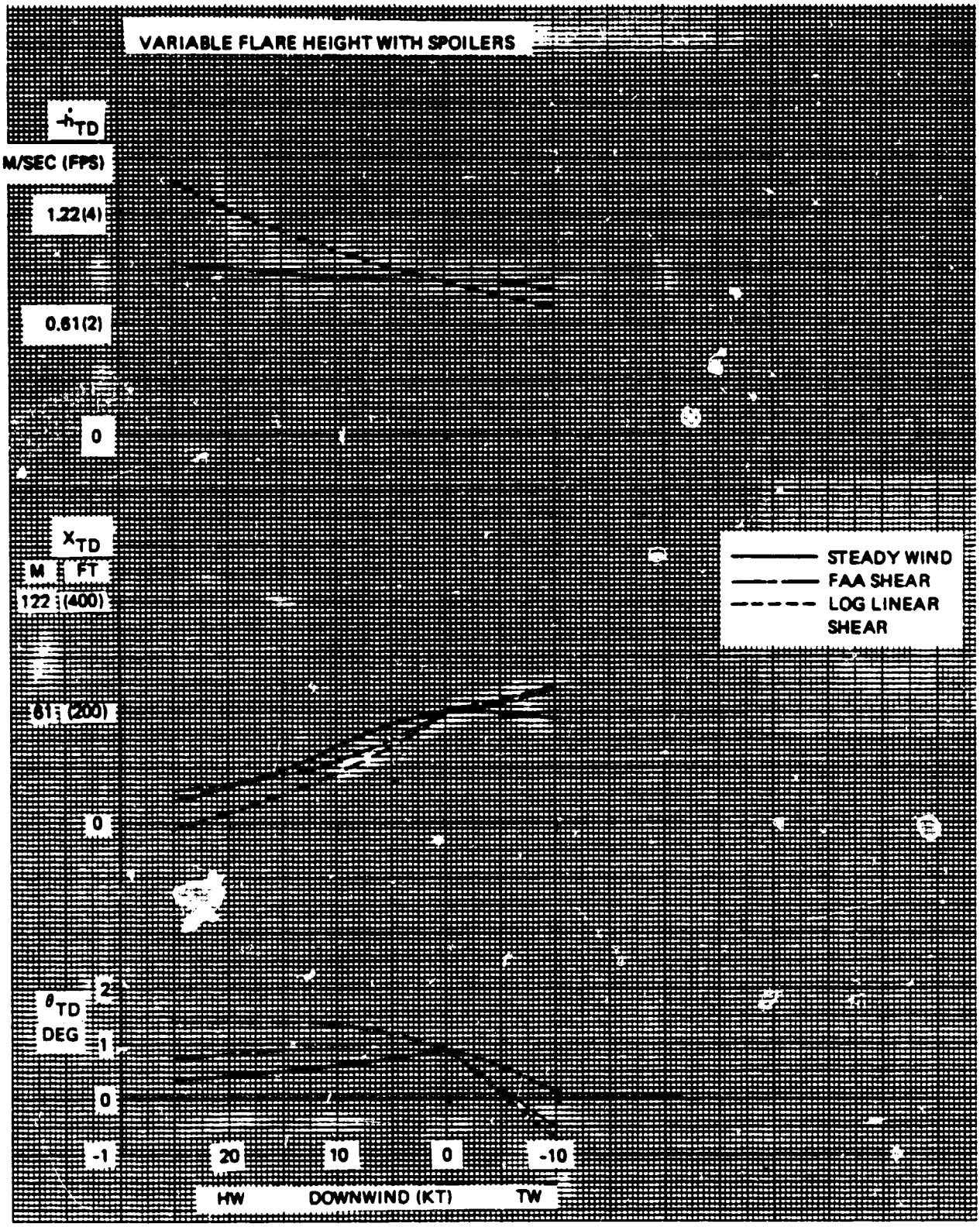

Figure 5-6. Effect of Deterministic Wind on Touchdown, Variable Flare Height With Spoilers

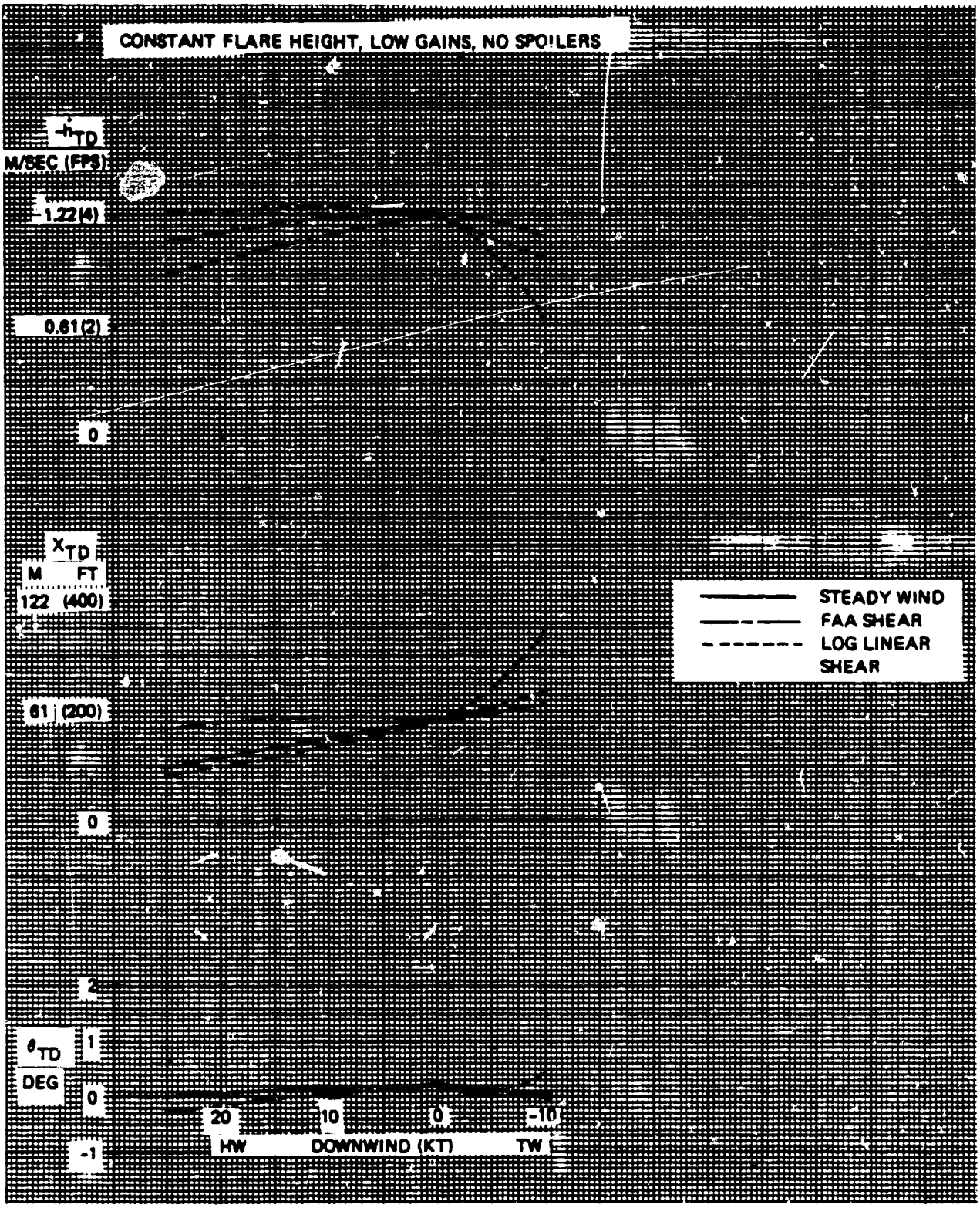

Figure 5-7. Effect of Deterministic Wind on Touchdown,Constant Flare Height, Low Gains, No Spoilers

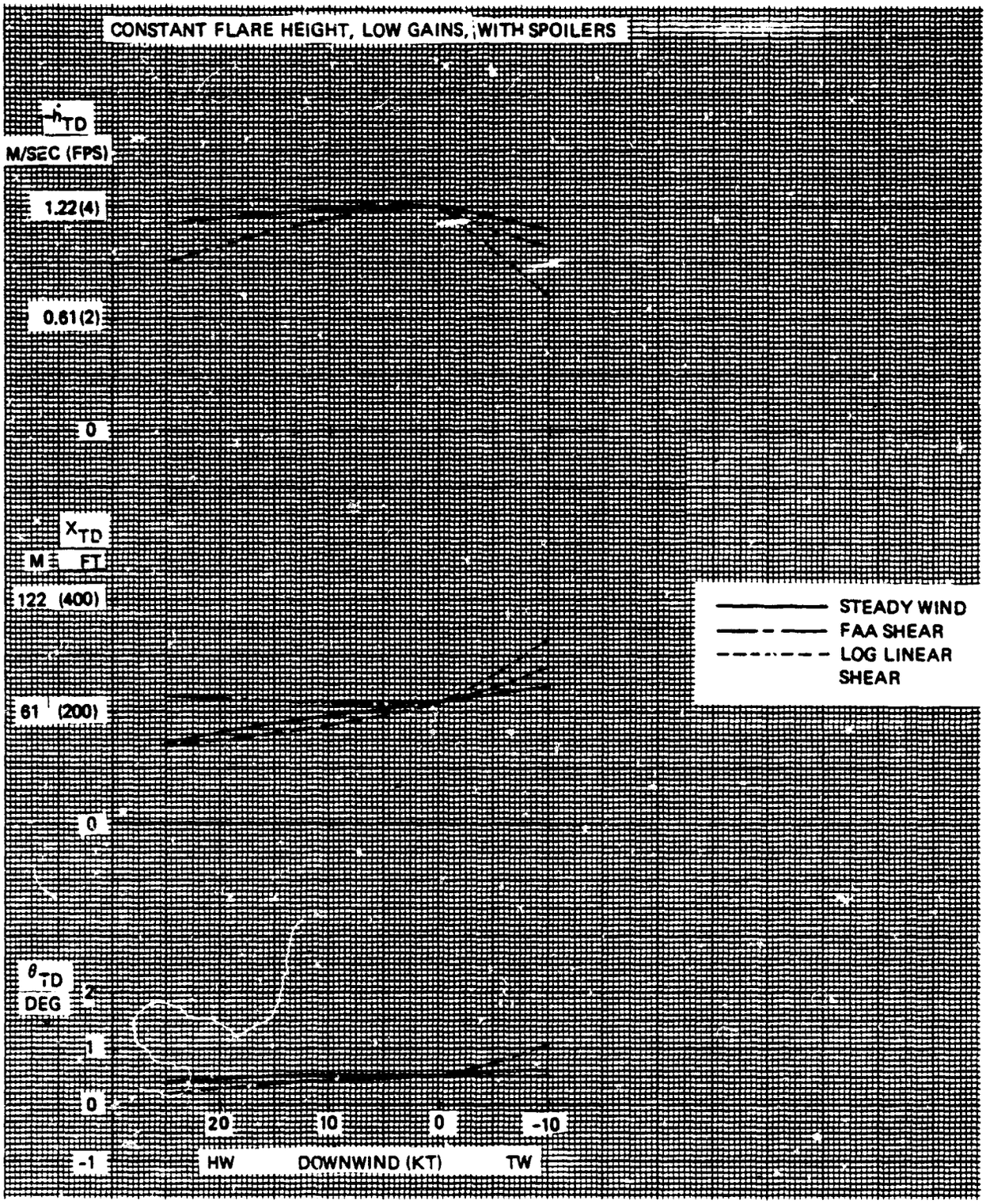

Figure 5-8. Effect of Deterministic Wind on Touchdown, Constant Flare Height, Low Gains With Spoilers

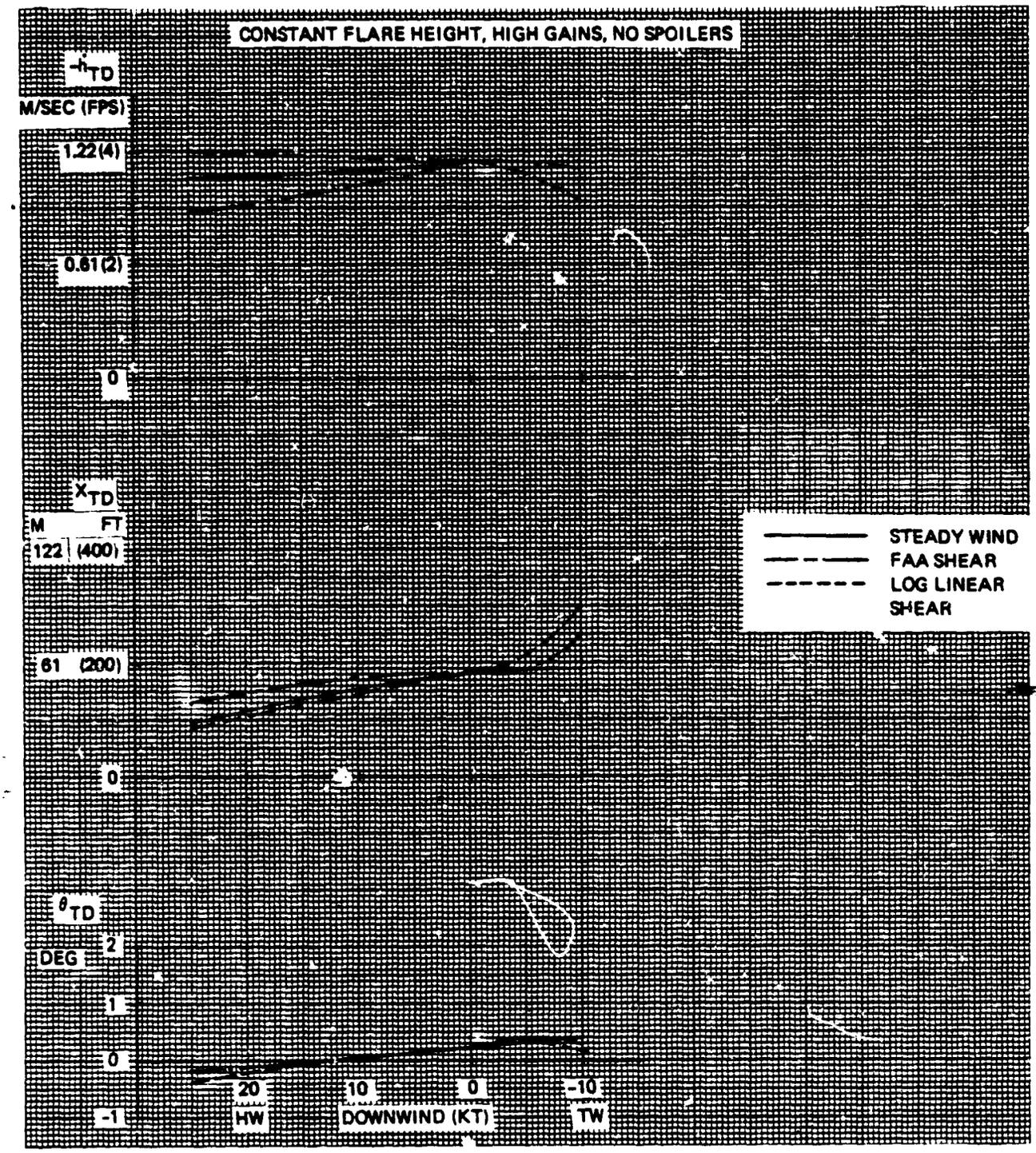

Figure 5-9. Effect of Deterministic Wind on Touchdown,Constant Flare Height, High Gains With Spoilers

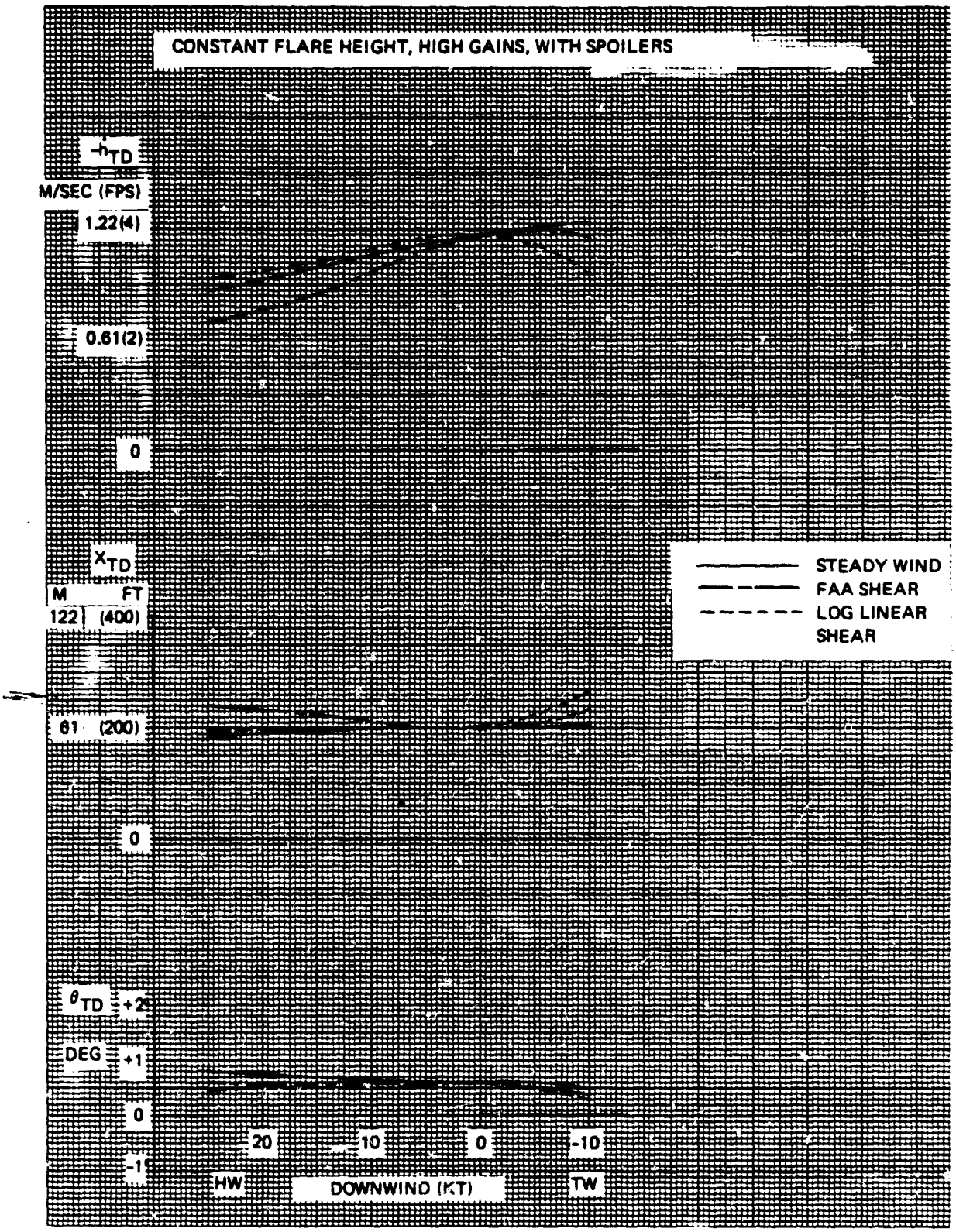

Figure 5-10. Effect of Deterministic Wind on Touchdown, Constant Flare Height With Spoilers High Gains

TABLE 5-VA DETERMINISTIC TOUCHDOWN SUMMARY
(METRIC UNITS)

		VARIABLE FLARE HEIGHT		CONSTANT FLARE HEIGHT LOW GAINS		CONSTANT FLARE HEIGHT HIGH GAINS	
SPOILERS		YES	NO	YES	NO	YES	NO
$\dot{h}_{TD}$ (m/sec)	MIN	0.701	0.671	0.914	0.640	0.701	0.884
	MAX	1.40	1.40	1.25	1.25	1.25	1.22
X_{TD} (m) BEYOND GPIP	MIN	-4.6	5.5	43.6	25.6	55.8	25.9
	MAX	74.7	88.4	101	107	81.1	91.4
θ_{TD} (deg)	MIN	-0.70	-0.36	0.20	-0.30	0.30	-0.40
	MAX	1.40	1.90	1.06	0.44	0.80	0.40
U_{TD} (kt)	MIN	59.0	56.0	58.5	54.6	58.5	54.5
	MAX	69.0	64.2	67.4	62.0	68.0	61.9

DISTURBANCES ARE STEADY WINDS, FAA SHEARS AND LOG LINEAR SHEARS VARYING FROM 25 kt HW TO 10 kt TW.

TABLE 5-VB DETERMINISTIC TOUCHDOWN SUMMARY
(ENGLISH UNITS)

		VARIABLE FLARE HEIGHT		CONSTANT FLARE HEIGHT LOW GAINS		CONSTANT FLARE HEIGHT HIGH GAINS	
SPOILERS		YES	NO	YES	NO	YES	NO
$\dot{h}_{TD}$ (fps)	MIN	2.3	2.2	3.0	2.1	2.3	2.9
	MAX	4.6	4.6	4.1	4.1	4.1	4.0
X_{TD} (ft)	MIN	-15	18	143	84	183	85
BEYOND GPIP	MAX	245	290	330	350	266	300
θ_{TD} (deg)	MIN	-0.70	-0.36	0.20	-0.30	0.30	-0.40
	MAX	1.40	1.90	1.06	0.44	0.80	0.40
U_{TD} (kt)	MIN	59.0	56.0	58.5	54.6	58.5	54.5
	MAX	69.0	64.2	67.4	62.0	68.0	61.9

DISTRUBANCES ARE STEADY WINDS, FAA SHEARS AND LOG LINEAR SHEARS VARYING FROM 25 kt HW TO 10 kt TW.

improved by 20 percent in comparison to the low gain version. The use of spoilers results in a further improvement of range control by 60 percent. Thus, the high gain constant flare height system with spoilers produces far better range control than the other configurations. The touchdown attitude results of Tabe 5-V indicate a somewhat uncomfortably low attitude for all configurations as an attitude greater than -1° is required to assure landing n the main gears first. The variable flare height with spoilers is worst in this respect at -0.7° and the constant flare height configurations with spoilers are the best, touching down at a minimum attitude of 0.2° or 0.3°. The targeted touchdown airspeed is 65 knots with the spoilers deployed and 60 knots with the spoilers retracted. The higher airspeed is used with spoilers to compensate for an increase in stall speed. The minimum touchdown speed for all spoiler configurations is 6.0 to 6.5 knots slow and for the no-spoiler configurations is 4.0 to 5.5 knots slow. The constant flare height configurations touchdown at about 1.5 knots slower than the variable flare height. All the minimum touchdown airspeeds are associated with the 25 knot log-linear headwind shear whereas other wind conditions result in higher touchdown airspeeds.

To summarize the results with deterministic winds, the low gain constant flare height control law provides somewhat better sink rate, range and attitude control than the variable flare height configuration. The high gain constant flare height system with spoilers provides much better range control than all the other configurations. The log-linear shear is the most demanding of the winds evaluated.

5.3 STOCHASTIC PERFORMANCE

The simulation that had been developed for this study was used to evaluate landing performance of the six longitudinal control law configurations with stochastic as well as deterministic disturbances. Horizontal turbulence, vertical turbulence and MLS beam noise according to the models that are defined in Appendix A were included in the simulation. Simulation runs were made with limiting FAA shear winds, moderate turbulence and beam noise. Probability distributions of the major touchdown variables were obtained and the results are summarized in this section. Data with respect to activity of the controlled variables and controllers on the glide slope with turbulence and beam noise were also obtained and are summarized here. Landing performance was also evaluated as a function of wind and turbulence level and the results are summarized in this section. Note that the limiting wind and turbulence levels are higher than the average levels that would be encountered in actual flight. While results using these levels provide a good

measure of the effectiveness of the control system being evaluated, they are a conservative indication of the ability to meet statistical criteria which are based on smaller average levels of disturbances.

5.3.1 LANDING PERFORMANCE WITH LIMITING WINDS

Table 5-VI is a summary of the longitudinal landing performance with limiting shearing winds, moderate turbulence and beam noise. The left most column of this table defines the performance goal that was used in this study. As explained in Reference 1, requirements for automatic landing systems of CTOL transport aircraft have been established but not for the STOL airplane. Consequently, performance goals had to be defined for this study, based on CTOL requirements scaled down to the STOL runway and landing geometry and taking into account geometrical and physical characteristics of the Twin Otter airplane. The mean targeted sink rate was selected to produce a comfortably soft landing. The two sigma land hard is a design objective which would produce acceptable sink rate control and a 10^{-6} hazard probability is attached to the exceedance of the Twin Otter airplane's gear strength. On range, the goal for the mean was computed assuming the airplane to be on the glide slope at flare initiation and executing the commanded $h/\dot{h}$ flare trajectory with no deviations. Two sigma dispersions of ±61 m (±200 ft) were scaled down from CTOL requirements. The 10^{-6} land short requirement provides for landing within the STOL runway's safety underrun area (Figure 3-1). The 10^{-6} land long requirement depends on the airplane's stopping distance and the runway length. Such considerations were outside the scope of this study and therefore the number shown in Table 5-VI is simply a linear extrapolation of the two-sigma dispersion to the 10^{-6} probability level. The 10^{-6} low attitude goal is based on the hazard of hitting the ground with the nose wheel first. All the control laws that were evaluated tended to produce flat touchdowns and therefore upper limits on attitude were not required.

The actual performance results that are given in Table 5-VI were computed assuming a 70 percent probability of encountering a 25 knot shearing headwind and 30 percent probability for a 10 knot shearing tailwind. The 70/30 split is based on the results of a survey of 79 major U.S. airports looking at runway orientation with respect to the prevailing winds. This ratio is applicable for airports that have bi-directional landing aids on the major runway. The assumption that each

TABLE 5-VIA LONGITUDINAL PERFORMANCE SUMMARY (METRIC UNITS)

(70% HW, 30% TW)

	VARIABLE	GOAL	VARIABLE FLARE HEIGHT		CONSTANT FLARE HEIGHT LOW GAINS		CONSTANT FLARE HEIGHT HIGH GAINS	
			WITH SPOILERS	WITHOUT SPOILERS	WITH SPOILERS	WITHOUT SPOILERS	WITH SPOILERS	WITHOUT SPOILERS
$\dot{h}_{TD}$ m/sec	μ	0.086	0.914	0.853	0.975	1.01	0.823	0.945
	2σ hard	<1.83	1.46	1.77	1.40	1.65	1.46	1.43
	10^{-6} hard	<3.05	3.29	3.35	2.16	2.80	2.07	2.19
X_{TD} (m) BEYOND GPIP	10^{-6} short	>-102	-39.6	-45.7	-45.7	-73.2	0	-51.8
	2σ short	>15.2	0	9.1	21.3	0	42.7	0
	μ	76.2	30.5	67.1	76.2	61.0	73.2	45.7
	2σ long	<137	94.5	162	143	146	116	134
	10^{-6} long	<226	287	354	344	335	198	277
θ_{TD} (deg)	10^{-6} low	>-1.5	-2.4	-3.0	-1.7	-1.7	-1.5	-1.9
	2σ low	-	-1.1	-1.2	-0.1	-0.7	-0.3	-0.8
	μ	> 0	0.2	0.6	0.7	0.1	0.4	0
	2σ high	-	1.4	2.4	1.7	1.0	1.3	0.9
	10^{-6} high	-	2.7	4.8	3.7	2.6	3.2	2.0
Δh_{WINDOW} (m)	2σ low	>-3.66	-3.51	-4.57	-1.83	-2.59	-1.01	-1.31
	μ	0	-0.762	-0.610	0	0.152	-0.091	-0.274
	2σ high	<3.66	1.37	3.20	1.83	3.20	0.792	0.823

DISTURBANCES:

70% PROBABILITY FOR 25 kt SHEARING HW, σ_u= 3.73 kt, σ_w = 1.48 kt, B.N.

30% PROBABILITY FOR 10 kt SHEARING TW, σ_u= 2.67 kt, σ_w = 1.48 kt, B.N.

TABLE 5-VI B LONGITUDINAL PERFORMANCE SUMMARY (ENGLISH UNITS)
(70% HW, 30% TW)

	VARIABLE	GOAL	VARIABLE FLARE HEIGHT		CONSTANT FLARE HEIGHT LOW GAINS		CONSTANT FLARE HEIGHT HIGH GAINS	
			WITH SPOILERS	WITHOUT SPOILERS	WITH SPOILERS	WITHOUT SPOILERS	WITH SPOILERS	WITHOUT SPOILERS
$\dot{h}_{TD}$ (fps)	μ	2.25	3.0	2.8	3.2	3.3	2.7	3.1
	2σ hard	< 6	4.8	5.8	4.6	5.4	4.8	4.7
	10^{-6} hard	< 10	10.8	11.0	7.1	9.2	6.8	7.2
x_{TD} (ft) BEYOND GPIP	10^{-6} short	> -335	-130	-150	-150	-240	0	-170
	2σ short	> 50	0	30	70	0	140	0
	μ	250	100	220	250	200	240	150
	2σ long	< 450	310	530	470	480	380	440
	10^{-6} long	< 740	940	1160	1130	1100	650	910
θ_{TD} (deg)	10^{-6} low	> -1.5	-2.4	-3.0	-1.7	-1.7	-1.5	-1.9
	2σ low	-	-1.1	-1.2	-0.1	-0.7	-0.3	-0.8
	μ	0	0.2	0.6	0.7	0.1	0.4	0
	2σ high	-	1.4	2.4	1.7	1.0	1.3	0.9
	10^{-6} high	-	2.7	4.8	3.7	2.6	3.2	2.0
Δh_{WINDOW} (ft)	2σ low	> -12	-11.5	-15	-6.0	-8.5	-3.3	-4.3
	μ	0	-2.5	-2.0	0	0.5	-0.3	-0.9
	2σ high	< 12	4.5	10.5	6.0	10.5	2.6	2.7

DISTURBANCES:
70% PROBABILITY FOR 25 kt SHEARING HW, σ_u = 6.3 fps, σ_w = 2.5 fps, B.N.
30% PROBABILITY FOR 10 kt SHEARING TW, σ_u = 4.5 fps, σ_w = 2.5 fps, B.N.

landing is made with either a limiting headwind or a limiting tailwind is conservative since the probability of encountering 25 knot headwinds or 10 knot tailwinds is significantly lower according to Reference 7. Simulation runs were made with 25 knot shearing headwind and 3.7 knot RMS horizontal turbulence or with 10 knots shearing tailwind and 2.7 knots RMS horizontal turbulence. All runs were made with 1.5 knots RMS vertical turbulence. Shears according to the FAA models only were used in obtaining the stochastic data.

The results of Table 5-VI indicate that the 10^{-6} land hard requirement is exceeded by the variable flare height control law with or without spoilers. All constant flare height configurations provide acceptable to very good sink rate control. The low gain system without spoilers is the poorest of the four in this respect but its performance is very significantly improved with the use of the DLC spoilers. Sink rate control with the high gain constant flare height control law is good even without the use of spoilers and it improves somewhat with spoilers.

All control law configurations meet the 10^{-6} land short requirement but the high gain configuration with spoilers is the only one to meet the 10^{-6} land long requirement. For the variable flare height control law, the use of spoilers improves range control by about 20 percent. Range control with the low gain constant flare height configuration without spoilers is about equivalent to that of the variable flare height without spoilers but the use of spoilers here fails to produce a significant improvement. It is suspected that switching of gains when transitioning from glide slope track to flare, adversely affects the range control with the low gain constant flare height configuration and therefore the improved sink rate control with spoilers does not translate to an equivalent improvement in range control. Range control with the high gain constant flare height system without spoilers is as good as with the variable flare height control law with spoilers. Excellent range control is obtained with the high gain constant flare height configuration with spoilers. The use of spoilers reduces range dispersion by 40 percent for this configuration.

The high gain constant flare height configuration with spoilers is the only one that meets the 10^{-6} low attitude requirement. All the configurations that were evaluated produced rather flat touchdown attitudes. Attempting to arbitrarily command a higher touchdown attitude with this light wing loading airplane, would result in a tendency towards long landings.

The nose down tendency was aggravated by the 4 knot increase in approach speed to account for a higher stall speed with spoilers deployed to their nominal value. If an automatic system were installed to close the spoilers for a downward gust or shear correction, the spoilers closed stall speed may be appropriate as the basis for establishing approach airspeed. When spoilers are used a lower approach speed would increase the approach pitch attitude and probably reduce the touchdown dispersions.

Deviations of more than 3.66 m (12 ft) from the glide slope at a decision height (Δh window) of 30.5 m (100 ft) would result in a requirement to abort the approach. The automatic landing system is required to be within this window on a two sigma basis. The variable flare height configuration without spoilers deviates somewhat from this requirement on the low side. (The asymmetrical nature of the deviations from the glide slope result from the dominant effect of the shearing headwind). All other configurations meet this glide slope window requirement. The low gain constant flare height system tracks the glide slope better than the variable flare height control law and the high gain version produces better glide slope tracking performance than the low gain version. The use of spoilers improves glide slope tracking performance with all configurations.

The probability distribution plots from which the data in Table 5-VI was extracted, are given in Appendix B.

5.3.2 CONTROL ACTIVITY

Activity data for controlled variables and controllers on the glide slope with moderate turbulence and MLS beam noise are summarized in Tables 5-VII and 5-VIII. Data were obtained from simulation and are given for all six evaluated control law configuraions. The results of Table 5-VII are with moderate turbulence and MLS beam noise, as defined in Appendix A. The results of Table 5-VIII are with turbulence only.

Table 5-VII indicates that glide slope track accuracy with the low gain constant flare height control law is slightly better than with the variable flare height configuration. The high gain configuration provides a glide slope tracking accuracy that is significantly better than with the other configuration. Glide slope tracking accuracy is improved by the use of the DLC spoilers. The improvement is significant for the variable flare height and the low gain system

TABLE 5-VII GLIDE SLOPE RMS ACTIVITY SUMMARY

TURBULENCE AND MLS BEAM NOISE

	VARIABLE FLARE HEIGHT		CONSTANT FLARE HEIGHT LOW GAINS		CONSTANT FLARE HEIGHT HIGH GAINS	
SPOILERS	ON	OFF	ON	OFF	ON	OFF
Δh_f m(ft)	2.19 (7.2)	2.68 (8.8)	1.95 (6.4)	2.44 (8.0)	1.52 (5.0)	1.58 (5.2)
$\dot{h}$ $\frac{m}{sec}$ (fps)	0.49 (1.6)	0.49 (1.6)	0.49 (1.6)	0.61 (2.0)	0.37 (1.2)	0.49 (1.6)
a_n $\frac{m}{sec^2}$ (fps^2)	0.61 (2.0)	0.67 (2.2)	0.61 (2.0)	0.67 (2.2)	0.61 (2.0)	0.67 (2.2)
U_A (kt)	2.8	3.0	2.8	3.0	2.6	2.8
θ deg	0.8	1.0	1.0	1.2	0.9	1.2
δ_e deg	1.0	1.3	1.2	1.4	1.3	1.6
δ_{th} deg	2.0	2.4	3.8	4.0	4.0	4.4
δ_{sp} deg	8.0	-	10.0	-	4.8	-

σ_u = 3.73 kt, σ_w = 1.5 kt, σ_{BN} = 0.06° @ h_G = 152 m (500 ft)

TABLE 5-VIII GLIDE SLOPE RMS ACTIVITY SUMMARY

TURBULENCE ONLY

	VARIABLE FLARE HEIGHT		CONSTANT FLARE HEIGHT LOW GAINS		CONSTANT FLARE HEIGHT HIGH GAINS	
SPOILERS	ON	OFF	ON	OFF	ON	OFF
Δh_f m(ft)	1.22 (4.0)	1.95 (6.4)	1.22 (4.0)	1.83 (6.0)	0.61 (2.0)	0.61 (2.0)
$\dot{h}$ $\frac{m}{sec}$ (fps)	0.37 (1.2)	0.49 (1.6)	0.43 (1.4)	0.61 (2.0)	0.27 (0.9)	0.37 (1.2)
a_n $\frac{m}{sec^2}$ (fps^2)	0.61 (2.0)	0.67 (2.2)	0.55 (1.8)	0.67 (2.2)	0.61 (2.0)	0.67 (2.2)
U_A kt	2.8	3.0	2.7	2.7	2.4	2.6
θ deg	0.64	0.8	1.0	1.0	0.75	1.1
δ_e deg	0.90	1.2	1.0	1.4	1.2	1.4
δ_{th} deg	2.0	2.4	3.4	3.8	4.0	4.2
δ_{sp} deg	8.0	-	8.4	-	4.8	-

σ_u = 3.73 kt, σ_w = 1.5 kt

but minor for the high gain version. Sink rate and normal acceleration activity are about equivalent with all configurations but the low gain control law has slightly higher sink rate activity and the high gain system has slightly lower sink rate activity than the other configurations. Airspeed control is also about equivalent for all configurations with the high gain configuration being slightly better than the others. Pitch attitude and elevator activity with the constant flare height control laws are somewhat higher than with the variable flare height system. Throttle activity with the constant flare height configurations is almost twice as high as with the variable flare height. This is a result of not using longitudinal acceleration feedback to the throttle in the constant flare height systems (see Table 5-III). Glide slope spoiler activity is 8° RMS with the variables flare height, somewhat higher (10°) with the low gain constant flare height system and much lower (4.8°) with the high gain configuration as a result of the higher pitch gains. The use of spoilers improves glide slope tracking accuracy and reduces sink rate, normal acceleration, airspeed, pitch attitude, elevator and throttle activities.

Table 5-VIII summarizes glide slope activity with horizontal and vertical turbulence but no beam noise. The difference between the results of Tables 5-VII and 5-VIII is a result of MLS beam noise being included in the former. Glide slope tracking accuracy without beam noise looks much better because Δh_f is raw glide slope deviation filtered with a 0.3 second first order lag, such that beam noise shows up directly on this variable. Without the beam noise, the improved glide slope tracking accuracy and sink-rate control with the high gain configuration are more apparent. Beam noise contributes some sink rate activity but little normal acceleration. It has a small impact on airspeed, pitch, elevator and throttle activities. Beam noise contributes to spoiler activity only with the low gain constant flare height control law.

The glide slope tracking accuracy given in Table 5-VIII is a good indication of anticipated accuracy at the 30.5 m (100 ft) decision height because the contribution of beam noise at 30.5 m (100 ft) is much smaller than at 152.4 m (500 ft) as a result of the proximity to the transmitting autenna. The RMS results of Table 5-VIII can be doubled to obtain an estimate of the two sigma excursions. Glide slope tracking accuracy is thus ±3.90 m (±12.8 ft), on a two sigma basis, for the variable flare height and ±3.66 m (12.0 ft) for the low gain constant flare configuration, both without spoilers. This is marginally acceptable in comparison to the required accuracy of ±3.66 m (±12 ft). With spoilers, glide slope tracking

accuracy of these two configurations is good. The performance of the high gain is excellent with, or without, spoilers.

5.3.3 LANDING PERFORMANCE WITH REDUCED WIND LEVELS

Landing performance results with limiting winds and moderate turbulence were given in Section 5.3.1. Results with reduced wind and turbulence levels are given and discussed here. Mean and two sigma touchdown results as a function of wind and turbulence level are given in Figure 5-11 for the variable flare height configuration without spoilers and in Figure 5-12 with spoilers. Data were taken with FAA wind shears of 25, 12.5, and 0 knots headwind and 5 and 10 knots tailwind. The magnitude of the horizontal turbulence was varied with the deterministic wind level as shown in the figures. A constant level of 1.5 knots vertical turbulence and beam noise were included in all cases. No horizontal turbulence was included with the zero headwind cases and therefore dispersions at this point are due to vertical turbulence and beam noise only, and vertical turbulence is the major contributor.

The results of Figure 5-11 indicate that the mean touchdown sink rate is essentially constant regardless of the wind magnitude. The two sigma land hard value is about 0.30 m/sec (1.0 fps) higher than the mean sink rate with zero wind (and horizontal turbulence). The worst case for sink rate control is at 25 knots headwind and the associated 3.73 knots of horizontal turbulence. The two sigma land hard value there is 1.83 m/sec (6.0 fps), or 0.98 m/sec (3.2 fps) harder than the mean sink rate. The mean touchdown range varies from 56.4 m (185 ft) with 25 knots shearing headwind to 88.4 m (290 ft) with 10 knots shearing tailwind. (Range is measured with respect to the GPIP). Touchdown range dispersion, from two sigma short to two sigma long, varies from 45.7 m (150 ft) at zero wind to 158.5 m (520 ft) with headwind and 3.73 knots of horizontal turbulence. The dispersion is smaller with tailwind (because of the smaller amount of turbulence). The mean touchdown pitch attitude is fairly constant at about 1° for all headwind magnitudes but it drops to [illegible] with the 10 knots shearing tailwind. Most of the attitude dispersion is caused by the vertical turbulence. It is 1.2° from the mean to the two sigma low attitude with zero headwind and 1.55° for the maximum headwind or tailwind. The lowest attitude on a two sigma basis is -1.55° with the 10 knots tailwind. Glide slope tracking dispersion at the 30.5 m (100 ft) decision height varies from 1.83 m (6 ft) with vertical turbulence and beam noise only, to 7.62 m (25 ft) with the full 25 knots headwind and the associated turbulence. The results

show a -0.76 m (-2.5 ft) mean deviation from the glide slope with zero wind. This is a result of an offset in the simulation affecting the beam complementary filter and resulting in a small constant beam error even in the absence of disturbences. The mean tends to be lower with the shearing headwinds and higher with the tailwinds.

The results for the same configuration with spoilers are given in Figure 5-12. All the dispersions are significantly reduced. Sink rate control is improved by more than 40 percent, range by 60 percent, attitude by more than 50 percent and glide slope track by 30 percent. The variation of the mean touchdown range and attitude as a function of wind has increased, however.

To summarize, all dispersions grow significantly with the magnitude of horizontal turbulence. Pitch attitude is the only touchdown variable evaluated that was more affected by vertical than by horizontal turbulance. The use of spoilers with this variable flare height control law produces a very marked improvement in the control of range, sink rate and glide slope deviations in the two sigma region.

The probability distribution curves, on which the data in Figures 5-11 and 5-12 are based, are given in Appendix B.

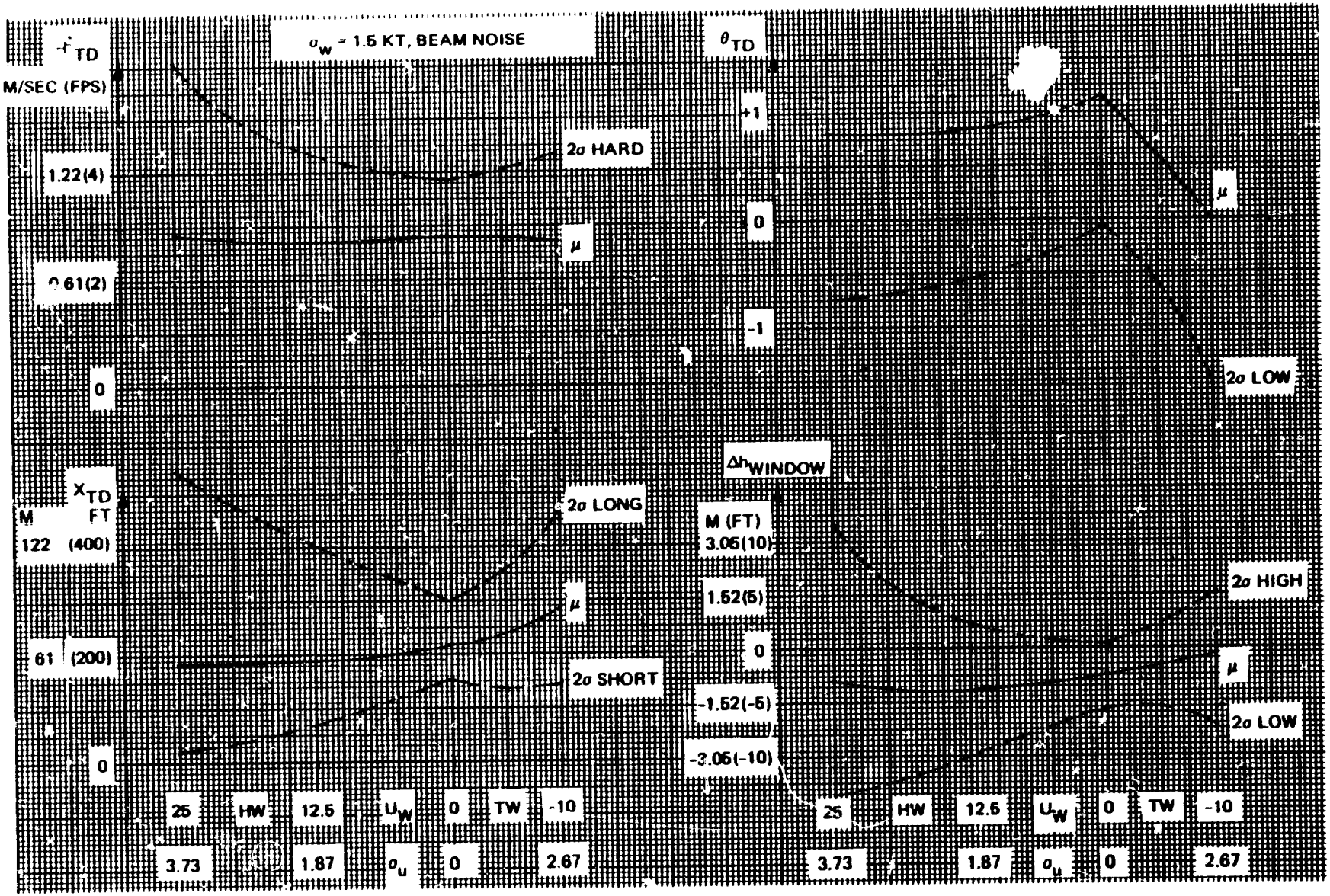

Figure 5-11. The Effect of Wind and Turbulence Level on Landing Performance, Variable Flare Height Without Spoilers

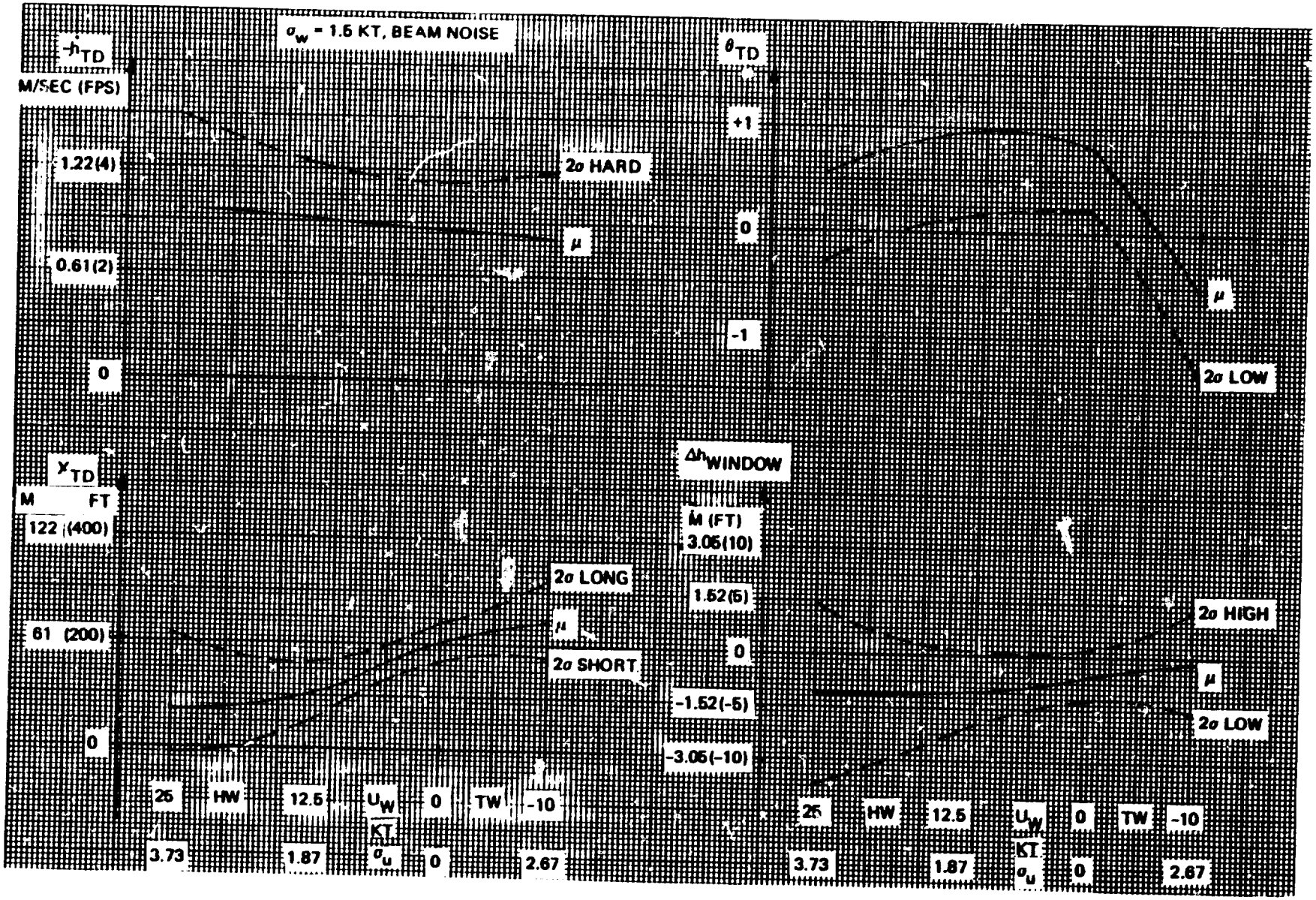

Figure 5-12. The Effect of Wind and Turbulence Level on Landing Performance, Variable Flare Height With Spoilers

6.0 LOCALIZER TRACK AND RUNWAY ALIGNMENT

For good lateral automatic landing prformance, the runway alignment maneuver must be initiated with the aircraft stabilized on beam certerline. Thus, the design of a stable, tight localizer track mode is a necessary prerequisite to defining an advanced automatic decrab control system. The assumption is made that even close in curved path approaches are selected so that the capture algorithm will place the aircraft on the localizer sufficiently early to allow transients to settle. Since the capture will have minimal impact on landing performance, it is not considered in this study. For Category IIIA landings, automatic roll-out guidance is not required, and it also is not included in this study.

During the design of the lateral landing system for the Augmentor Wing STOL vehicle, Reference 3, extensive tradeoff and optimization studies were performed to define the recommended forward slip algorithms. With few exceptions, the Twin Otter lateral directional dynamics and system requirements are very similar to the Augmentor Wing. Thus, maximum useage was made of the tradeoffs conducted during the previous work to provide a sound basis for this Advanced Autoland lateral landing study. This allowed a more extensive evaluation of the Twin Otter peculiarities, with tradeoffs and optimization directed specifically toward the problems peculiar to a light wing loading STOL aircraft.

This section describes the performance of the recommended localizer track and runway alignment control laws that are described in Section 4. Performance was evaluated through the use of simulation with deterministic and stochastic disturbances. The effects of sensor errors, trim changes and system variations were evaluated and the results are given and discussed here. Control law variations that were studied in the process of defining the recommended control law are also discussed in this section, as well as failure effects and system limitations.

6.1 PERFORMANCE

A performance summary of the recommended lateral landing system as described in Section 4 is presented here, with the detailed supporting data included in Appendix C.

The following subjects are presented and discussed here:

1. Landing time histories.
2. Statistical landing performance in stochastic disturbances only.
3. Landing performance over the total landing environment.
4. Deterministic variations and off-nominal conditions.
5. Localizer track activity in stochastic disturbances.

Landing Time Histories

Landing time histories, as obtained from simulation, with the recommended control law are given in Figure 6-1 (A and B). Six time histories are shown, starting at a C.G. height of 91.4 m (300 ft) above the ground and terminating at touchdown. The first three are all with 15 knots right shearing crosswind and the first is with 10 knots shearing tailwind, the second is with zero headwind and the third is with 25 knots shearing headwind. The second group of three landings is with 15 knots right steady crosswind and the same headwinds. Wind shears are patterned after FAA models as described in Appendix A. The initial crab angle is 20° with the shearing crosswind and 12° with the steady crosswind because the crosswind magnitude is higher at altitude with the shear. At touchdown, the airplane is aligned with the runway heading , within one degree, for all wind cases. There are no heading overshoots. Crosstrack velocity at touchdown is less than -0.114 m/sec (-0.375 fps away from the wind). Bank angle at touchdown is less than 5° (into the wind) for all cases. The control law does not have a wing leveling mode. The sideslip induced lateral acceleration is about -0.087 g for all wind cases. Ten degrees of rudder are needed to maintain runway heading and control wheel excursions of less than 10° are used. The crosstrack displacement at touchdown varies from 0.61 m (2 ft) to the right to 1.07 m (3.5 ft) to the left. Additional variables for the same six landings are shown in Figure 6-1B. The H_{CG} traces clearly show the impact of the headwind variations. The alignment model, ψ_M, as defined in Figure 4-7 starts out being equal to the crab angle above 45.7 m (150 ft) and it is reduced to zero at 15.2 m (50 ft). The rudder alignment command, $\delta_{C\ ALIGN}$, (which is the rudder command during alignment, excluding the yaw rate path) hits the 16° limit ($R_{LIM} \times K_{rL}$, Figure 4-7) for shearing crosswind cases. The δ_C trace is the total rudder command, including the yaw rate path. Rudder command does not exceed 11° for any landing.

Statistical Landing Performance

The landing performance of the recommended lateral landing system is summarized in Table 6-I both for stochastic disturbances only and over the total landing environment including the deterministic disturbances defined in Table 6-II. These data were obtained with limiting atmospheric and MLS disturbance levels, with average limiting longitudinal winds and shears, without accounting for the low occurrence probability of these disturbance levels, and thus it represnets a conservative estimate of landing performance. Moreover, Crows Landing Stolport (the airport at which the Twin Otter was tested) geometry, with localizer antenna placement of 1356 m (4450 ft) with respect to the elevation antenna location was

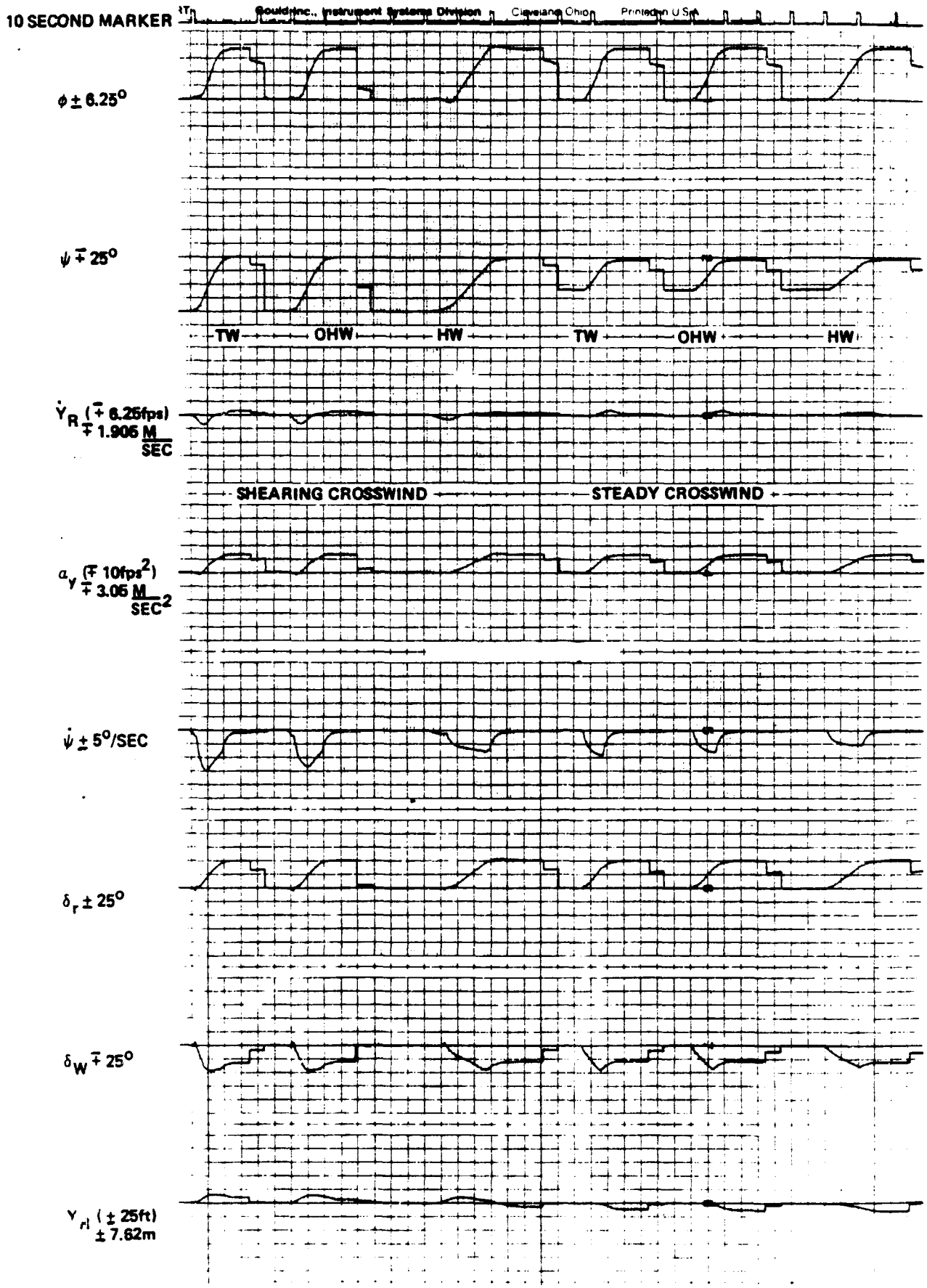

Figure 6-1A. Landing Time Histories – Nominal Configuration

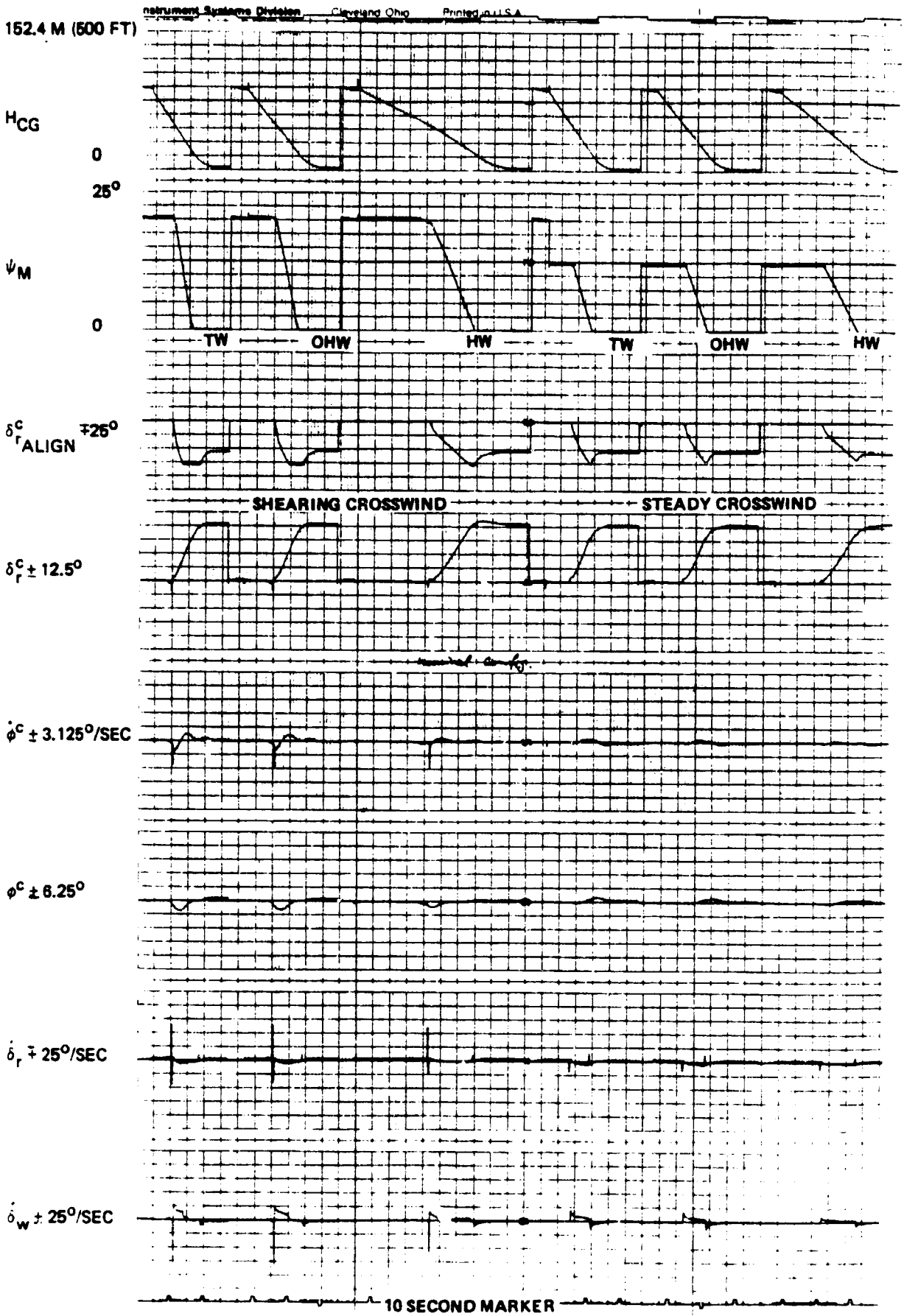

Figure 6-1B. Landing Time Histories - Nominal Configuration

used to give 1σ = 2.91 m (9.55 ft) lateral beam noise level at an altitude of 30.5 m (100 ft). In an actual STOL port installation a number less than 1356 m (4450 ft) can probably be established.

The lateral performance goals are given in the first column of Table 6-I. Performance requirements for Category III automatic landing systems have been defined for CTOL transports but not for STOL aircraft, as discussed in Reference 1. Thus, design goals had to be defined for this study. Most of these goals were specified by the NASA Statement of Work (SOW) or are determined by vehicle constraints. The allowed lateral two sigma landing dispersion was specified as ±4.57 m (15 ft) in the SOW. However, the FAA AC20-57A (Reference 7) requirement for not landing any closer than five feet to the runway edge, effectively specifies that for the Twin Otter vehicle on a 30.5 m (100 ft) runway, the probability of exceeding 11.88 m (39.0 ft) of lateral deviation at touchdown must be less than 10^{-6}, which is equivalent to a two sigma dispersion of ±4.86 m (15.9 ft). In Table 6-I, this 10^{-6} value is being used along with the SOW requirement for two sigma lateral dispersion. Applying the above 11.88 m (39.0 ft) constraint to lateral deviation during rollout, the touchdown heading error becomes 10.8°. This is based on the assumption that lateral rate just after touchdown is approximately equal to $U_o/57.3$ times the touchdown course error, and that a correcting lateral acceleration of 0.2 g's is applied to arrest the lateral velocity. The corresponding 2 sigma value for $\Delta\psi_{TD}$ is 4.40 degrees. The touchdown bank angle requirement is based on aircraft geometry. Wing contact for the Twin Otter airplane occurs at 19° of bank. The touchdown crosstrack velocity limit is normally dependent on touchdown bank angle. For conservatism, a one gear touchdown lateral velocity limit of 3.048 m/s (10 fps) was considered as the 10^{-6} requirement. The results of Table 6-I indicate that the landing performance satisfied all the design goals by wide margins. The probability distributions for the landing parameters of Table 6-I are given in Appendix C.

Deterministic Variations

Many deterministic variations were considered during this study. Those which significantly impact lateral landing performance are listed in Table 6-II along with their effect on the aircraft performance indication parameters, with a more complete discussion given in the next section.

TABLE 6-I LATERAL PERFORMANCE SUMMARY

PARAMETER	GOAL	ACTUAL	
		STOCHASTIC ONLY	TOTAL POPULATION
Y_{TD} m (ft)	μ -	-0.365 (-1.2)	-0.365 (-1.2)
	2σ <4.57 (15.0)	-3.35 (-11.0)	-4.419 (-14.5)
	10^{-6} <11.88 (39.0)	-6.58 (-21.6)	-8.9 (-29.2)
$\dot{Y}_{TD}$ m/sec (fps)	μ -	-0.122 (-0.4)	-0.122 (-0.4)
	2σ -	±0.518 (±1.7)	±0.518 (±1.7)
	10^{-6} <3.048 (10.0)	-1.37 (-4.5)	-1.37 (-4.5)
$\Delta\psi_{TD}$	μ -	0.0	0.0
	2σ -	+2.2 -0.8	+2.4 -1.3
	10^{-6} <10.8	+7.2	+7.7
ϕ_{TD} deg	μ -	+4.7	+4.7
	2σ -	±2.0	±2.1
	10^{-6} <19.0	+9.4	+9.8
ΔY_{WINDOW} m (ft)	μ	+0.457 (+1.5)	+0.457 (+1.5)
	2σ (±25.0)	±3.81 (±12.5)	±4.11 (±13.4)

NOTES:
1. This table defines both stochastic only and total population landing performance, where the latter includes deterministic disturbance effects.
2. Only those requirements specified in the SOW or dictated by aircraft/geometry limitations are listed.
3. For the lateral axis, means should all be zero when evaluated over the total environment. Since actual results are presented for limiting wind from the right, significant mean values are obtained.
4. ΔY_{WINDOW} is lateral tracking error at the 30.48m (100 ft) approach window.
5. For conservatism, results are presented for limiting crosswind, shear, turbulence, and MLS noise levels for averaged limiting headwind and tailwind conditions, without accounting for the ≈4% probability of occurrence of these limiting atmospheric disturbances.
6. Deterministic variations included in total population distributions are MLS azimuth bias, course datum error, accelerometer and gyro errors, and approach speed variations.

TABLE 6-II LATERAL DETERMINISTIC DISTURBANCE EFFECTS

DISTURBANCE	STANDARD DEVIATION	CUTOFF	ΔY_{TD}	$\dot{\Delta Y}_{TD}$	$\Delta\psi_{TD}$	$\Delta\phi_{TD}$	ΔY_{WINDOW}
1. Azimuth Bias	0.0935°	@3σ	0.994 m (3.26 ft)	-	-	-	1.372 m (4.5 ft)*
2. Compass System	0.889°	No	0.042 m (0.139 ft)	-	.498°	0.21°	0.042 m (0.139 ft)
3. Accelerometer Errors	0.0031 g	No	0.45 m (1.48 ft)	-	-	0.25°	0.45 m (1.48 ft)
4. Vertical Gyro Errors	0.35°	No	0.66 m (2.16 ft)	-	-	0.35°	0.66 m (2.16 ft)
5. Rudder Trim Shift	0.5°	No	0.356 m (1.17 ft)	0.05 m (0.17 fps)	-	-	0.091 m (0.3 ft)

NOTES:
1. Normal distributions are assumed for all deterministic variations, and performance effects are for 1σ disturbance levels.
2. Azimuth bias distribution is cut off at 3σ level since it is assumed that the near field monitor would detect variations of more than 0.3° (see Figure C-30).
3. Accelerometer and gyro errors depend on dynamics, and the equivalent worst case value is indicated.
4. The azimuth distribution is assumed normal to the cutoff point, and no cutoff is used on the other distributions for conservatism.
5. Blank entries indicate no significant contribution due to that disturbance.
6. The ΔY_{window} due to azimuth bias (*) does not contribute to window accuracy since it is measured with respect to the beam, not extended runway center line.
7. These results are graphically presented in Appendix C.
8. See discussion of Rudder Trim Shift in paragraphs 6.2.3 and 6.3.2.

The performance impact of these deterministic variations is relatively small compared to atmospheric disturbance induced landing dispersions. However, the lateral displacement error at the intended touchdown point due to the 0.0935° one sigma azimuth bias is significant.

Activity in Disturbances

A summary of aircraft state variations and control activity as obtained from simulation with limiting turbulence levels and beam noise is given in Table 6-III. All activity levels are acceptable.

TABLE 6-III LOCALIZER RMS ACTIVITY

Φ	deg	0.85	
ψ	deg	1.60	
$\dot{y}$	m/s (fps)	0.427	(1.40)
a_y	g	0.010	
$\dot{\psi}$	deg/s	0.68	
δ_R	deg	0.80	
δ_w	deg	2.0	
y	m (ft)	1.34	(4.40)

NOTE : σ_{BN} = 2.9 m (9.5 ft), $\sigma_{\beta G}$ = 1.83°

In summary, the recommended system provides landing performance compatible with Cat IIIA landing requirements.

6.2 SENSOR ERRORS AND SYSTEM VARIATIONS

The following sensor and system errors and off-nominal conditions were evaluated as part of this study and are discussed here:

1. MLS guidance system errors
2. Sensor errors
3. Rudder trim changes

4. Sensitivity analysis
5. MODILS discretization effects

6.2.1 MLS ERRORS

For a Cat IIIA lateral automatic landing system, only DME and azimuth errors can impact landing performance. The effects of DME bias is small, and only azimuth variations need be considered. Assuming that the azimuth antenna is located 609.6 m (2000 ft) from the nominal touchdown point, the 0.0935° one sigma bias level directly yields ±0.99 m (±3.26 ft) 1σ lateral touchdown variations; and 4.88 m (16.0 ft) if extrapolated linearly to the 10^{-6} (4.9σ) probability level. Thus, this term alone is as significant as limiting wind levels on lateral touchdown dispersion. To limit the impact of this bias in the low probability region, a 0.3° 3σ cutoff level was used, since it appears reasonable that the near field beam monitor threshold should be no greater than 0.3°. With this assumption, the lateral deviation due to stochestic and deterministic disturbances at the 10^{-6} probability level is 8.9 m (29.2 ft), as shown in Table 6-I.

6.2.2 SENSOR ERRORS

The three sensor on board the aircraft which contribute significantly to landing performance are the compass system, the lateral accelerometer, and the vertical gyro.

Since the compass system signal provides the main input to the align maneuver, its errors are significant. The expected accuracy is ±4.0 degrees on a 4.5σ basis. As expected, it yields touchdown misalignment on a one to one basis, with relatively small impact on other landing parameters.

The runway axis lateral acceleration signal is used both for navigation filter augmentation and wing down compensation, and its error characteristics are of a dynamic nature. An equivalent offset of ±0.014 g, 4.5σ (or 0.0031 g, 1σ as shown in Table 6-II) was assumed. The induced landing variations are very dependent on landing system design; for the recommended configuration with washed out acceleration, this acceleration inaccuracy yields 0.45 m (1.48 ft) one sigma lateral dispersion as discussed in detail in Appendix C.

The roll attitude vertical gyro errors are also dynamic in nature, a combination of steady errors and acceleration induced erection and drift errors as discussed in Appendix C. The ±0.35° equivalent 1σ error has about the same landing performance impact as the accelerometer (see Table 6-II).

6.2.3 RUDDER TRIM CHANGES

The usage of the rudder command signal for crossfeed purposes, has an impact on the landing accuracy as discussed in paragraph 6.3.2. The effect is dynamic in nature and is a function of the glide slope capture maneuver characteristics and the altitude at which this maneuver is executed. A ±1.5° rudder deflection on a 3σ basis was determined (as shown in paragraph 6.3.2) as the effective error introduced via this path. The impact on lateral touchdown deviation is ±1.07 m (±3.5 ft) three sigma.

6.2.4 SENSITIVITY ANALYSIS

A sensitivity analysis study was conducted to examine the effect of gain and time constant variation on system performance. The analysis included the variation of most of the gains by ±6 db around nominal, with the exception of the yaw to roll crossfeed gains for which the variation was ±20 percent. The landing time histories are given in Appendix C. As expected, none of the variables has a pronounced effect, with K_ϕ and τ_2 having similar impact as crossfeed parameters variations.

6.2.5 MODILS DISCRETIZATION EFFECTS

MODILS is an experimental microwave landing aid that was used initially in flight tests. It has a narrow azimuth coverage and a granular azimuth signal. The impact of MODILS finite resolution (refer to Appendix A) was investigated to establish the feasibility of using higher guidance proportional loop gain (K_y). The MODILS beam resolution of 0.1°, renders 4.72 m (15.5 ft) lateral deviation discretization effect at an altitude of 274 m (900 ft). Localizer track performance with the discretization incorporated into the simulation is given as Figure 6-2 where a rudder ramp going from zero to 1.5° in 10 seconds was used as the disturbance. The results are optimistic since a discretization level of ±3.28 m (±10 ft) was used. Note that for a doubled proportional gain, absolutely no lateral deviation performance improvement is gained. On the contrary, a higher limit cycle frequency is observed.

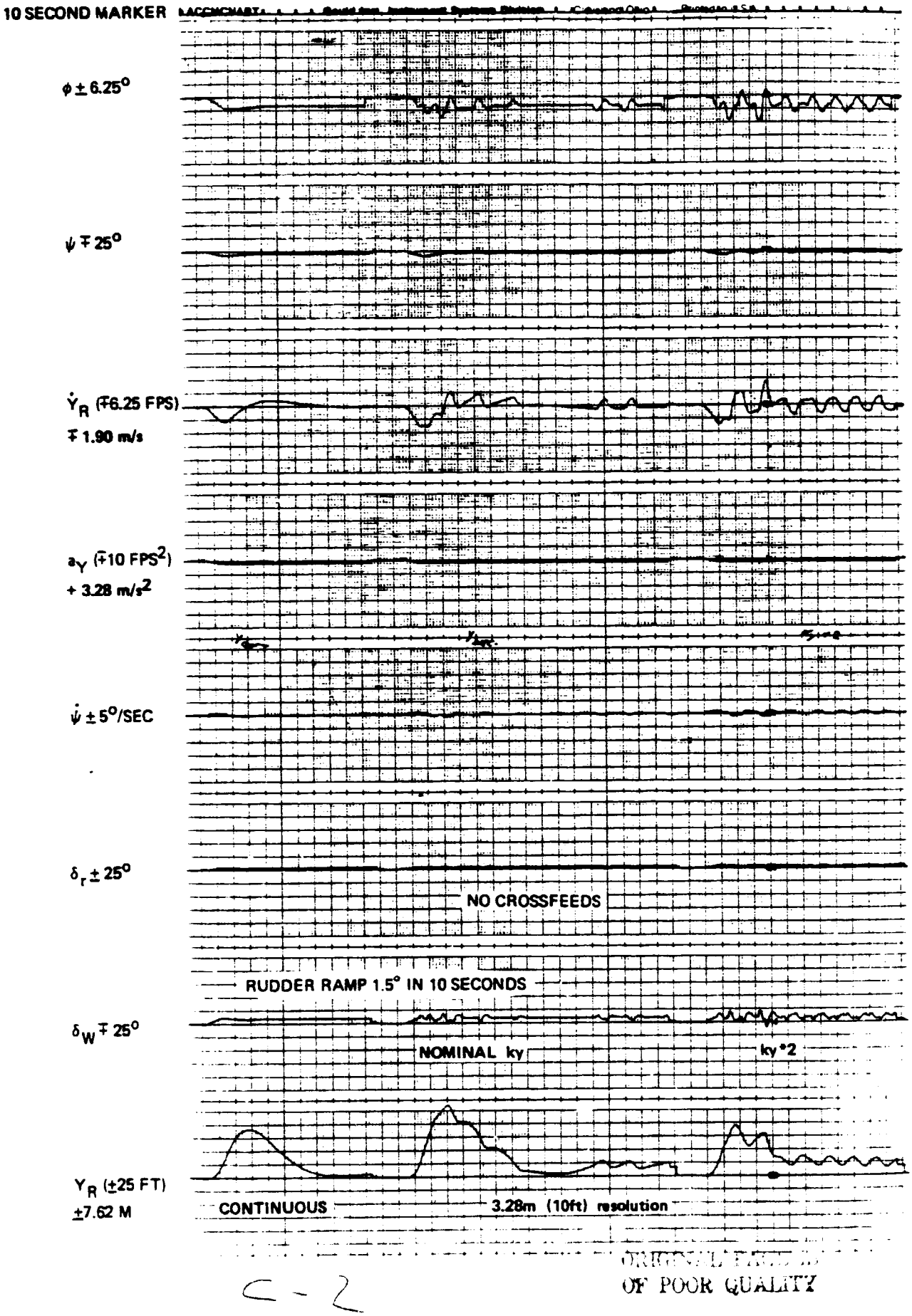

C-2

Figure 6-2. Effect of Beam Discretization, Yawing Moment Disturbance

The resolution of the MLS guidance system is 0.01° in azimuth, an order of magnitude better than MODILS, yielding 0.457 m (1.5 ft) steps at an altitude of 274 m (900 ft). The scaling of the digital autopilot is 1.22 m/bit (4 ft/bit) with MODILS but it has been changed to 0.0762 m/bit (0.25 ft/bit) for the final approach phase with MLS guidance. Thus, the MLS beam information can be considered continuous.

Figure 6-3 summarizes the effect of MODILS resolution on statistical landing performance. Results are given for the discretized beam signal and for a continuous signal. Data were taken with turbulence and beam noise and repeated with turbulence only because beam noise acts as a dither, masking the effects of the poor resolution. This is most obvious on y_{TD}. With the beam noise the results for the discrete and the continuous signal are very similar. Without the noise, the continuous beam yields a much smaller lateral dispersion than the discretized signal. The same effect is apparent to a smaller degree on the touchdown bank angle.

6.3 SYSTEM OPTIMIZATION

This section describes the results of tradeoff studies that were carried out in order to arrive at the recommended localizer track and runway alignment control laws that are described in Section 4. Extensive tradeoff studies were made in the course of a previous automatic landing study for the Augmentor Wing airplane which is a powered lift experimental STOL airplane. Some of the major results of that study are considered to be directly applicable to the Twin Otter. They are listed here and described in detail in Reference 3. This section concentracts on presenting the results of tradeoff studies that were directed at problems peculiar to the Twin Otter as a representative light wing loading STOL airplane.

6.3.1 RESULTS BASED ON THE AUGMENTOR WING STUDY

The study of the lateral automatic landing control laws for the Augmentor wing airplane is described in Reference 3. Several control law alternatives were evaluated in that work. Some of these results are applicable to the Twin Otter because both are STOL aircraft flying a 6° to 7.5° final approach at about 70 knots.

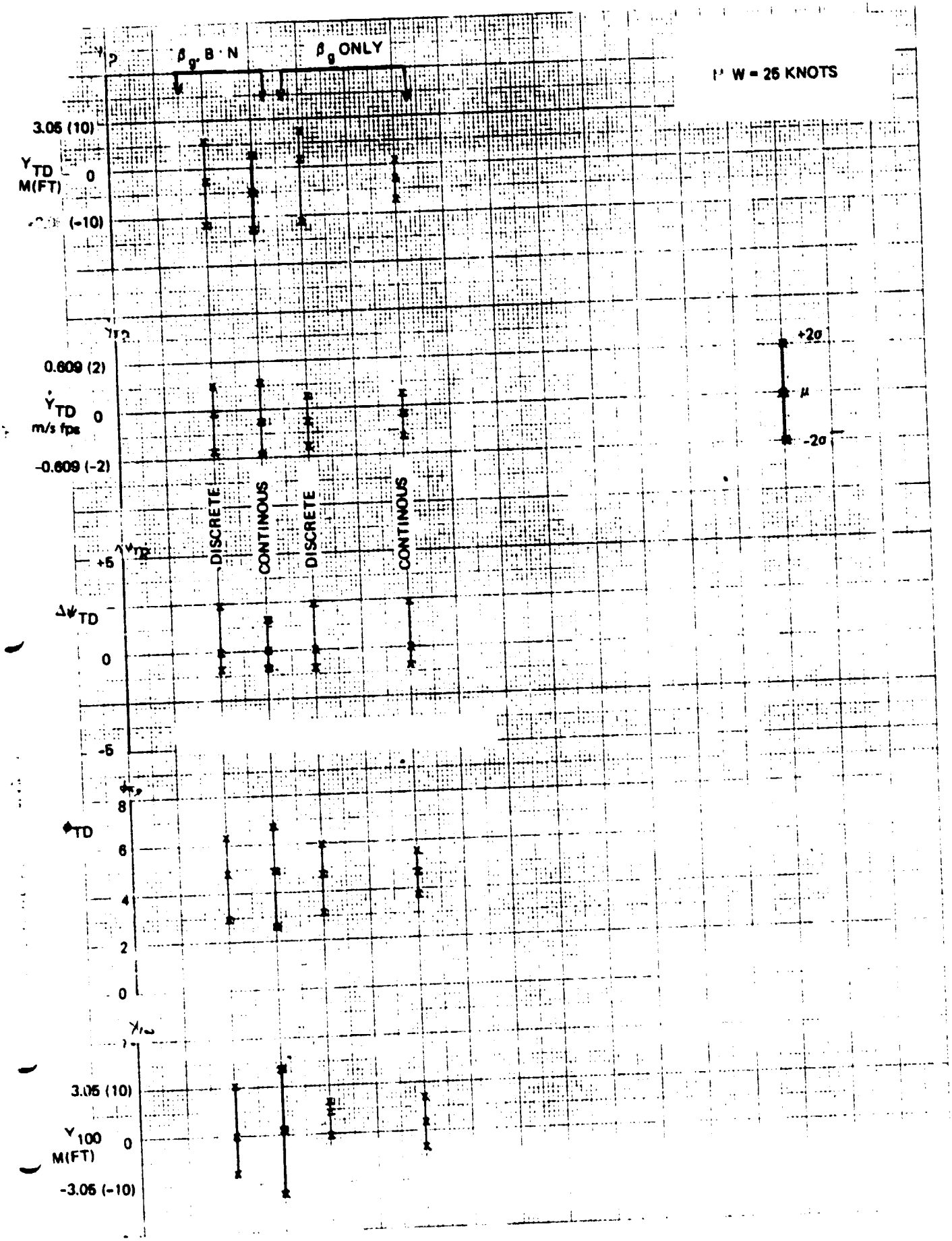

Figure 6-3. The Effect of MODILS Discretization on Statistical Performance

Differences between the powered lift and light wing loading aircraft in pitch are very significant but in roll and yaw both vehicles use the same basic control techniques.

The runway alignment results that were obtained for the Augmentor Wing and applied to the Twin Otter are listed here and the tradeoff studies leading to these results are described in detail in Reference 3.

Runway Alignment Configuration

A forward slip technique was traded against the flat decrab, resulting in a clear superiority of the forward slip since the alignment initiation timing is not critical and touchdown performance is less dependent on vehicle and wind variations.

Align Entry

Two schemes were evaluated. One relied on a command rate limiter to slow the forward slip entry rate while permitting a reasonably high heading loop gain. Although landing performance with this configuration was satisfactory it had some drawbacks which included overshoots of both the reference heading and the required steady state bank angle. Also, full crab angle was reached at a relatively high altitude, requiring the full wing down compensation for up to 10 seconds which may negatively impact ride quality. The altitude scheduled reference heading error trajectory described in Section 4 was selected as the preferred configuration as it eliminated the drawbacks of the rate limited align entry.

Rudder Bias Generation

A sideslip angle is generated while aligning the airplane with the runway in the presence of a crosswind. This sideslip must be held with the rudder. Three methods for generating the steady state rudder deflection were evaluated. An open loop rudder predict term, based on heading error at align entry, was evaluated in conjunction with the flat decrab configuration and was found to be subject to limitations inherent in most open loop compensation. In the second technique the steady state rudder command was obtained from a crosswind estimate. Good performance

was obtained with this method for the Augmentor Wing airplane, but the computation is fairly complex and it requires a prior knowledge of several of the airplane's stability derivatives. The third method that was implemented in the recommended control law is a closed loop rudder control using heading reference trajectory error and its integral to drive the rudder (as described in 4.2). The aircraft is able to track the model trajectory with only small errors, thus allowing the use of a high gain integral term to provide the required steady rudder during the alignment.

Wing Down Compensation

A roll command is needed at align entry to minimize the roll transient due to the align rudder kick. Three techniques were considered for the Augmentor Wing airplane. An open loop wing down predictor, a crosstrack acceleration referenced signal and one based on pseudo crosstrack acceleration computed from bank angle and rudder deflection. The last two methods produced good results and the accelerometer referenced signal was selected for the recommended signal because the Augmentor Wing airplane (and the Twin Otter) have three axis accelerometers and the accelerations are resolved into runway axes as part of the navigation computations. An additional compensation signal, based on rudder and yaw rate to roll wheel crossfeeds, was needed for the Twin Otter, as described in a following section.

The following sections described tradeoff studies and alternative methods that were used to solve problems that were peculiar to the Twin Otter.

6.3.2 ROLL WHEEL CROSSFEEDS

The recommended Twin Otter lateral/directional control law includes crossfeeds of rudder command and yaw rate to the wheel, as shown in Figure 4-7. These crossfeeds were needed to minimize a pronounced tendency of the airplane to deviate from the localizer, away from the wind, during runway alignment. A sequence of alignment time histories without the crossfeeds and with 15 knots steady crosswind is shown in Figure 6-4. The first time history is with all the nominal Twim Otter stability derivatives. During the first two or three seconds into the alignment the airplane banks in the wrong direction and a lateral deviation developes and reaches -5.18 m (-17 ft, away from the wind) at touchdown. In the following time histories one airplane stability derivative is set to zero for

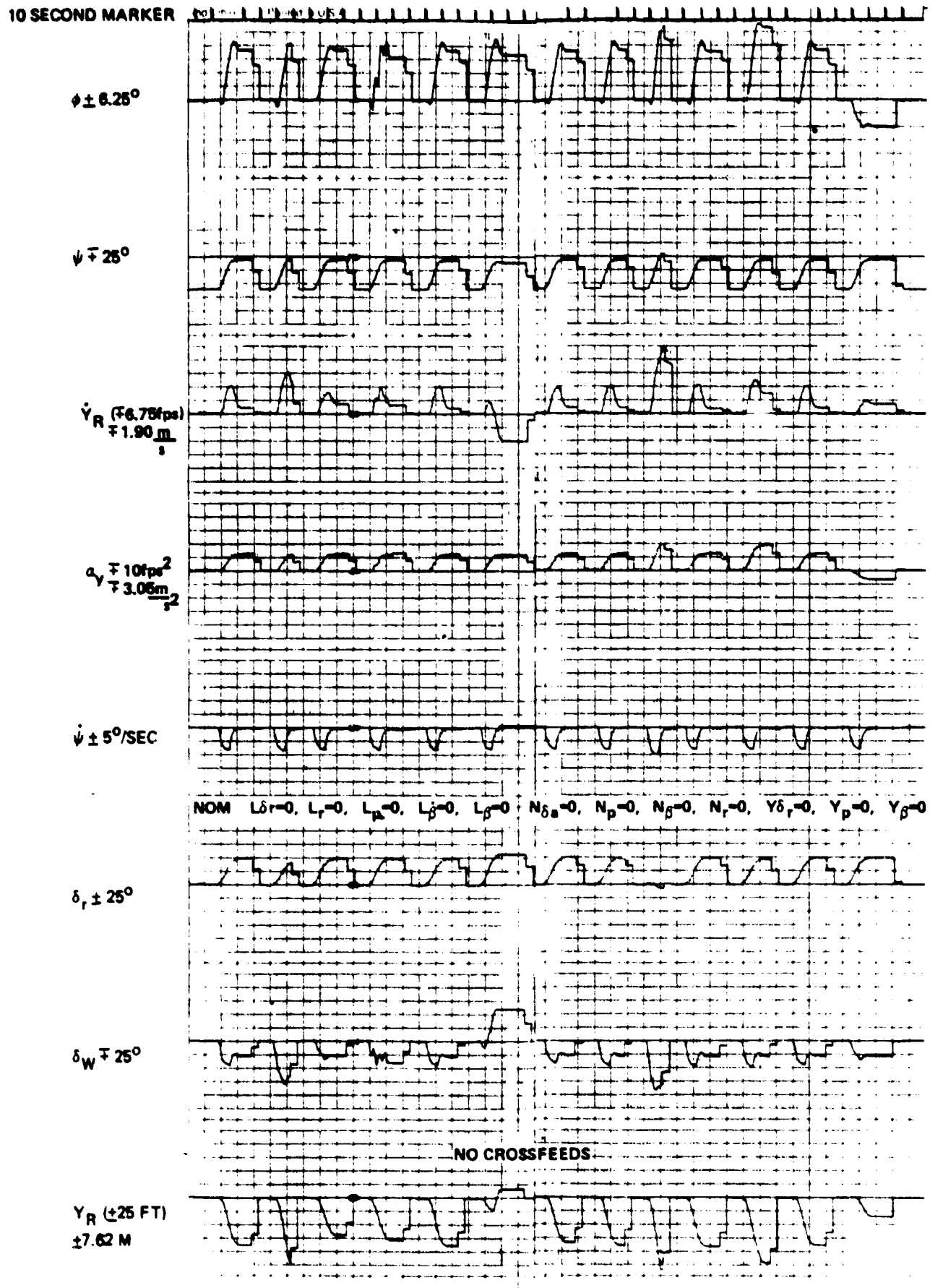

Figure 6-4. The Effect of Stability Derivatives on Lateral Deviation

each run in order to identify the airframe parameter that contributes the most to the problem. It is quite obvious that the dihedral effect, L_β, is the most significant single contributor.

Crossfeeding yaw rate to the wheel proved to be effective in controlling the adverse roll in alignment but it did not reduce the problem to a satisfactory low level and therefore additional crossfeeds were considered.

Sideslip to Wheel Crossfeed

All wheel and rudder control laws for this configuration are as shown in Figure 4-7 with the exception of the substitution of sideslip angle for rudder command, as shown in Figure 6-5.

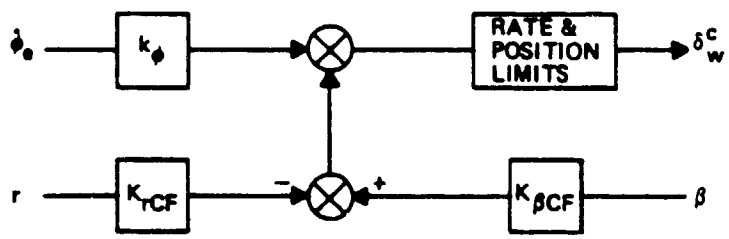

$$K_{rCF} = 4.0 \frac{\text{deg}}{\text{deg/sec}}, \qquad K_{\beta CF} = 0.6 \frac{\text{deg}}{\text{deg}}$$

FIGURE 6-5. SIDESLIP TO WHEEL CROSSFEED BLOCK DIAGRAM

An alignment time history with these crossfeeds is shown in Figure 6-6 and it is obvious that the results are very good as the lateral deviation is kept below 0.76 m (2.5 ft).

Sideslip angle, however, is not directly available on the Twin Otter. It can be computed through the use of the following equation:

$$\beta = \int \left(\frac{a_y}{U_o} + \frac{g\phi}{U_o} - r \right) dt$$

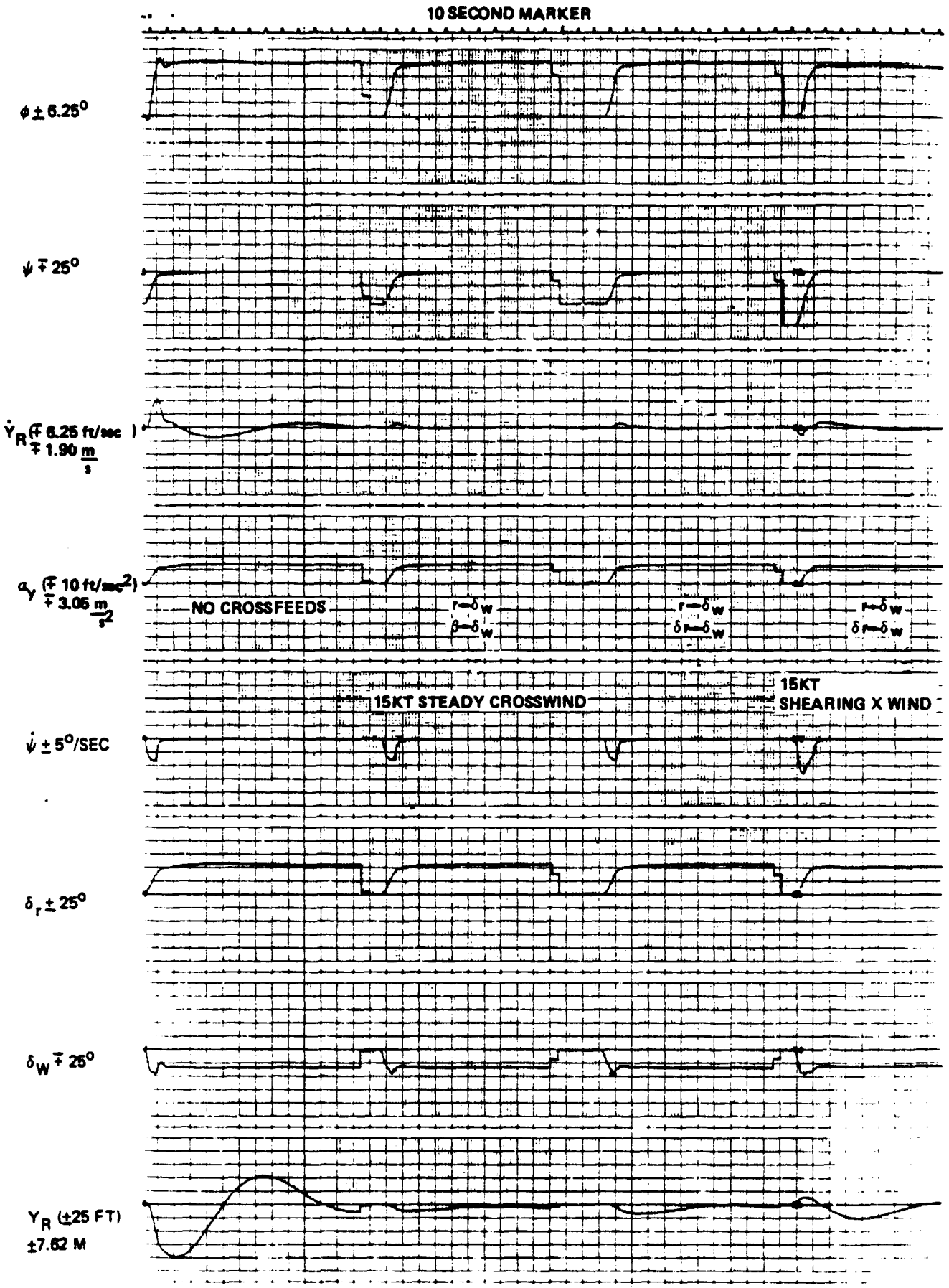

Figure 6-6. Alignment Time Histories with Various Crossfeeds

But the signal obtained this way is susceptible to drift problems and it was therefore not adopted in the recommended control law.

Heading Error to Wheel Crossfeed

Heading change during alignment is a reasonably good approximation for slidslip in the case of a steady crosswind. An attempt was made to use $\Delta\psi_i - \Delta\psi$ (see Figure 4-7) instead of β in the block diagram of Figure 6-5. Alignment time histories with β and $\Delta\psi_i - \Delta\psi$ used as crossfeed to the wheel, are given in Figure 6-7. The heading error crossfeed results in centerline tracking accuracy with a steady crosswind that is as good as with the sideslip crossfeed. Significant excursions occur, however, with a shearing crosswind and therefore this crossfeed has been discarded.

Rudder Command to Wheel Crossfeed

A crossfeed of rudder command, along with yaw rate, to the wheel produces good tracking accuracy as seen in Figure 6-6 and these crossfeeds were included in the final configuration as shown in Figure 4-7.

One problem associated with the use of rudder command to roll crossfeed is a non zero rudder trim value which could introduce a disturbance into the roll axis during glide slope capture. An attempt was made to incorporate a washout on δ_R^c to δ_w^c but even unreasonably long washout time constants (100 seconds) resulted in a pronounced degradation of runway alignment performance, as can be seen in Figure 6-8, precluding the use of a washout. The impact of rudder trim on landing performance is therefore evaluated. Assume that most of the rudder trim change on final approach is a result of thrust asymmetry that occurs while thrust is reduced in the glide slope capture maneuver. The thrust variation between straight flight and a 7.5° descent is:

$\Delta T = W \sin \gamma$

$W = 5000$ kg (11,000 lb) $\qquad \gamma = -7.5°$

result in $\Delta T = -652.6$ kg $\qquad$ (-1436 lb)

Further assuming 10 percent thrust asymmetry and with the moment arm of 2.56 m (8.4 ft) the total yawing moment is:

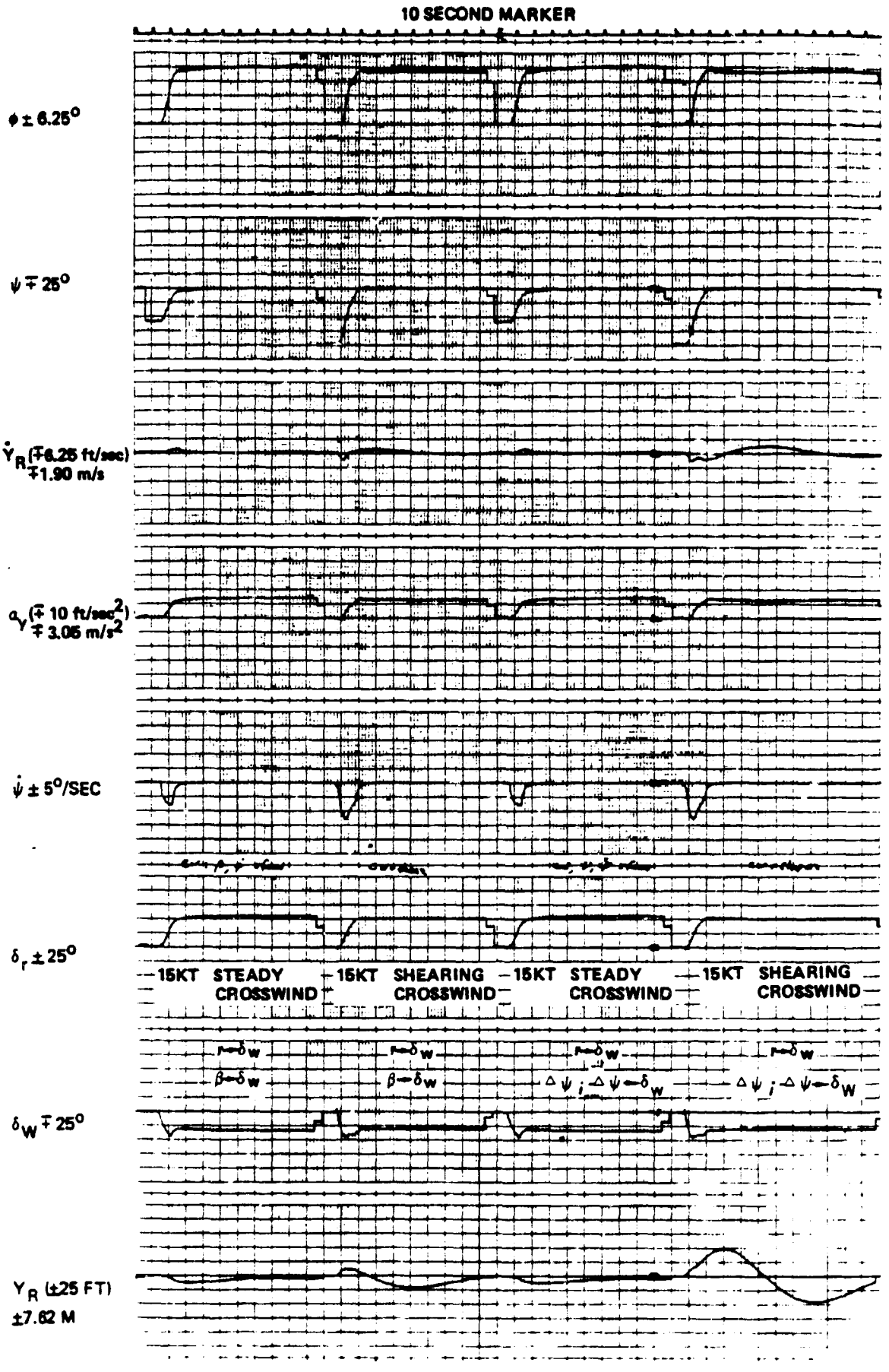

Figure 6-7. Alignment Time Histories with Various Crossfeeds

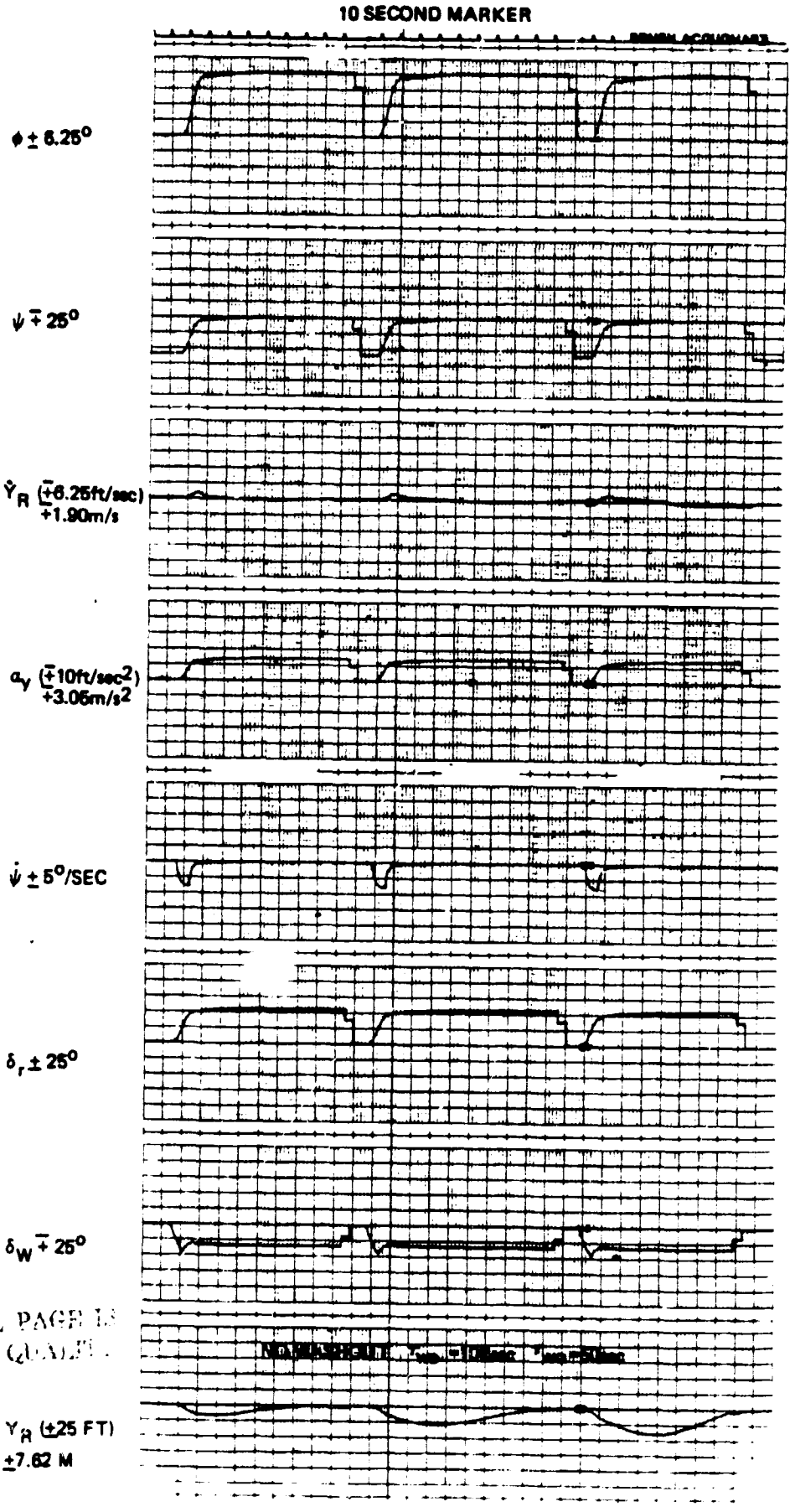

Figure 6-8. The Effect of a Washout on δ_R^c to δ_W^c

$$N = \Delta T * L_{ENGINE} = 65.3 * 2.56 = 167 \text{ kg - m } (1206 \text{ ft-lb})$$

The rudder deflection required to compensate for this moment is computed from:

$$\Delta N + qsb\, C_{n\delta R}\delta_R = 0$$

The result is 1° of rudder. This effect was simulated by inserting a ramp of rudder command in the crossfeed path going from zero to 1.5° (for conservatism) in 10 seconds. The lateral touchdown deviation induced by the rudder trim change was determined to be less than 1.07 m (3.5 ft) for a glide slope capture maneuver at 274 m (900 ft) height, as seen in Figure 6-9.

6.3.3 RUDDER AND ALIGN LIMITS

The rudder authority limit and the yaw rate command limit (R_{LIM} in Figure 4-7) have a significant impact on runway alignment performance. Initially, software rudder limits in the Twin Otter automatic landing system were set at ±5° (out of a mechanical travel of 21° to the right and 17° to the left). Statistical landing results were obtained for several levels of rudder and yaw rate command limits and the results are summarized in Table 6-IV. Data were taken with the recommended alignment control law but with ψ_0 (the alignment model value at low altitude; see Figure 4-7) of 2° and therefore a 1° mean touchdown heading deviation is obtained even without limits. The ±2σ heading dispersion increases by a factor of 4 when the yaw rate command is limited to ±3.125° instead of being unlimited. No degradation is apparent when the unlimited rudder authority limit is narrowed to ±12° and the align limit to ±2.5°/s. Table 6-V summarizes the results with a fixed rudder limit of ±7° and an alignment limit of ±1.25°/sec as a function of wind and turbulence level. Even with 5 knots of crosswind the touchdown heading dispersion is much worse than with the unlimited system with 15 knots of crosswind. The results clearly indicate that ±5° of rudder authority is inadequate. A 12° to 15° authority is needed with a high align rate limit. The recommended control law uses 12° rudder authority and a 4°/sec align limit. Since the rudder authority is a function of dynamic pressure, data were taken for both 12° authority and 10° which is considered to be the worst case. The results are summarized in Figure 6-10 and the 10° authority is marginal with 15 knots crosswinds.

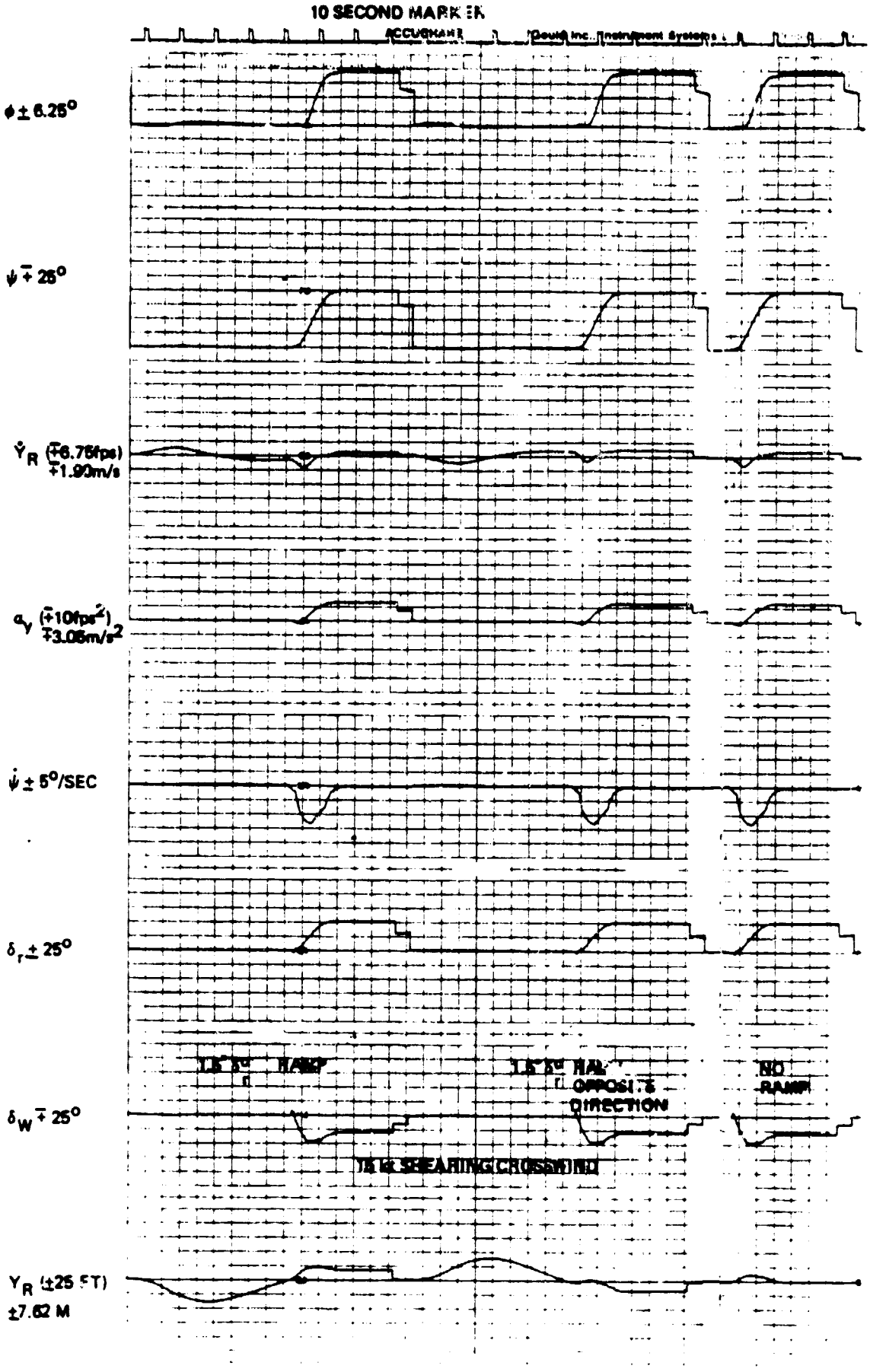

Figure 6-9. Alignment Time Histories with δ_R^C Ramps

TABLE 6-IV ALIGN PERFORMANCE WITH VARYING RUDDER AUTHORITY

Align Limit R_{LIM} (deg/sec)	1	1.25	2.5	3.125	3.125	∞
Rudder Limit (deg)	5	10	12	15.0	∞	∞
ψ_{TD} (deg)	$9.8^{+2.6}_{-2.8}$	9.4 ±2.6	$4^{+2.5}_{-3.2}$	$1.9^{+2.0}_{-1.1}$	$1.9^{+2.3}_{-1.1}$	2±0.8

NOTE: 1. Data obtained with 15 knots shearing crosswind and corresponding turbulence.

2. Results are given as $\mu \pm 2\sigma$.

3. $\psi_0 = 2°$.

TABLE 6-V ALIGN PERFORMANCE WITH 7° RUDDER AUTHORITY

Cross Wind (knots)	5	10	15
ψ_{TD} (deg)	$1.5^{+1.5}_{-0.7}$	5 ±2.8	9.4 ± 2.6

NOTE: 1. Rudder align and position limits of 1.25°/sec and 7° respectively were used.

2. The crosswind level also defines the appropriate turbulence and shear.

3. $\psi_0 = 2°$.

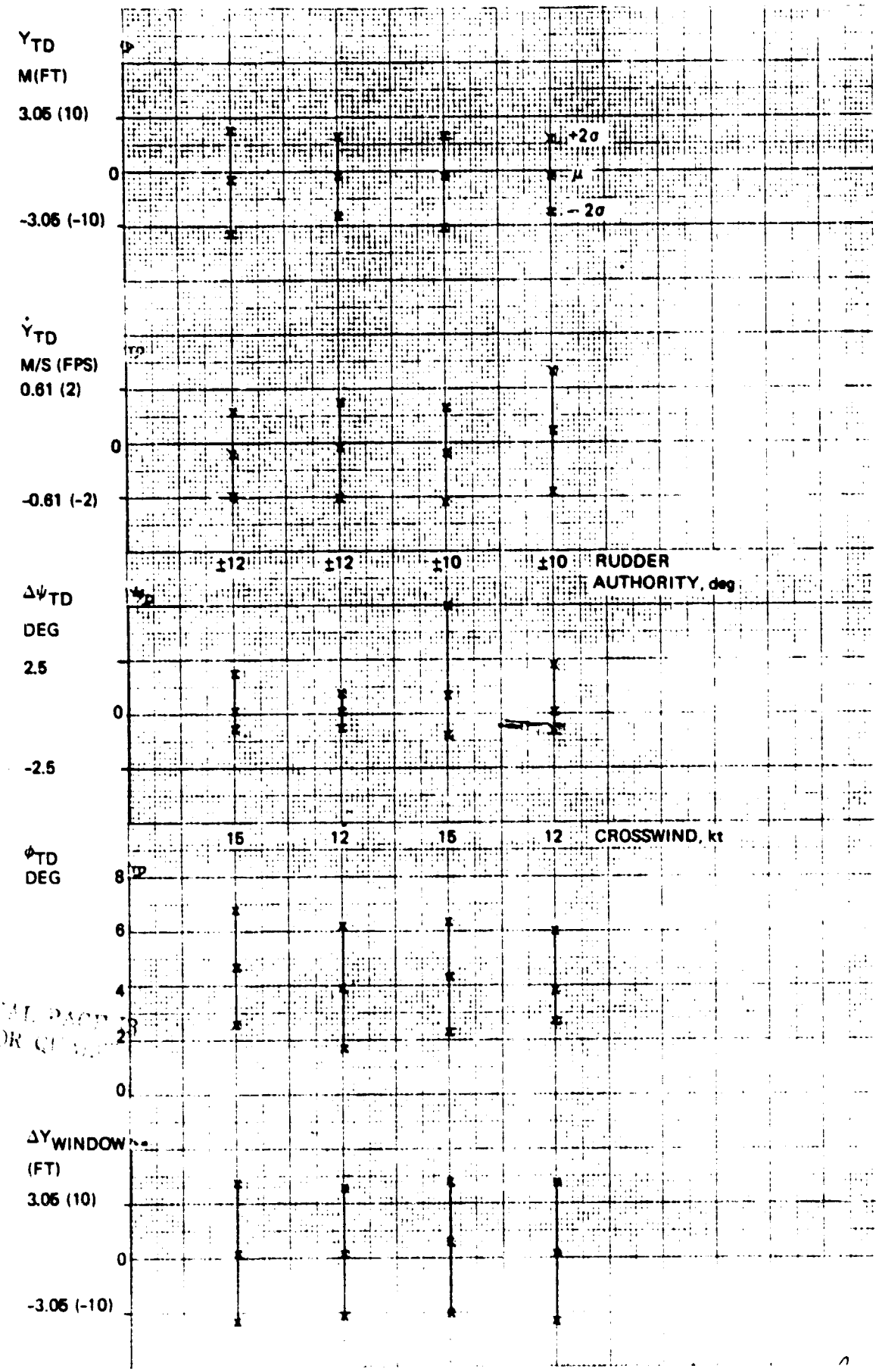

Figure 6-10. Statistical Landing Performance Summaries, Effect of Rudder Authority and Crosswind

The steady state rudder deflection required to handle a 15 knot crosswind is readily computed from:

$$N_{\beta}\,\beta + N_{\delta R}\,\delta_R = 0$$

The result is 11.7° which suggests that the recommended 12° rudder limit is the minimum allowable value and any lower value will be detrimental to performance.

6.3.4 ADDITIONAL VARIATIONS

Minimum Heading Reference ψ_0

The recommended alignment control law utilizes a reference trajectory for runway alignment as shown in Figure 4-7. This trajectory starts out with ψ_i, the pre-align heading error, at a gear height of 45.72 m (150 ft) and it decreases and levels off at the final value of ψ_0 at 15.24 m (50 ft). A non zero value of ψ_0 results in an alignment command that is ψ_0 degrees short of the runway heading such that the alignment is not complete at 15.24 m (50 ft) but the integrator reduces the heading error to zero at touchdown. This is done to eliminate possible overshoots of the runway heading. Alignment time histories for the Twin Otter with 15 knot shearing crosswind are shown in Figure 6-11 with ψ_0 of 2° and 0. No overshoot tendency is apparent and the airplane touches down about 1.5° short of the runway heading with the non zero ψ_0. Therefore, ψ_0 is zero for the recommended system.

MLS Receiving Antenna Location

Most of the work in this study was done assuming that the nose located antenna is C.G. corrected such that the input to the lateral navigation filter is lateral deviation at the airplane's center of gravity. Landing time histories with a nose mounted uncorrected antenna are given in Figure 6-12. The first three of the six traces are with 15 knots shearing crosswind and the second group of three traces is with 15 knots steady crosswind. The first and fourth traces are with 10 knots shearing tailwind, the second and fifth are with zero headwind, and the third and sixth are with 25 knots shearing headwind. With the uncorrected antenna, the airplane's nose tracks the localizer and since during alignment it tends to rotate about its center of gravity it is displaced from the centerline at touchdown by up to 1.52 m (5 ft) away from the wind. Lateral displacement with steady crosswind is larger than with shearing crosswind.

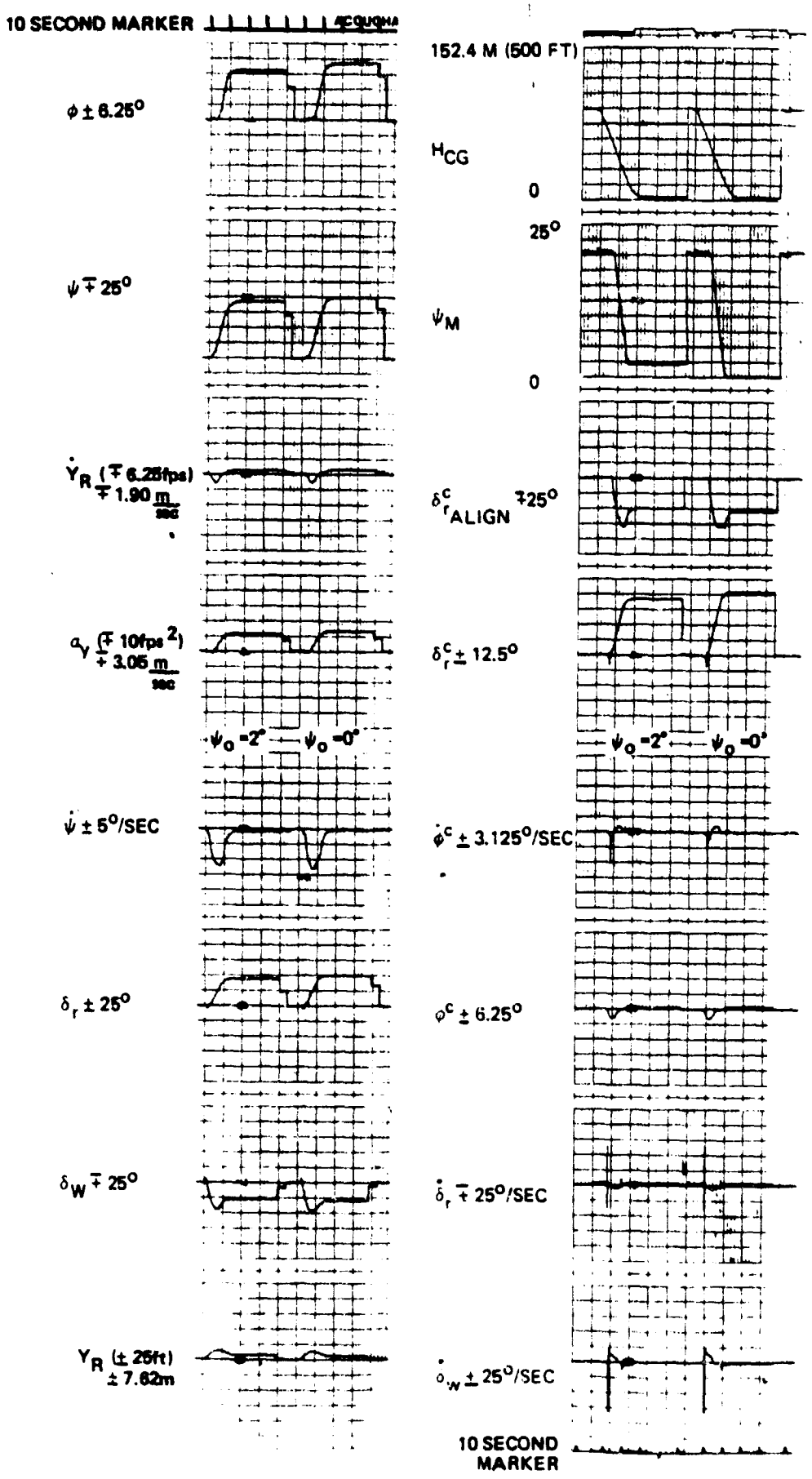

Figure 6-11. Landing Time Histories – Impact of ψ_o

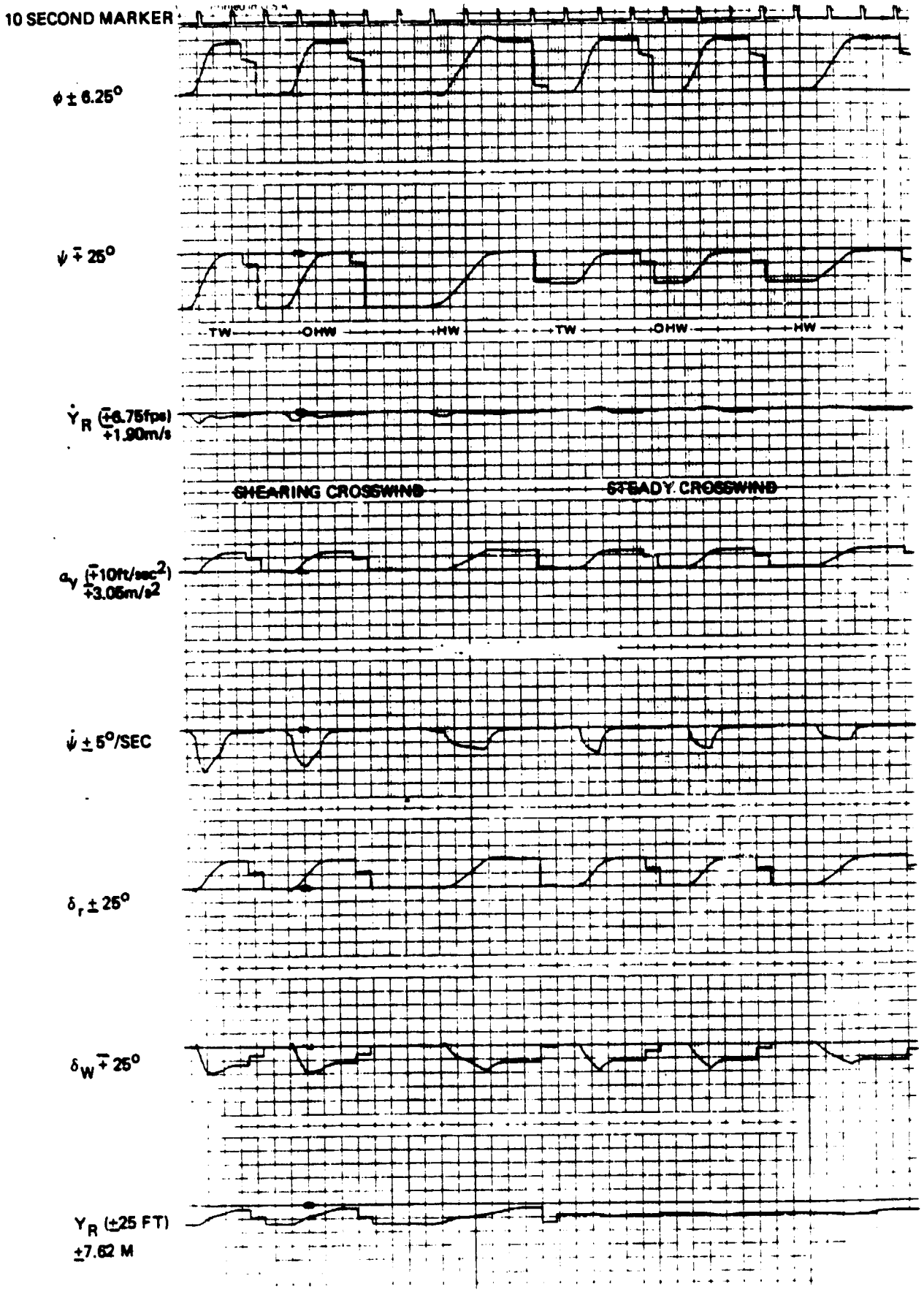

Figure 6-12A. Landing Time Histories Impact of Nose Located Antenna

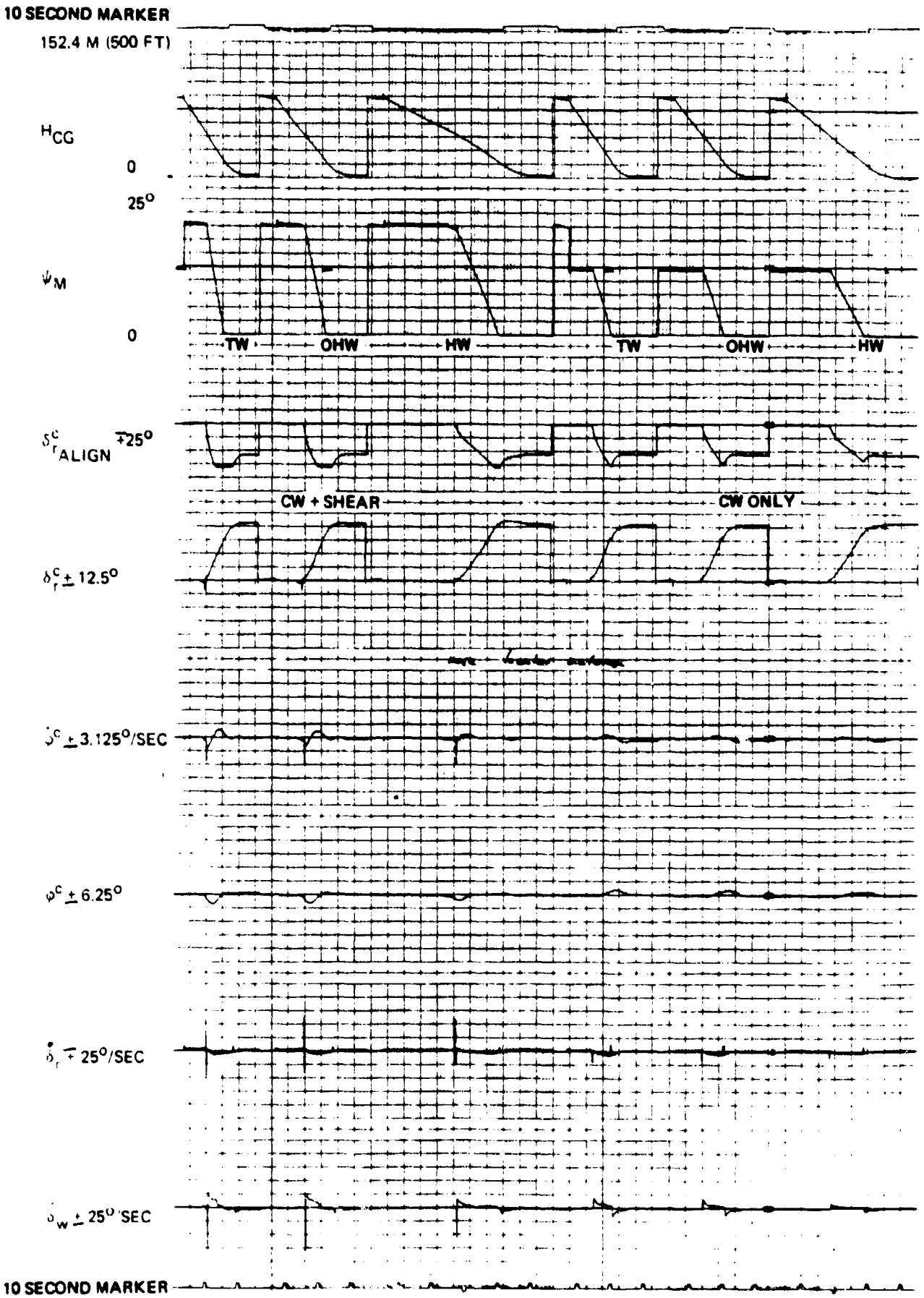

Figure 6-12B. Landing Time Histories, Impact of Nose Located Antenna

Increased Gains

The impact of increased gains on lateral landing deviations had been studied prior to the determination to use yaw to roll crossfeeds to improve control.

K_ϕ	increased from 4 to 24 deg/deg
K_R	increased from 2.14 to 3.0 deg/deg/sec
K_y	increased from 0.197 (0.06) to 0.656 (0.30) deg/m (deg/ft)

Time histories with the increased K_ϕ and K_R are given in Figure 6-13. These gains improve lateral control but a touchdown deviation of 2.13 m (7 ft) still occurs with 15 knot shearing crosswind. Time histories with the increased K_ϕ, K_R and K_y are given in Figure 6-14. Control is improved but it is not so good as with the crossfeeds (see Figure 6-1). Also, these high gains result in excessive wheel activity and they are therefore not utilized in the final system configuration.

The label "Hold at T.D." in Figure 6-13 means that the simulation computer is switched to the Hold Mode at touchdown which is the way the simulation is normally operated. "No Hold at T.D." means that the simulation was allowed to run past the touchdown altitude as if the runway was not there, in order to evaluate system dynamics by allowing more time in which transients can develop.

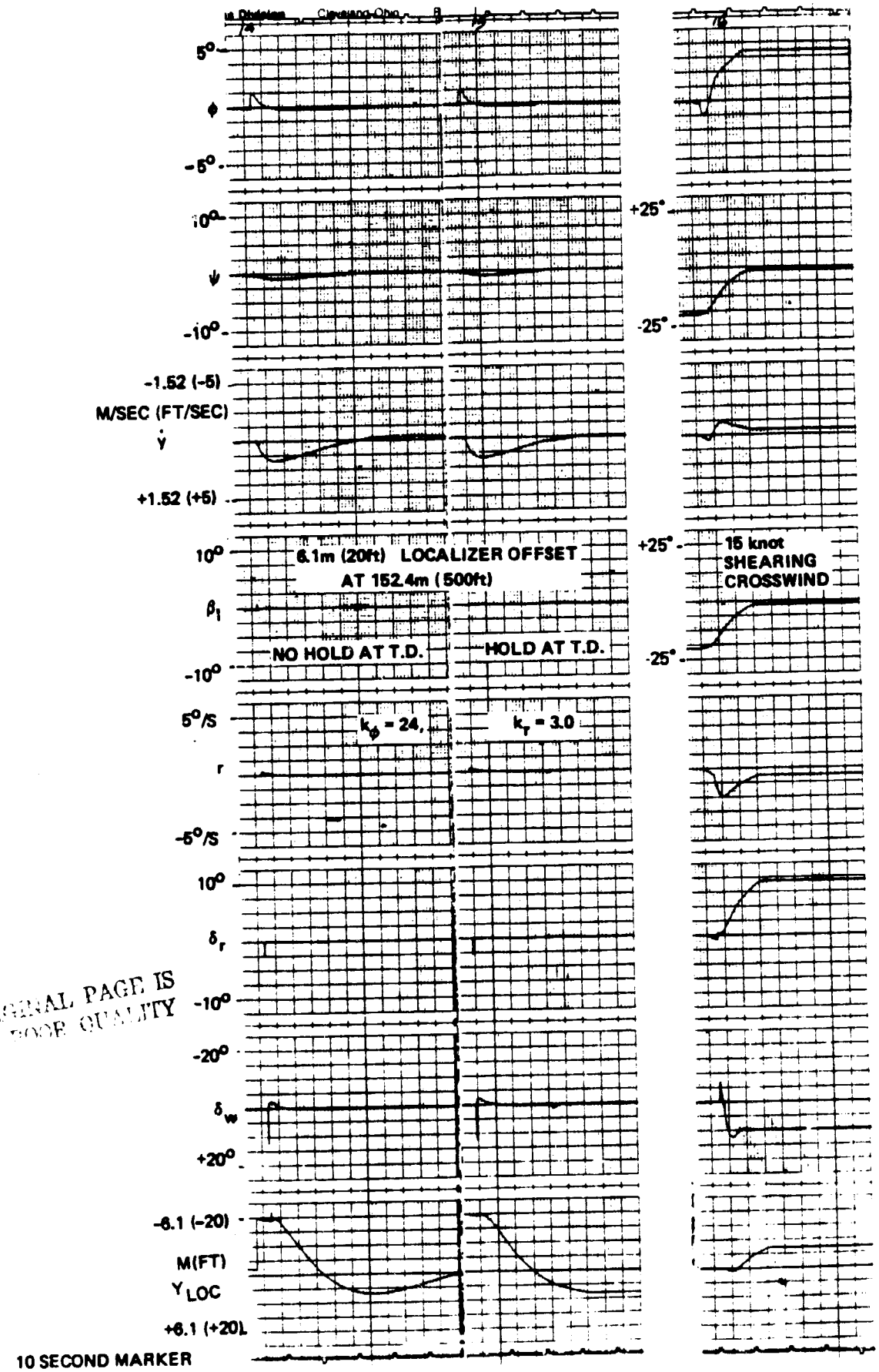

Figure 6-13. Time Histories with Increased K_ϕ and K_R

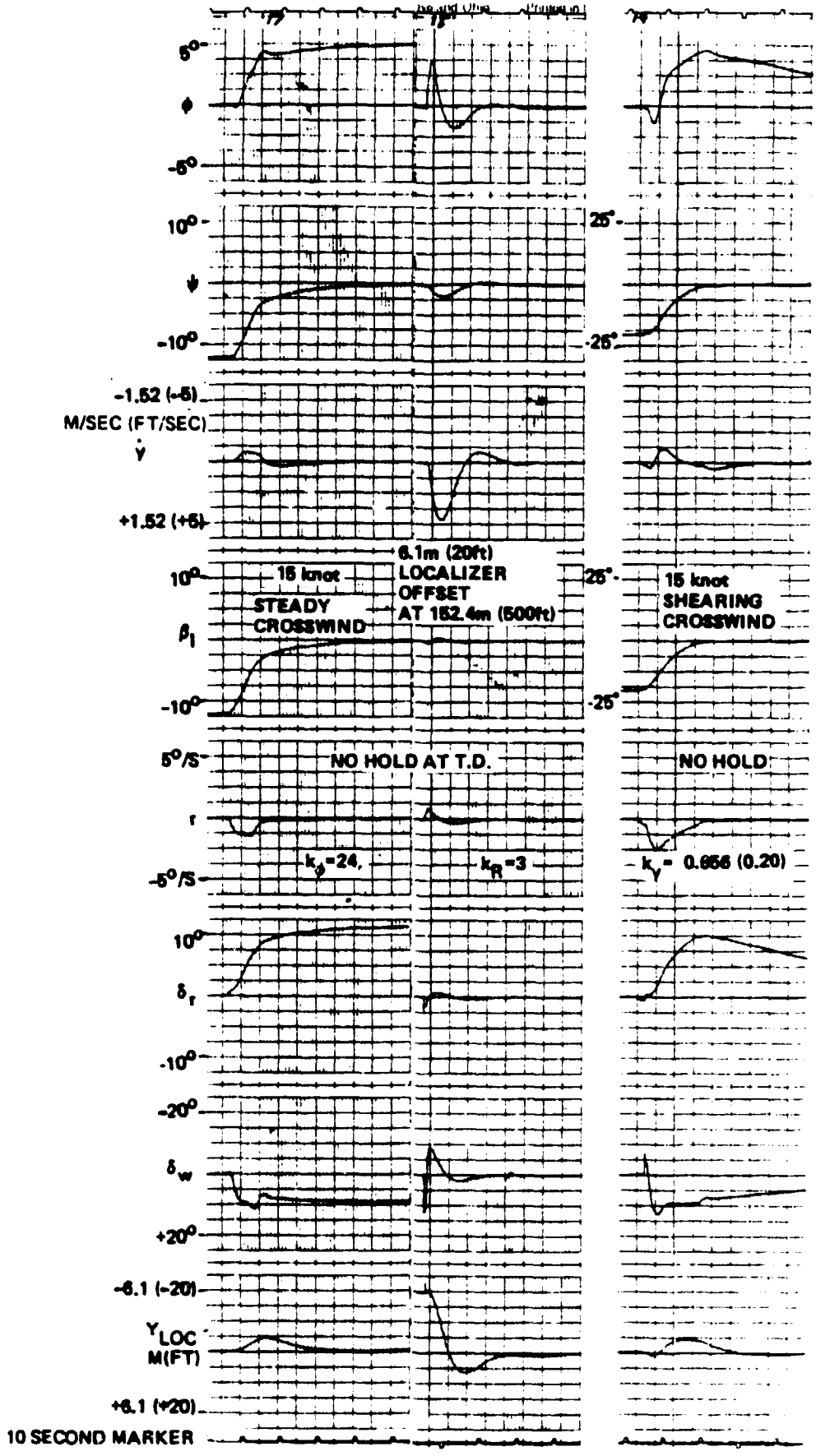

Figure 6-14. Time Histories with Increased K_{ϕ}, K_R and K_Y

7.0 CONCLUSIONS

The conclusions of this light wing loading STOL aircraft automatic landing study results are given here. These conclusions are based on results obtained from simulation.

1. This light wing loading airplane operates on the front side of the required power curve and therefore a conventional control strategy can be used. Flight path is effectively controlled with the elevator and airspeed with the throttles. This is in contrast with the situation of the powered lift STOL airplane operating on the back side of the power curve. There, the throttles are used for flight path control and the elevator for airspeed as described in Reference 1.

2. The control laws that were developed are capable of producing landing performance that is consistent with Category III operation into STOL runways as defined in Reference 9.

3. The use of the fast responding DLC spoilers enhances flight path control bandwidth and improves landing performance. The improvement is mostly in sink rate for the constant flare height configuration and mostly in range for the variable flare height control law.

4. All the control laws that were evaluated resulted in a flat touchdown attitude with this light wing loading airplane. Attempts to arbitrarily command a higher attitude resulted in excessively long landings. The lift reduction capability of the Twin Otter spoilers was approximately 0.13 g. A higher lift reduction capability, if available, would have probably allowed rotation to higher attitudes without floating. Lower approach airspeed for spoilers might have also been beneficial.

5. The constant flare height closed loop longitudinal control laws produce equal or better landing accuracy and are much simpler in structure than the variable flare height control laws, using predictive pitch and elevator terms.

6. Landing performance results that were obtained for the light wing loading Twin Otter are very similar to these obtained in a previous study (Reference 1) for the powered lift Augmentor Wing airplane despite almost a factor of

two difference in wing loading between the two aircraft. The two aircraft approach to land at approximately the same speed.

7. Turbulence and winds are the major contributors to landing dispersions. Beam disturbances have no significant impact on the longitudinal axis but they do affect lateral performance.

8. Yaw rate and rudder to wheel crossfeeds were used to overcome the adverse effect of a pronounced dihedral effect on lateral landing performance.

APPENDIX A

SIMULATION DEFINITION

TABLE OF CONTENTS
APPENDIX A

LIST OF FIGURES

APPENDIX A

LIST OF TABLES
APPENDIX A

APPENDIX A

SIMULATION DEFINITION

The non-piloted simulation of the modified DeHavilland DHC-6-100 Twin Otter research STOL aircraft and its automatic landing system are defined in this appendix. This simulation definition includes:

1. Airframe Dynamics
2. Control Dynamics
3. Geometry and Sensors
4. Beam Noise Model
5. Wind Models

A-1 Airframe Dynamics

The three nominal flight conditions for this study are defined below.

	LONGITUDINAL		LATERAL/DIRECTIONAL
	NO DLC	DLC	
Weight, kg (lb)	4990 (11000)	4990 (11000)	4990 (11000)
Speed, kt	71	75	70.5
Angle of Attack, deg	-3	-3	-3.8
Glide Slope, deg	-6	-6	-7.5
Flaps, deg	35.4	35.4	35.4
Spoilers, deg	0	20	0

It should be noted that the glide slope angle for the longitudinal studies is 6° whereas 7.5° was used for the lateral/directional work. This is due to the fact that the lateral studies were conducted earlier when 7.5° was planned to be used as the nominal approach angle. Later on, the 6° glide slope was selected as a more appropriate value.

The approach speed with spoilers is higher in order to provide adequate stall margin with the wing spoilers extended.

A-1.1 Equations of Motion

The normal set of uncoupled, linearized, small perturbation aerodynamic equations of motion were used as documented in Tables A-I and A-III. The aircraft equations and stability derivatives included in the separate longitudinal and lateral landing simulations are described in detail along with representative time responses. Note that the important aerodynamic nonlinearities, such as ground effect, were also included in the simulation.

A-1.2 Stability Derivatives

Twin Otter longitudinal dimensional stability derivatives and other pertinent data are included in Table A-II and the lateral directional data are in Table A-IV. The aerodynamic data are based on NASA's simulation documentation. Spoiler derivatives were obtained from flight tests by NASA.

A-1.3 Airframe Response Characteristics

Characteristic roots for the nominal approach cases are given below.

Longitudinal (75 kt)	$\zeta_{sp} = 0.605$	$\omega_{sp} = 2.24$ rps
	$\zeta_{ph} = 0.141$	$\omega_{ph} = 0.313$ rps
Lateral (70.5 kt)	$\zeta_{DR} = 0.301$	$\omega_{DR} = 1.467$ rps
	$\tau_s = -11.27$ sec	$\tau_R = 0.246$ sec

The longitudinal free airframe responses to step elevator, throttle and DLC spoilers are given in Figure A-1 and responses to u and α gust inputs are given in Figure A-2. Lateral/directional free airframe responses to wheel, rudder and β gust steps, as well as roll rate and yaw rate initial condition, are given in Figure A-3.

A-2 Control System Dynamics

For the Twin Otter vehicle, control surface aerodynamic and inertia loads were sufficiently small that acceleration limits and detailed actuator models

TABLE A-I. LONGITUDINAL EQUATIONS OF MOTION

$$\dot{u} = X_u u_A + X_w w_A - g \cos\gamma_o \theta + \Delta X_{GE} HF + X_{\delta th} \delta_{th} + X_{\delta SP} \delta_{SP}$$

$$\dot{w} = Z_u u_A + Z_{\dot{w}} \dot{w} + Z_w w_A + (U_1 + Z_q) q + \Delta Z_{GE} HF + Z_{\delta e} \delta_e + Z_{\delta th} \delta_{th} + Z_{\delta SP} \delta_{SP}$$

$$\dot{q} = M_u u_A + M_{\dot{w}} \dot{w} + M_w w_A + M_q q + \Delta M_{GE} HF + M_{\delta e} \delta_e + M_{\delta th} \delta_{th} + M_{\delta SP} \delta_{SP}$$

$$a_{NACC} \simeq (U_1 q - \dot{w}) \cos\alpha_O - \dot{u} \sin\alpha_O + \ell_{ACC} \dot{q}$$

$$a_{XACC} \simeq \dot{u} + g\theta$$

$$\dot{h}_{CG} = U_1 (\theta_T - \alpha_O) - w_1 \cos\gamma_O$$

$$h_G \simeq h_{CG} - Z_G \cos\theta_O + X_G \theta_T$$

$$h_{RA} \simeq h_G$$

$$\Delta h_B \simeq h_G - R_G \sin\gamma_O + X_{RG} (\theta_T - \gamma_O) - Z_{RG} \cos\theta_O$$

$$u_A = U_1 - U_O + u_{WIND}$$

$$w_A = w_1 + w_{WIND}$$

$$HF = e^{-h_G/h_{GE}}$$

NOTES: u_A, w_A are incremental aerodynamic values about trim.

θ is incremental pitch attitude about trim.

the subscripts "o" and $_T$ indicate trim and total values respectively. The subscript $_1$ indicates inertial quantity.

TABLE A-II. LONGITUDINAL STABILITY DERIVATIVES

W kg, (lb) = 4990 (11,000), α_o = -3°, γ_o = -6°, Flap = 35.4°

I_y kg-m^2 (slug-ft^2) = 33082 (24400)

		WITHOUT SPOILERS	WITH SPOILERS
U_o	kt	71	75
δ_{spo}	deg	0	20
X^*_u	1/sec	-0.0883	-0.0911
X_w	1/sec	0.1346	0.1423
$X_{\delta th}$	m/sec^2/rad (fps^2/rad)	4.356 (14.29)	4.866 (15.96)
$X_{\delta sp}$	m/sec^2/rad (fps^2/rad)	-	-0.3573 (-1.172)
Z^*_u	1/sec	-0.4836	-0.4578
Z_w	1/sec	-1.009	-1.066
$Z^{\cdot}_w$		-0.0086	-0.0086
Z_q	m/sec^2/rps (fps^2/rps)	-0.953 (-3.127)	-1.007 (-3.304)
$Z_{\delta e}$	m/sec^2/rad (fps^2/rad)	-2.896 (-9.50)	-3.234 (-10.61)
$Z_{\delta th}$	m/sec^2/rad (fps^2/rad)	-5.360 (-17.59)	-5.989 (-19.65)
$Z_{\delta sp}$	m/sec^2/rad (fps^2/rad)	-	3.566 (11.70)
M^*_u	rps^2/m/sec (rps^2/fps)	0.00478 (0.00146)	0.00533 (0.00163)
M_w	rps^2/m/sec (rps^2/fps)	-0.09161 (-0.02792)	-0.09677 (-0.02949)
$M^{\cdot}_w$	rps^2/m/sec^2 (rps^2/fps^2)	-0.1006 (-0.00306)	-0.1006 (-0.00306)
M_q	1/sec	-1.203	-1.271
$M_{\delta e}$	$1/sec^2$	-3.384	-3.778
$M_{\delta th}$	$1/sec^2$	-0.6096	-0.6808
$M_{\delta sp}$	$1/sec^2$	-	0.213
ΔX_{GE}	m/sec^2 (fps^2)	0.179 (0.589)	0.200 (0.657)
ΔZ_{GE}	m/sec^2 (fps^2)	-1.02 (-3.36)	-1.14 (-3.75)
ΔM_{GE}	rps^2	-0.551	-0.615
h_{GE}	m (ft)	3.66 (12)	3.66 (12)

NOTE: ALL DERIVATIVES ARE IN STABILITY AXES

TABLE A-III. LATERAL/DIRECTIONAL EQUATIONS OF MOTION

Lateral/Directional

$$U_o \cdot \dot{\beta}_I = Y_p \cdot P_A + Y_r \cdot r_A - U_o \cdot r + Y_\beta \cdot \beta_A + g \cos \gamma_o \cdot \phi + Y_{\delta R} \cdot \delta_R + Y_{\delta A} \cdot \delta_A$$

$$\dot{p} = L_p \cdot P_A + \frac{I_{xz}}{I_x} \cdot \dot{r} + L_r \cdot r_A + L_{\dot{\beta}} \cdot \dot{\beta} + L_\beta \cdot \beta_A + L_{\delta R} \cdot \delta_R + L_{\delta A} \cdot \delta_A$$

$$\dot{r} = N_p \cdot p_A + \frac{I_{xz}}{I_z} \cdot \dot{p} + N_r \cdot r_A + N_{\dot{\beta}} \cdot \dot{\beta} + N_\beta \cdot \beta_A + N_{\delta R} \cdot \delta_R + N_{\delta A} \cdot \delta_A$$

$$\begin{bmatrix} p \\ r \end{bmatrix}_B = \begin{bmatrix} \cos \alpha_o & -\sin \alpha_o \\ \sin \alpha_o & \cos \alpha_o \end{bmatrix} \begin{bmatrix} p \\ r \end{bmatrix}_S$$ Body axes rates

$$\dot{\phi} = p_B + \tan \theta_o \cdot r_B$$ Euler rates

$$\dot{\psi} = r_B$$

$$a_y = U_o (\dot{\beta} + r_B) - g\phi$$ Lateral acceleration

$$\ddot{Y}_R = (a_y + g\phi) \cos \phi \cos \Delta\psi$$ Runway crosstrack acceleration

$$\beta_A = \beta_I + \beta_{WIND}$$

$$\Delta\psi = \psi - \psi_{RUNWAY}$$

The A and o subscripts denote aerodynamic and trim quantities, respectively.
The B subscript denotes body axes quantities.
The subscript I indicates inertial quantity.

TABLE A-IV. LATERAL DIRECTIONAL STABILITY DERIVATIVES

U_o	kt	70.5
α_o	deg	-3.8
I_X	kg-m^2 (slug-ft^2)	22776 (16800)
I_Z	kg-m^2 (slug-ft^2)	50908 (37550)
I_{XZ}	kg-m^2 (slug-ft^2)	1898 (1400)
y_p/U_o	-	-0.00473
y_r/U_o	-	0.0236
y_β/U_o	1/sec	-0.1756
$y_{\delta R}/U_o$	1/sec	0.068
$y_{\delta A}/U_o$	1/sec	0.00059
L_p	1/sec	-4.089
L_r	1/sec	2.9896
$L_{\dot{\beta}}$	1/sec	0
L_β	1/sec^2	-2.052
$L_{\delta R}$	1/sec^2	1.321
$L_{\delta A}$	1/sec^2	-5.473
N_p	1/sec	0.0067
N_r	1/sec	-0.6880
$N_{\dot{\beta}}$	1/sec	0
N_β	1/sec^2	1.75
$N_{\delta R}$	1/sec^2	-1.818
$N_{\delta A}$	1/sec^2	-0.4872

NOTE: 1. All derivatives and inertias are given in stability axes.
2. All angles are in radians unless otherwise noted.

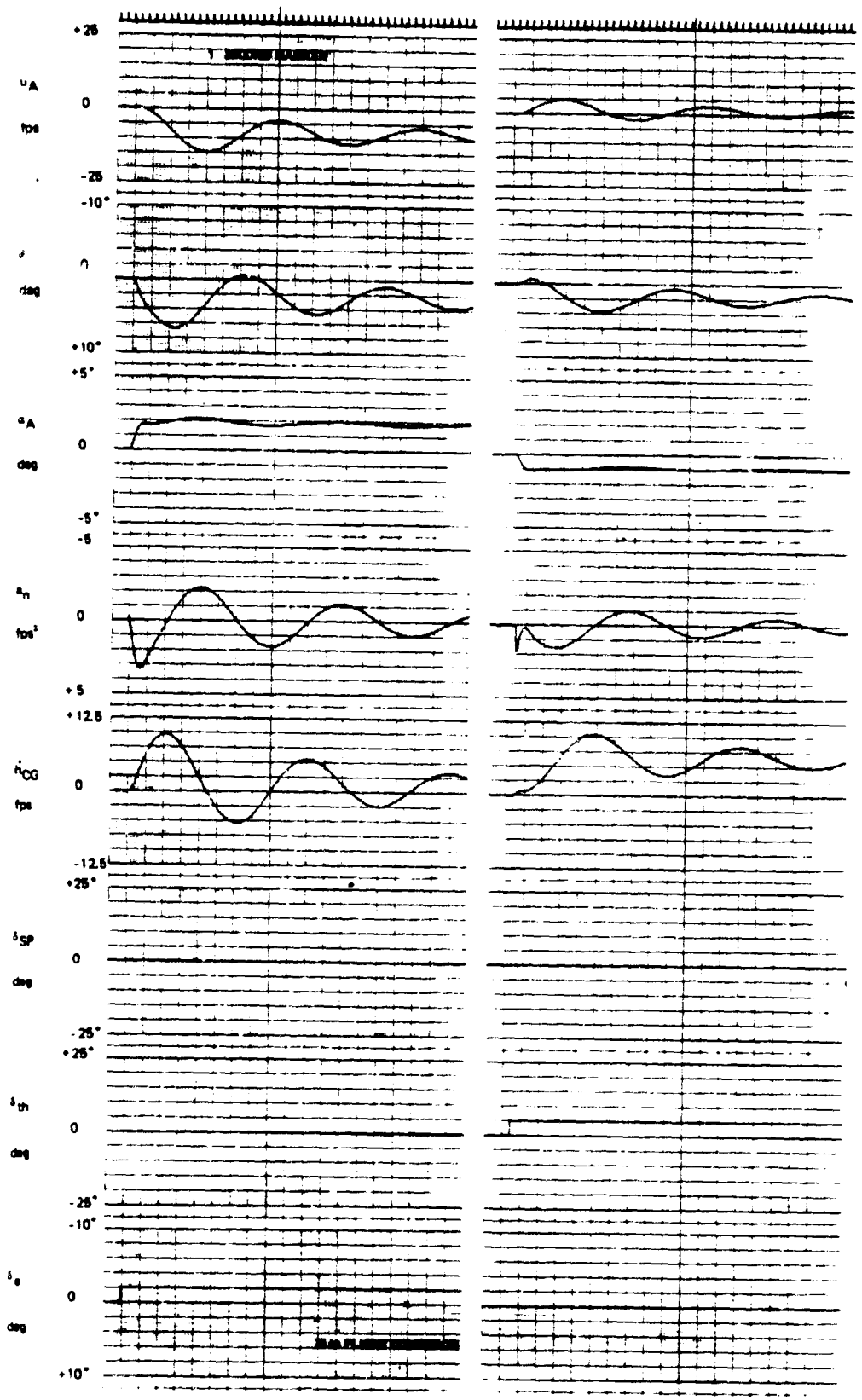

Figure A-1A. Free Airframe Responses to Control Steps - Longitudinal

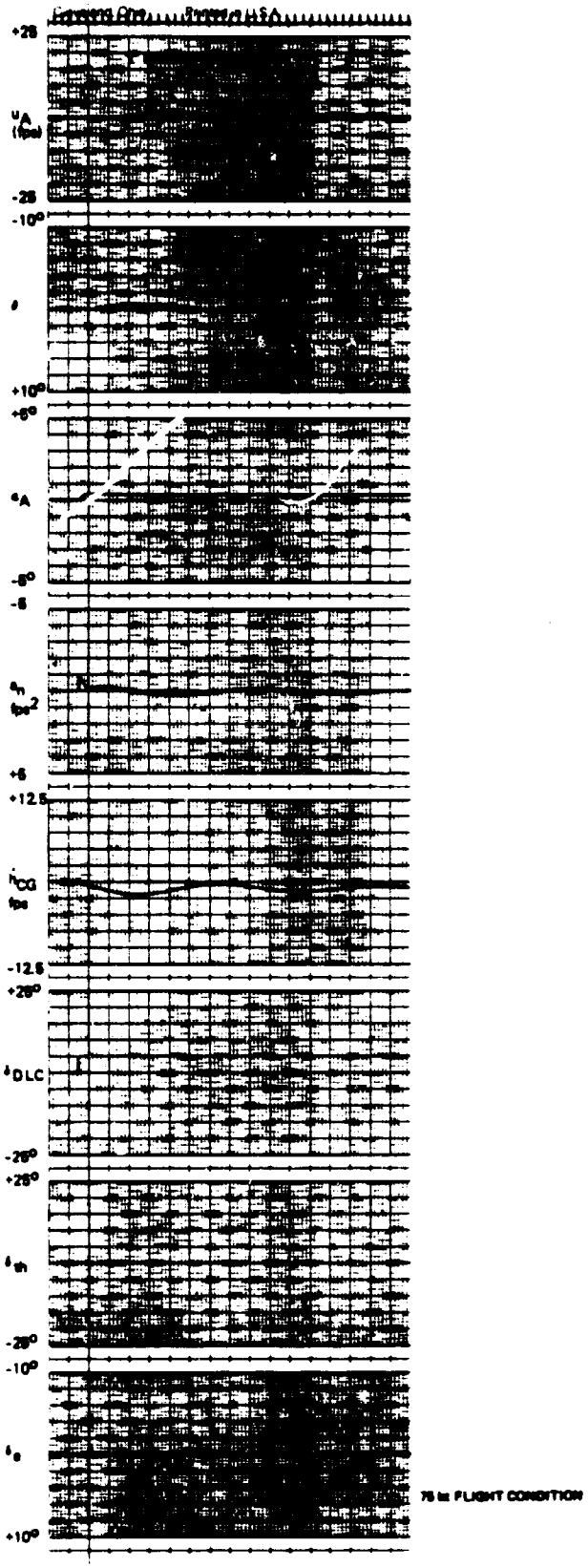

Figure A-1B. Free Airframe Responses to Control Steps - Longitudinal

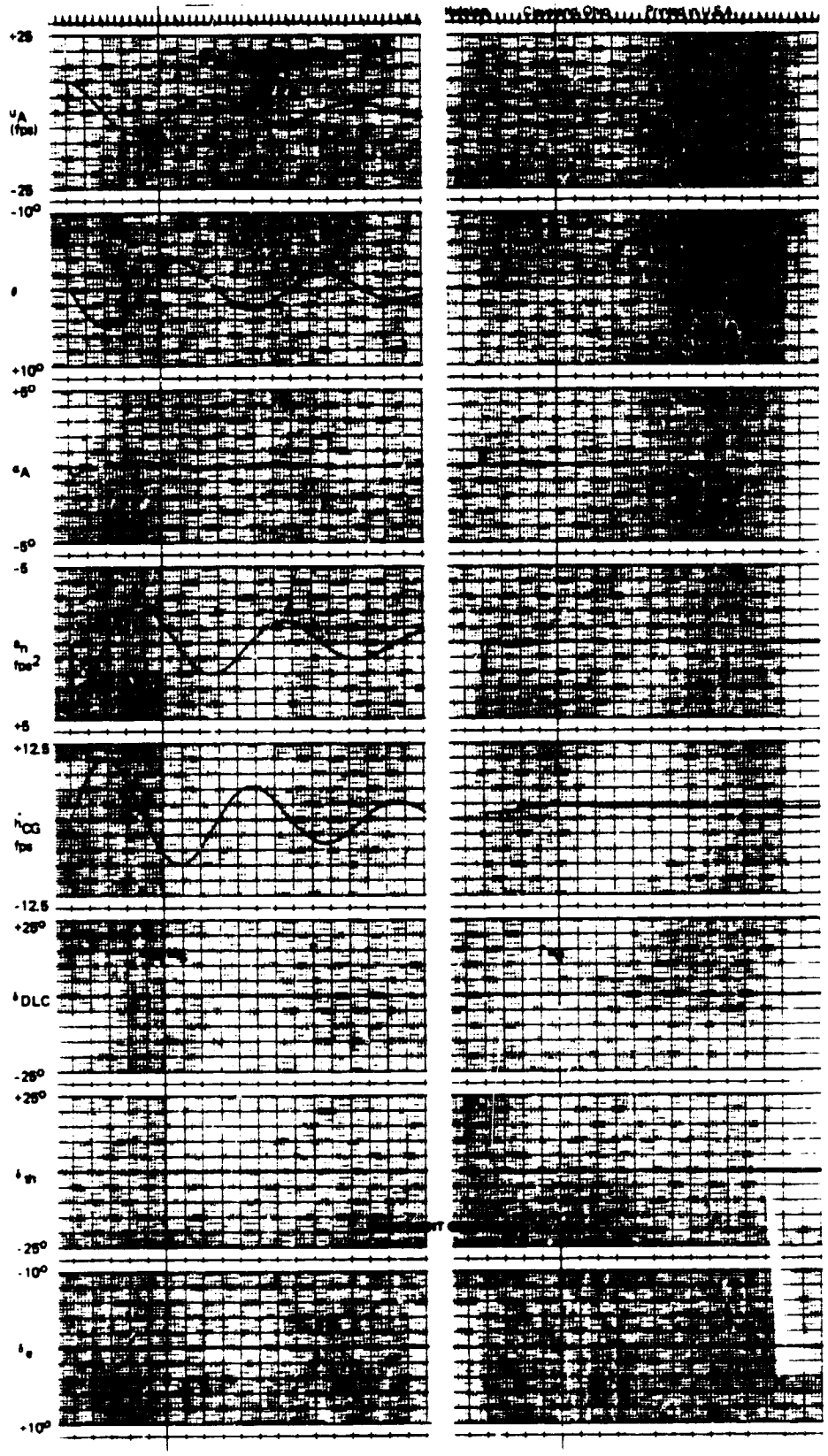

Figure A-2. Free Airframe Responses to Wind Steps - Longitudinal

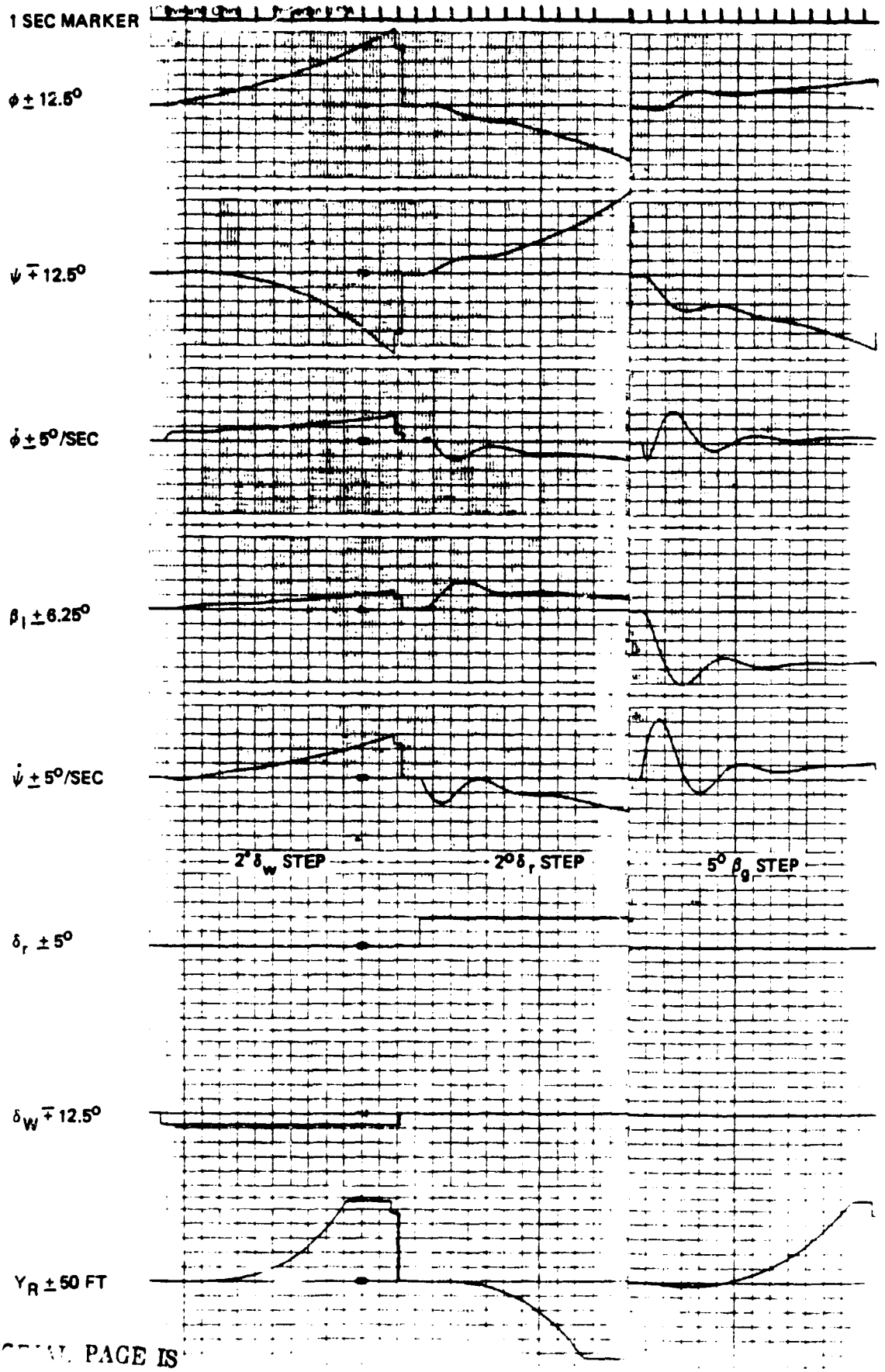

Figure A-. Free Airframe Responses – Lateral/Directional

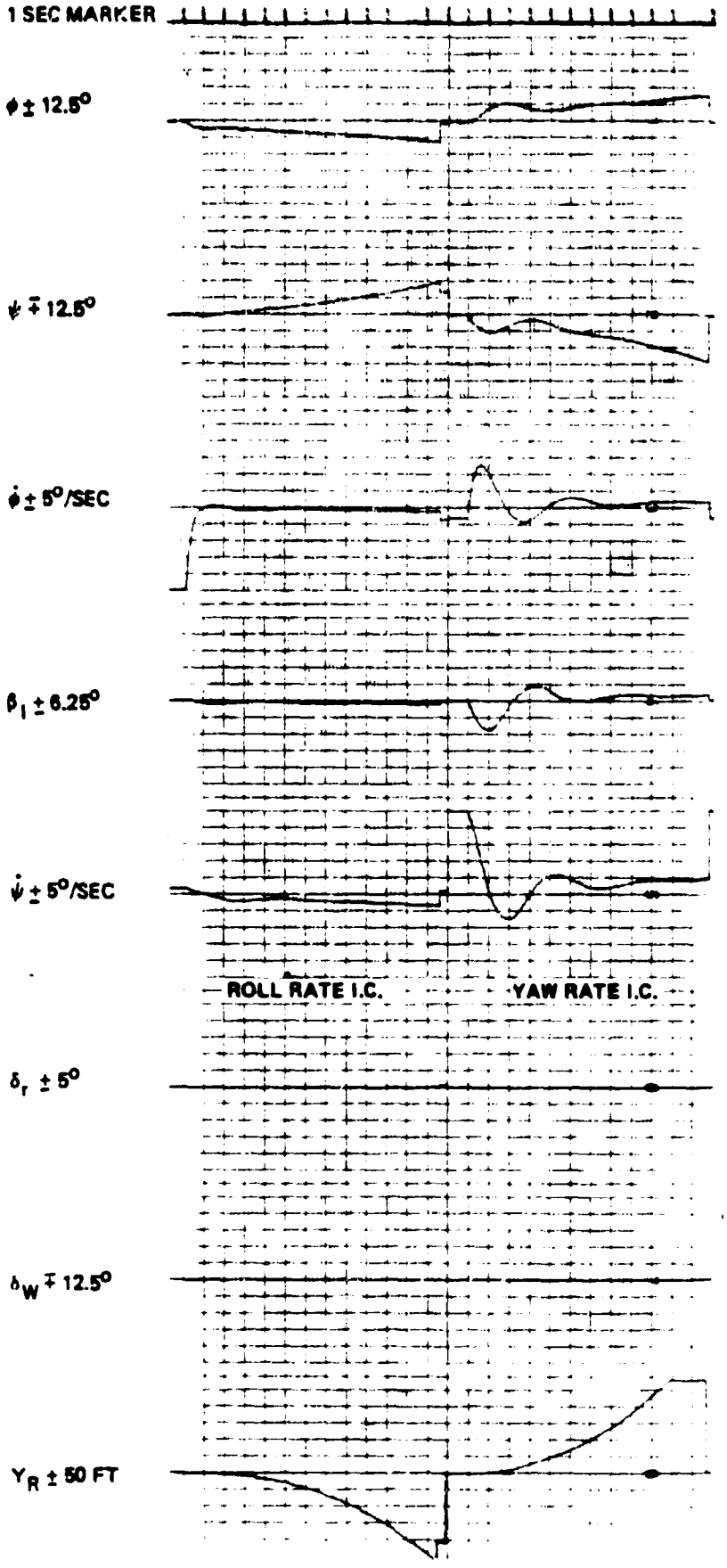

Figure A-3B. Free Airframe Responses - Lateral/Directional

were not required. Thus only important nonlinearities as rate and position limits were included in this study. The simplified actuator models are described in this section.

The throttle, engine, elevator and spoiler actuator models are given in Figure A-4. The one second lag in the throttle servo, as shown in the Figure, was included with the variable flare height and the low gain constant flare height control law configurations. The high gain constant flare height configuration assumed a high bandwidth throttle servo but the same engine dynamics as shown in the Figure. The turboprop engine dynamics are different for throttle advance or retard. The throttle and elevator position limits of Figure A-4 are with respect to a zero wind nominal trim position. Spoiler limits are in terms of actual spoiler deflection.

The wheel-aileron and rudder models are shown in Figure A-5. Note that initially mechanized rudder limits had been ±5° and were found to be inadequate for the 15 knot crosswind landing requirement. Accordingly, the rudder limits were modified to ±12°. The limits are dependent on dynamic pressure and a ±10° worst case limit was assumed during part of the simulations.

A-3 Geometry and Sensors

A-3.1 Sensor Geometry

The relative geometry of the gear, c.g., and MLS antenna are illustrated in Figure A-6. The gear and MLS receiver location are expressed in terms of cg height above the runway by the expressions:

$$h_G = h_{cg} - Z_G \cos\theta + X_G \sin\theta \qquad X_{REC} = 5.97\text{m } (19.58\text{ ft})$$

$$h_{REC} = h_{cg} - Z_{REC} \cos\theta + X_{REC} \sin\theta \qquad Z_{REC} = 0.78\text{m } (2.56\text{ ft})$$

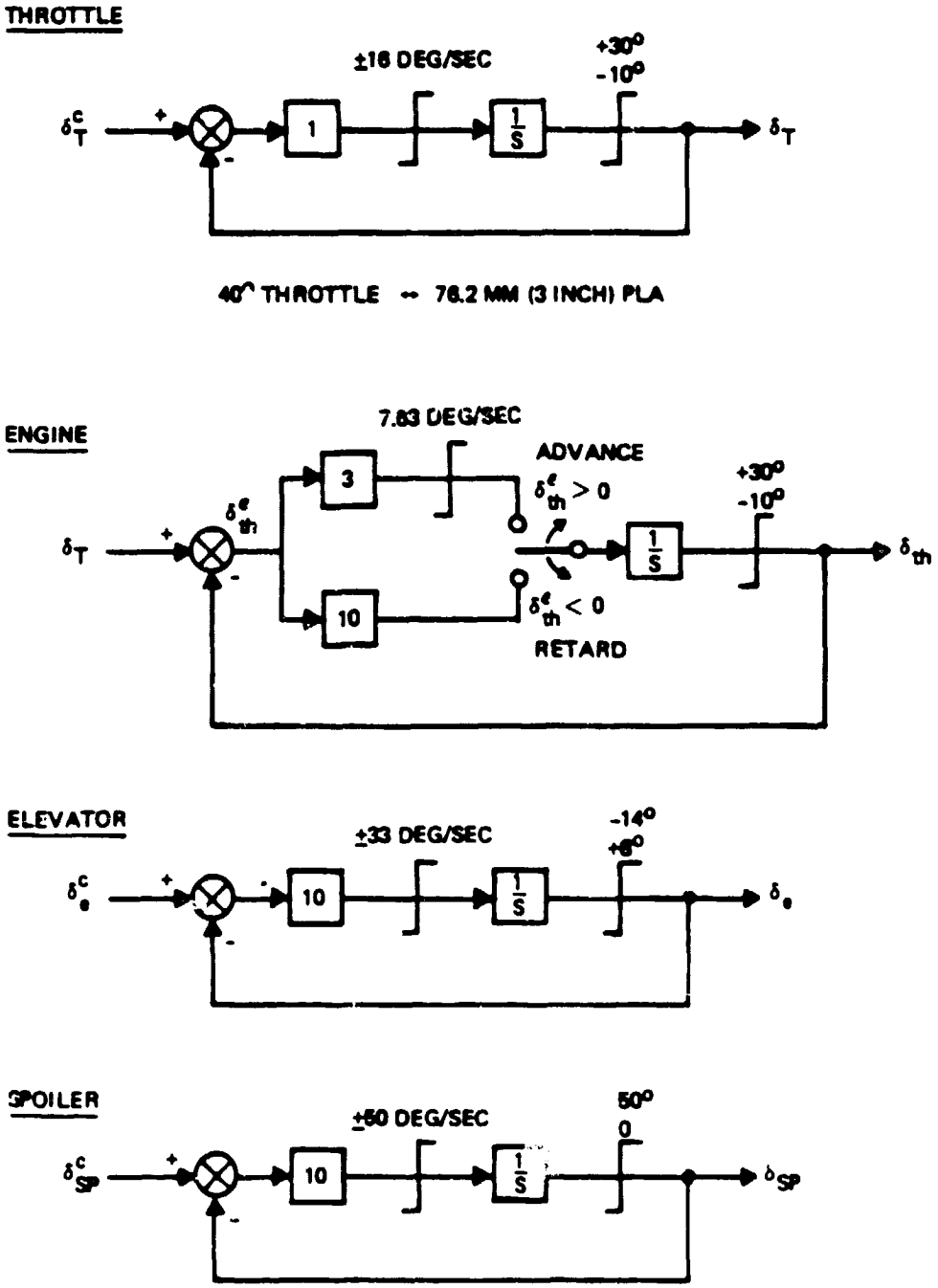

Figure A-4. Longitudinal Actuator Models

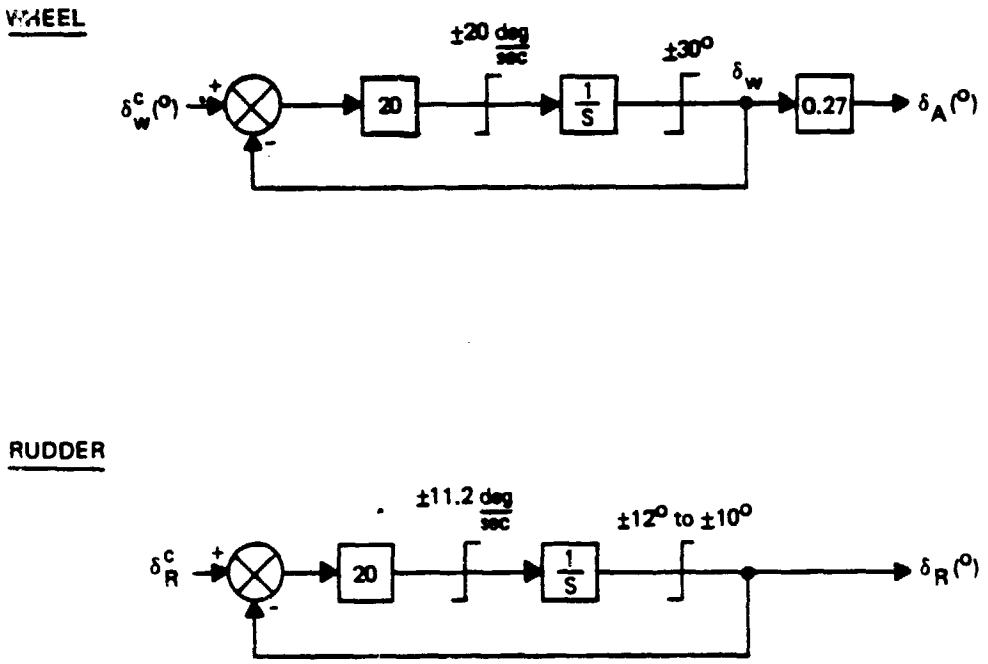

Figure A-5. Lateral-Directional Actuator Models

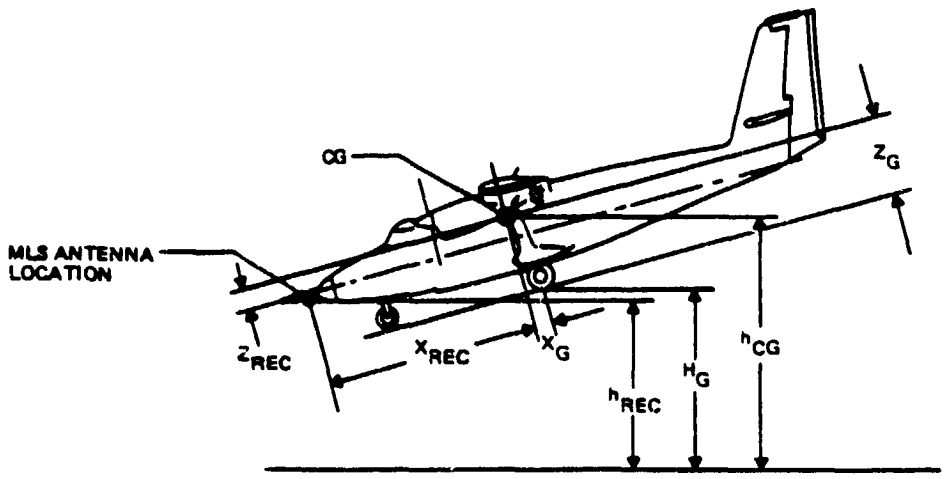

FIGURE A-6. AIRPLANE GEOMETRY

A-3.2 Physical Data

Sensor location, landing gear geometry and the weight, moments of inertia and dimensions of the Twin Otter airplane in the landing configuration are given in Table A-V. This geometry defines the following absolute touchdown constraints for this vehicle:

θ_{TD} max	12°
θ_{TD} min	-1.5°
ϕ wing scrape	19°

A-3.3 Sensor Models

Only those sensors whose dynamics or errors impact landing performance are discussed in this section. Also, only the errors which affect landing performance are included. The properties of the sensors which impact landing performance are summarized in Table A-VI.

Although MLS yields discrete information at 5 scans per second for elevation 1 and azimuth guidance, and 40 per second for DME, continuous position inputs were used during these studies. During the previous glide slope

TABLE A-V. PHYSICAL DATA FOR LANDING CONFIGURATION

Sensor Location	FS	WL	BL
CG (26% MAC)	529.64 (208.52)	254 (100)	0
MLS Antenna	-67.31 (-26.5)	177.8 (70)	0
Radar Altimeter	589.28 (232)	127 (50)	0
Accelerometers	458.88 (180.66)	254 (100)	0

GEAR GEOMETRY

	Nose	Right	Left
X_G	3.937 (12.9)	-0.596 (-1.956)	-0.596 (-1.956)
Y_G	0.0	1.828 (6.0)	-1.828 (-6.0)
Z_G	1.99 (6.53)	1.99 (6.53)	1.99 (6.53)
$Z_{Compression}$	.253 (0.83)	.311 (1.02)	.311 (1.02)

AIRCRAFT DIMENSIONS

W	48947	N	(11,000	lb)
I_X	22776	$Kg\text{-}m^2$	(16,800	$slug\text{-}ft^2$)
I_Y	33079	$Kg\text{-}m^2$	(24,400	$slug\text{-}ft^2$)
I_Z	50908	$Kg\text{-}m^2$	(37,550	$slug\text{-}ft^2$)
I_{XZ}	1898	$Kg\text{-}m^2$	(1,400	$slug\text{-}ft^2$)
S_{wing}	39.02m^2		(420 ft^2)	
b	19.812 m		(65 ft)	
$\bar{C}$	1.98 m		(6.5 ft)	

NOTES: 1) Sensor location is expressed in centimeters (inches)
2) Gear geometry is expressed in meters (feet)
3) WLCG is estimated.

and localizer track MLS studies reported in Reference A-1, it was determined that these update rates provided control activity and landing performance identical to a continuous guidance signal, especially if beam filtering is used. Although continuous position signals were used to limit simulation complexity, the actual MLS error models defined below were included to maintain fidelity in the results. In addition, the effect of guidance signal resolution was investigated using the model described in the following section. Only azimuth effects were considered since the effects of the elevation signal resolution are minimal.

TABLE A-VI. SENSOR CHARACTERISTICS

SENSOR	DYNAMICS	ERRORS
Radar Altimeter	$\frac{1}{.1S + 1}$	Bias - ±1.03m (±3.4 ft)
GS/LOC Receiver	$\frac{1}{.1S + 1}$	Figure A-7
Vertical Gyro		Verticality - ±.6° False erection - ±1.0°
Accelerometers		Cross axis sensitivity .01
Course Datum		Equivalent Bias - ±4.0°

NOTE: All errors are given as 4.5σ values.

A-4 Beam Disturbance Models

1-4.1 Beam Noise

In this study, both MODILS and MLS error models were used. The azimuth, elevation, and DME error amplitudes, spectral characteristics, and resolution are given in Figure A-7. It should be noted that the effect of DME inaccuracies is small with respect to the angular errors during the final approach. The noise and bias values for the MLS are based on the preliminary specification for the system at the Navy Crows Landing Auxiliary Landing Field.

ELEVATION

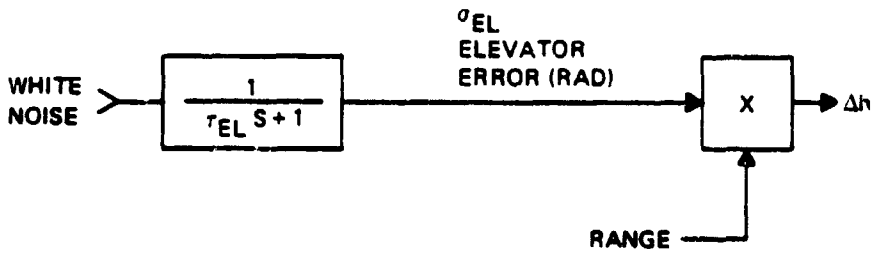

AZIMUTH

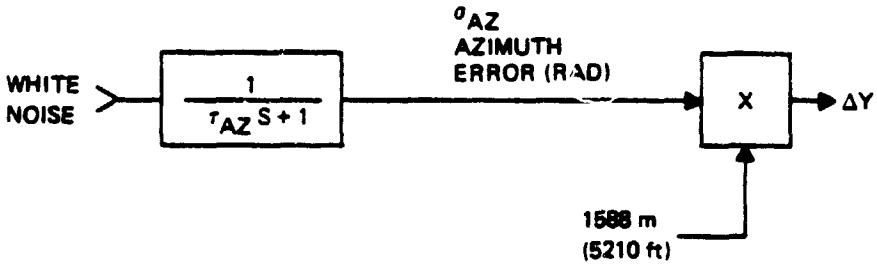

	τ	σ_{NOISE}	σ_{BIAS}	RESOLUTION
		MODILS		
Elevation	10.0 sec	0.07°	0.05°	0.01°
Azimuth	4.0 sec	0.03°	0.17°	0.1°
DME	-	12.19m (40 ft)	6.10m (20 ft)	18.29m (60 ft)
		MLS		
Elevation	0.5 sec	0.0625°	0.0375°	0.01°
Azimuth	0.5 sec	0.105°	0.0935°	0.01°
DME	0.5 sec	12.19m(40 ft)	15.24m (50 ft)	1.83m (6 ft)

FIGURE A-7 MODILS AND MLS ERROR MODELS

A-4.2 Azimuth Signal Discretization

Two significant sources of discretization exist in the lateral guidance signal:

i) Azimuth resolution of .1 degrees for MODILS, .01 degrees for MLS.
ii) Digital autopilot scaling of 1.22 m (4 ft) per bit.

The MODILS lateral deviation resolution is a function of slant range. Assuming the typical STOL-port geometry shown in Section 3, with a 7.5 degree descent path, the .1 degree discretization yields about 1.07 m (3.5 ft) at touchdown and 6.1 m (20 ft) at 304.8 m (1000 ft) altitude. Thus the azimuth resolution is the major contributor to lateral discretization with MODILS, and its impact on track and align performance was determined. The implementation diagram and discretization effects with sinusoidal input are given as Figure A-8.

With MLS, the azimuth resolution is improved by an order of magnitude. To take advantage of this improved guidance signal quality, the digital signal resolution was increased for approach. A resolution of better than .305 m (1 ft) would provide an essentially continuous guidance signal. Thus a continuous azimuth signal adequately models the MLS system characteristics.

A DME resolution of 18.532 m (.01 N.miles) yields only .305 m (1 ft) discretization error at a 1 degree azimuth error. Since aircraft azimuth deviation is always less than 1 degree during final track and alignment, the DME resolution has insignificant impact on lateral signal discretization.

A-5 Atmospheric Disturbance Models

In these landing studies, both a standard atmospheric disturbance model and specific deterministic wind inputs were considered. The final performance determination was based on the standard disturbance model.

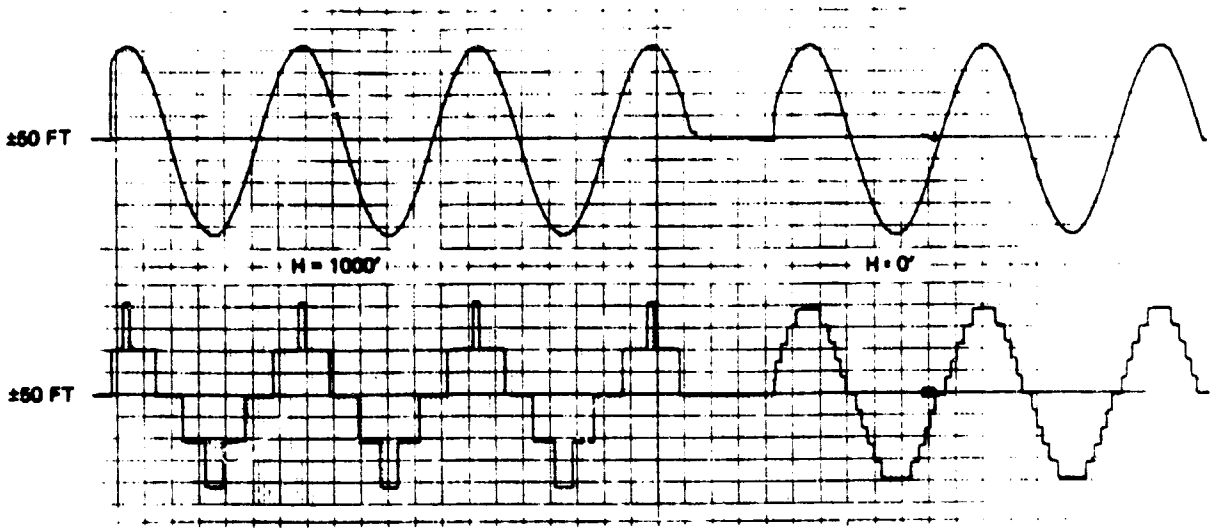

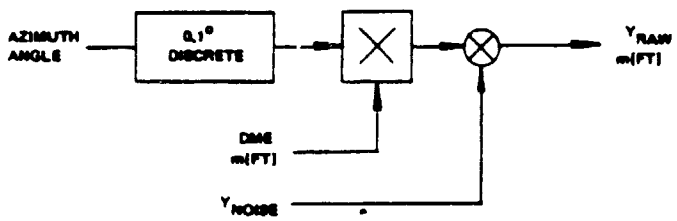

LATERAL GUIDANCE SIGNAL GENERATION

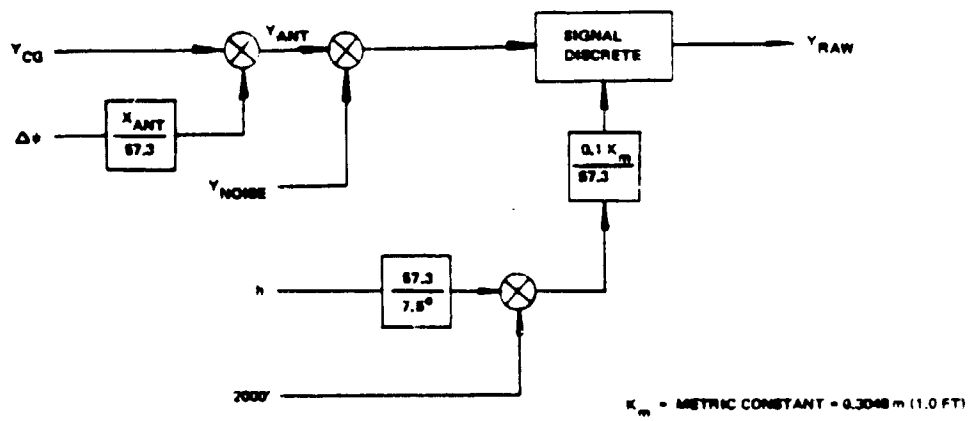

Figure A-8. MODILS Signal Discretization

A-5.1 Standard Wind Model

The wind model used for obtaining all the statistical data is closely patterned after the standard FAA wind model specified in AC-20-57A (Reference 7) and described more fully in References 4 and 5. The total wind level also determines the turbulence amplitudes, while the shear corresponds to the headwind and crosswind components. A summary of the standard wind model is shown as Figure A-9. The wind shear of this model consists of a steady wind at altitude down to 61 m (200 ft.) at which point the wind decreases linearly with decreasing altitude all the way to the ground. The nominal wind magnitude is given as the value at the 7.62 m (25 ft) reference altitude. Thus, a 25 knot shearing headwind has a 42.5 knot magnitude at altitude, decreasing to 22.5 knots at zero height. Similarly, a 10 knot shearing tailwind decreases in magnitude from 17 to 9 knots and a 15 knot crosswind shears from 25.5 to 13.5 knots. The magnitude of the horizontal turbulence, according to this model, is proportional to the wind level, as shown in Figure A-9. For conservatism, most statistical data in this study were taken assuming a 70 percent probability of encountering a 25 knot shearing headwind with the associated σ_u of 3.75 knots and a 30 percent probability of encountering a 10 knot shearing tailwind with a turbulence level of 2.70 knots RMS. The horizontal turbulence levels given above were computed from the formula σ_u = 0.15 WINDV given in Figure A-9. WINDV is the total wind velocity and in the case of the 25 knot headwind, WINDV is 25 knots. The 10 knot tailwind is assumed to be associated with a 15 knot crosswind, resulting in a total wind of 18 knots. These maximum conditions are referred to as limiting winds in the body of the report. The localizer track and runway alignment data were taken with 15 knots shearing crosswind and σ_v of 2.25 knots. Reference 7 assigns a 1 percent probability with headwinds in excess of 25 knots and 4 percent with crosswinds exceeding 15 knots. The much higher probabilities used in this study produce conservative results. A constant level of 1.5 knots RMS vertical turbulence (invariable with altitude or wind conditions) was used. For this study, winds were assumed to be in earth local level axes and transformed into aircraft axes. No pitch rate gusts were used, since their effects are negligibly small compared to horizontal and vertical turbulence. Uncorrelated white noise generators were used for longitudinal, lateral, vertical, and roll rate gusts.

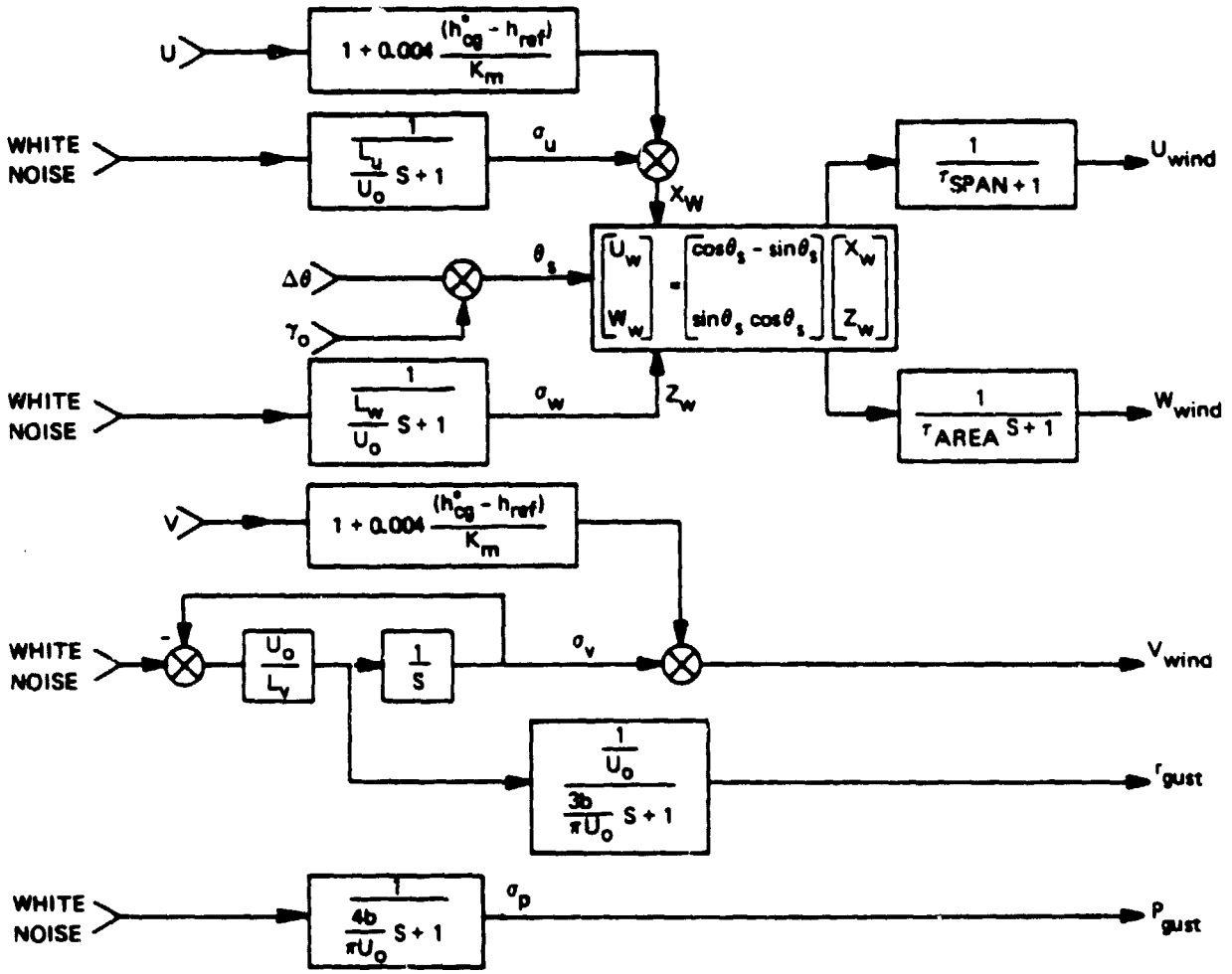

	u	V	w	P
L(SCALE LENGTH)	182.88m (600 ft)	182.88m (600 ft)	9.14m (30 ft)	———
τSPAN, AREA	$\frac{27.66K_m}{U_o}$	———	$\frac{12.39K_m}{U_o}$	———
σ	0.15WINDV	0.15V	$0.773 \frac{m}{sec}$ (1.5 kt)	$.00953 \frac{\sigma_w}{K_m} \frac{RAD}{sec}$
Mean Wind Limit	+12.88 +25kt -5.15 m/sec -10 kt	±7.73 m/sec (±15kt)	———	———
Prob of Exceedance	1%	4.5%	———	———

9/78/668

h_{cg}° = CG Height (200 ft maximum)
h_{ref} = Wind Reference Altitude = 7.62m (25 ft)
K_m = Metric Constant = 0.3048m (1.0 ft) for metric (English) units
b = Wing Span = 19.81m (65 ft)
U_o = Approach speed
U = Down Wind Speed; V = Crosswind Speed; WINDV = Total Wind Speed (25 kt Limit)

Figure A-9. Standard Wind Model

A-5.2 Logarithmic Wind Shear

The performance of the various glide slope track and flare control laws was evaluated deterministically with the standard linear wind shears described above and also with the logarithmic shears, as defined by the following expression:

$$U_{WIND} = U_{REF} [0.4512 \log_{10} (3.28084*h) + 0.3692]$$

h is expressed in meters.

$$U_{WIND} = U_{REF} \text{ at } 7.62 \text{ m } (25 \text{ ft})$$

Twenty five knot standard and logarithmic shear profiles are shown in Figure A-10. The logarithmic shear is a more severe disturbance during the flare because of its steeper gradient below 15.24 m (50 ft).

A-5.3 Altitude Profiles for Lateral Landings

Since the time between align initiate and touchdown can have a significant impact on landing performance, the effect of longitudinal winds and shears on lateral performance was included in the simulation.

A simplified flare model was constructed, with the altitude trajectory varying with inertial velocity and flare time constant in a manner very similar to the actual pitch approach and flare control system. The altitude profile generator block diagram is given as Figure A-11, with sample profiles for limiting headwind and tailwind shown in Figure A-12.

This altitude trajectory is used to drive the sidewind shear and the align model, and to indicate touchdown. Thus the proper relationship is maintained between altitude and time for all downwind conditions, to allow realistic determination of lateral landing performance.

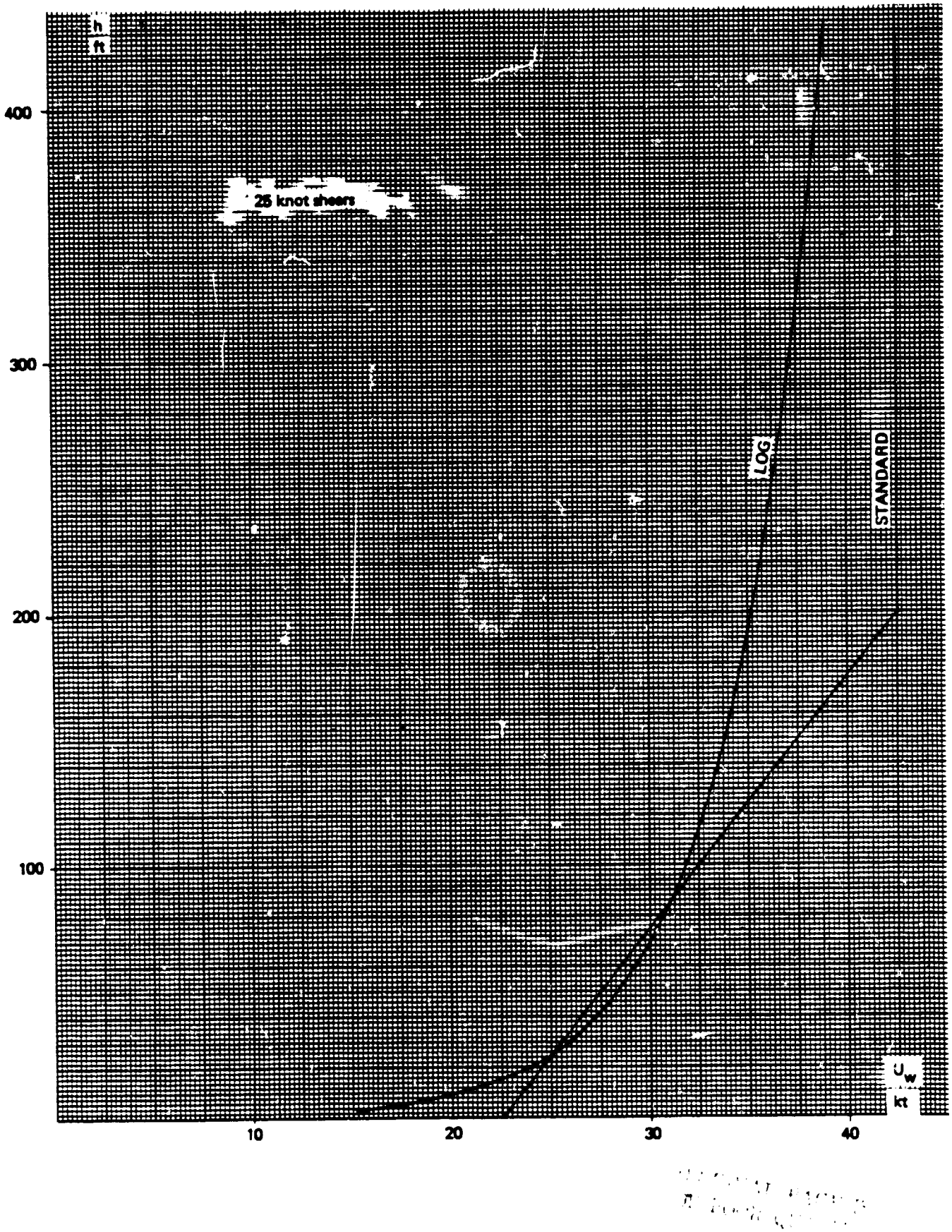

Figure A-10. Linear and Logarithmic Shear Profiles

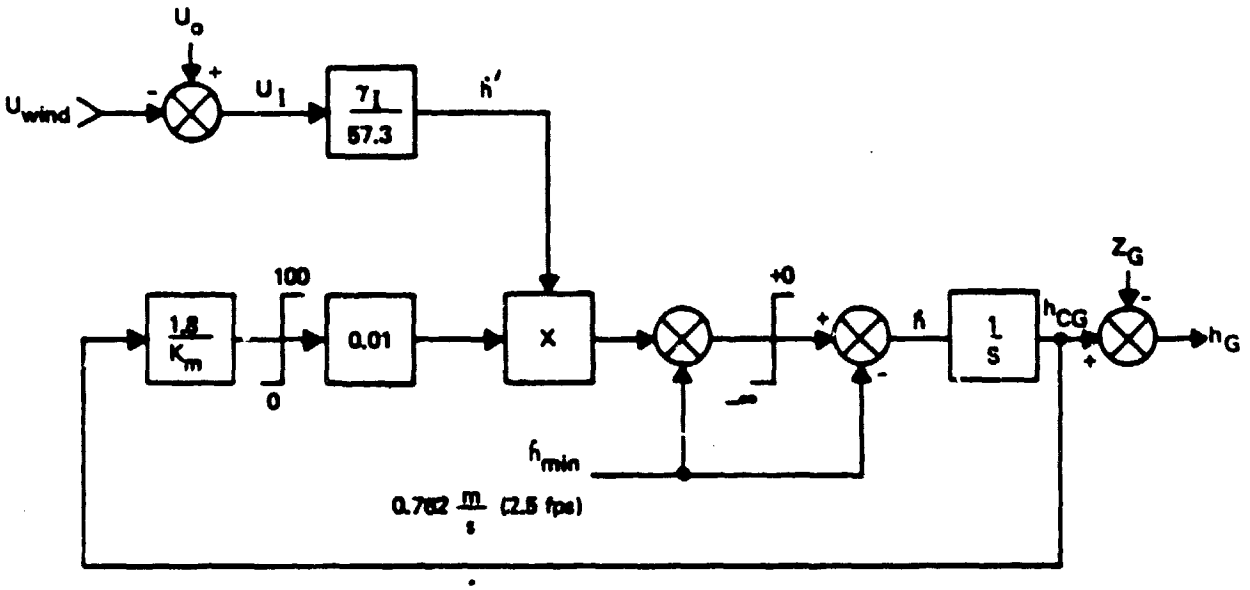

K_m = metric constant = 0.3048 (1.0) for metric (English) units

Z_G = 1.98m (6.53 ft)

Figure A-11. Altitude Profile Generation

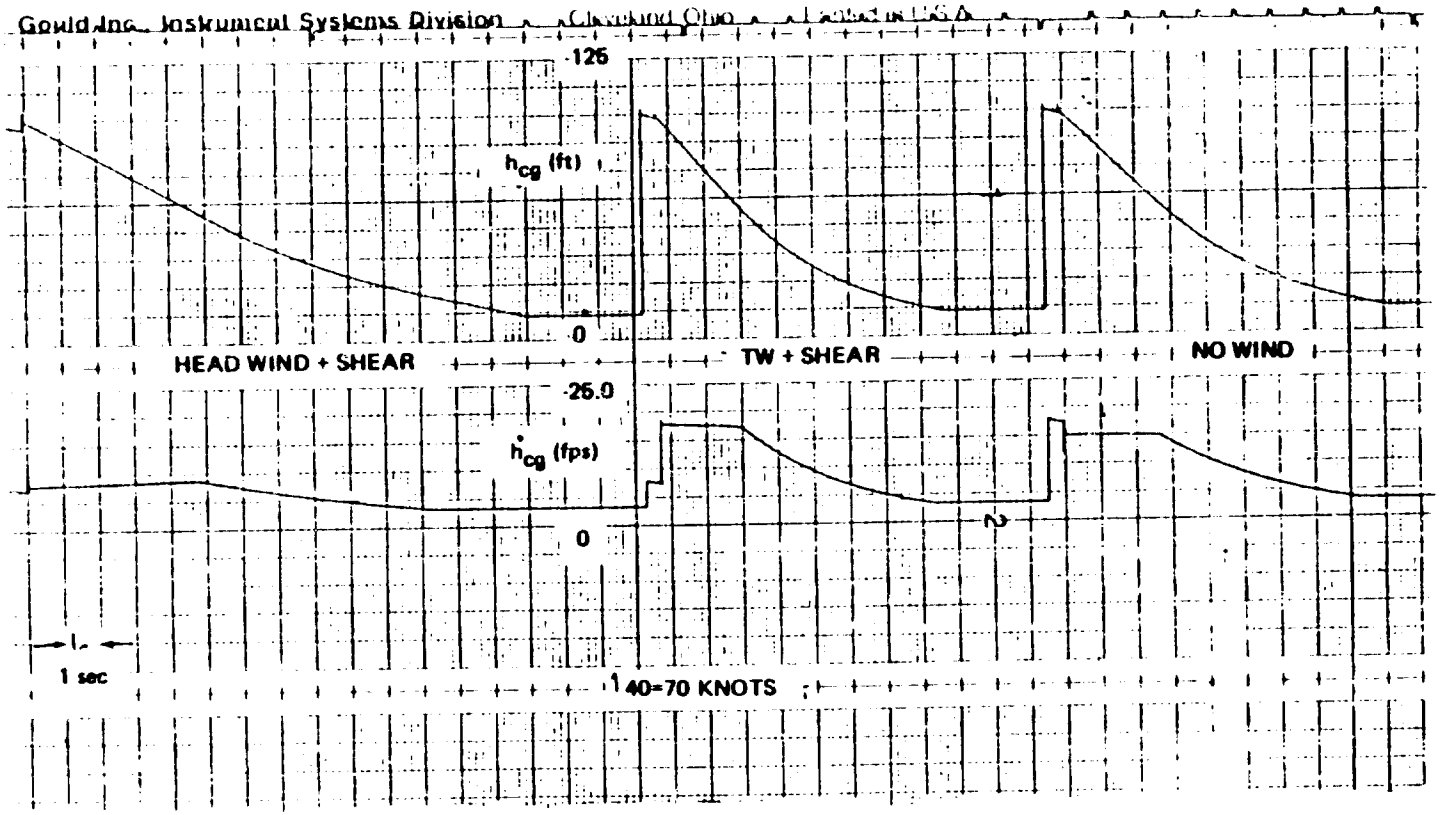

Figure A-12. Typical Altitude Profiles

APPENDIX B

SUPPLEMENTARY GLIDE SLOPE TRACK

AND FLARE SIMULATION RESULTS

LIST OF FIGURES

Probability Distributions

* 70% probability for 25 knot shearing HW with σ_u = 3.75 kt, σ_w = 1.5 kt and 30% probability for 10 knot shearing TW with σ_u = 2.70 kt, σ_w = 1.5 kt

LIST OF FIGURES (CONTINUED)

Probability Distributions (continued)

LIST OF FIGURES (CONTINUED)

Probability Distributions (continued)

Figure	System Configuration			Variable	Wind (kt)	σ_u (kt)	σ_w (kt)	BN	Page
	Flr Hgt	Gains	Spoilers						
B-71	Variable	-	No	$\dot{h}$	12.5	1.87	1.50	✓	B-77
B-72				X	-10	2.70	1.50	✓	B-78
B-73				θ					B-79
B-74				U					B-80
B-75				Δh_{WINDOW}					B-81
B-76	Variable	-	No	$\dot{h}$	-5	1.35	1.50	✓	B-82
B-77				X	0	0	1.50	✓	B-83
B-78				θ					B-84
B-79				U					B-85
B-80				Δh_{WINDOW}					B-86
B-81	Constant	Low	Yes	$\dot{h}$	25	3.75	1.50	✓	B-87
B-82				X	-10	2.70	1.50	✓	B-88
B-83				θ					B-89
B-84				U					B-90
B-85				Δh_{WINDOW}					B-91
B-86	Constant	Low	No	$\dot{h}$	25	3.75	1.50	✓	B-92
B-87				X	-10	2.70	1.50	✓	B-93
B-88				θ					B-94
B-89				U					B-95
B-90				Δh_{WINDOW}					B-96
B-91	Constant	High	Yes	$\dot{h}$	25	3.75	1.50	✓	B-97
B-92				X	-10	2.70	1.50	✓	B-98
B-93				θ	0	0	1.50	✓	B-99
B-94				U					B-100
B-95				Δh_{WINDOW}					B-101

Probability Distributions (continued)

APPENDIX B
SUPPLEMENTARY GLIDE SLOPE TRACK AND FLARE SIMULATION RESULTS

This Appendix contains simulation generated landing time histories and flare trajectories that supplement these given in Section 5 to cover all the major longitudinal control law configurations and deterministic disturbances that were evaluated. The simulation generated probability distributions of longitudinal landing variables, on which the Section 5 summaries are based, are also given here.

The landing time histories of the variable flare height configuration and the low gain constant flare height configuration, both with spoilers and standard wind shears (as defined in Appendix A) were given in Section 5 as Figures 5-1 and 5-2. Landing time histories for all the remaining combinations of evaluated configurations and deterministic disturbances, including logarithmic wind shears (defined in Appendix A) are given here as Figures B-1 through B-10.

Similarly, the $\dot{h}/h$ flare trajectories for the variable flare height configuration and the low gain constant flare height configuration, both without spoilers and with logarithmic wind shears, are given in Section 5 as Figures 5-3 and 5-4. The flare trajectories for the remaining configurations and disturbances are given here as Figures B-11 through B-20.

Figures B-21 through B-110 are the probability distributions of the longitudinal landing variables. These variables are touchdown sink rate, range (measured from the GPIP), pitch attitude and airspeed, and the deviation from the glide-slope at the 30.48 m (100 ft) window height is also given. In Figures B-21 through B-50 one curve is given per variable, obtained by combining results obtained for 25 knot shearing headwind and a horizontal turbulence level of 3.75 kt rms, with results for 10 knots shearing tailwind and a horizontal turbulence level of 2.70 knots. Both headwind and tailwind results were obtained with 1.50 knots of vertical turbulence and MLS beam noise. The results were combined assuming 70% probability for the headwind and 30% for the tailwind. Figures B-51 through B-110 have two or three curves for each variable, where each curve represents one specific set of deterministic and stochastic disturbances, as indicated on the figure or in the list of figures. All statistical data for the Twin Otter were obtained with the standard wind models that are defined in Appendix A.

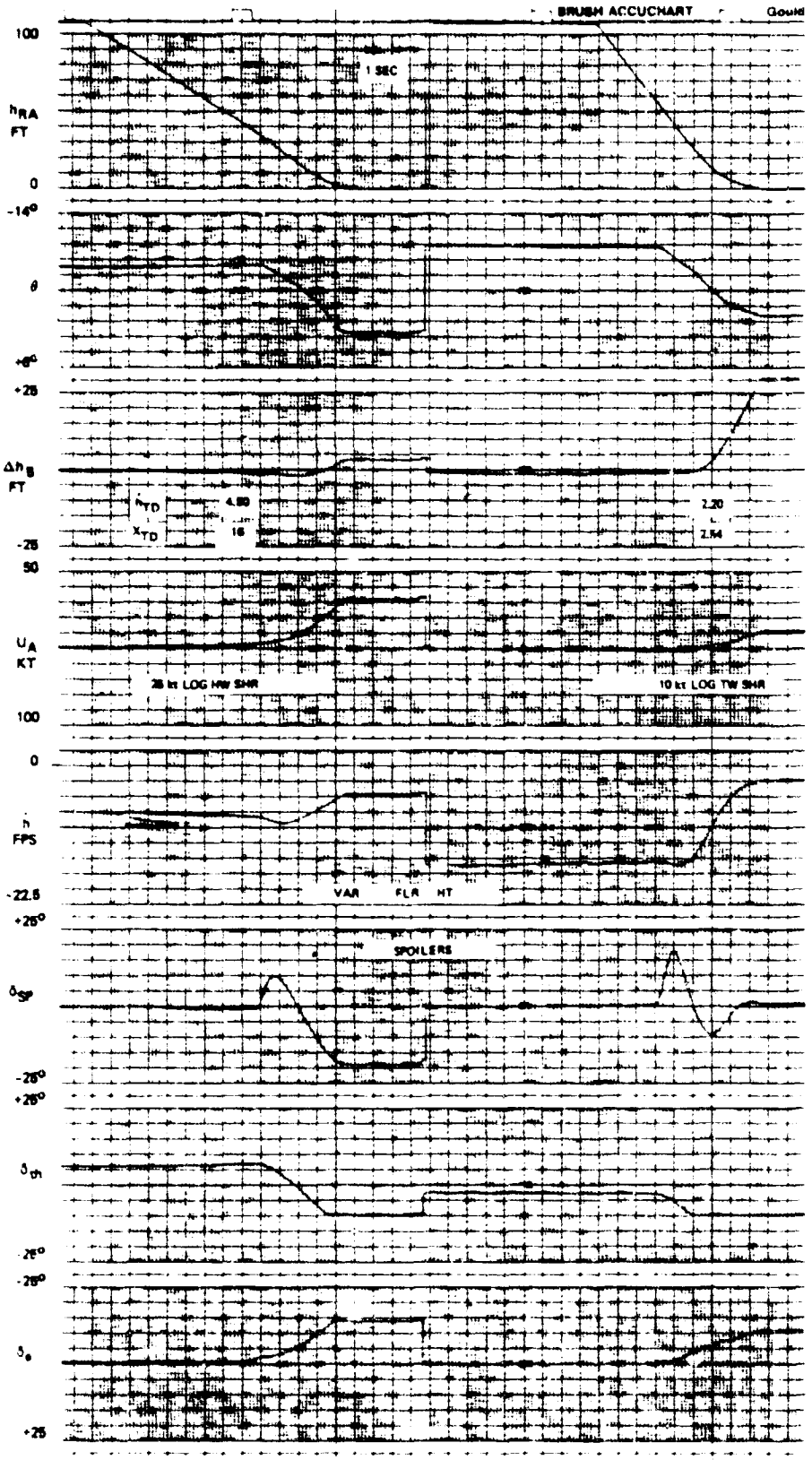

Figure B-1A. Landing Time Histories: Variable Flare Height with Spoilers Logarithmic Shears

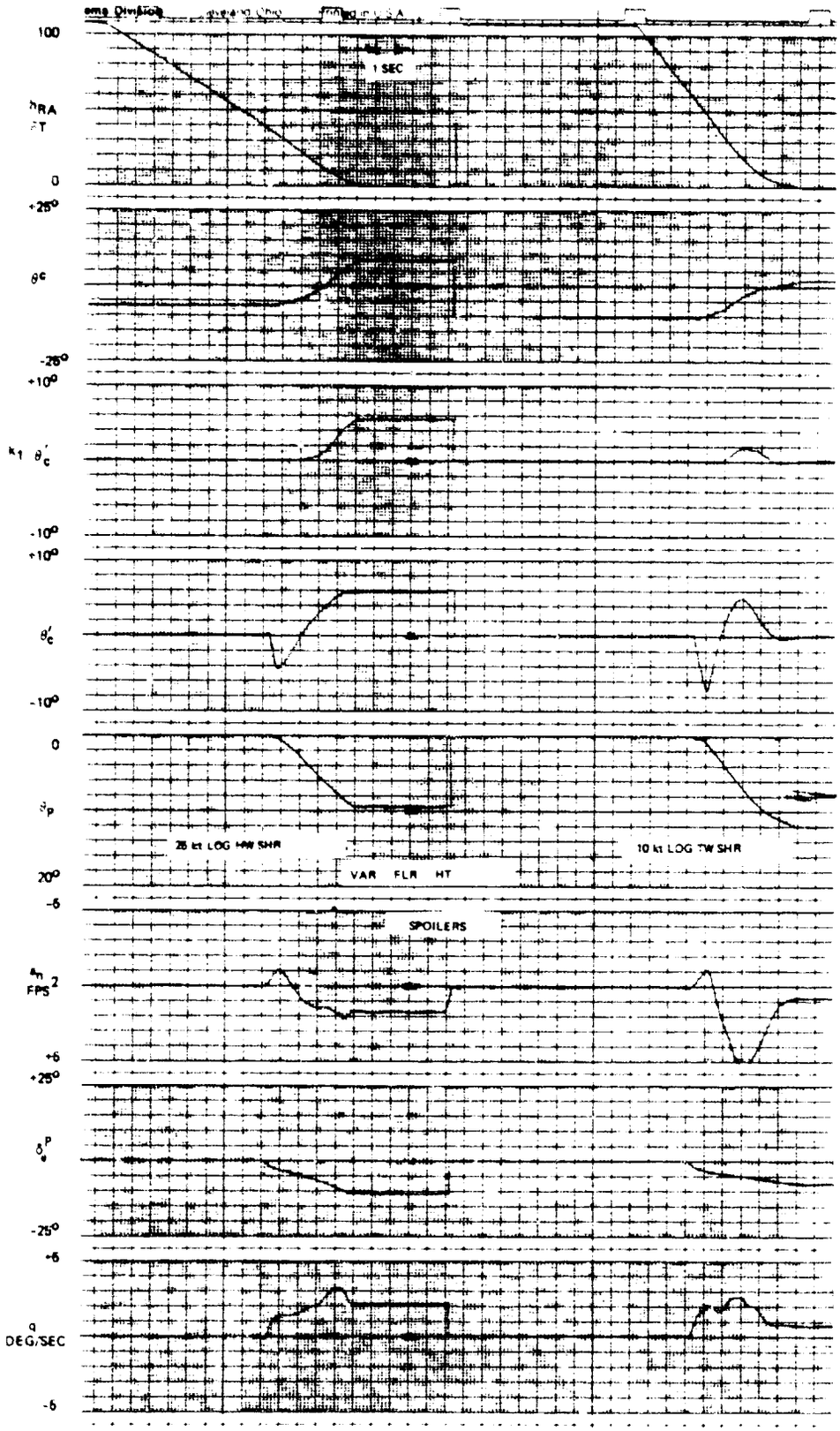

Figure B-1B. Landing Time Histories: Variable Flare Height with Spoilers, Logarithmic Shears

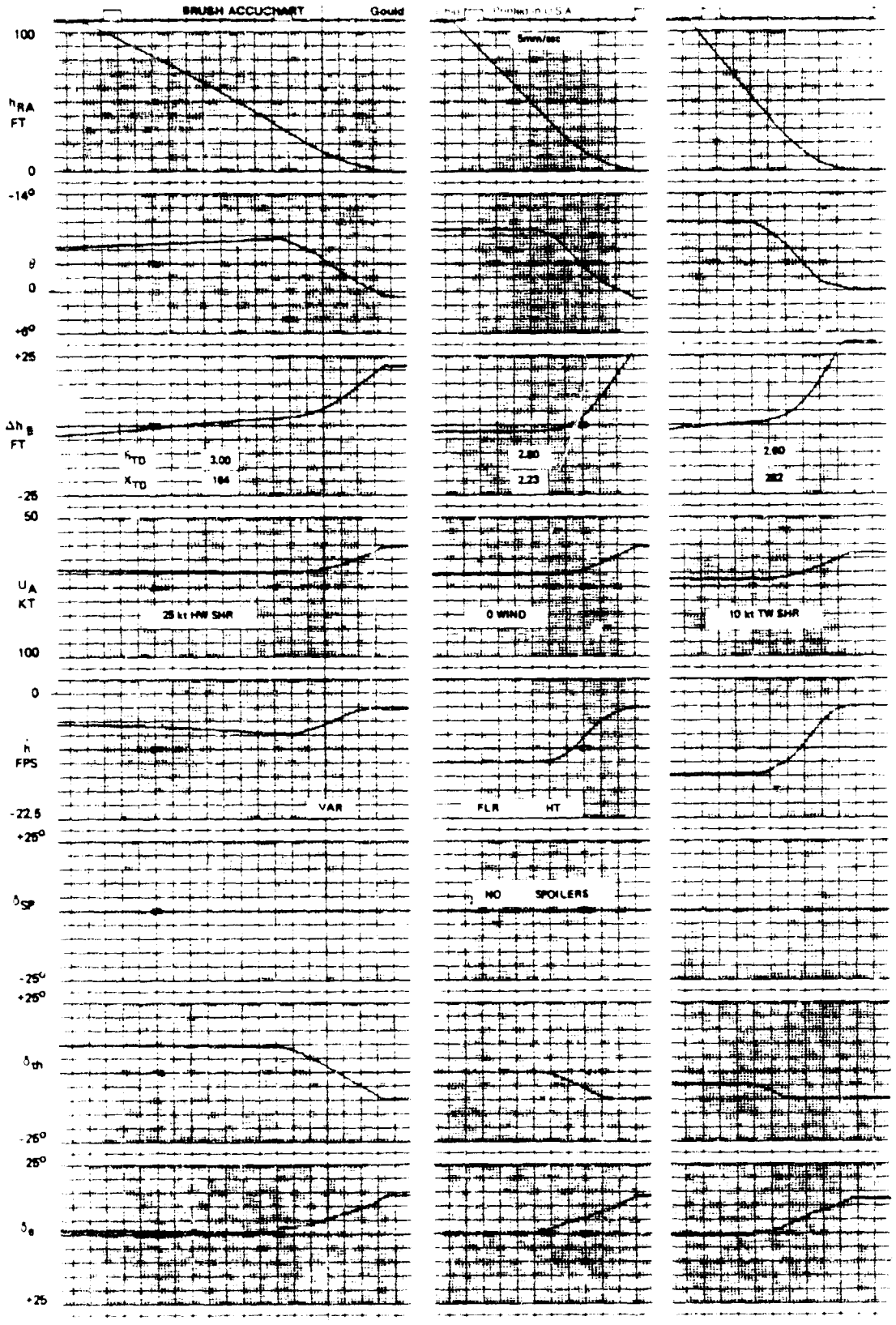

Figure B-2A. Landing Time Histories; Variable Flare Height; No Spoilers

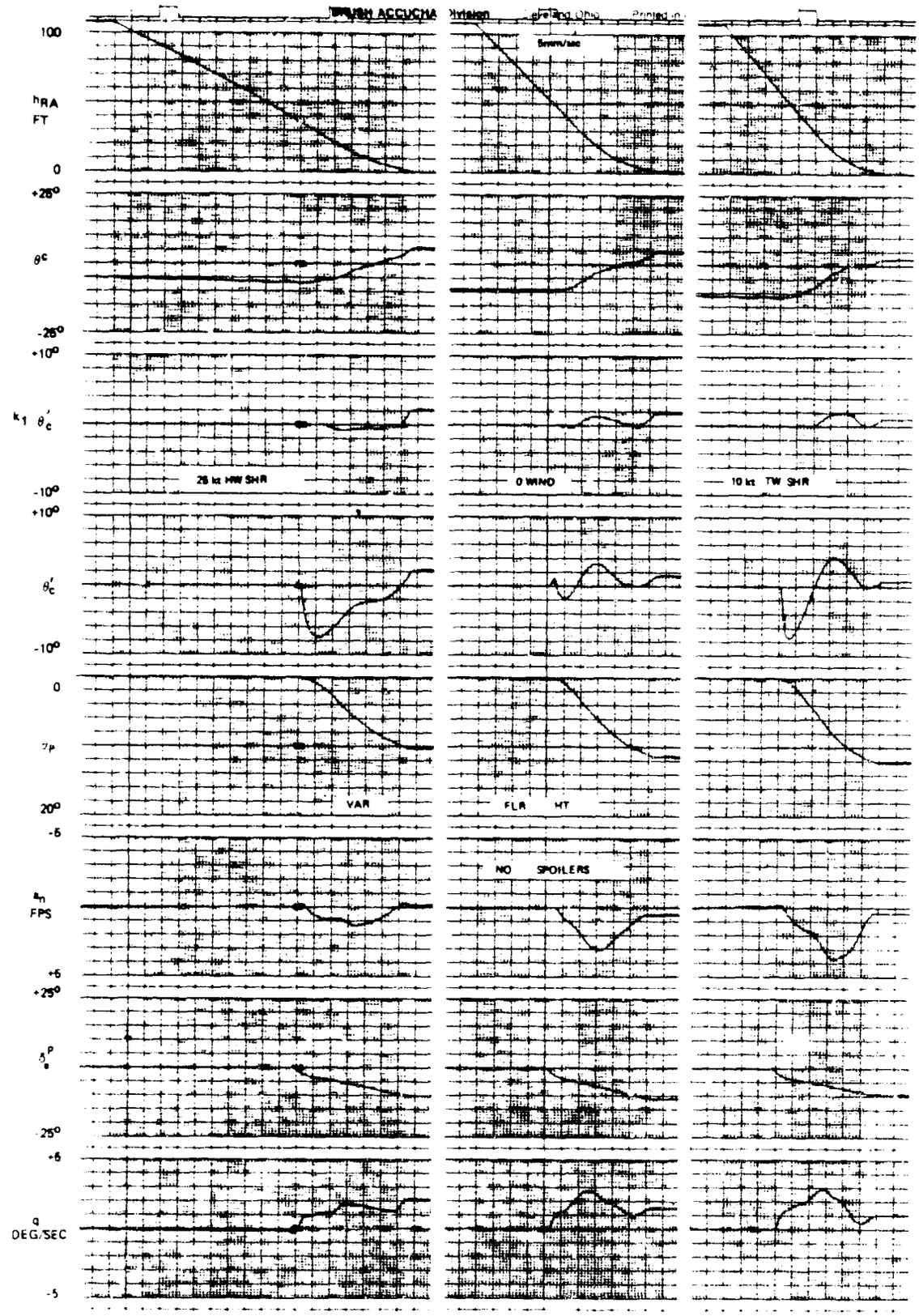

Figure B-2B. Landing Time Histories; Variable Flare Height; No Spoilers

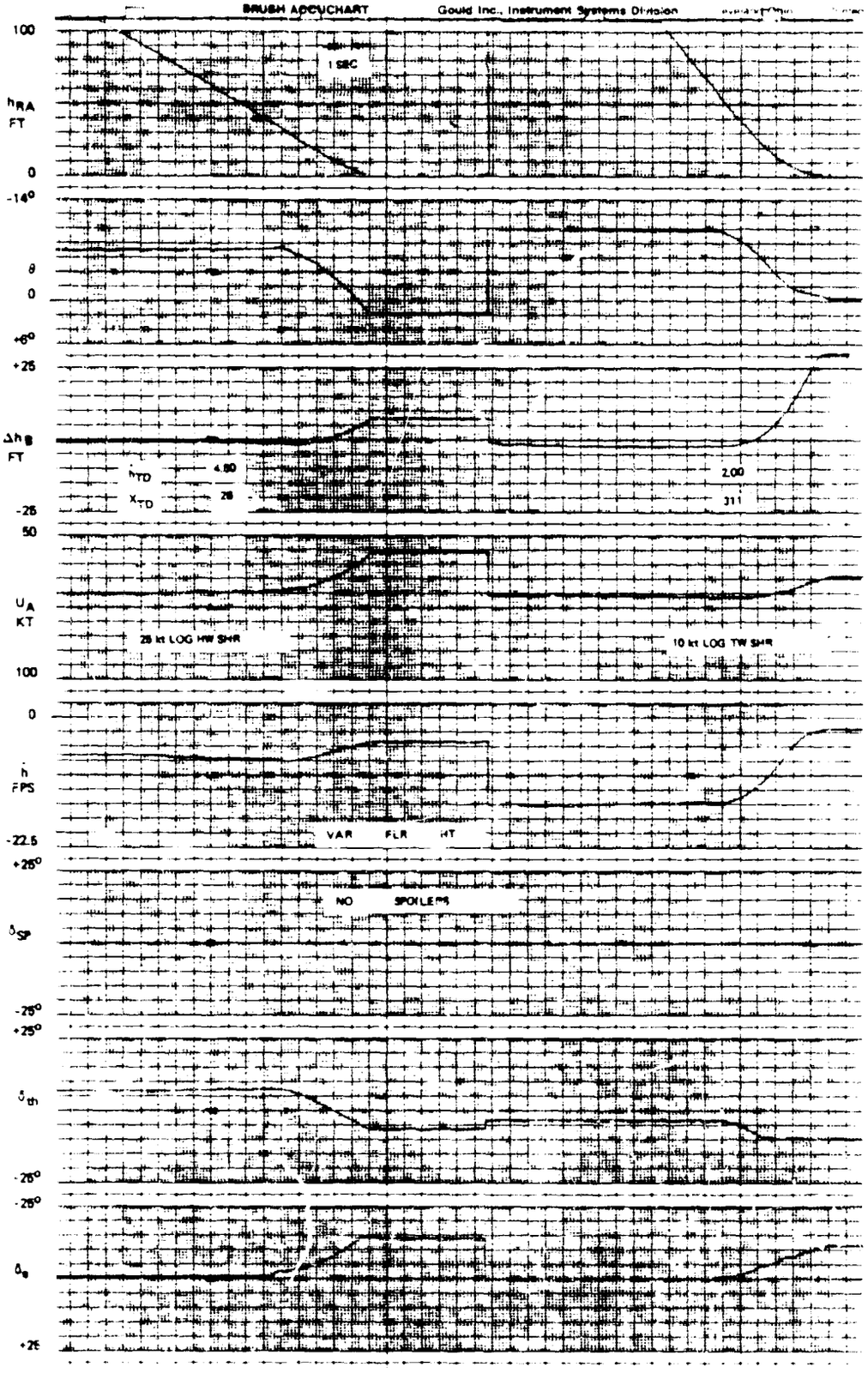

Figure B-3A. Landing Time Histories: Variable Flare Height: No Spoilers
Logarithmic Shears

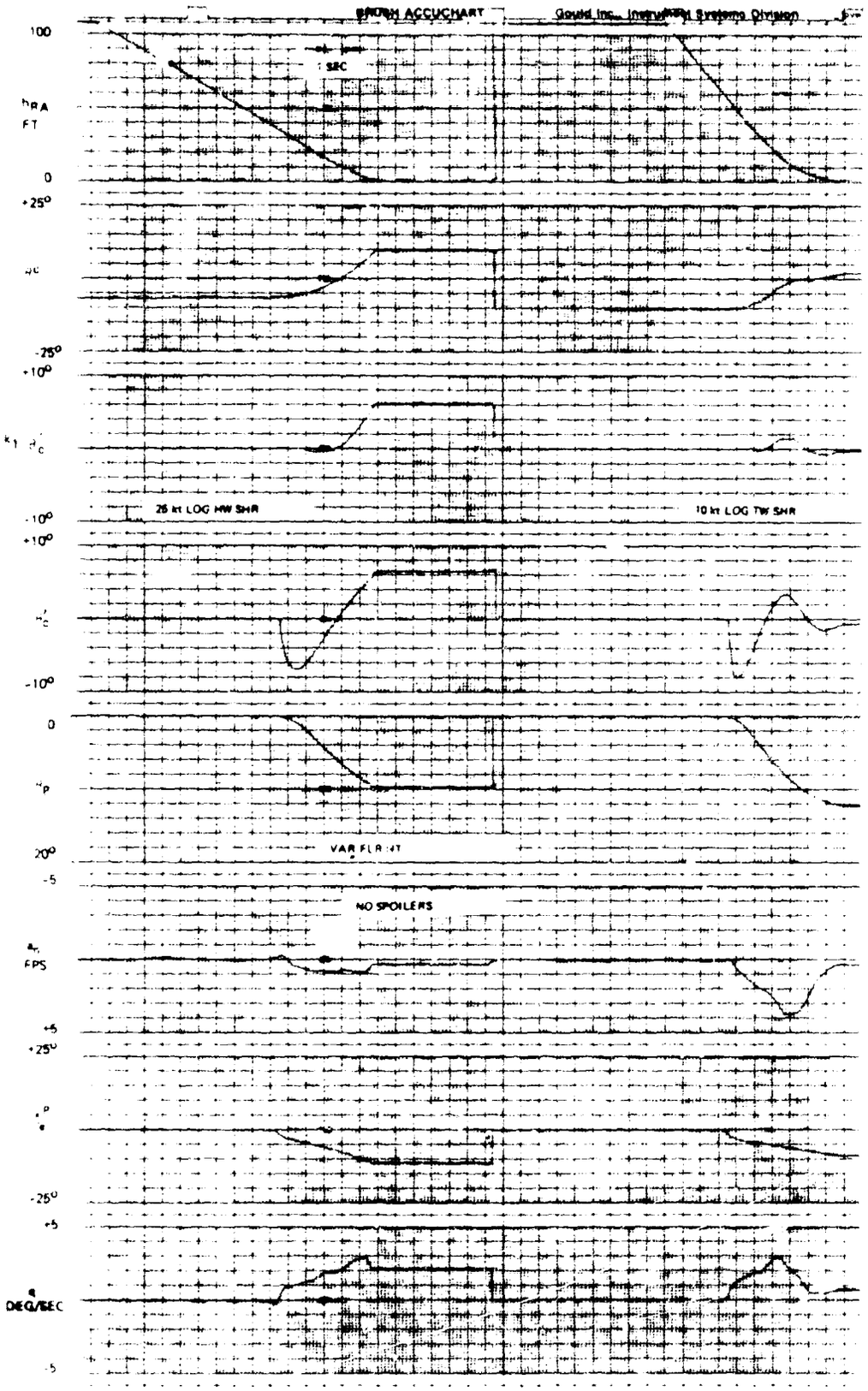

Figure B-3B. Landing Time Histories: Variable Flare Height; No Spoilers
Logarithmic Shears

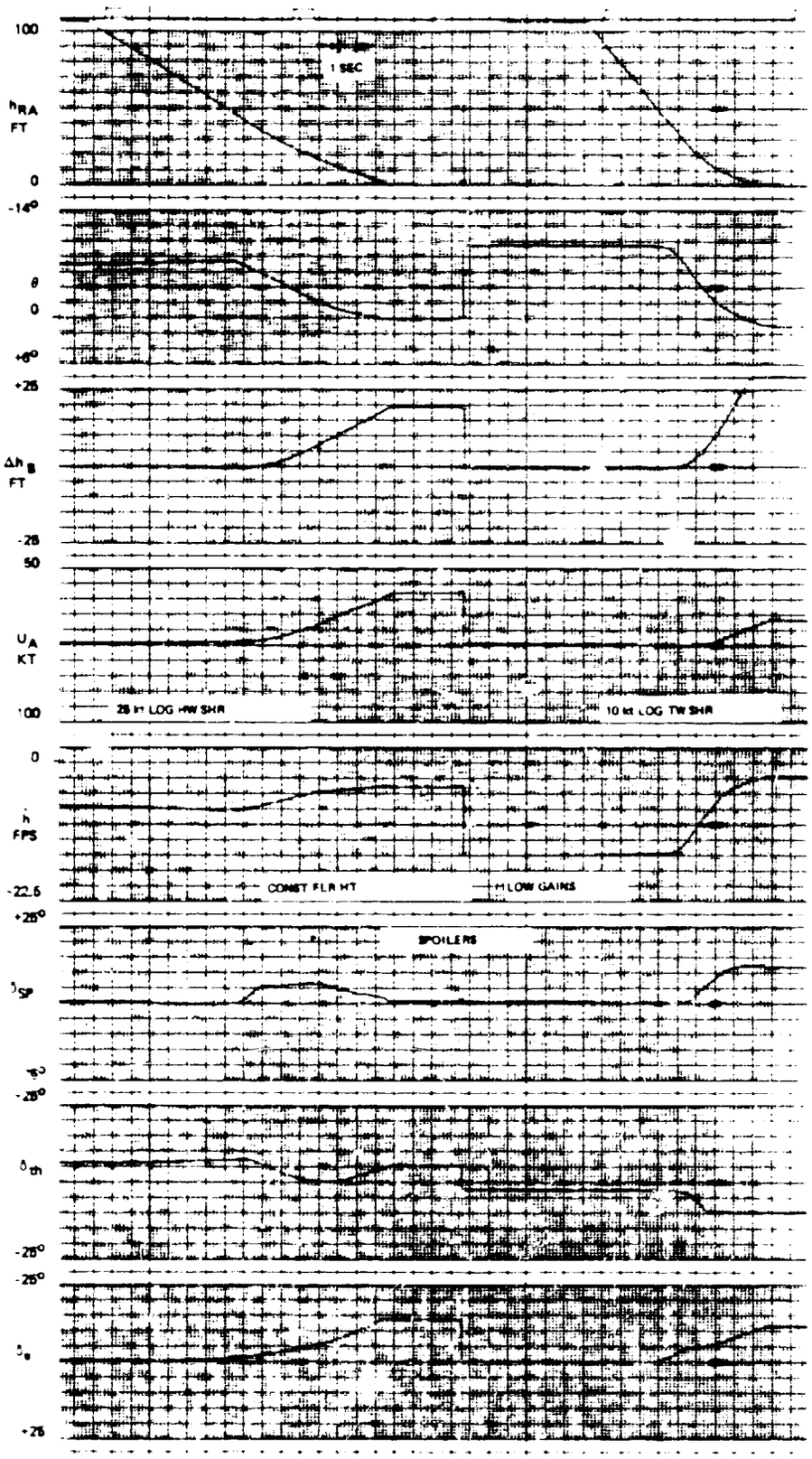

Figure B-4. Landing Time Histones. Constant Flare Height, Low Gains with Spoilers. Loganthmic Wind Shears

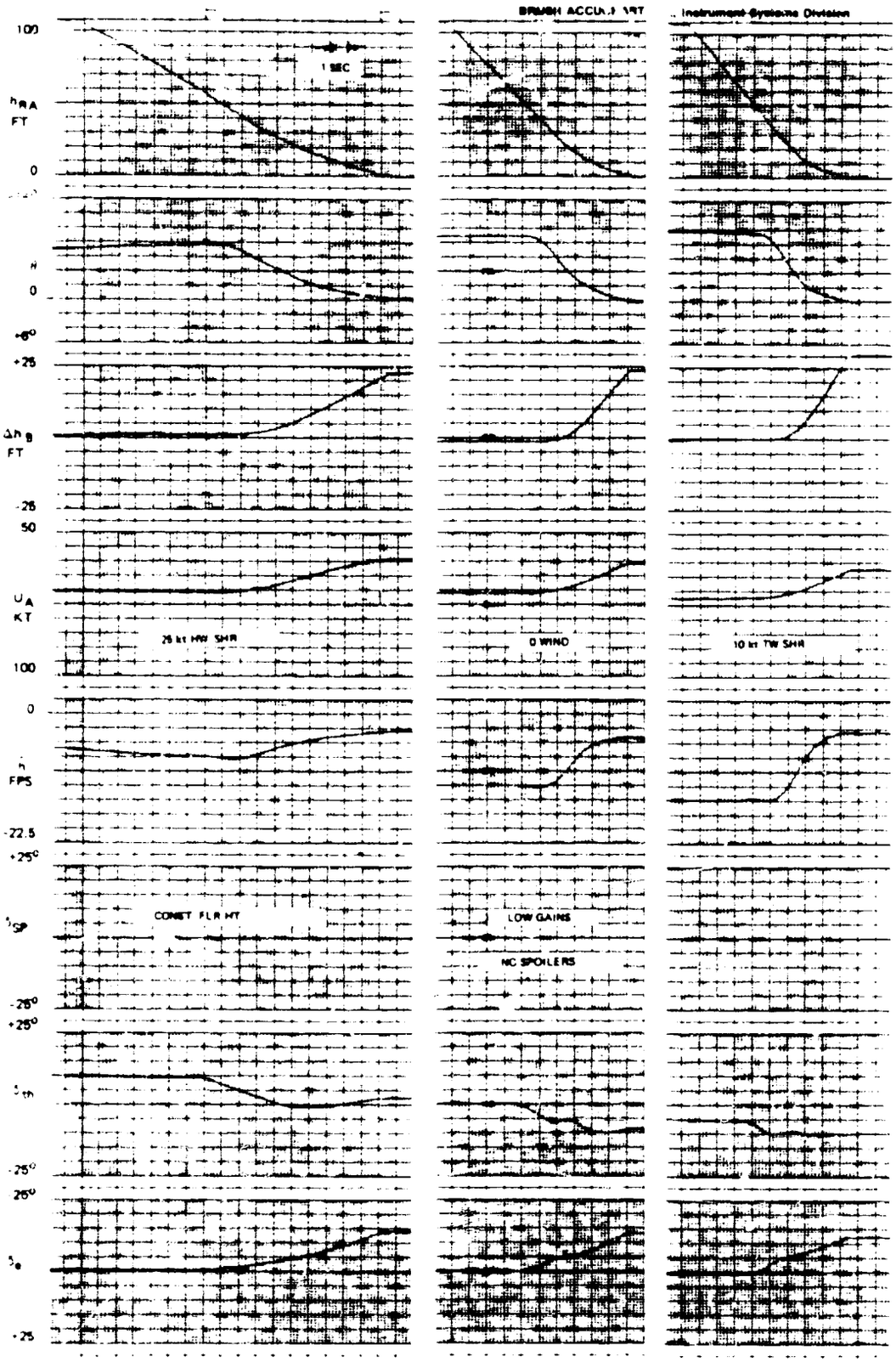

Figure B-5. Landing Time Histories, Constant Flare Height, Low Gains, No Spoilers

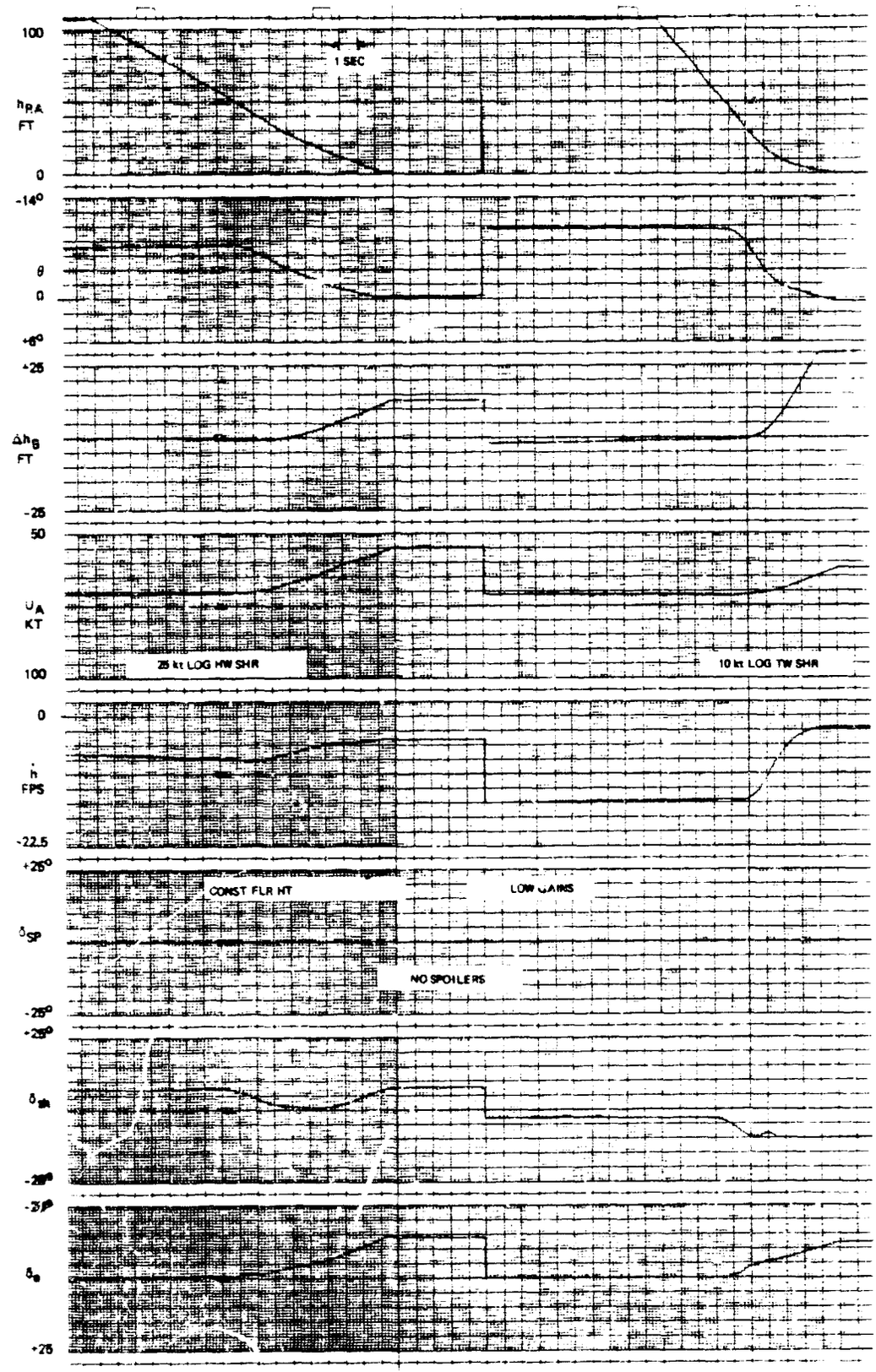

Figure B-6. Landing Time Histories, Constant Flare Height, Low Gains, No Spoilers Logarithmic Wind Shears

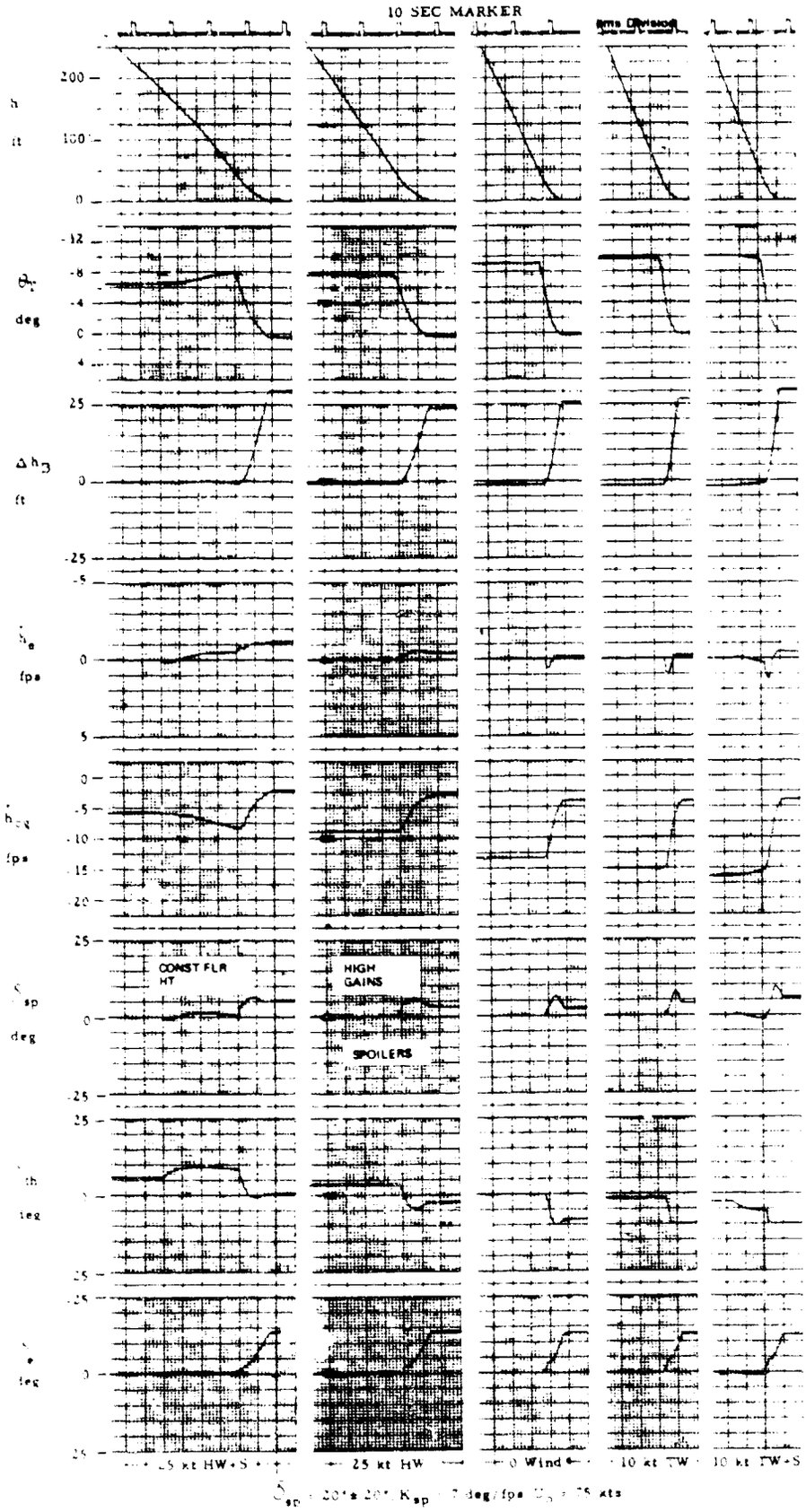

Figure B-7A. Landing Time Histories; Constant Flare Height, High Gains with Spoilers, FAA Winds

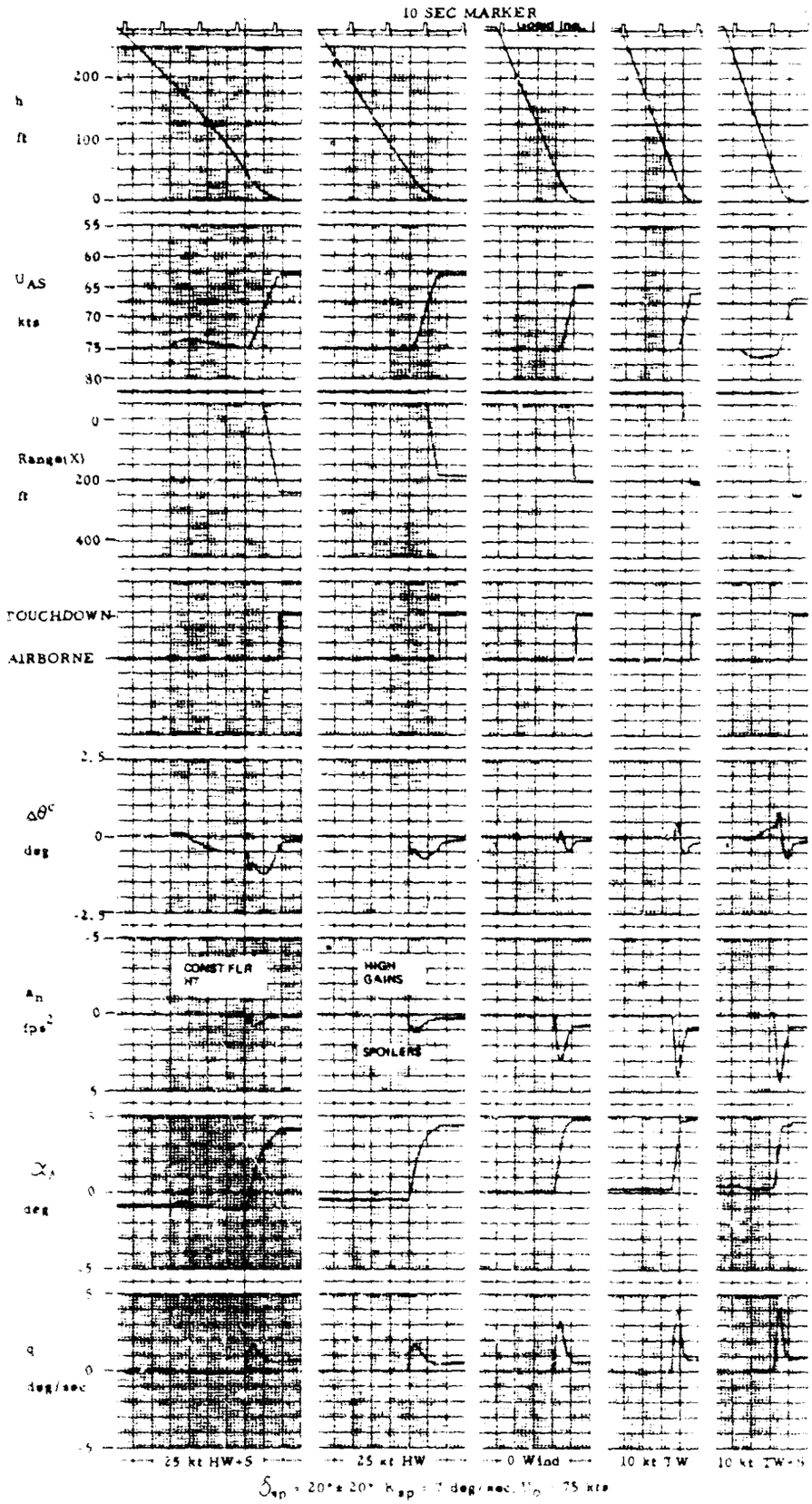

Figure B-7B. Landing Time Histories; Constant Flare Height, High Gains, with Spoilers FAA Winds

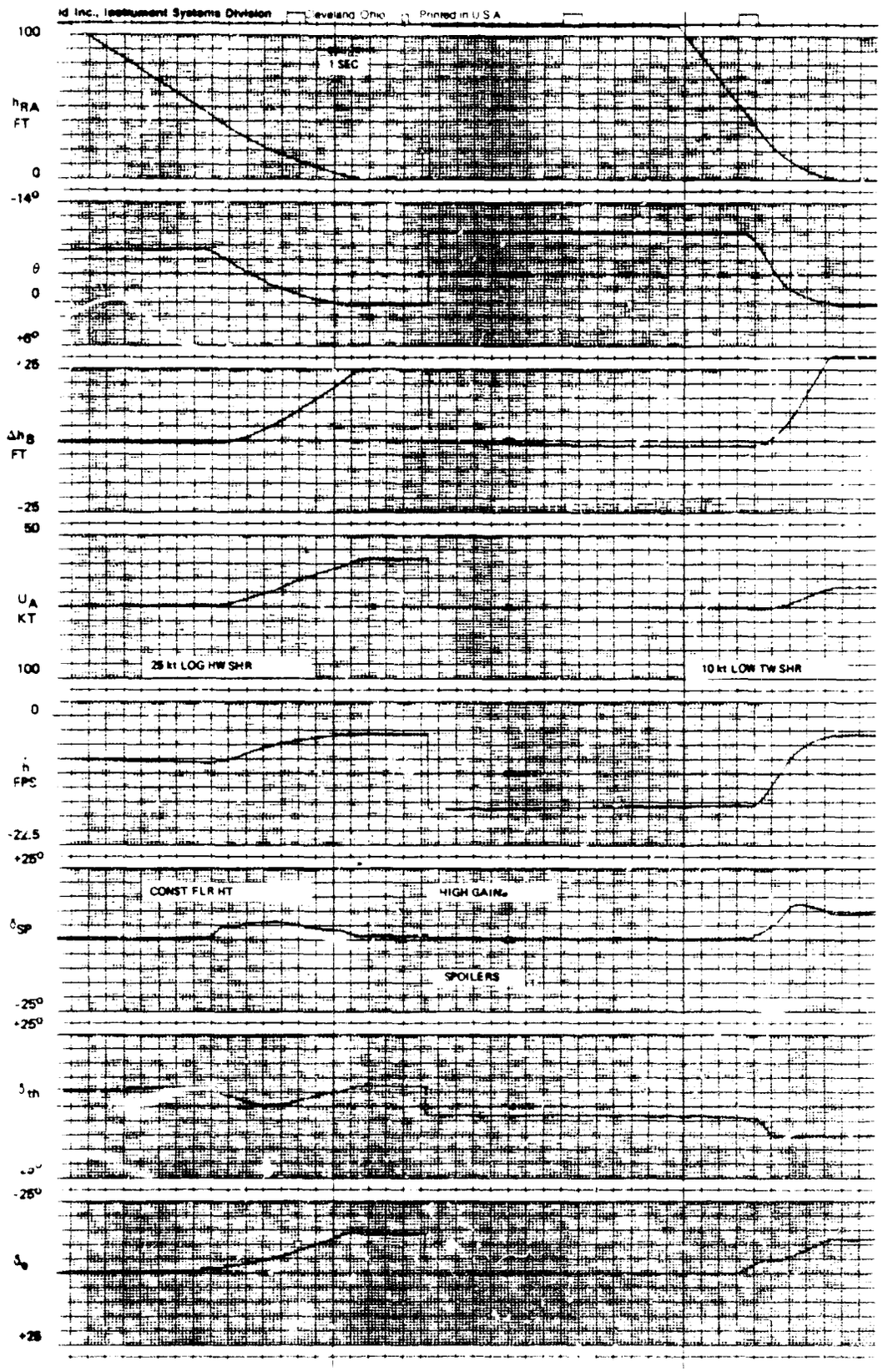

Figure B-8. Landing Time Histories: Constant Flare Height, High Gains, with Spoiler Logarithmic Wind Shears

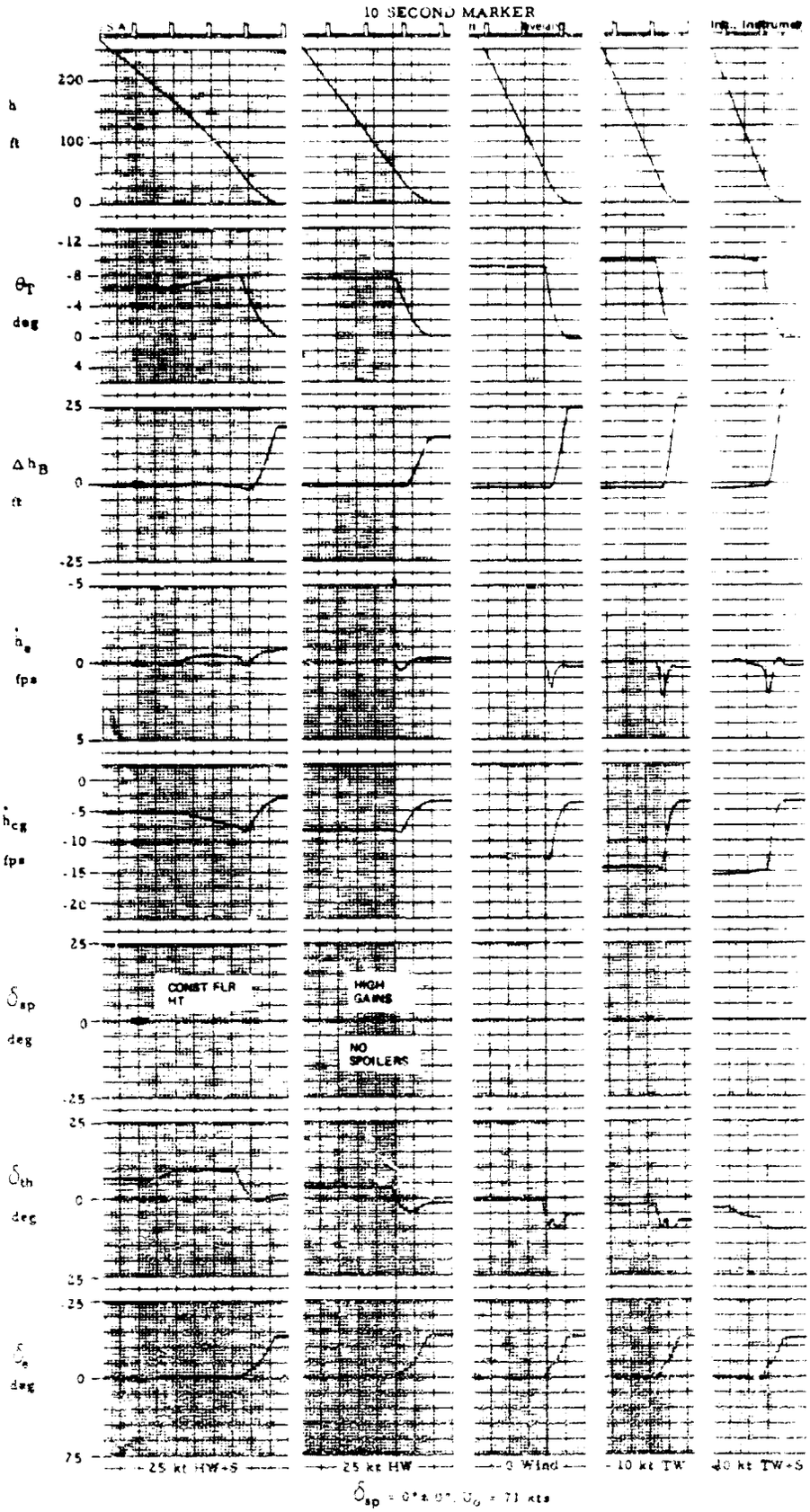

Figure B-9A. Landing Time Histories; Constant Flare Height, High Gains, No Spoilers FAA Winds

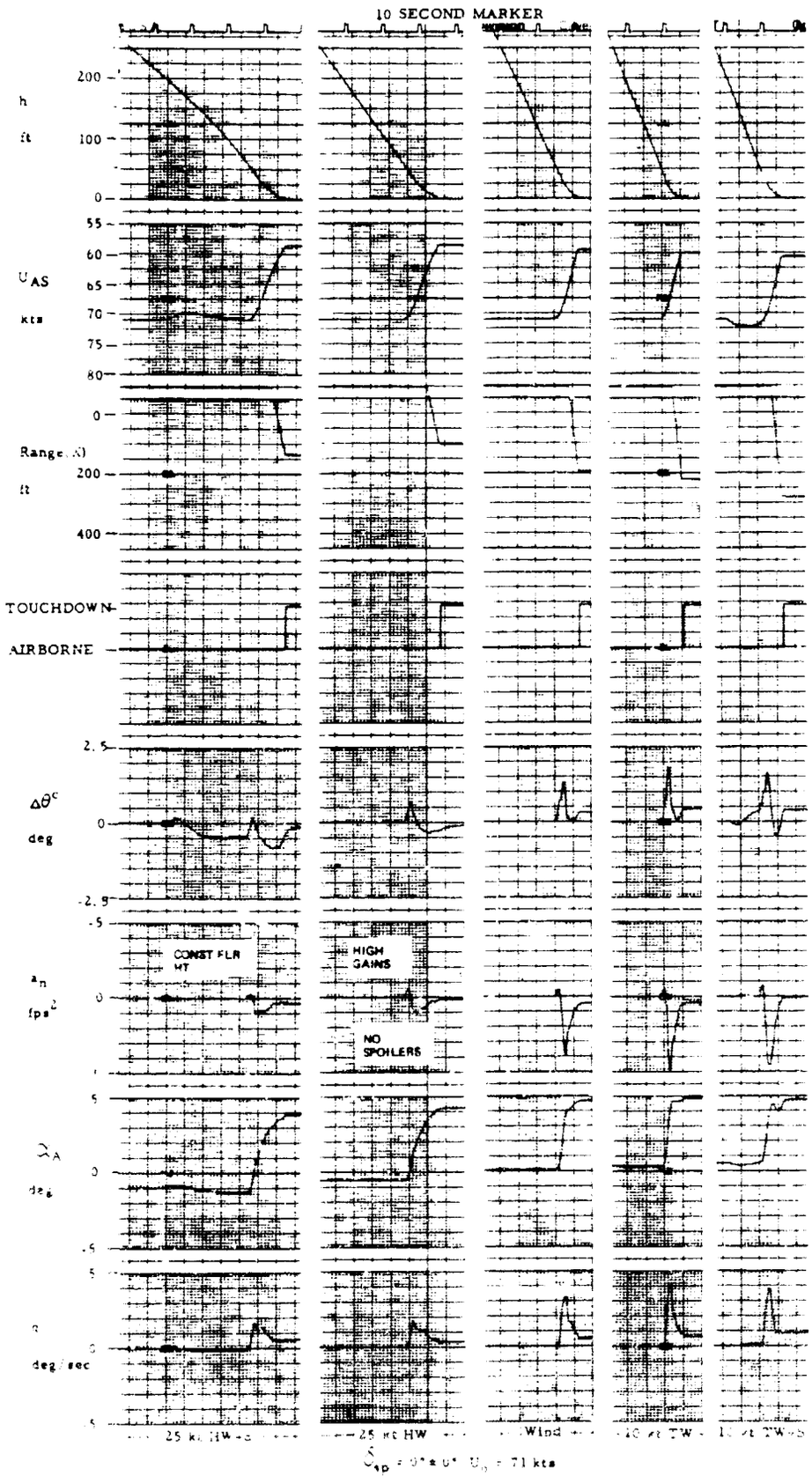

Figure B-9B. Landing Time Histories: Constant Flare Height, High Gains, No Spoilers
FAA Winds

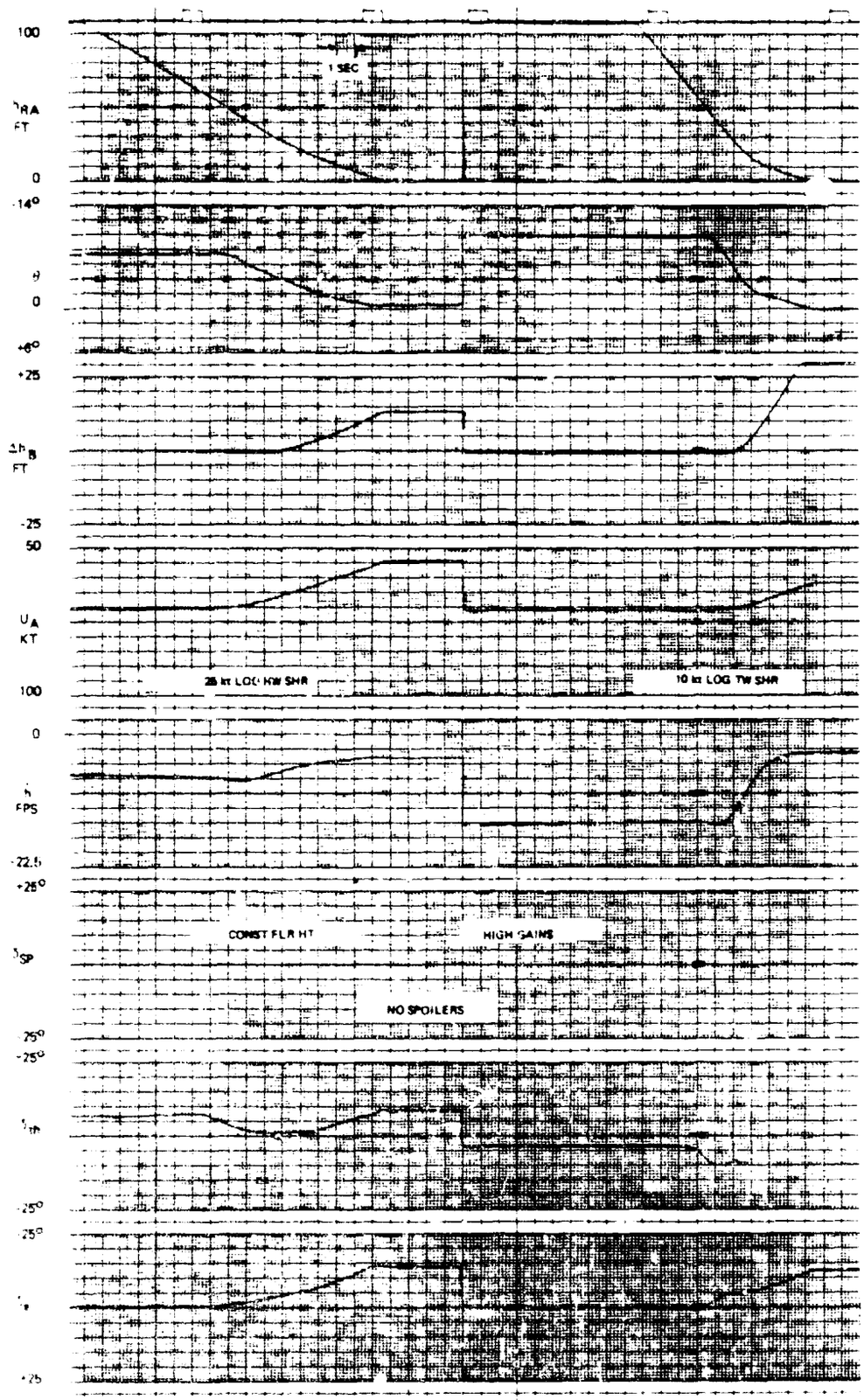

Figure B-10. Landing Time Histories, Constant Flare Height, High Gains No Spoilers Loganthmic Wind Shears

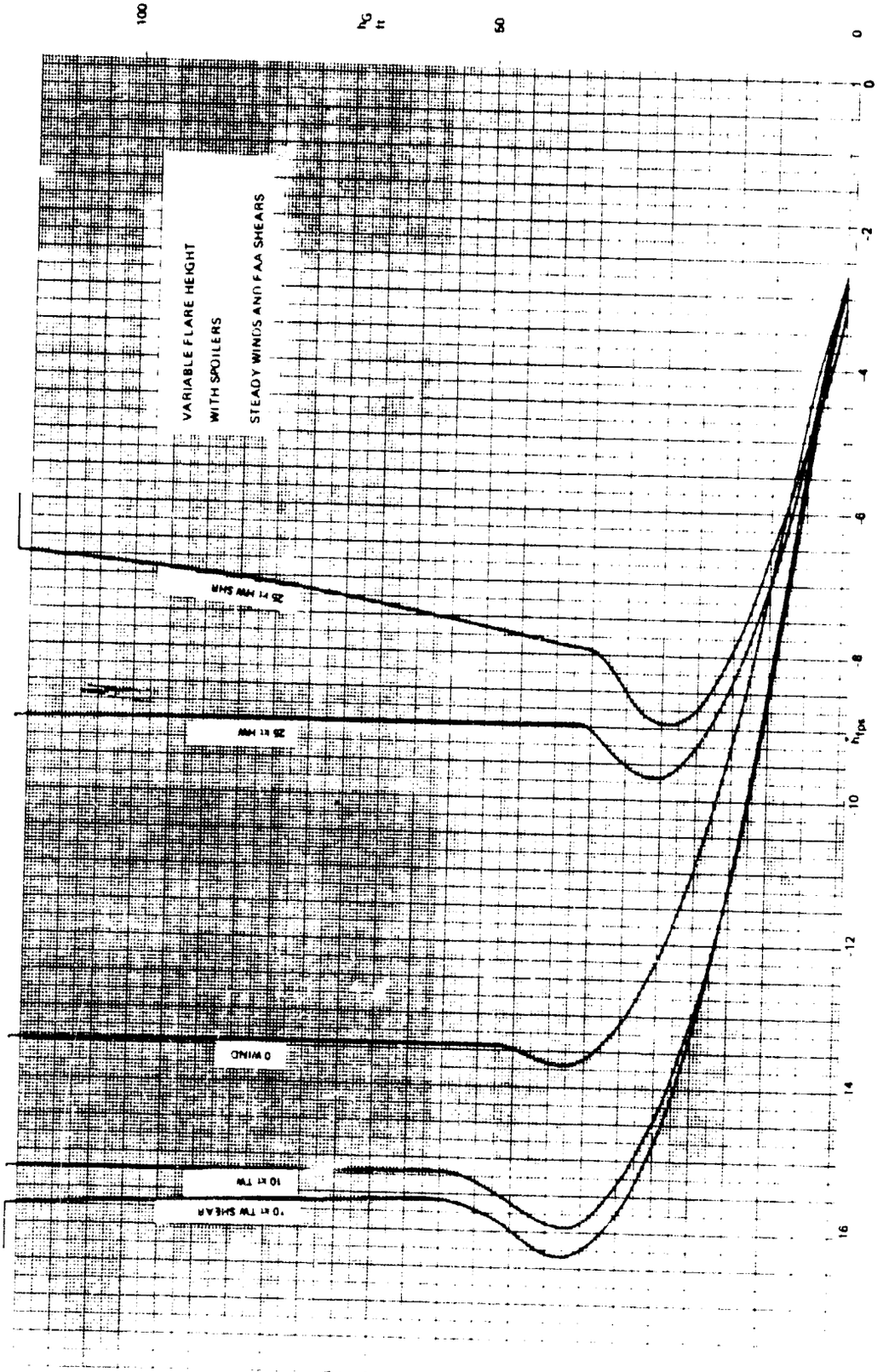

Figure B-11. Flare h/ḣ Trajectories, Variable Flare Height, Spoilers

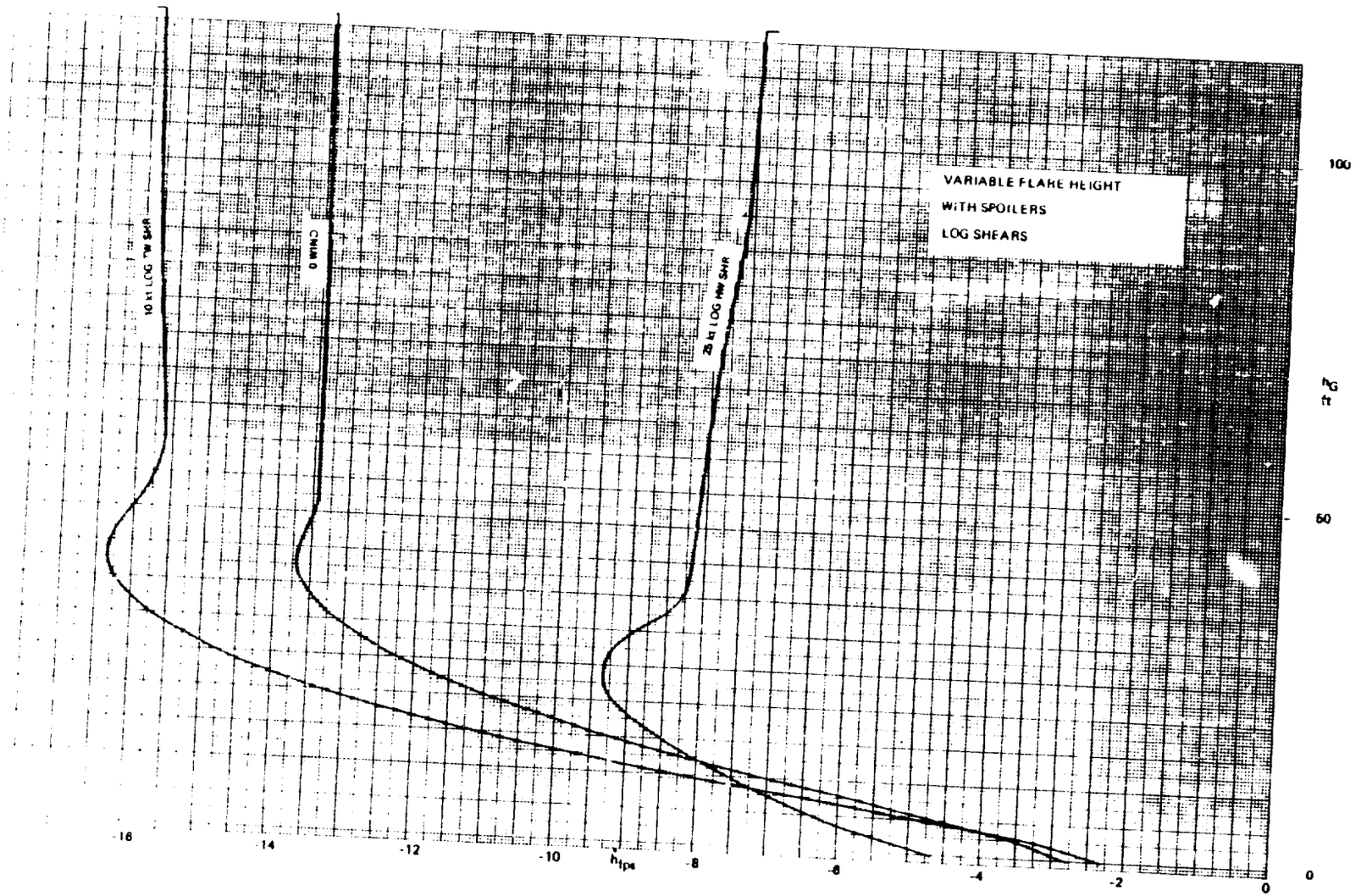

Figure B-12. Flare h/h̄ Trajectories, Variable Flare Height, Spoilers

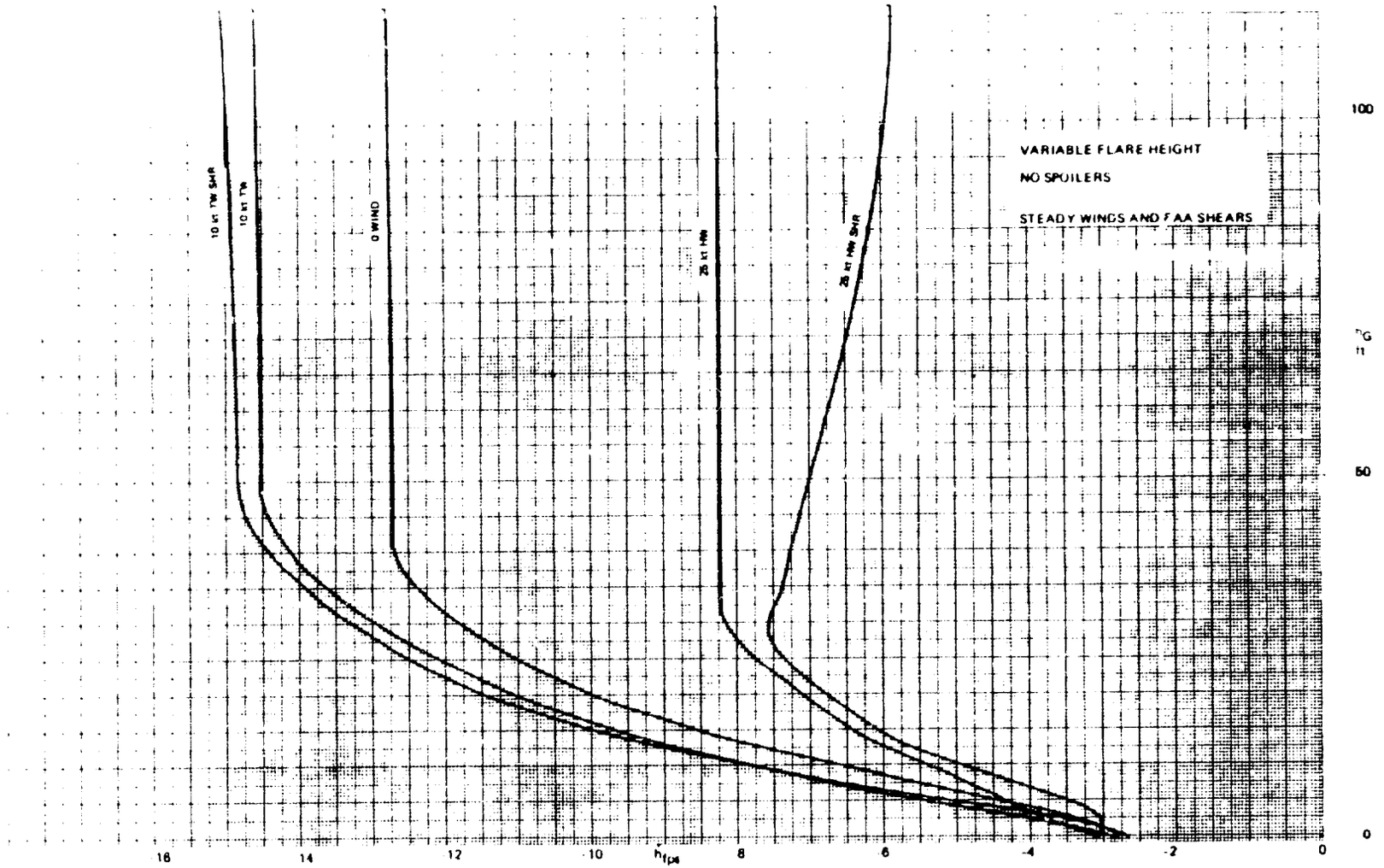

Figure B-13. Flare h/ḣ Trajectories, Variable Flare Height, No Spoilers

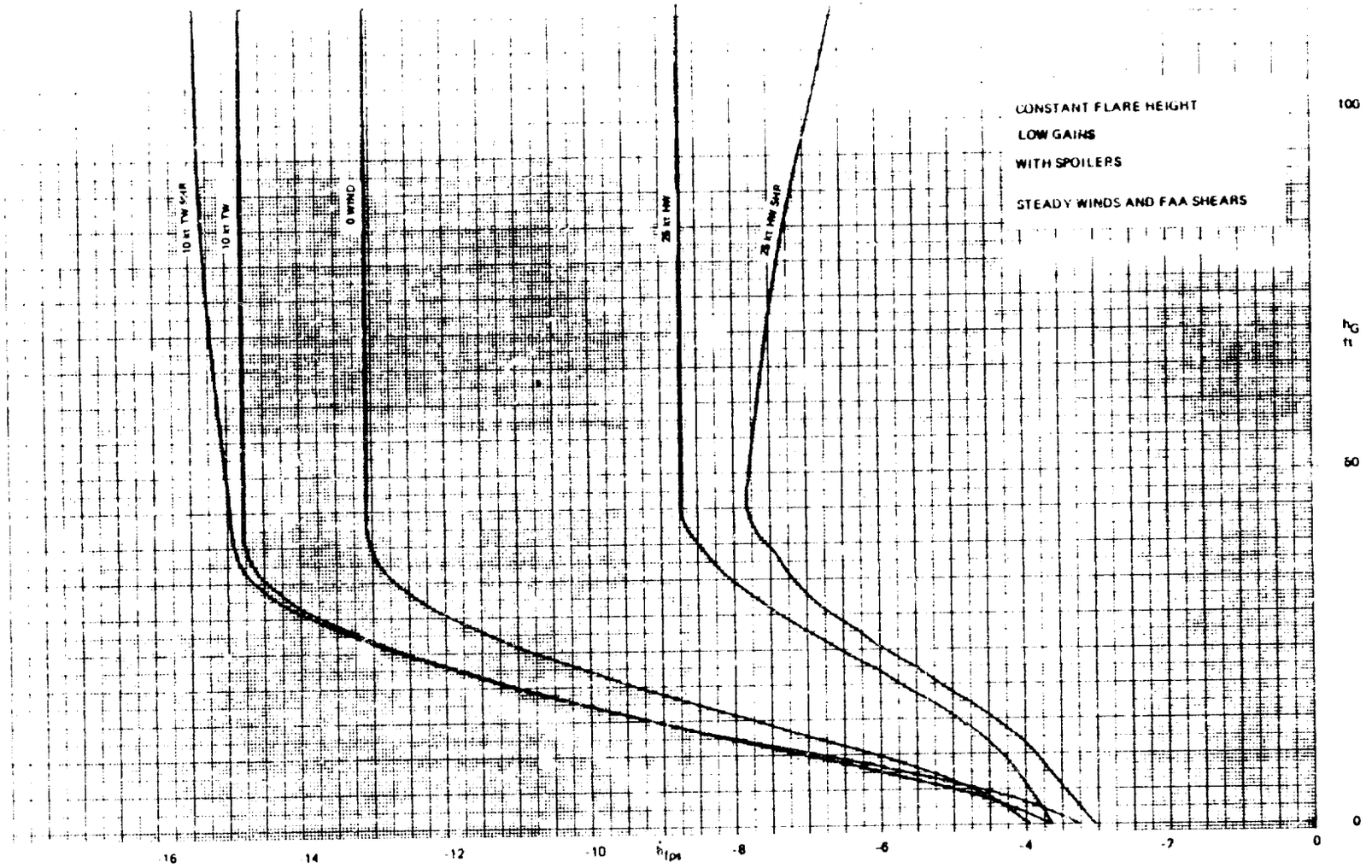

Figure B-14. Flare h/ḣ Trajectories, Constant Flare Height, Low Gains, Spoilers

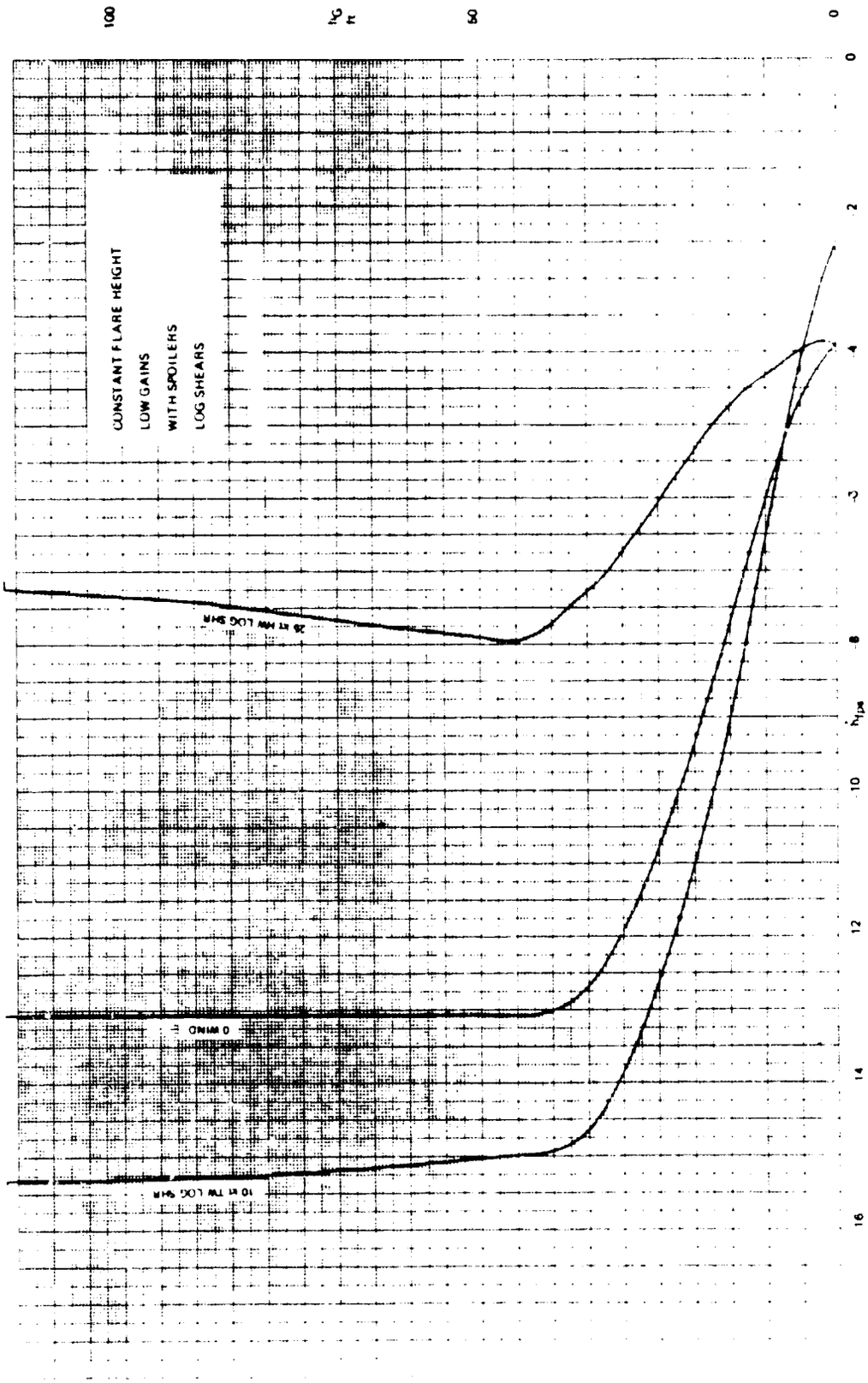

Figure B-15. Flare h/ḣ Trajectories, Constant Flare Height, Low Gains, Spoilers

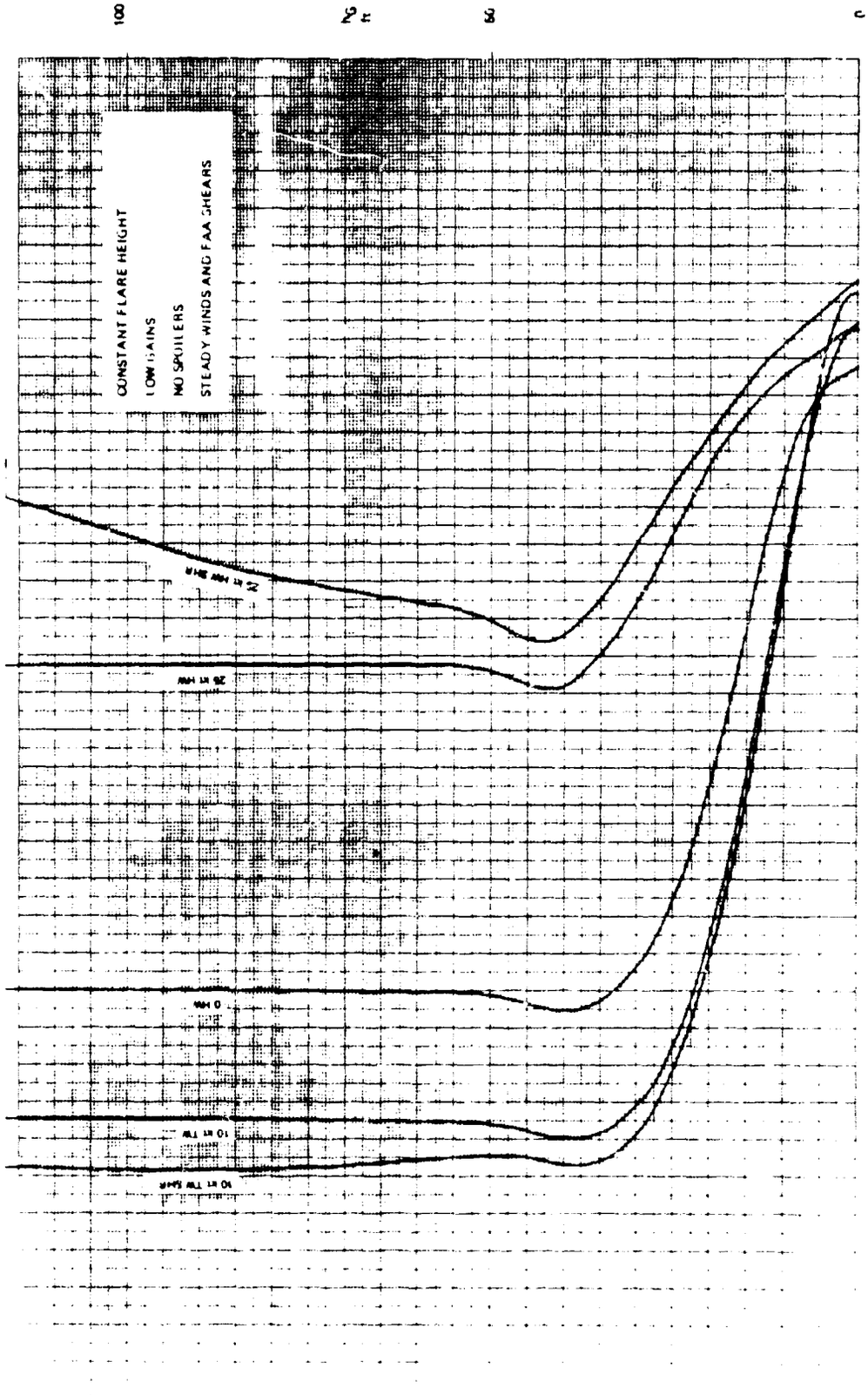

Figure B-16. Flare h/ḣ Trajectories, Constant Flare Height, Low Gains, No Spoilers

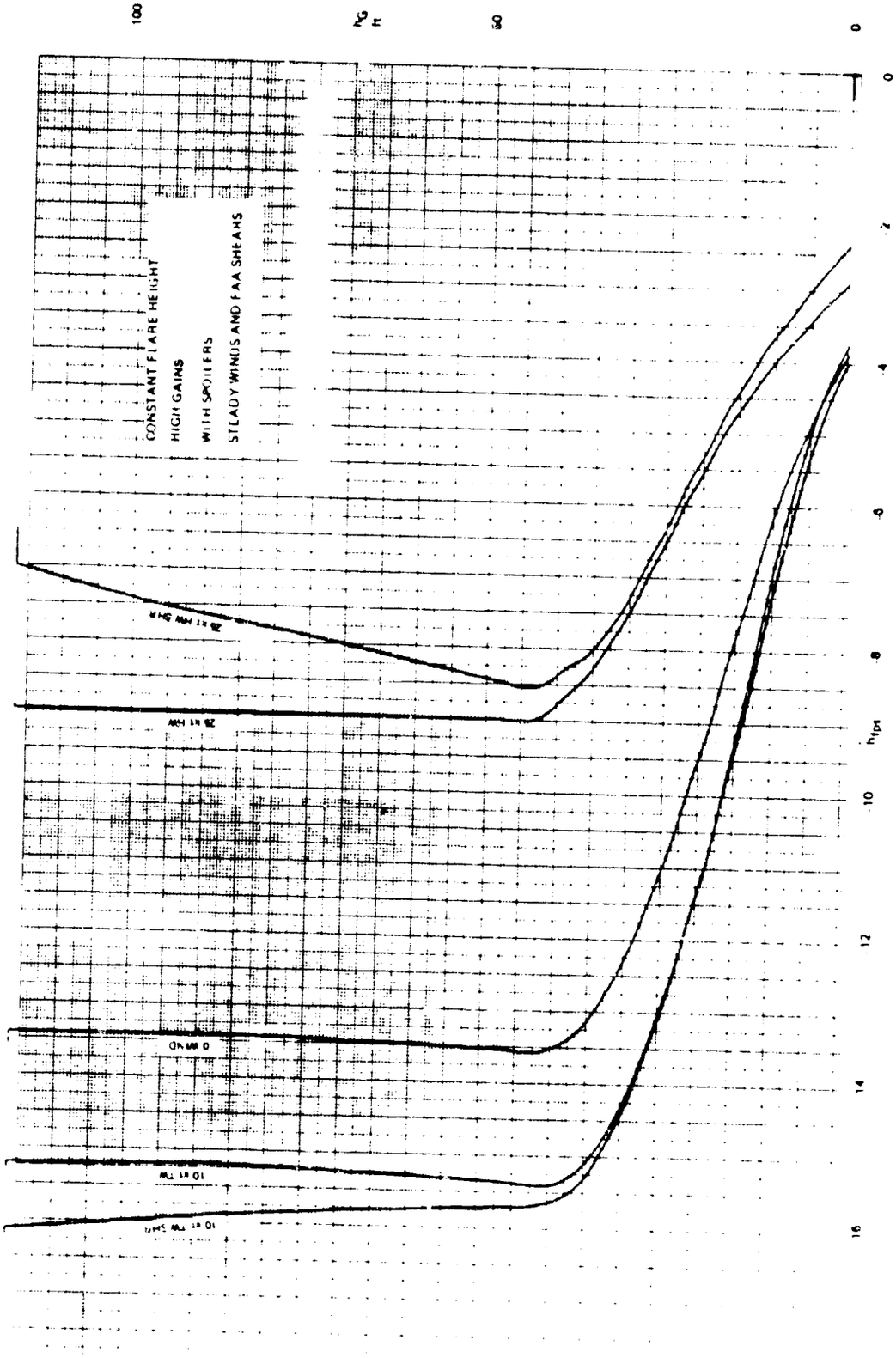

Figure B-17. Flare h/ḣ Trajectories, Constant Flare Height, High Gains, Spoilers

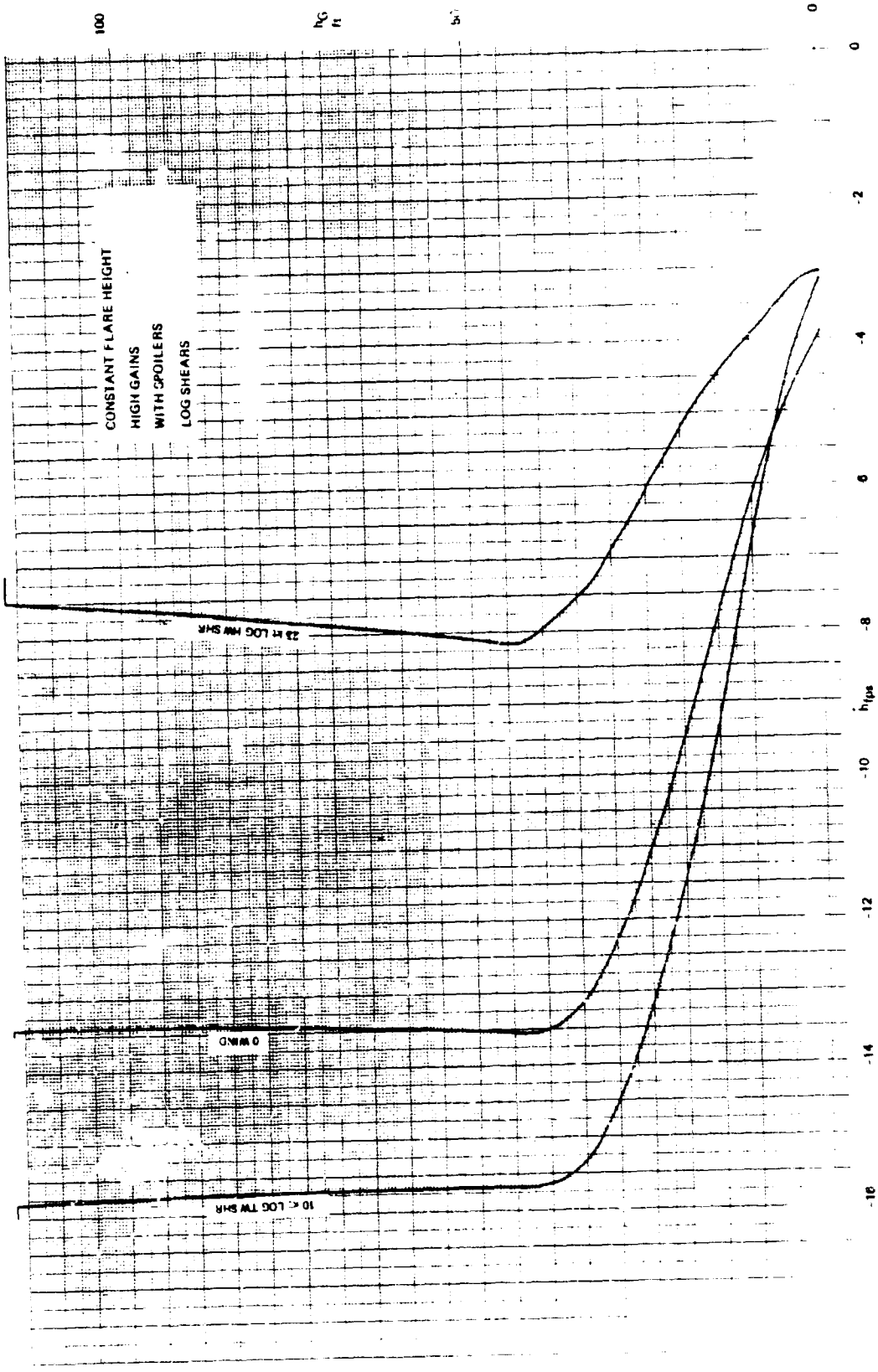

Figure B-18. Flare h/ḣ Trajectories, Constant Flare Height, High Gains, Spoilers

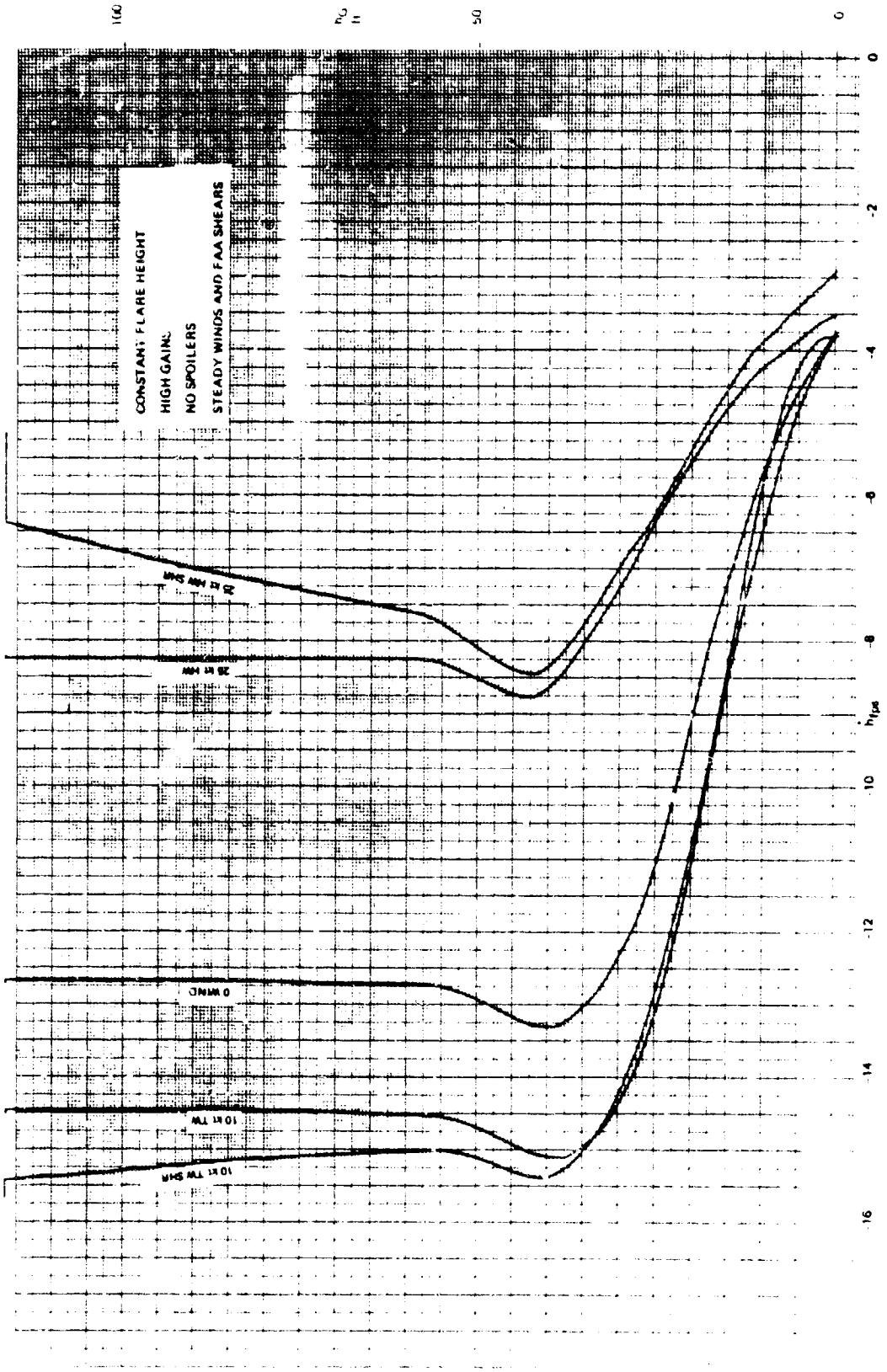

Figure B-15. Flare h/ḣ Trajectories, Constant Flare Height, High Gains, No Spoilers

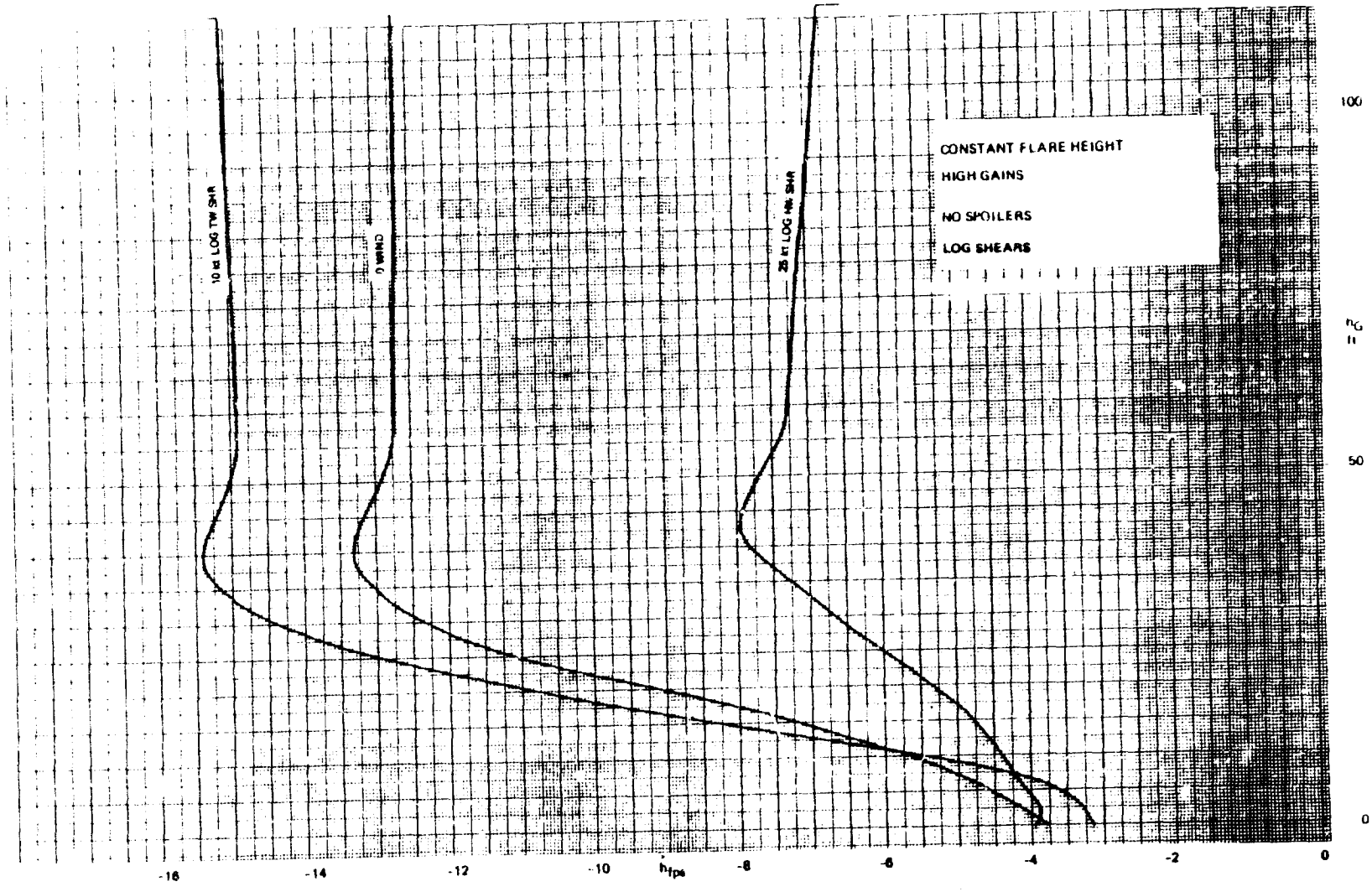

Figure B-20. Flare h/ḣ Trajectories, Constant Flare Height, High Gains, No Spoilers

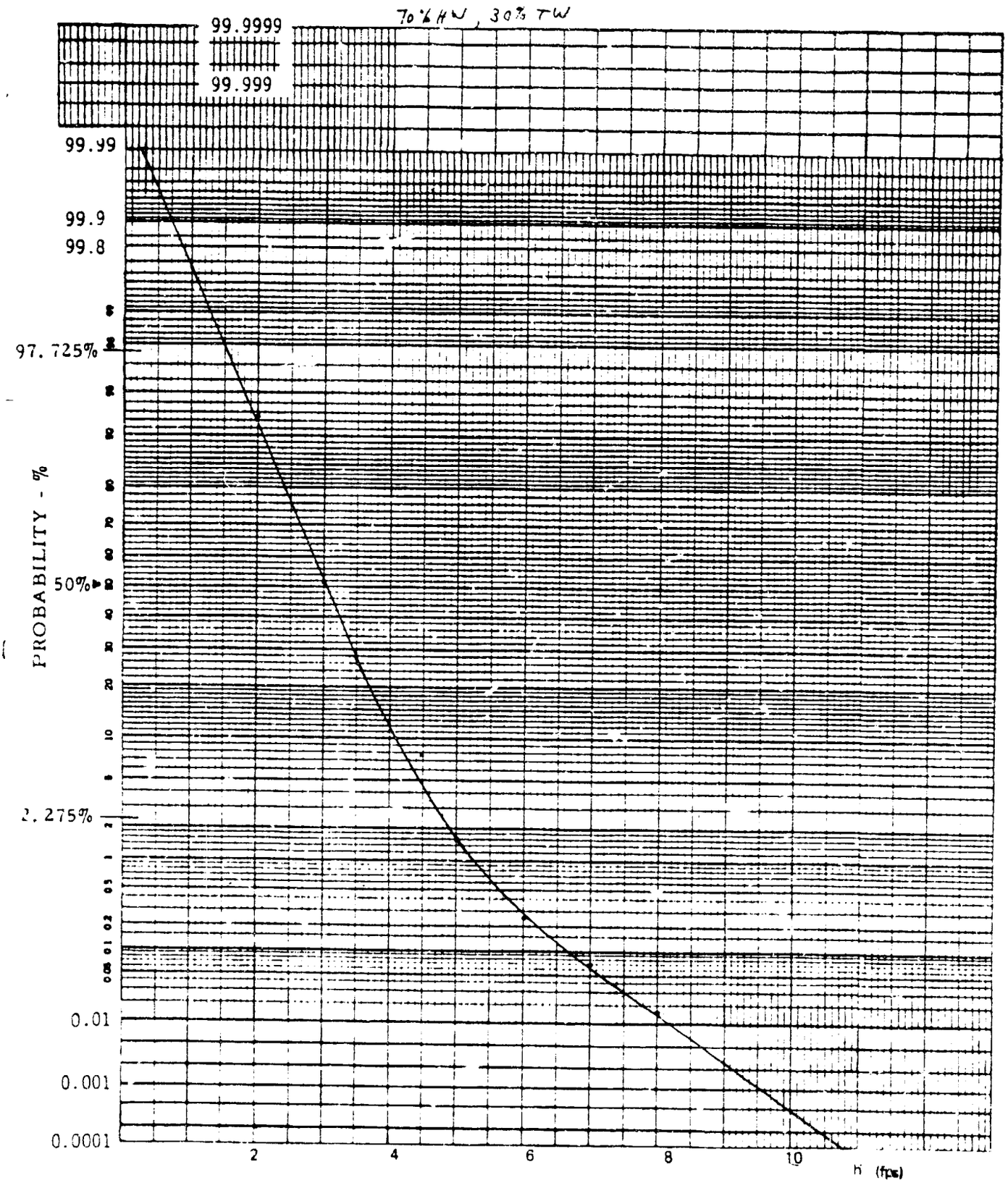

Figure B-21. Variable Flare Height, Spoilers

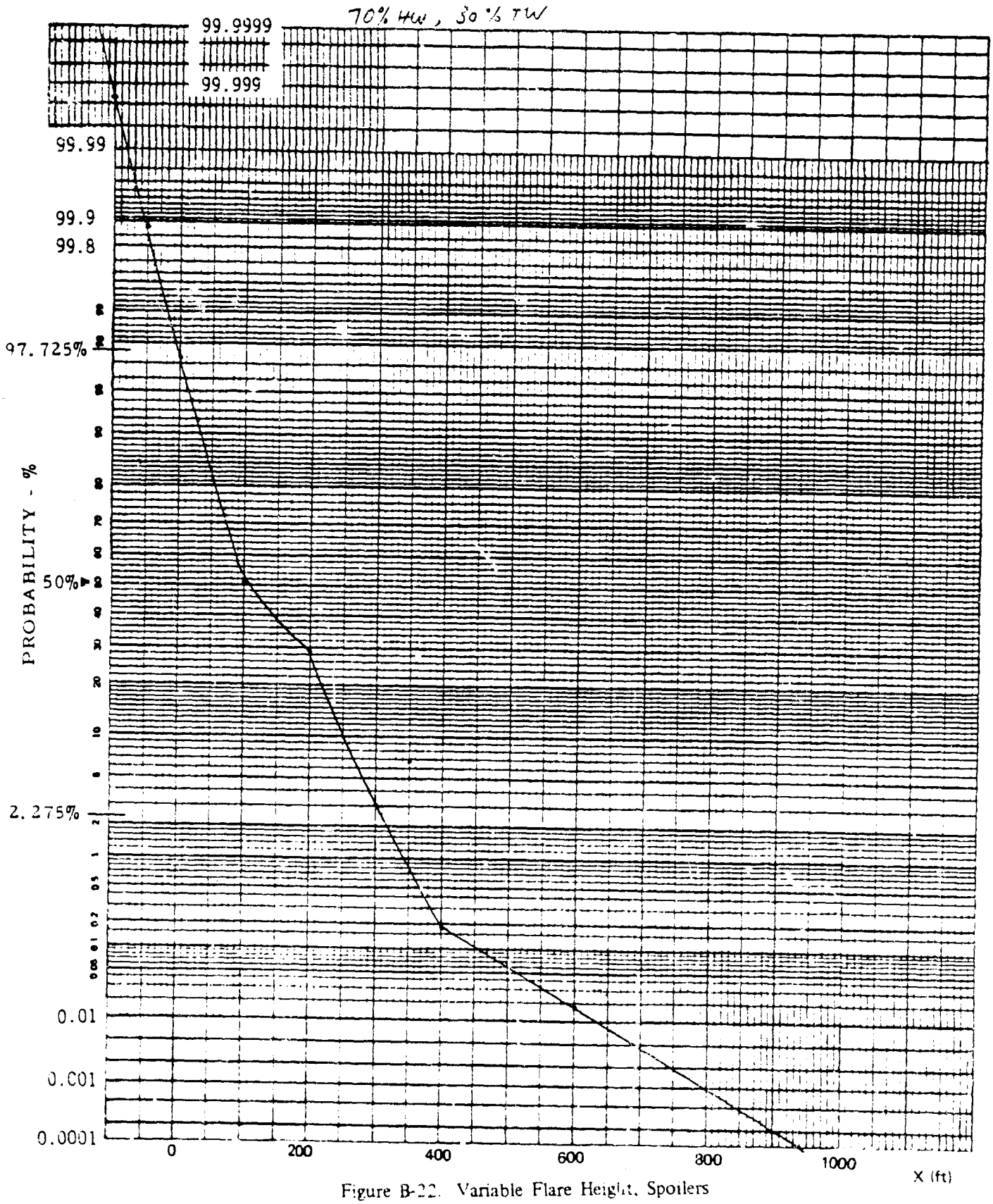

Figure B-22. Variable Flare Height, Spoilers

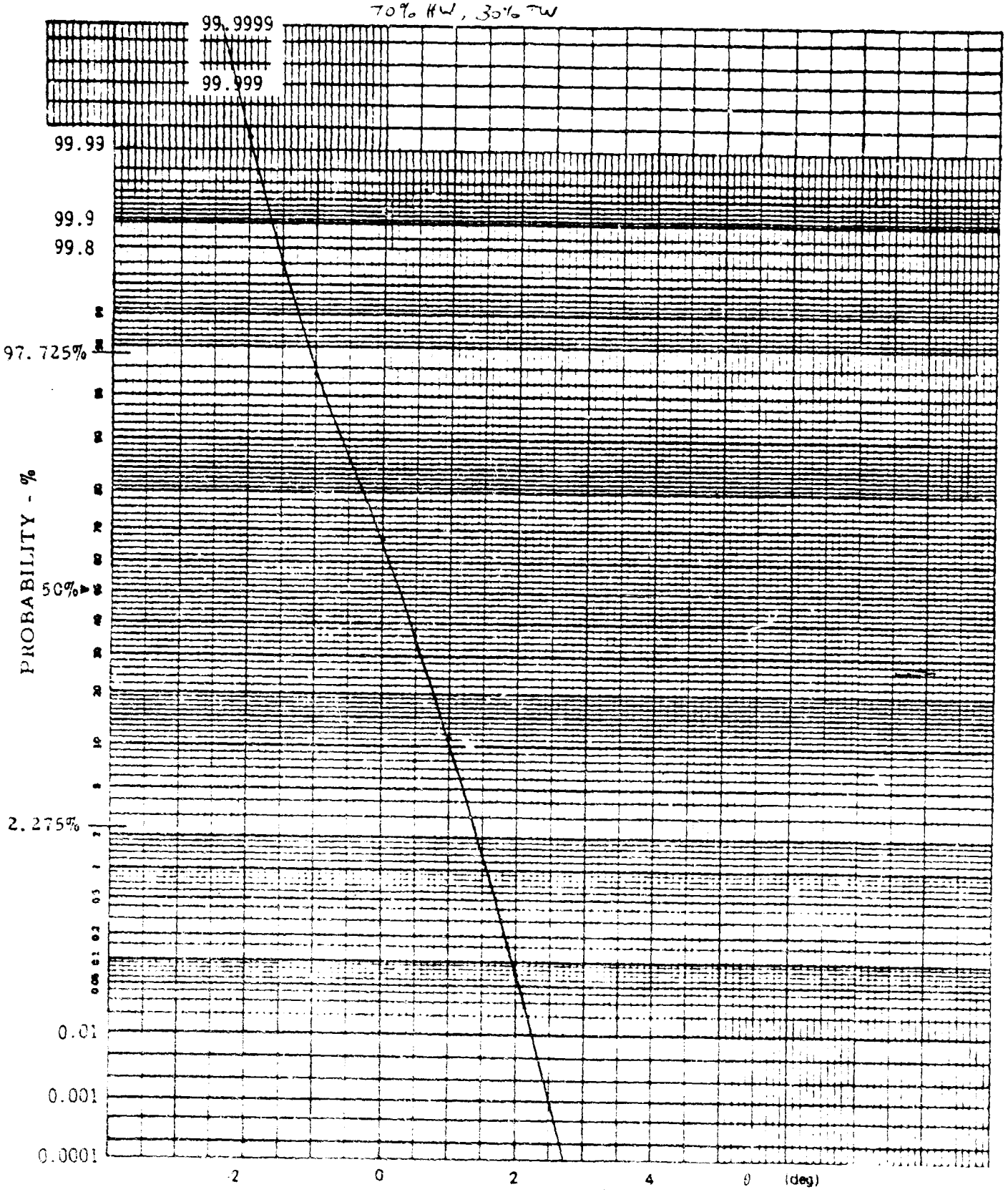

Figure B-23. Variable Flare Height Spoilers

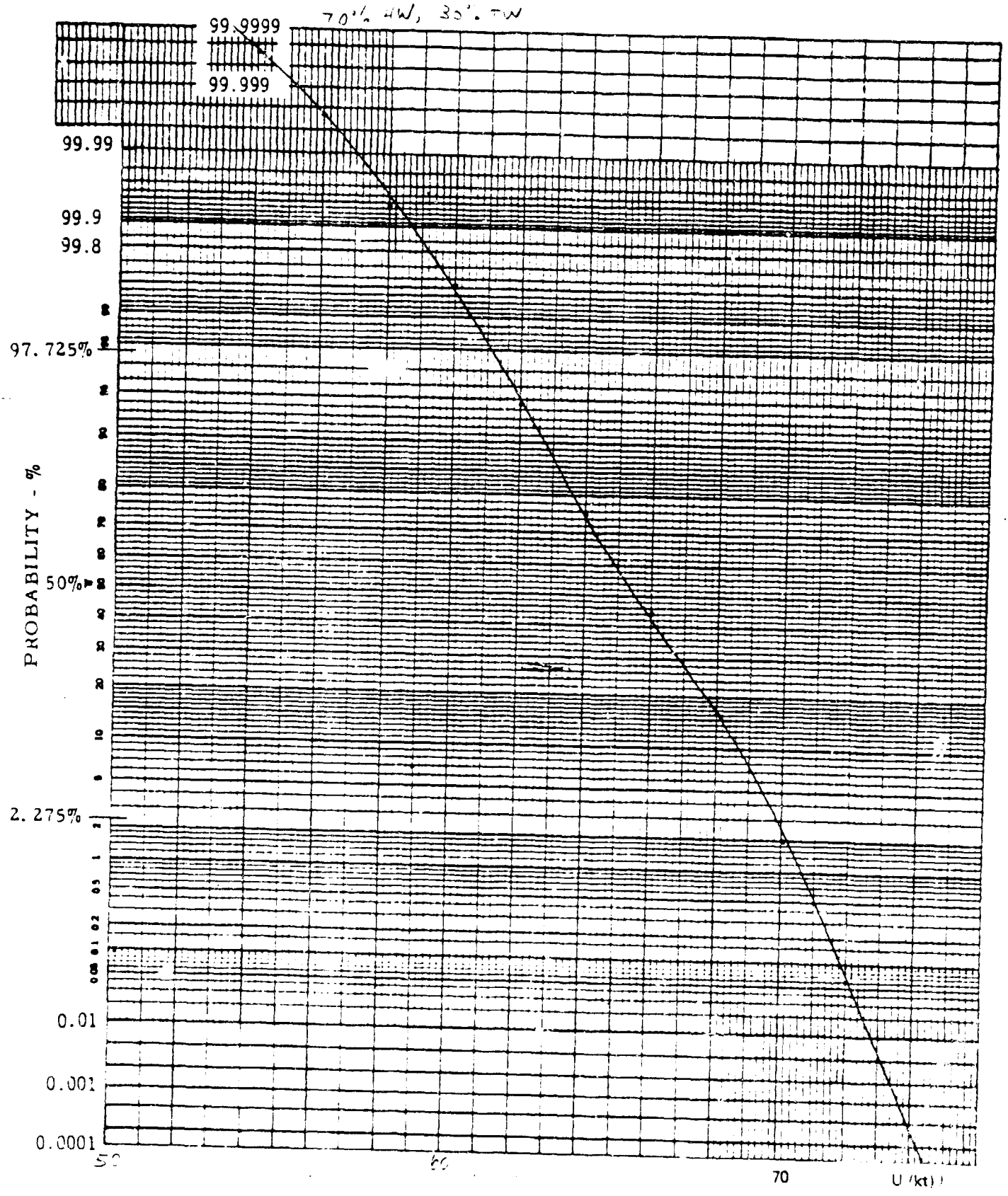

Figure B-24. Variable Flare Height, Spoilers

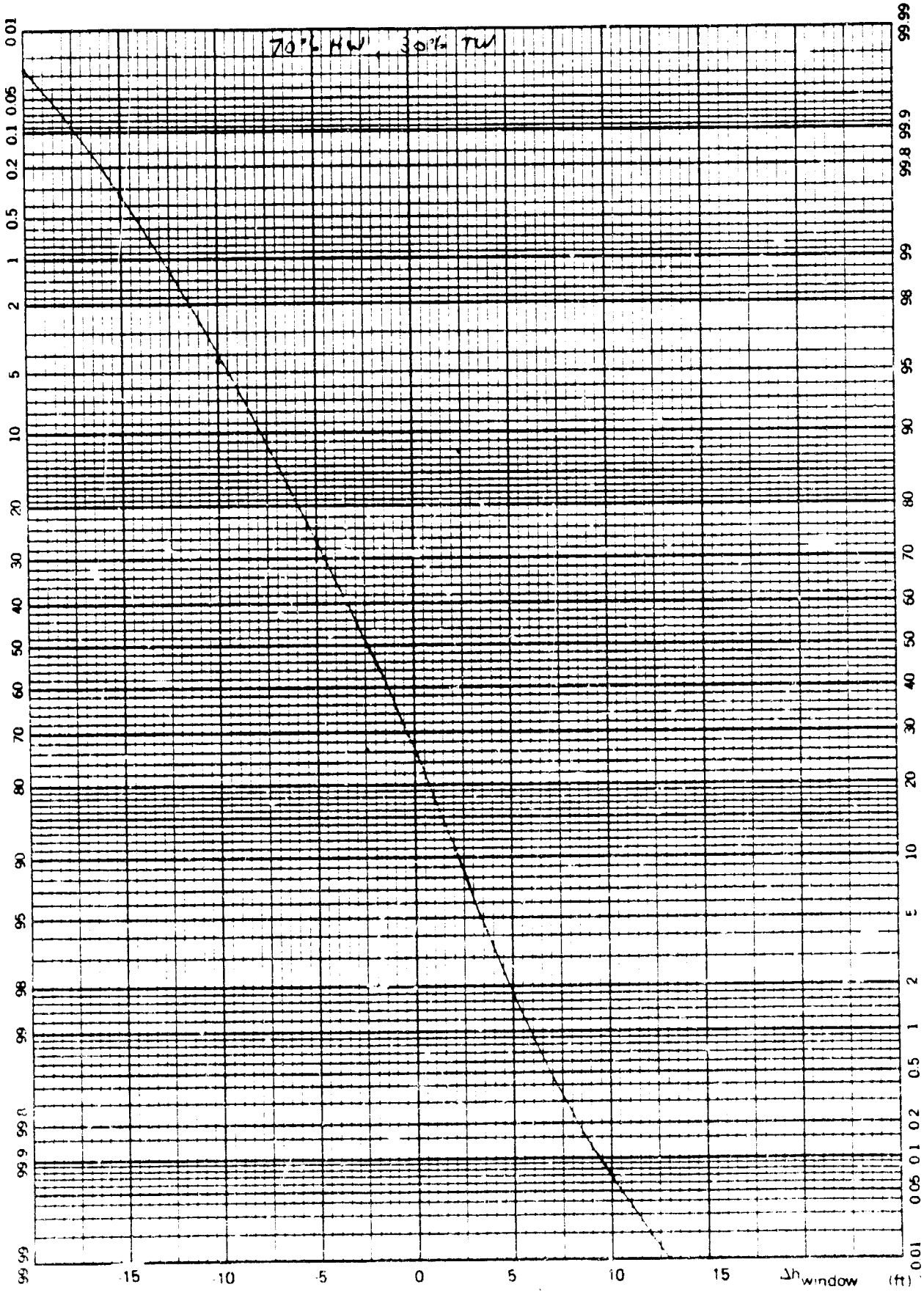

Figure B-25. Variable Flare Height, Spoilers

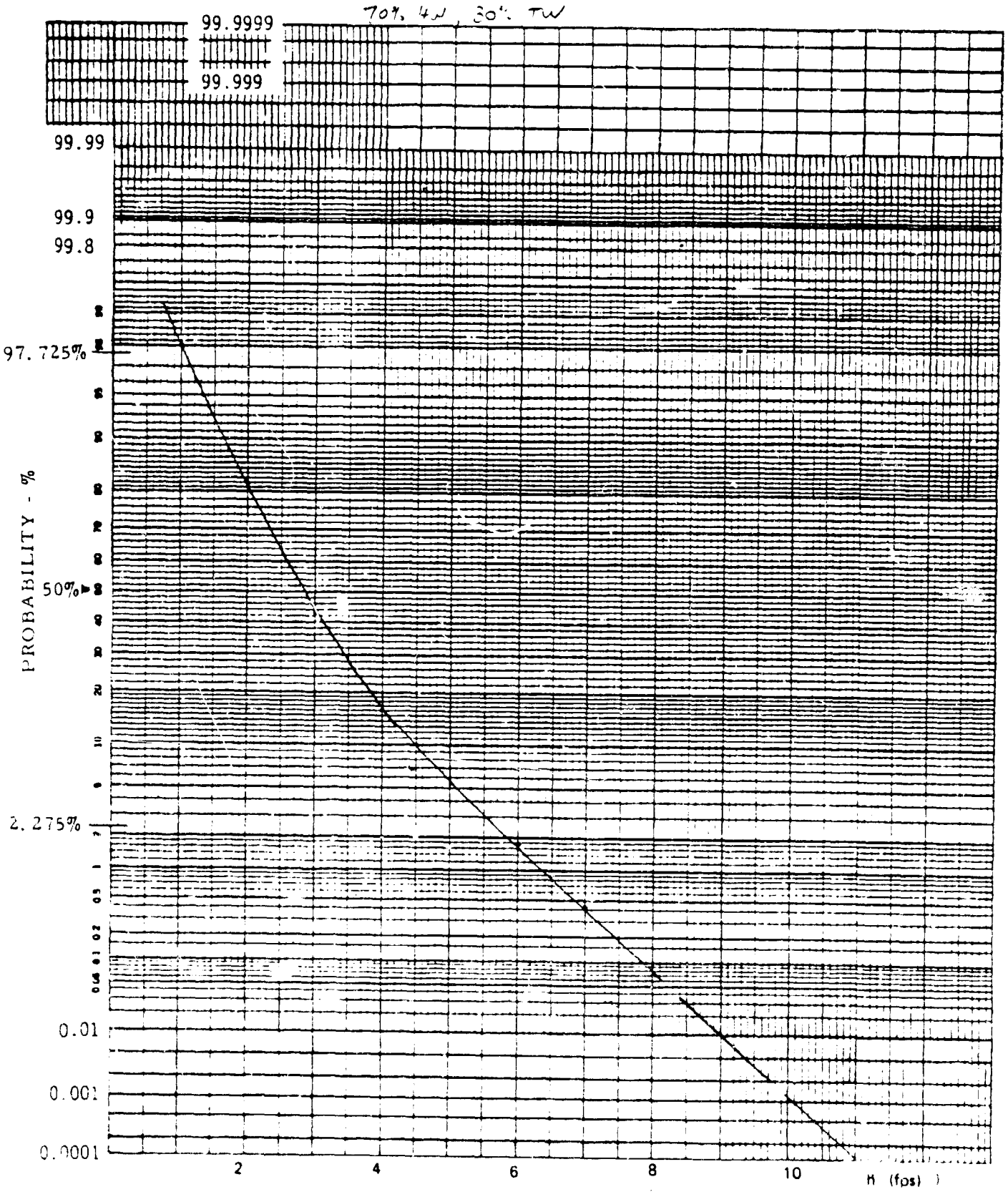

Figure B-26. Variable Flare Height, No Spoilers

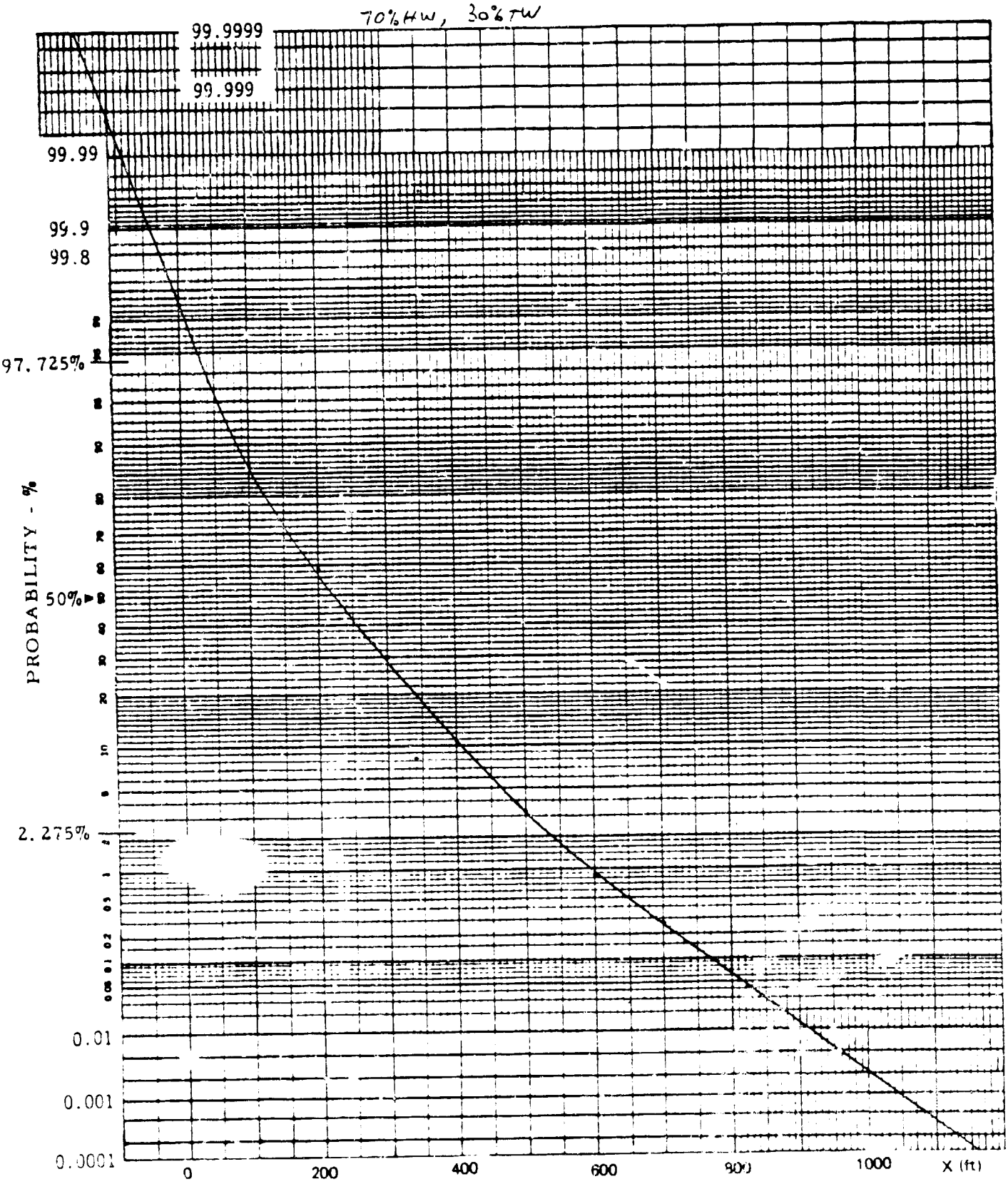

Figure B-27. Variable Flare Height, No Spoilers

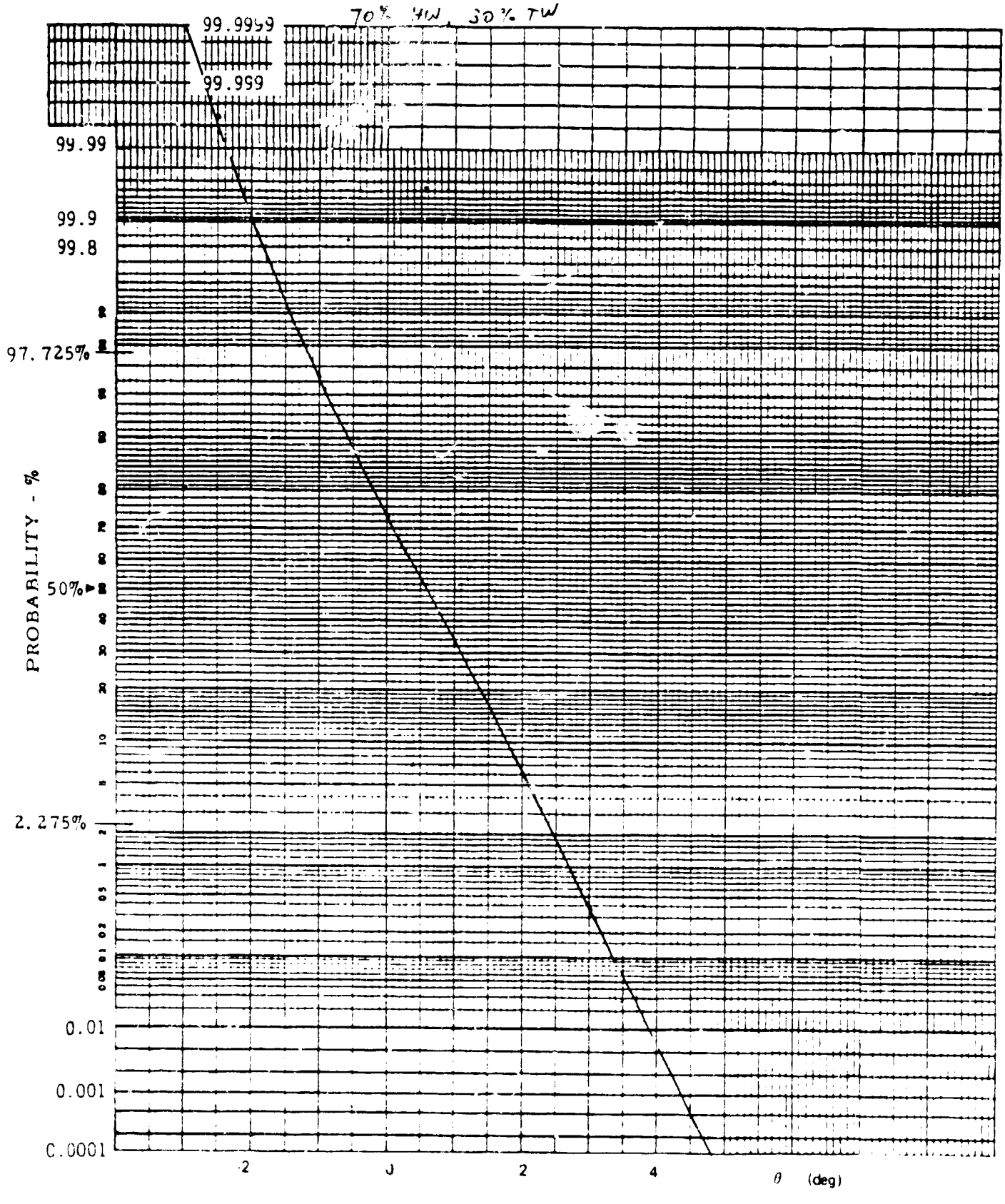

Figure B-28. Variable Flare Height, No Spoilers

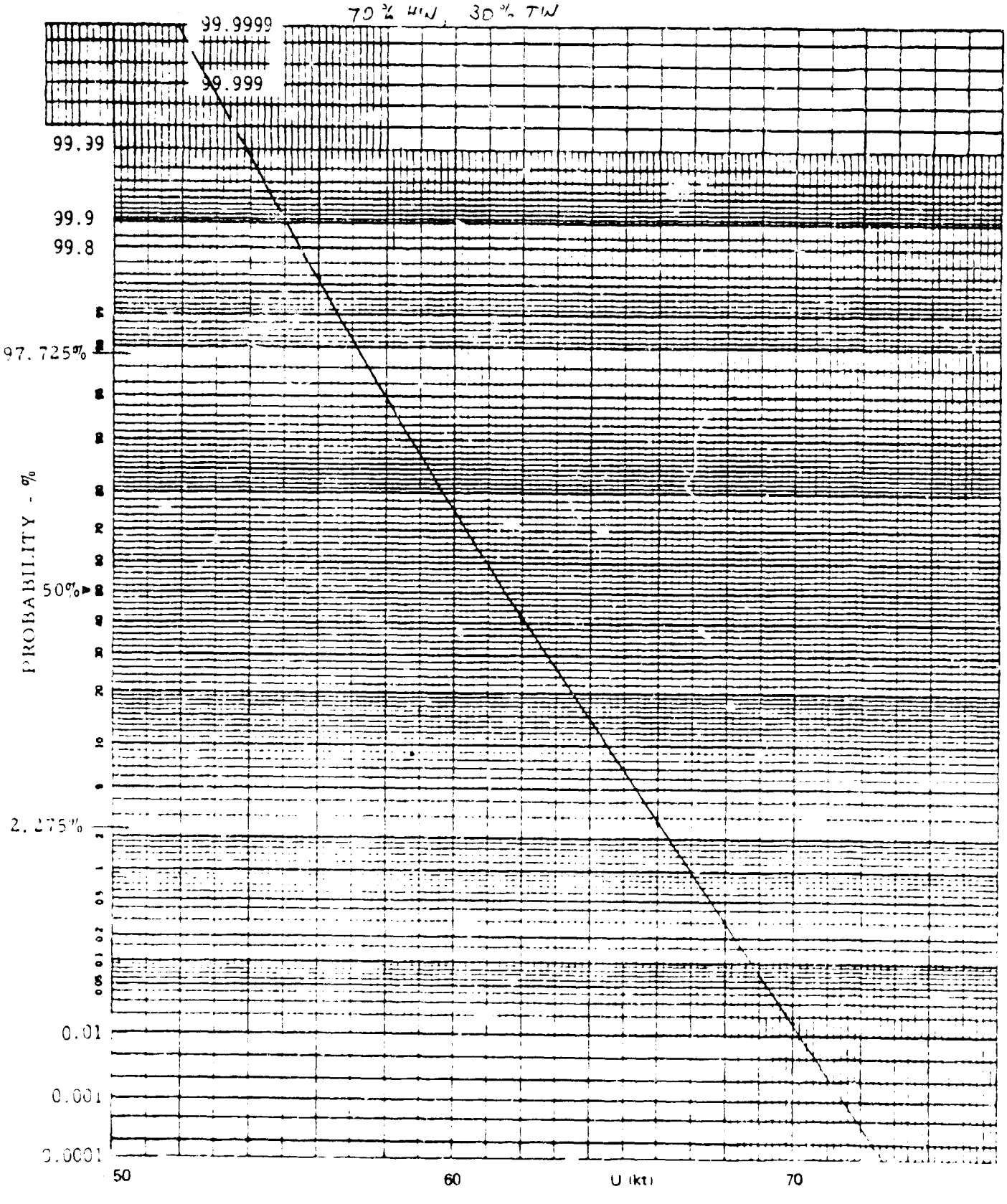

Figure B-29 Variable Flare Height, No Spoilers

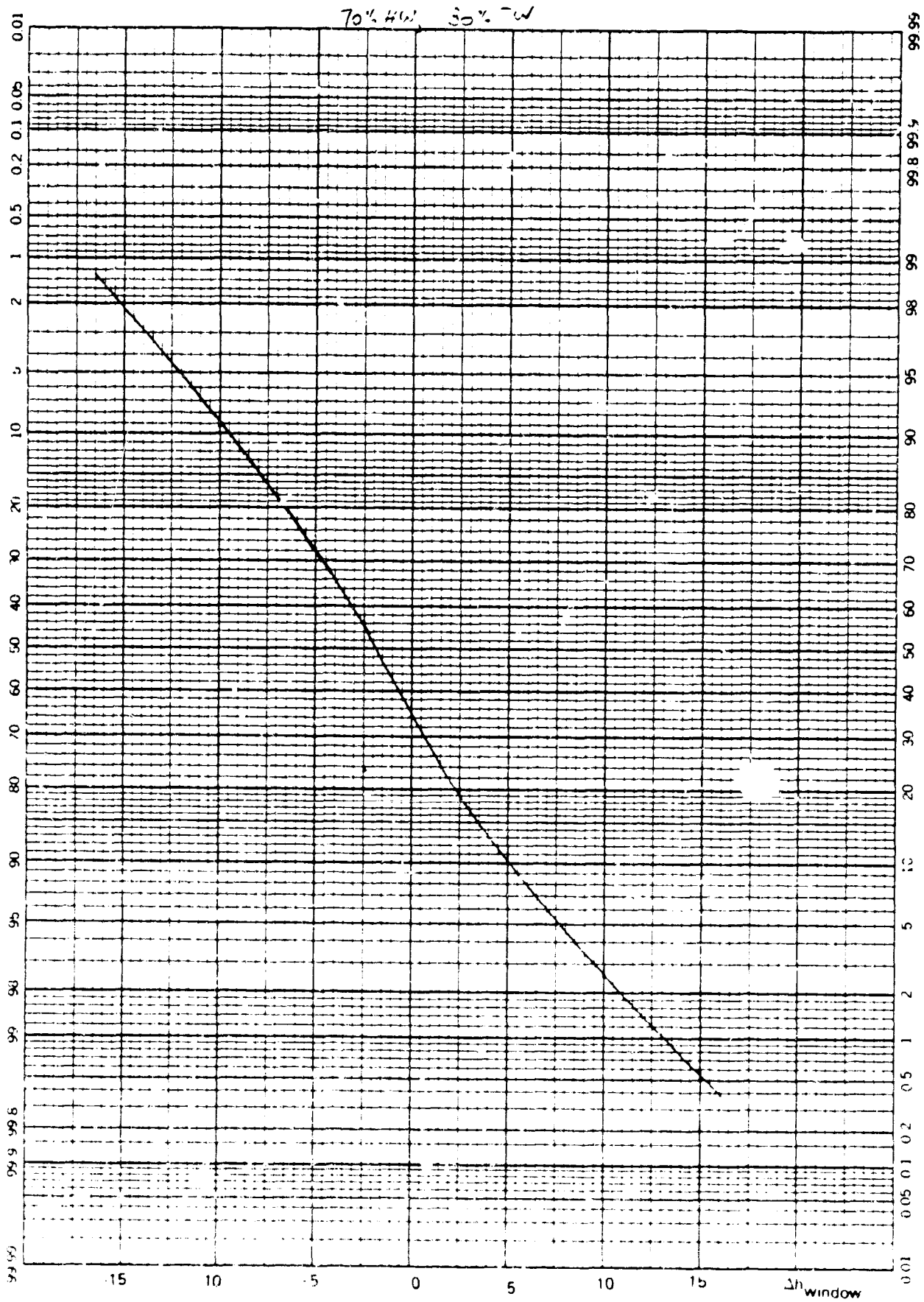

Figure B-30. Variable Flare Height, No Spoilers

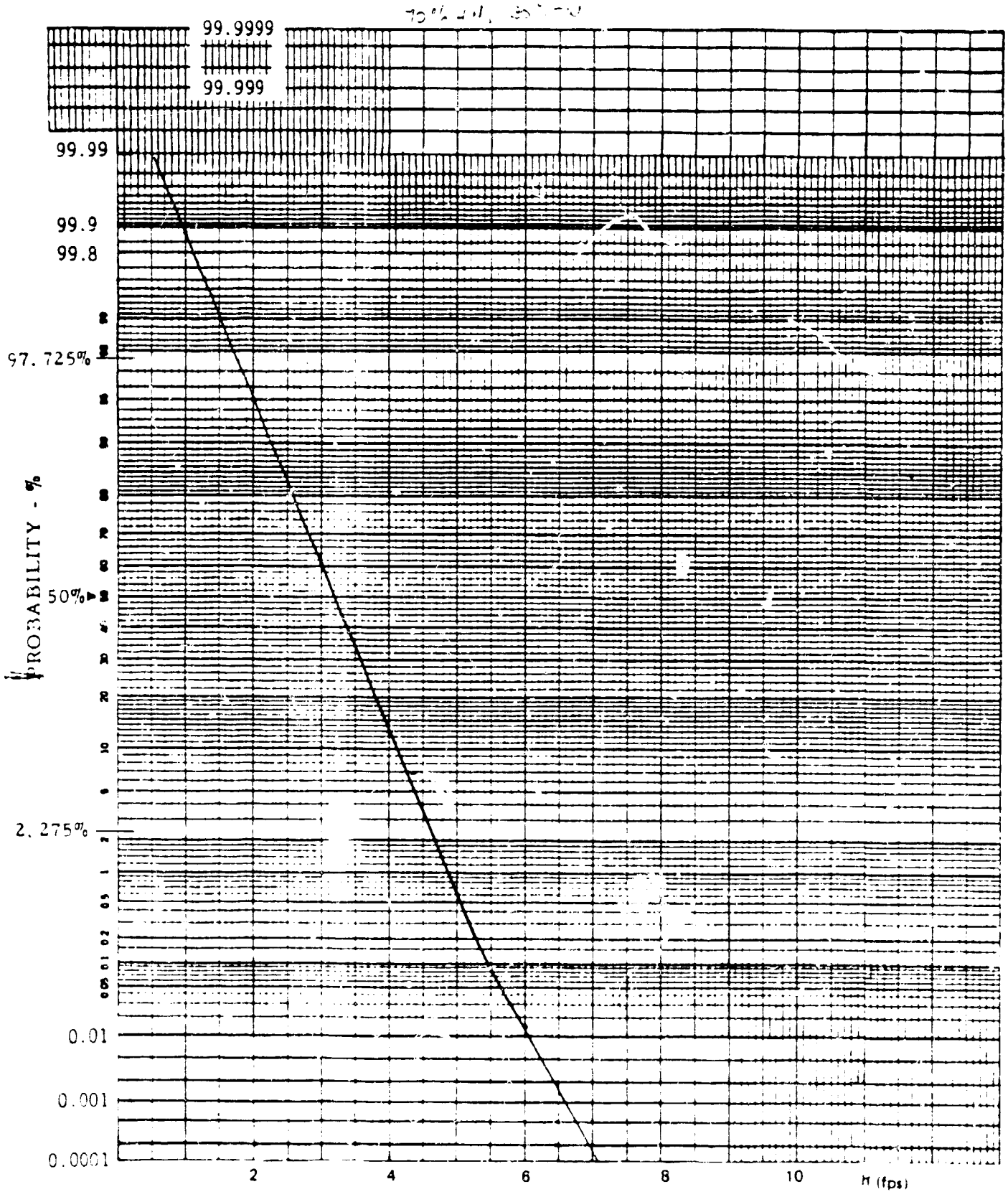

Figure B-31. Constant Flare Height, Low Gains Spoilers

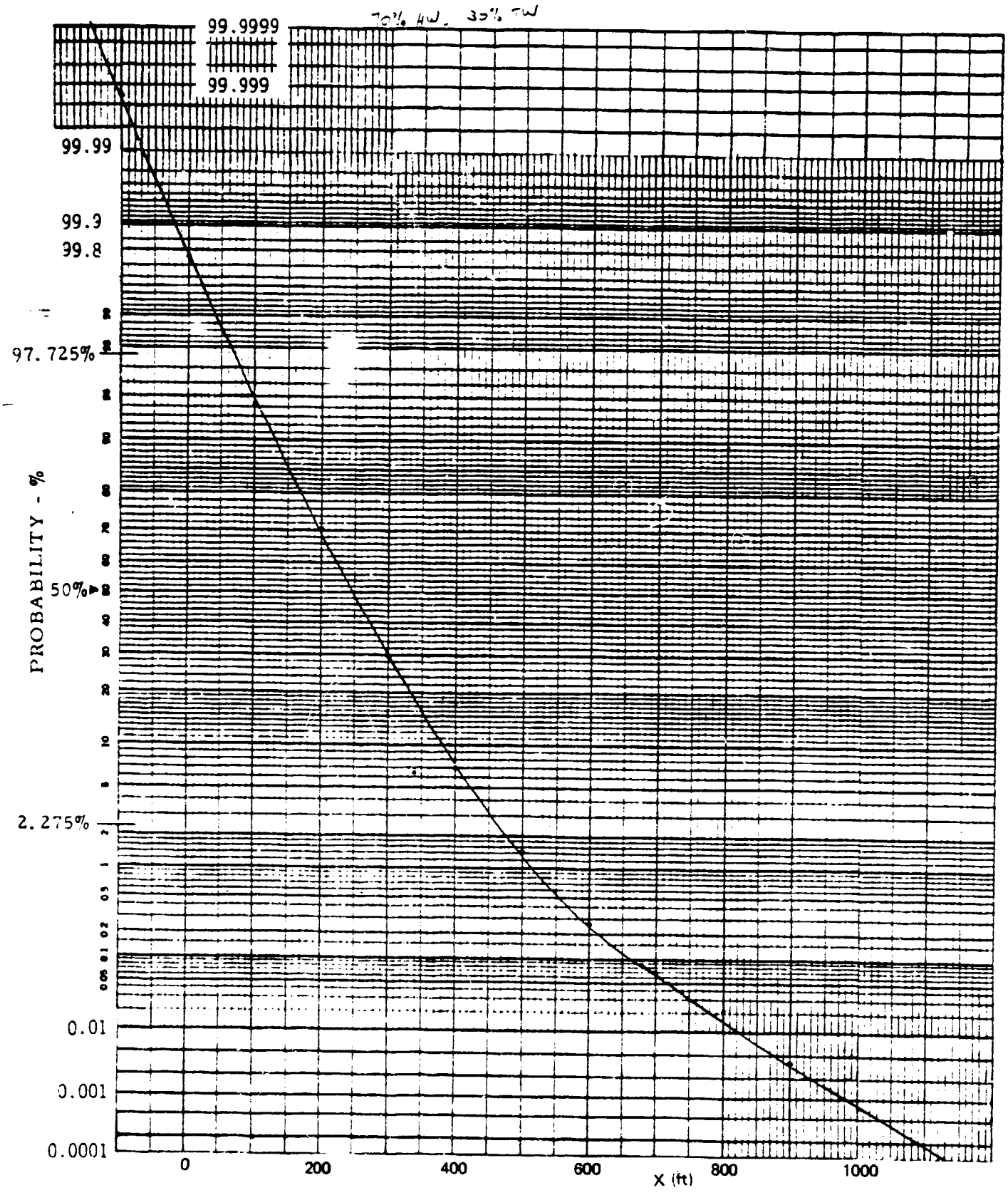

Figure B-32. Constant Flare Height, Low Gains, Spoilers

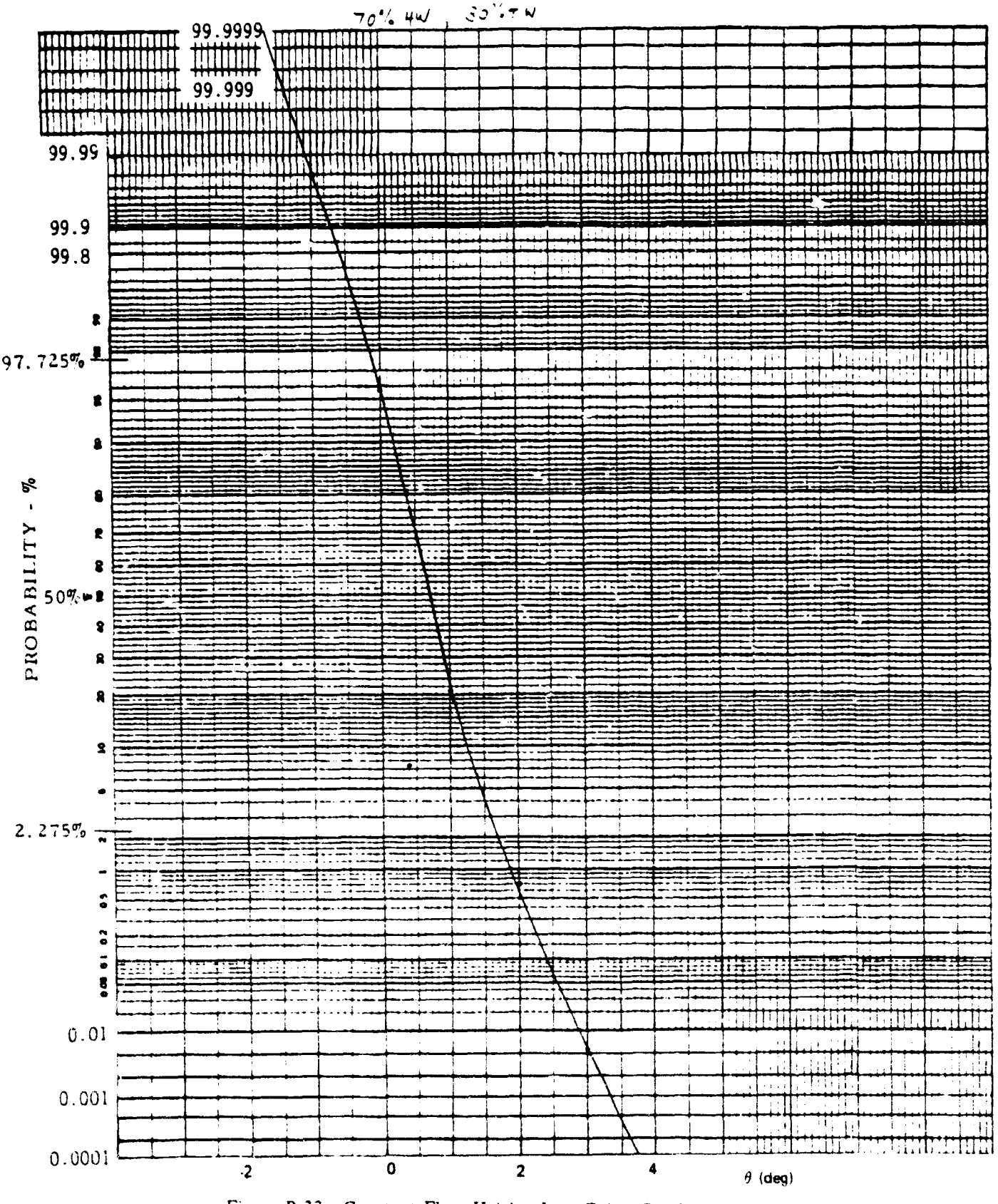

Figure B-33. Constant Flare Height, Low Gains, Spoilers

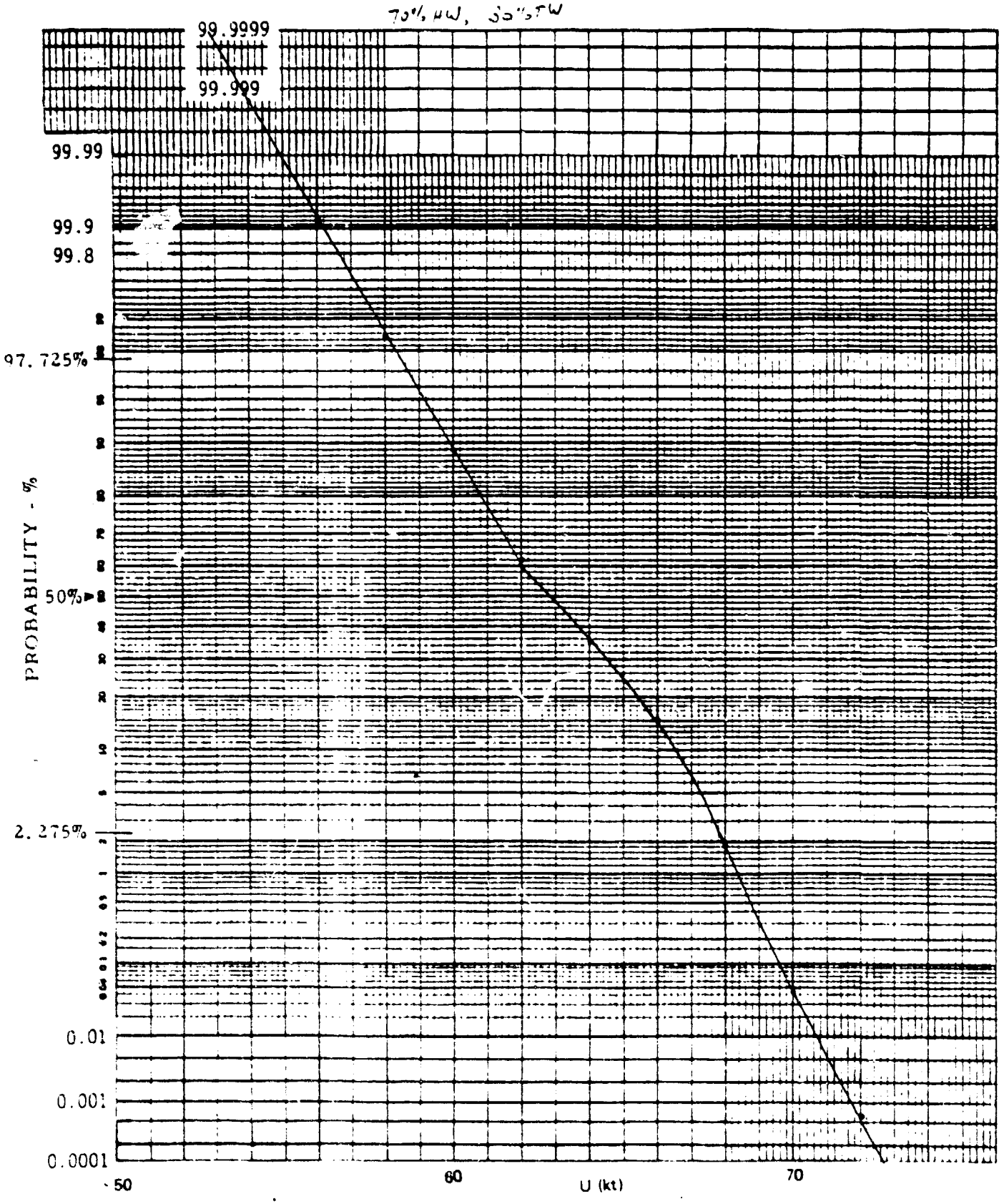

Figure B-34. Constant Flare Height, Low Gains, Spoilers

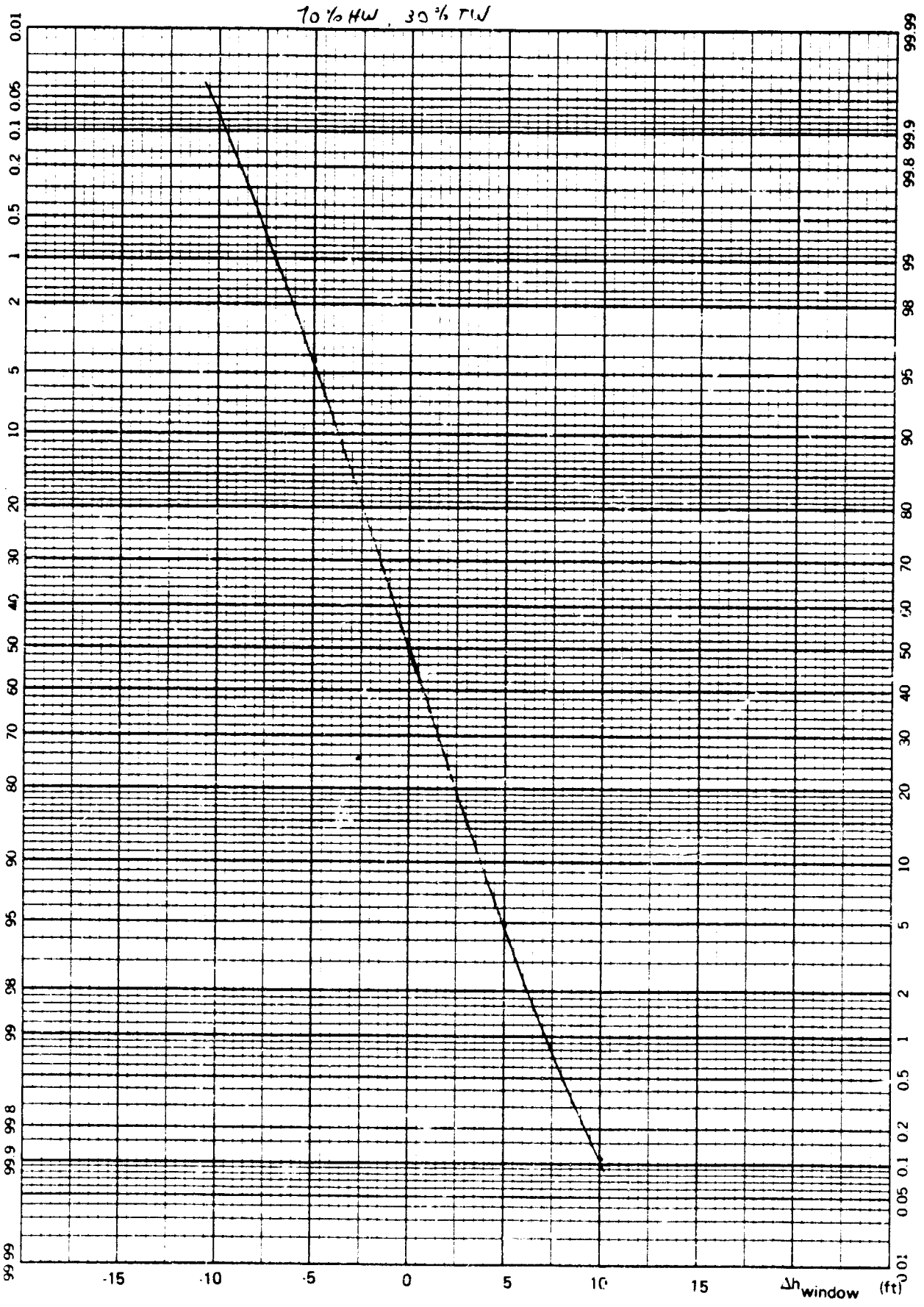

Figure B-35. Constant, Flare Height, Low Gains, Spoilers

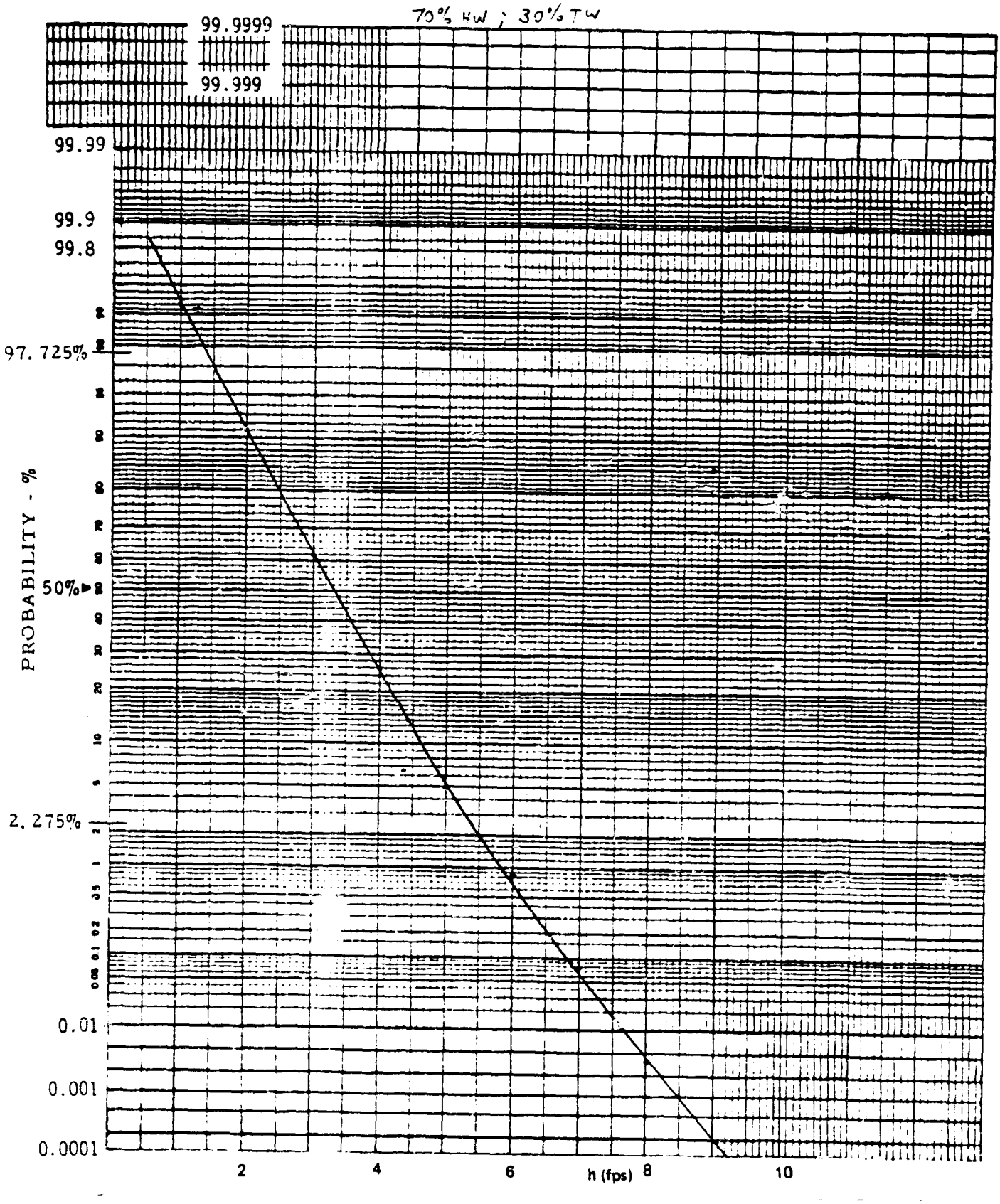

Figure B-36. Constant Flare Height, Low Gains, No Spoilers

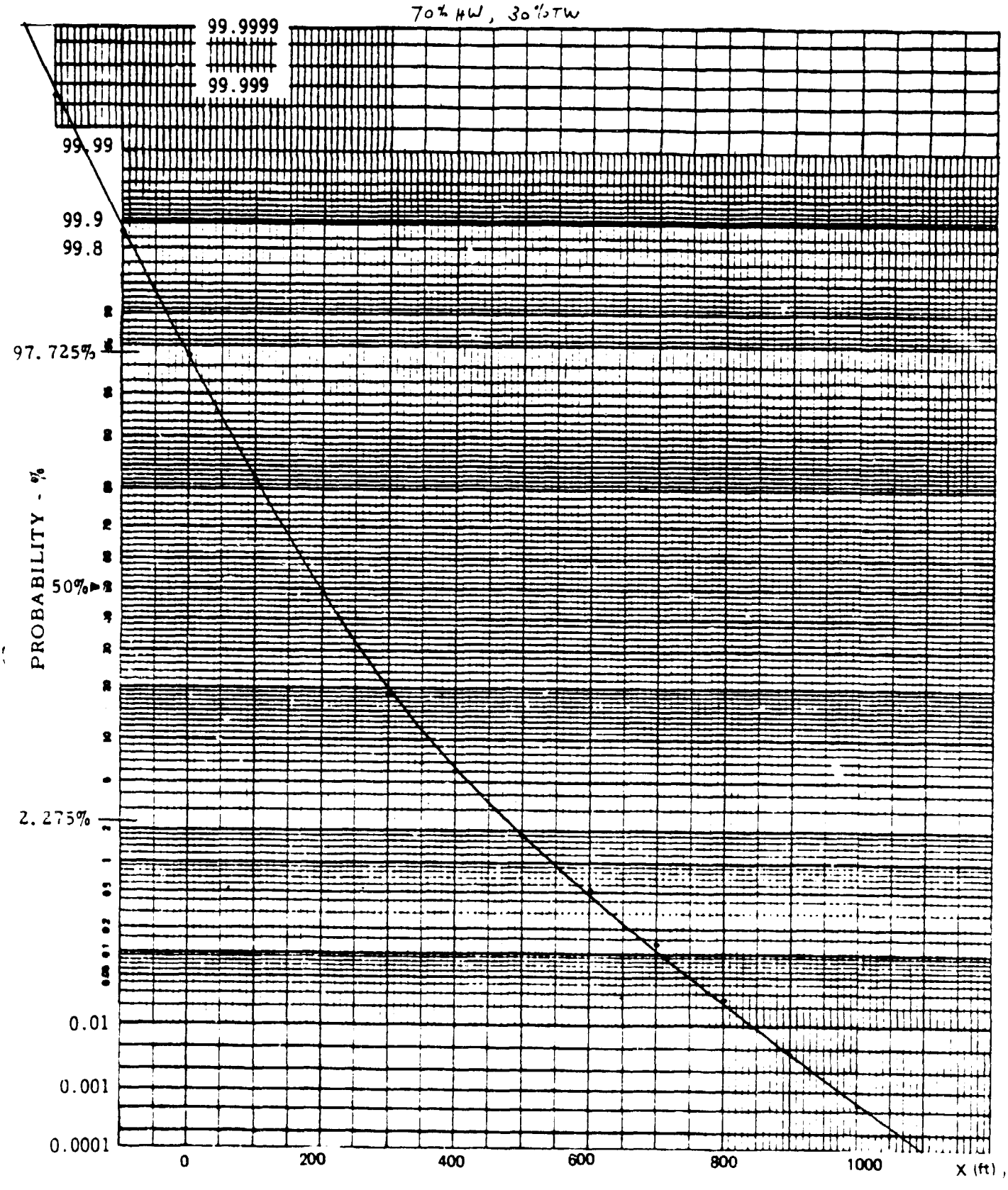

Figure B-37. Constant Flare Height, Low Gains, No Spoilers

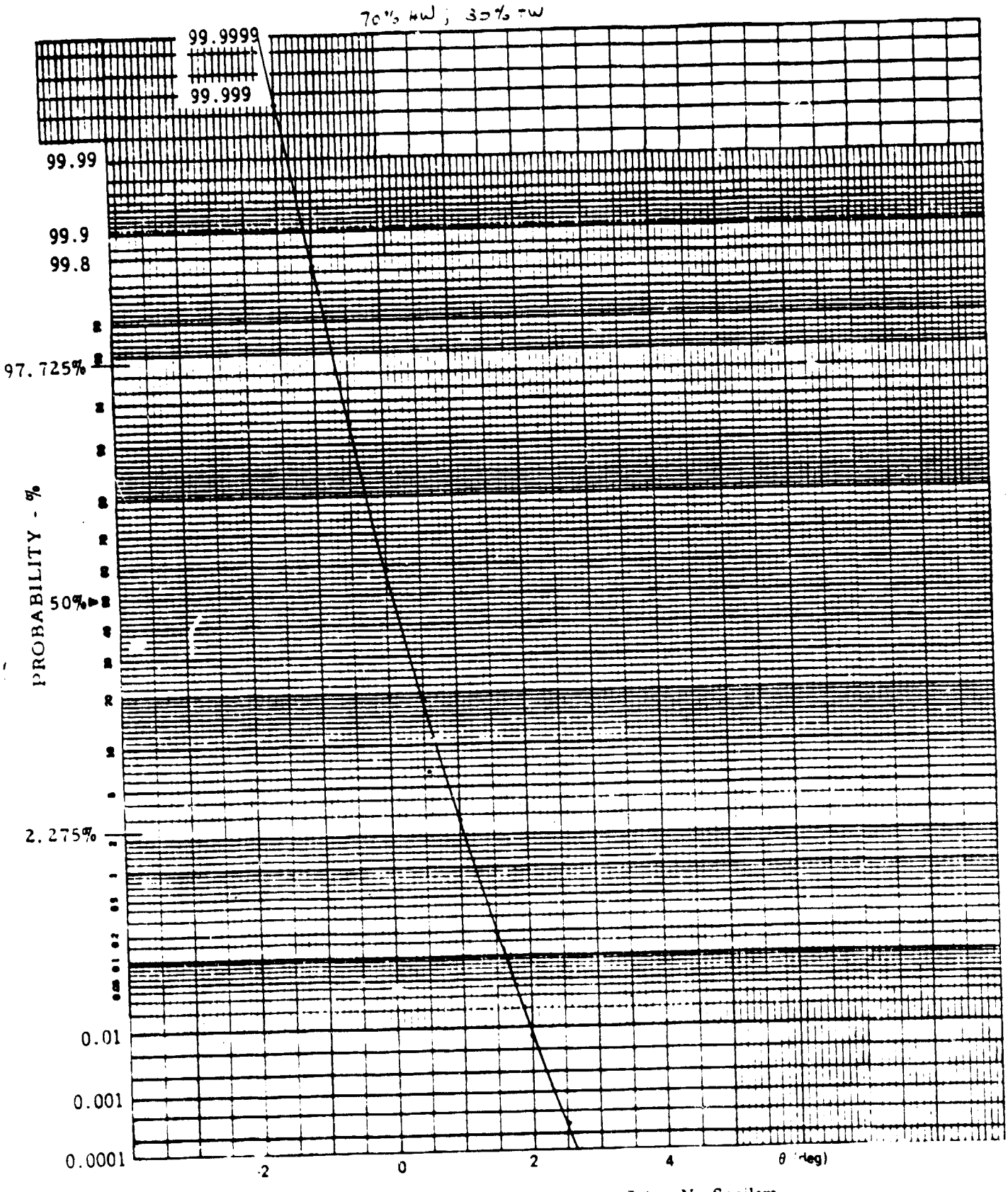

Figure B-38. Constant Flare Height, Low Gains, No Spoilers

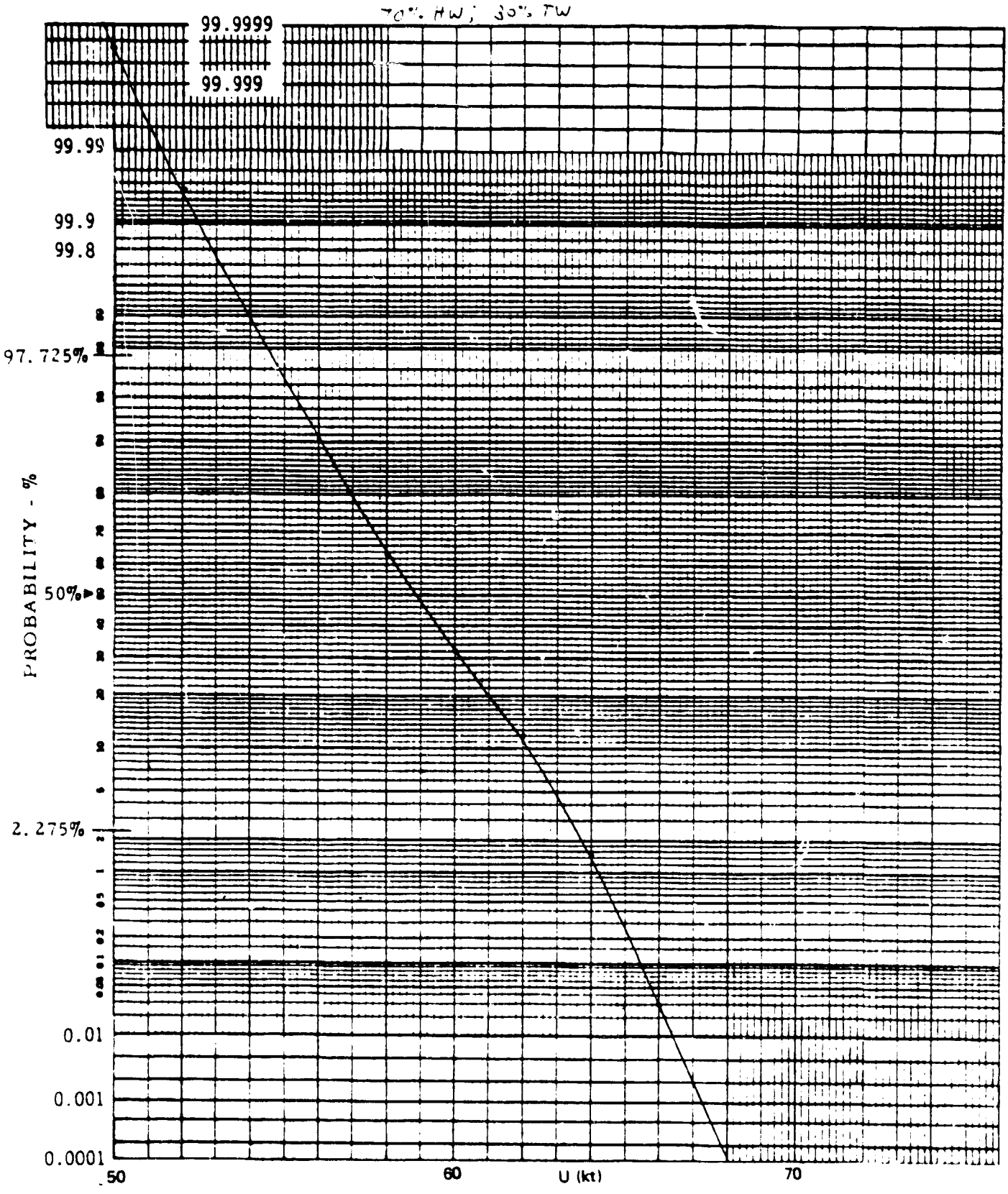

Figure B-39. Constant Flare Height, Low Gains, No Spoilers

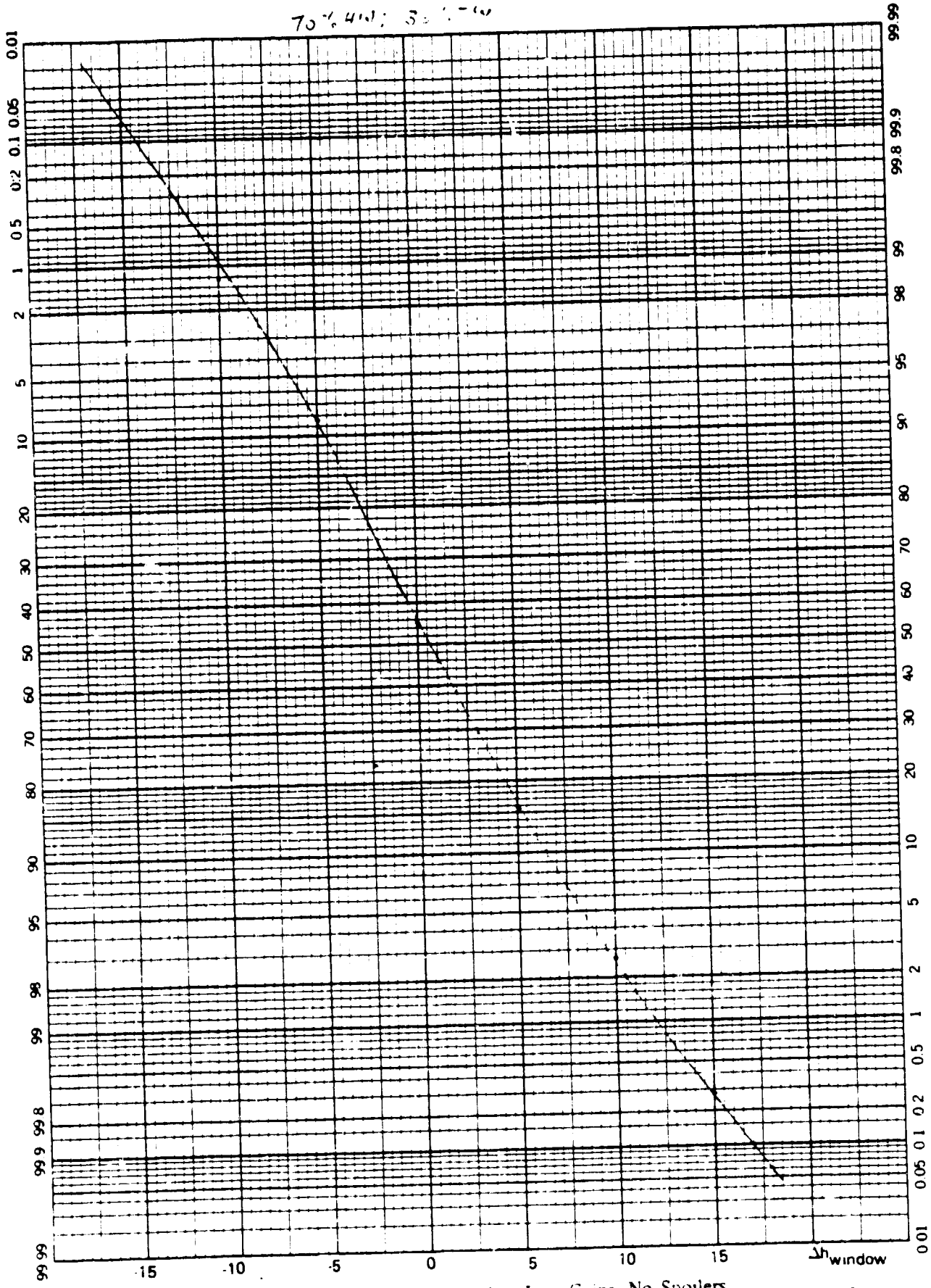

Figure B-40. Constant Flare Height, Low Gains, No Spoilers

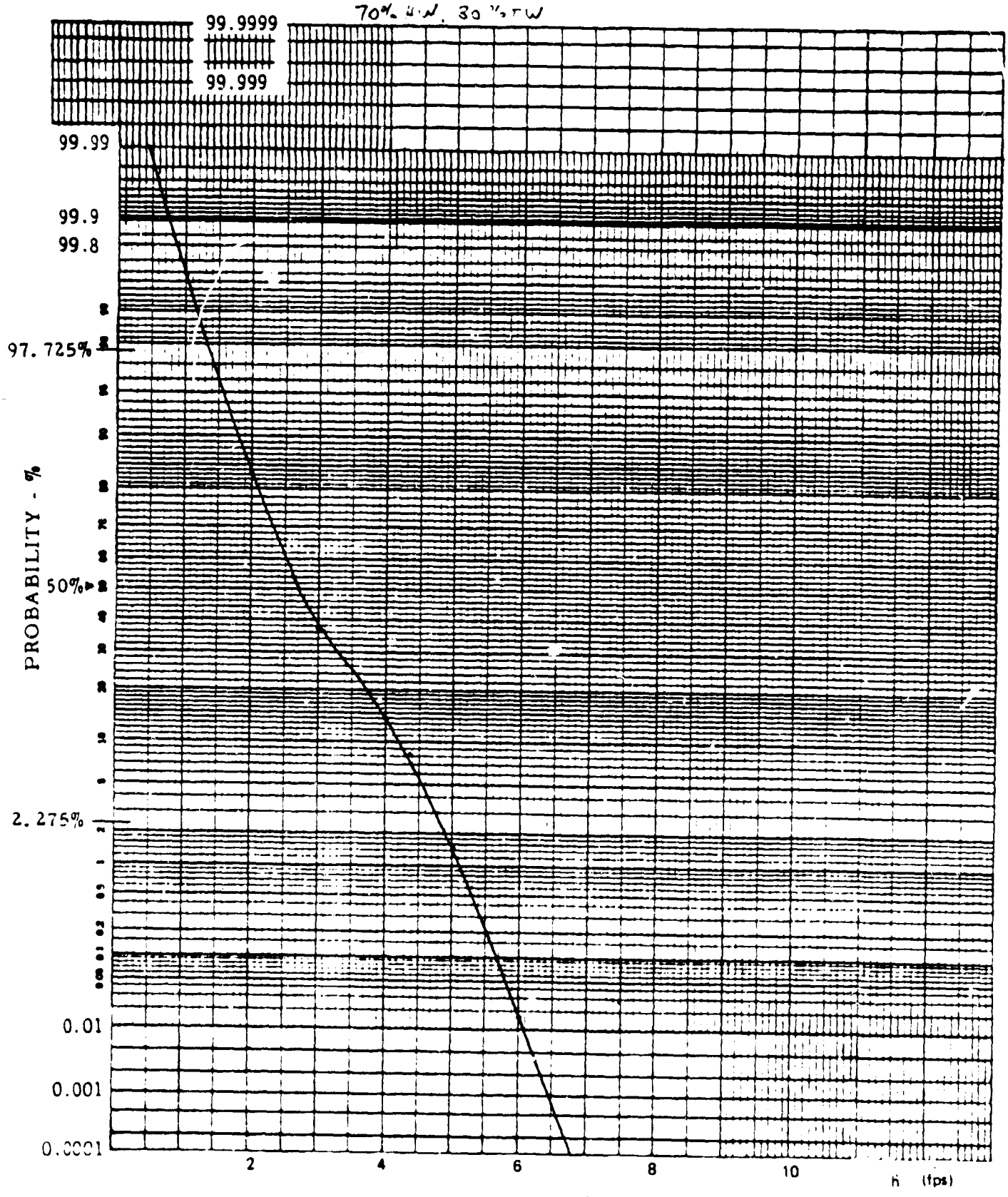

Figure 3-41. Constant Flare Height, High Gains, Spoilers

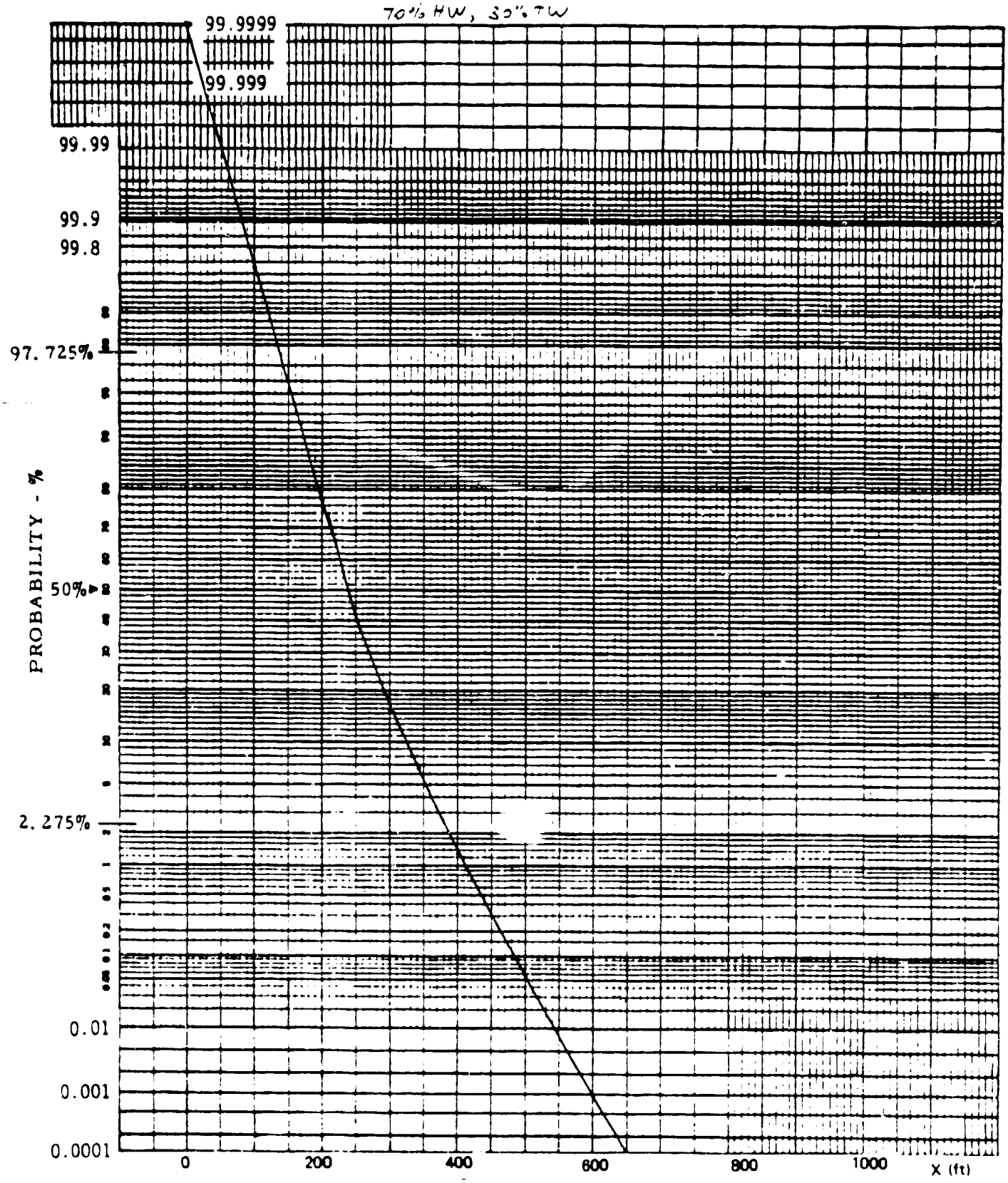

Figure B-42. Constant Flare Height, High Gains, Spoilers

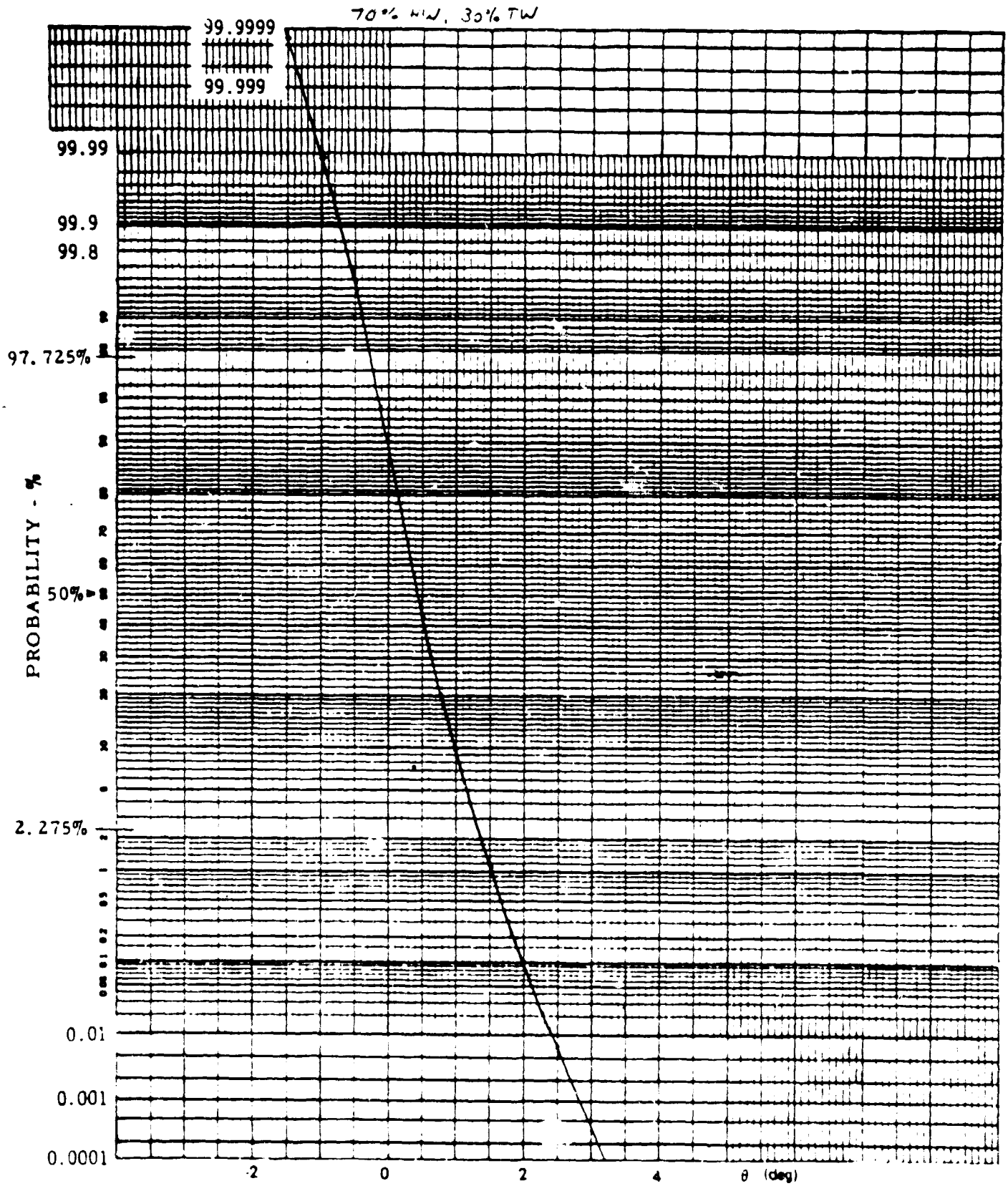

Figure B-43. Constant Flare Height with Spoilers, High Gains

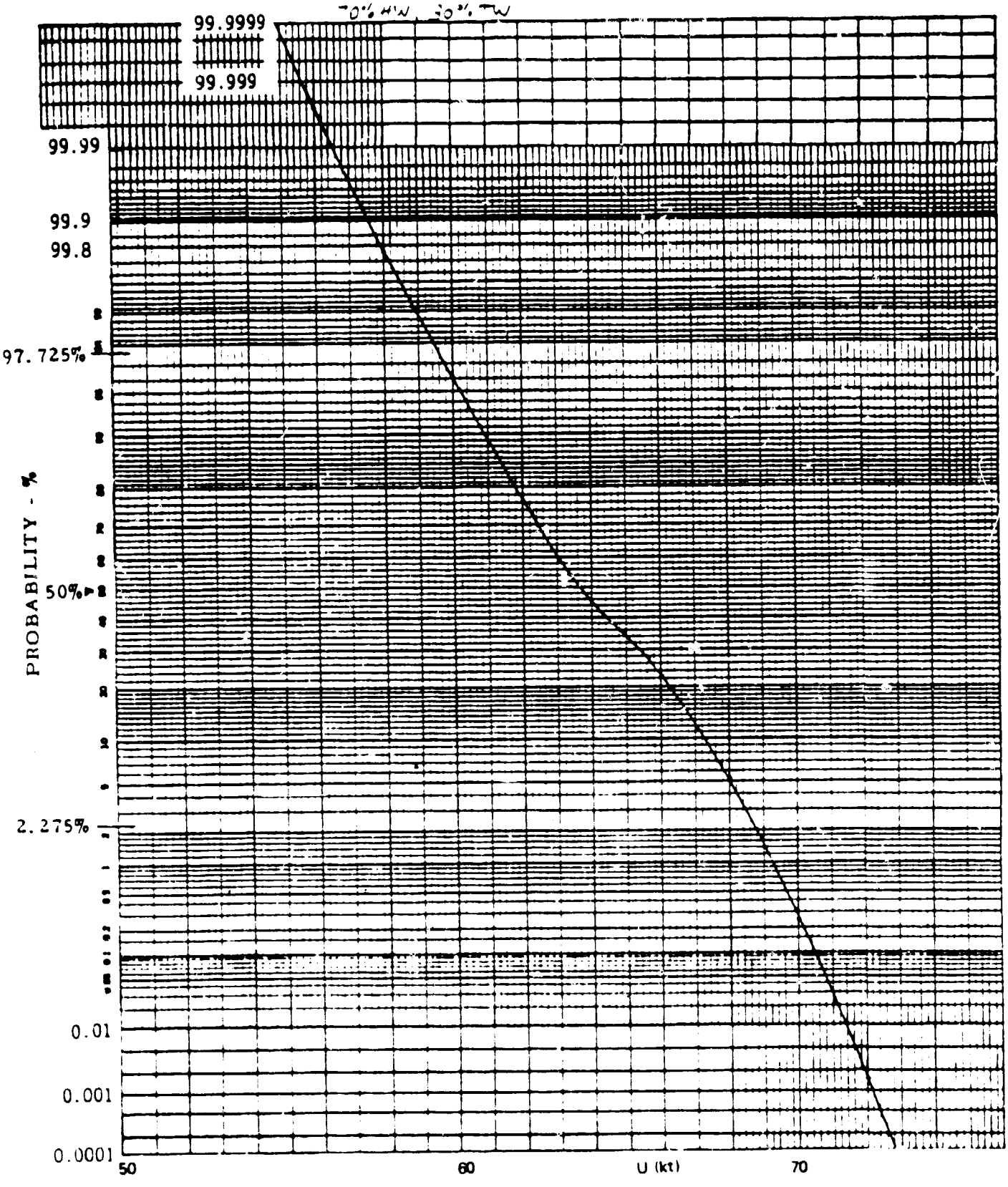

Figure B-44. Constant Flare Height with Spoilers, High Gains

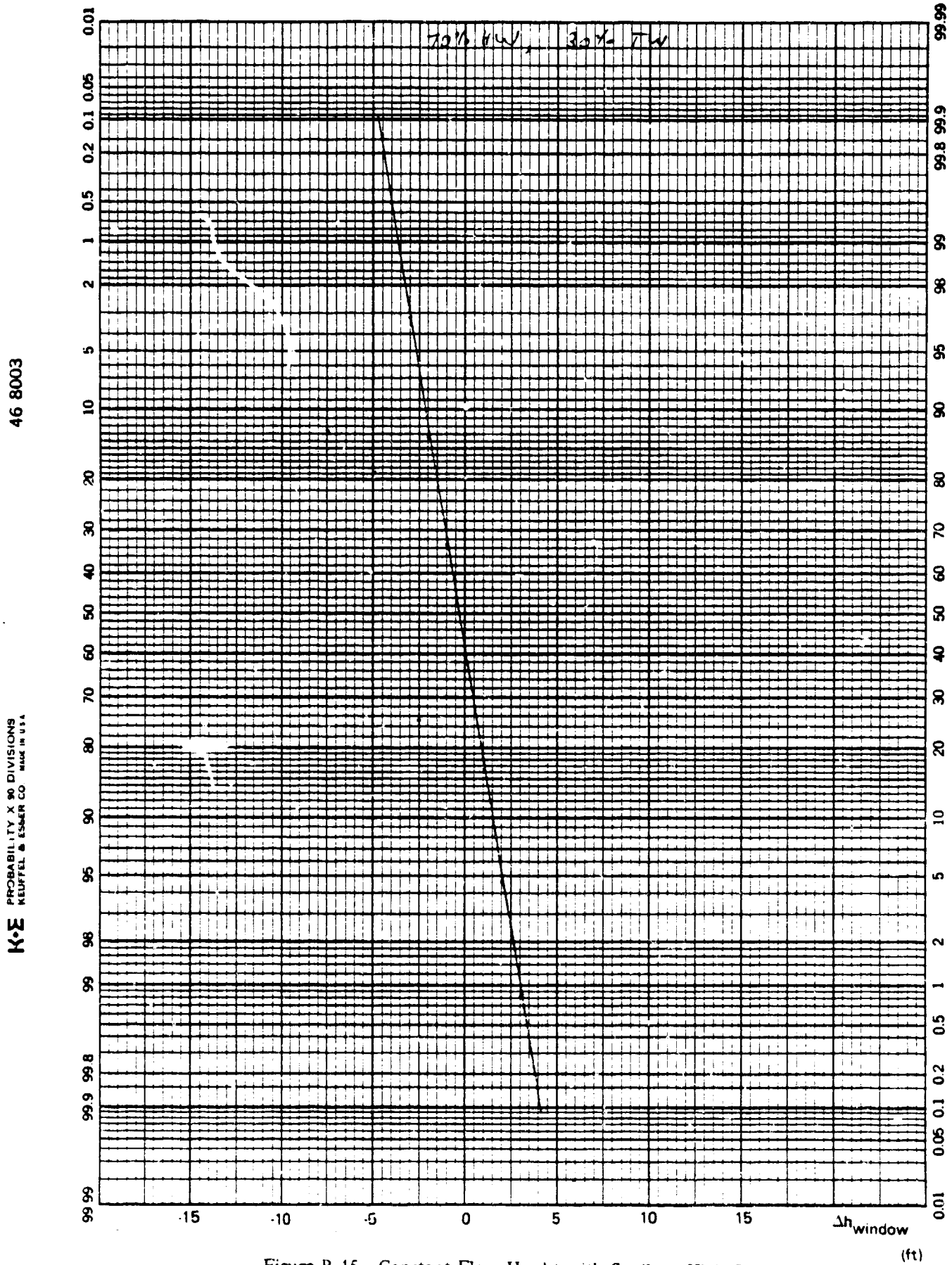

Figure B-45. Constant Flare Height with Spoilers, High Gain

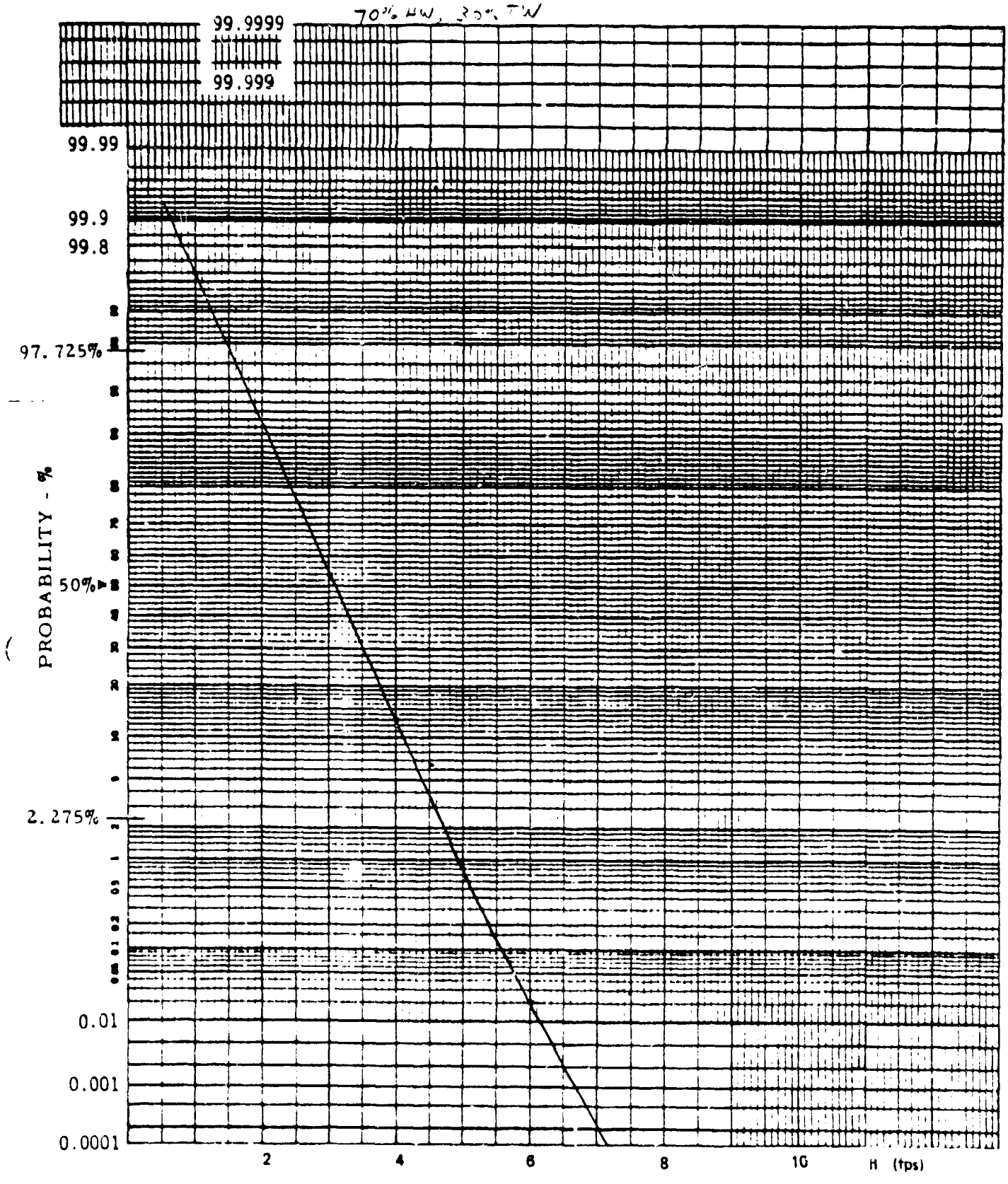

Figure B-46. Constant Flare Height, No Spoilers, High Gains

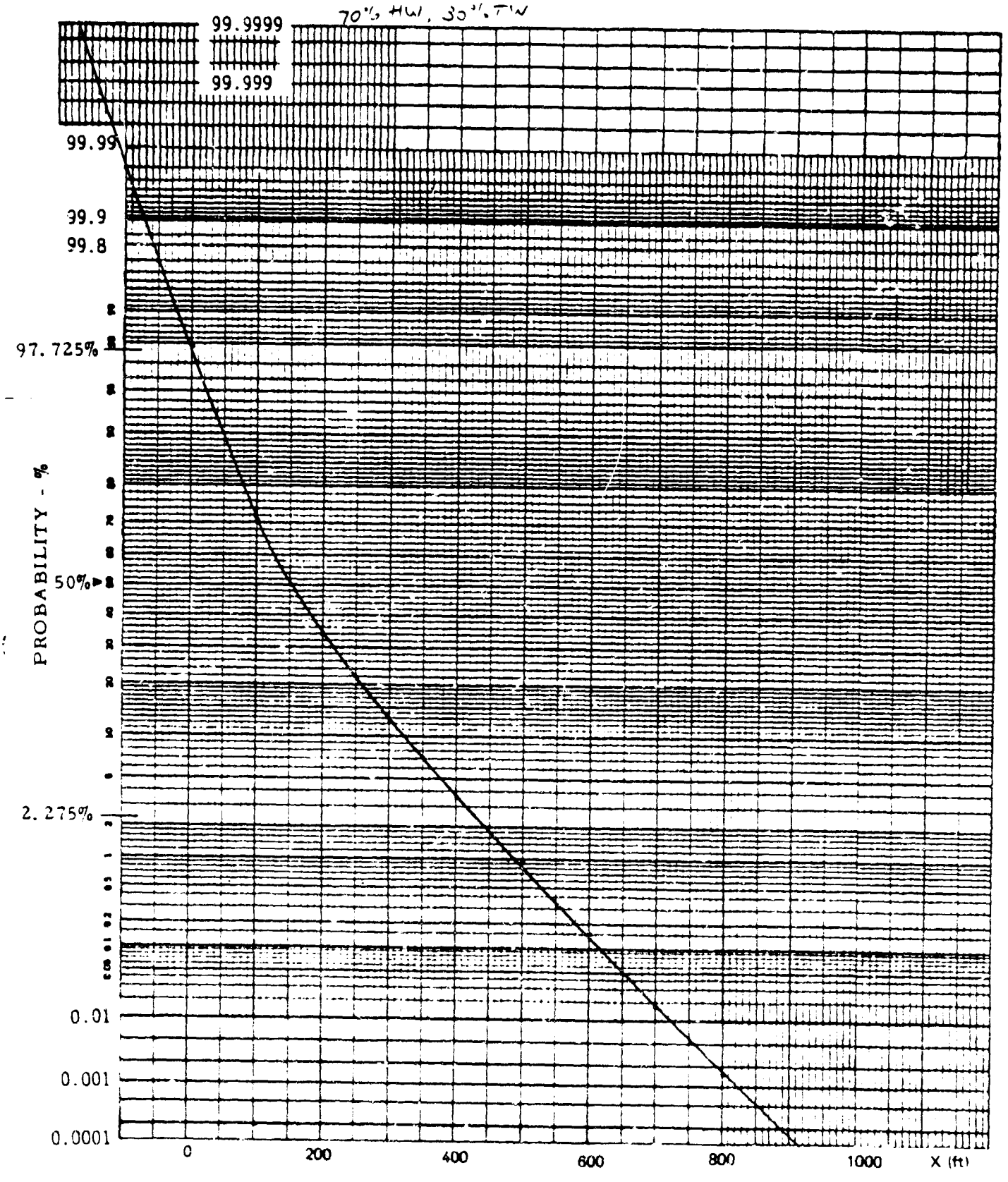

Figure B-47. Constant Flare Height, No Spoilers, High Gains

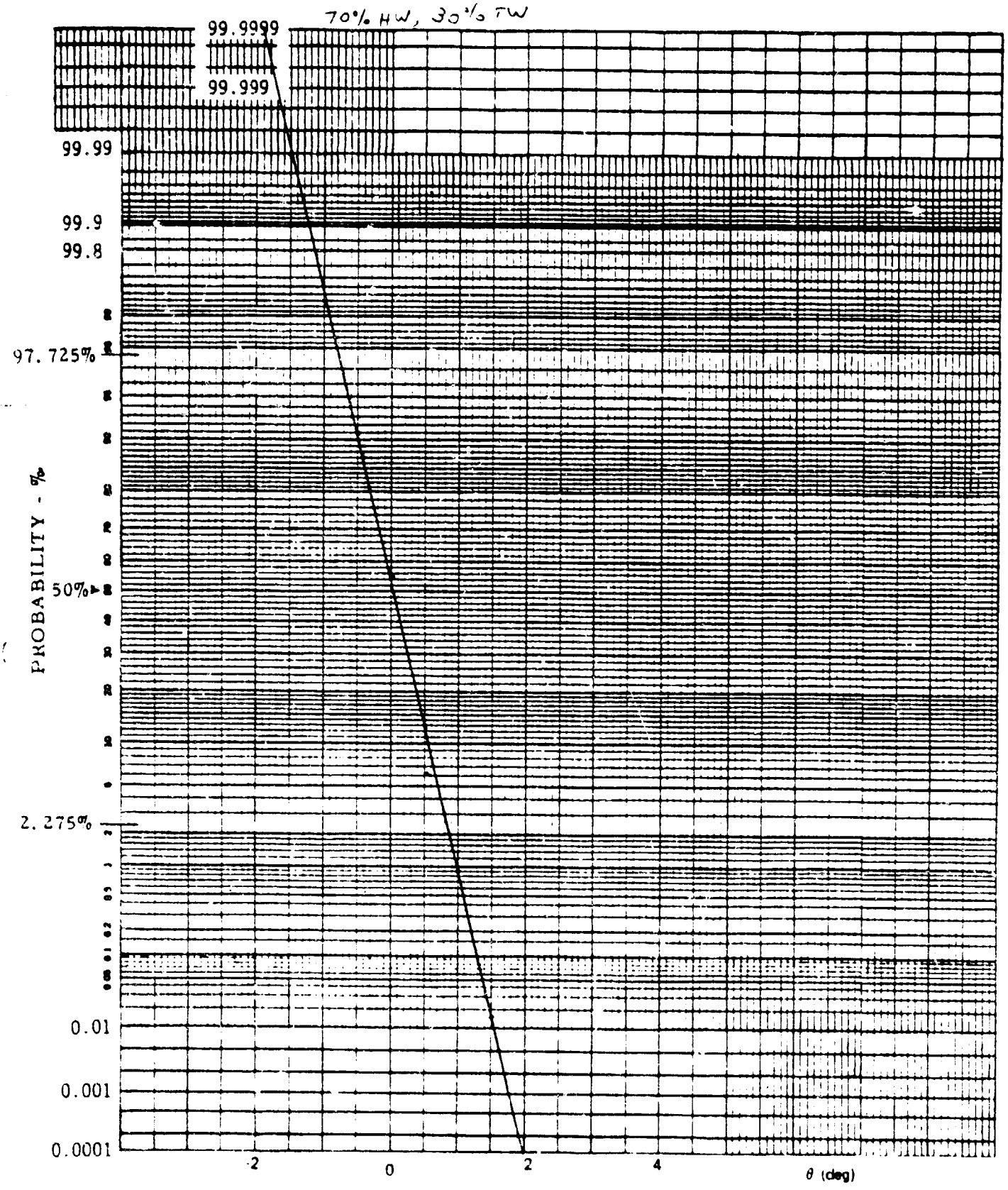

Figure B-48. Constant Flare Height, No Spoilers, High Gains

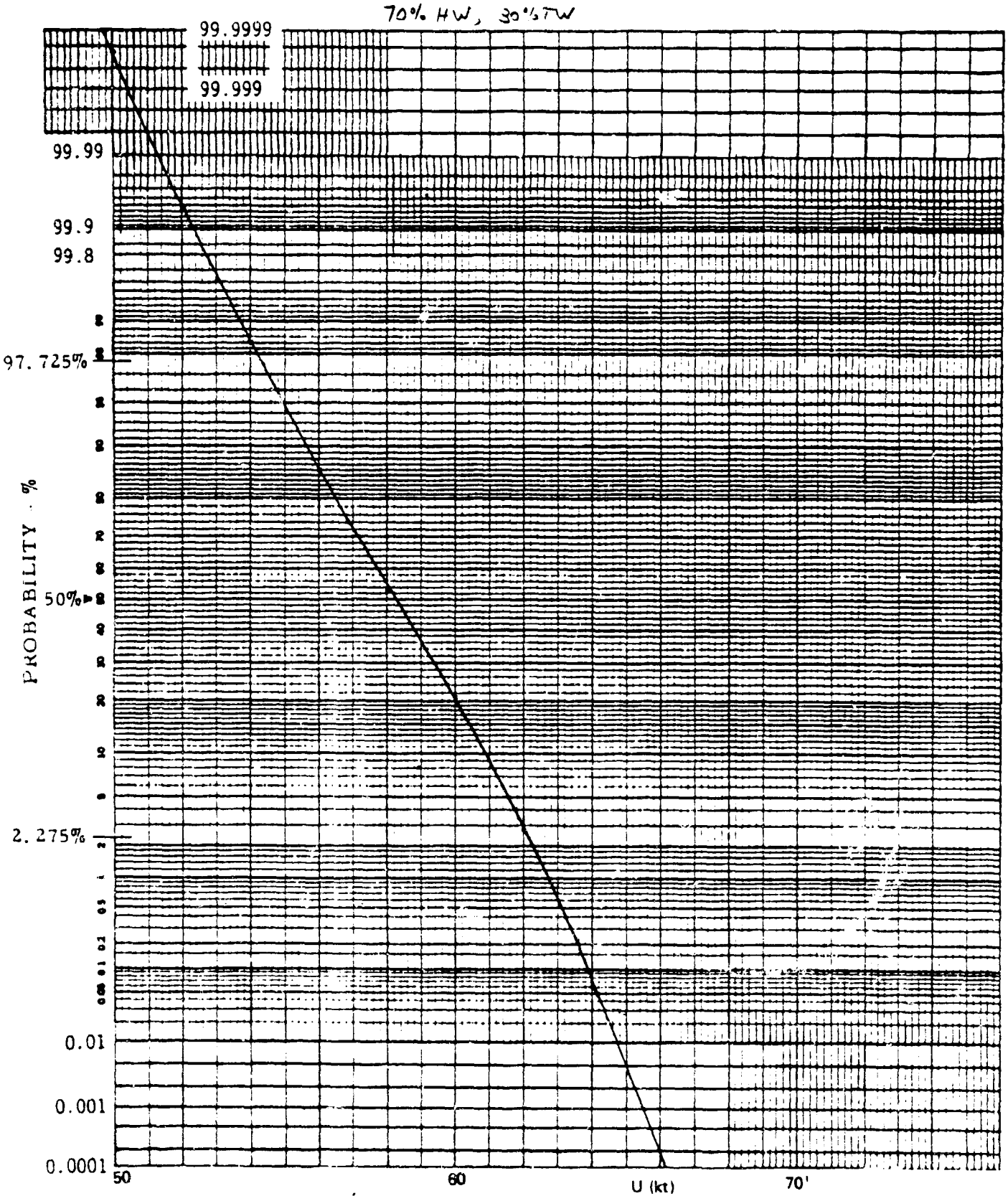

Figure B-49. Constant Flare Height, No Spoilers, High Gains

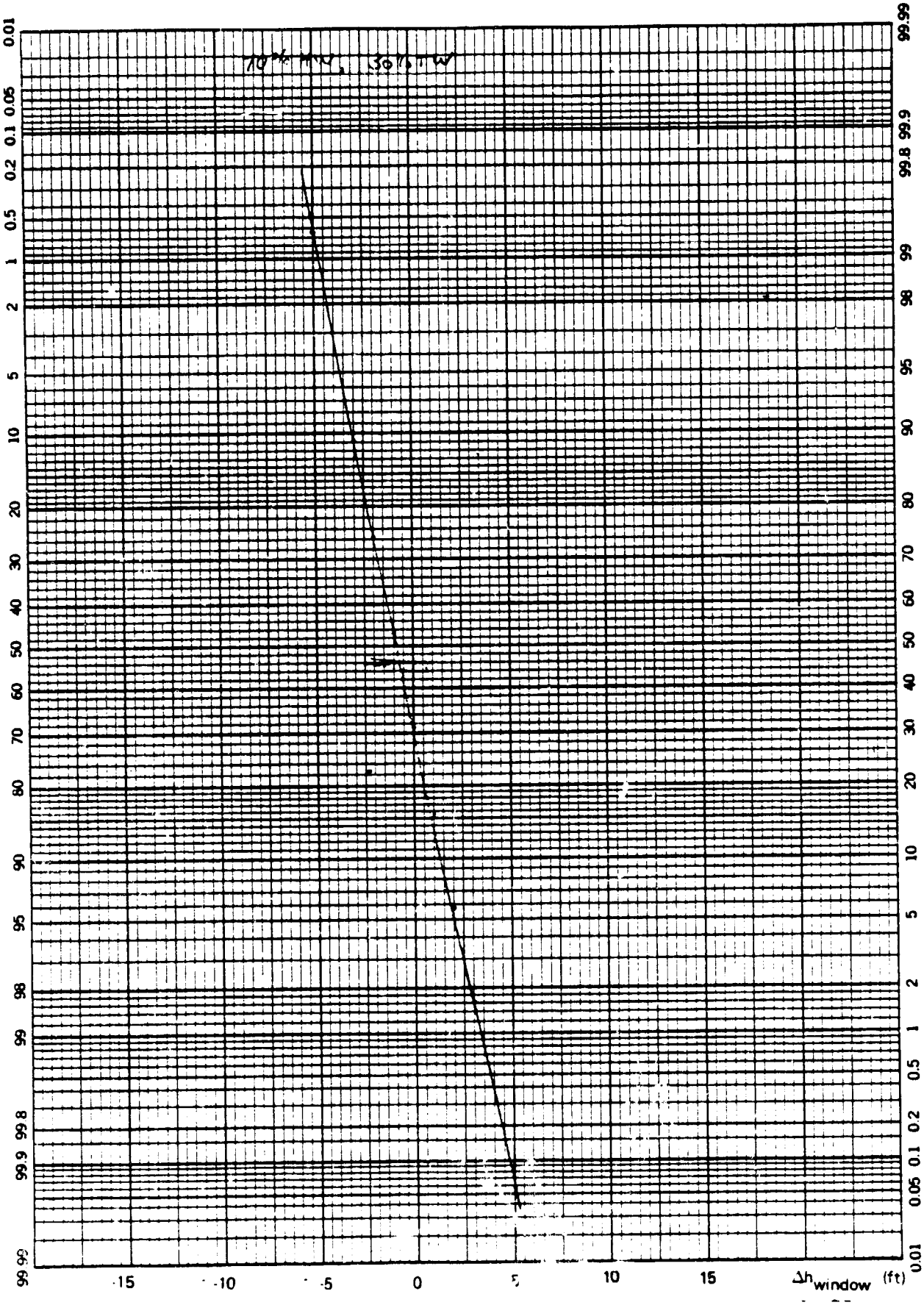

Figure B-50. Constant Flare Height, High Gains, No Spoilers

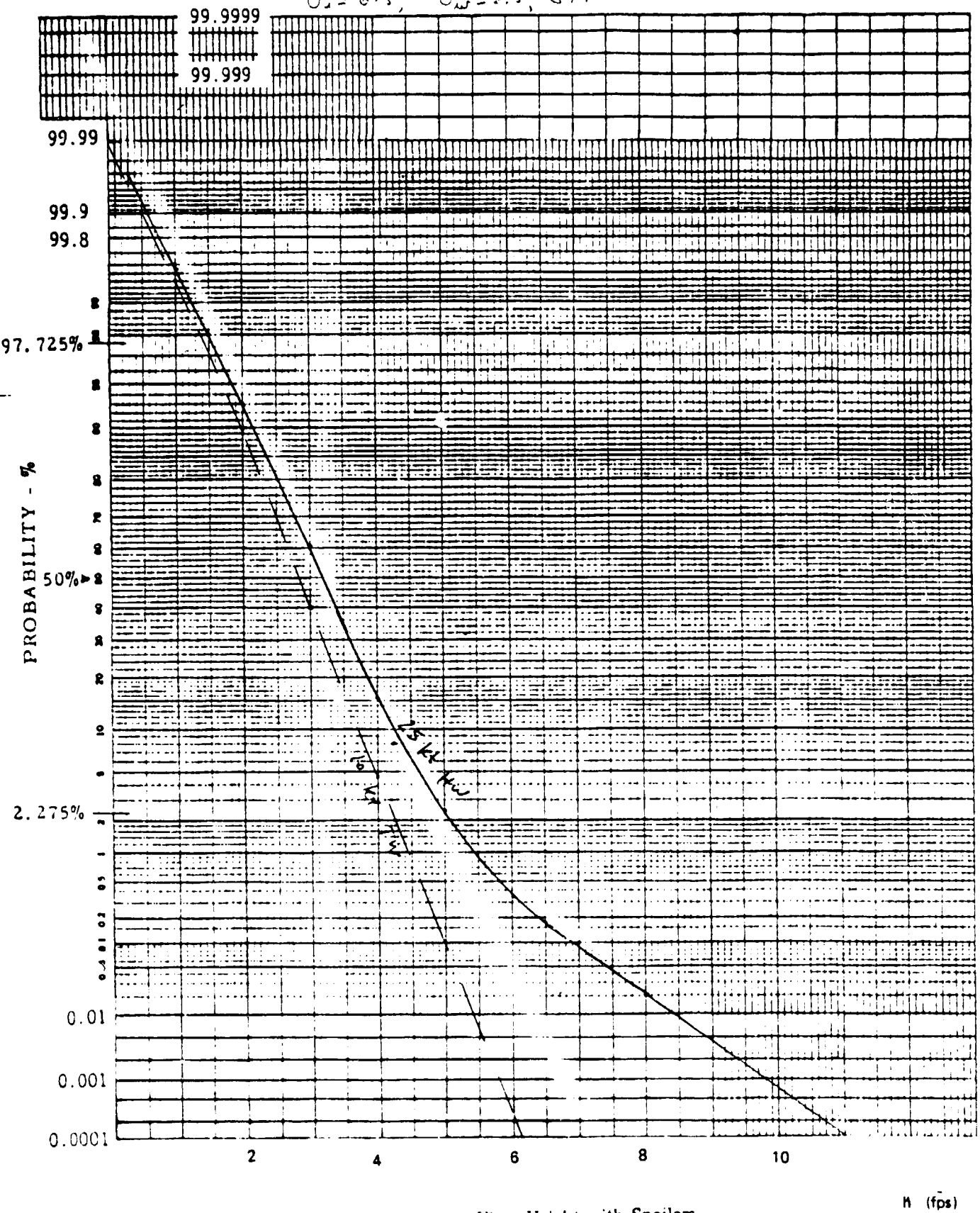

Figure B-51. Variable Flare Height with Spoilers

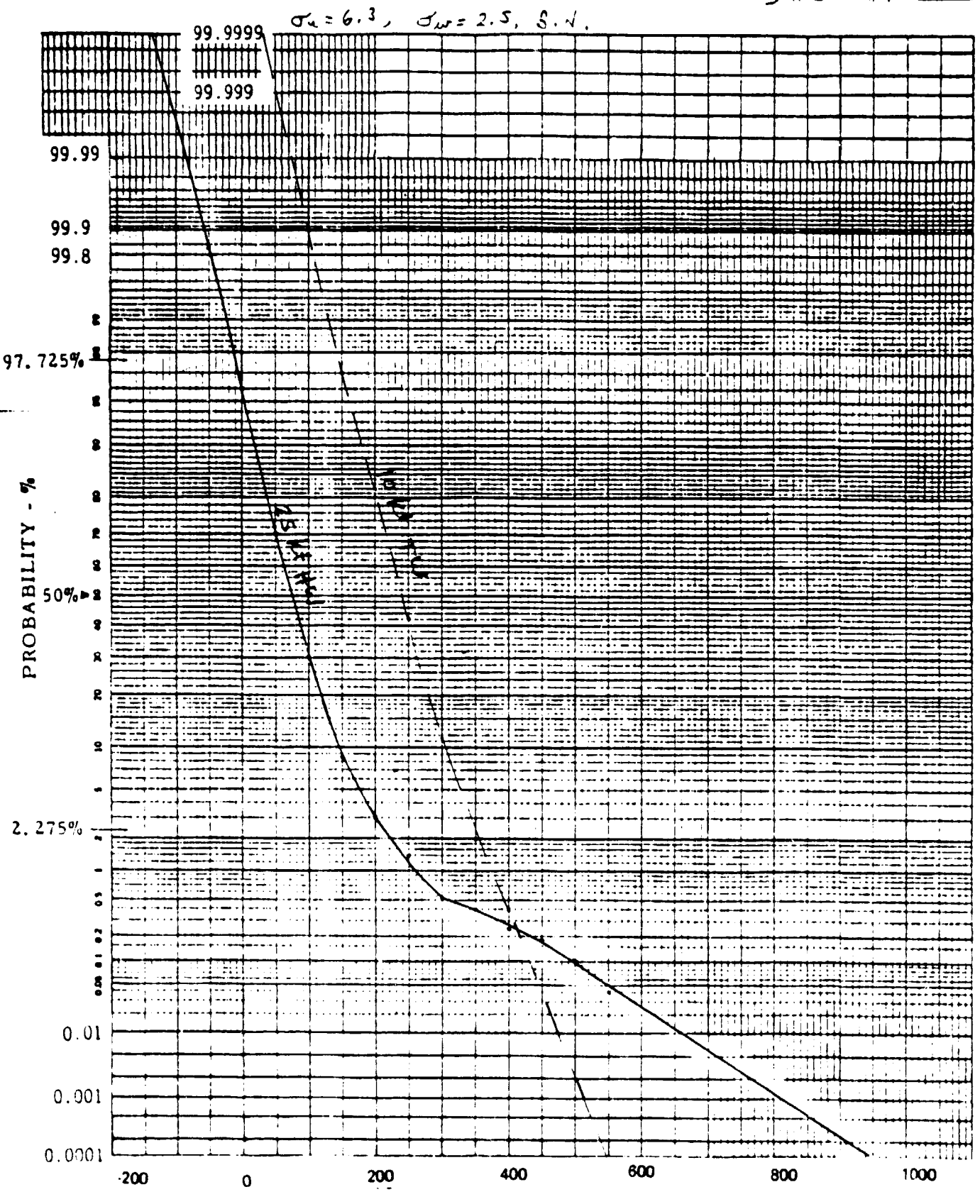

Figure B-52. Variable Flare Height with Spoilers

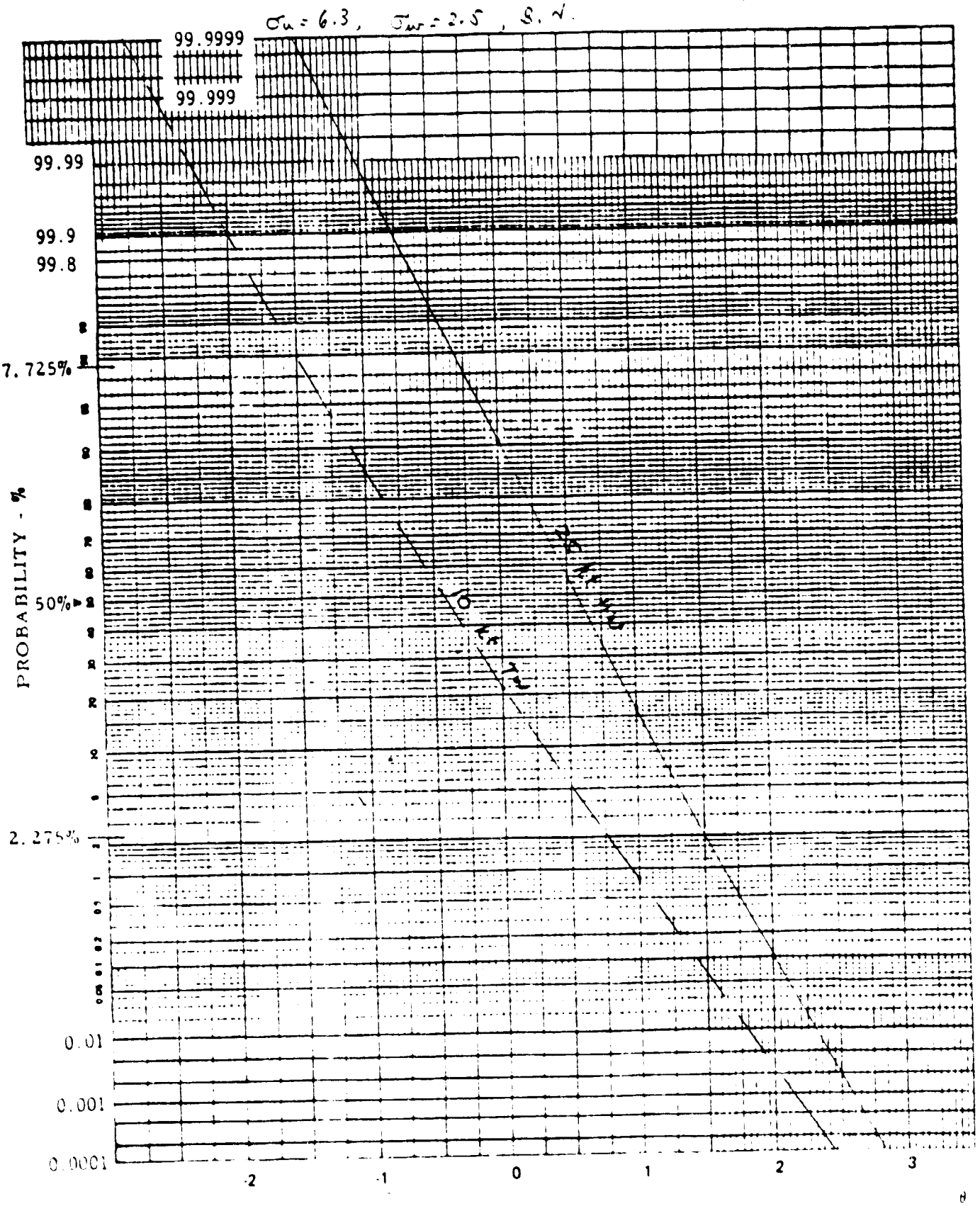

Figure B-53. Variable Flare Height with Spoilers

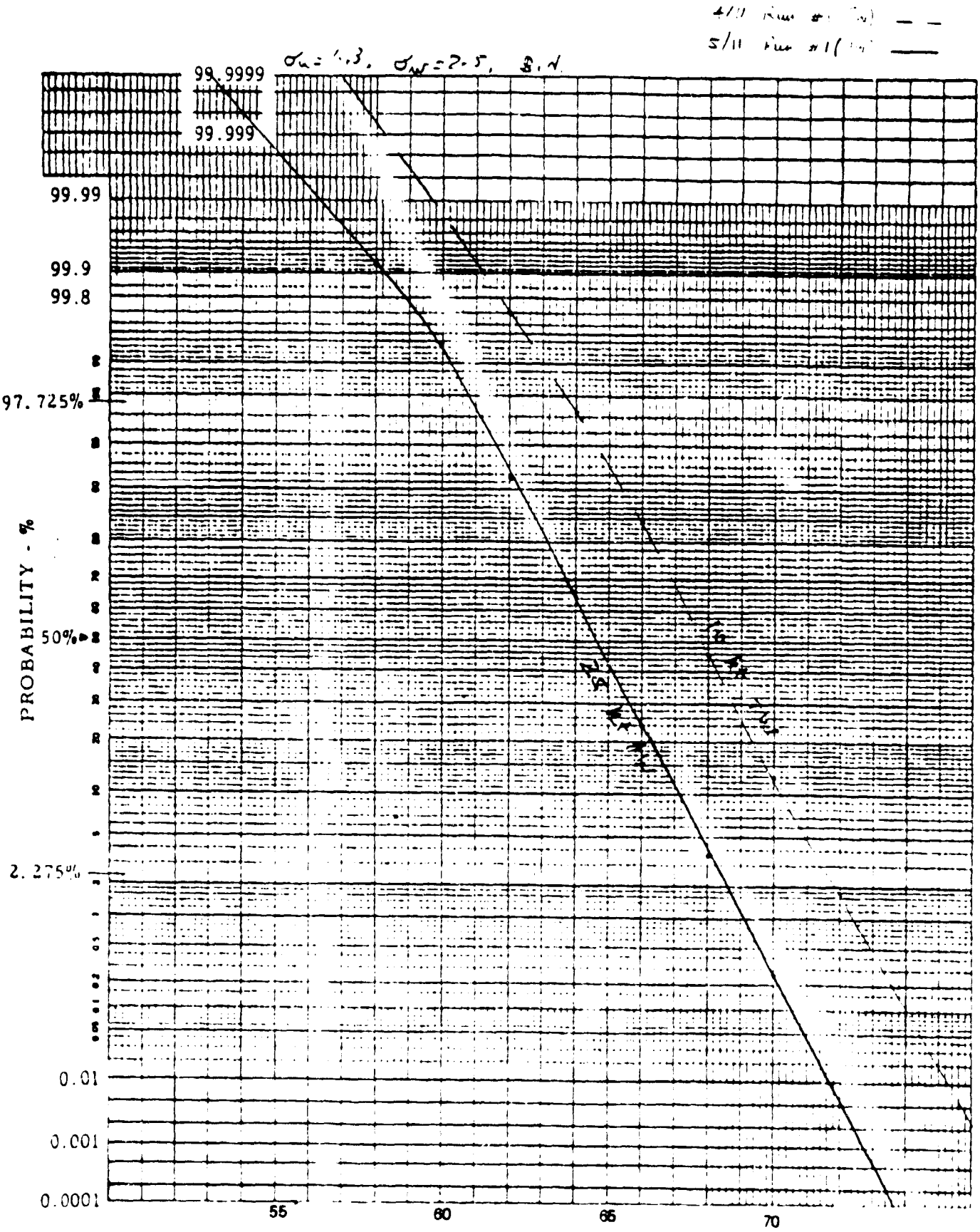

Figure B-54. Variable Flare Height with Spoilers

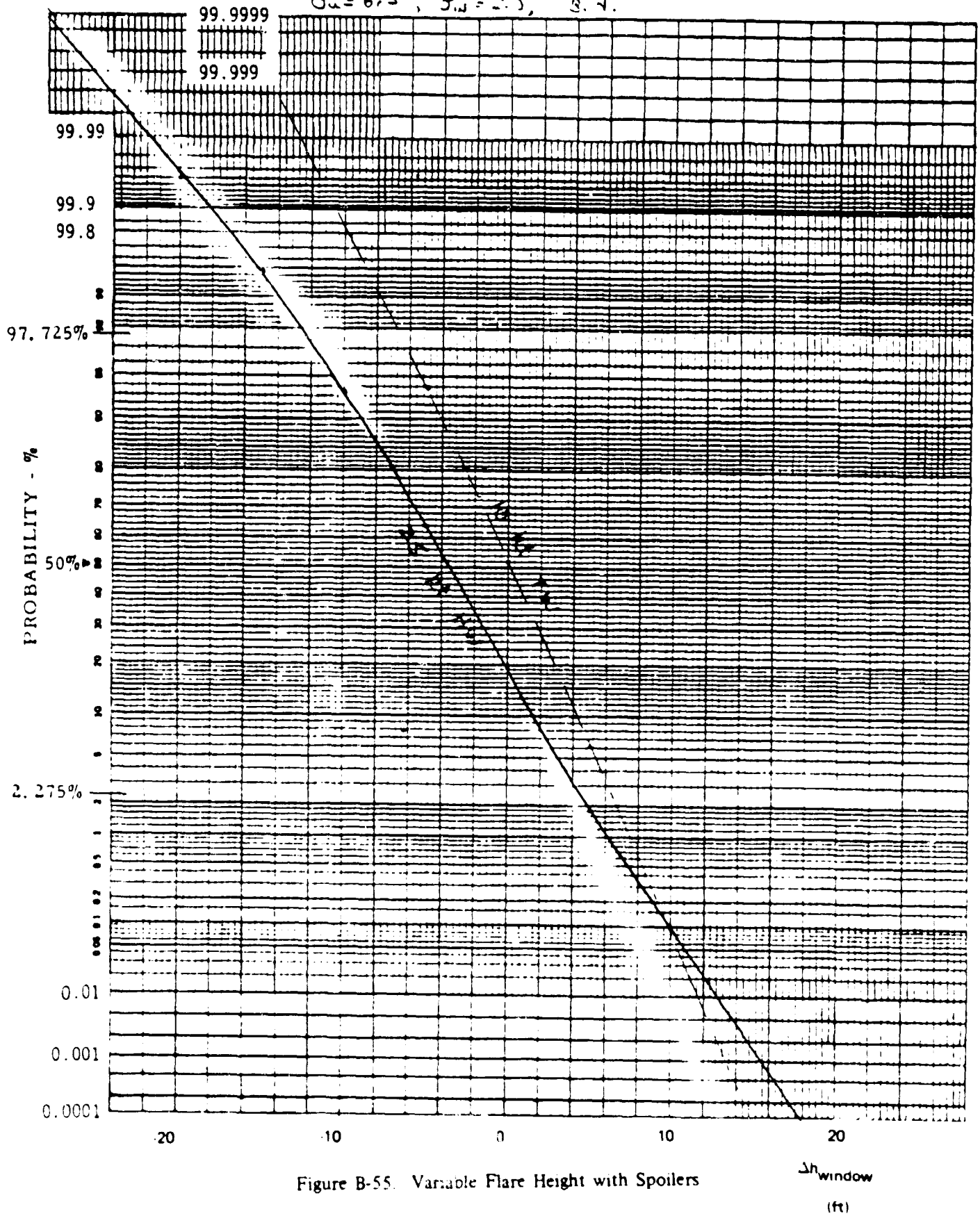

Figure B-55. Variable Flare Height with Spoilers

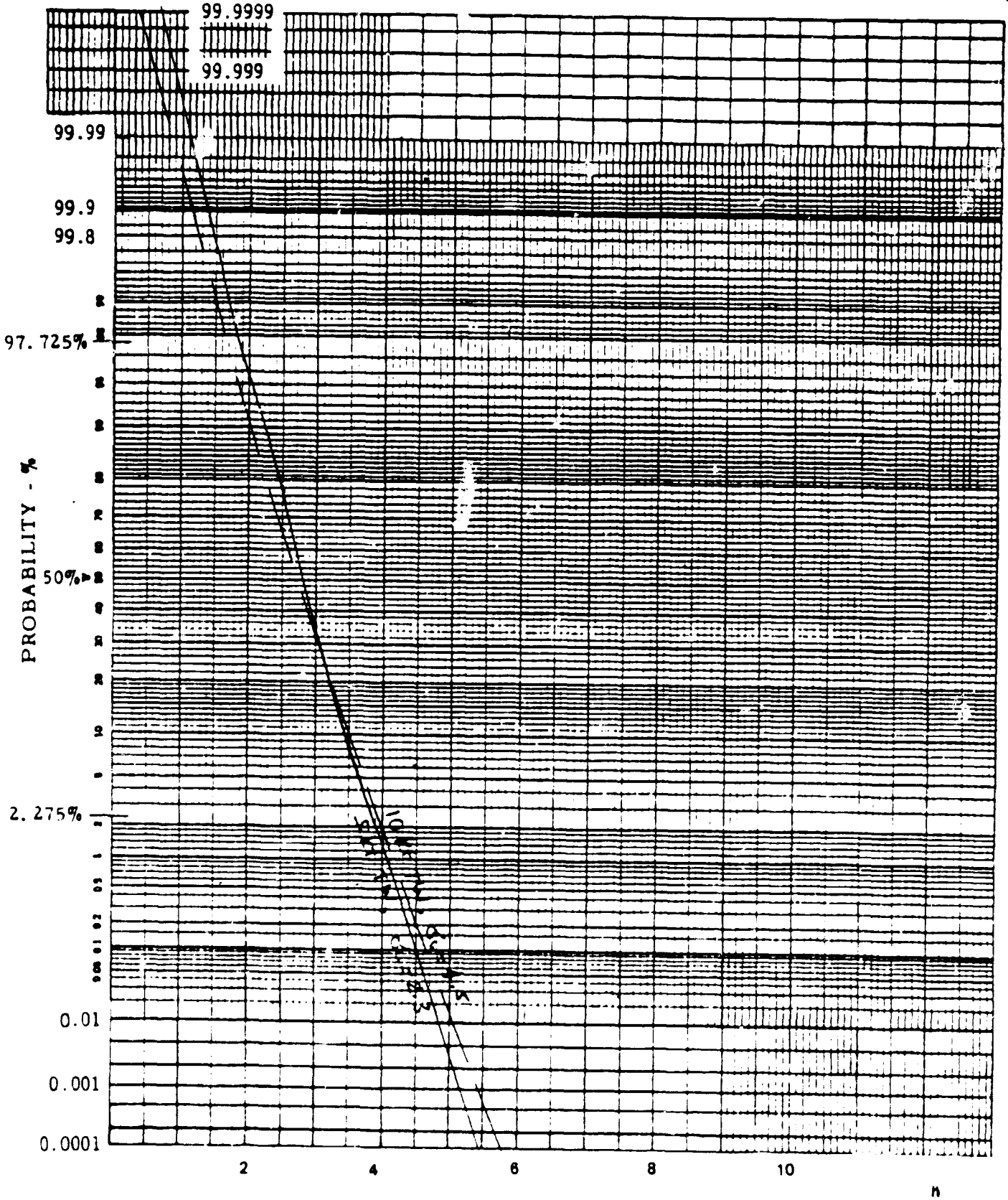

Figure B-56. Variable Flare Height with Spoilers

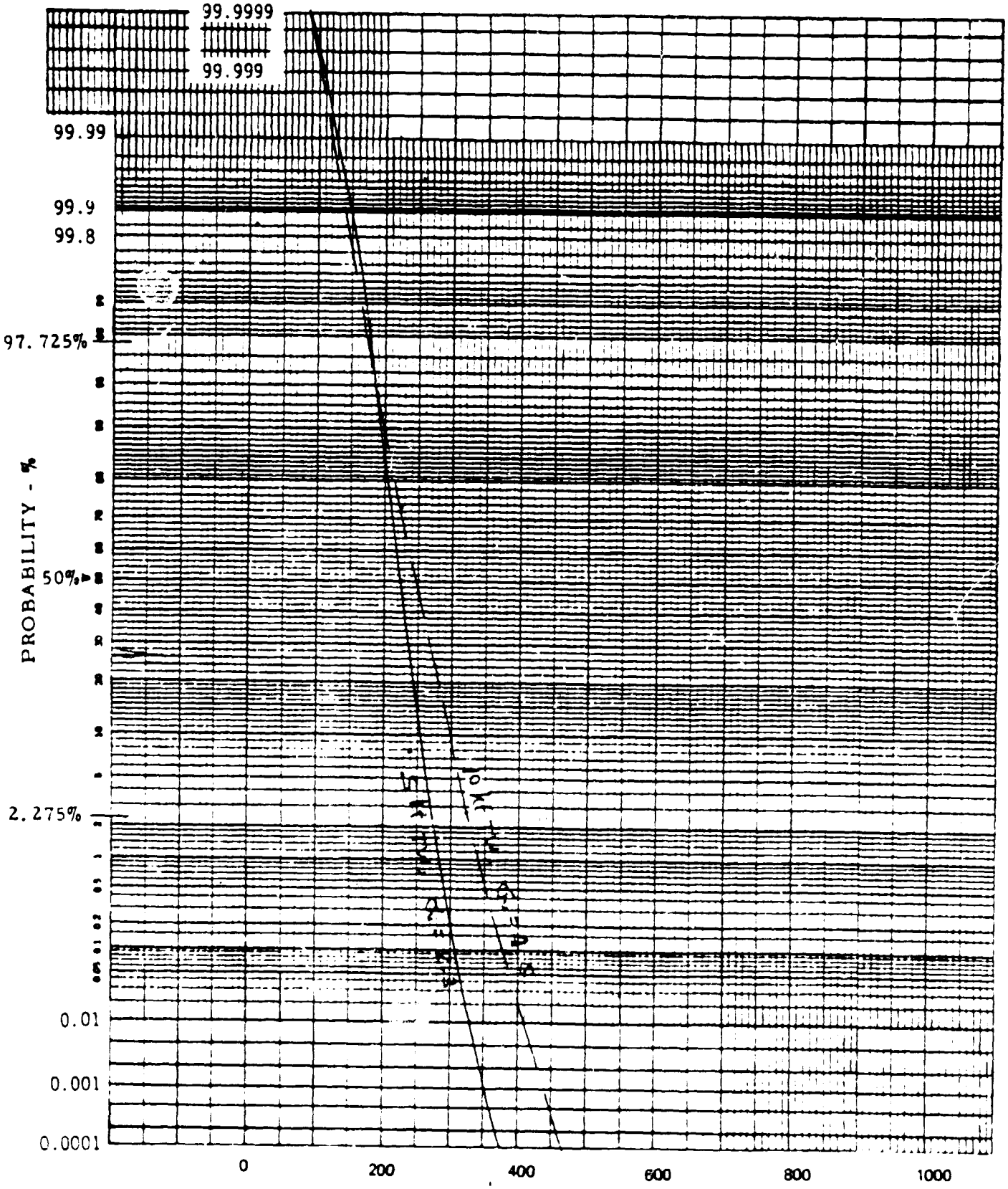

Figure B-57. Variable Flare Height with Spoilers

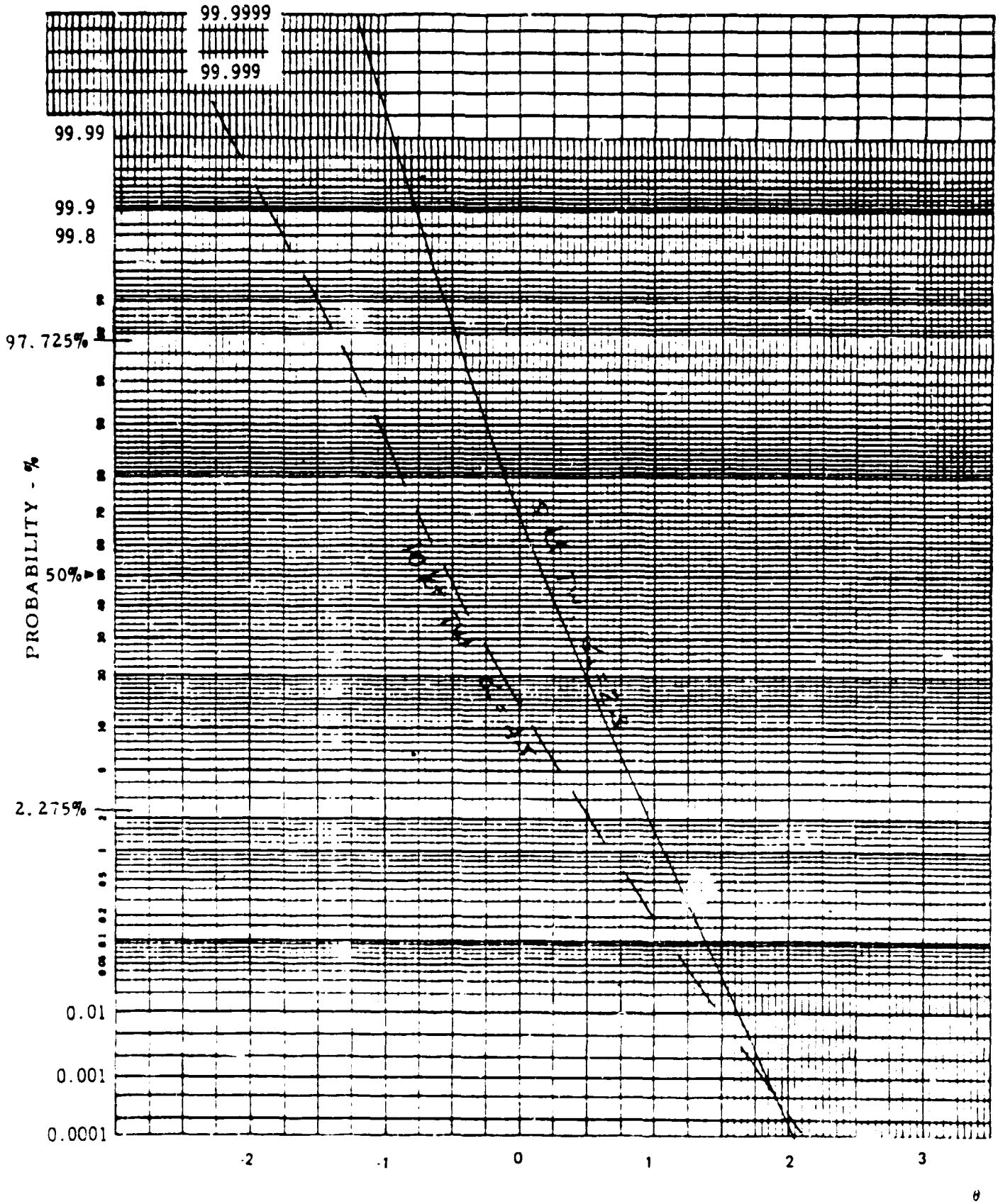

Figure B-58. Variable Flare Height with Spoilers

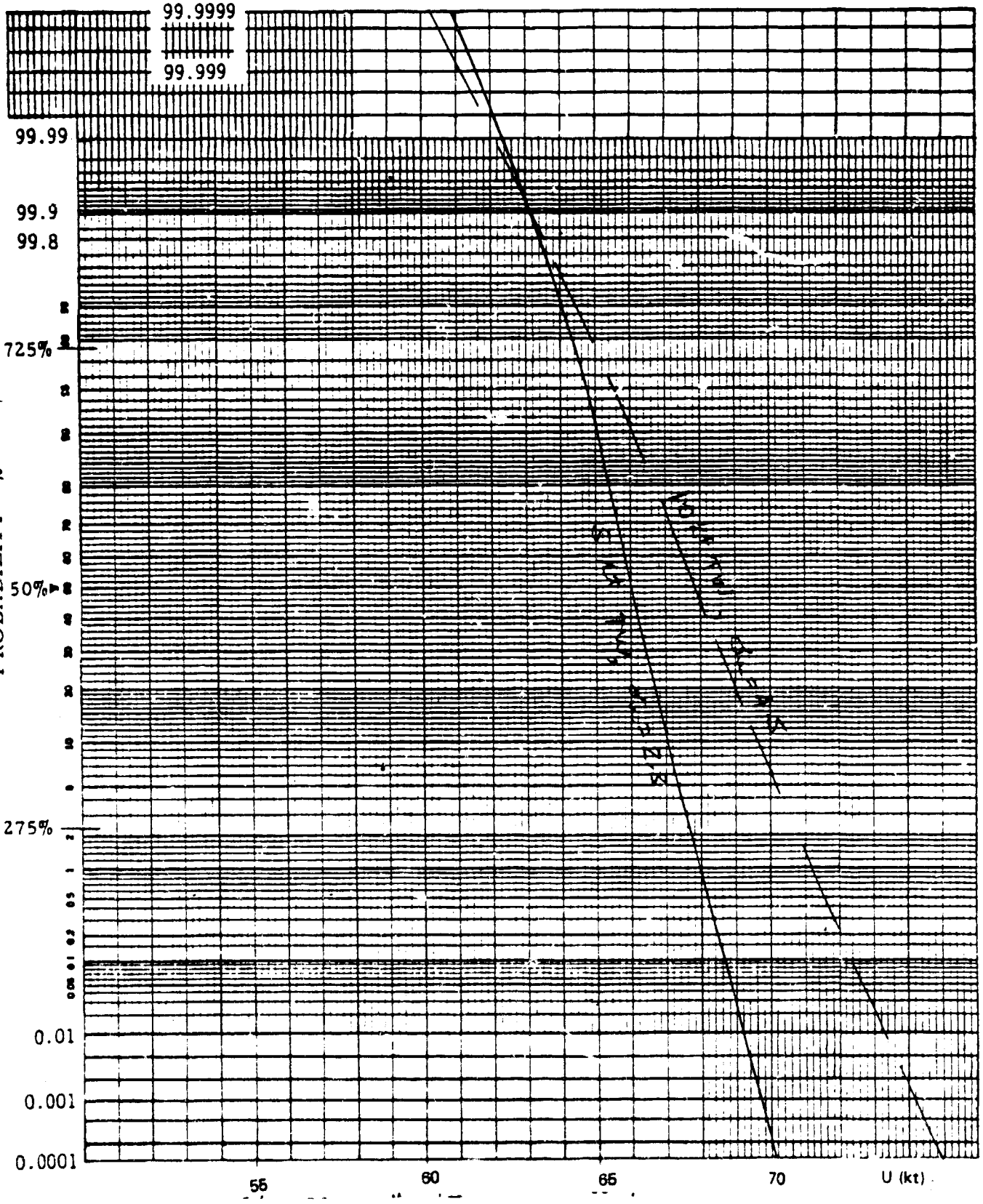

Figure B-59. Variable Flare Height with Spoilers

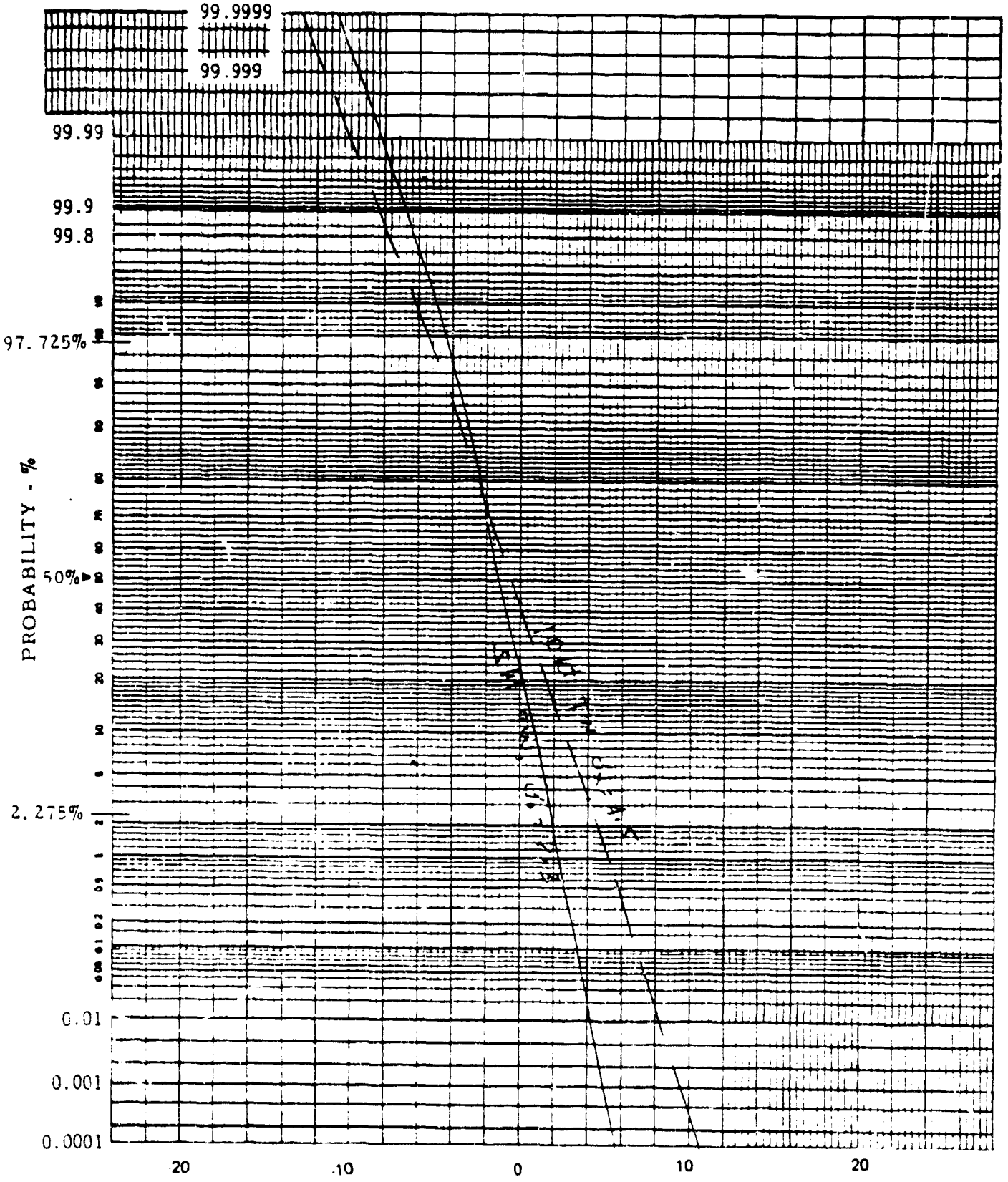

Figure B-60. Variable Flare Height with Spoilers

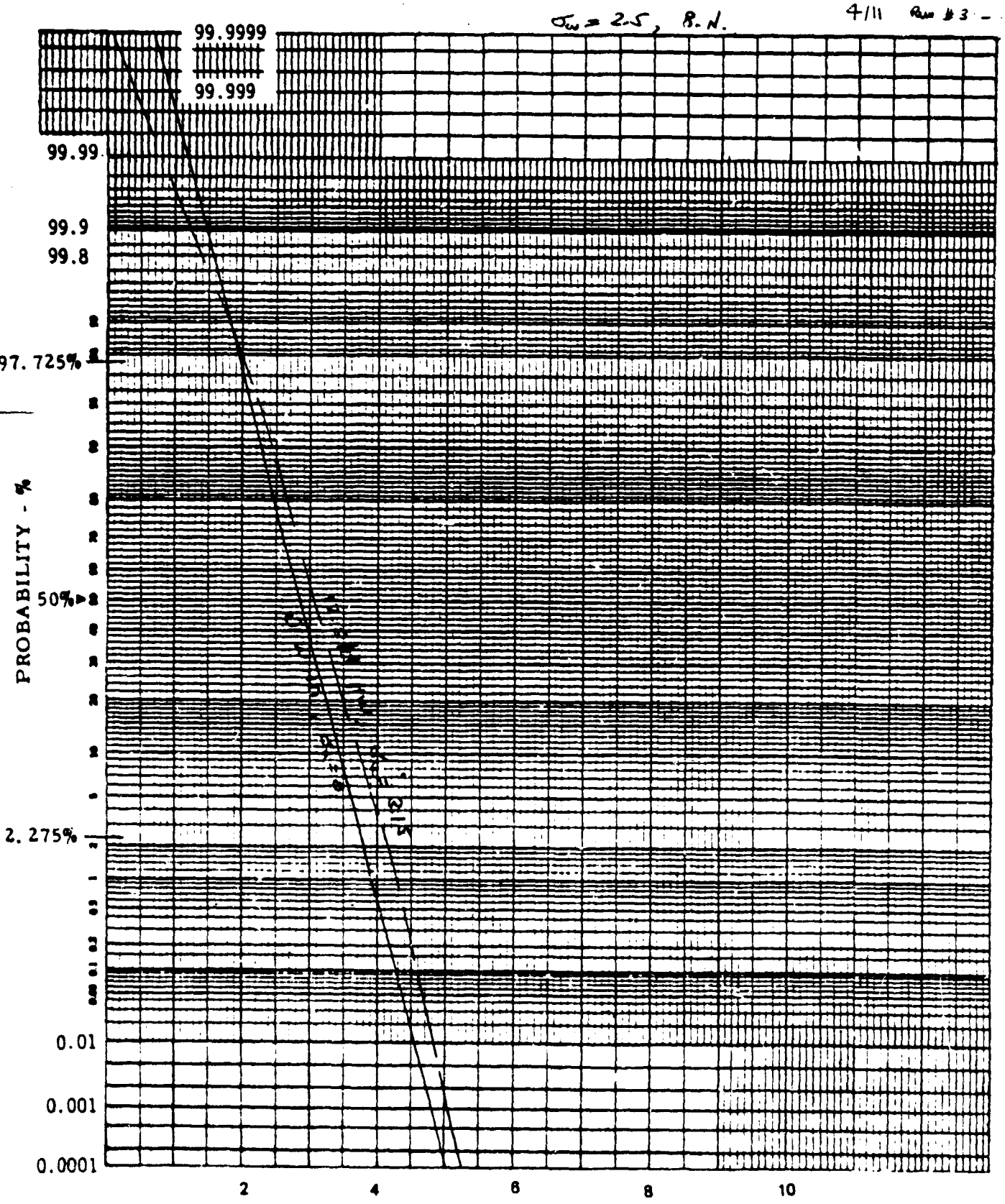

Figure B-61. Variable Flare Height with Spoilers

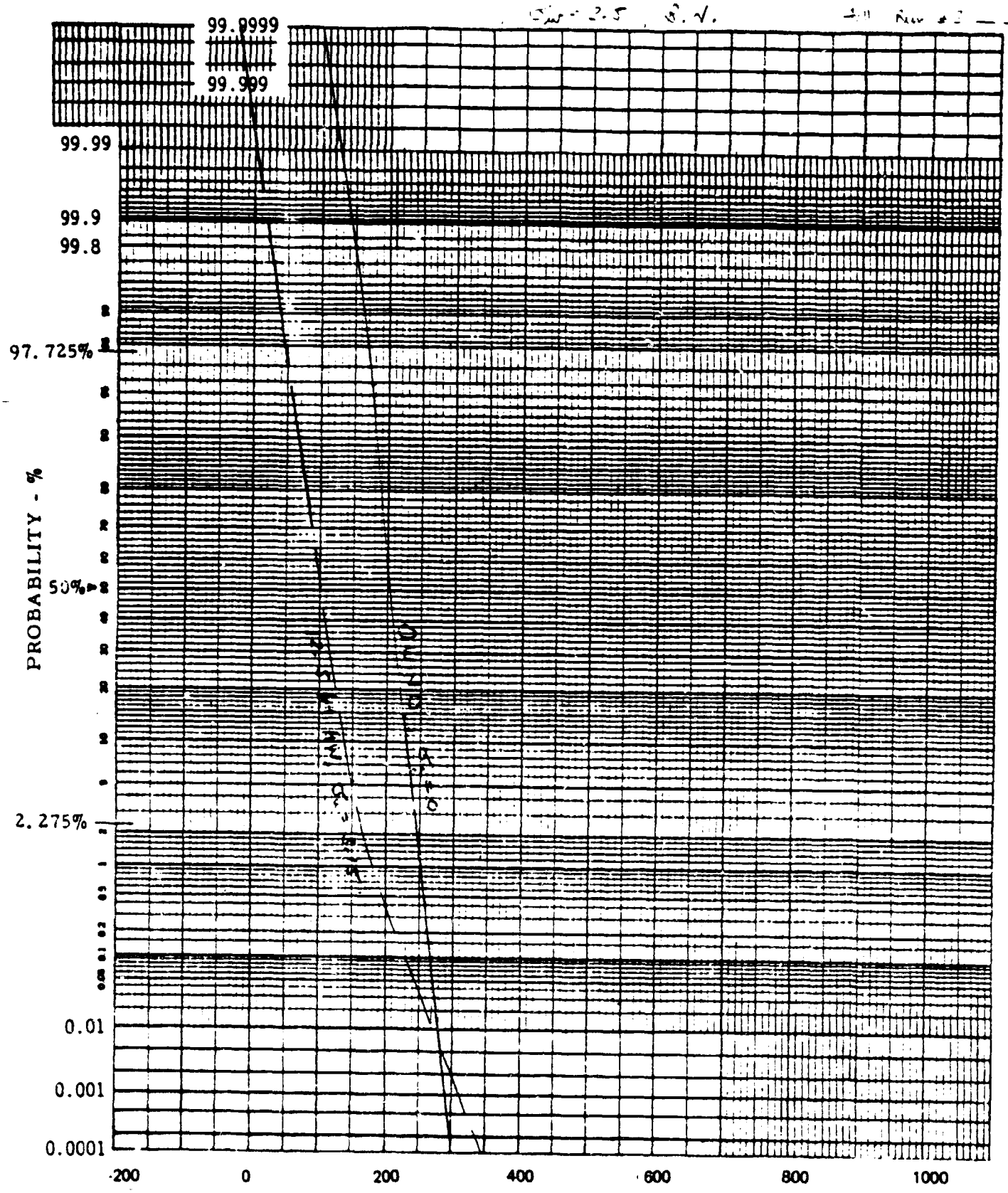

Figure B-62. Variable Flare Height with Spoilers

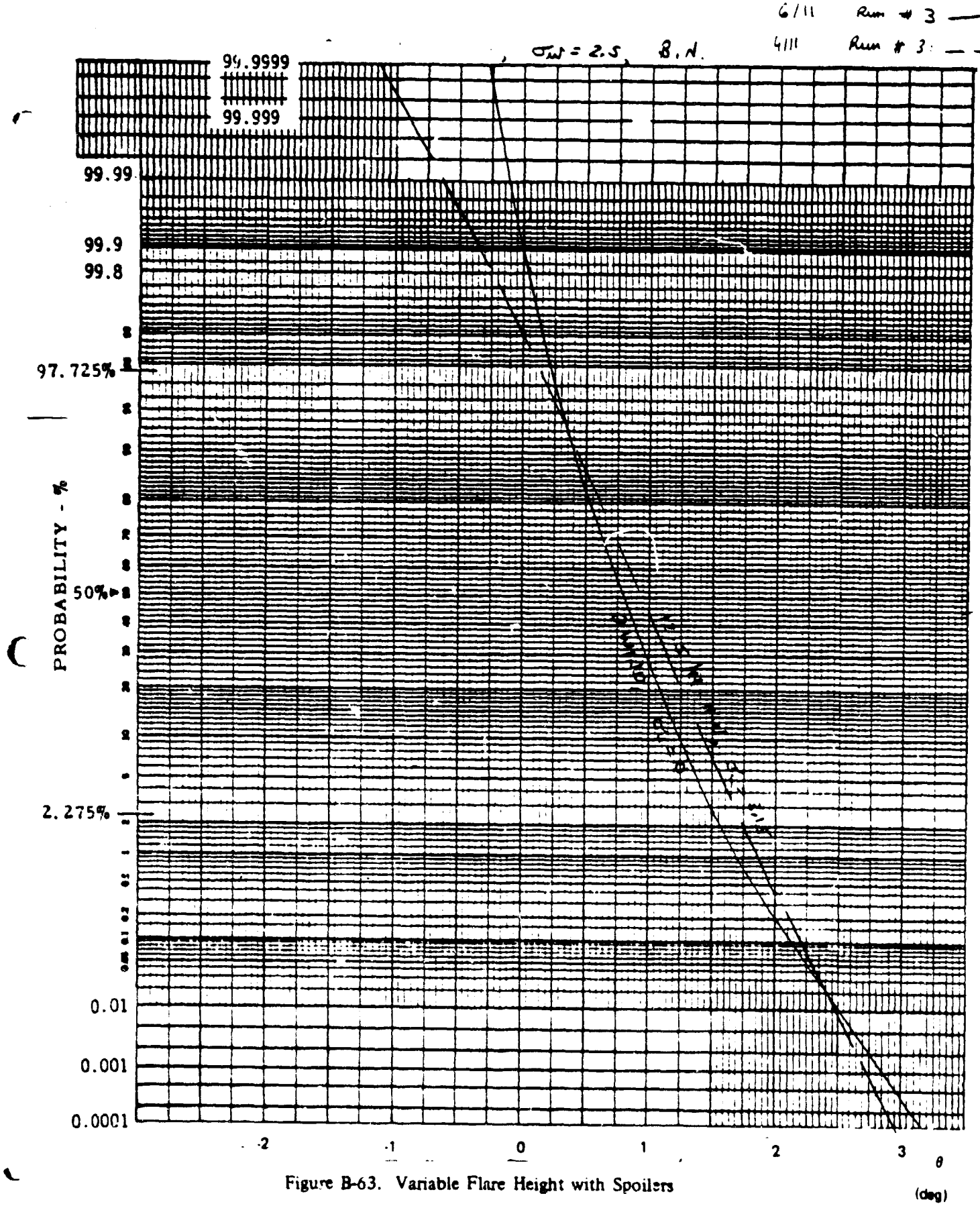

Figure B-63. Variable Flare Height with Spoilers

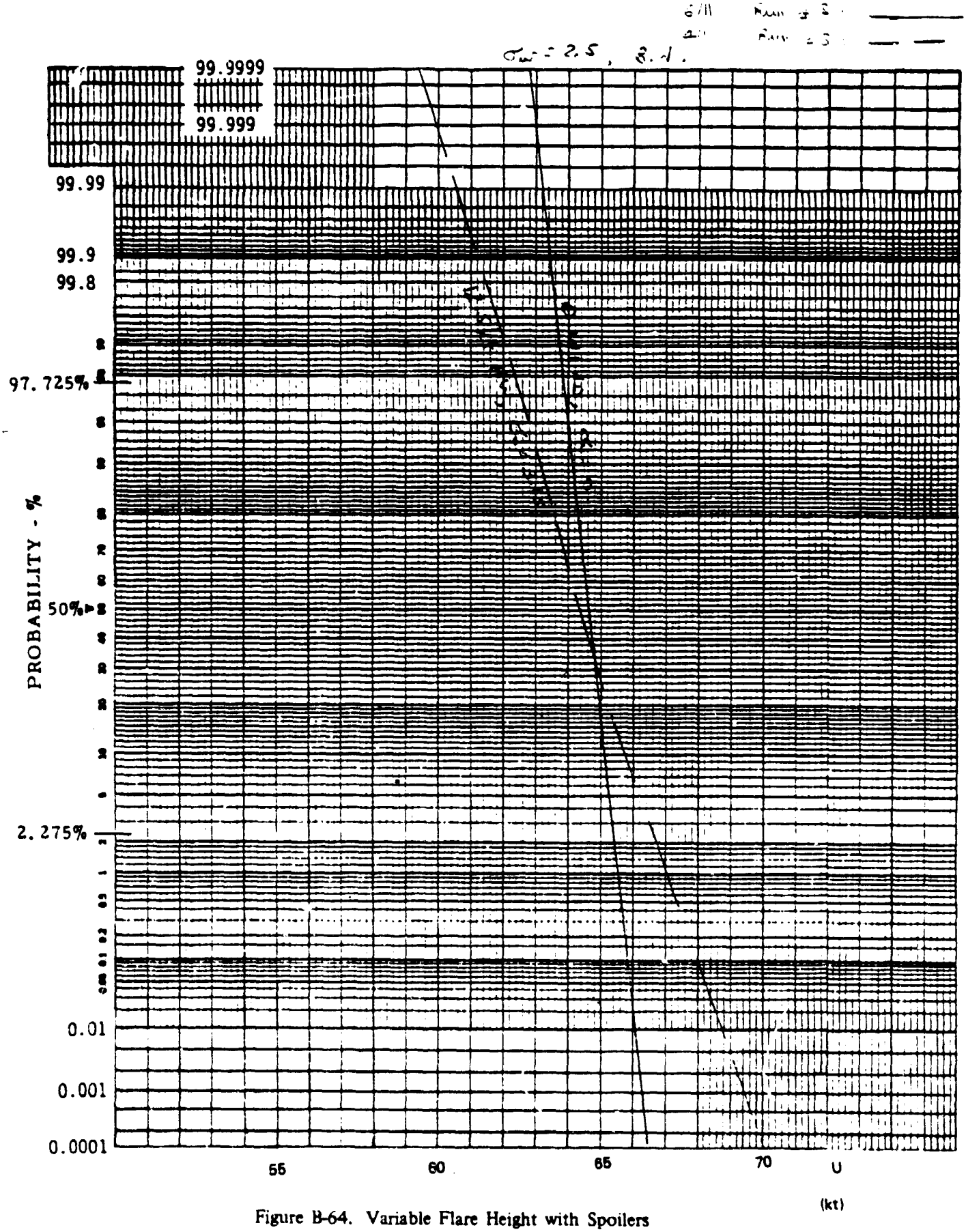

Figure B-64. Variable Flare Height with Spoilers

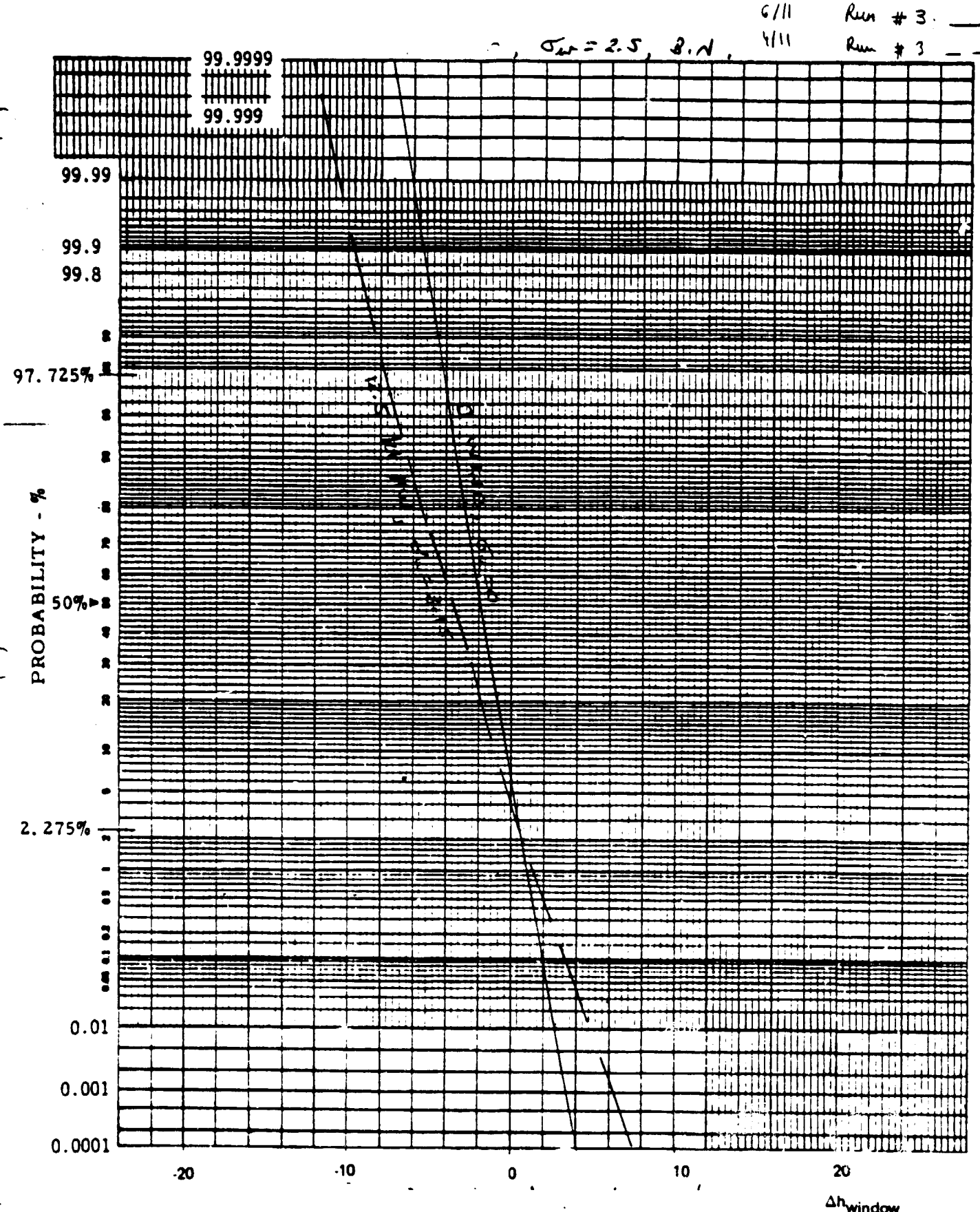

Figure B-65. Variable Flare Heigh: with Spoilers

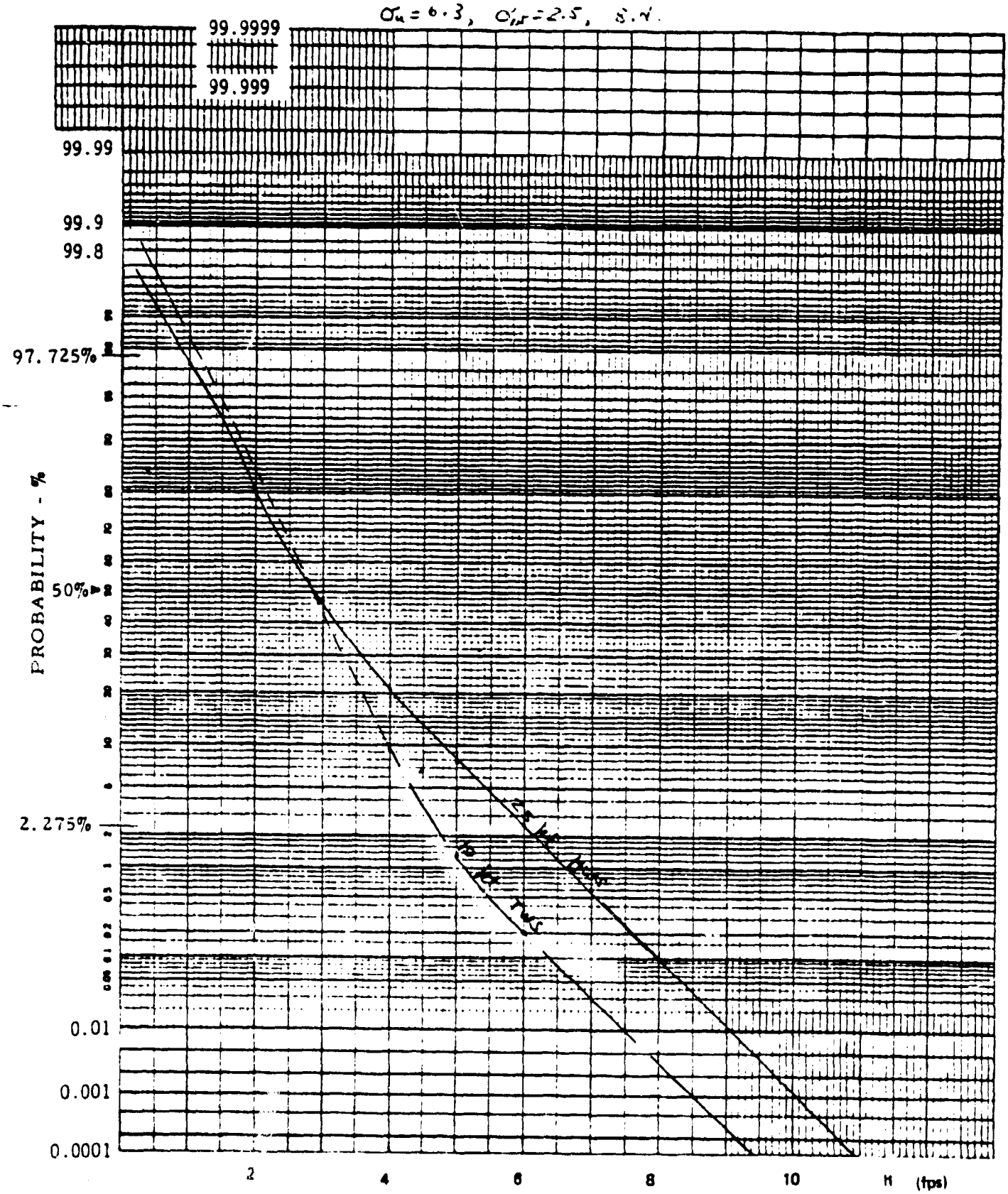

Figure B-66. Variable Flare Height; No Spoilers

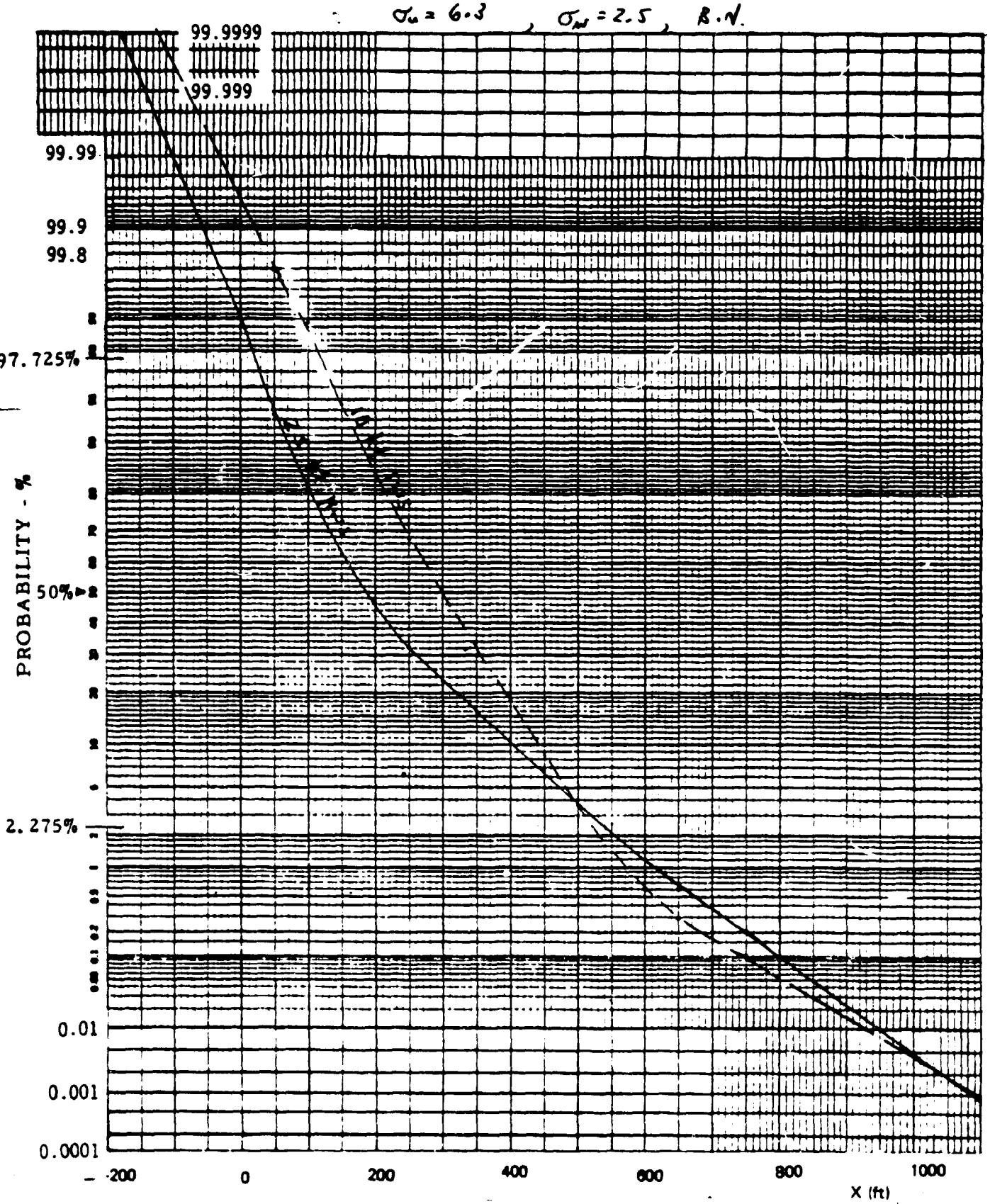

Figure B-67. Variable Flare Height; No Spoilers

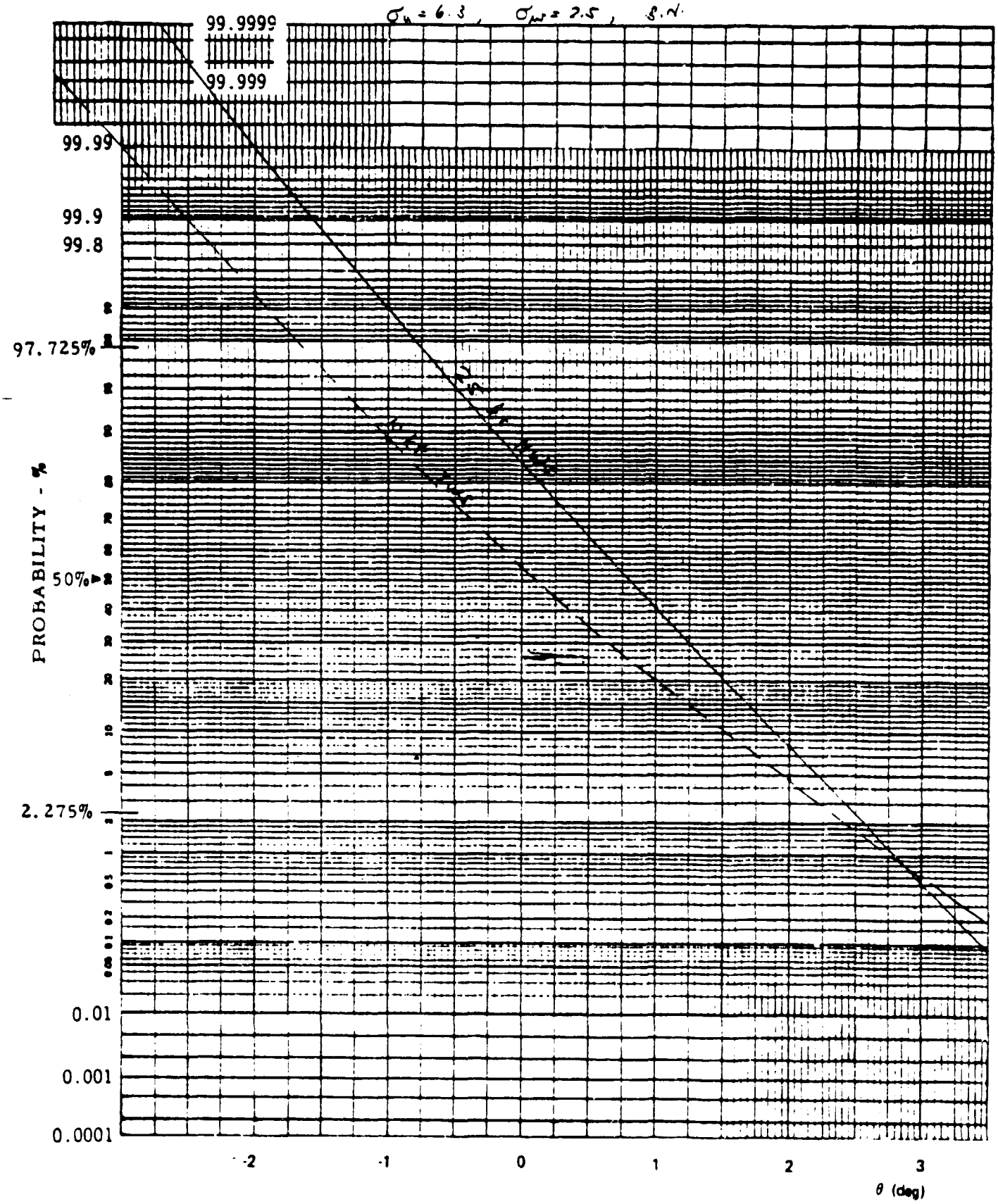

Figure B-68. Variable Flare Height; No Spoilers

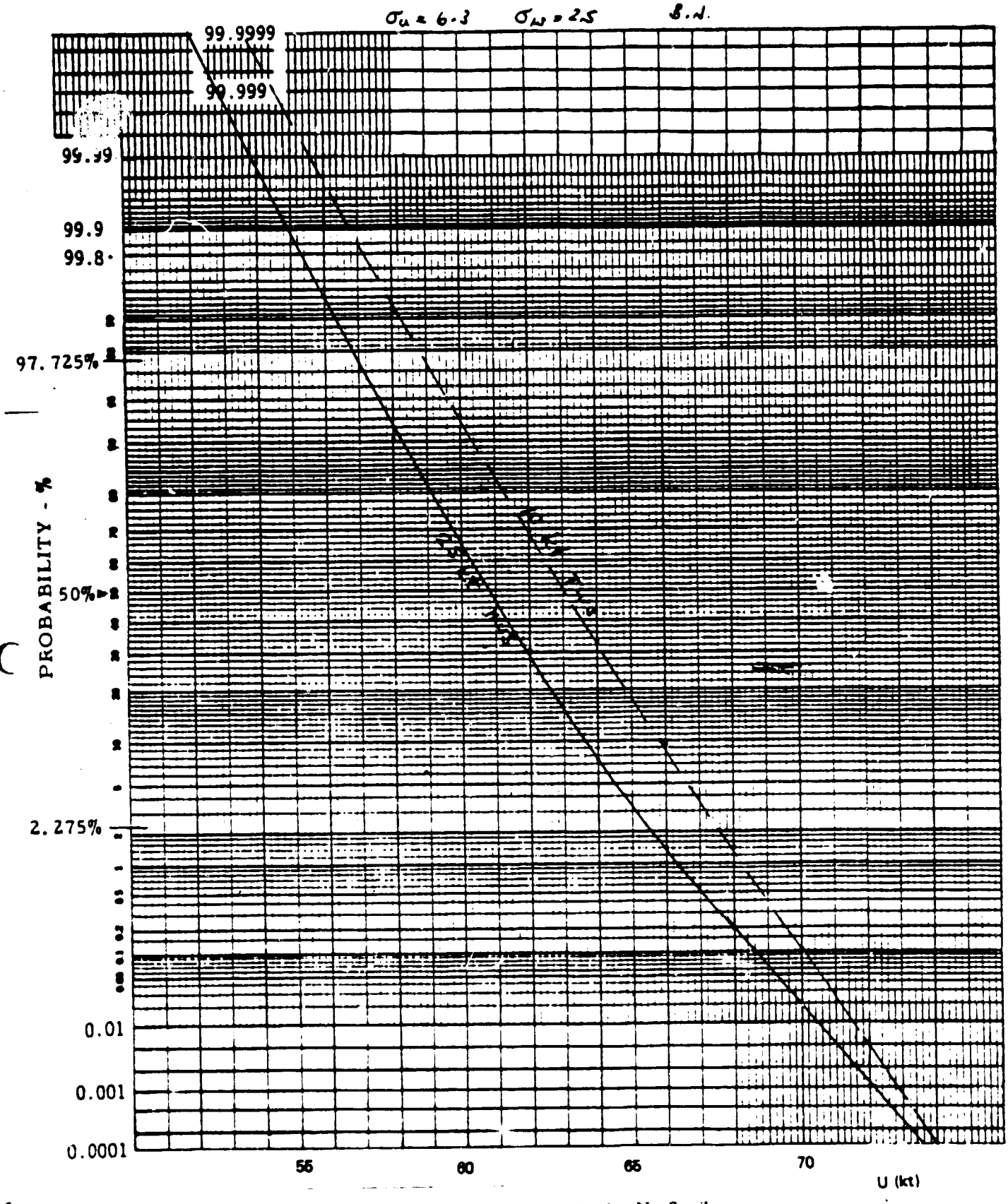

Figure B-69. Variable Flare Height; No Spoilers

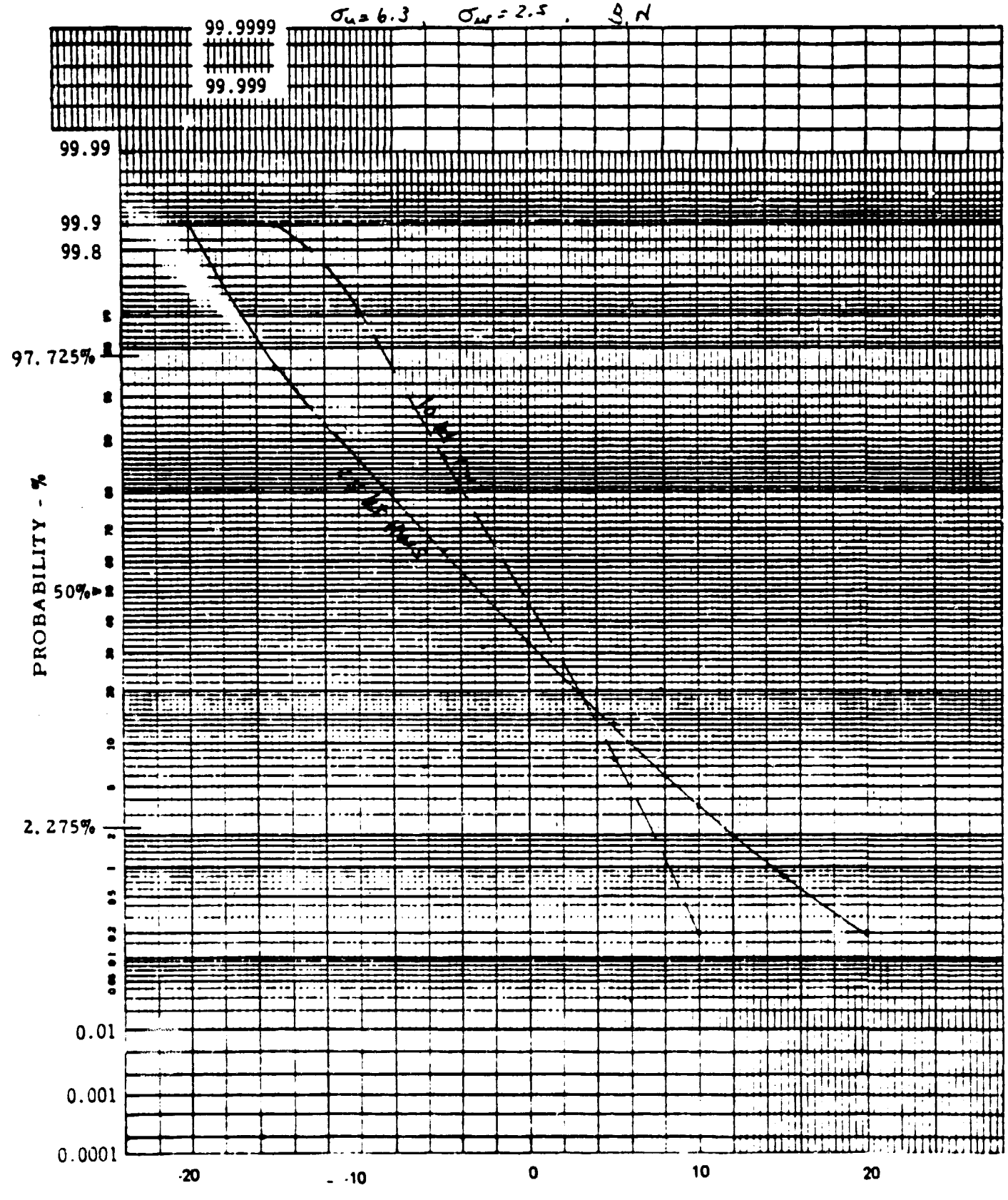

Figure B-70. Variable Flare Height; No Spoilers

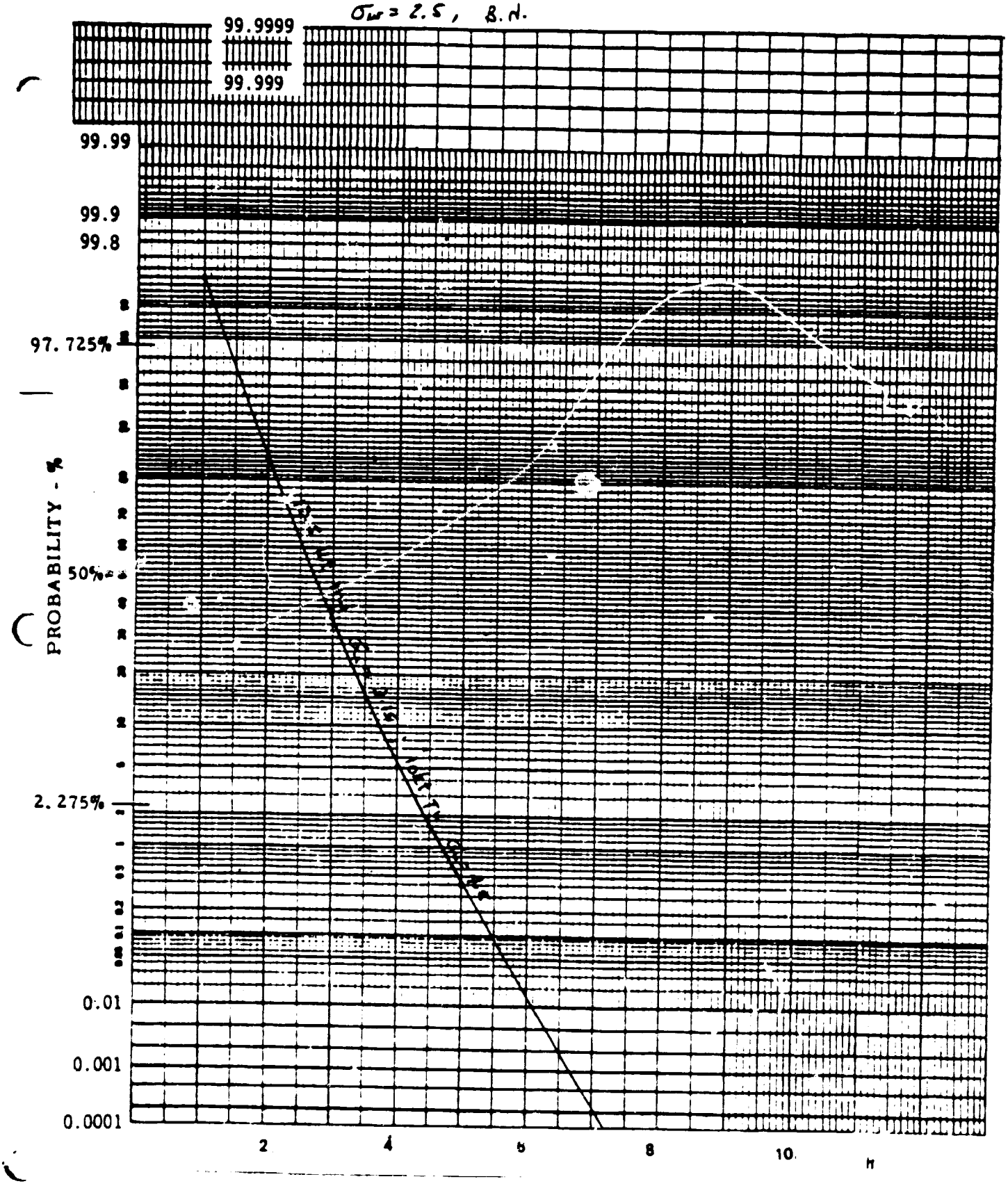

Figure B-71. Variable Flare Height; No Spoilers

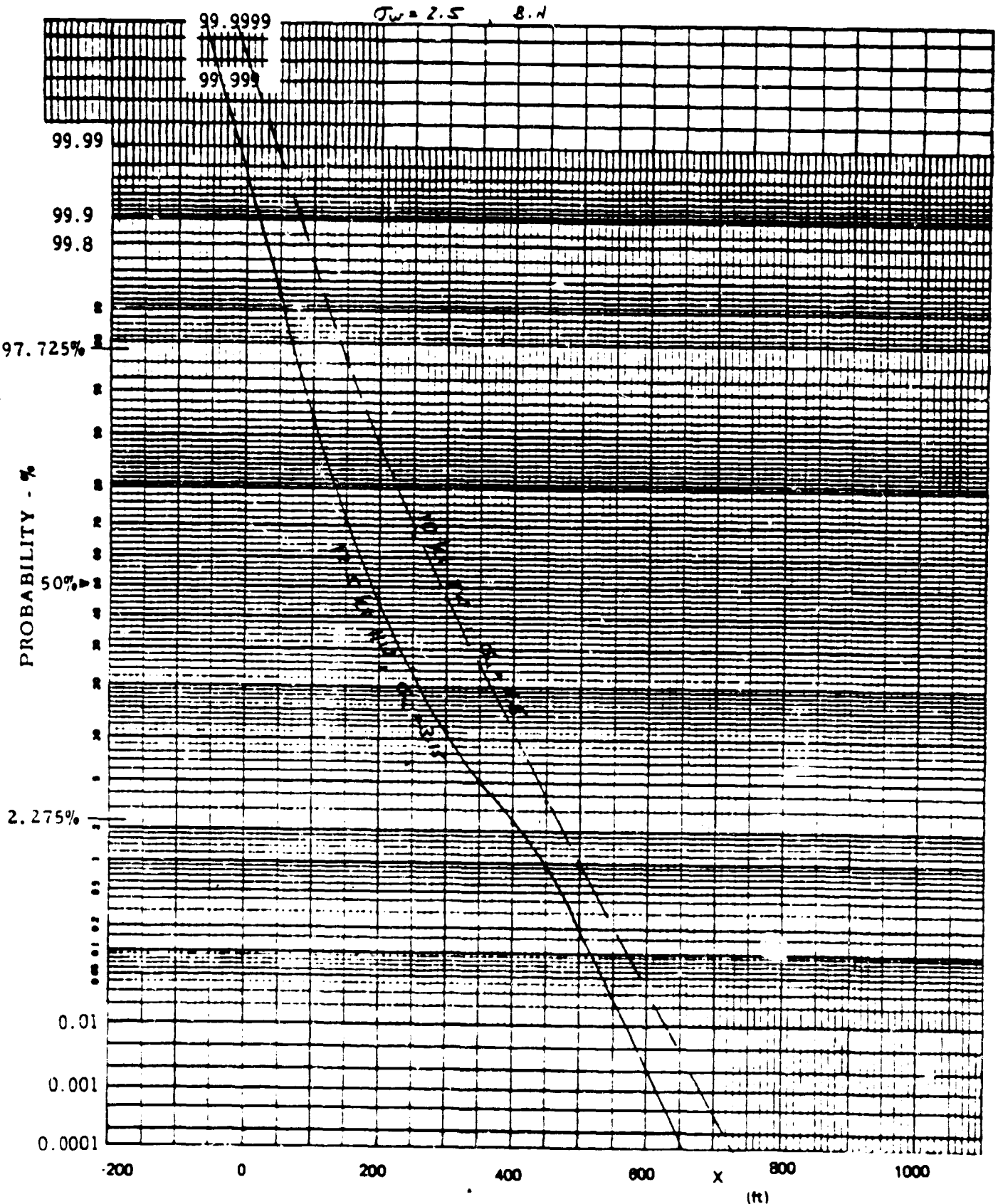

Figure B-72. Variable Flare Height; No Spoilers

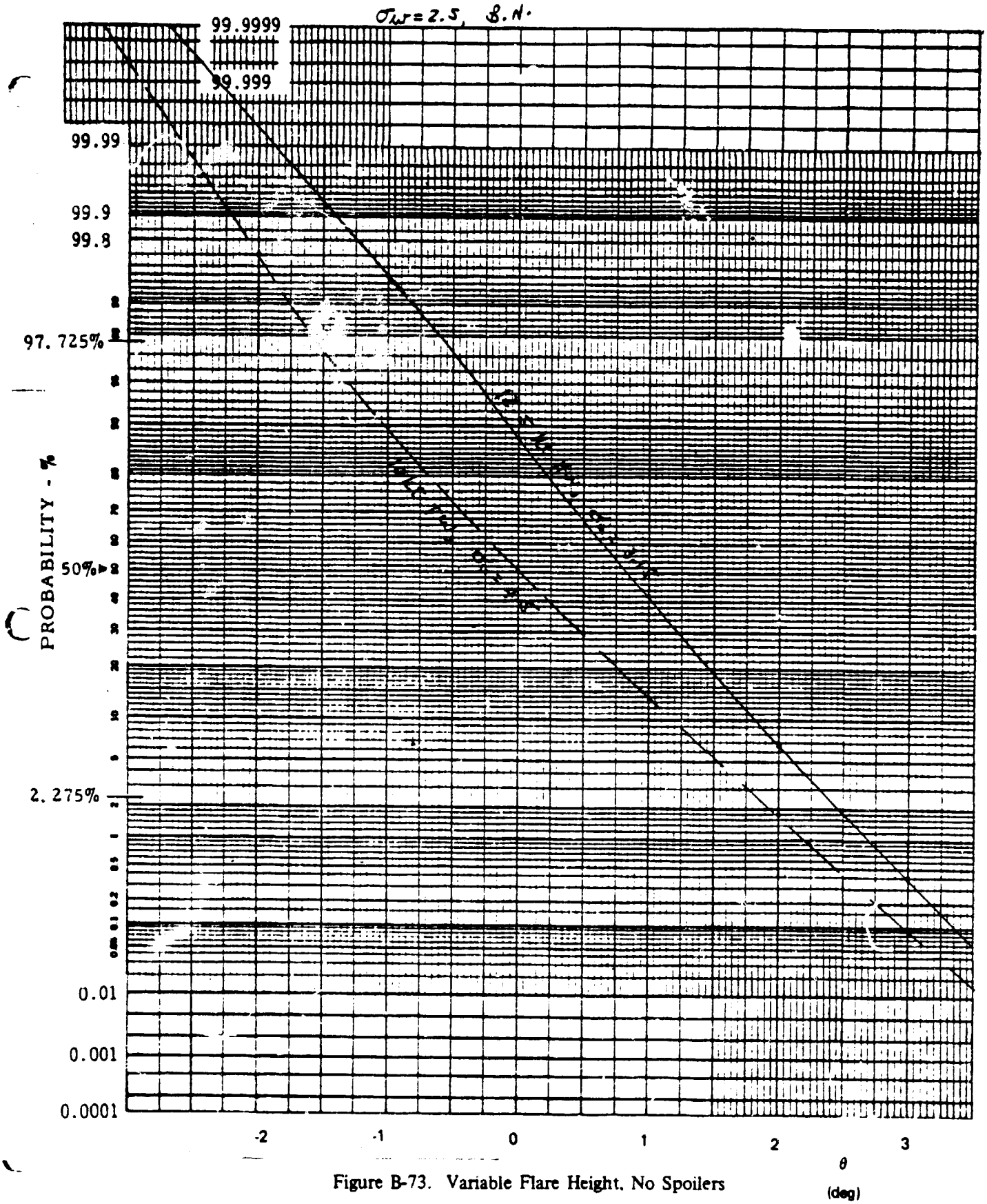

Figure B-73. Variable Flare Height, No Spoilers

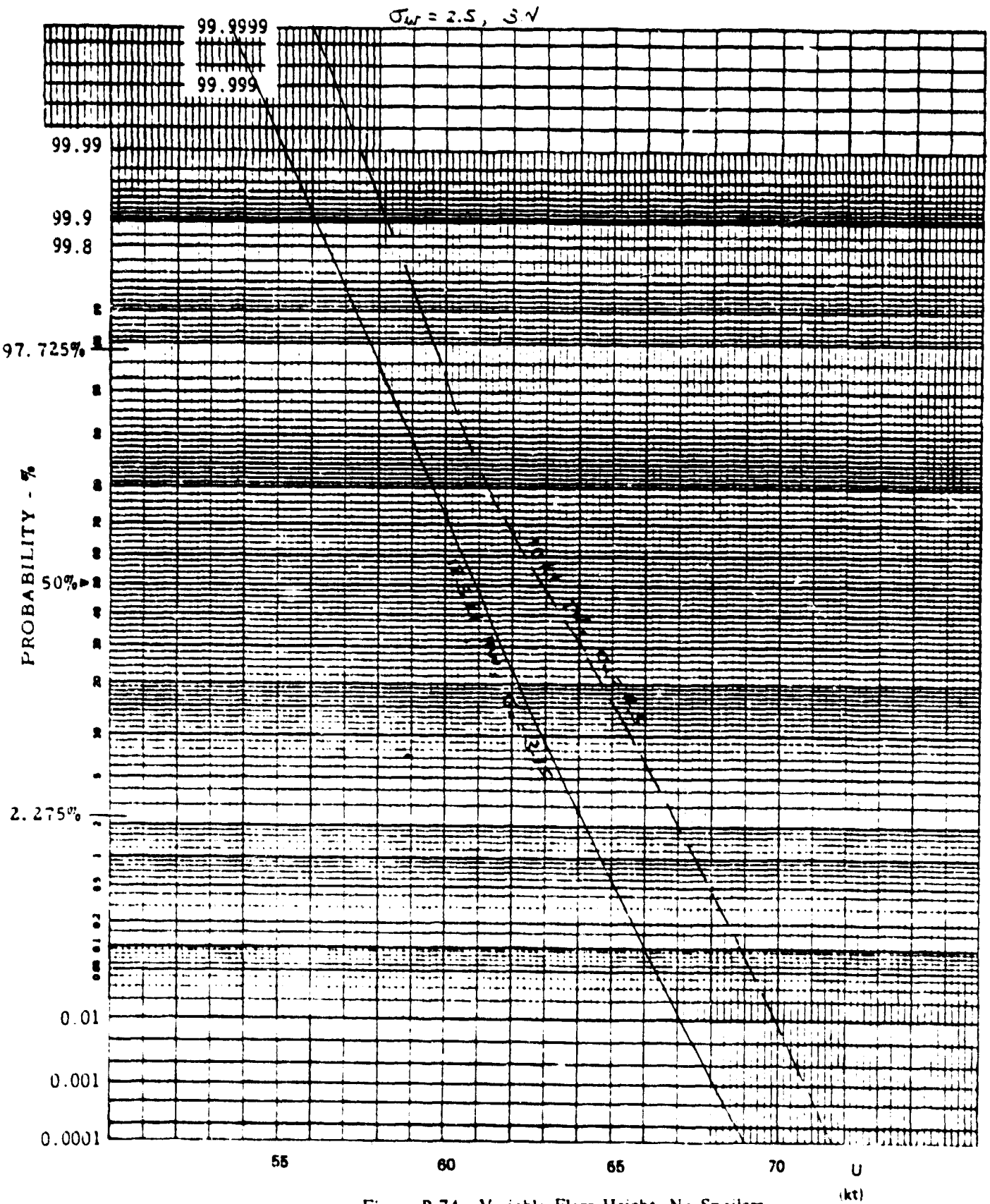

Figure B-74. Variable Flare Height, No Spoilers

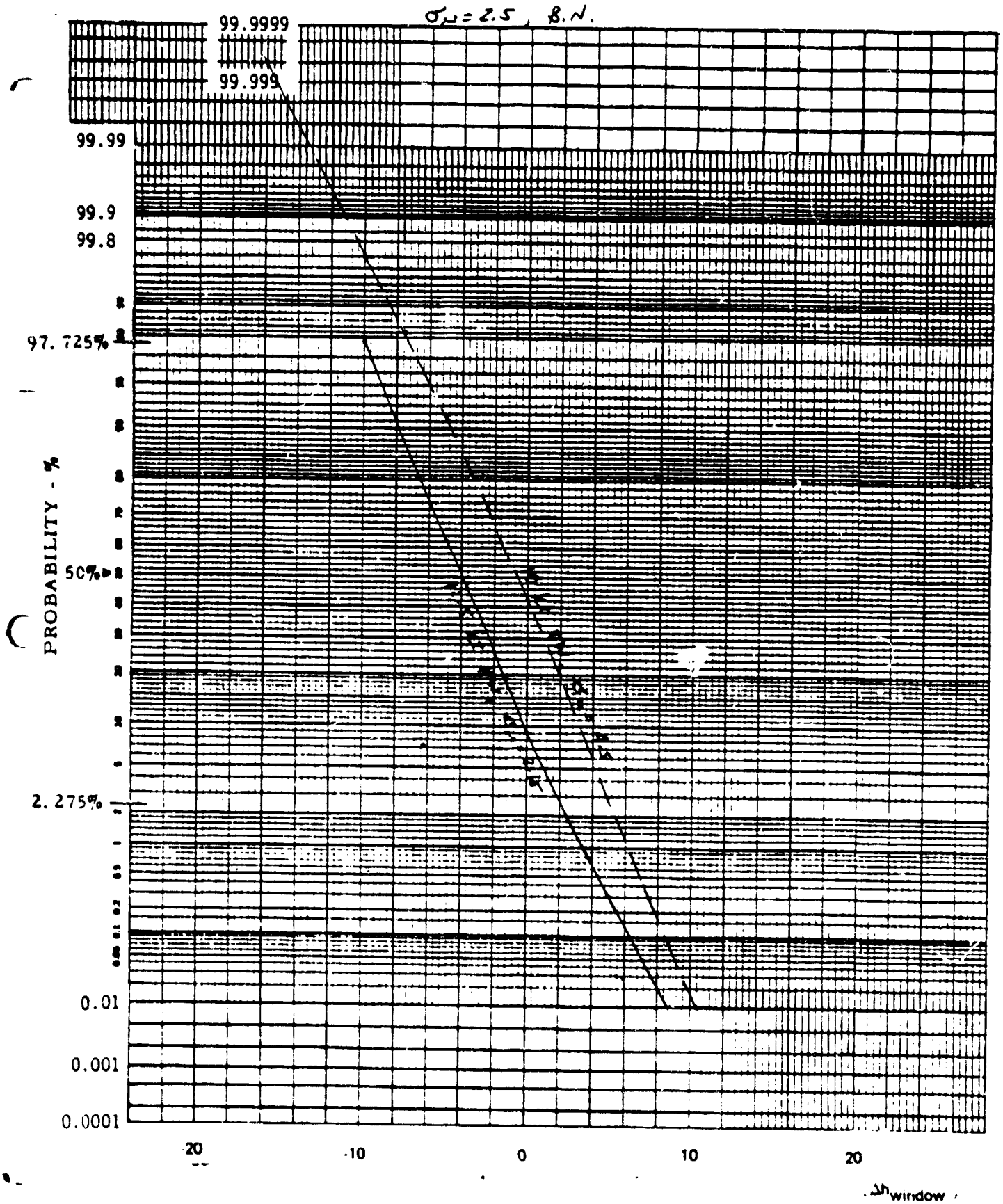

Figure B-75. Variable Flare Height, No Spoilers

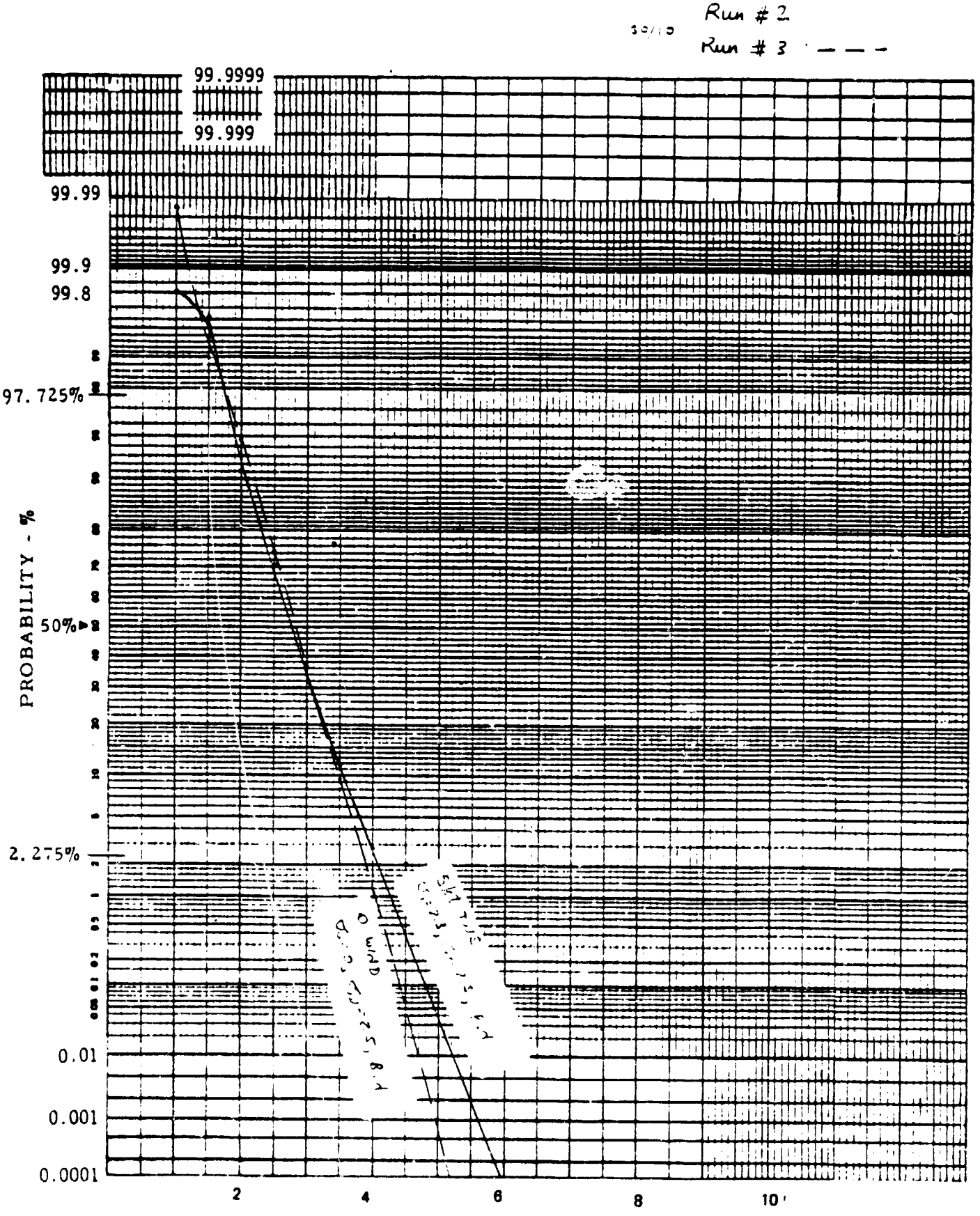

Figure B-76. Variable Flare Height, No Spoilers

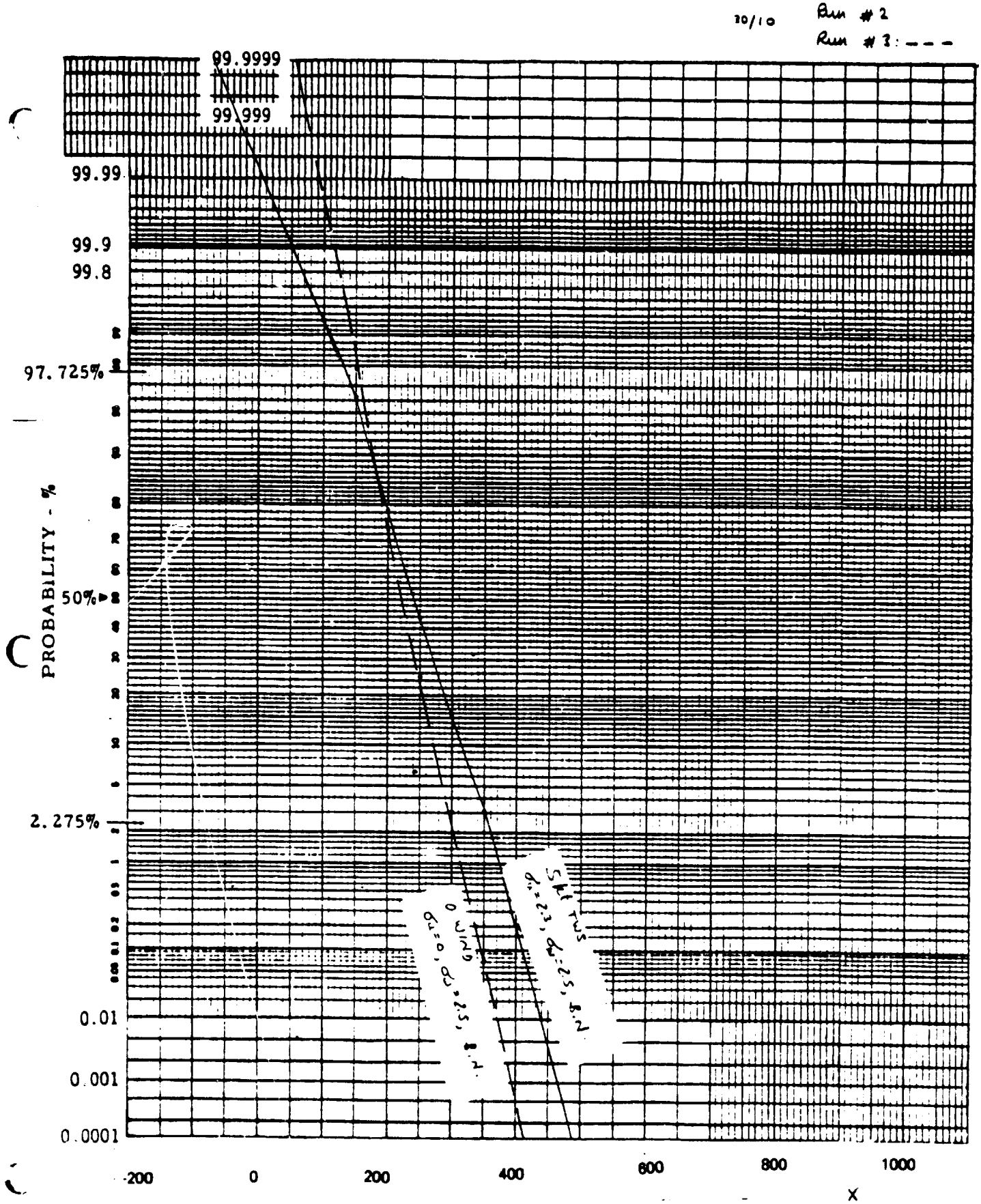

Figure B-77. Variable Flare Height, No Spoilers

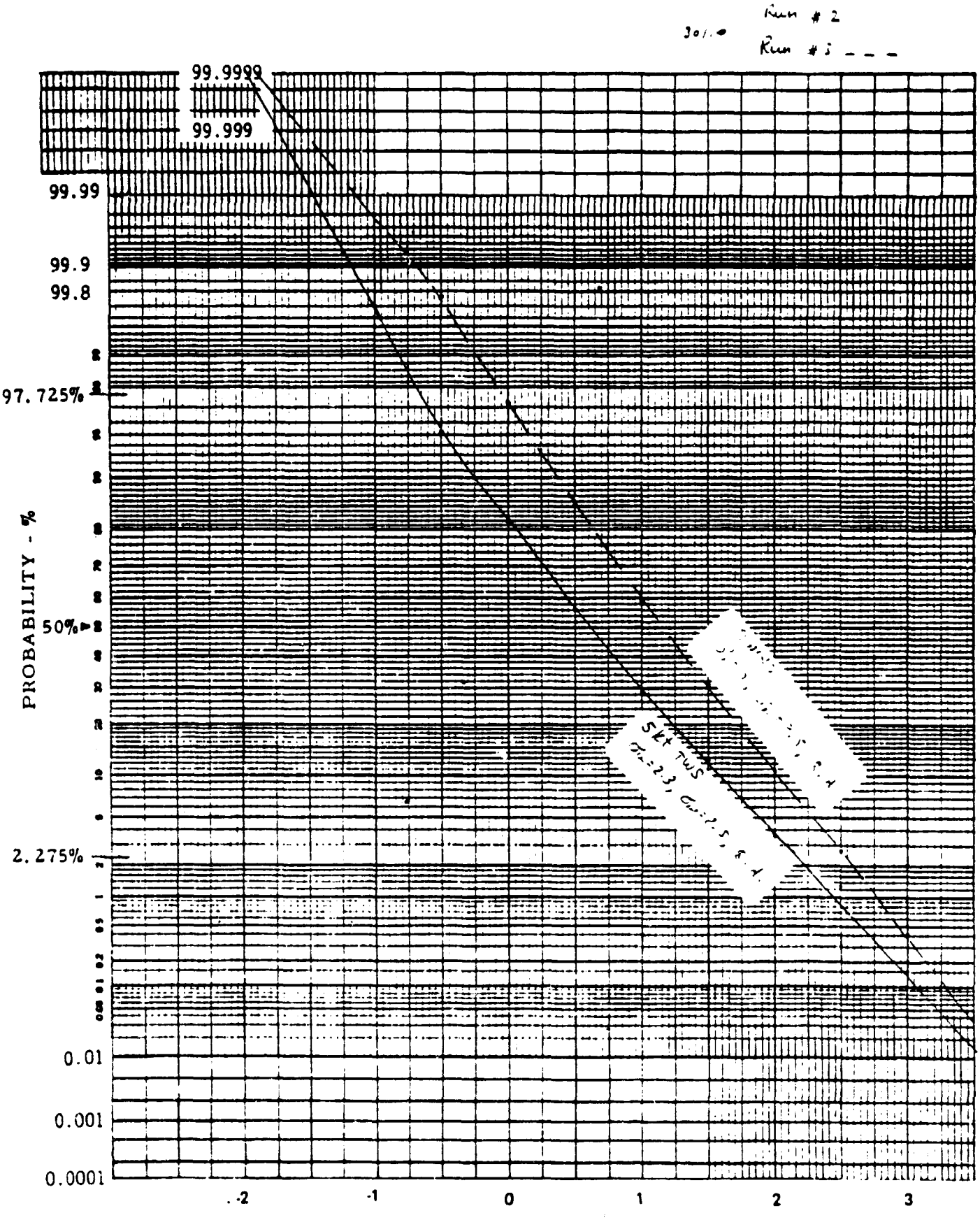

Figure B-78. Variable Flare Height, No Spoilers

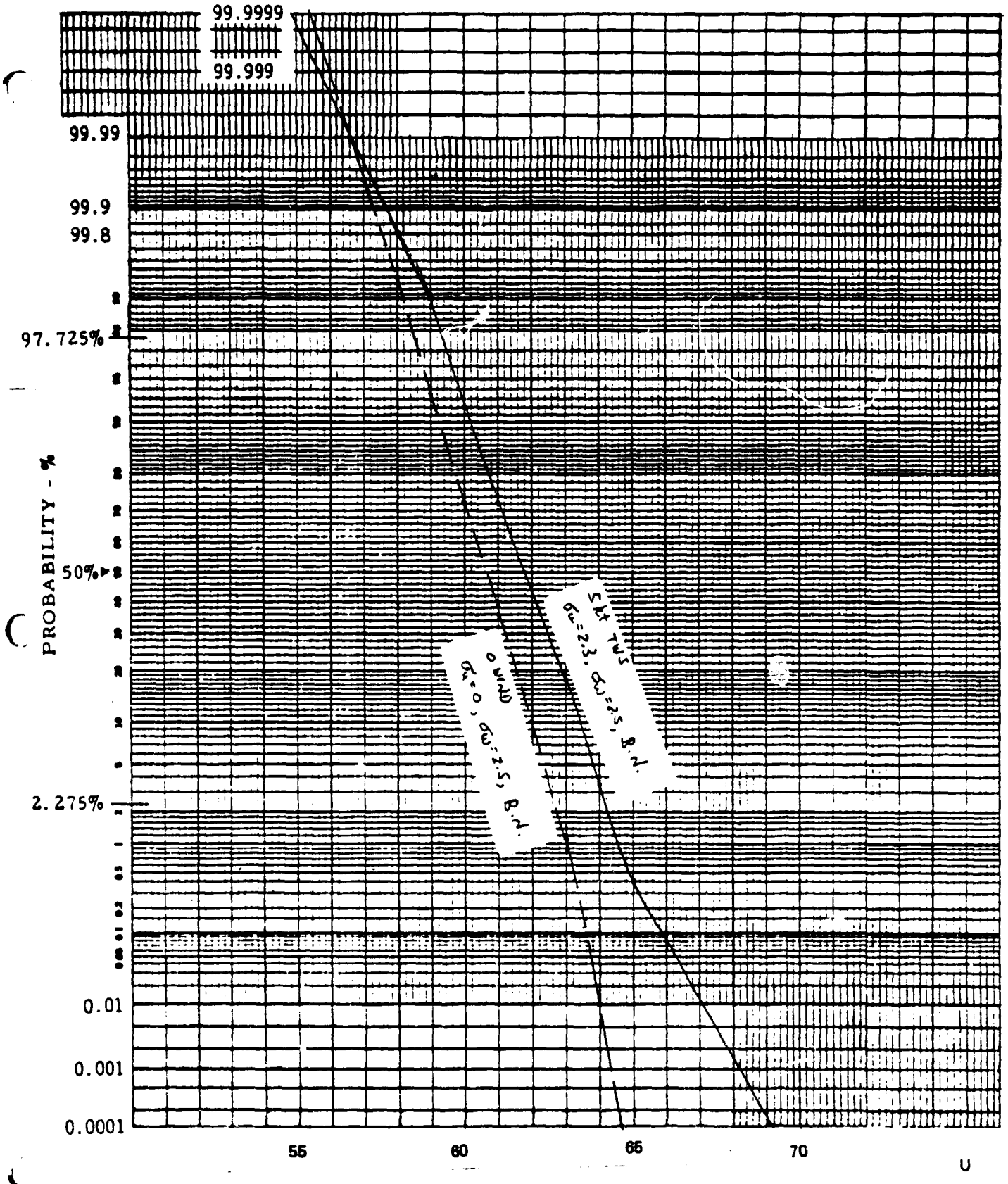

Figure B-79. Variable Flare Height, No Spoilers

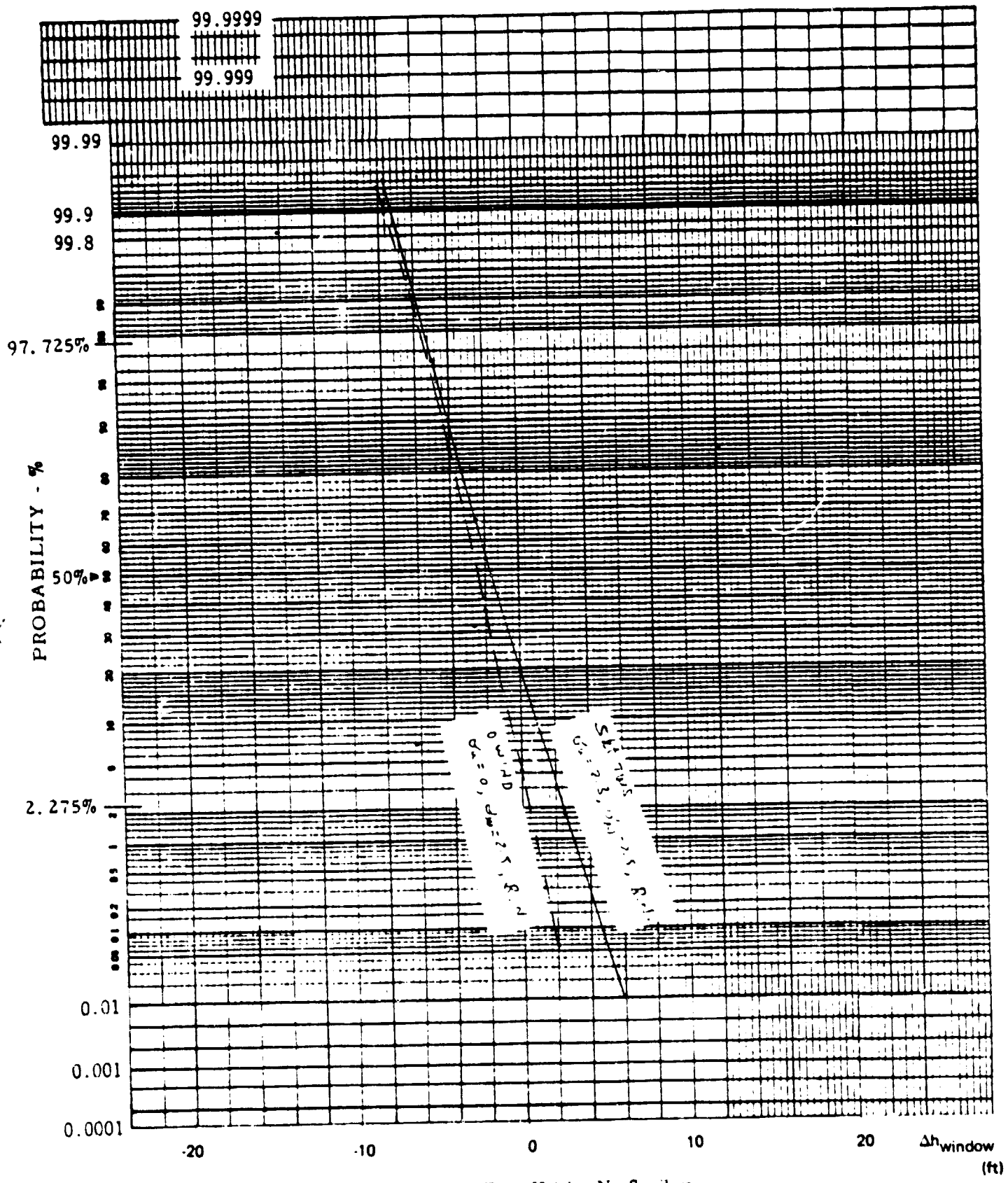

Figure B-80. Variable Flare Height, No Spoilers

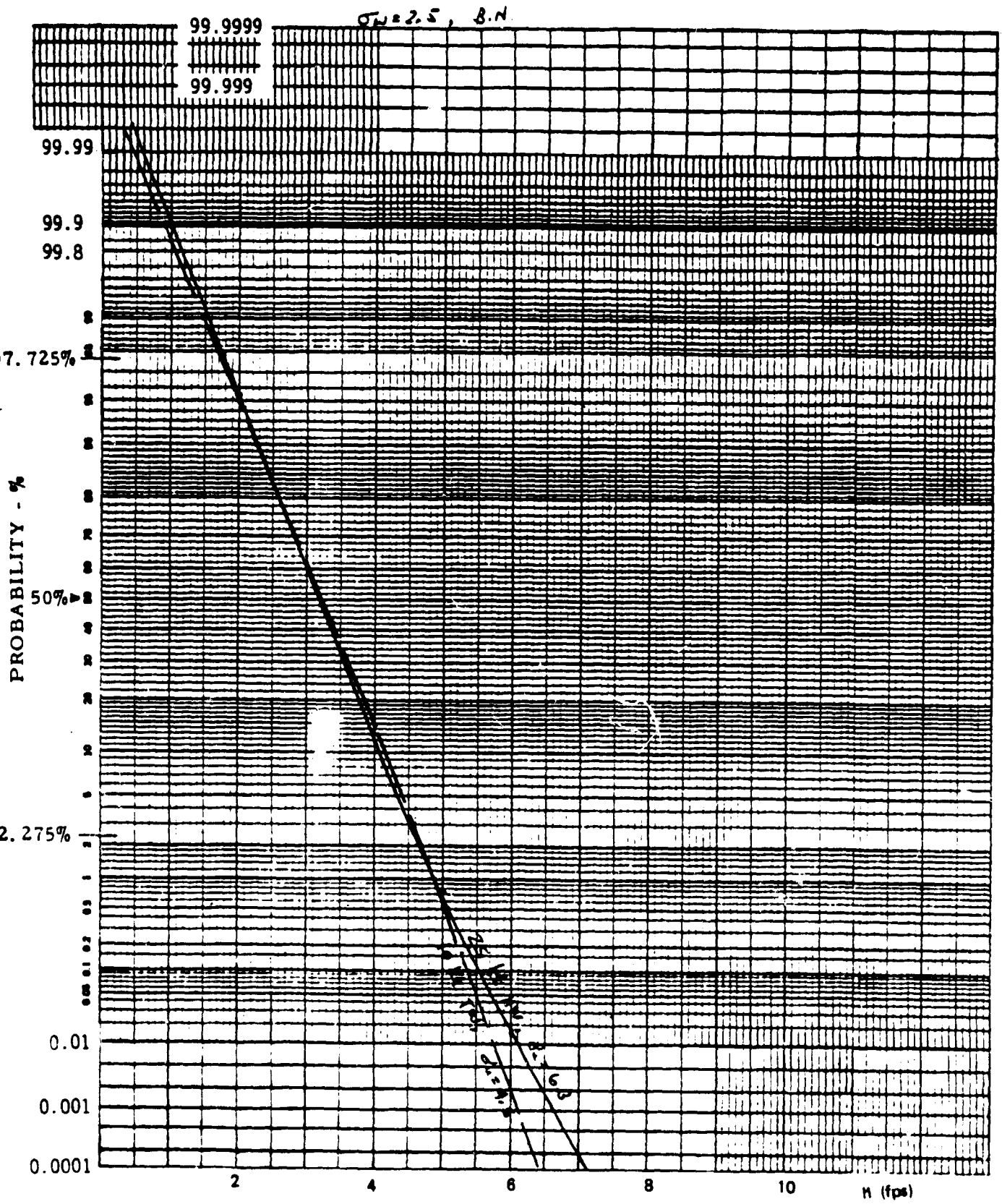

Figure B-81. Constant Flare Height, Spoilers, Low Gains

3DEC#1
9DEC#1

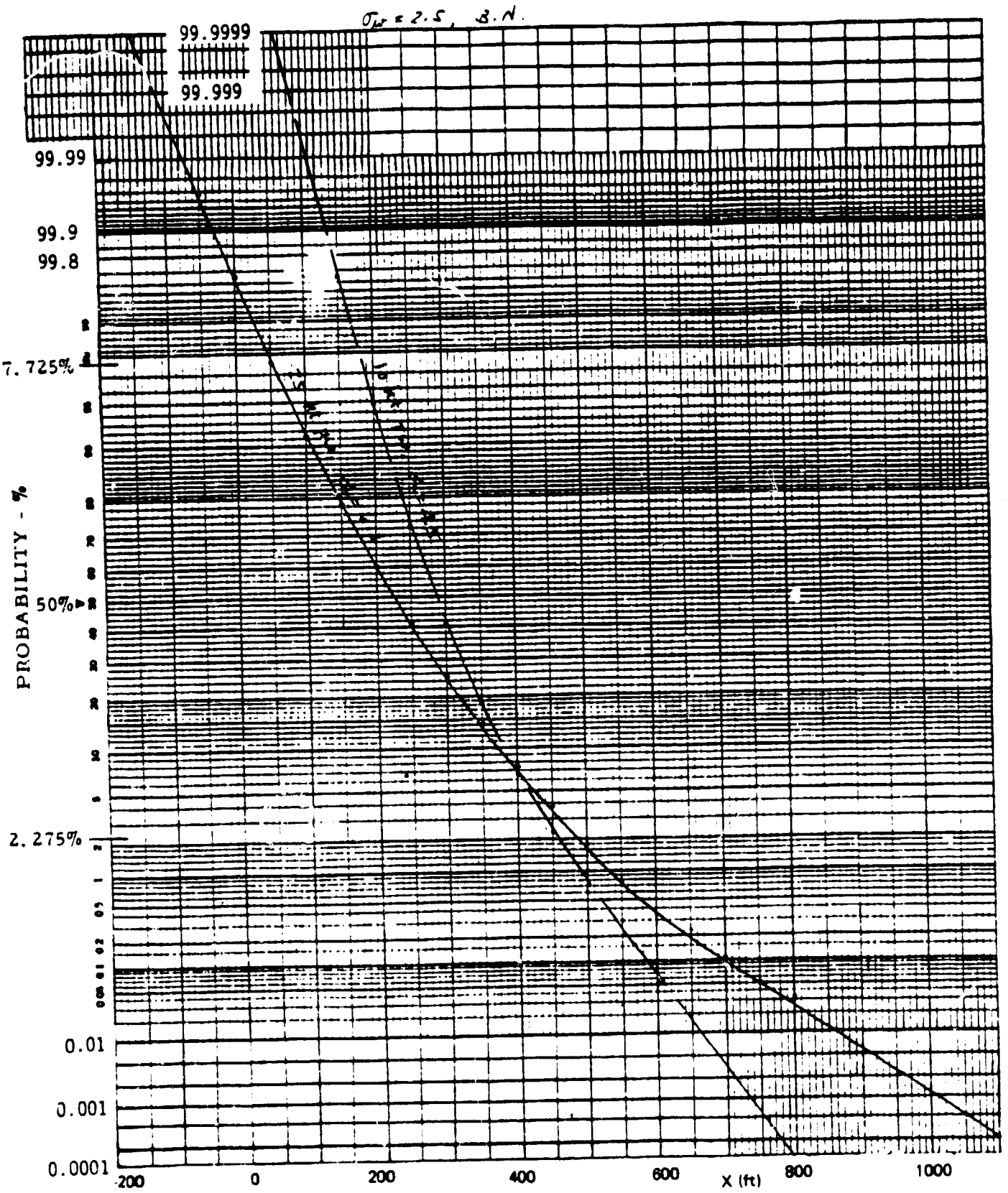

Figure B-82. Constant Flare Height, Spoilers, Low Gains

8 DEC #1
9 DEC #1

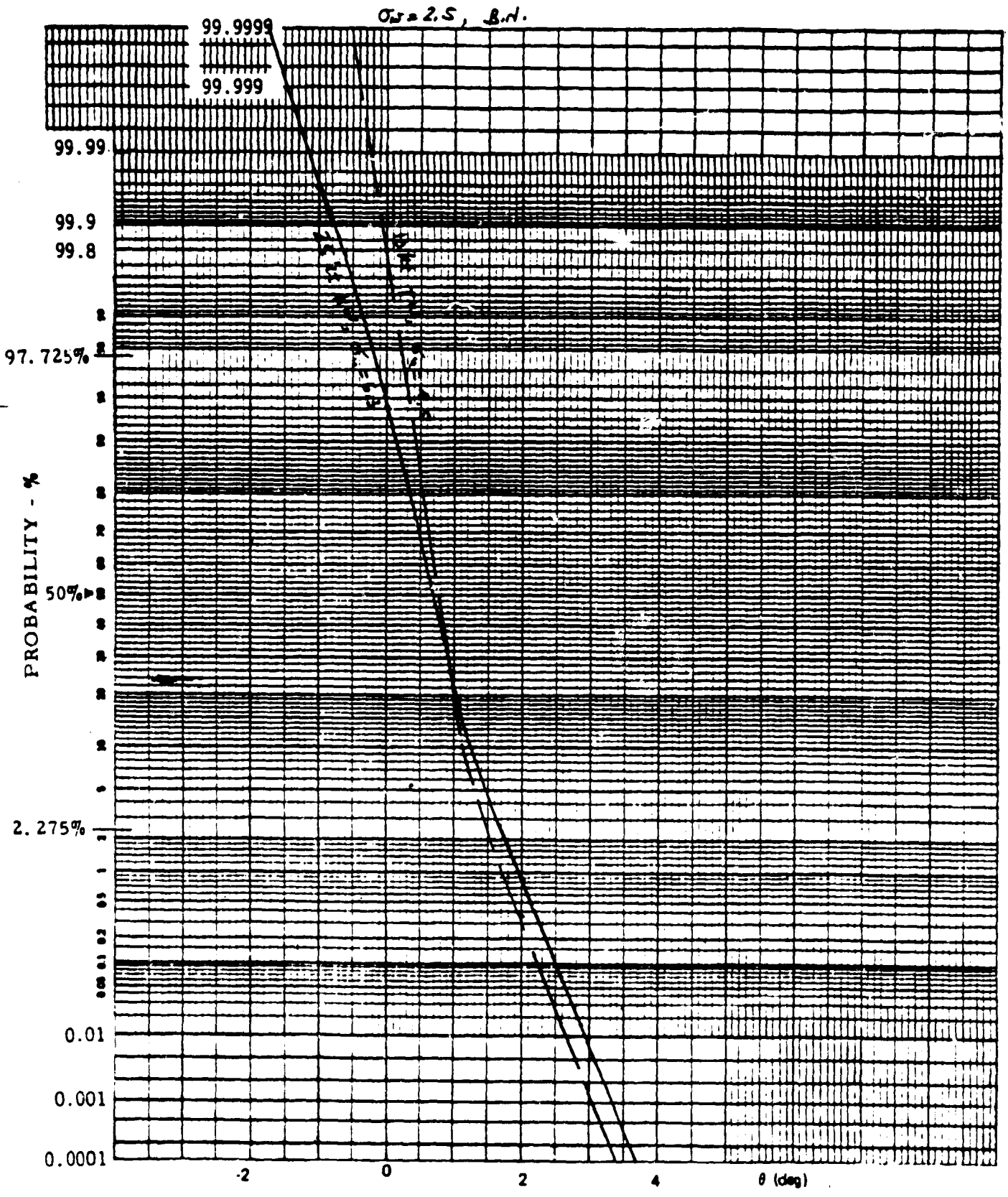

Figure B-83. Constant Flare Height, Spoilers, Low Gains

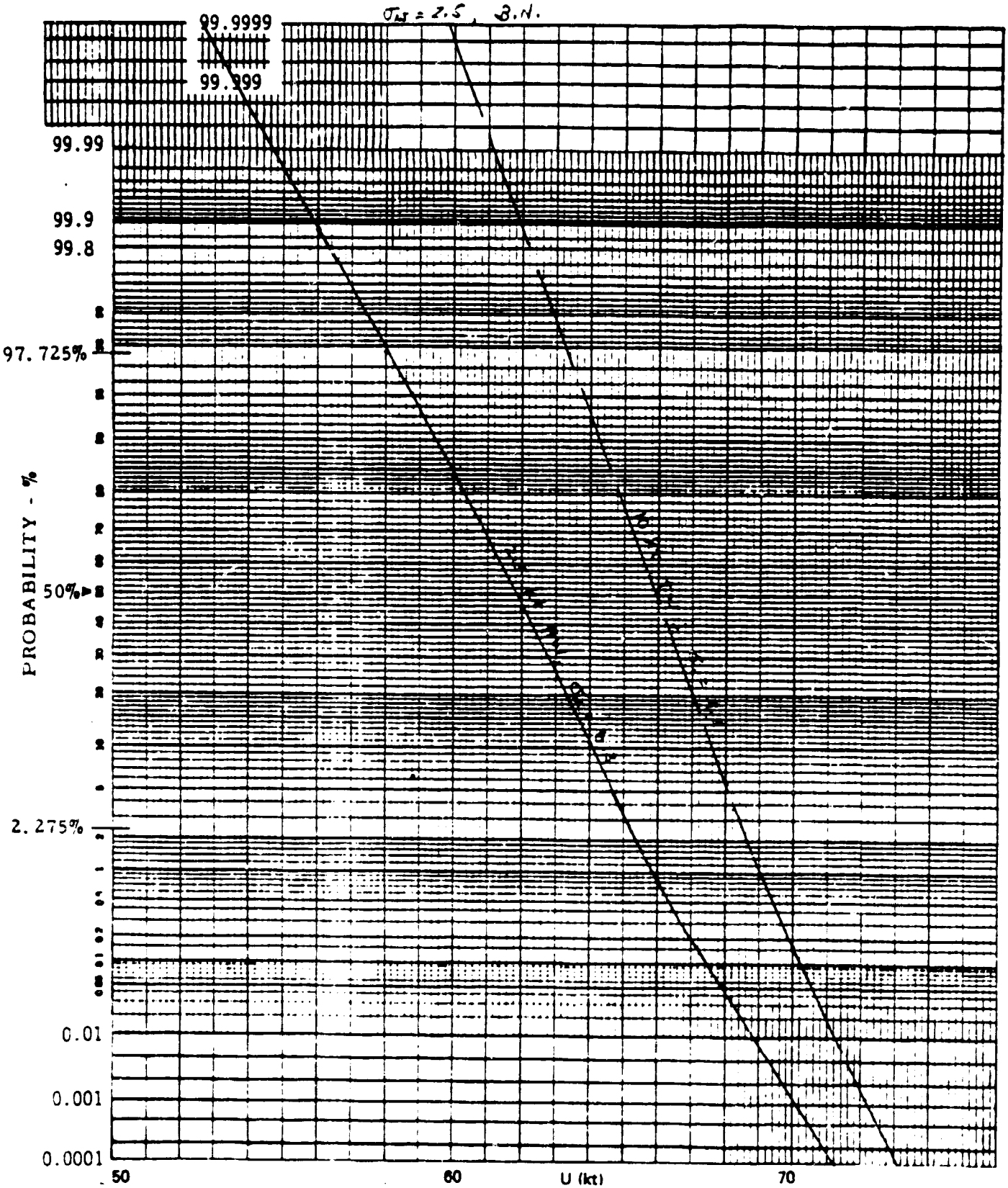

Figure B-84. Constant Flare Height, Spoilers, Low Gains

8 DEC # 1
9 DEC # 1

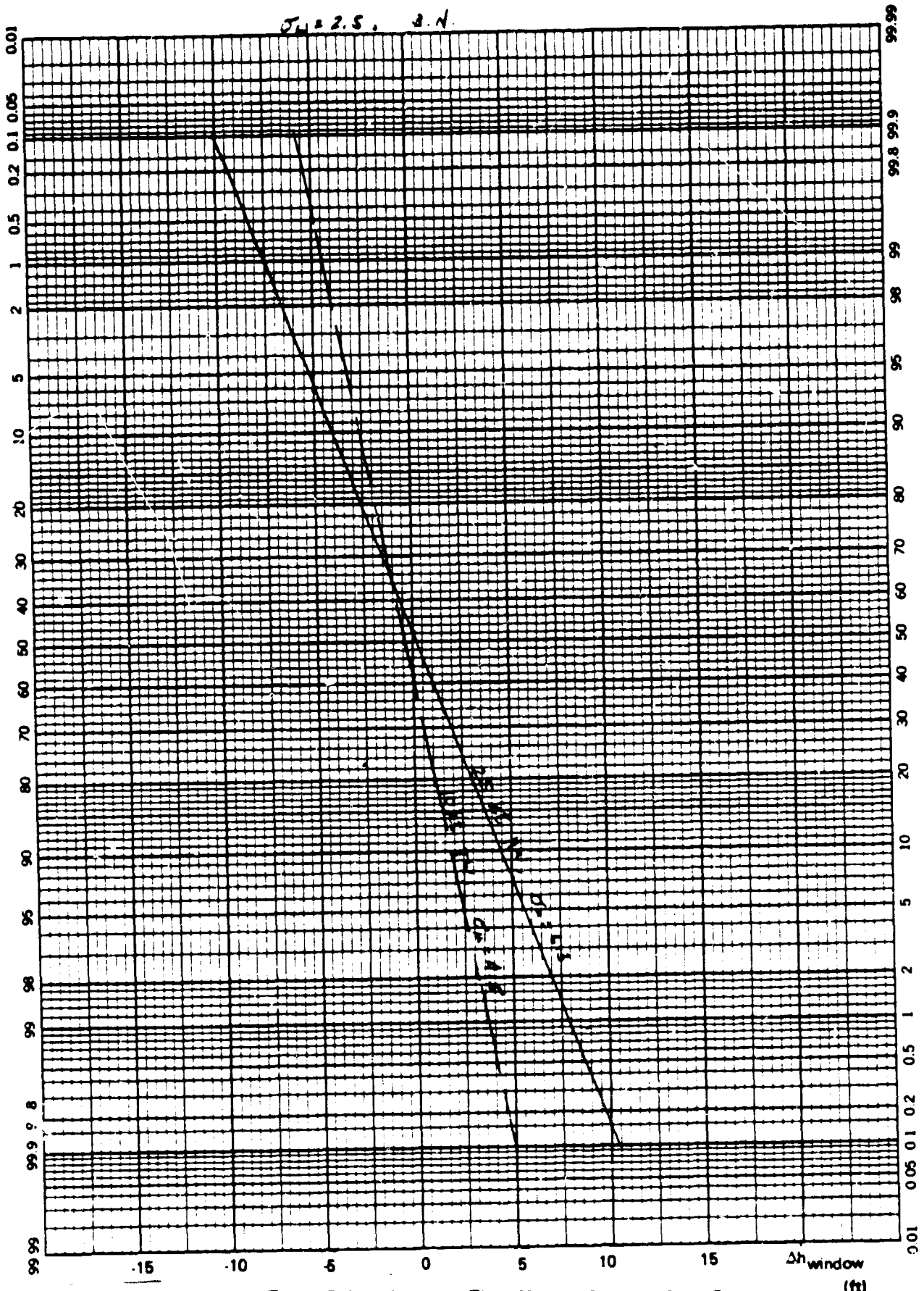

Figure B-85. Constant Flare Height, Spoilers, Low Gains

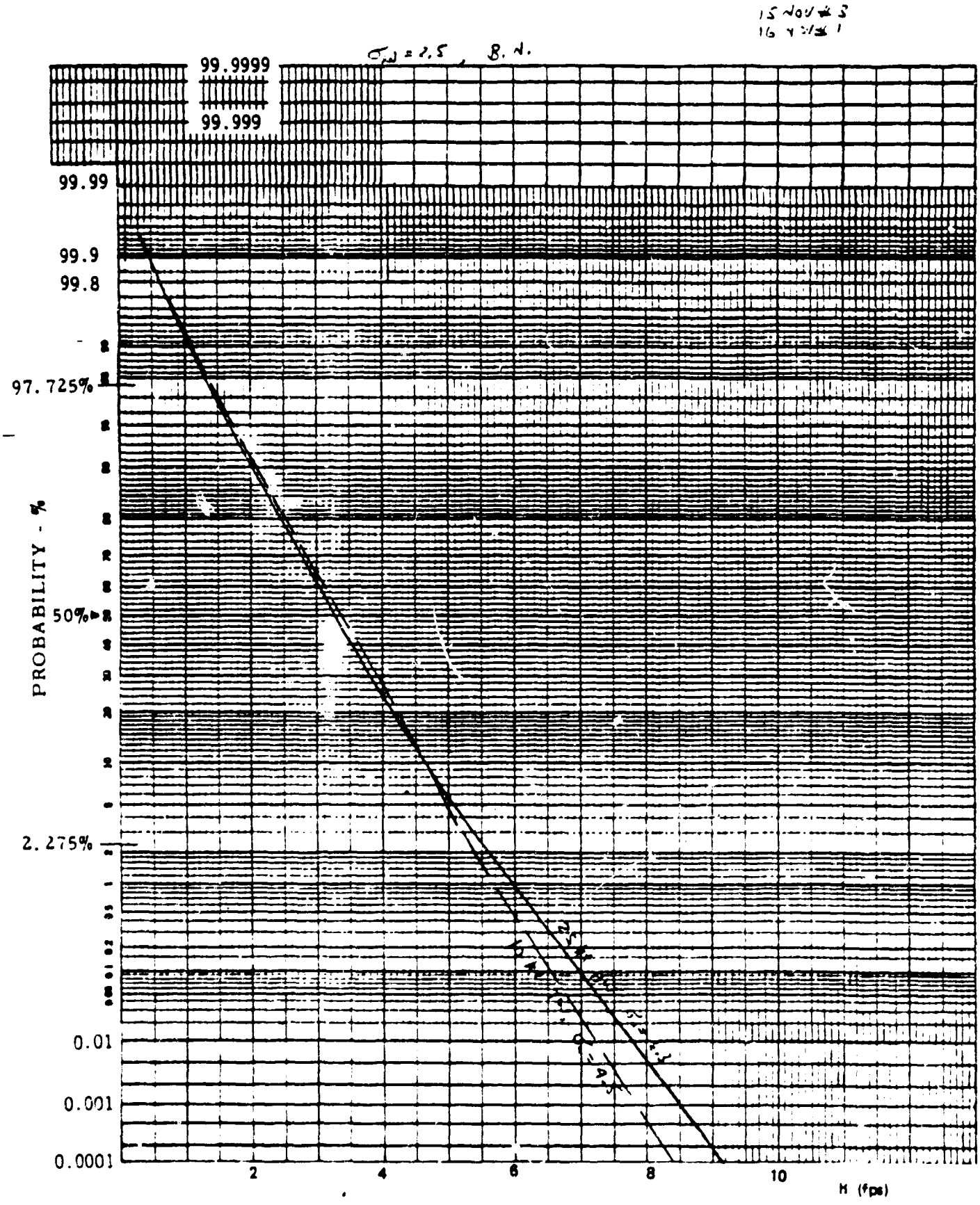

Figure B-86. Constant Flare Height, No Spoilers, Low Gains

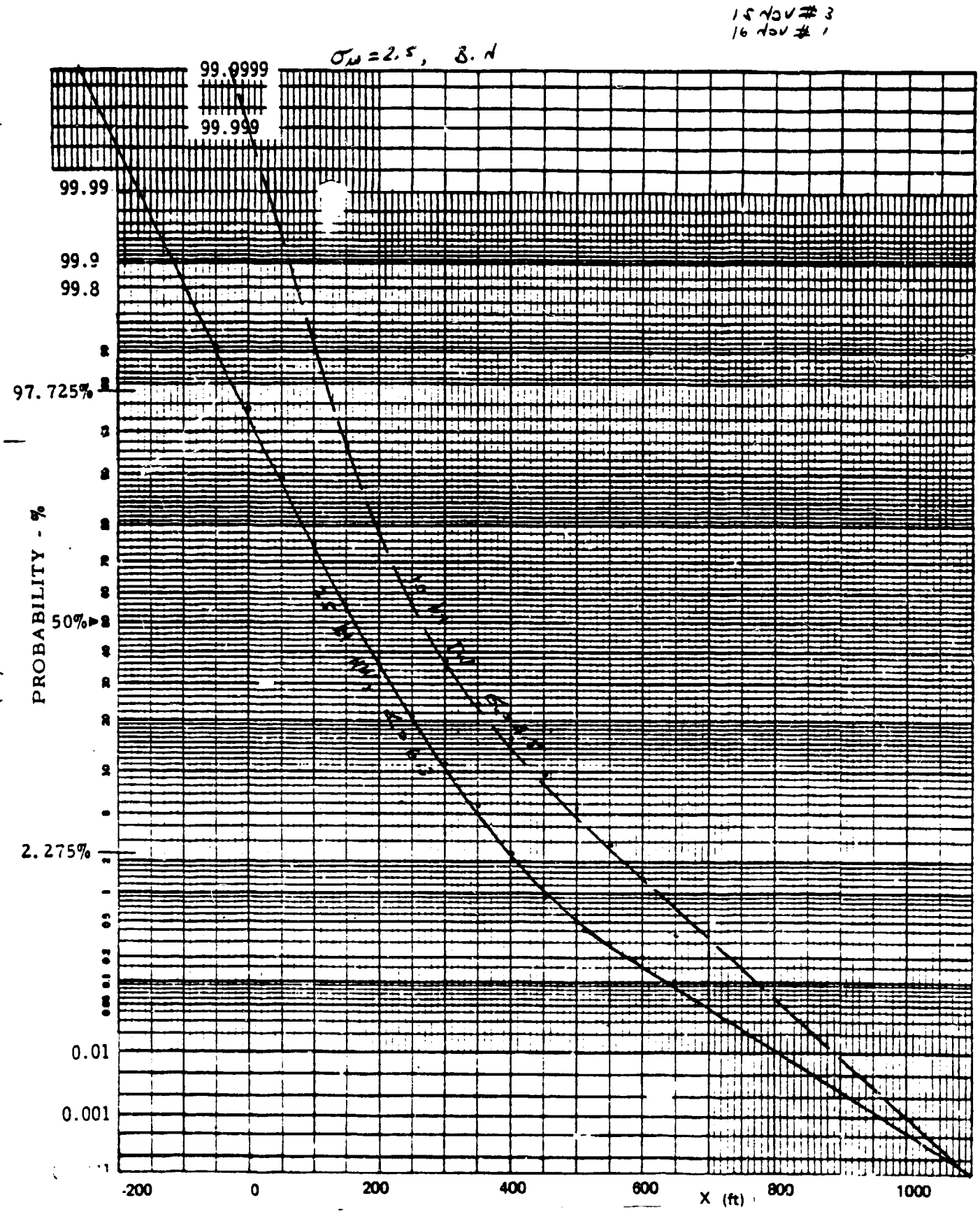

Figure B-87. Constant Flare Height, No Spoilers, Low Gains

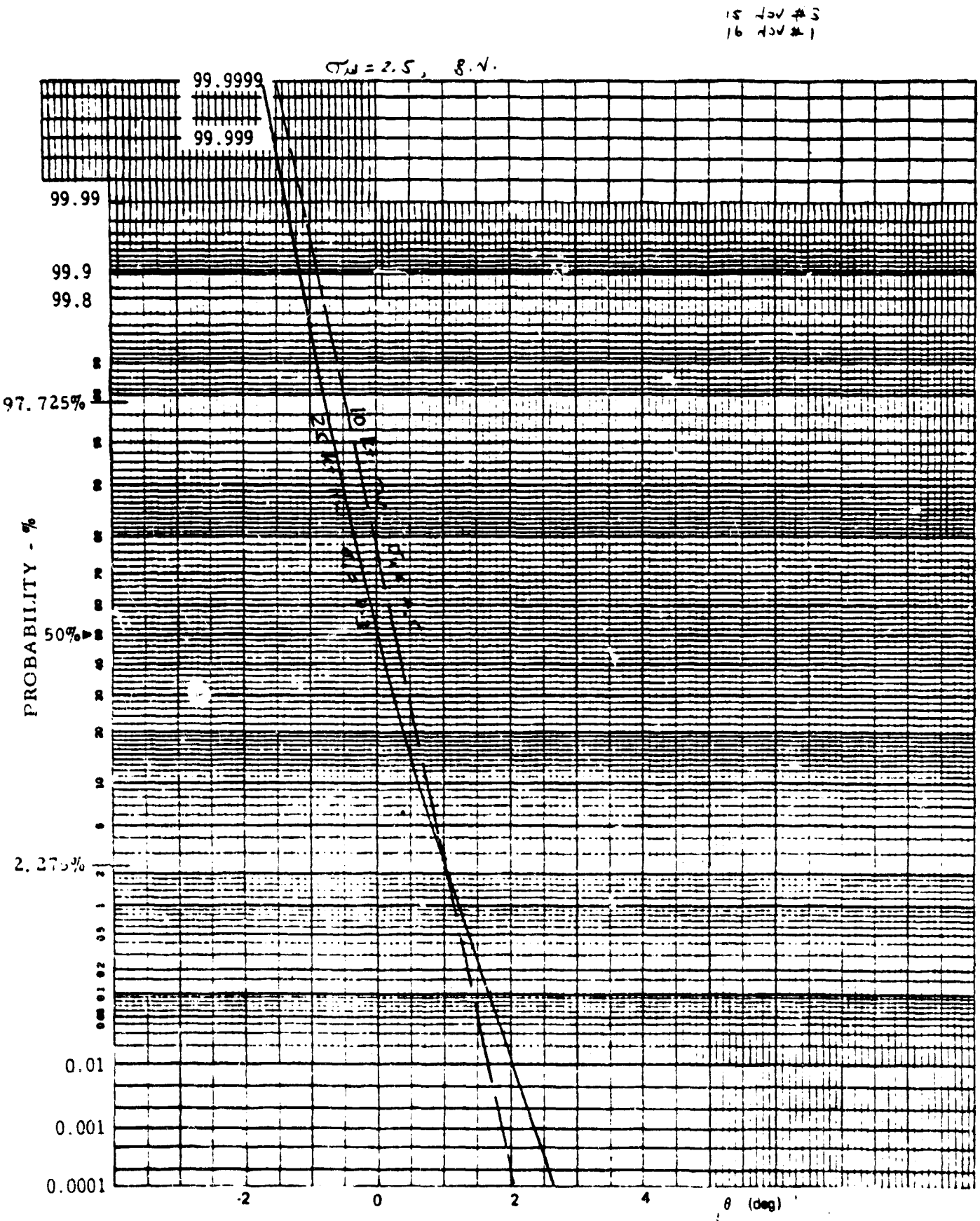

Figure B-88. Constant Flare Height, No Spoilers, Low Gains

15 NOV #3
16 NOV #1

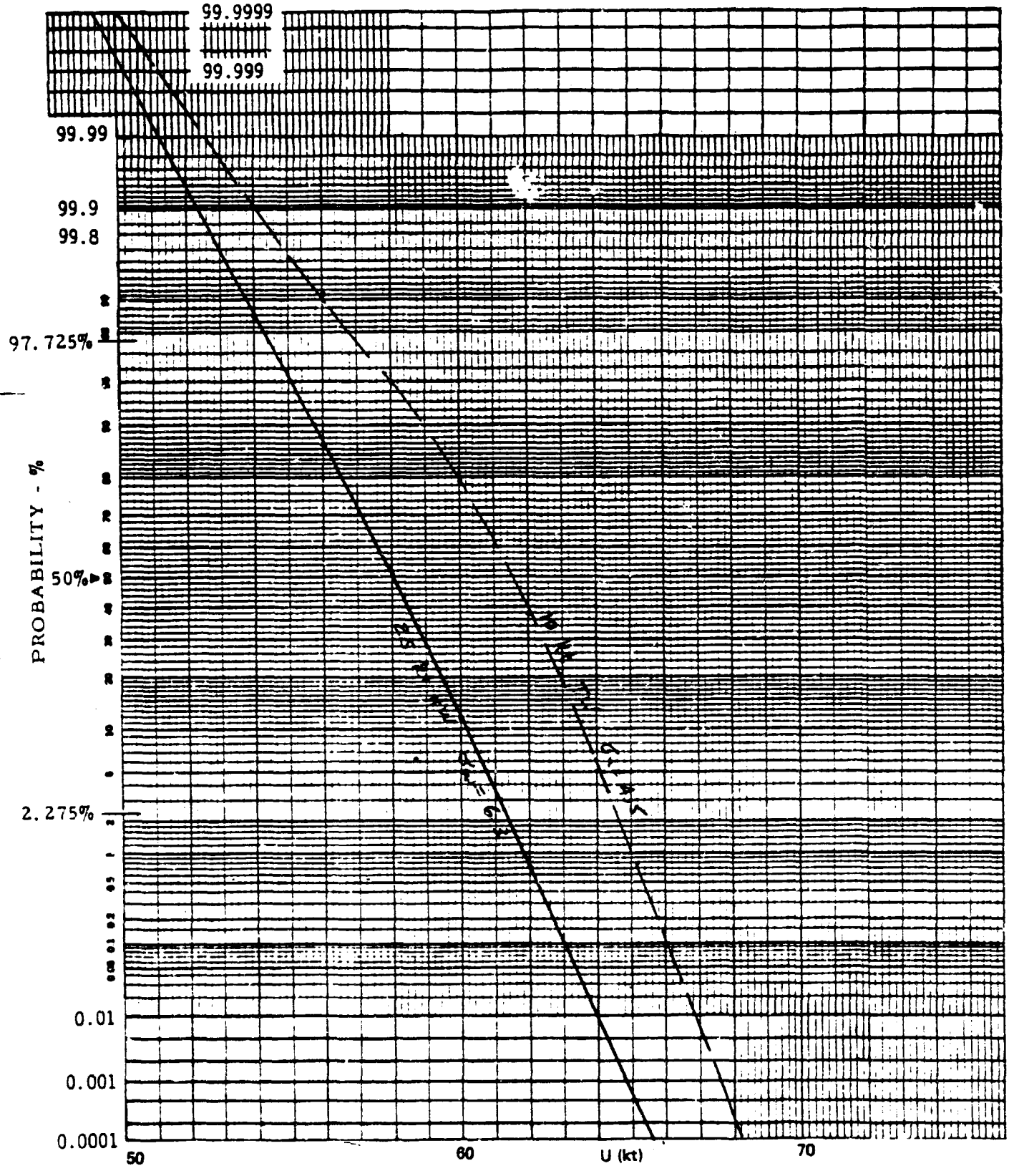

Figure B-89. Constant Flare Height, No Spoilers, Low Gains

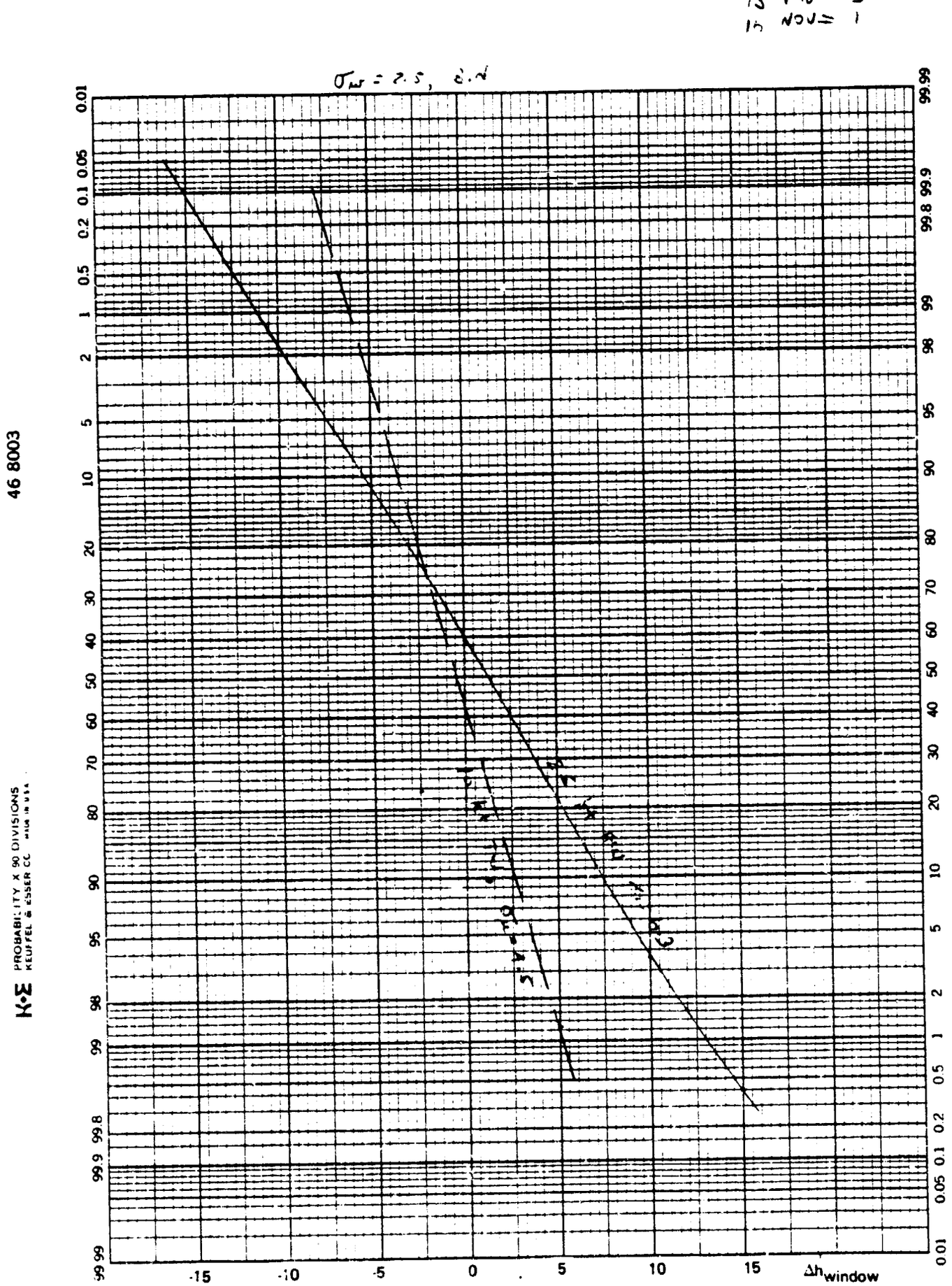

Figure B-90. Constant Flare Height, No Spoilers, Low Gains

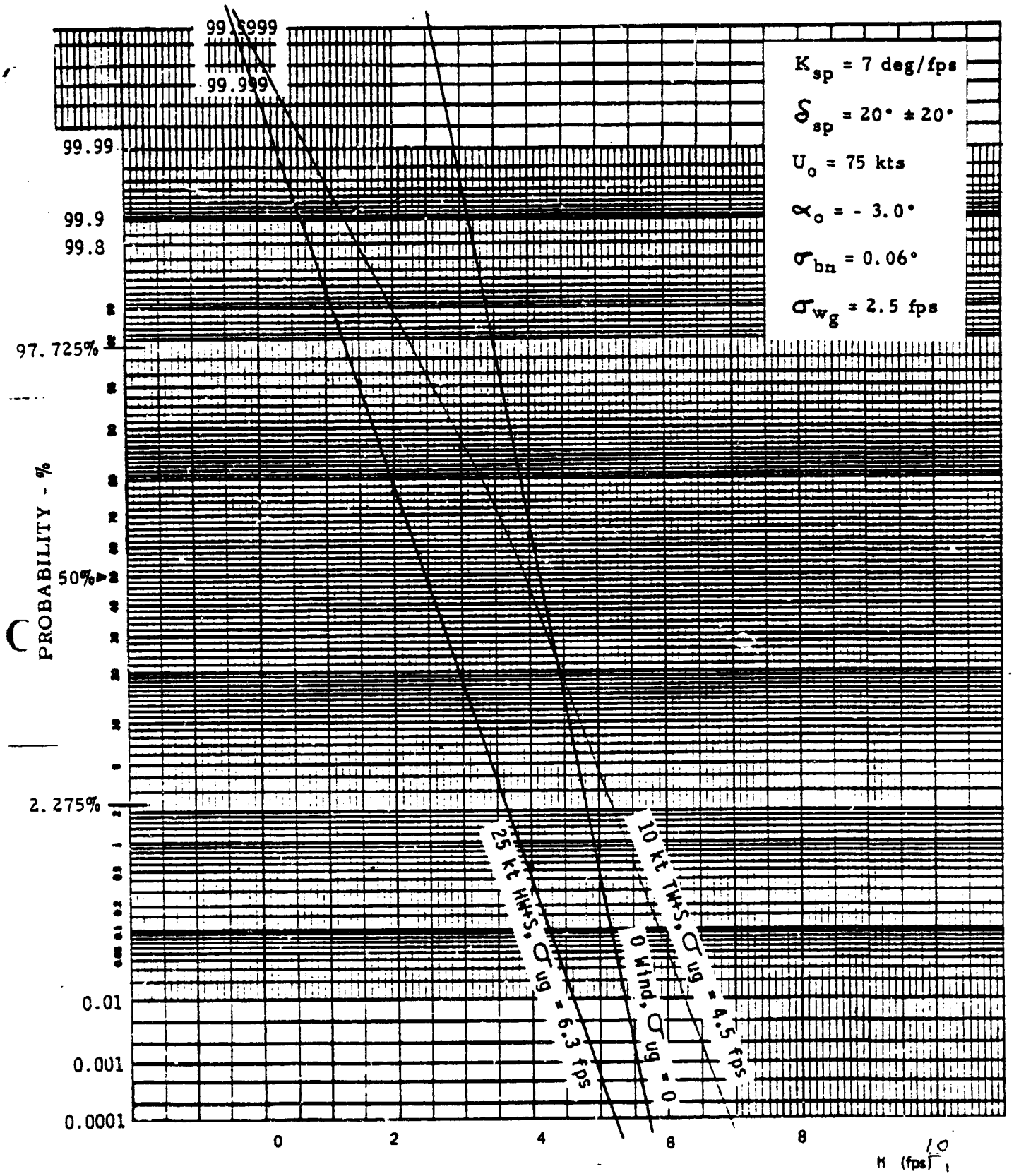

Figure B-91. Constant Flare Height, High Gains, Spoilers

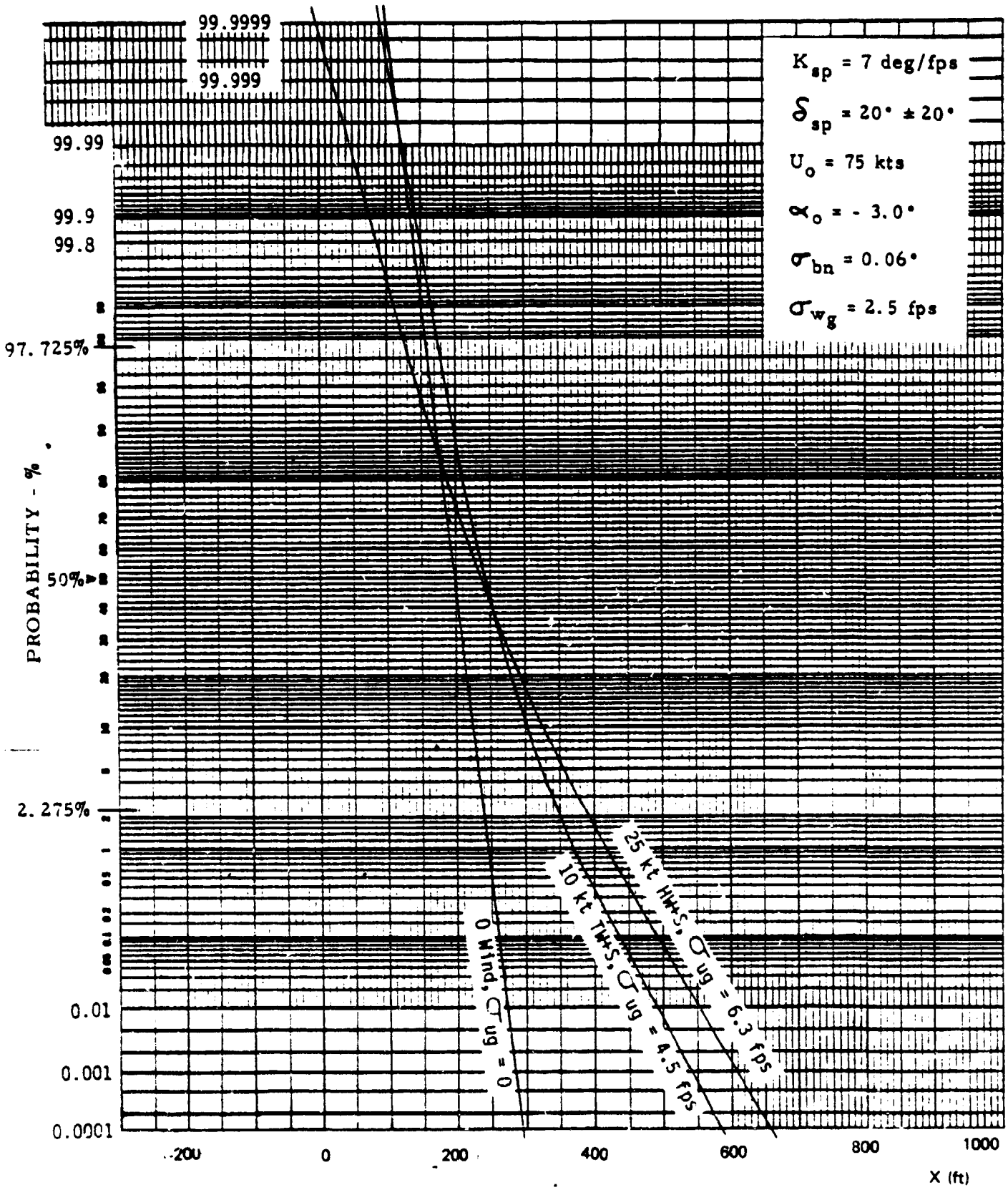

Figure B-92. Constant Flare Height, High Gains, Spoilers

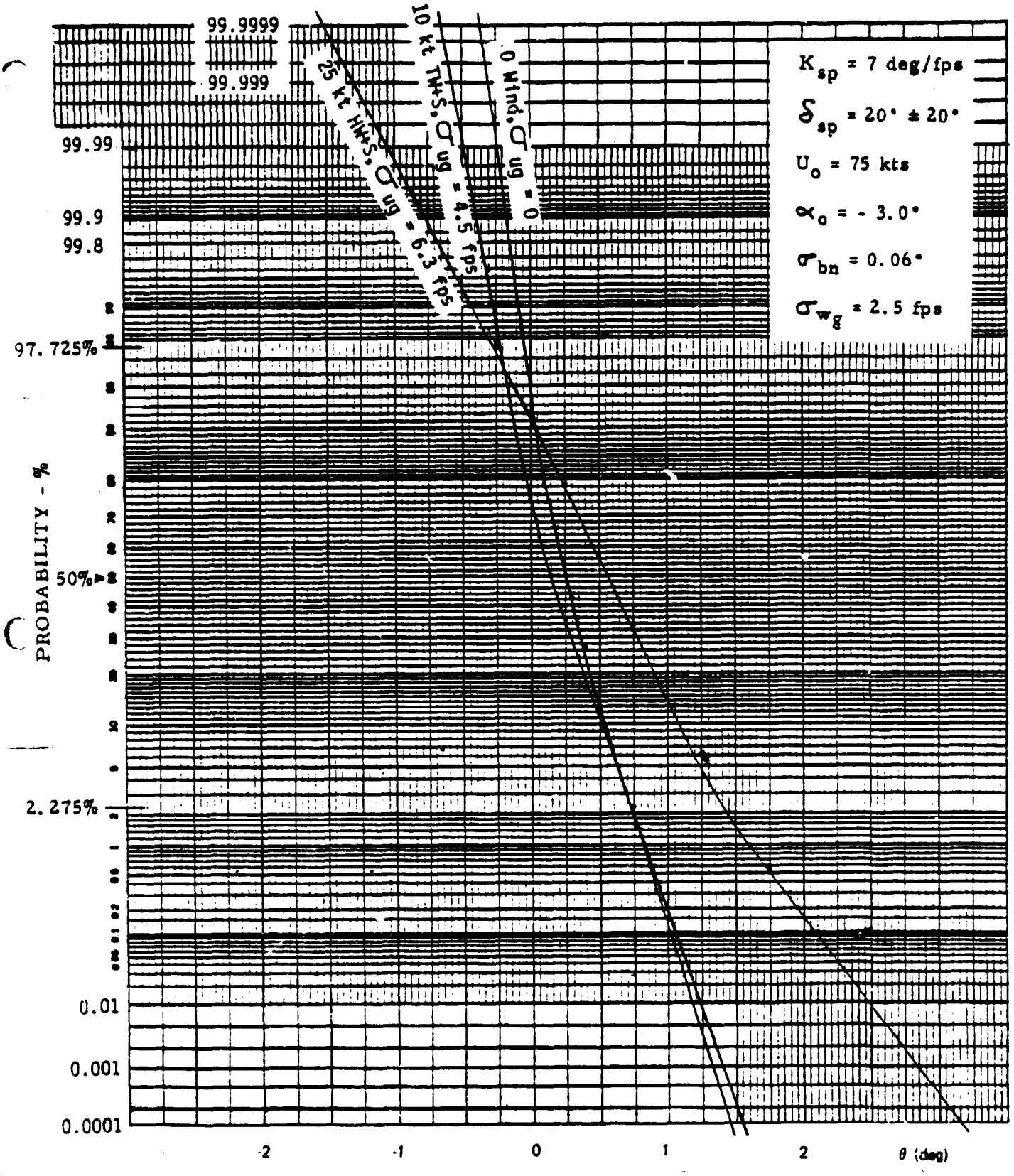

Figure B-93. Constant Flare Height, High Gains, Spoilers

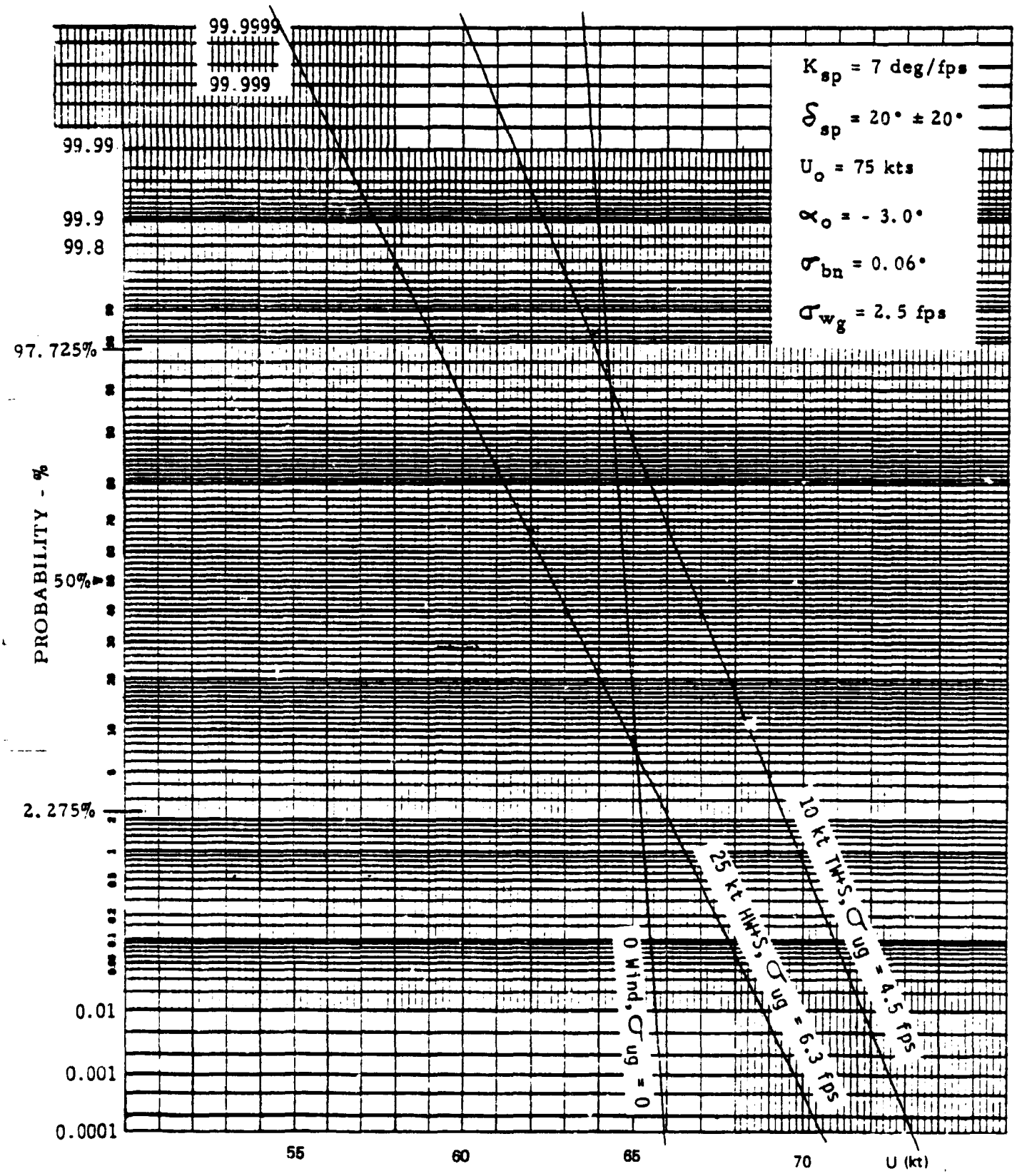

Figure B-94. Constant Flare Height, High Gains, Spoilers

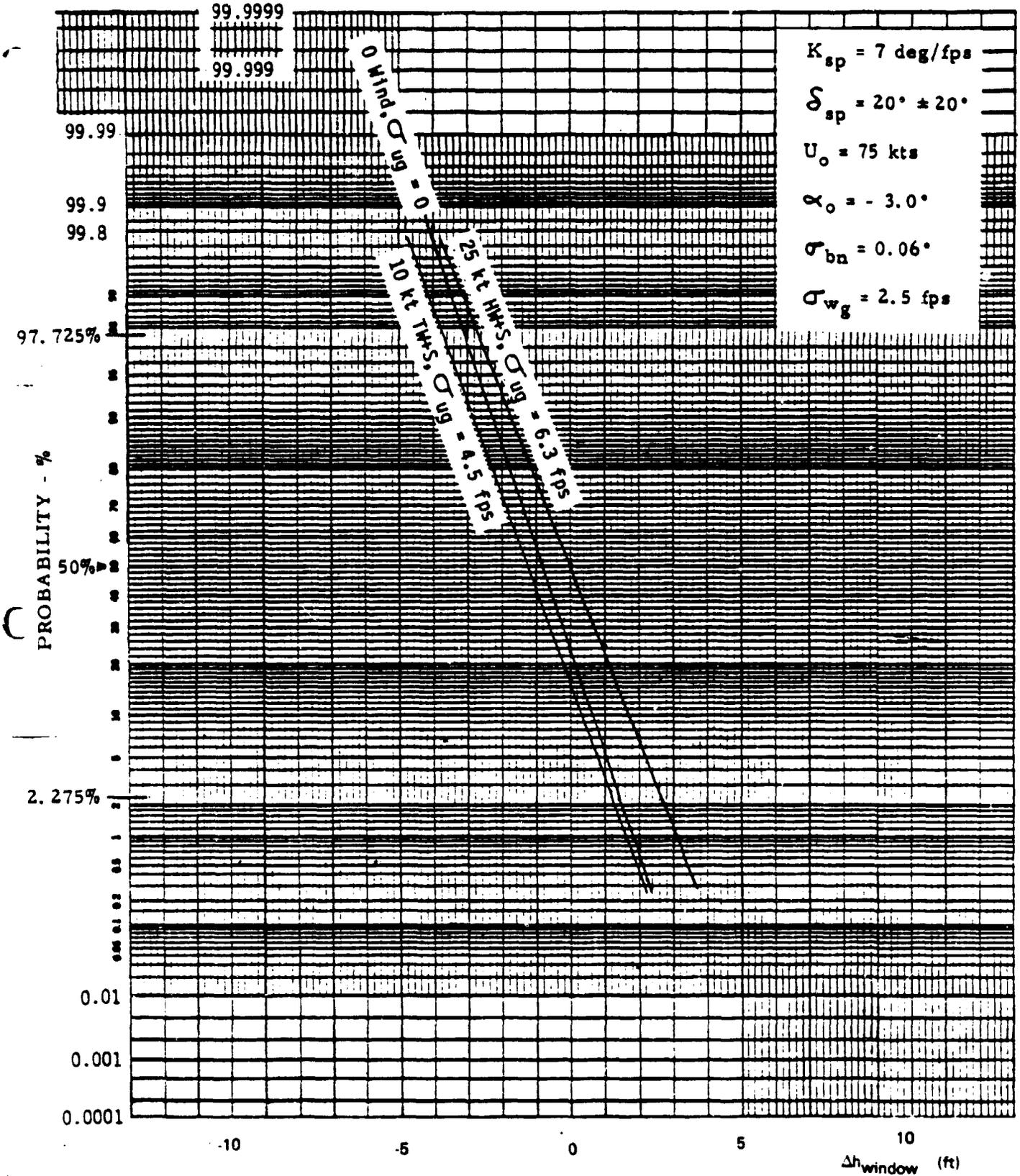

Figure B-95. Constant Flare Height, High Gains, Spoilers

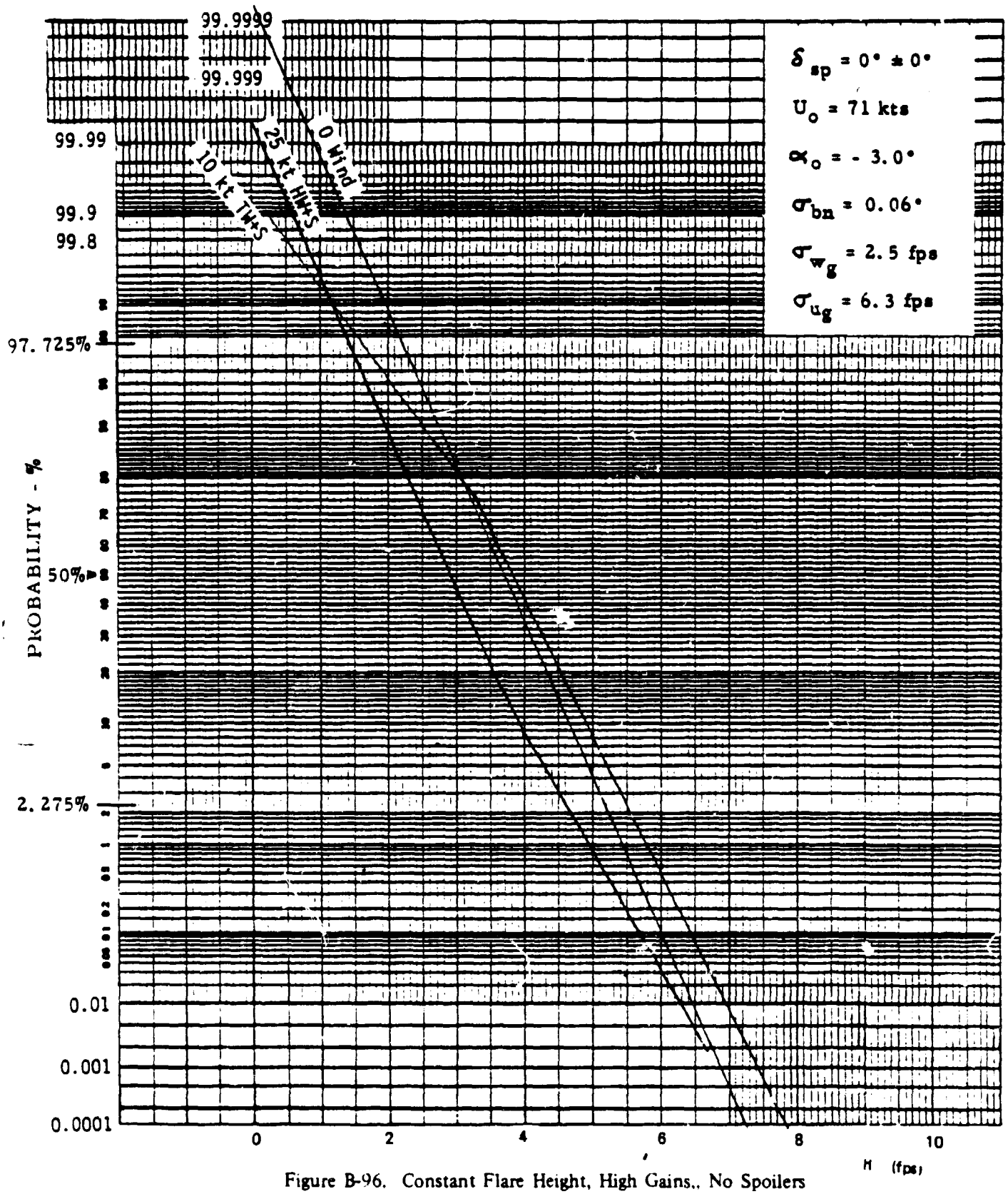

Figure B-96. Constant Flare Height, High Gains., No Spoilers

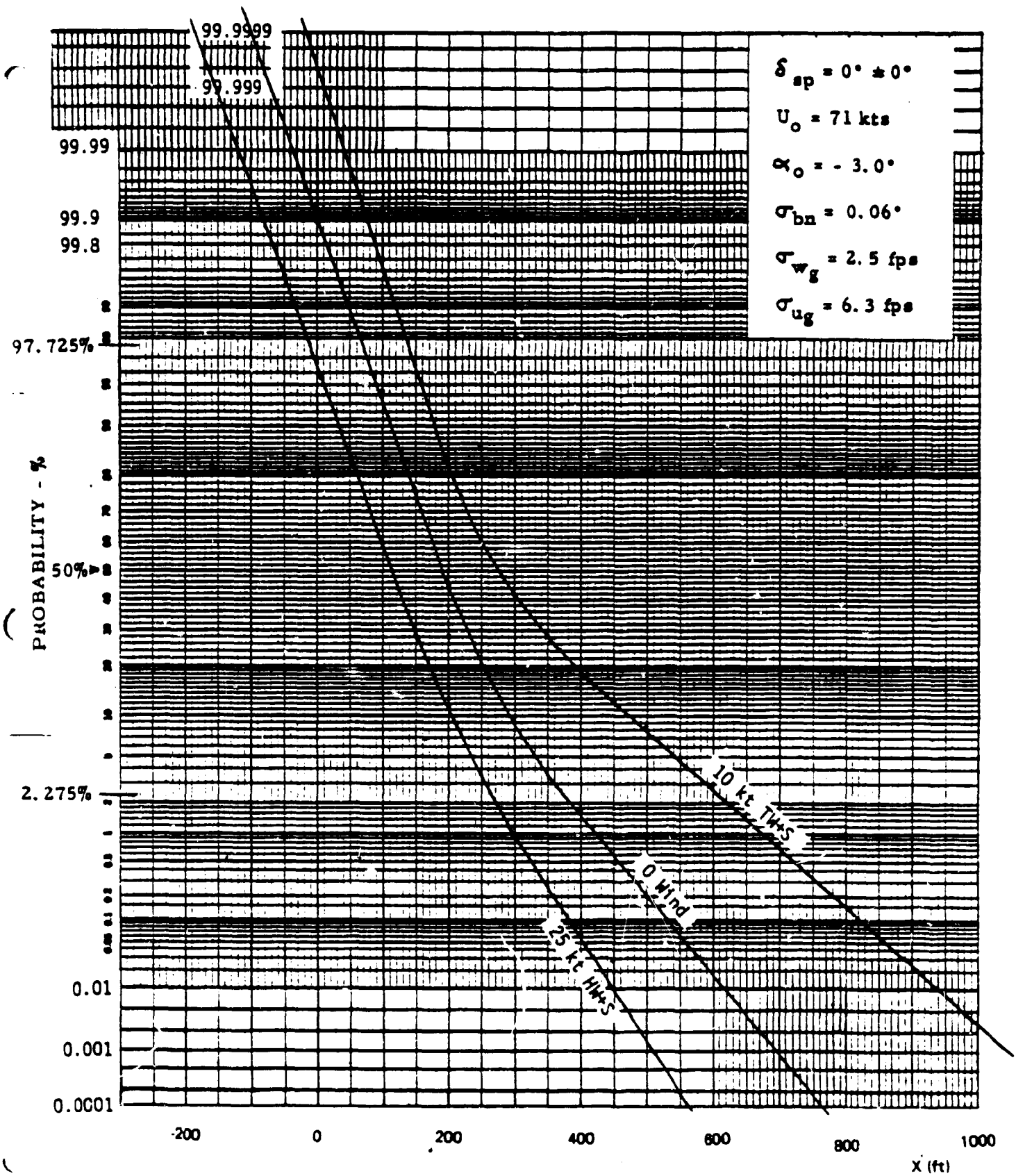

Figure B-97. Constant Flare Height, High Gains, No Spoilers

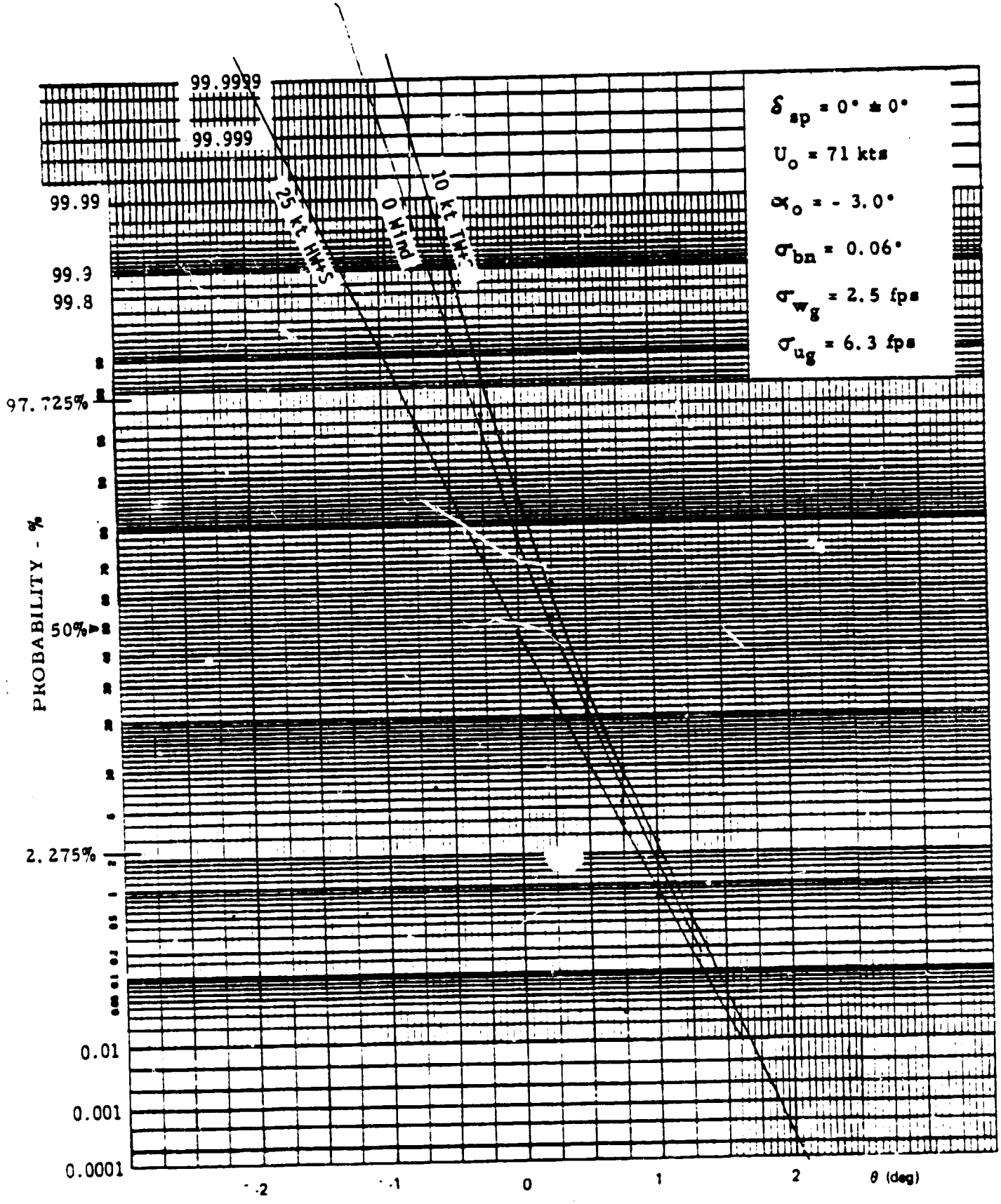

Figure B-98. Constant Flare Height, High Gains, No Spoilers

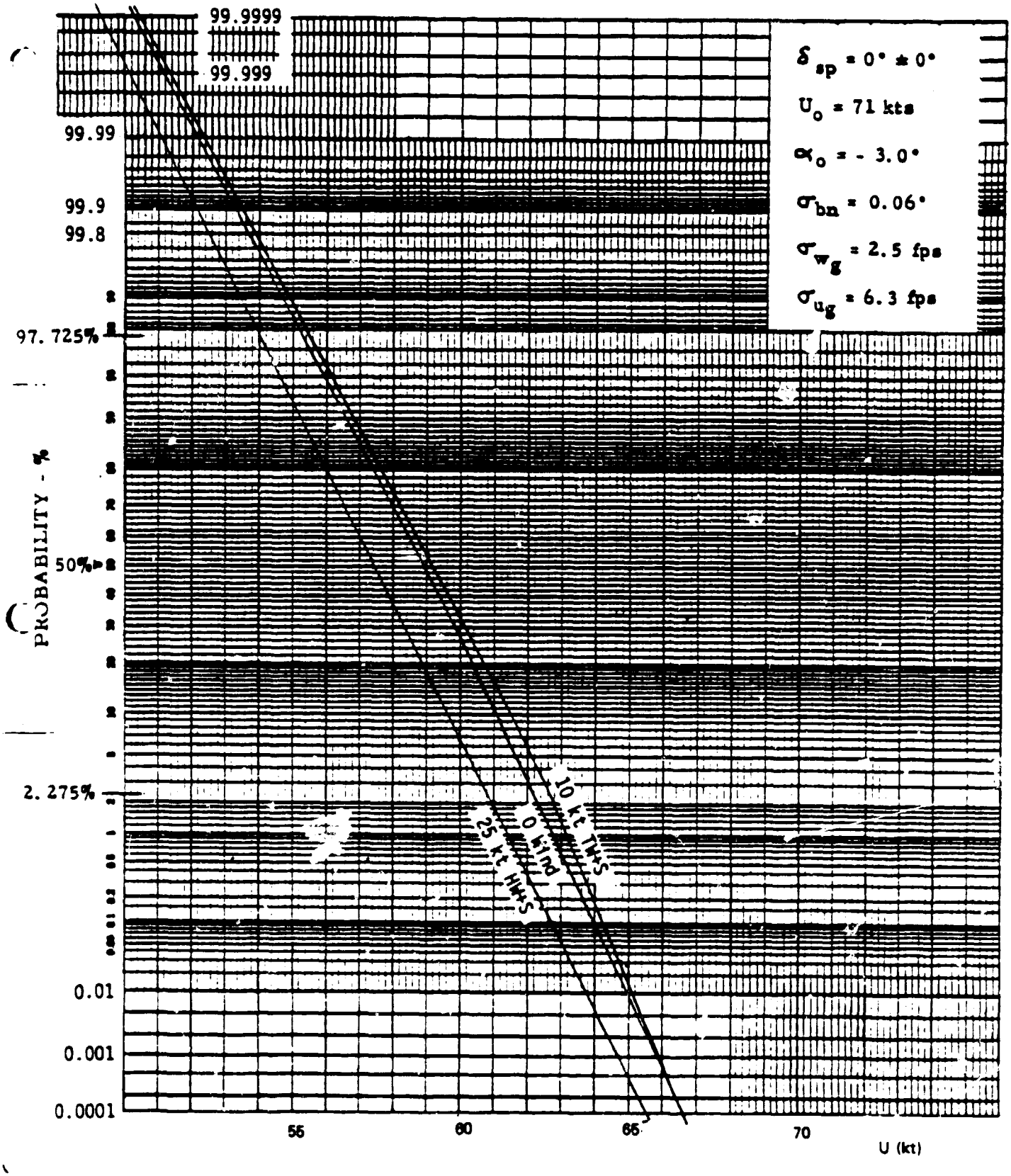

Figure B-99. Constant Flare Height, High Gains, No Spoilers

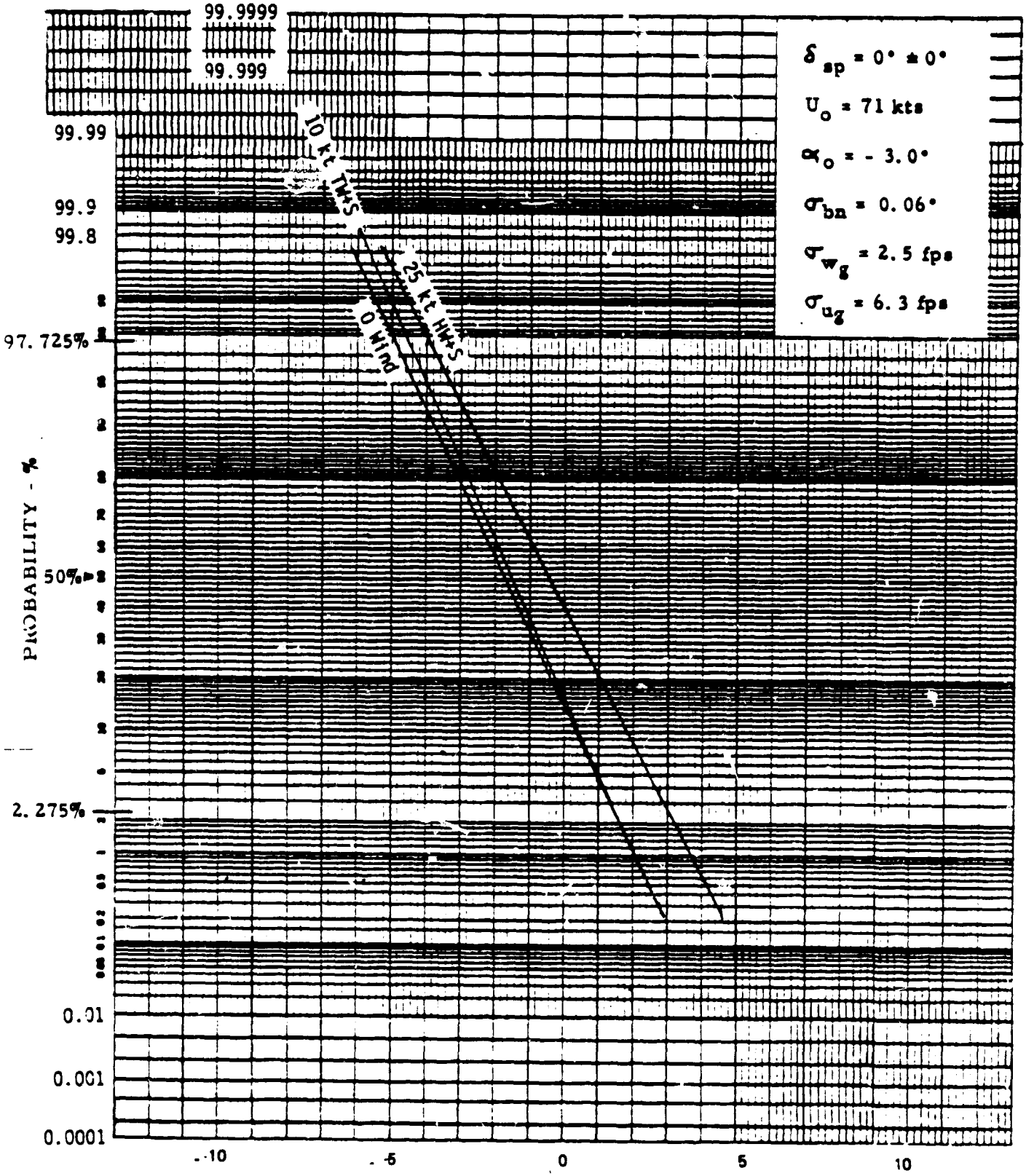

Figure B-100. Constant Flare Height, High Gains, No Spoilers

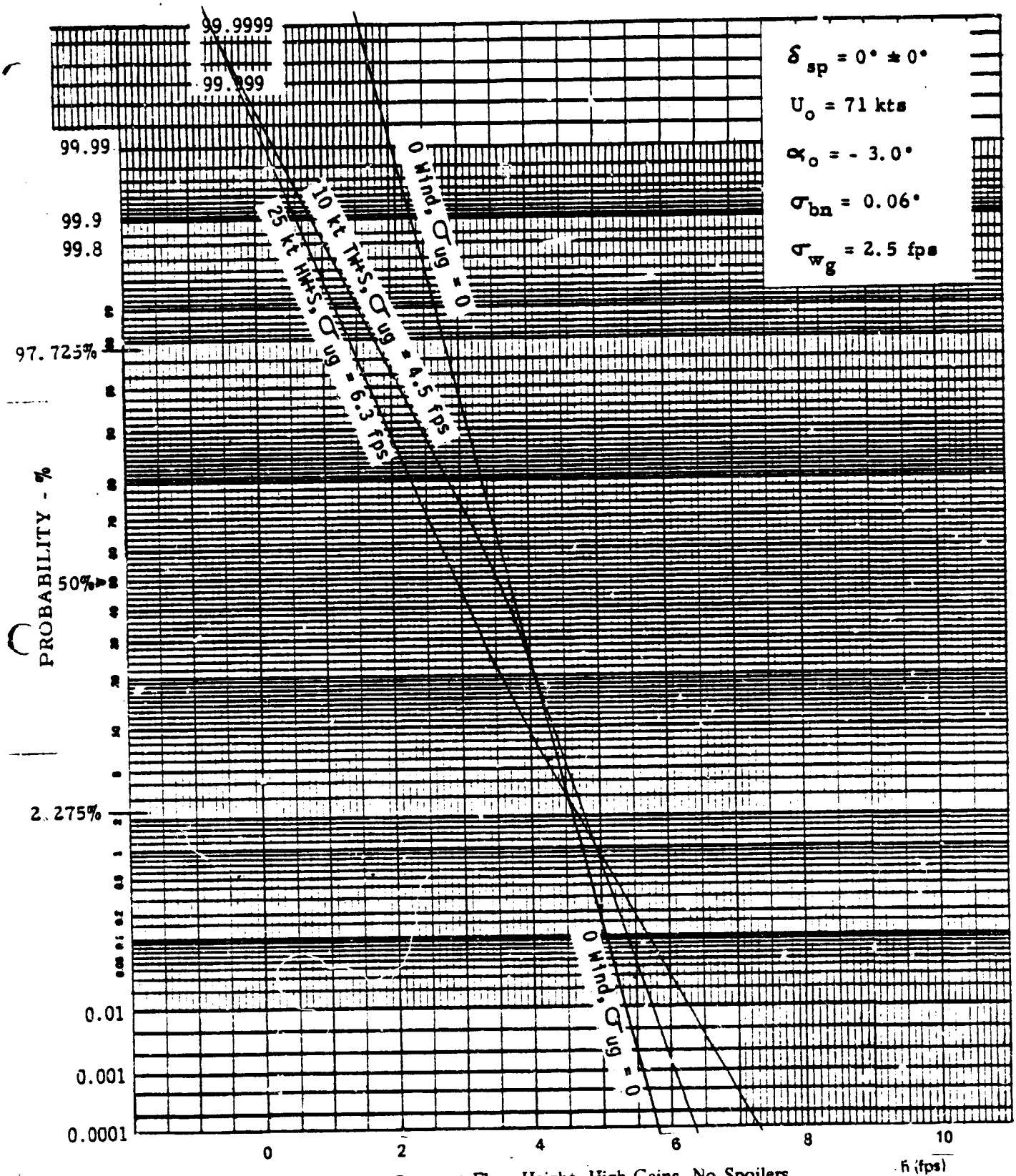

Figure B-101. Constant Flare Height, High Gains, No Spoilers

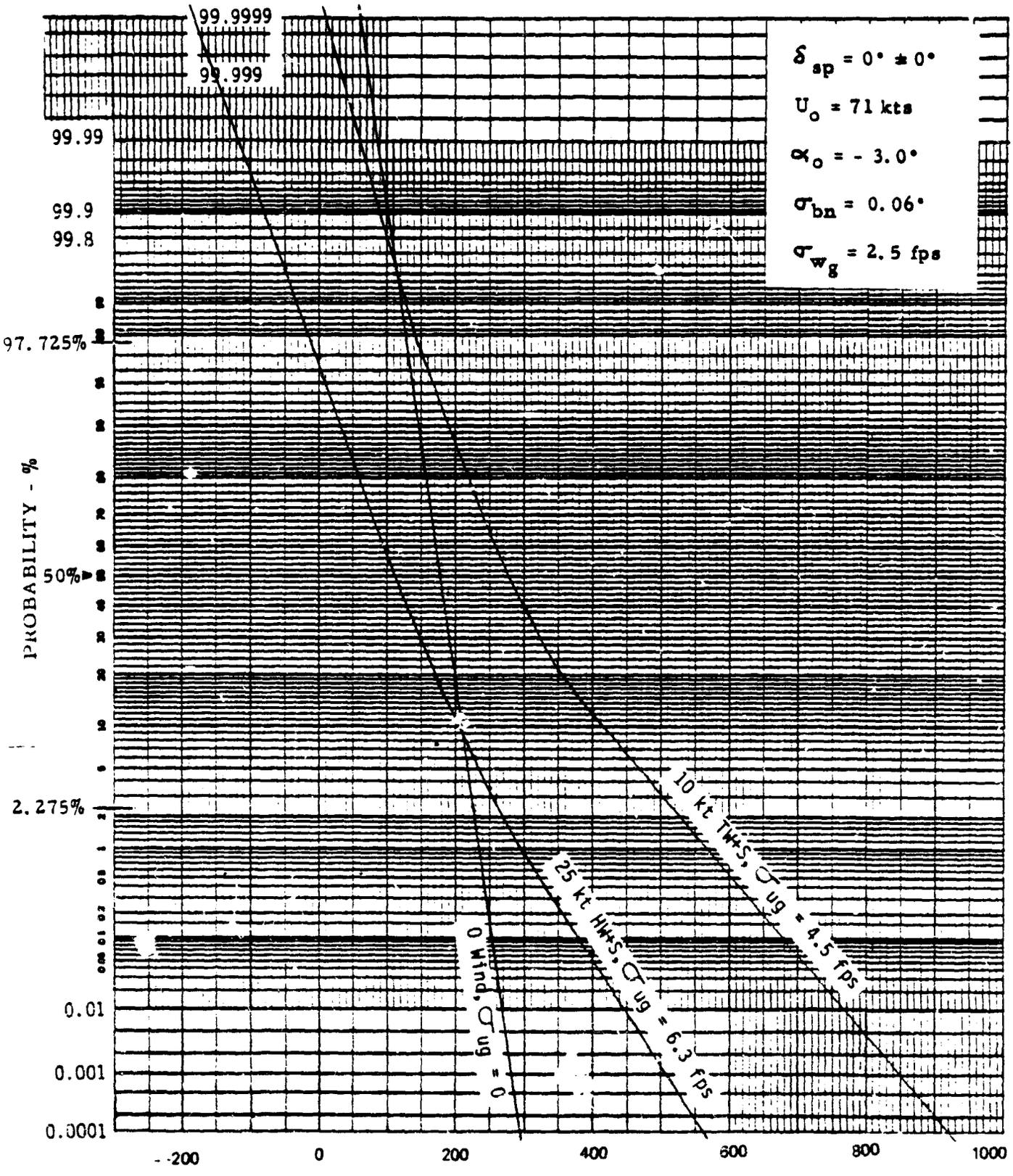

Figure B-102. Constant Flare Height, High Gains, No Spoilers

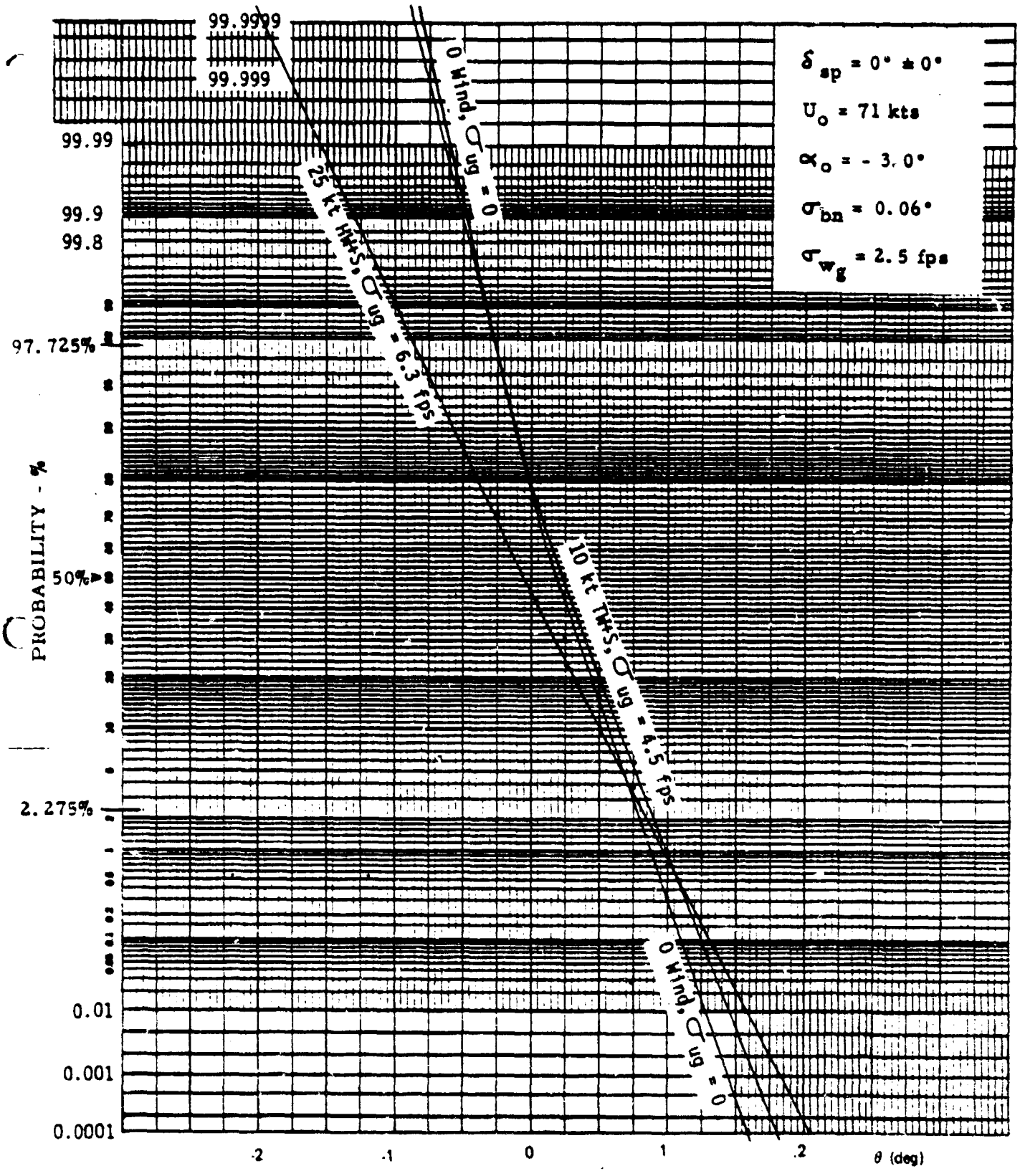

Figure B-103. Constant Flare Height, High Gains, No Spoilers

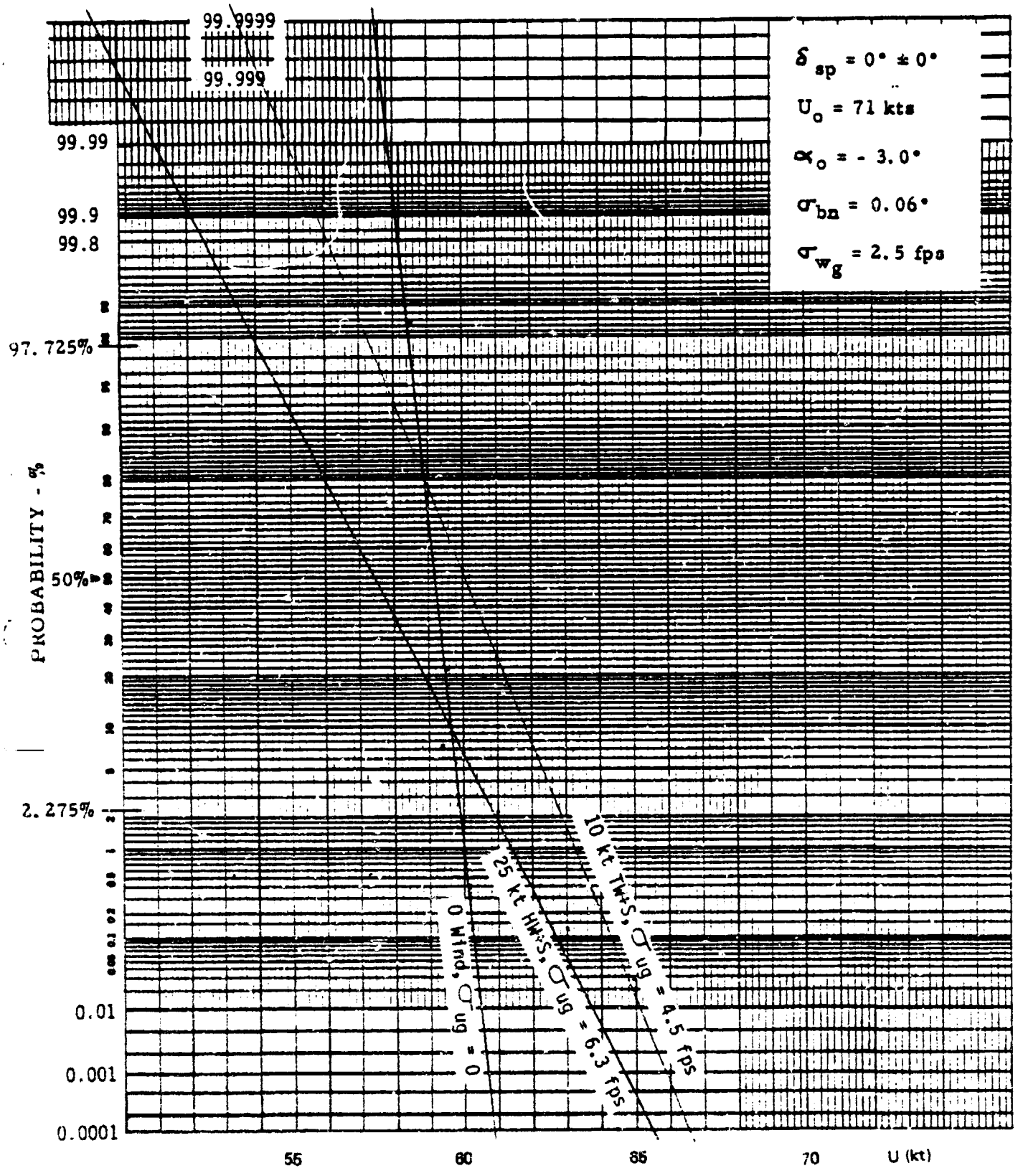

Figure B-104. Constant Flare Height, High Gains, No Spoilers

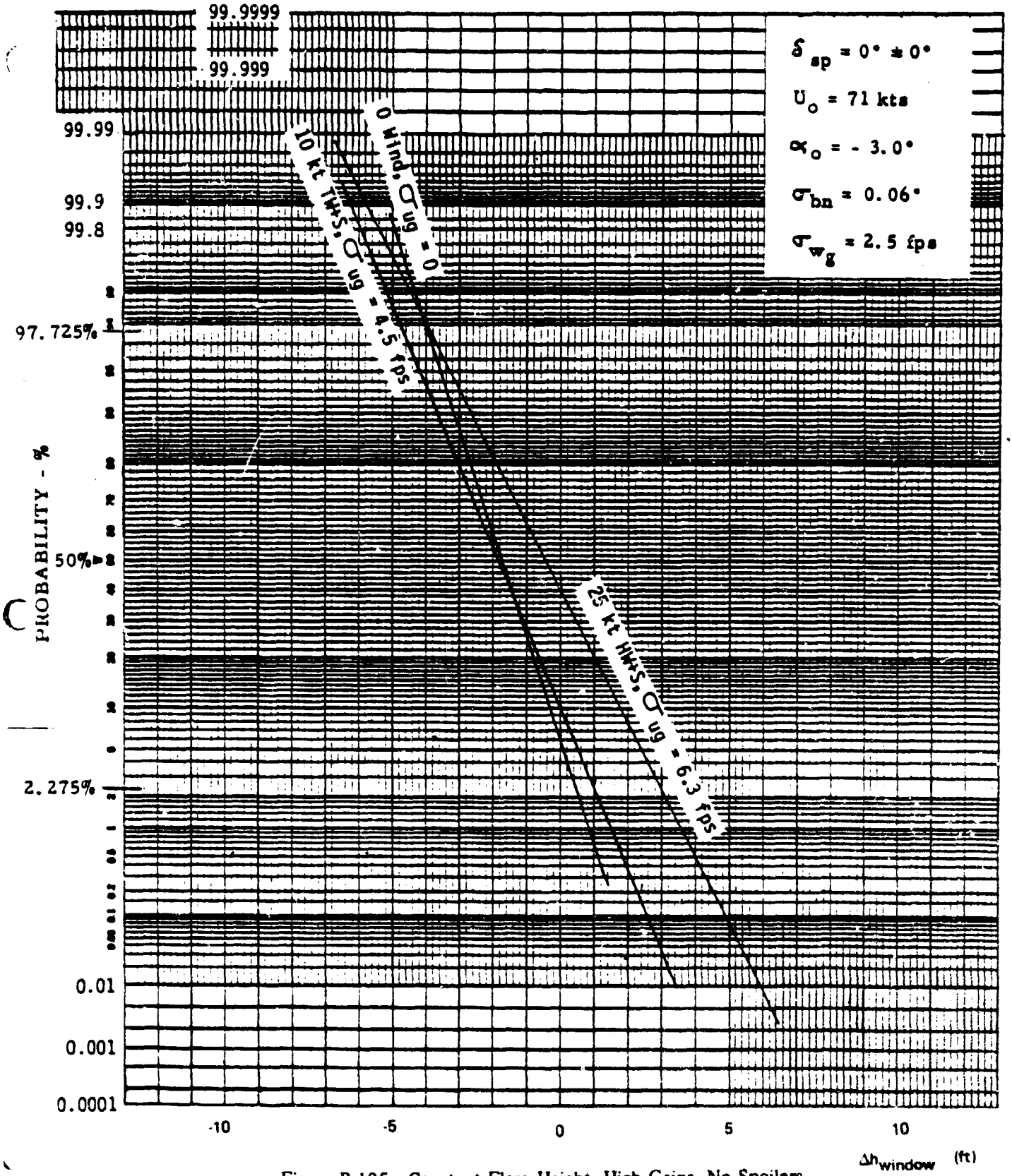

Figure B-105. Constant Flare Height, High Gains, No Spoilers

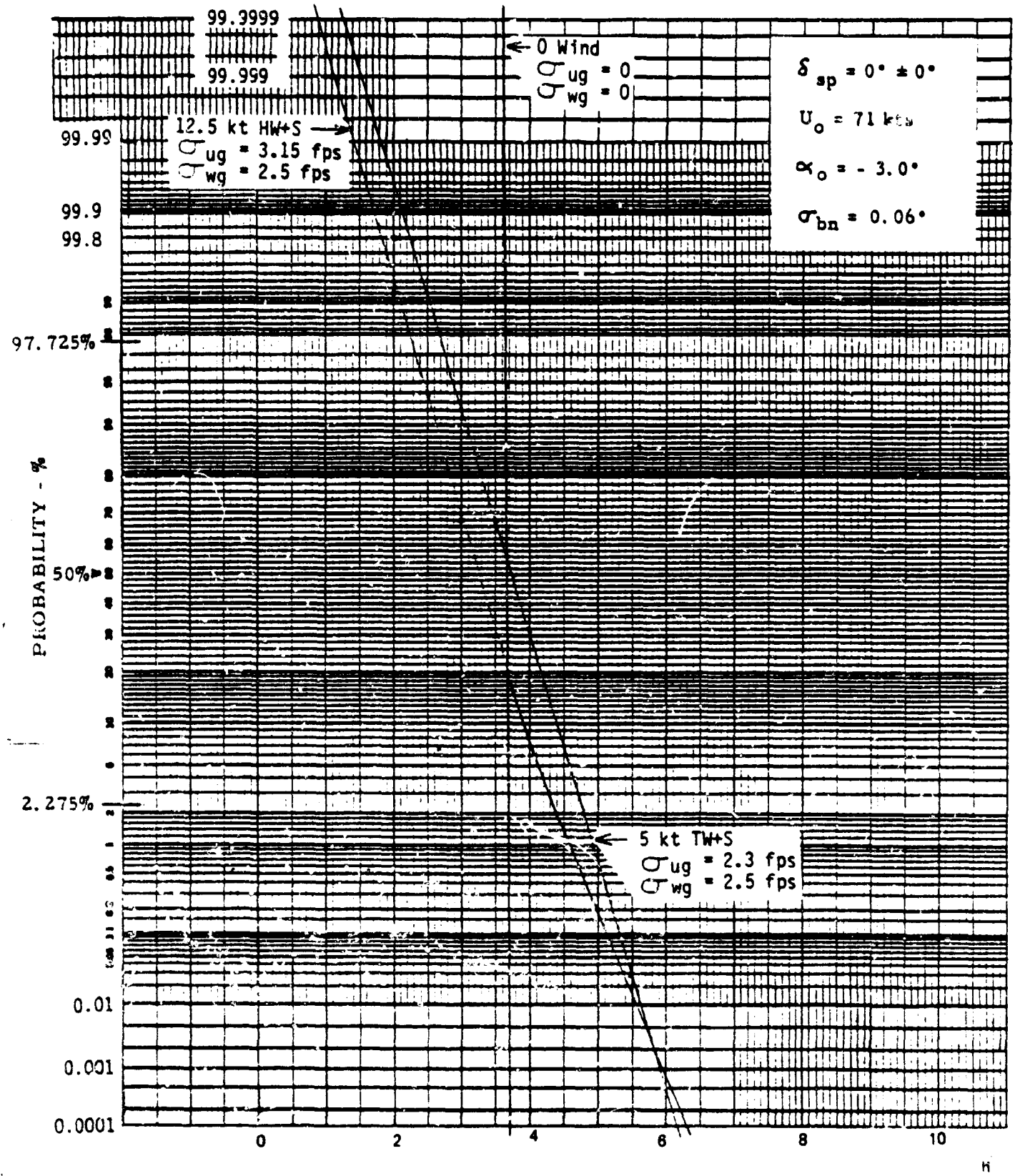

Figure B-106. Constant Flare Height, High Gains, No Spoilers

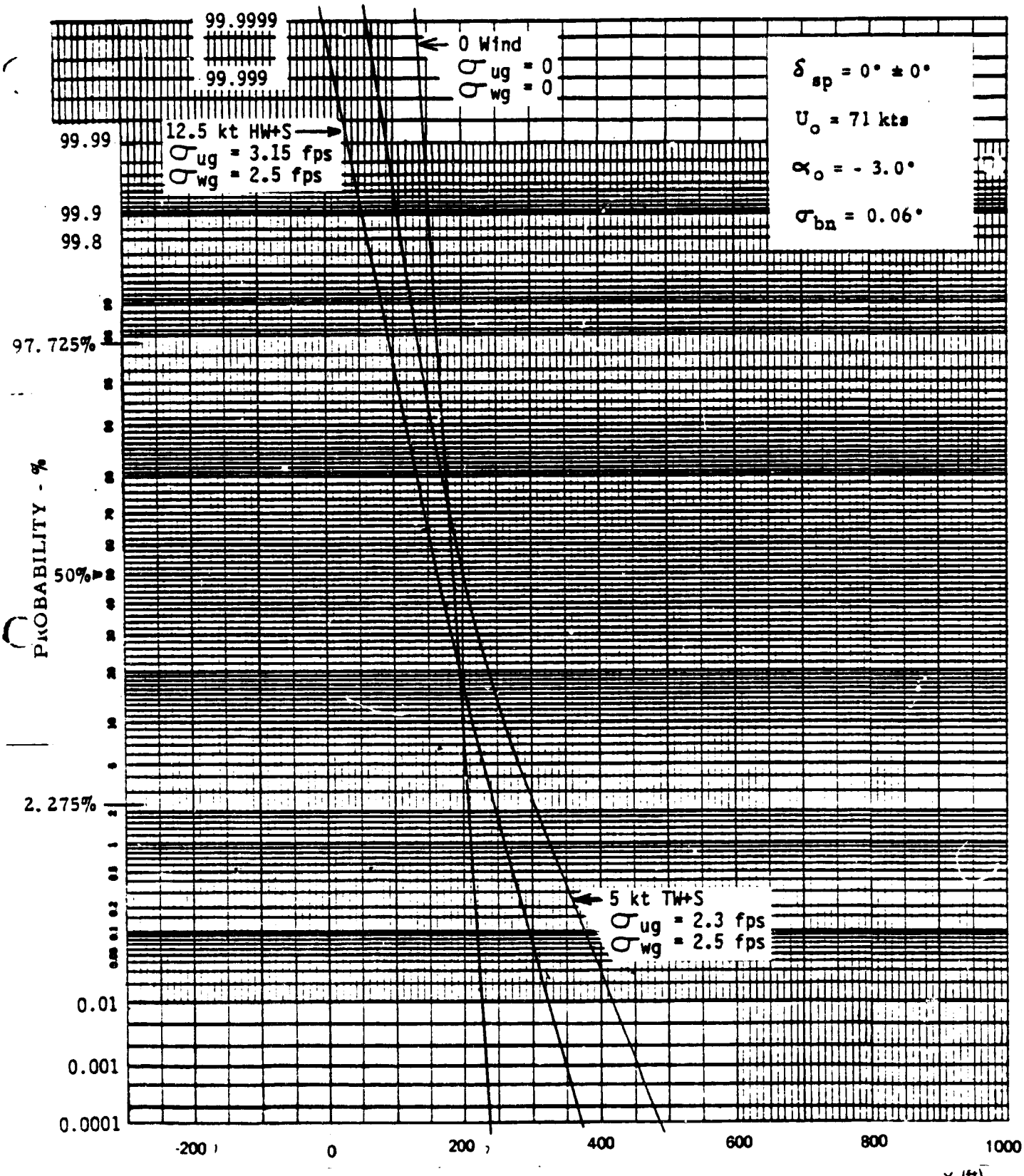

Figure B-107. Constant Flare Height, High Gains, No Spoilers

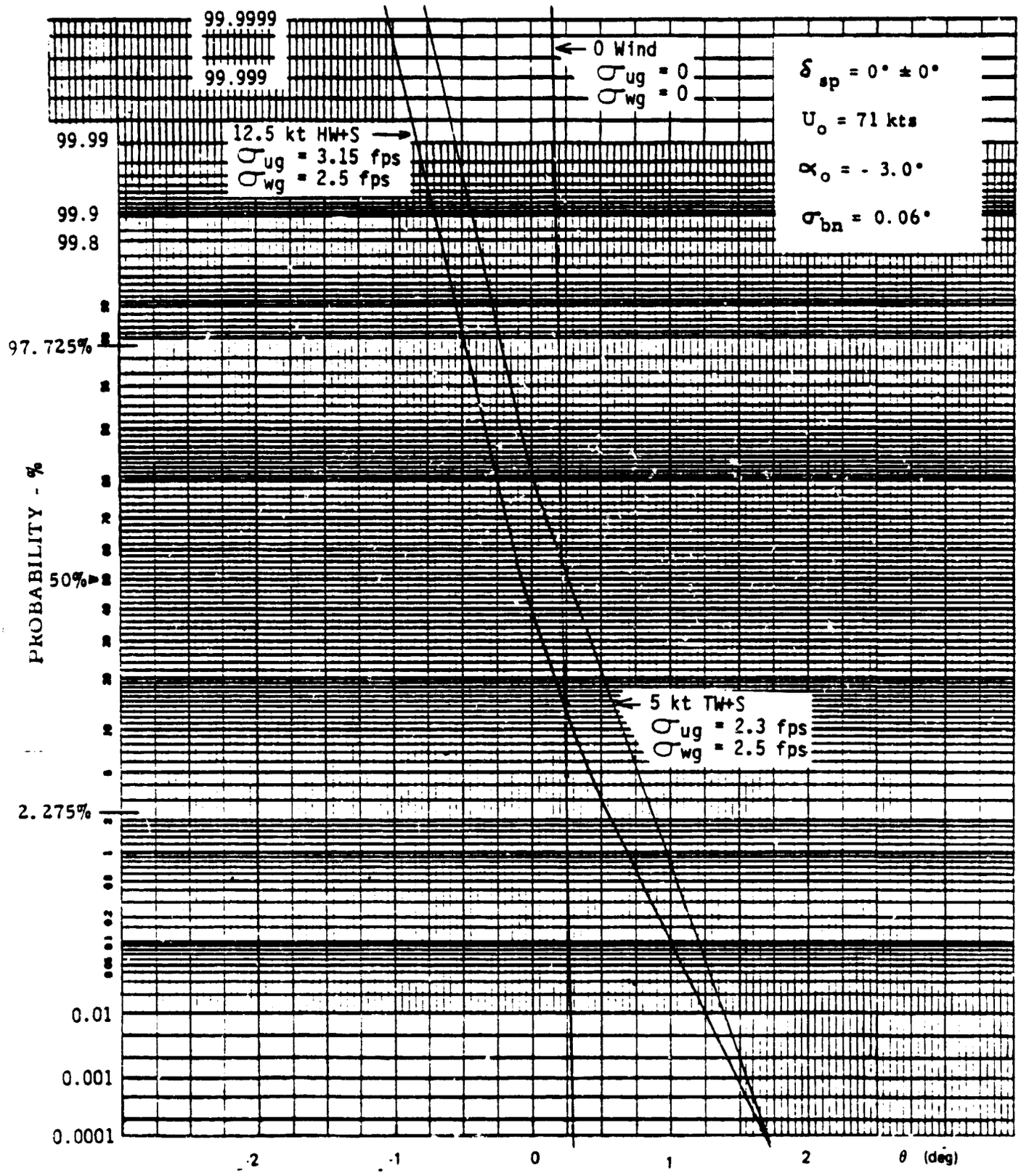

Figure B-108. Constant Flare Height, High Gains, No Spoilers

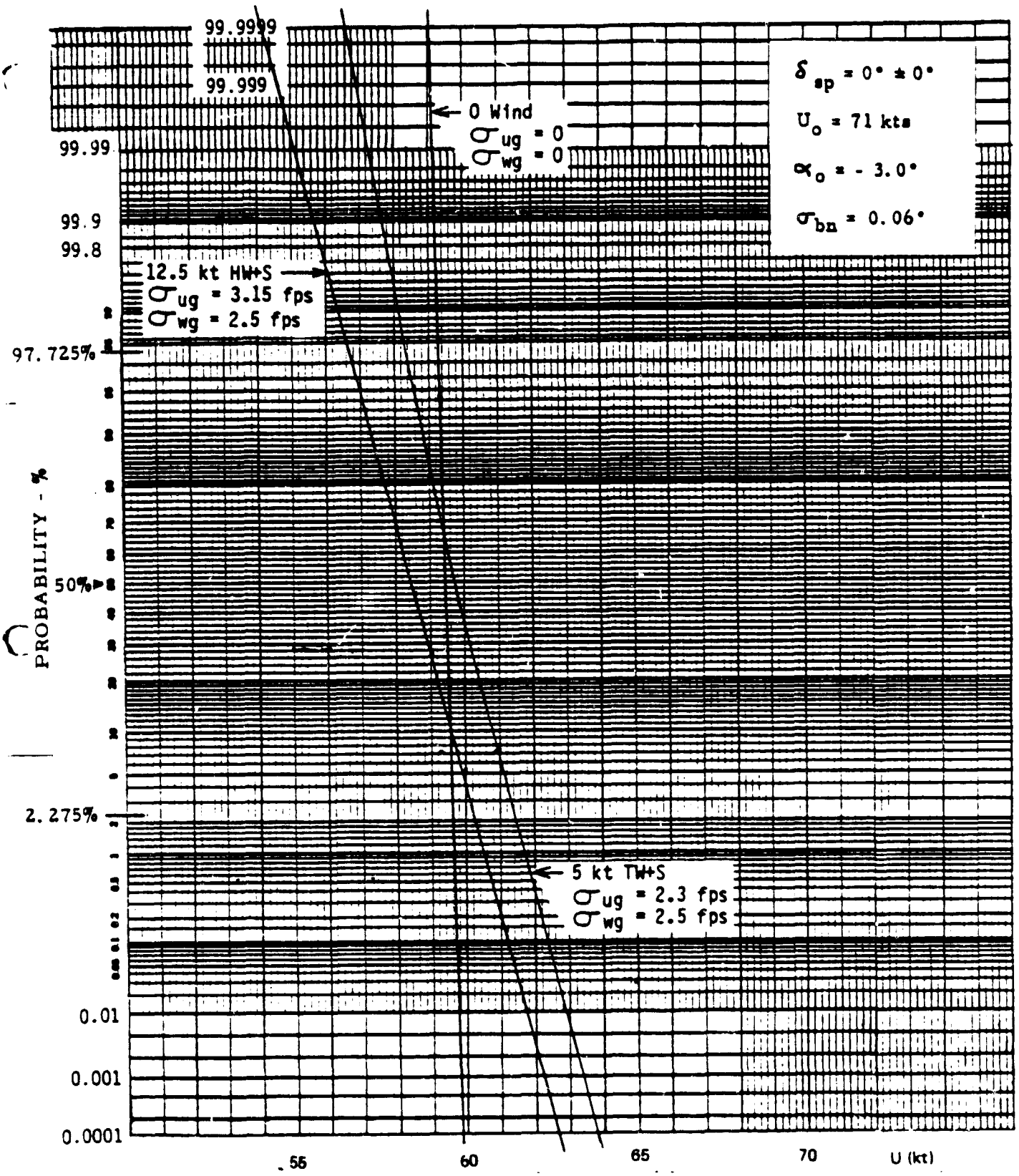

Figure B-109. Constant Flare Height, High Gains, No Spoilers

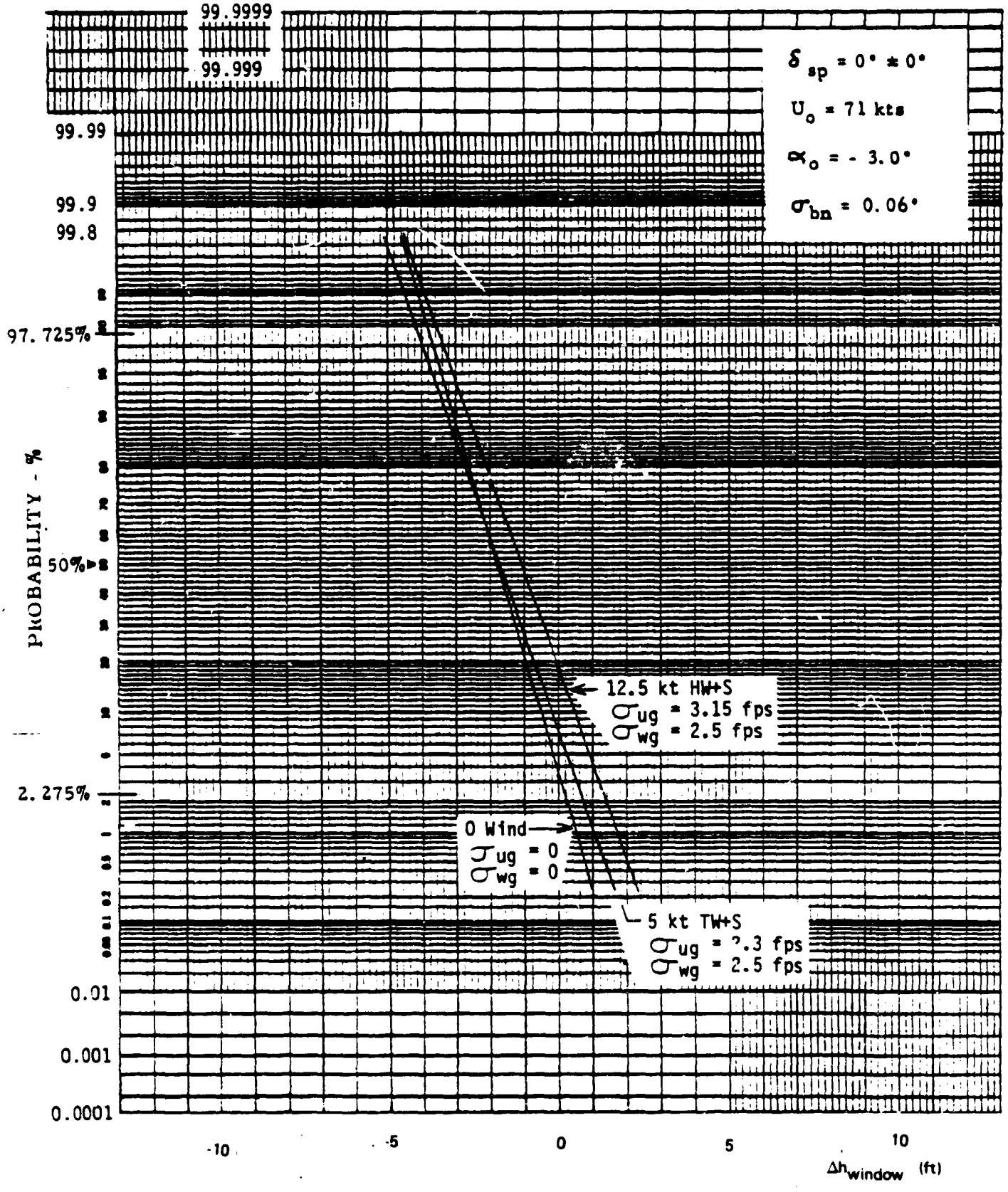

Figure B-110. Constant Flare Height, High Gains, No Spoilers

APPENDIX C

SUPPLEMENTARY LOCALIZER TRACK

AND RUNWAY ALIGNMENT SIMULATION RESULTS

LIST OF FIGURES

LANDING TIME HISTORIES

LOCALIZER TRACK ACTIVITY AND FAILURE EFFECTS

LIST OF FIGURES (CONTINUED)

EFFECTS OF SENSOR ERRORS

PROBABILITY DISTRIBUTIONS

LIST OF FIGURES (CONTINUED)

PROBABILITY DISTRIBUTIONS

LIST OF FIGURES (CONTINUED)

PROBABILITY DISTRIBUTIONS (continued)

APPENDIX C

SUPPLEMENTARY LOCALIZER TRACK AND RUNWAY ALIGNMENT SIMULATION RESULTS

This Appendix contains a discussion of the effects of gyro and accelerometer errors on lateral landing performance. Simulation generated landing time histories to supplement these given in Section 6, are also included here. Landing time histories are given for the various control law variations that were evaluated during these studies. Localizer track activity traces and time histories of responses to various failures are given, as well as responses to sensor errors. Simulation generated probability distributions of the lateral/directional landing variables are also given here. Probability distributions for various system and disturbance variations are included. Performance results that are summarized in Section 6, are based in part on these data.

C-1 DISCUSSION OF GYRO AND ACCELEROMETER ERROR EFFECTS ON LATERAL AXIS PERFORMANCE

The lateral axis control law accepts as inputs the following signals:

1. Roll attitude
2. Roll rate
3. Runway axis lateral acceleration
4. Pos ⌝ and rate data from the navigation filter (Y_f, $\dot{Y}_f$)

These signals are necessarily corrupted by a finite amount of noise and errors of various kinds. The most commonly discussed noise is that associated with the localizer deviation signal and is the reason for the use of the navigation filter. The sensitivity of the autoland system to this source of noise is assessed with the simulation by applying random gaussian noise through the appropriate filter and summing this with the Y deviation data. The attitude, attitude rate, and acceleration signals are normally characterized as having a bias (null error). Slow time varying attitude errors due to gyro drift and erection to a false vertical also must be considered. Furthermore, the runway axis lateral acceleration signal, which is used for wing down compensation in align and for localizer signal augmentation in the navigation filter, includes signal product terms such as $a_x \Delta\psi$ and therefore will contain time varying error signals due to bias errors in either signal.

The following material will evaluate these errors quantitatively and a summary of the analysis will be offered at the end of this section.

C-1.1.1 ACCELEROMETER ERRORS

Accelerometer errors effect the aircraft through the $\ddot{y}_R$ path. The expression for $\ddot{y}_R^{\epsilon}$ was developed in Reference 3 where it is shown that the dominant terms are:

$$\ddot{Y}_R^{\epsilon} = a_y' + a_{x_1} \Delta\psi' + a_{z_1} \phi'$$

where the prime indicates the error components and the 1 indicates the correct value. Each of these terms is being effected by accelerations occurring at

different times:

$a_{y'}$ - occurs mainly due to accelerometer cross axis sensitivity and therefore will be affected whenever sustained forward or normal acceleration exist. Such accelerations may occur under the following conditions:

a) During the pushover manuever (H < 1000 ft)

Mainly the forward acceleration is affected, and the estimated value is $a_{x_1} = 1$ ft/sec^2. It is also assumed that this change occurs as a step for a duration of 20 sec (estimated time for the pushover maneuver to be completed).

b) Due to wind shear

According to the defined wind model, wind shear will affect the forward acceleration starting at 200 ft through touchdown. The estimated value is $a_{x_1} = 1$ ft/sec^2.

c) During Flare (H < 50 ft)

During this phase, the normal and longitudinal accelerations are present and the maximum estimated value is

$$a_{z_1} = 5 \text{ ft/sec}^2 \ (4.5\sigma)$$

$$a_{x_1} = 2 \text{ ft/sec}^2$$

$a_{x_1}\ \Delta\psi'$ - The maximum (4.5σ) estimated compass system error is 4°. This term will affect the aircraft whenever linear accelerations (a_{x_1}) exist according to the list above.

$a_{z_1}\ \phi'$ - The maximum estimated roll angle error is 1.6° (4.5σ). This term will affect the aircraft during the flare maneuver only because of the associated normal acceleration.

Figure C-17 shows the effect of a .5 fps^2 step in $\ddot{y}_R$ error inserted at an altitude of H = 1000'. In the first two traces, the step was removed after 20 sec and in the other two the step was maintained through touchdown. The worst case, which is a combination of sustained acceleration error and shearing crosswind is 70 ft/fps^2 and will be assessed on a 4.5σ basis. Figure C-18 shows the effect of steps inserted at altitudes of H = 200 feet (effect of shear) and H = 50 feet (flare) respectively. The touchdown deviation is 60 ft/fps^2 and 8 ft/fps^2, respectively.

Errors Due to the $a_{y'}$ term

The cross axis sensitivity is estimated to be 0.01 g/g on a 4.5σ basis. Therefore, the total lateral deviation will be:

a)	Pushover maneuver:	$1\ ft/sec^2 * 0.01 * 70 = 0.7$ ft
b)	Wind shears:	$1\ ft/sec^2 * 0.01 * 60 = 0.6$ ft
c)	During flare:	$5\ ft/sec^2 * 0.01 * 8 = 0.4$ ft
		$2\ ft/sec^2 * 0.01 * 8 = 0.16$ ft
		RSS total 1.02 ft (4.5σ)

Errors Due to $a_{x_1}\ \Delta\psi'$ term

a)	Pushover maneuver:	$1\ ft/sec^2 * \frac{4°}{57.3} * 70 = 4.9$ ft
b)	Wind shears:	$1\ ft/sec^2 * \frac{4°}{57.3} * 60 = 4.2$ ft
		RSS total 6.45 ft

Errors Due to $a_{z_1}\ \phi'$ term

This term exists only during flare; to give:

$$5\ ft/sec^2 * \frac{1.6°}{57.3} * 8 = 1.12\ ft$$

The different contributors to the touchdown error are also RSS ed to give a total estimated touchdown deviation of 6.62 ft on a 4.5σ basis or 2.95 ft on a 2σ basis.

C-1.1.2. GYRO ERRORS

Gyro errors may arise because of:

a) Verticality error
b) False erection

Gyro data suggests max. verticality error of 0.6 degree (4.5σ) and a maximum error of 1. degree due to false erection to give a total of 1.60° (4.5σ). It is assumed that the rate of erection is in the order of 1.0 to 2.0 degrees per minute.

False erection may occur due to uncoordinated maneuvers which cause lateral accelerations, followed by erection to a false vertical. Such maneuvers may occur prior to final approach and during the align maneuver. The same maximum errors, as stated above, will be assumed for both cases. It is also assumed that final approach and localizer mode initiation occur at an altitude of H = 1000 ft.

Figure C-19 shows the response to an existing 1.0 degree error prior to localizer mode initiation. A steady state defined by $y = \frac{\phi^{\epsilon}}{k_y} = \frac{1}{0.06} = 16.7$ ft is maintained. The first trace shows the response following the mode initiation and the second trace shows the same, this time with the gyro erecting back at the rate of 1.0 degree per minute. If a worst case of tailwind is assumed, the elapsed time from H = 1000 ft to touchdown will be about 60 sec which will leave a lateral deviation error of 6 ft/degree. As a point of interest, Fig C-20 shows the same response carried throughout the align maneuver with limiting crosswind and crosswind shear. The touchdown error is 5 ft/degree.

Fig C-21 shows the same response, this time with a gyro erection rate of 2°/min. Although the lateral deviation is peaking earlier, the same 6 ft/degree touchdown deviation remains after 60 sec.

Fig C-20 also shows the response to the erection cycle occurring at the align altitude (H = 150 ft). It is assumed that the aircraft is centered on

the beam prior to align and the only disturbance is due to the rate of erection trying to respond to the lateral acceleration. The max. error at touchdown is about 1.5 ft. For reference, the same response with limiting crosswind and crosswind shear is also shown.

Summary of Gyro Errors

Errors existing prior to mode initiation:

6 ft/deg X 1.6° = 9.6 ft

Errors at align:

	1.5 ft
RSS total	9.72 ft (4.5σ)

C-1.1.3 SUMMARY OF TOTAL ERRORS (Accelerometer and Gyro)

Total accelerometer errors:	6.62 ft
Total gyro errors:	9.72 ft
RSS total:	11.76 ft

or, a total touchdown error of 5.23 ft on a 2σ basis.

C-1.2 INCREASED K_y

Since a higher lateral deviation proportional gain (K_y) was considered, error analysis is performed for a $K_y' = 2K_y$. Figures C-22 through C-24 repeat most of the traces for this higher gain and the following is the error calculation based on the same assumptions as were defined above.

C-1.2.1 ACCELEROMETER ERRORS:

Cross Axis Sensitivity

.) Pushover maneuver: $1\ ft/sec^2 \times 0.01 \times 48\ ft/ft/sec^2 = .48\ ft$
(continuous step, worst case)

b) Wind shears (H < 200 ft): $1\ ft/sec^2 \times 0.01 \times 46\ ft/ft/sec^2 = .46\ ft$

c) During flare: $5\ ft/sec^2 \times 0.01 \times 5\ ft/ft/sec^2 = .30\ ft$

$2\ ft/sec^2 \times 0.01 \times 6\ ft/ft/sec^2 = .12\ ft$

RSS total .74 ft

Errors Due to the $a_{x_1}\ \Delta\psi'$ term:

a) Push over maneuver: $1\ ft/sec^2 \times \frac{4°}{57.3} \times 48\ ft/ft/sec^2 = 3.35\ ft$

b) Wind shears: $1\ ft/sec^2 \times \frac{4°}{57.3} \times 46\ ft/ft/sec^2 = 3.21\ ft$

RSS total 4.64 ft

Error Due to $a_{z_1}\ \phi'$ term:

$5\ ft/sec^2 \times \frac{1.6°}{57.3} \times 6\ ft/ft/sec^2 = 0.84\ ft$

Total 4.5σ RSS ed accelerometer errors is: 4.77 ft, or a 2σ value of 2.12 feet.

C-1.2.2 GYRO ERRORS

Errors existing prior to mode initiation:

1 ft/deg X 1.6° = 1.6 ft

Error at align:

(due to max. erection rate)

1.0 ft

RSS total 1.9 ft

C-1.2.3 SUMMARY OF TOTAL ERRORS (Accelerometer and Gyro)

for the $K_y' = 2K_y$ case:

Total accelerometer errors:	4.77 ft (4.5σ)
Total gyro errors:	1.9 ft (4.5σ)
RSS total:	5.13 ft (4.5σ)

or, a total touchdown error of 2.28 ft on a 2σ basis.

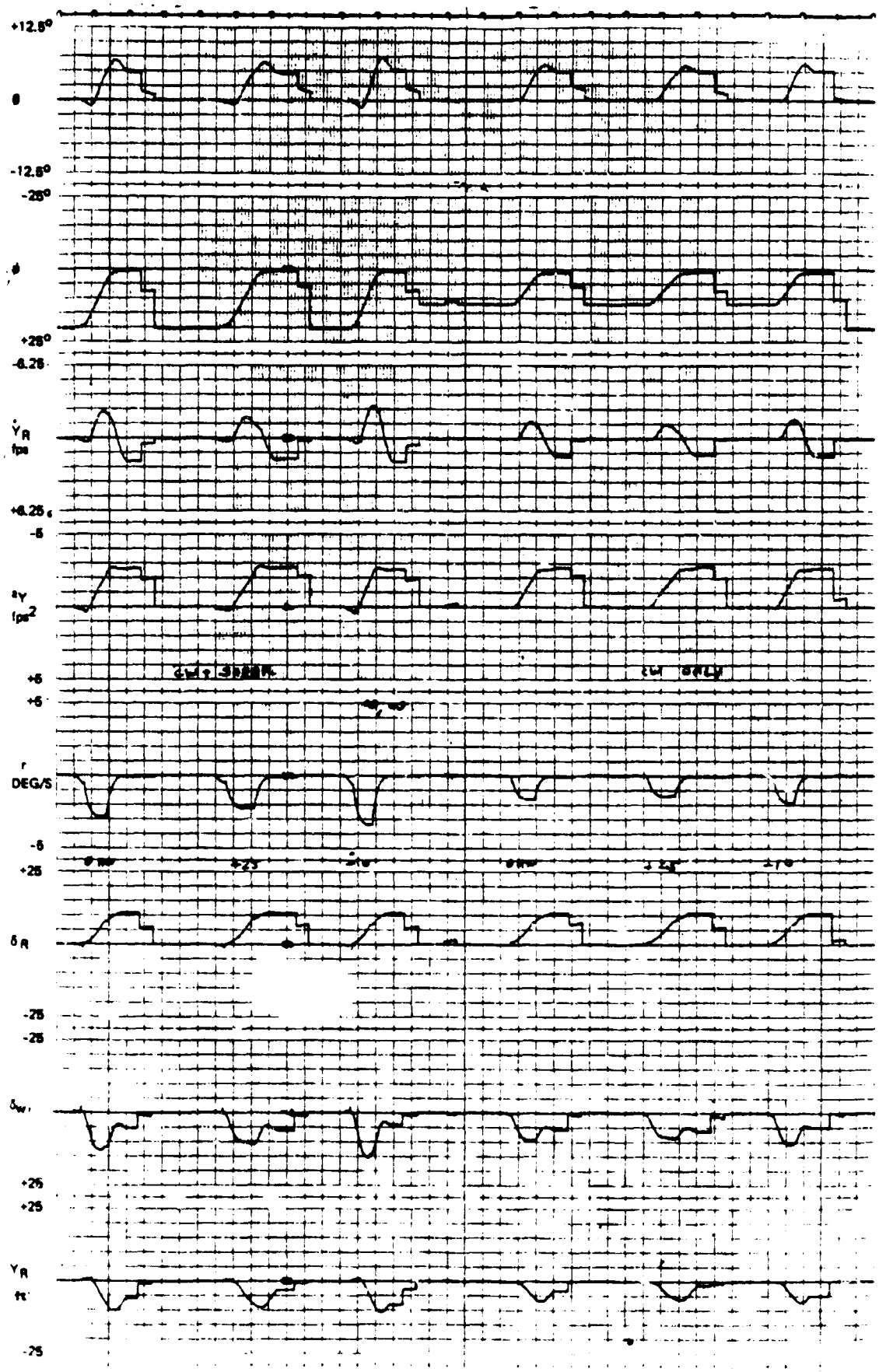

Figure C-1. Unlimited Rudder and Align

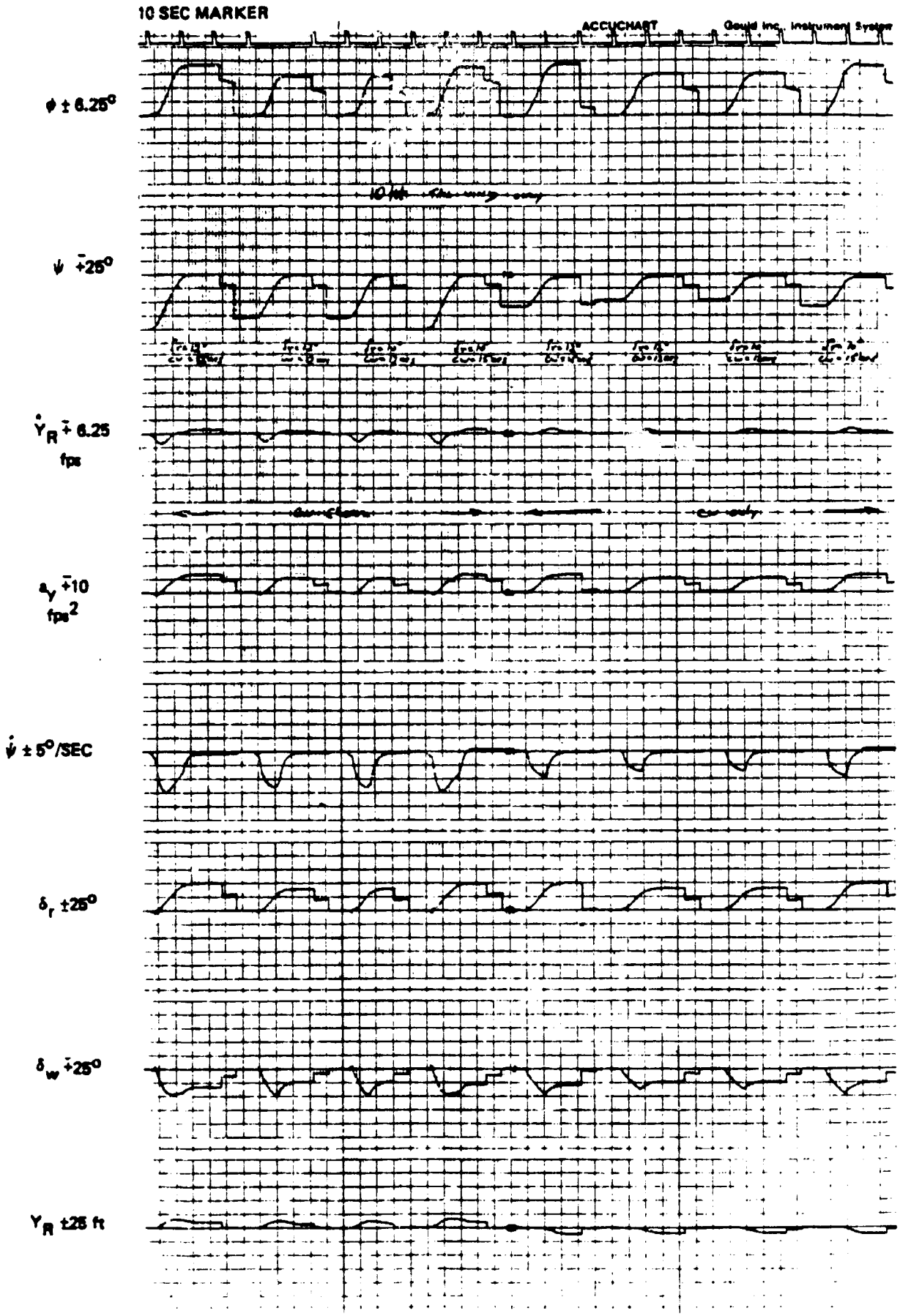

Figure C-2A. Rudder Limit and Crosswind Variations

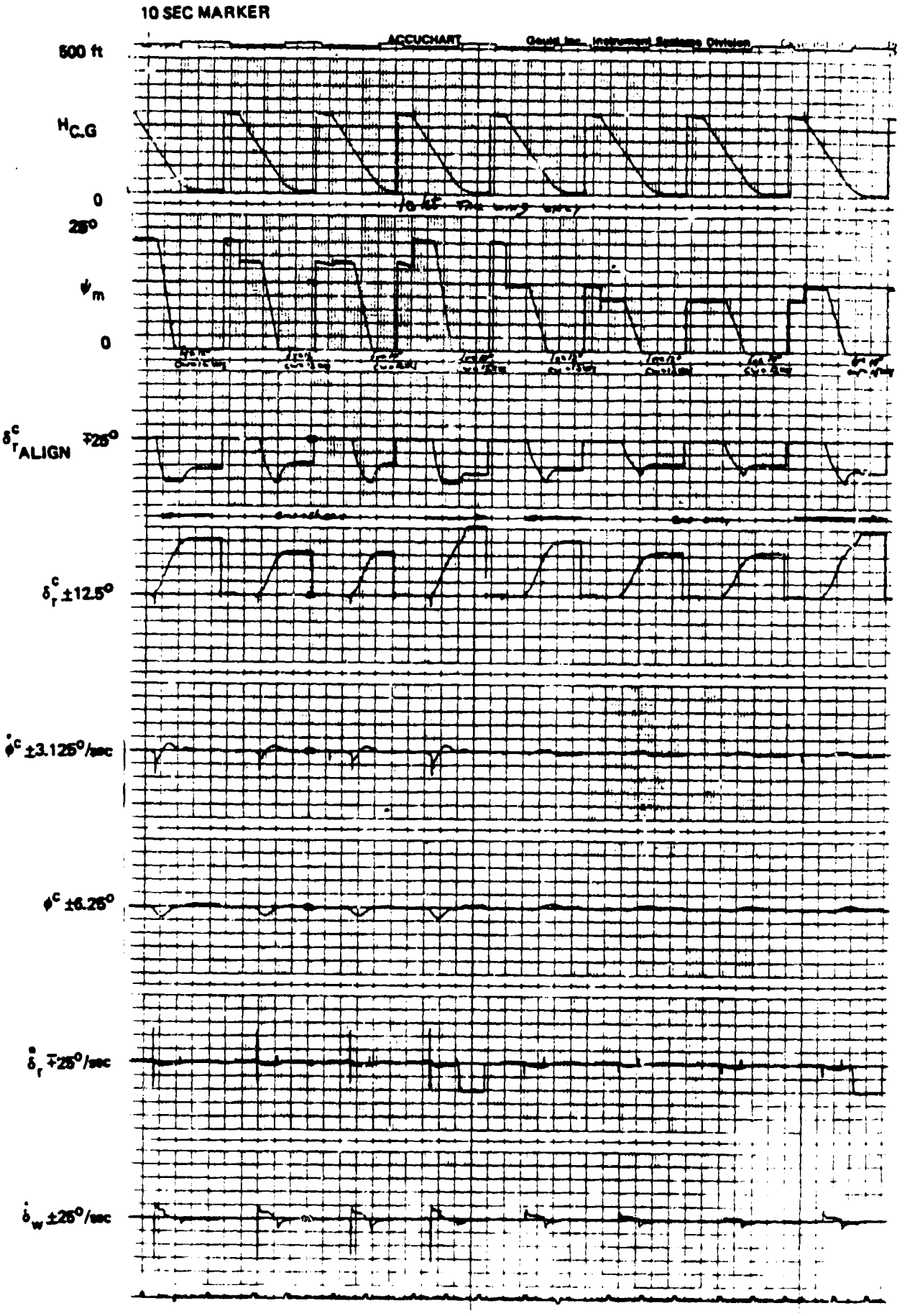

Figure C-2B. Rudder Limit and Crosswind Variations

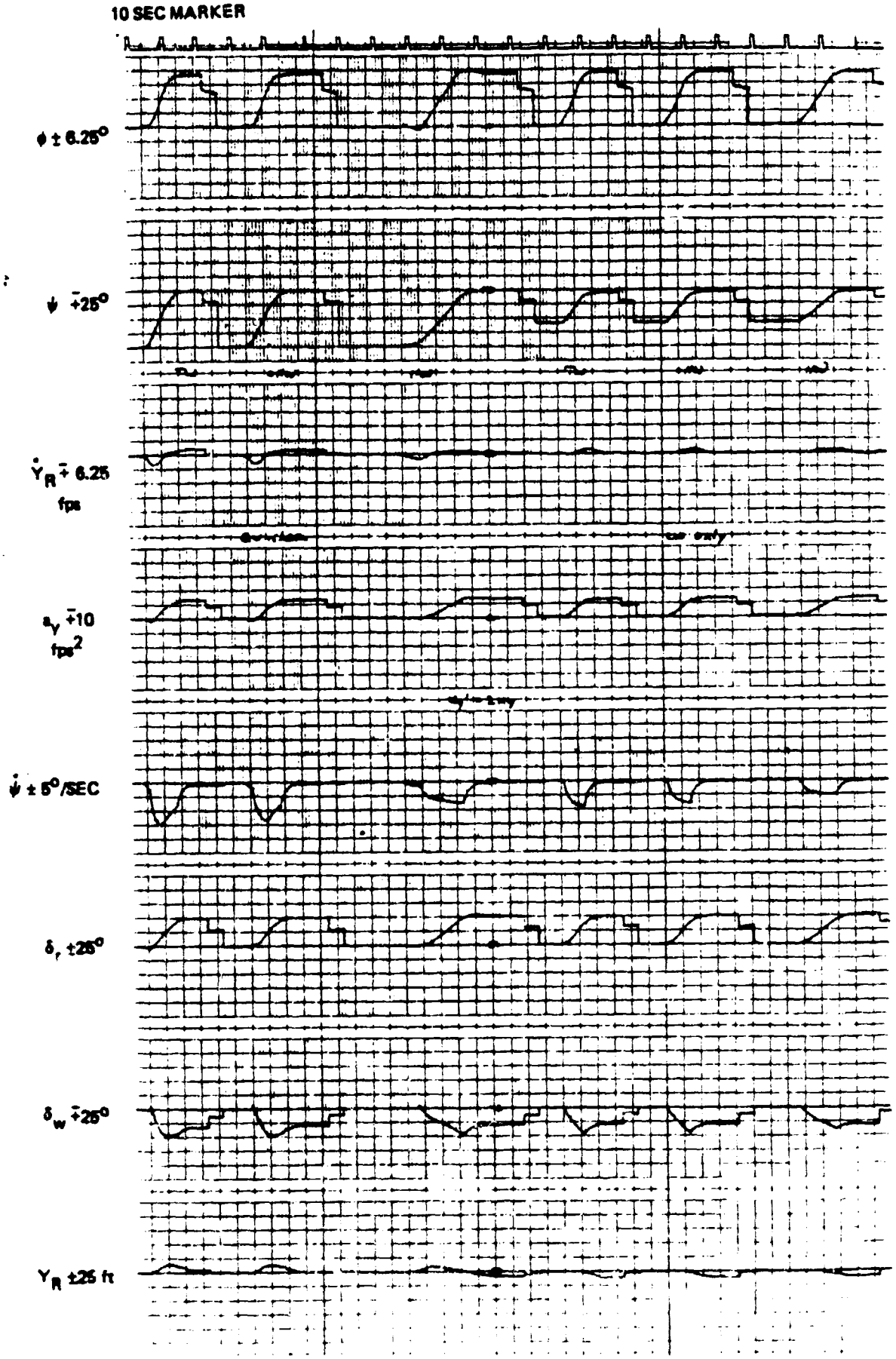

Figure C-3A. Doubled Lateral Position Gain

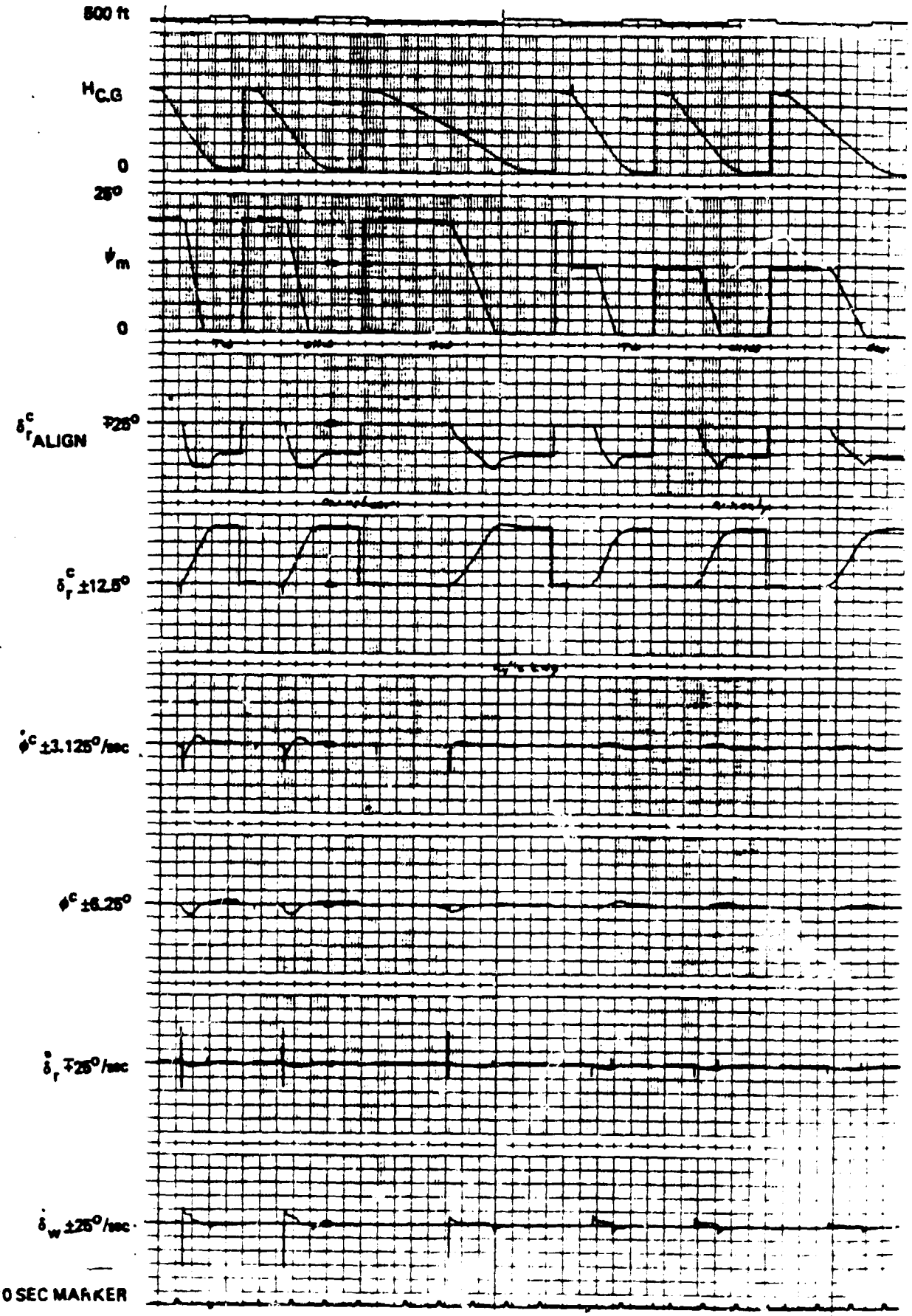

Figure C-3B. Doubled Lateral Position Gain

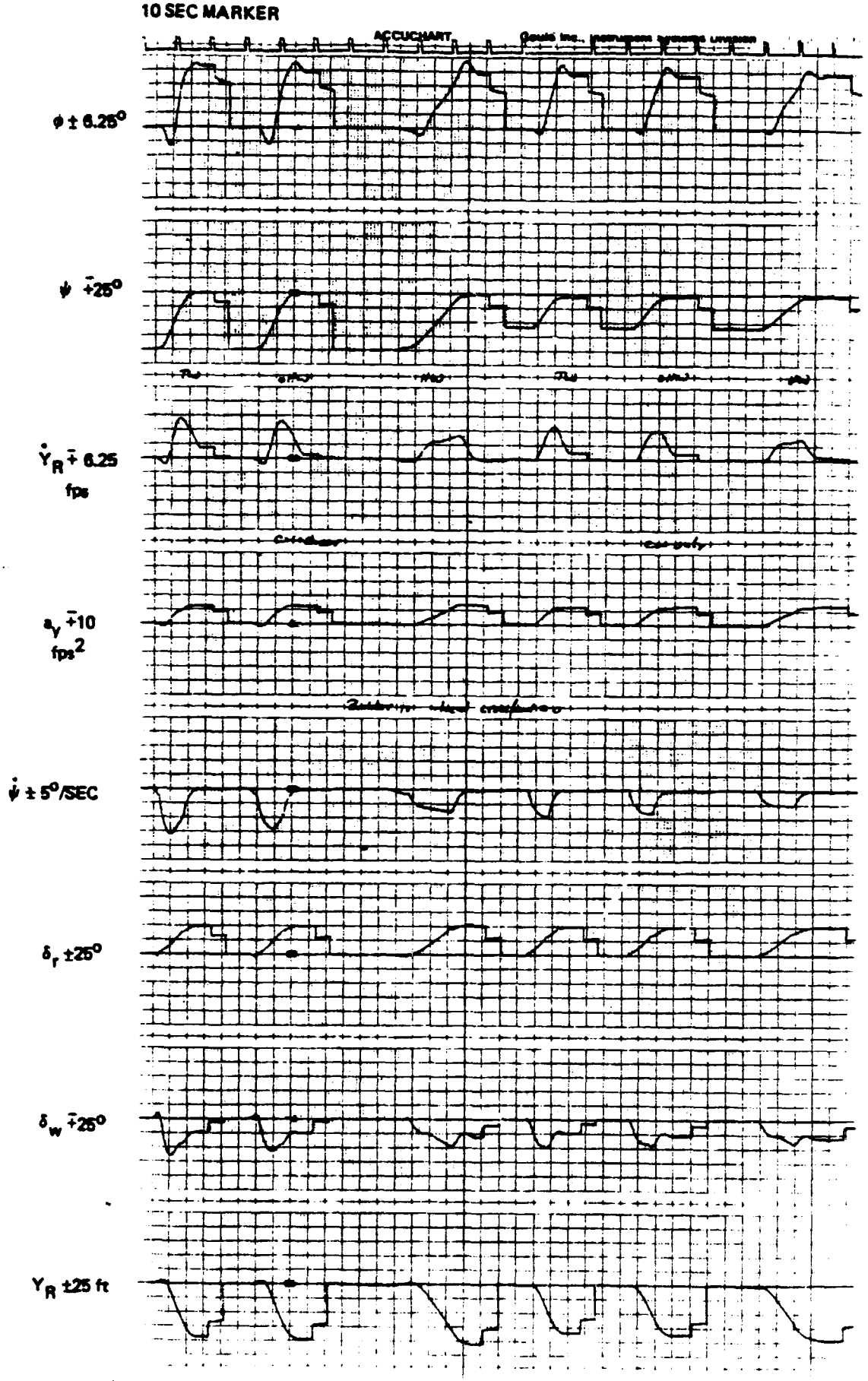

Figure C-4A. No Rudder to Wheel Crossfeed

C-14

C-4

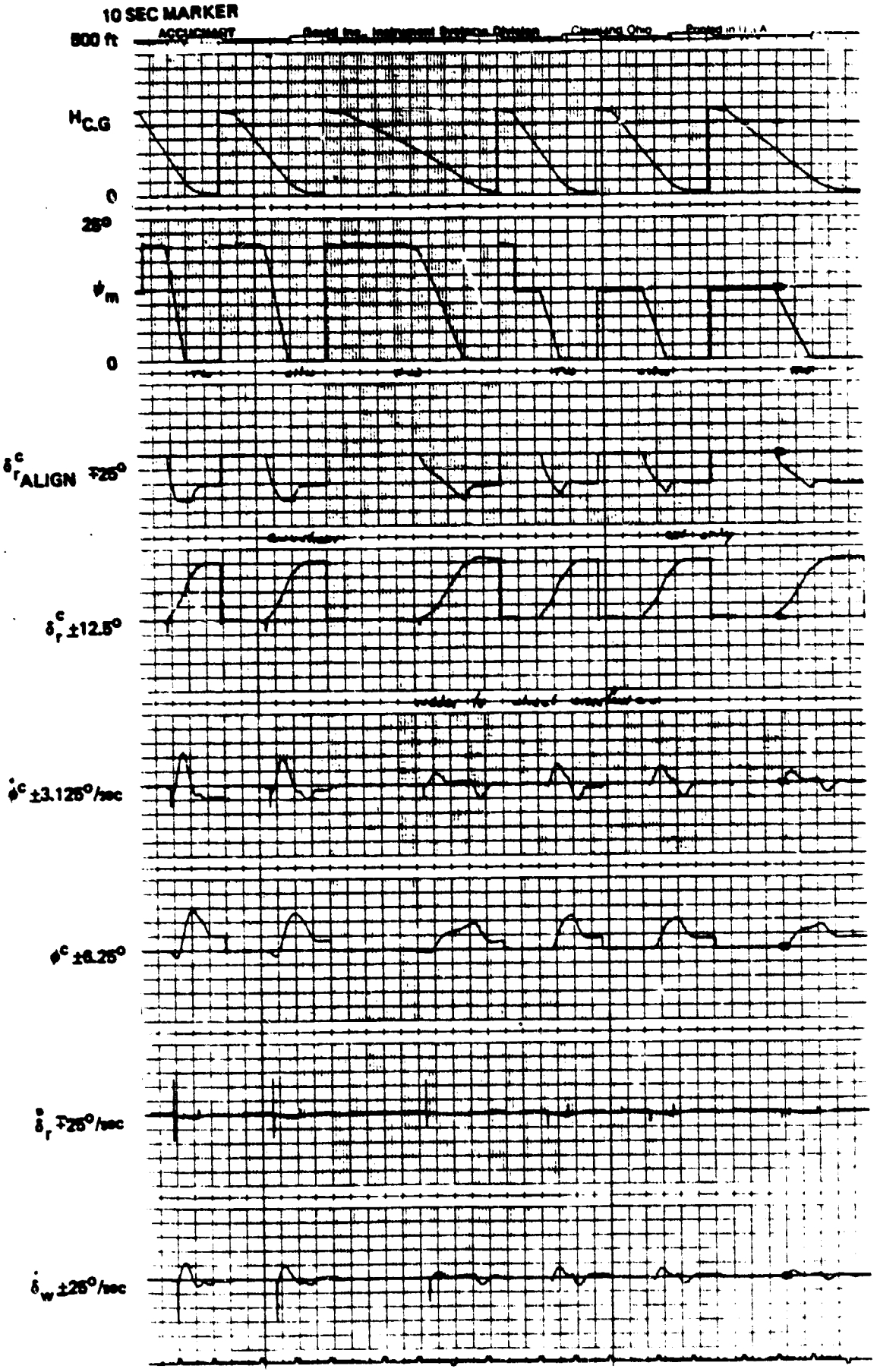

Figure C-4B. No Rudder to Wheel Crossfeed

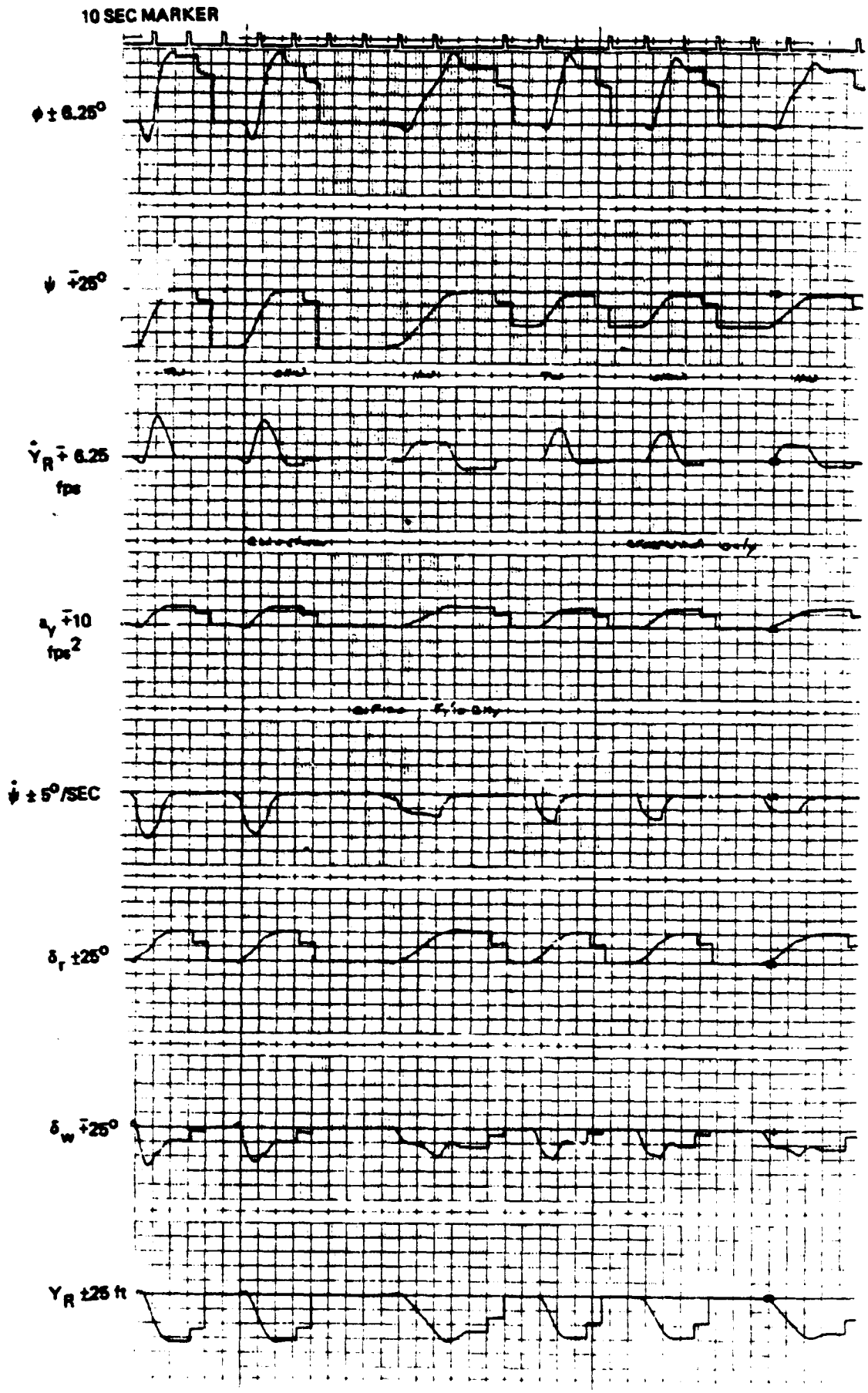

Figure C-5A. Doubled Ky and No Rudder to Wheel Crossfeed

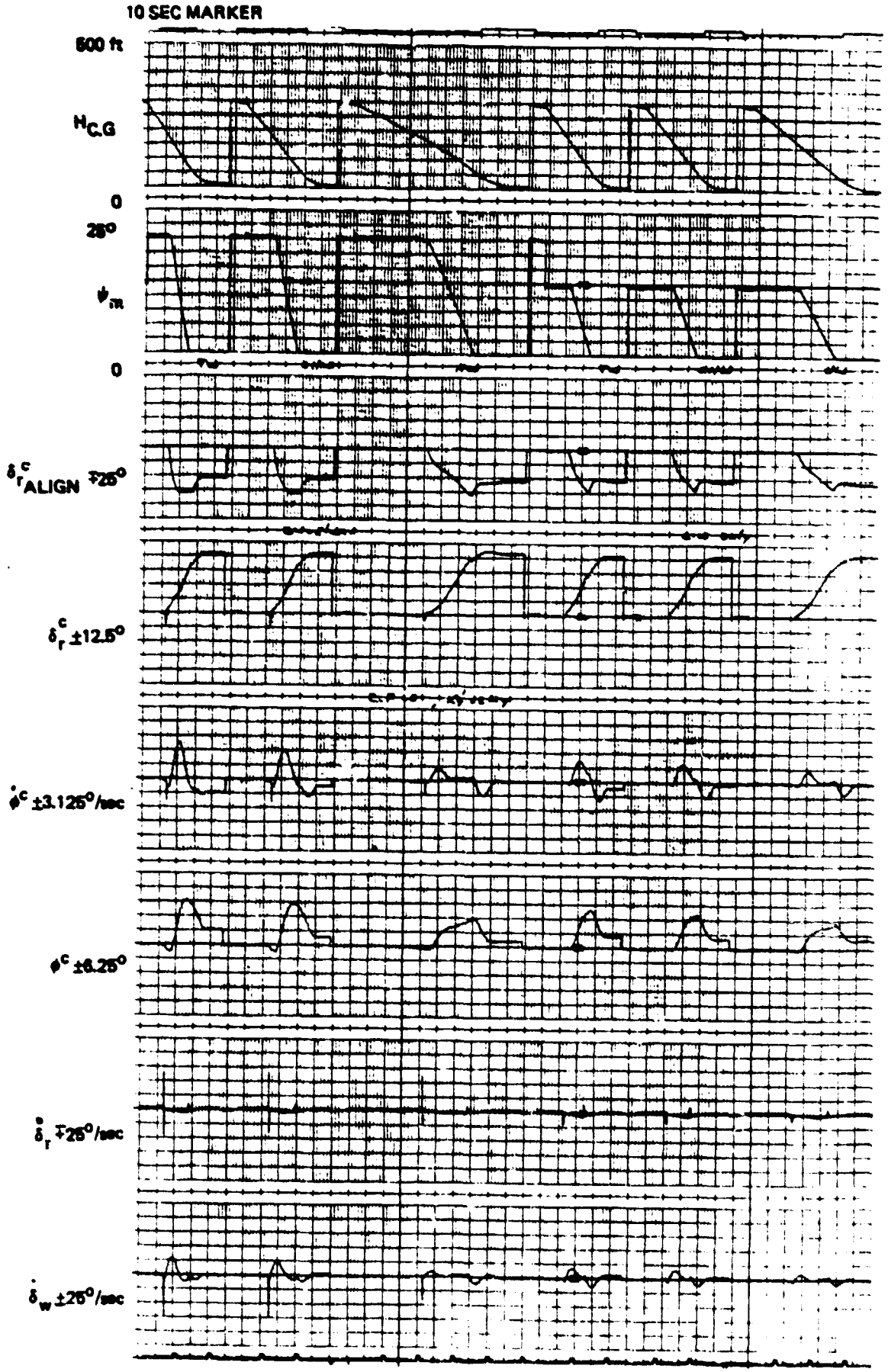

Figure C-5B. Doubled Ky and No Rudder to Wheel Crossfeed

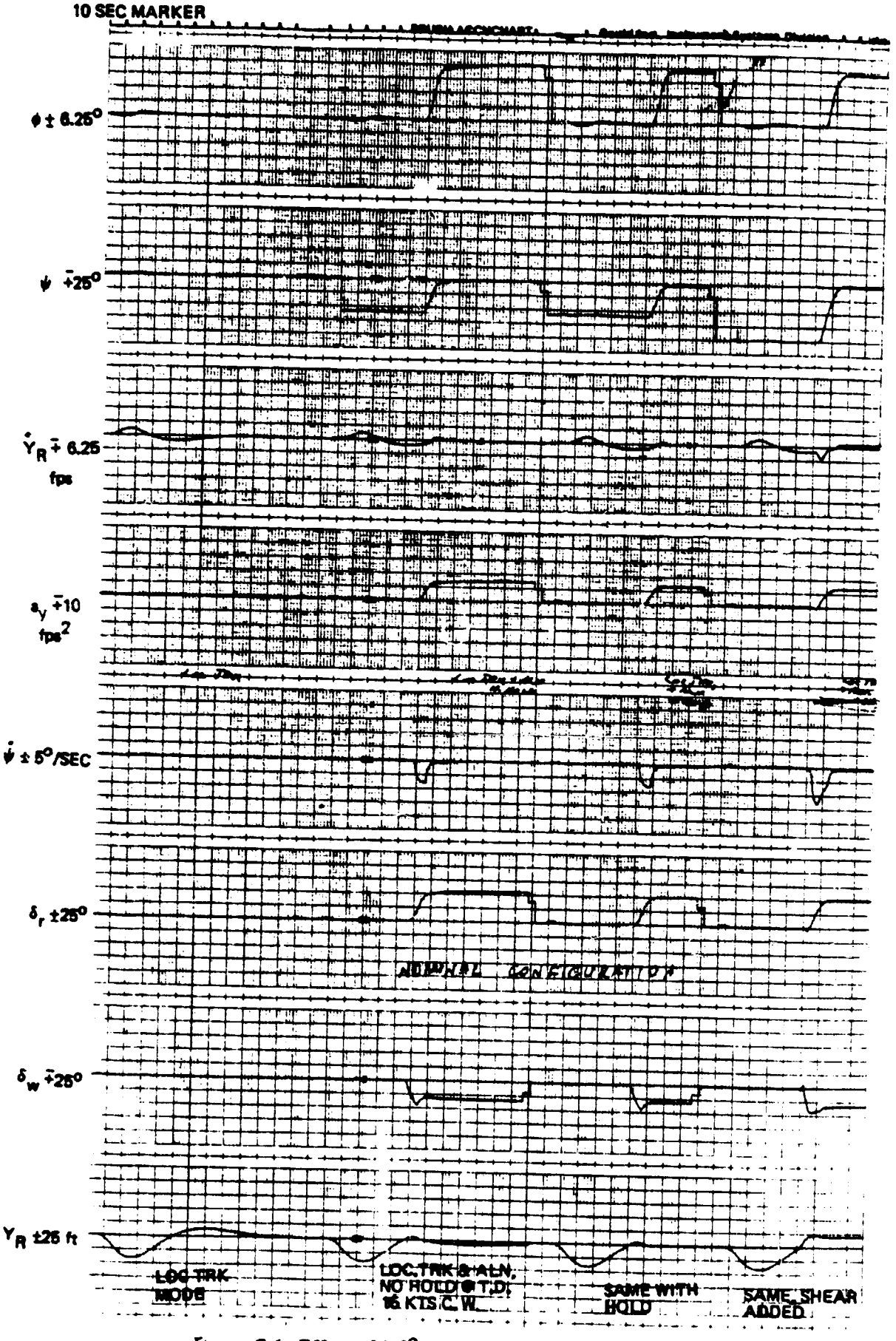

Figure C-6. Effect of 1.5° (max) Rudder Ramp into $\delta_r \rightarrow \delta_w$

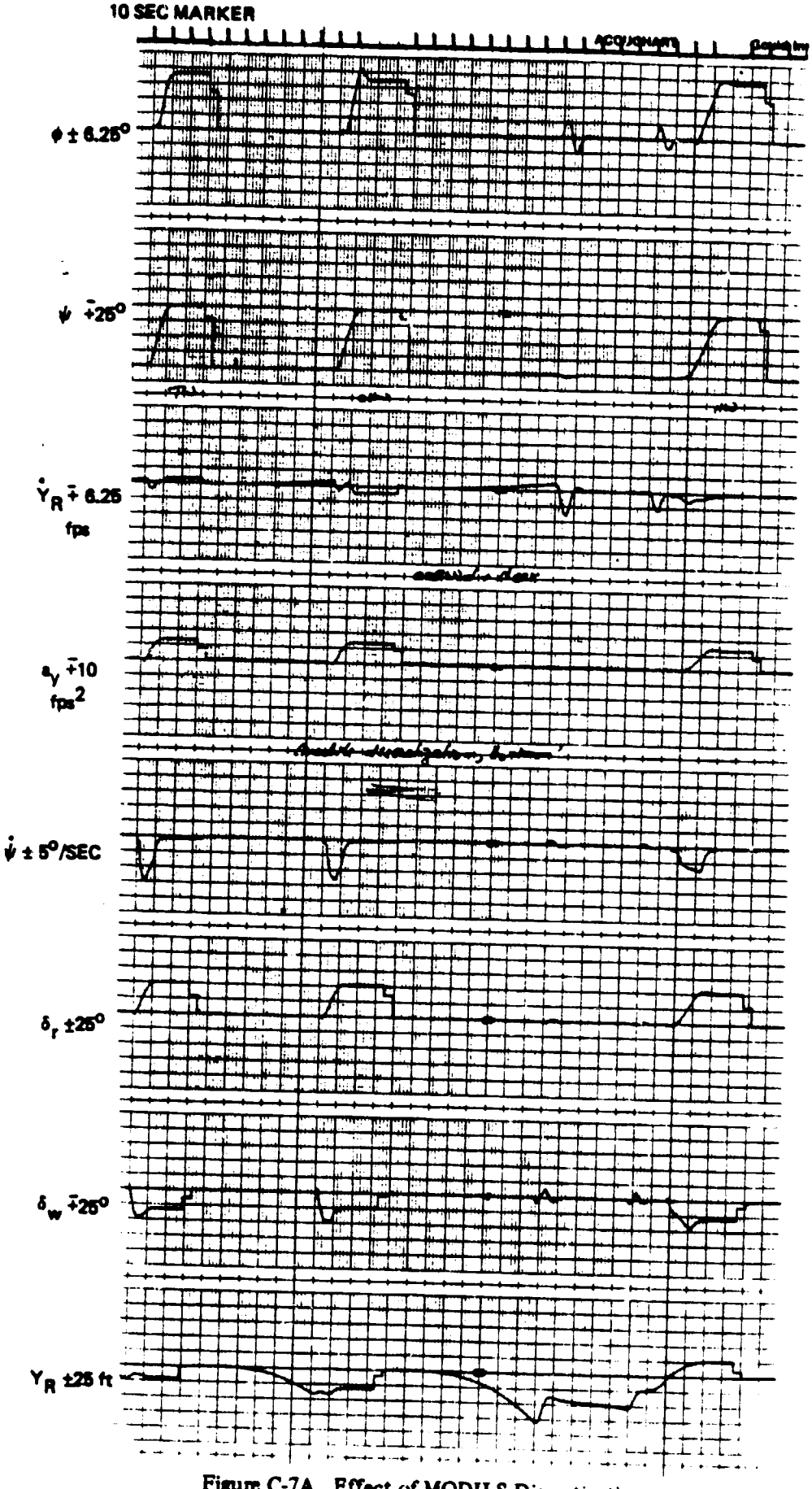

Figure C-7A. Effect of MODILS Discretization

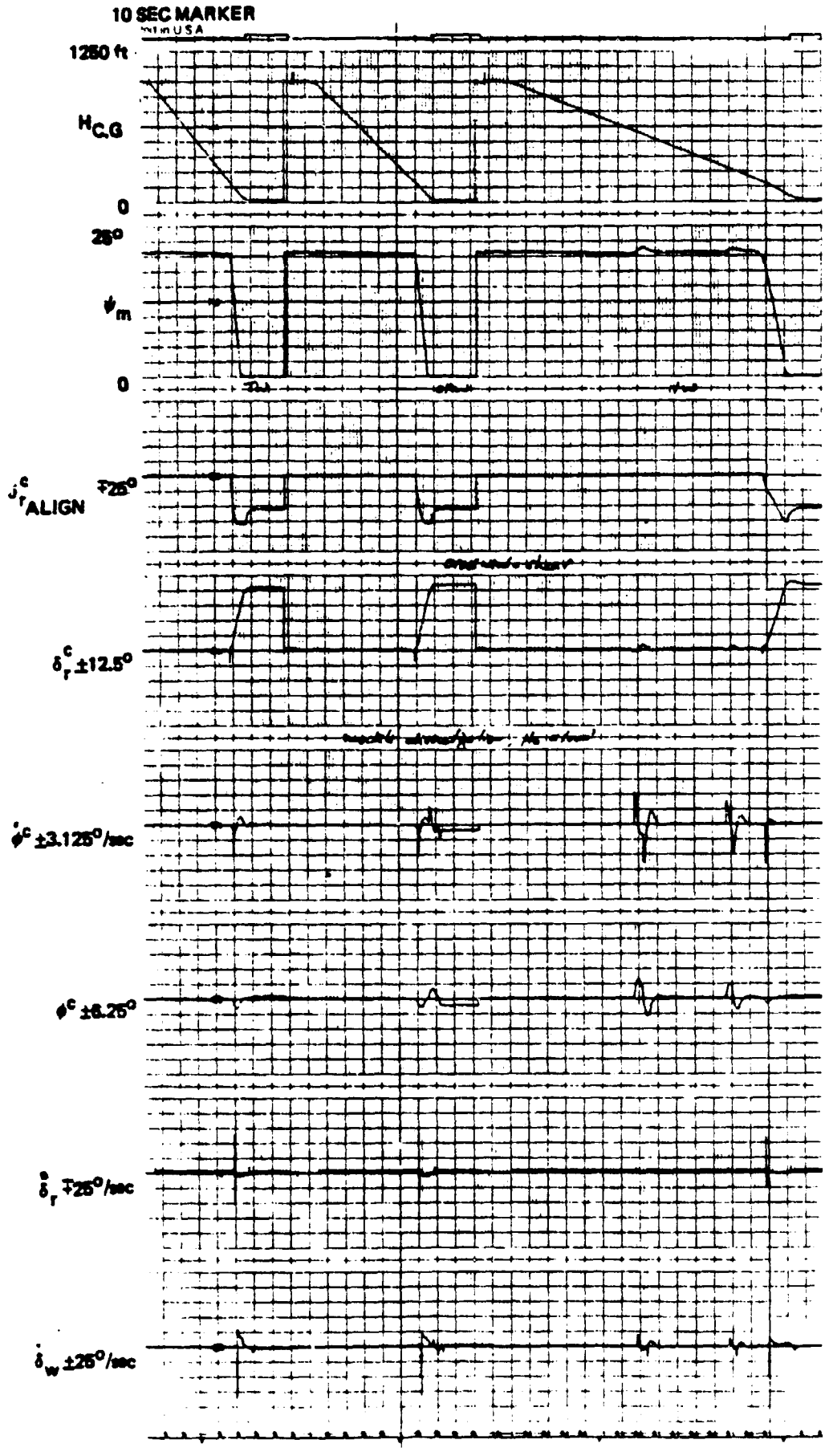

Figure C-7B. Effect of MODILS Discretization

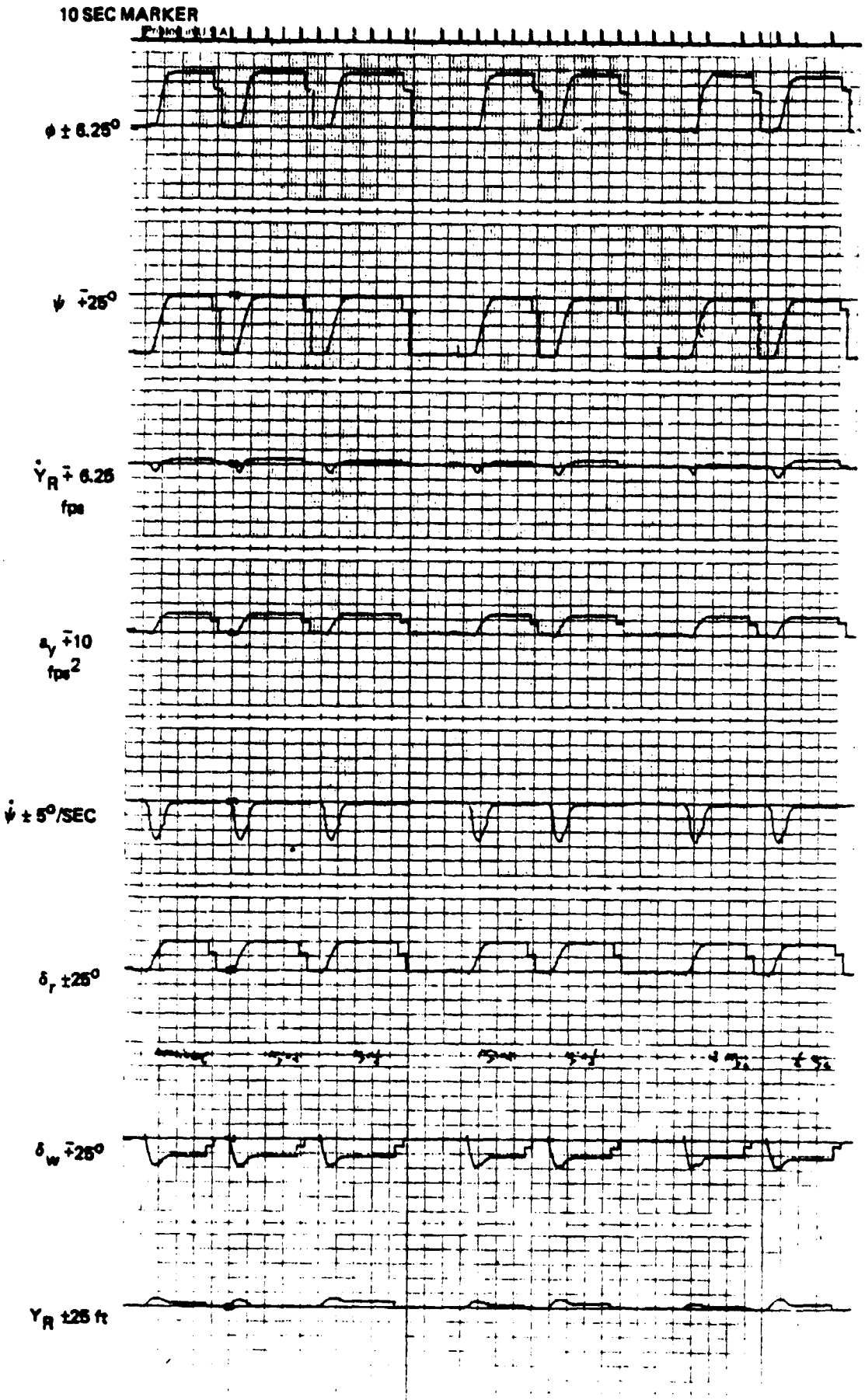

Figure C-8. Effect of Outer Loop Lateral Gain Variations

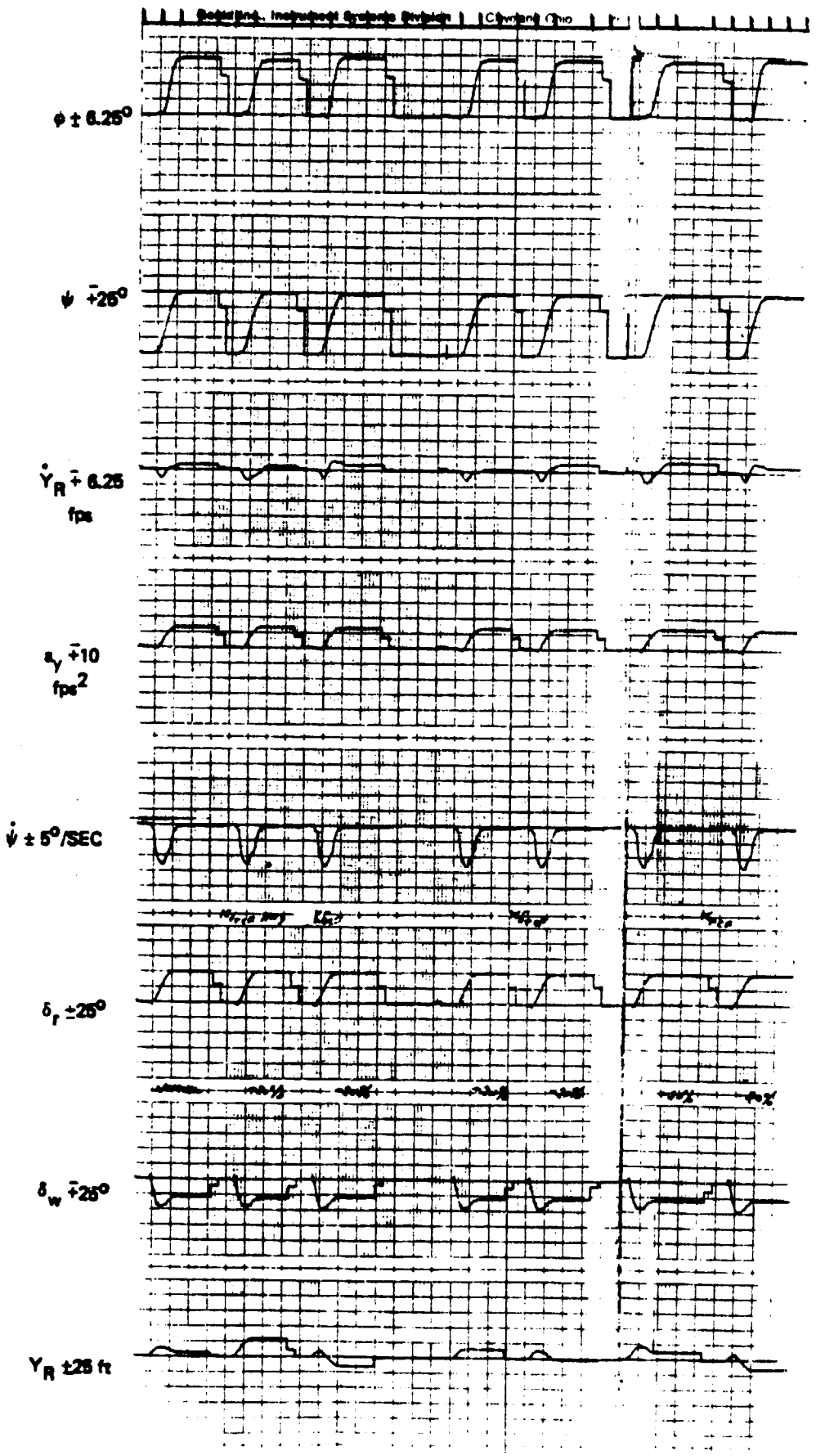

Figure C-9. Effect of Yaw to Roll Crossfeed Gain Variations

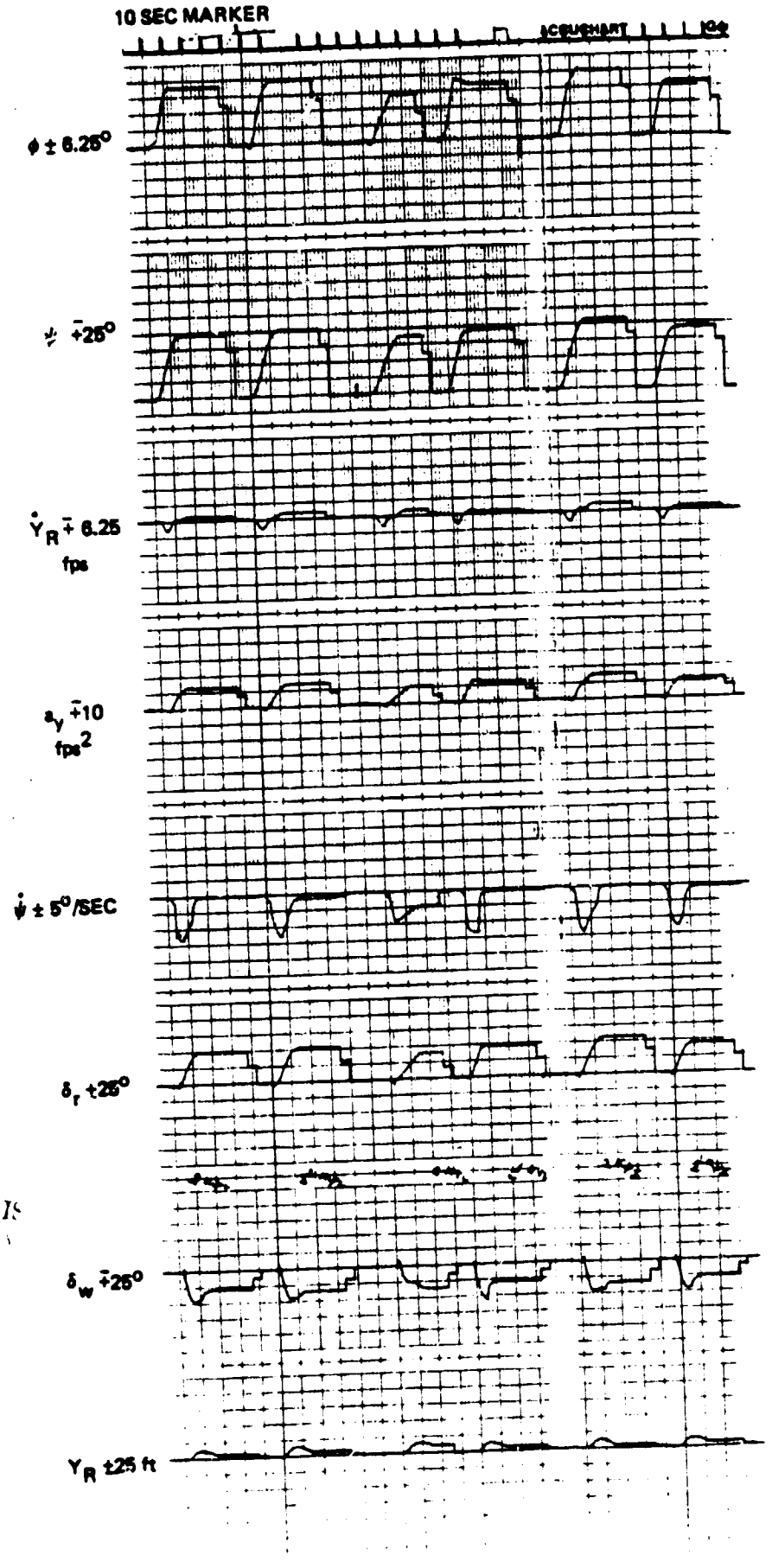

Figure C-10. Effect of Align Gain Variations

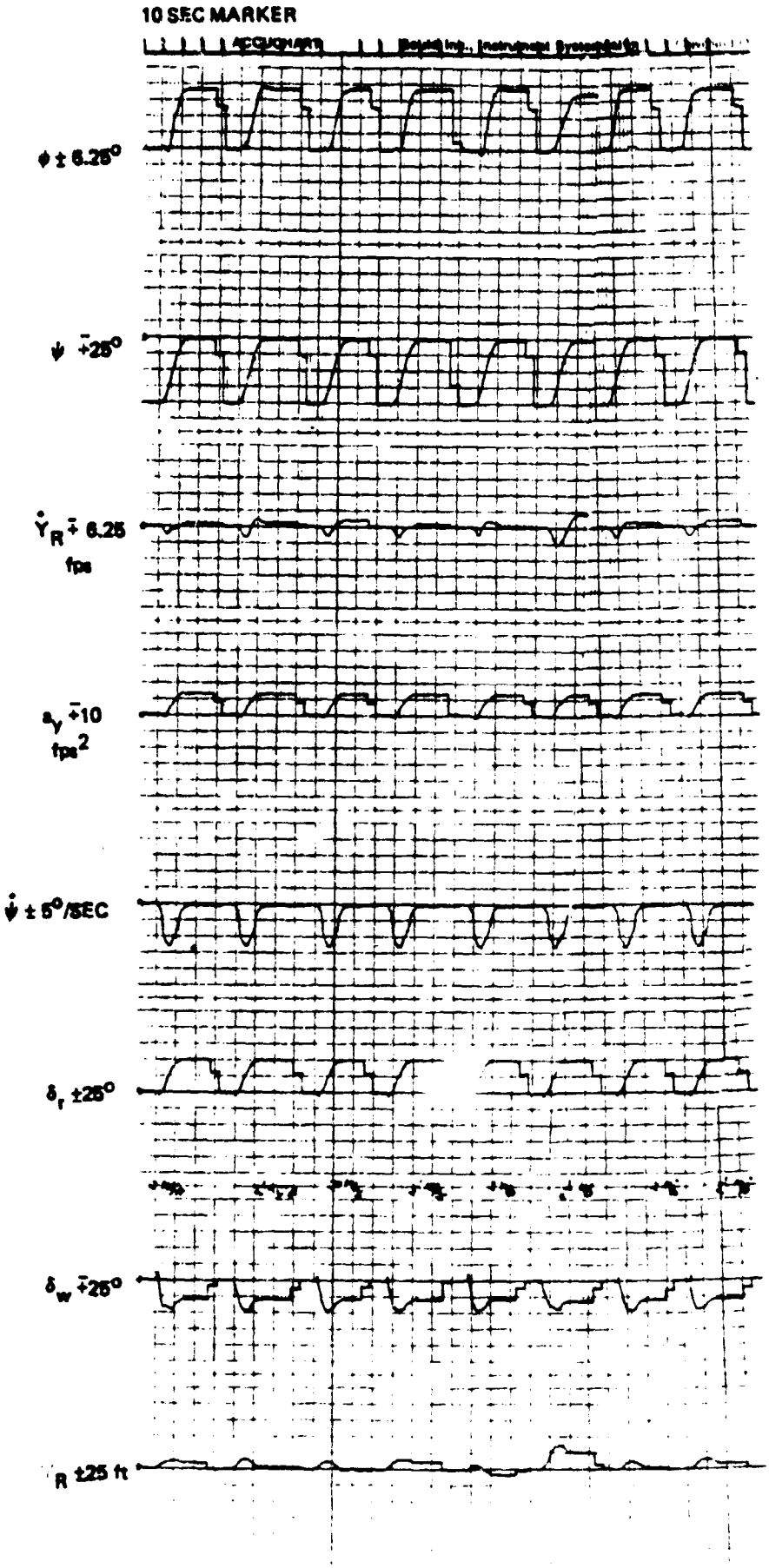

Figure C-11. Effect of Wind Down Compensation and Inner Roll Loop Gain Variations

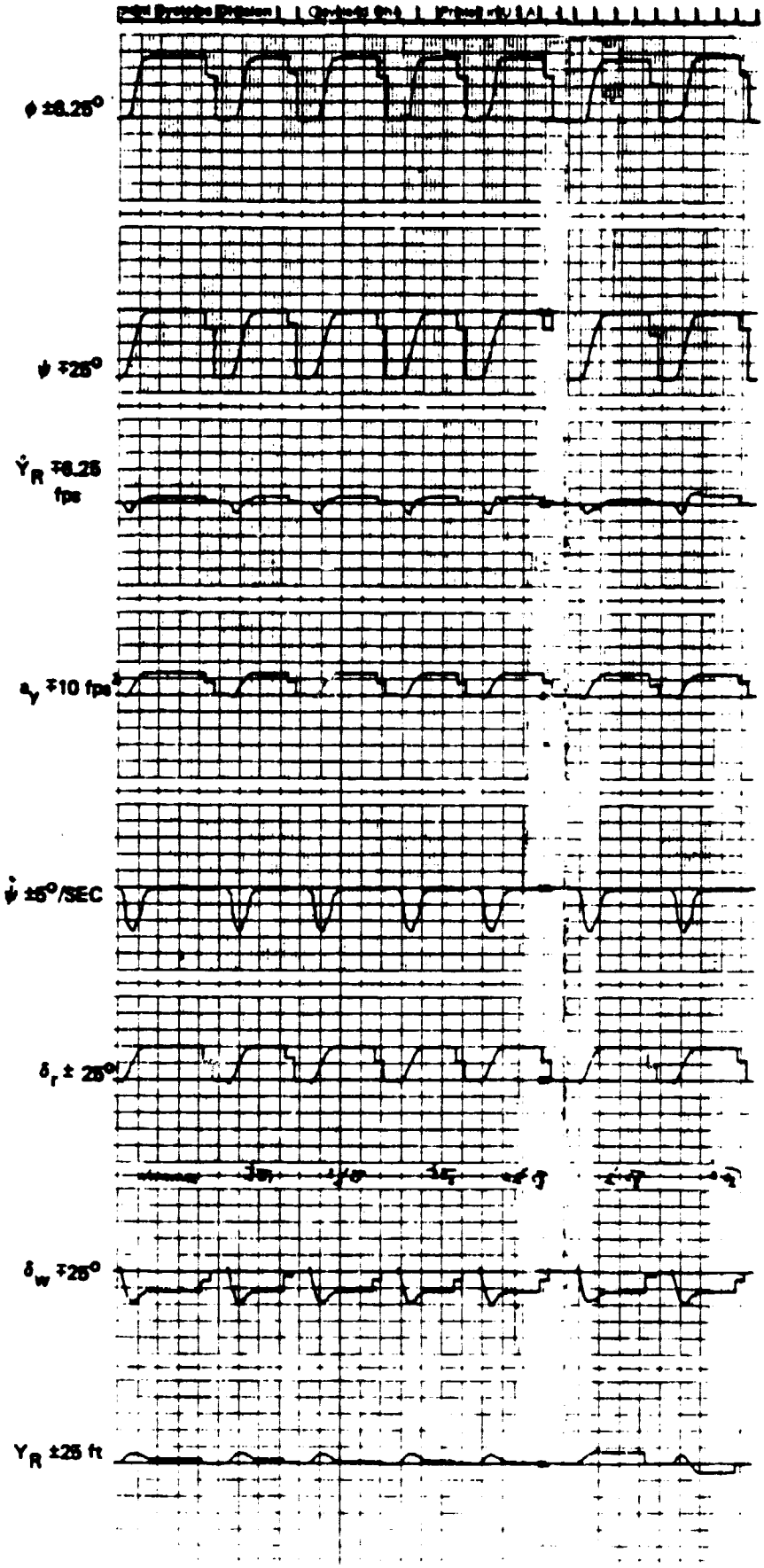

Figure C-12. Effect of Time Constant Variations

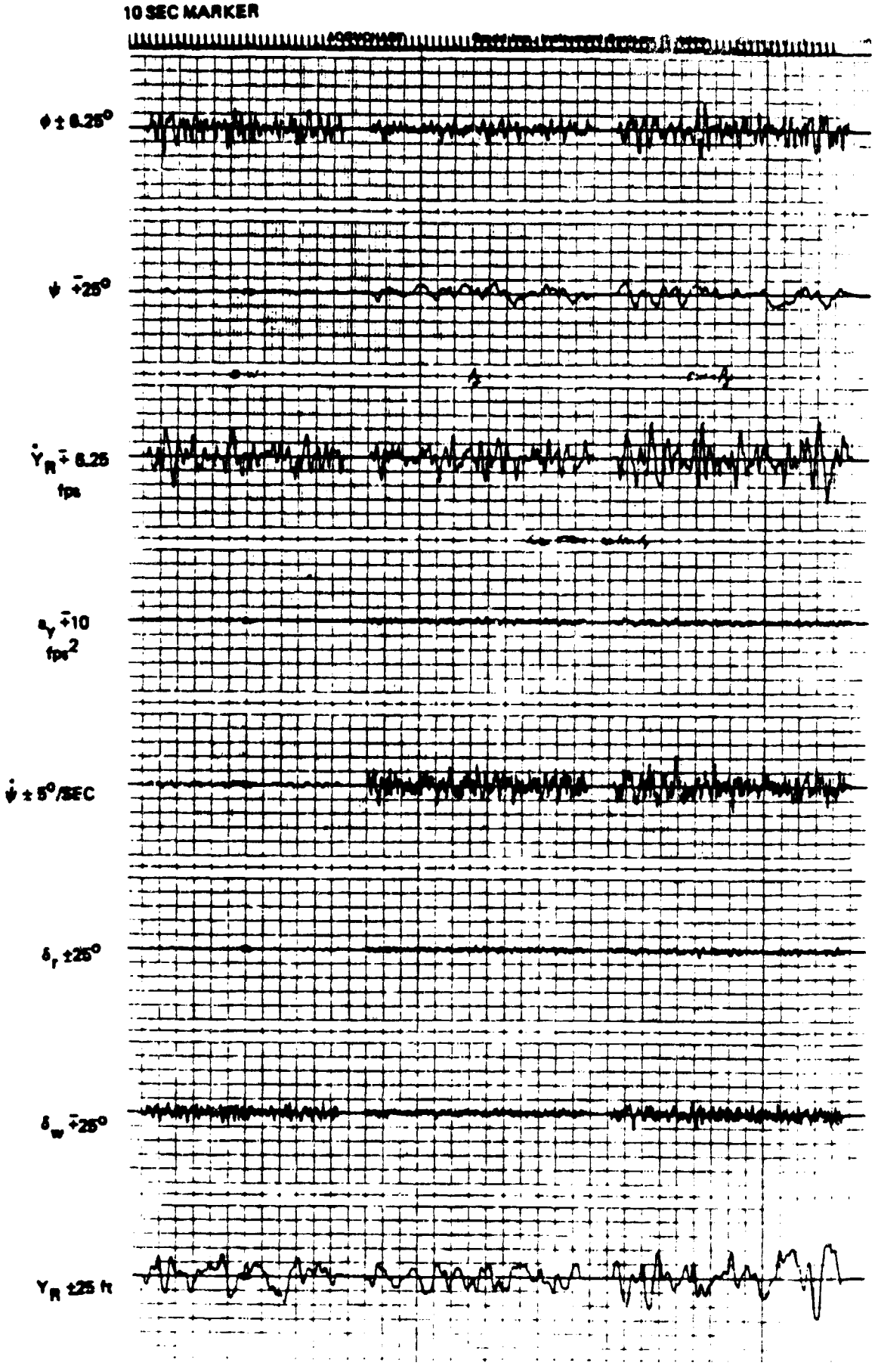

Figure C-13A. Localizer Track Activity

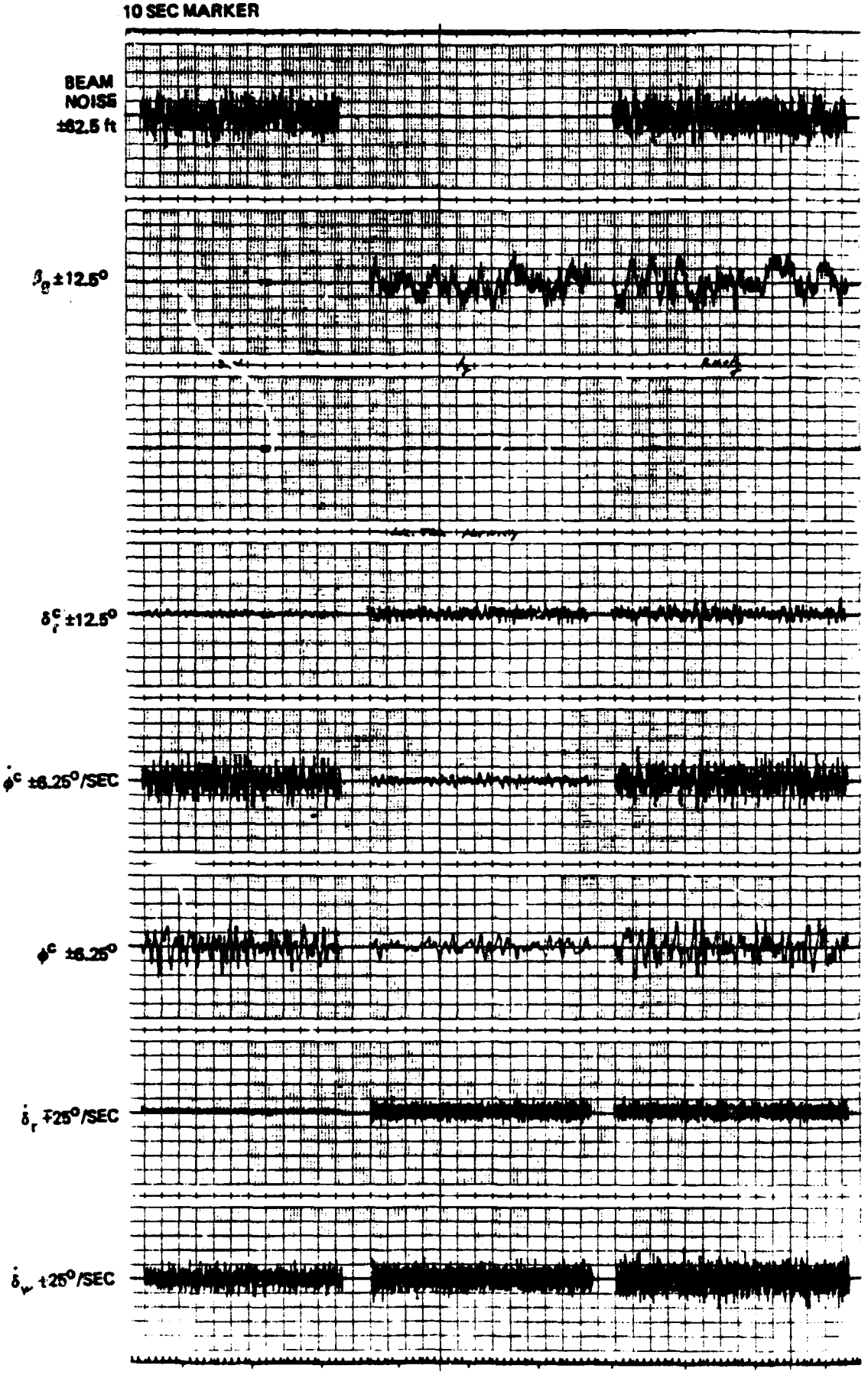

Figure C-13B. Localizer Track Activity

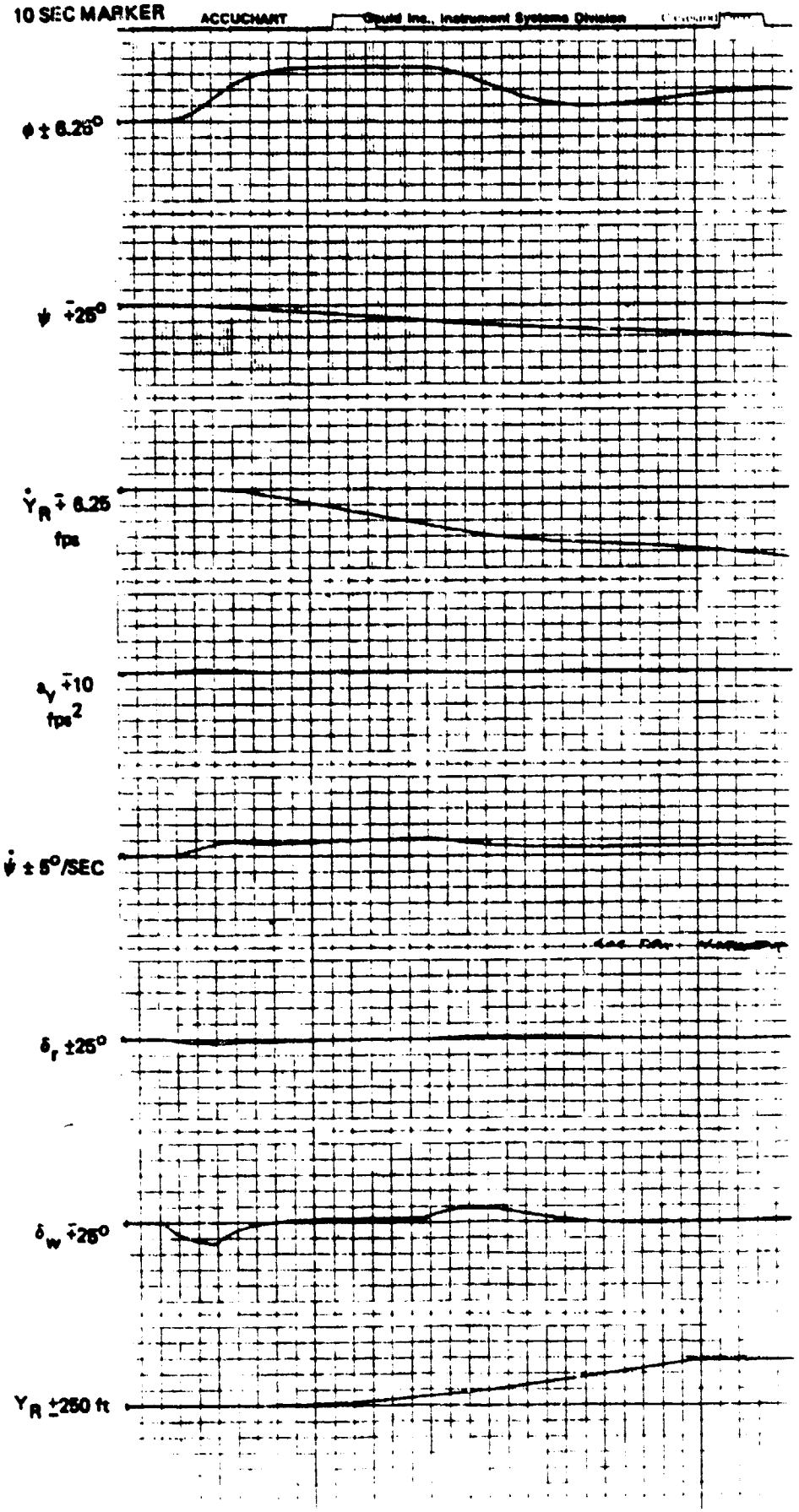

Figure C-14. Effect of Localizer Receiver Hardover Loc TRK Mode

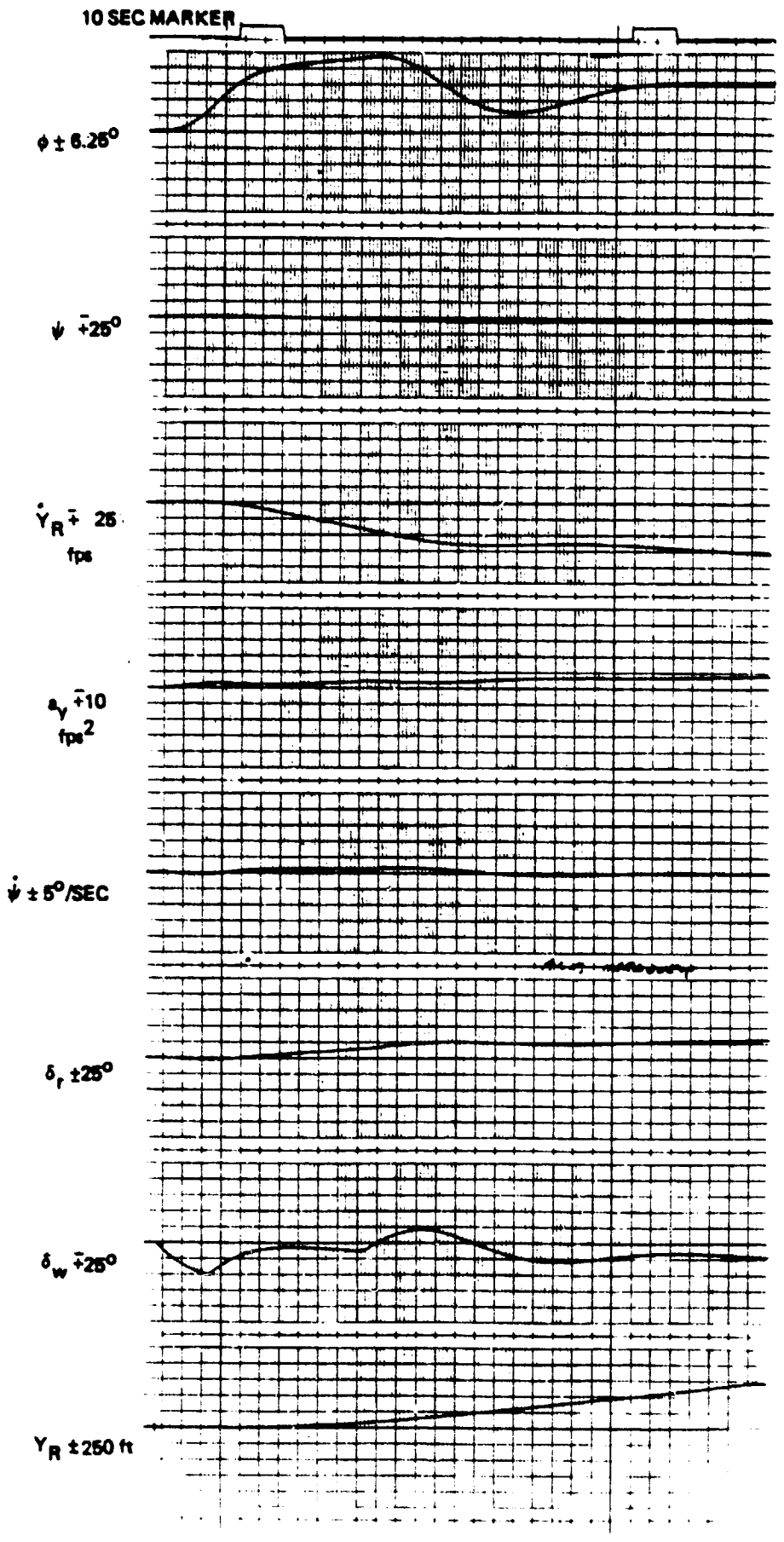

Figure C-15. Effect of Localizer Receiver Hardover; ALN Mode

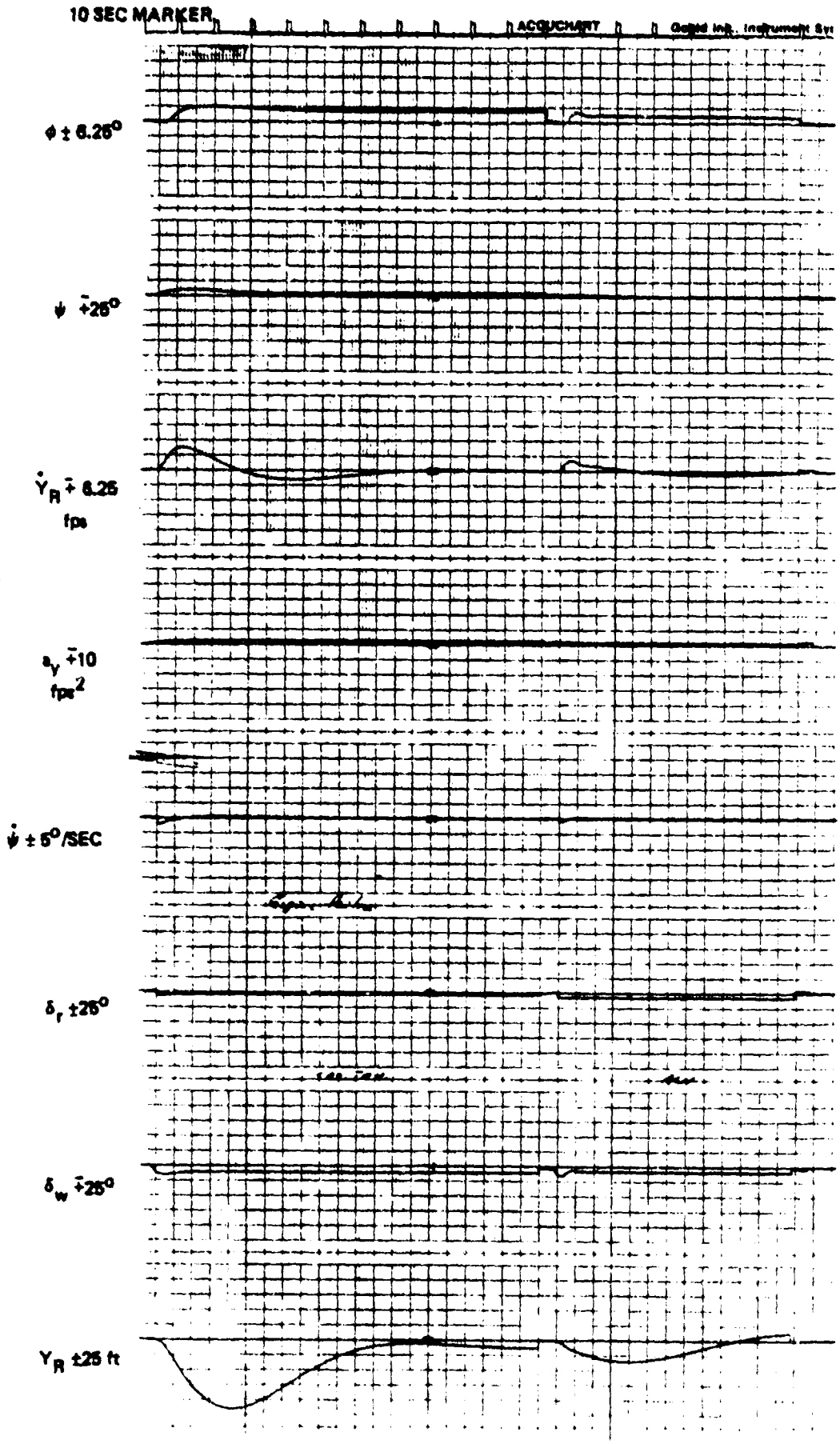

Figure C-16. Effect of Engine Failure

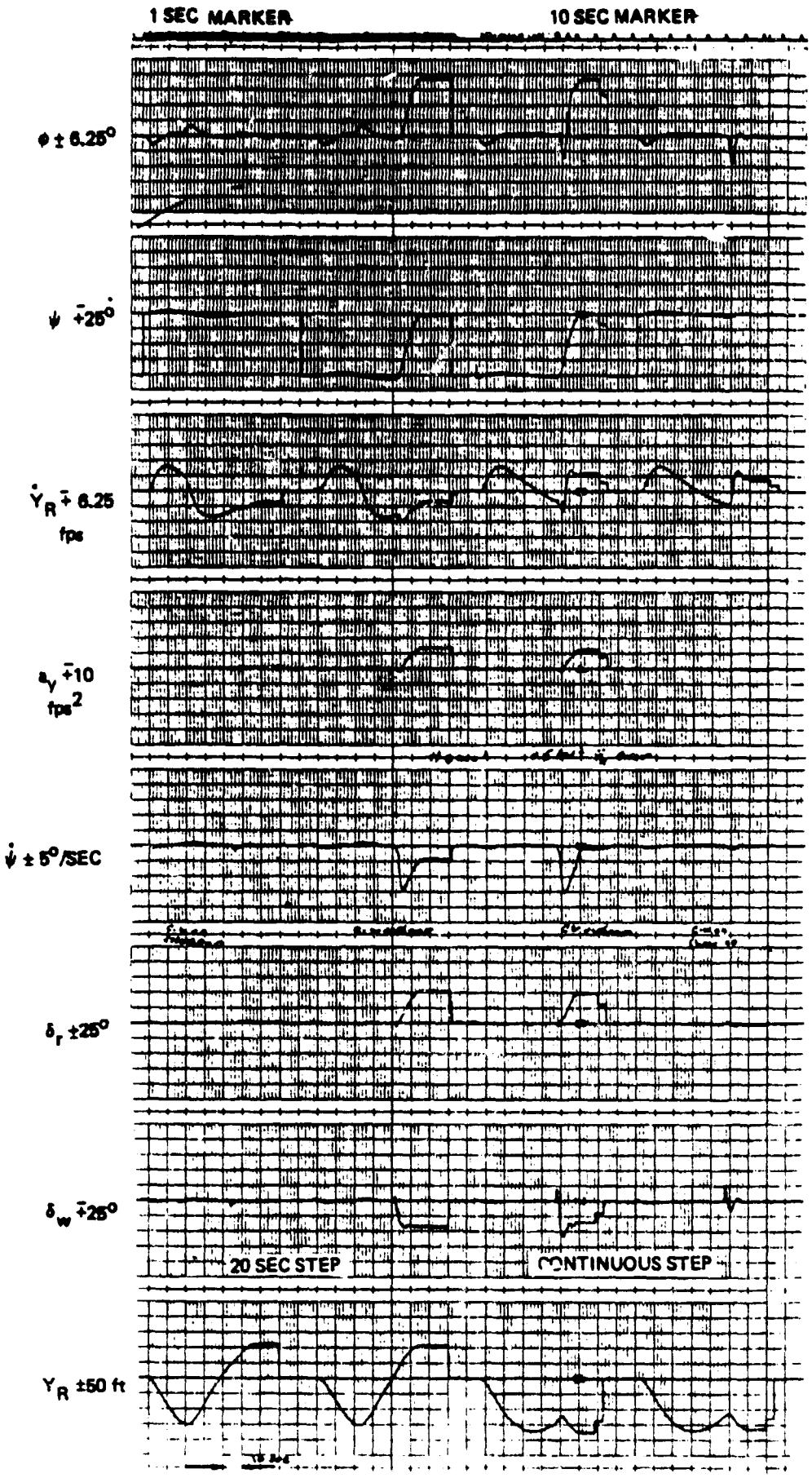

Figure C-17. Response to 0.5 fps^2 $\ddot{Y}_R$ Error at h=1000 ft.

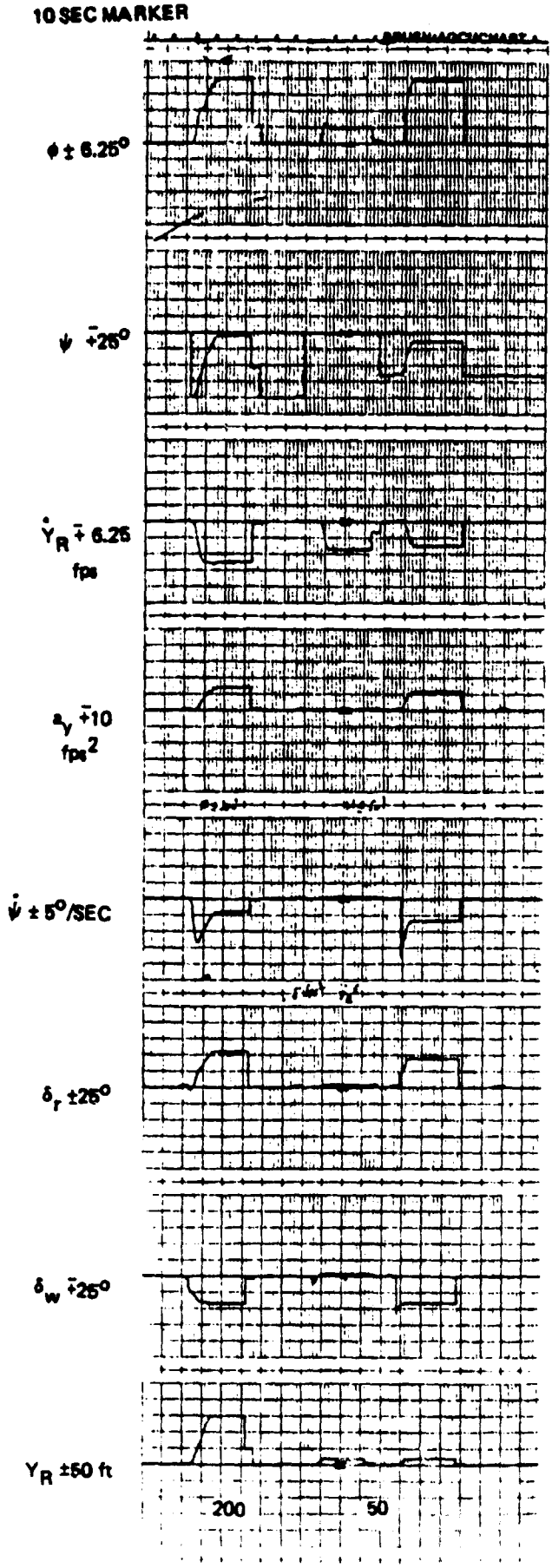

Figure C-18. Response to 0.5 fps^2 Step Y_p at 200 and 50 ft

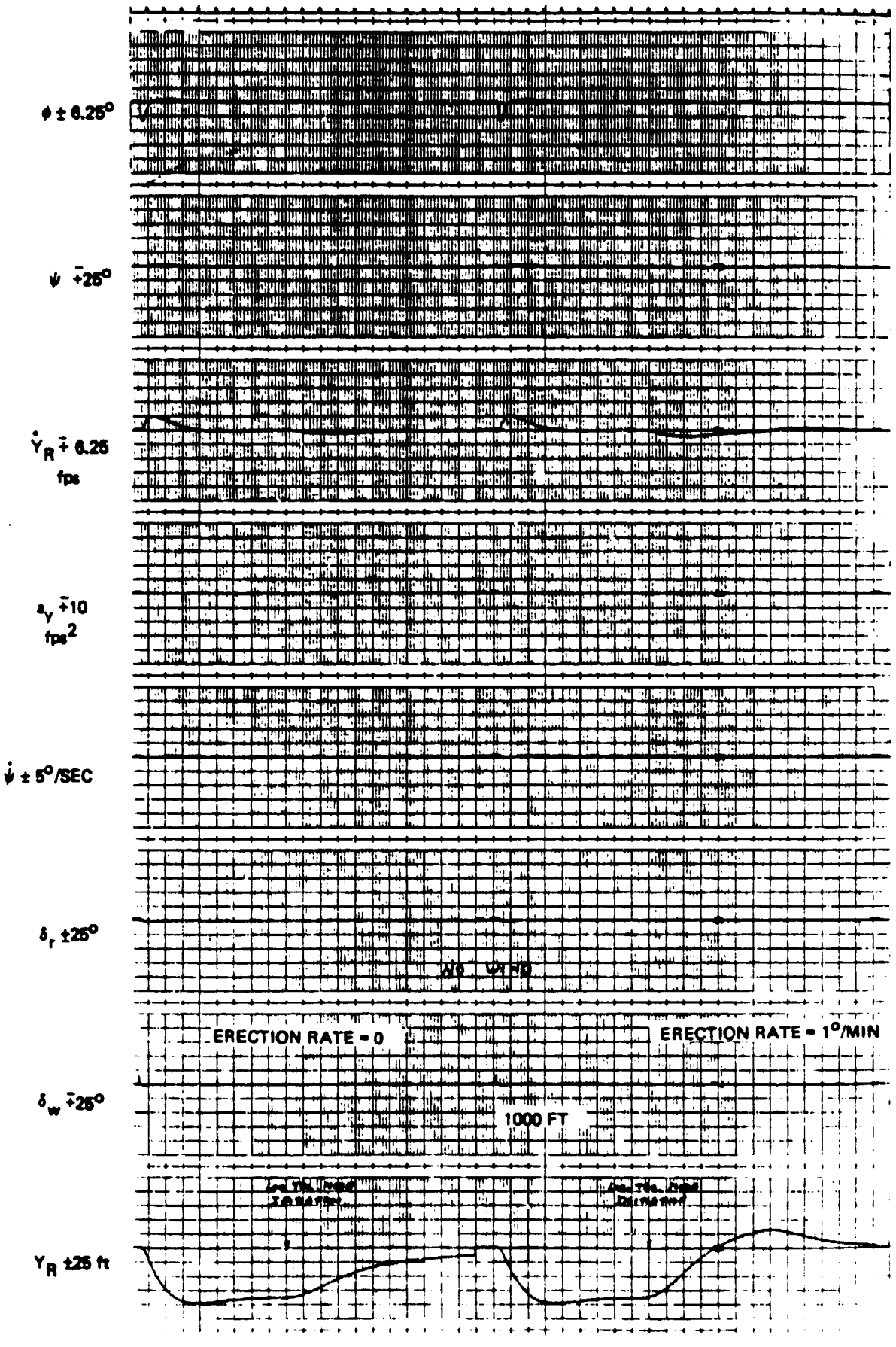

Figure C-19. Response to 1° Gyro Error, No Wind

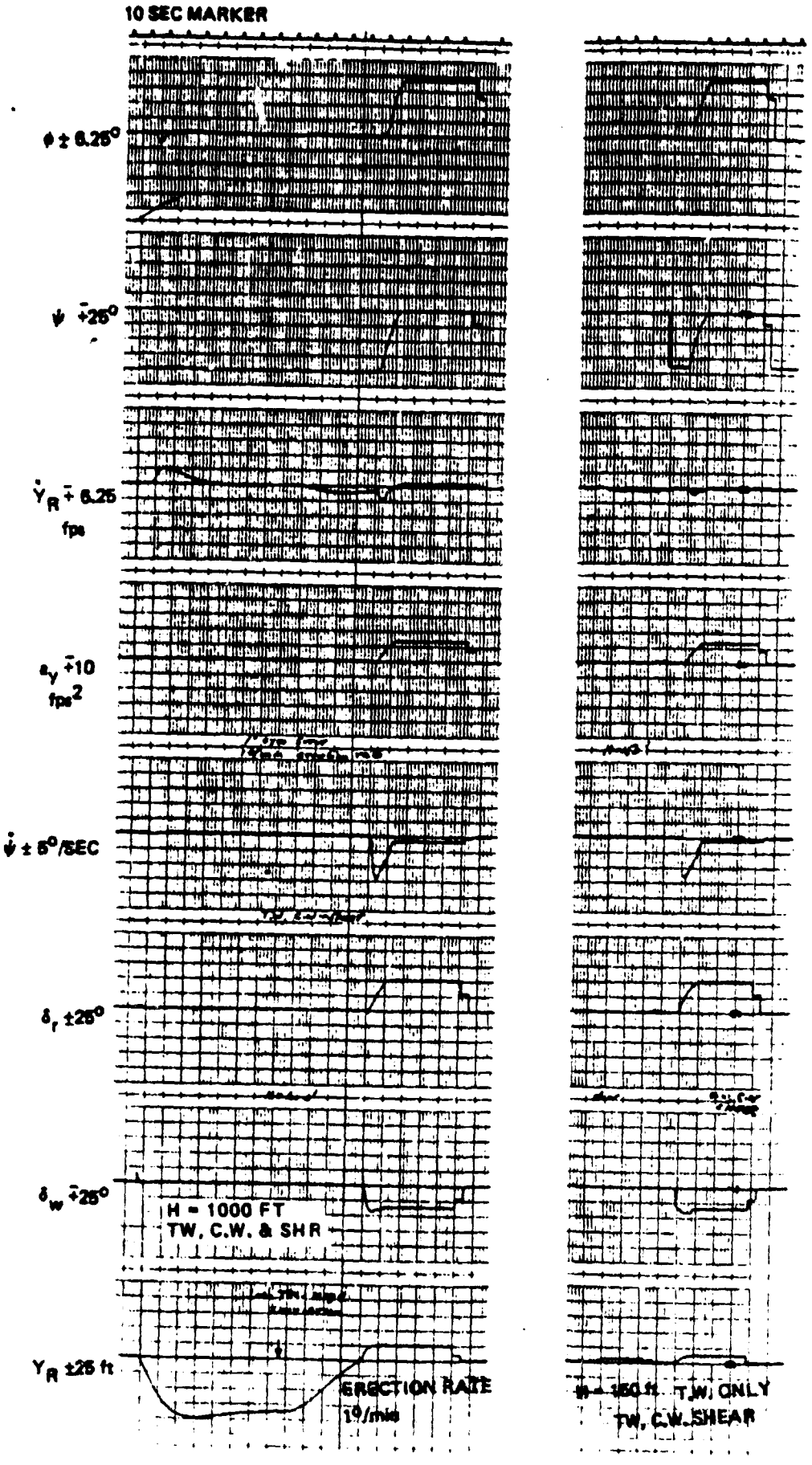

Figure C-20. Response to 1° Gyro Error With Winds

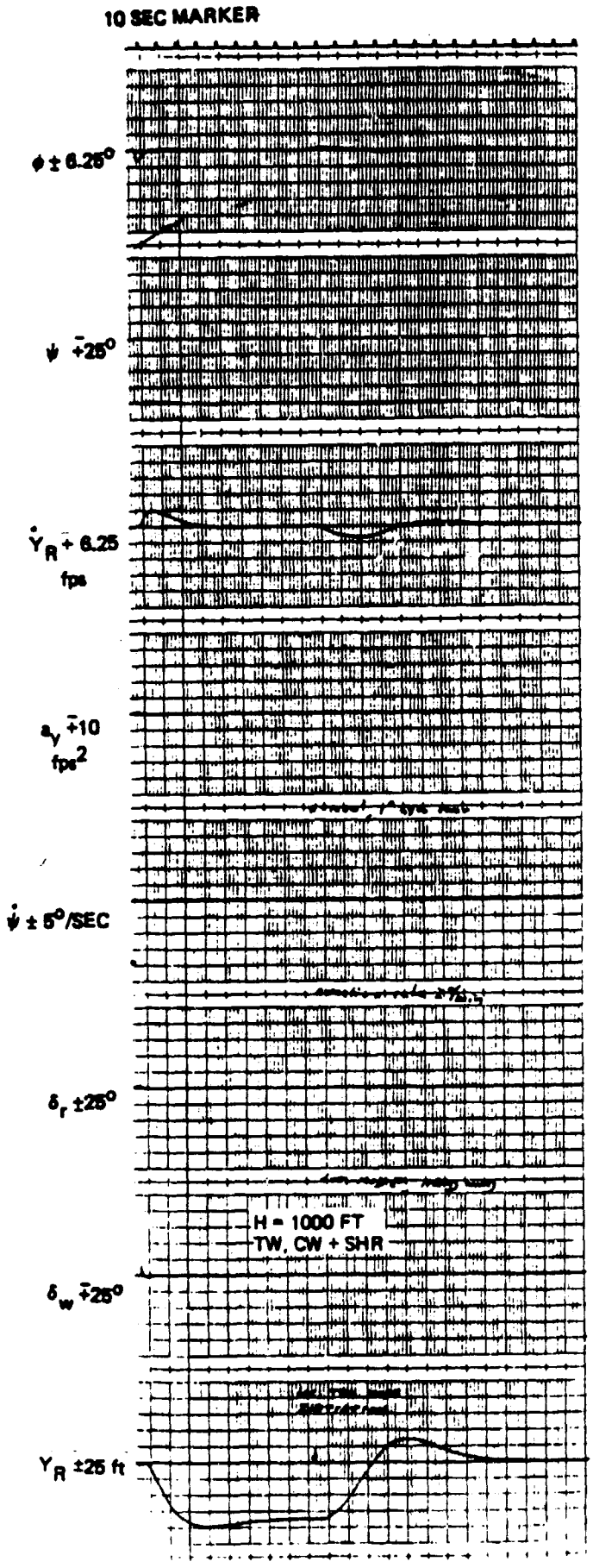

Figure C-21. Response to 1° Gyro Error, 2°/min Erection

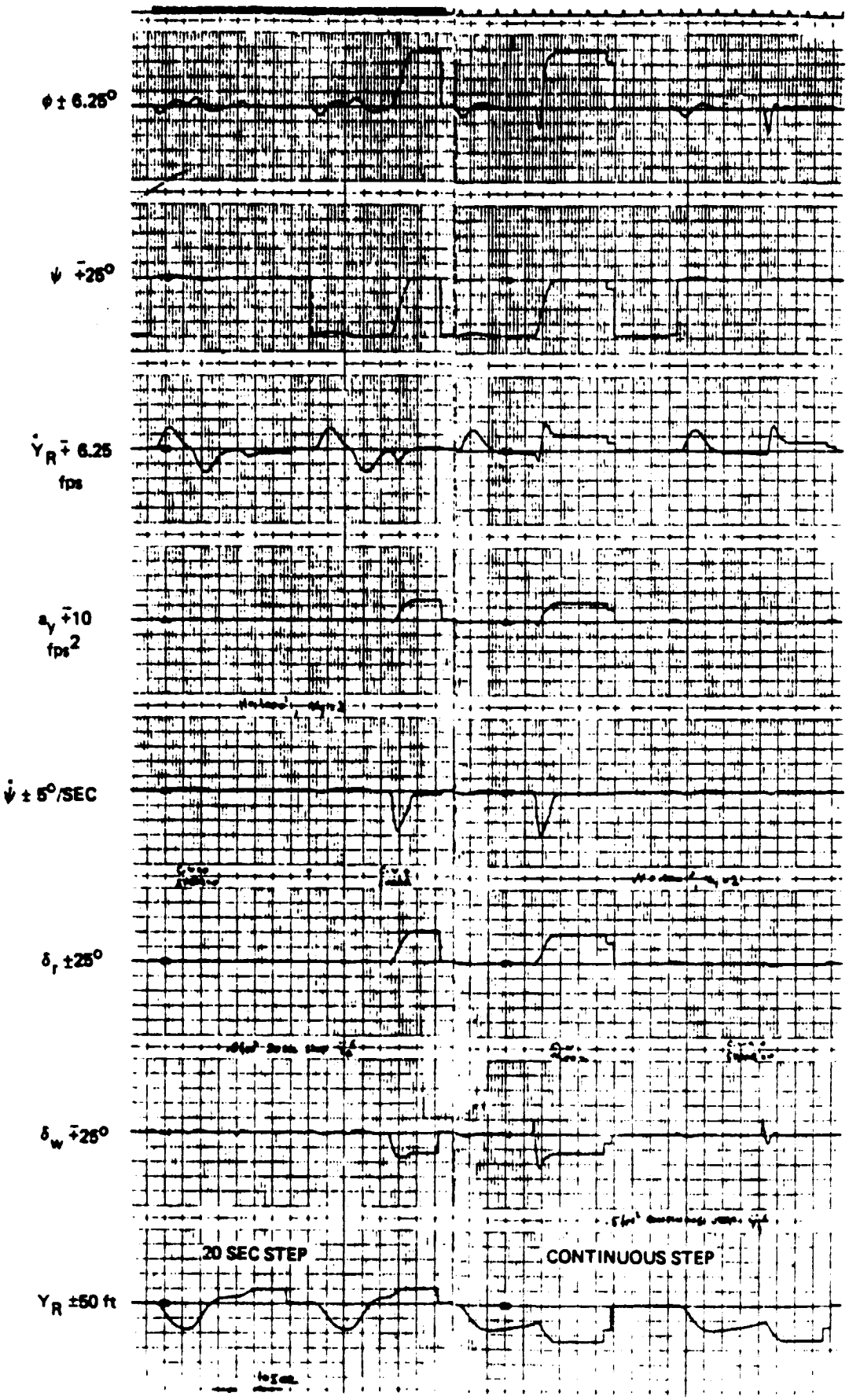

Figure C-22. Response to $0.5 fps^2 \ddot{Y}_R$ Error, 2*ky, h=1000 ft.

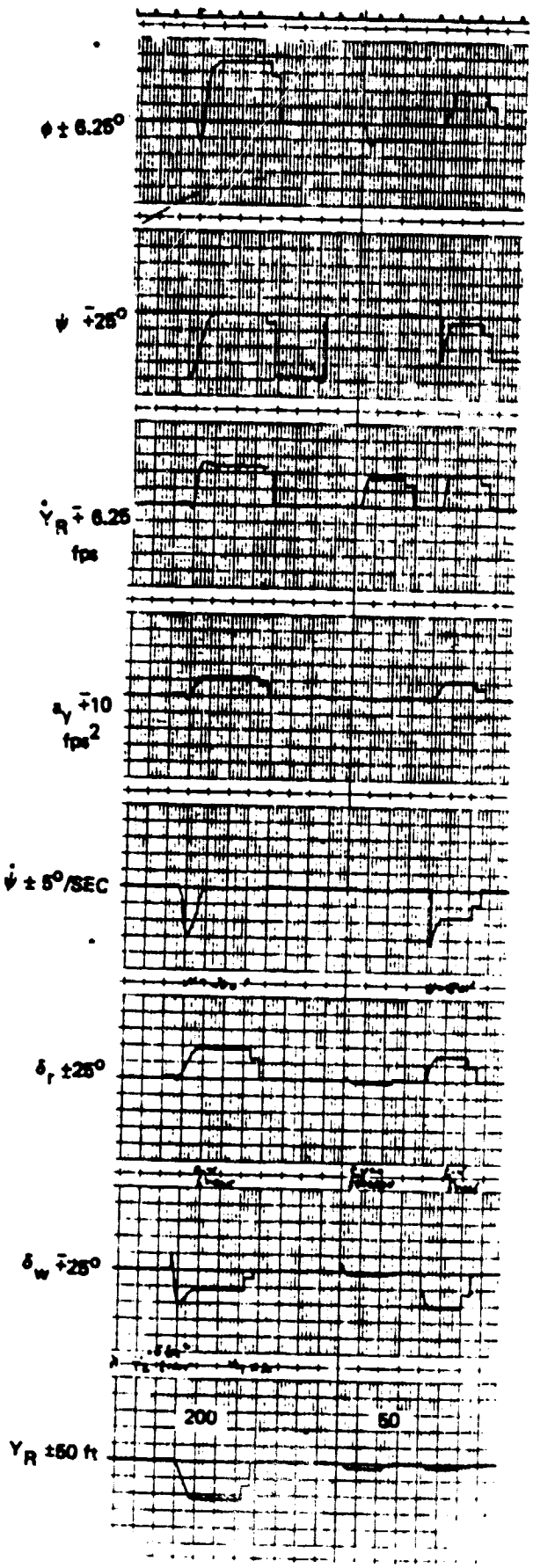

Figure C-23. Response to 0.5fps^2 $\ddot{Y}_R$ Error, 2°ky, h=200 and 50ft.

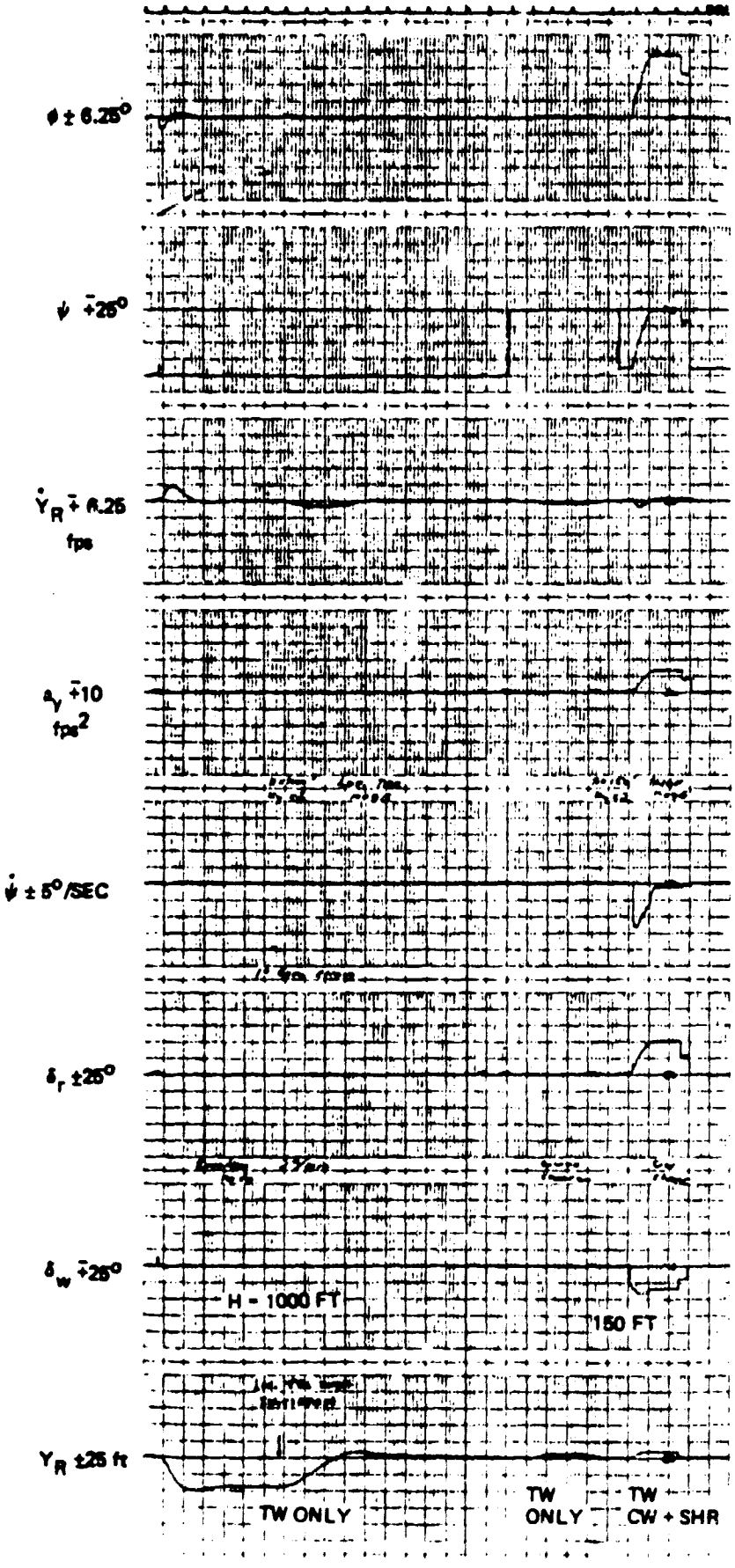

Figure C-24. Response to 1° Gyro Error, 2°ky, 2°/min Erection

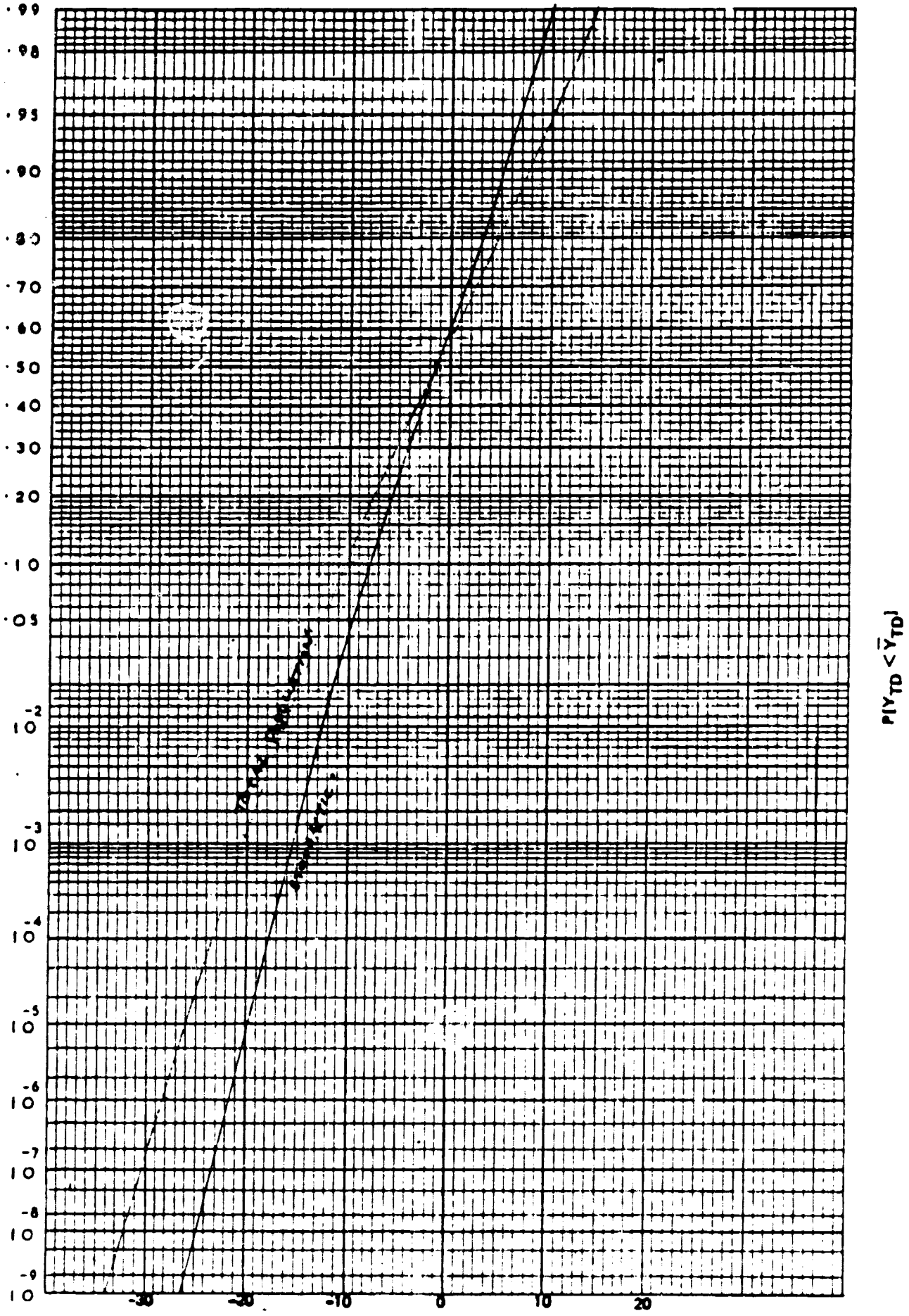

Figure C-25. Nominal Configuration, Y_{TD} (ft)

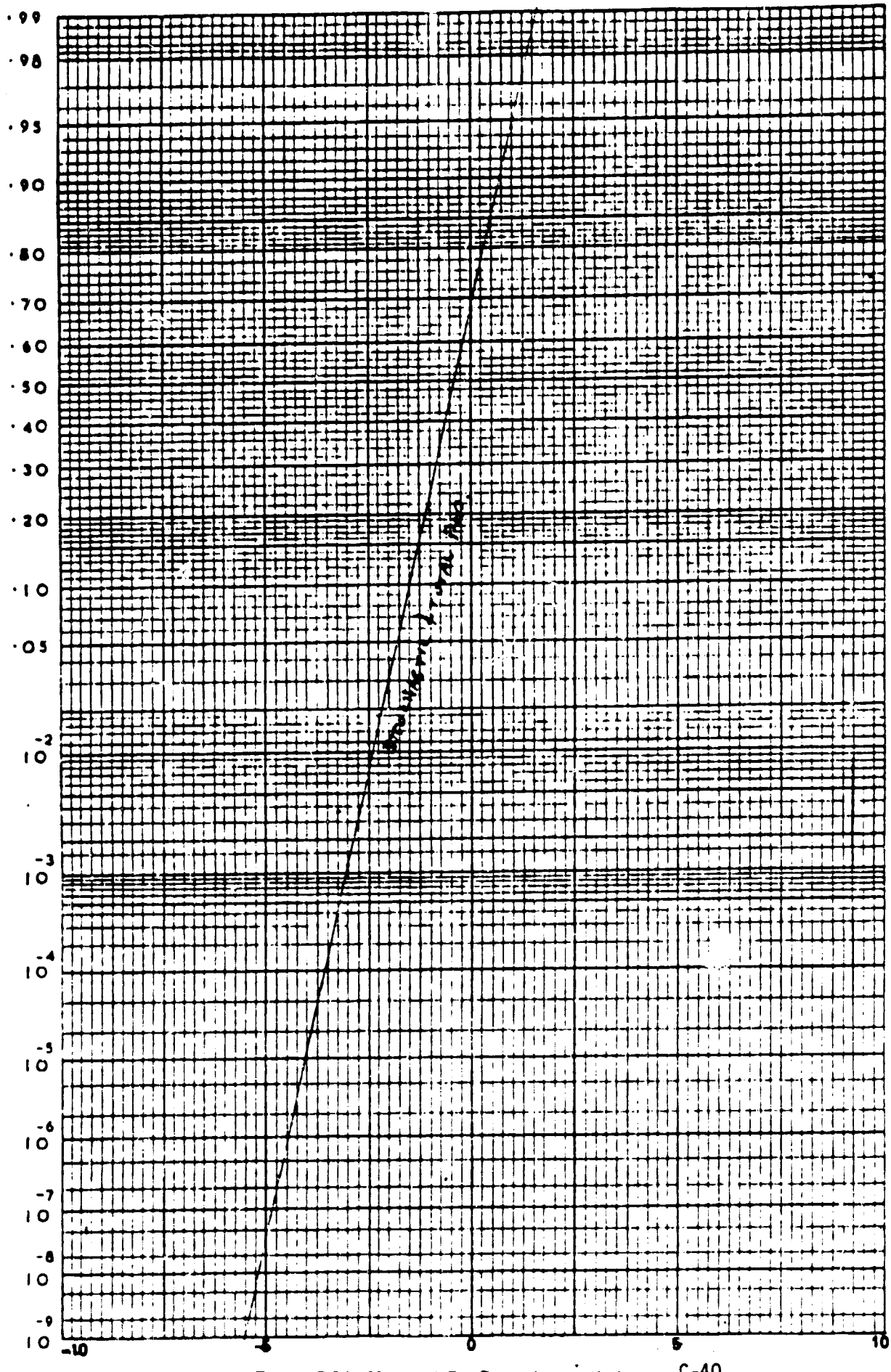

Figure C-25. Nominal Configuration, $\dot{Y}$ (fps)

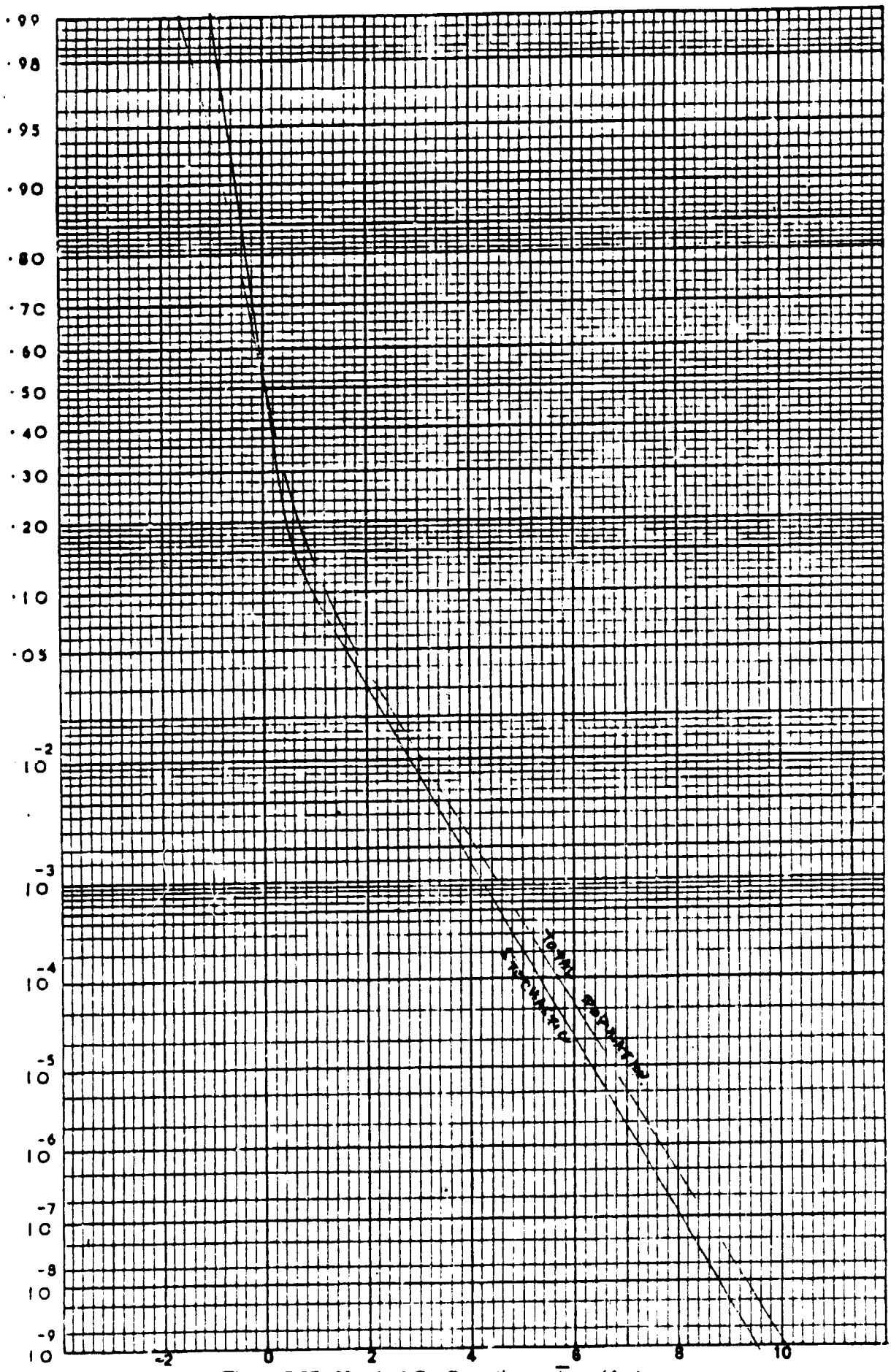

Figure C-27. Nominal Configuration, $\bar{\psi}_{TD}$ (deg)

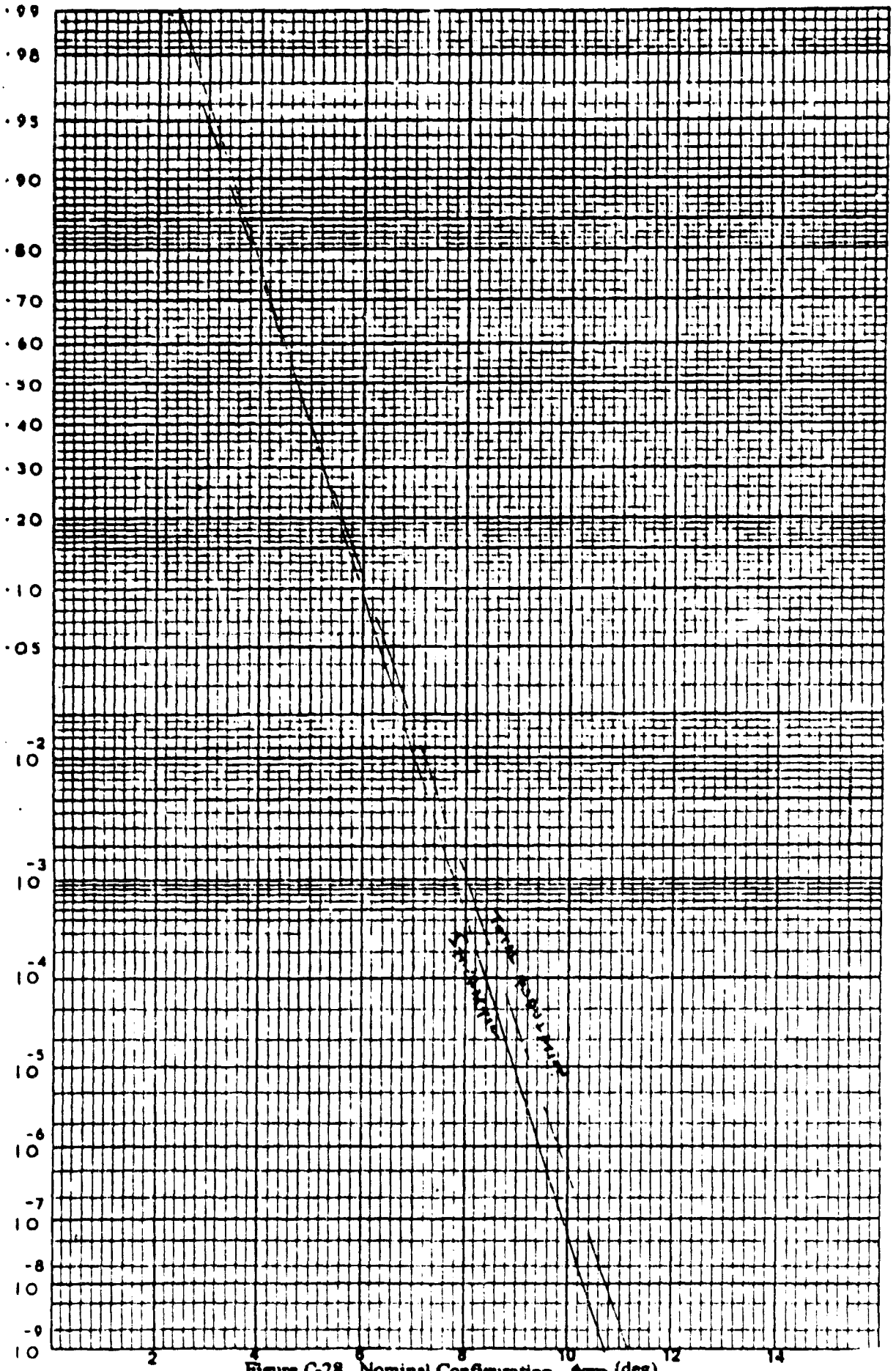

Figure C-28. Nominal Configuration, ϕ_{TD} (deg)

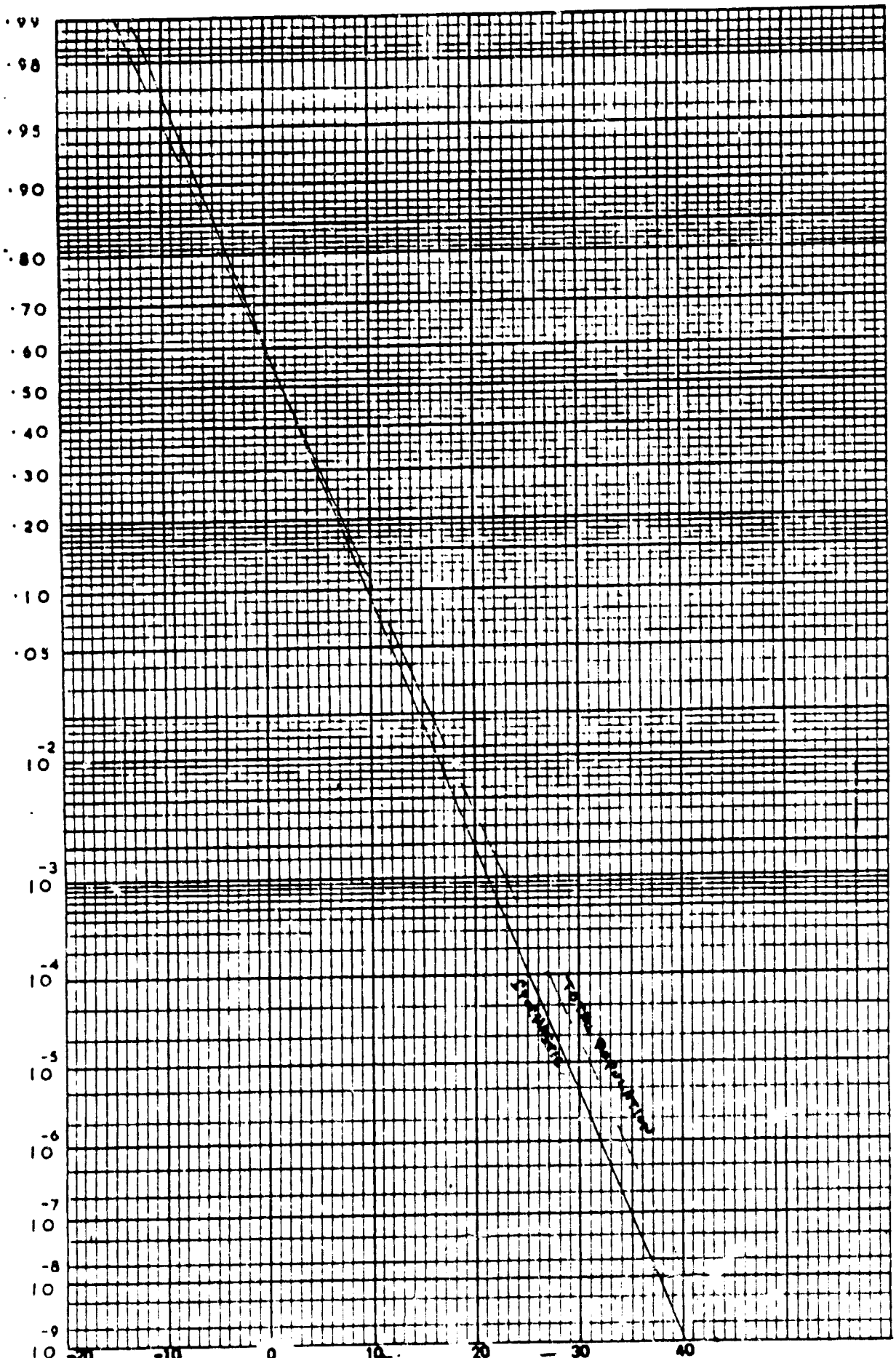

Figure C-29. Nominal Configuration, $\bar{Y}_{100}$ (ft)

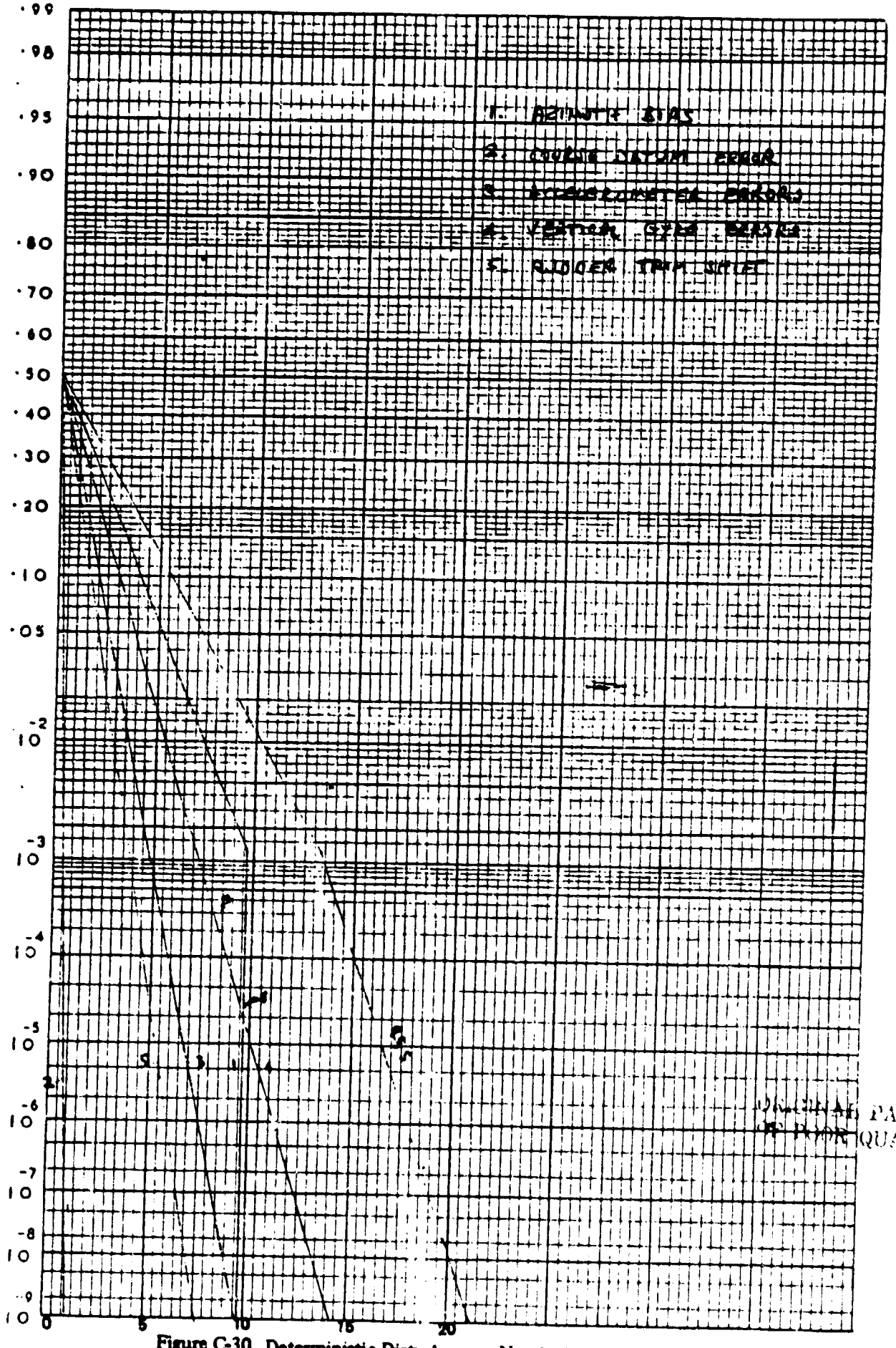

Figure C-30. Deterministic Disturbances–Nominal, ΔY_{TD} (ft)

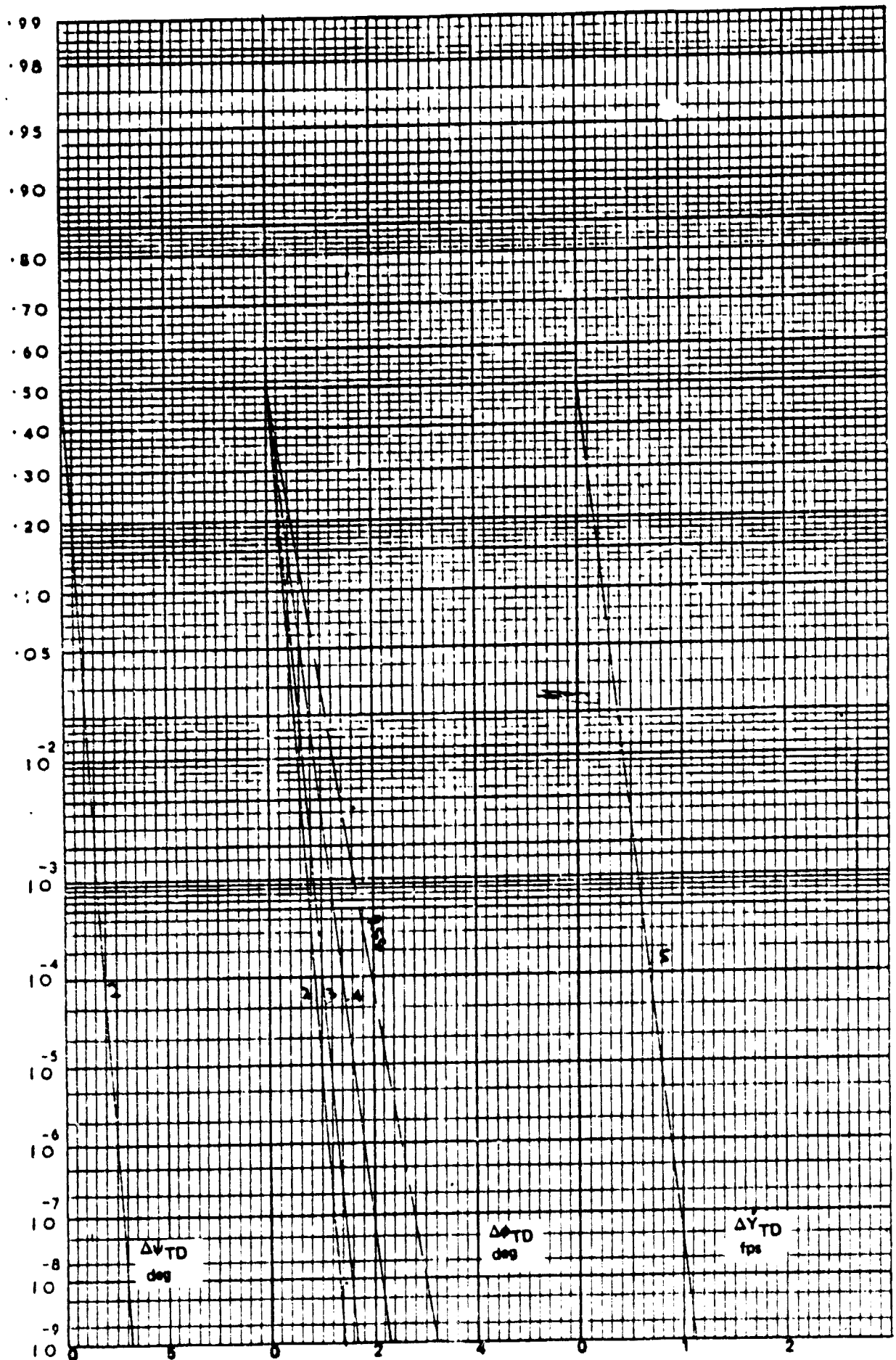

Figure C-31. Deterministic Disturbances, Nominal

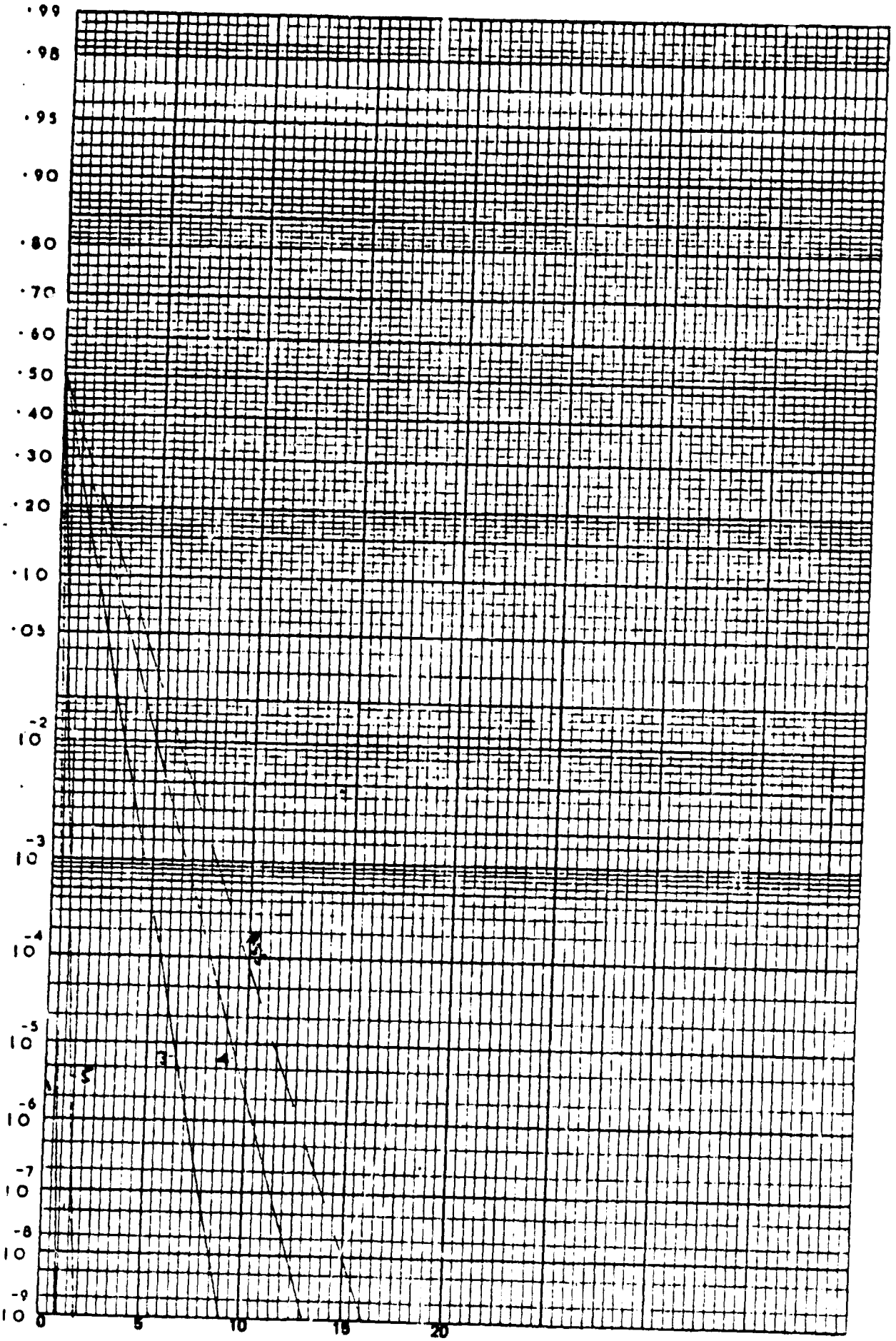

Figure C-32. ΔY_{WINDOW} (ft) Deterministic Variations, Nominal

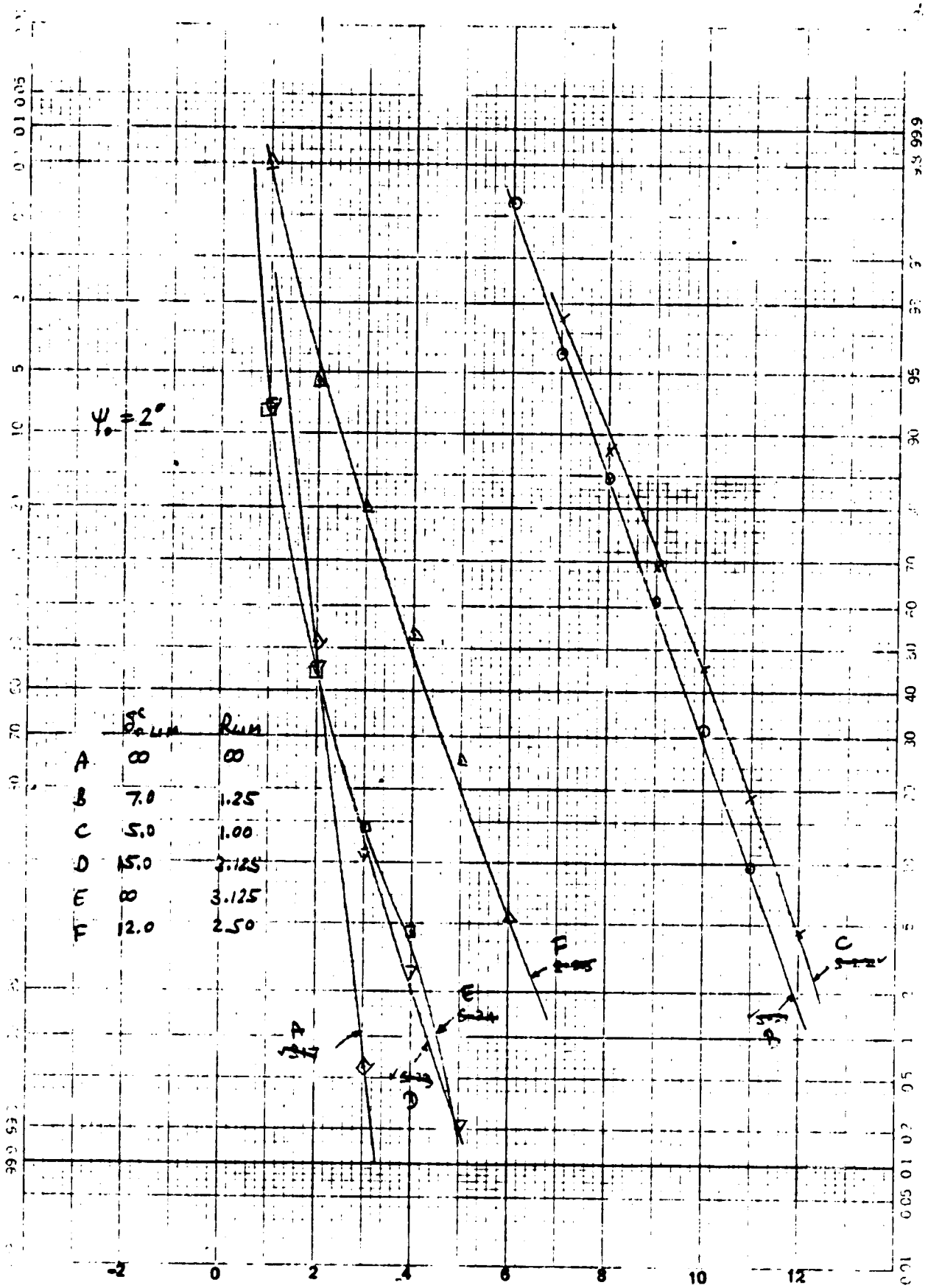

Figure C-33. Effect of Rudder and ALIGN Limits, ψ_{TD} (deg)

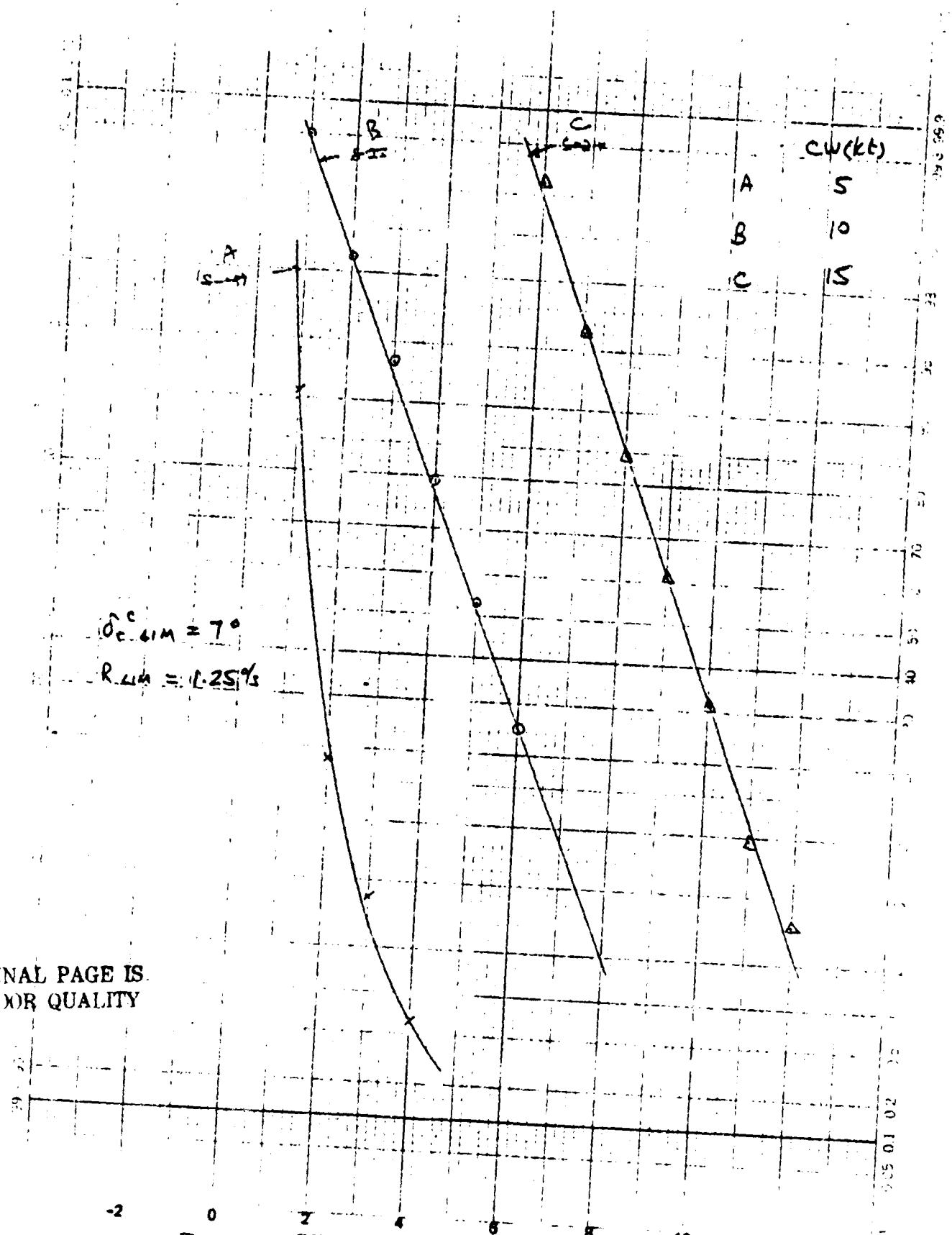

ORIGINAL PAGE IS
OF POOR QUALITY

Figure C-34. Effect of Varying Cross Wind, Ψ_{TD} (deg)

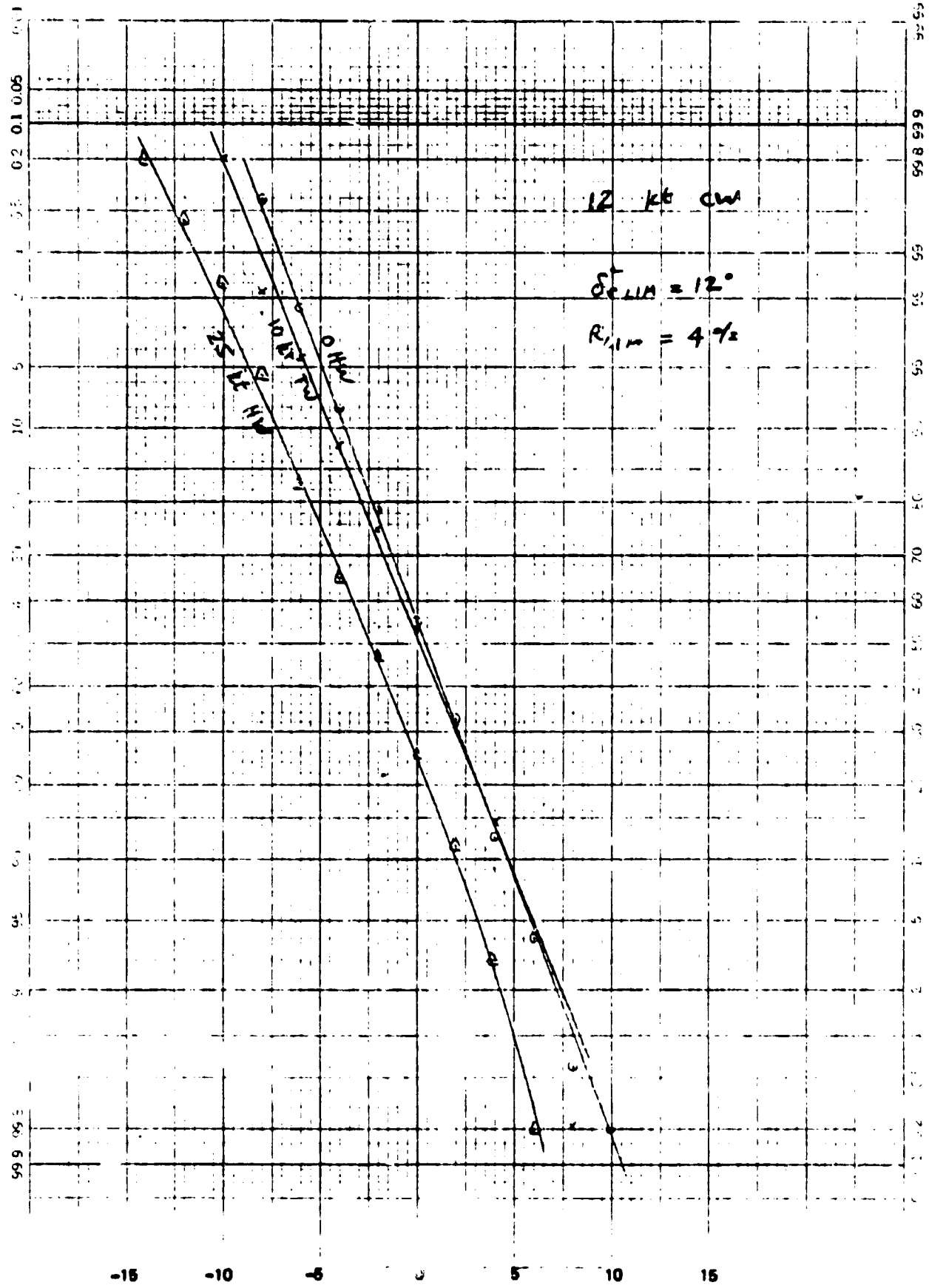

Figure C-35. Nominal Configuration Headwind Variations, Y_{TD} (ft)

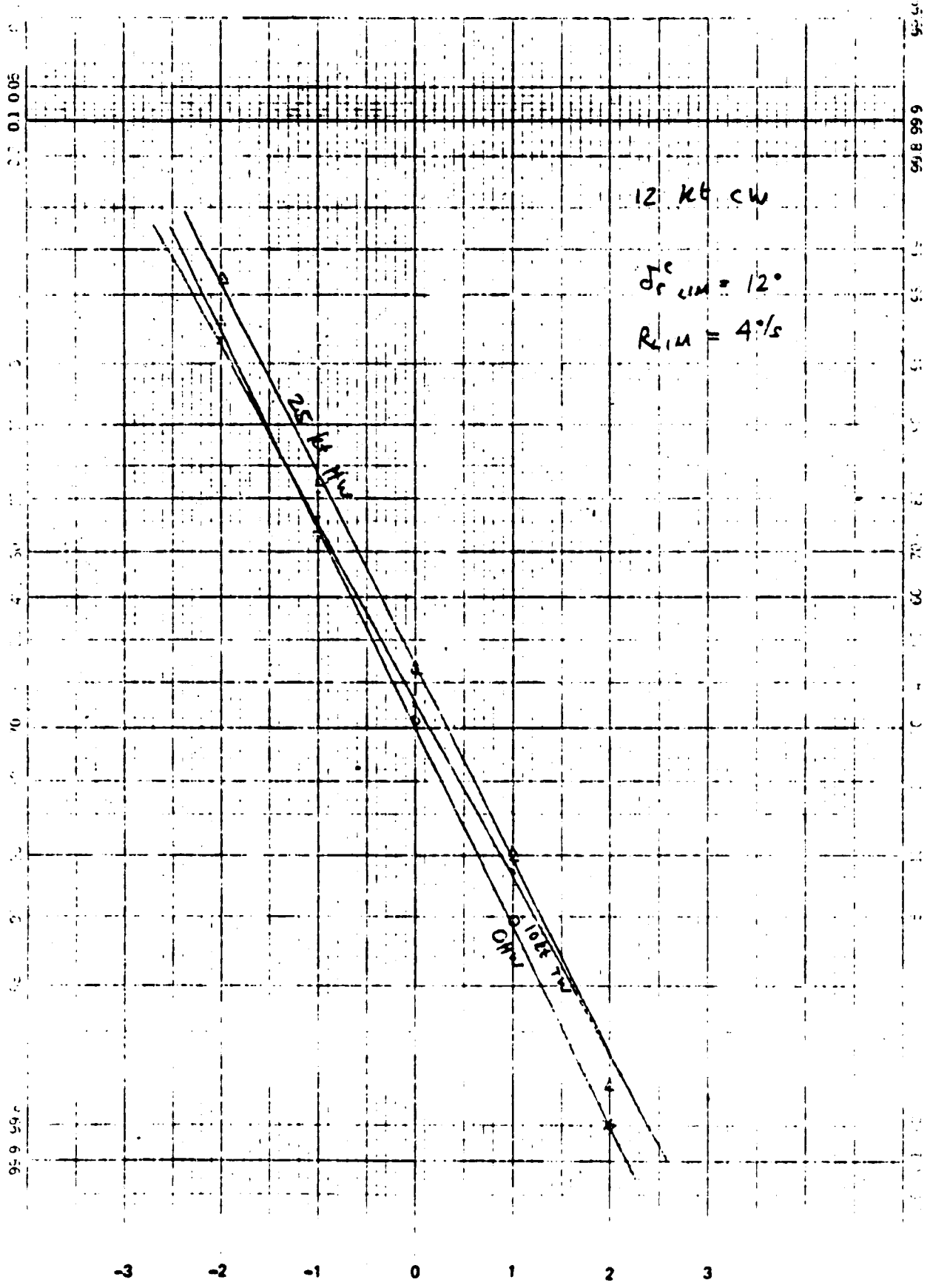

Figure C-36. Nominal Configuration Headwind Variations, $\dot{Y}_{TD}$ (fps)

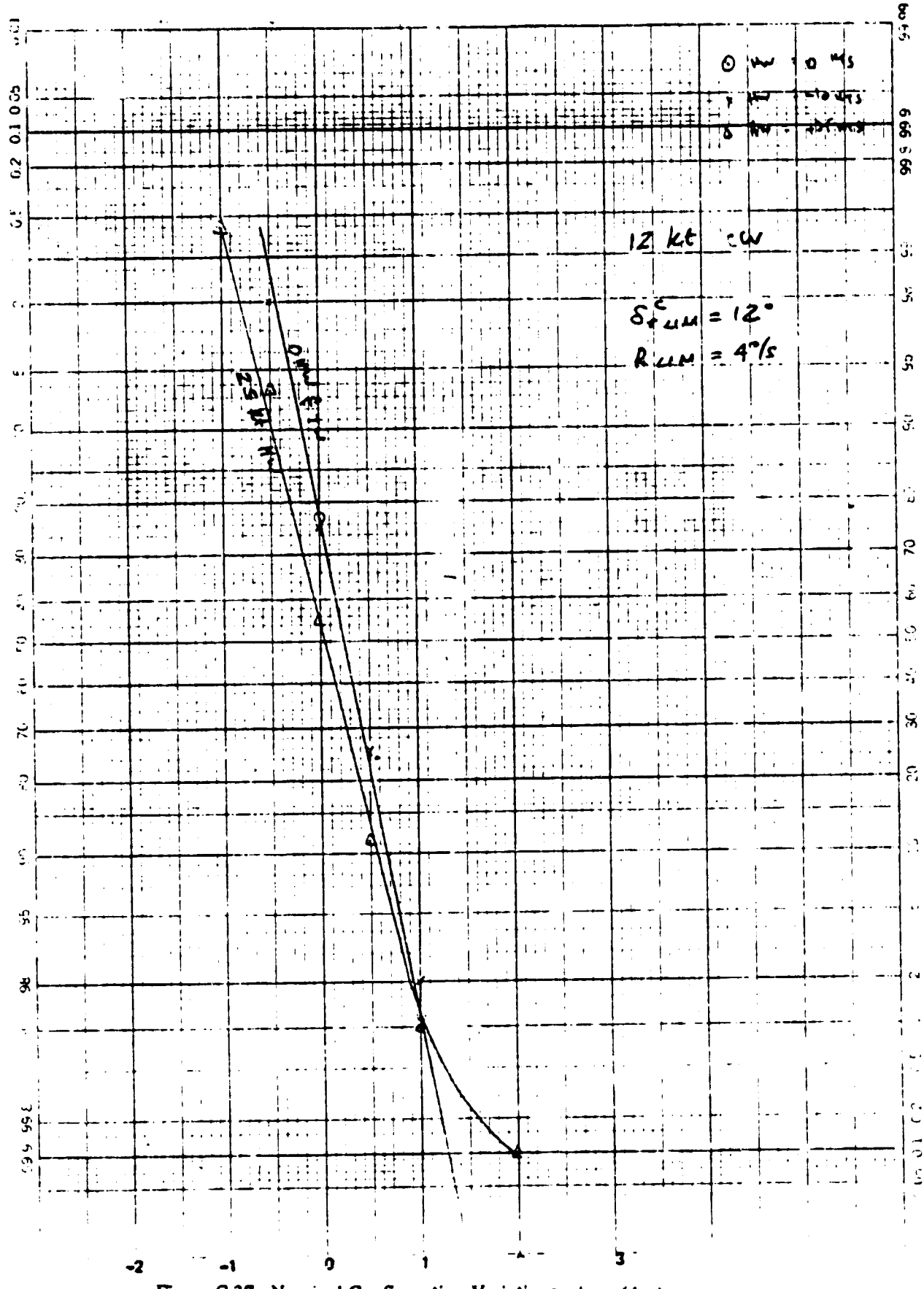

Figure C-37. Nominal Configuration Variations, ψ_{TD} (deg)

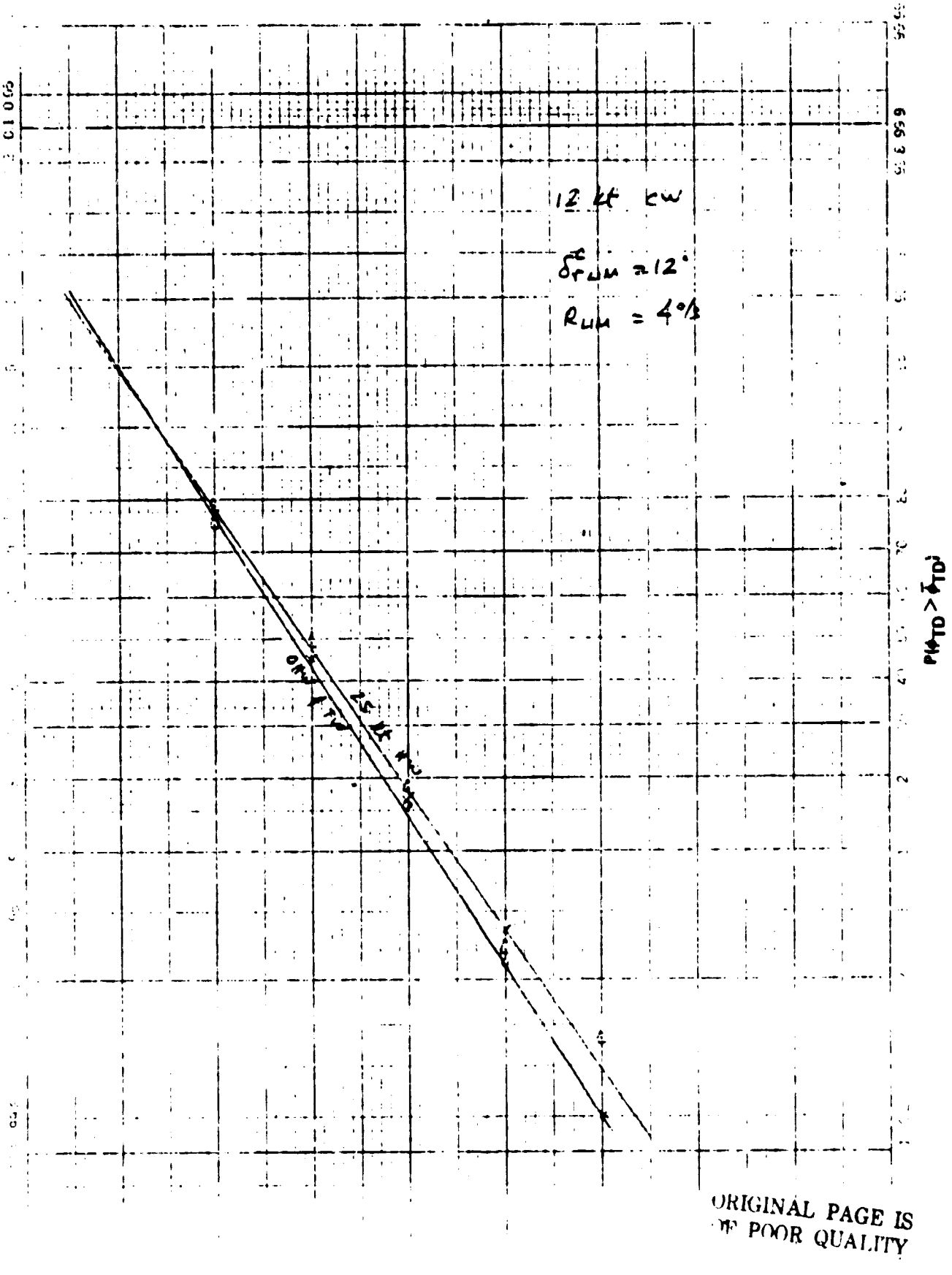

Figure C-38. Nominal Configuration Headwind Variations, ϕ_{TD} (deg)

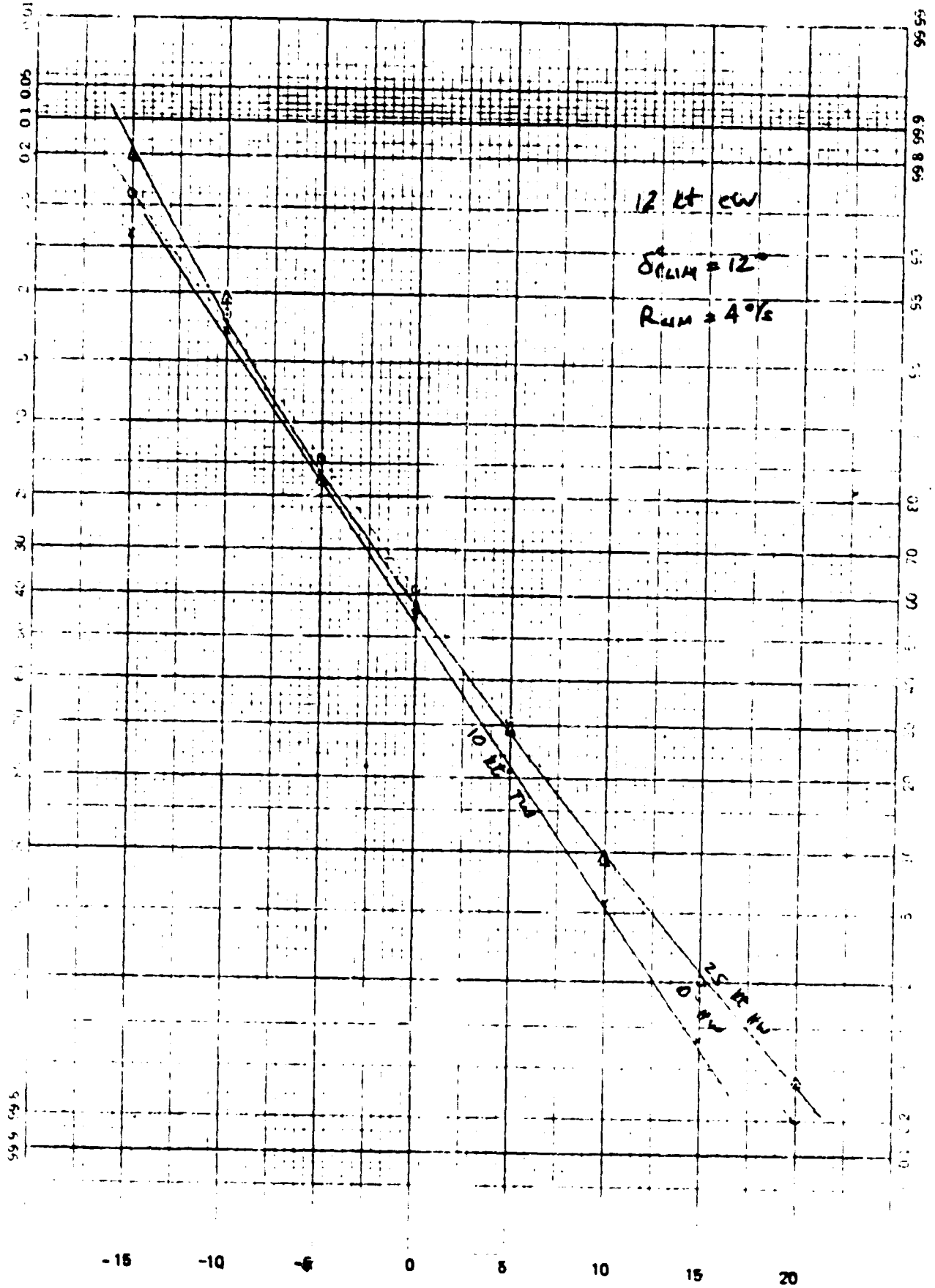

Figure C-39. Nominal Configuration, Headwind Variations

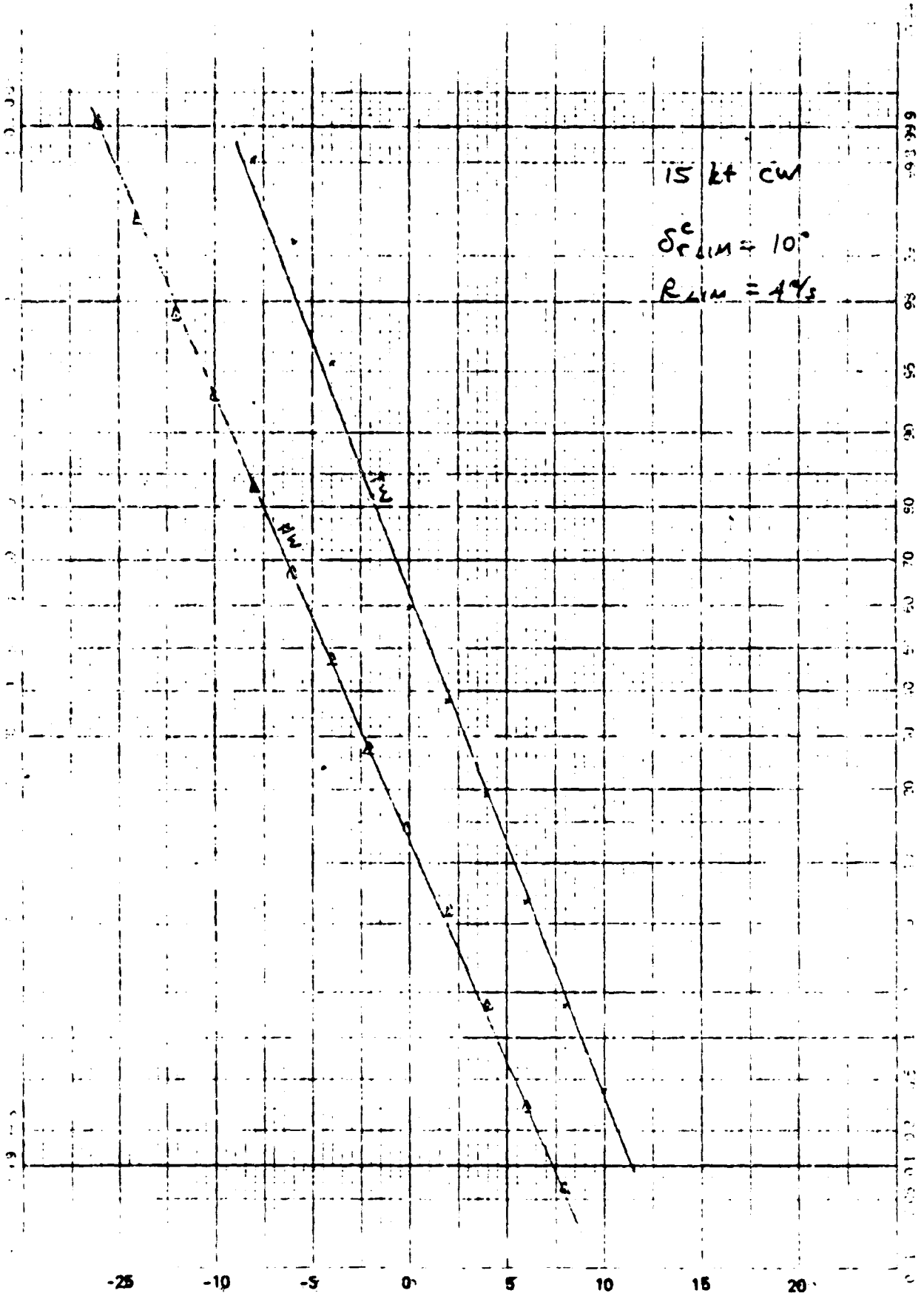

Figure C-40. Nominal Configuration Headwind Variation Y_{TD}

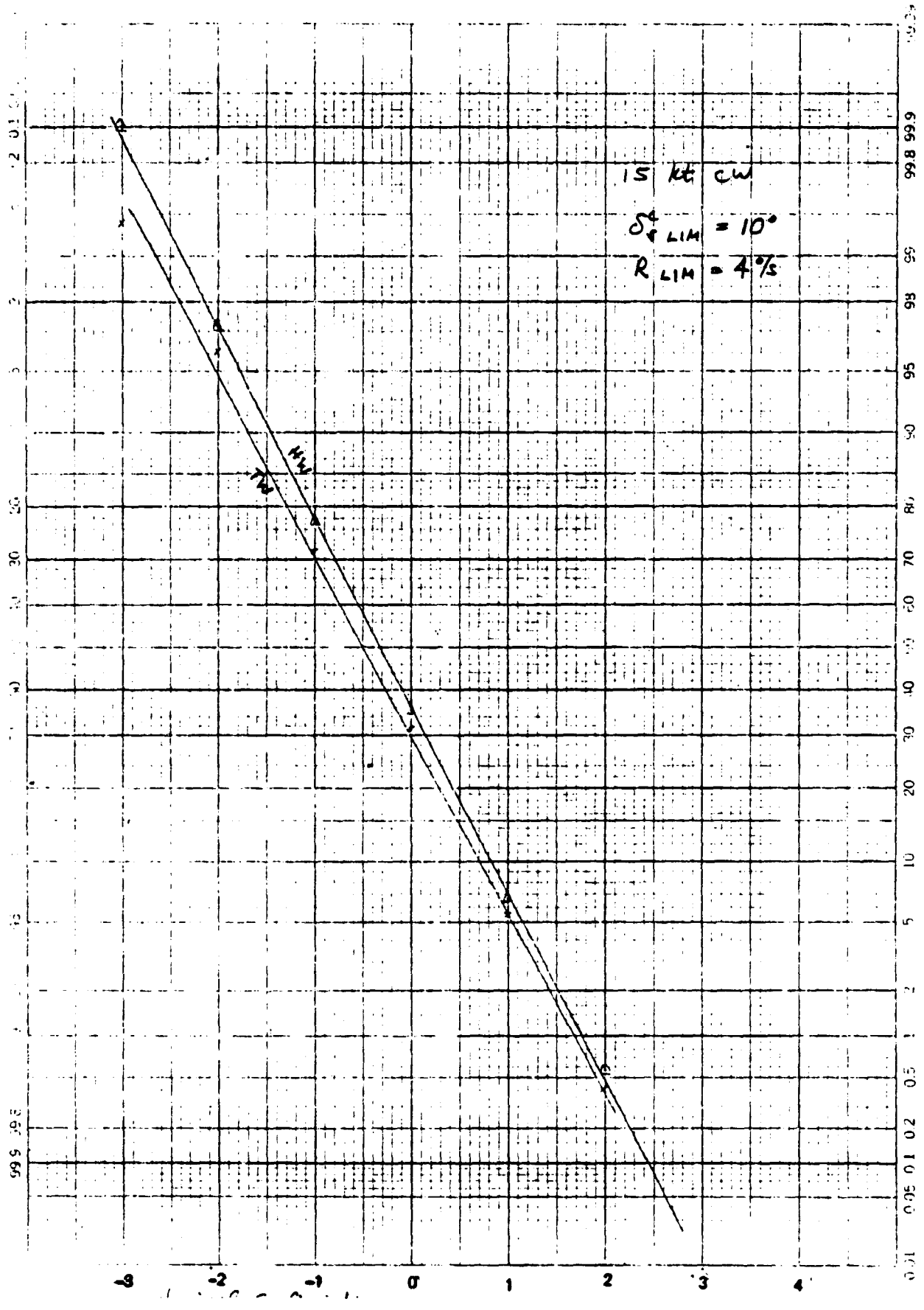

Figure C-41. Nominal Configuration Headwind Variation $\dot{Y}_{TD}$

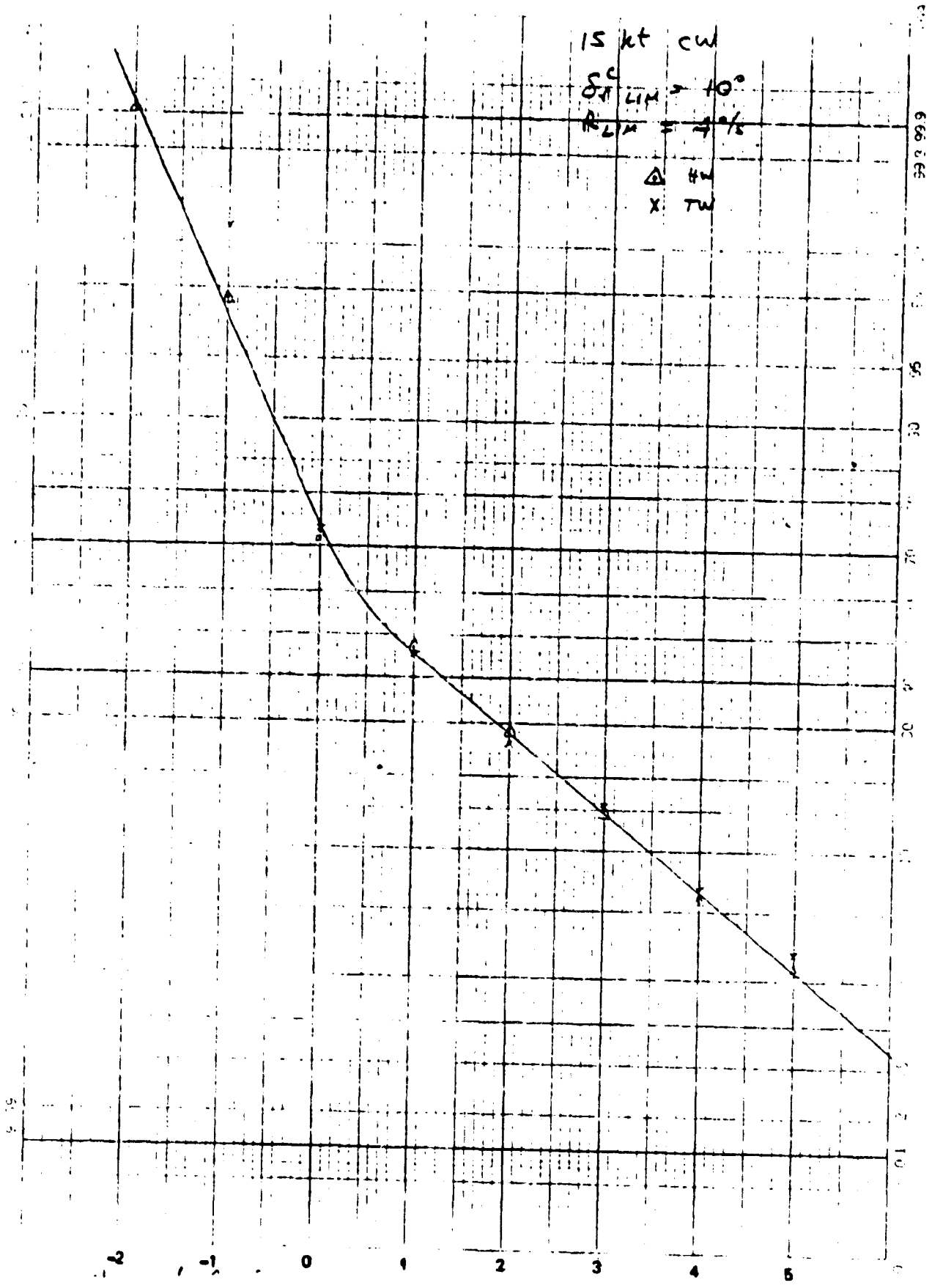

Figure C-42. Nominal Configuration Headwind Variation

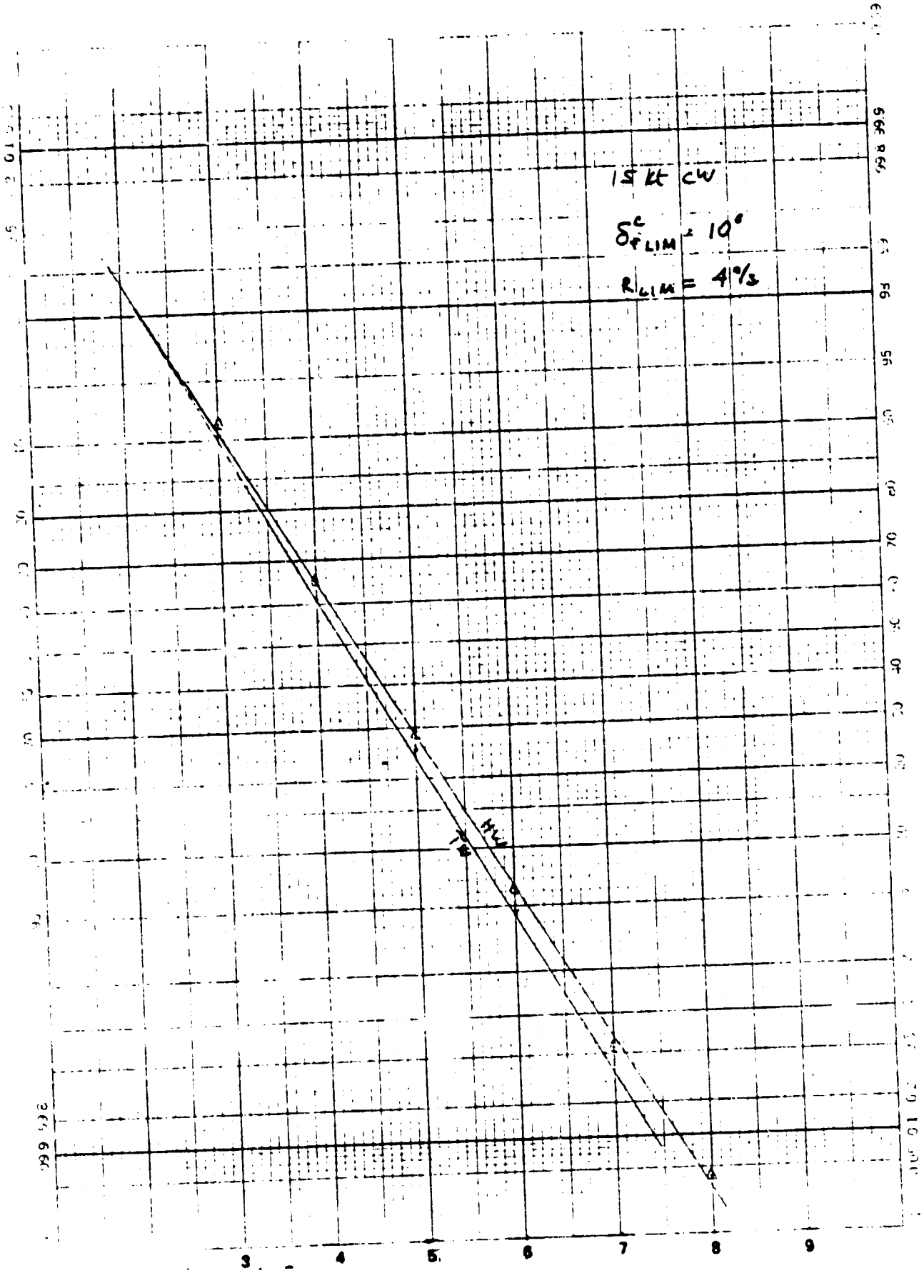

Figure C-43. Nominal Configuration Headwind Variation

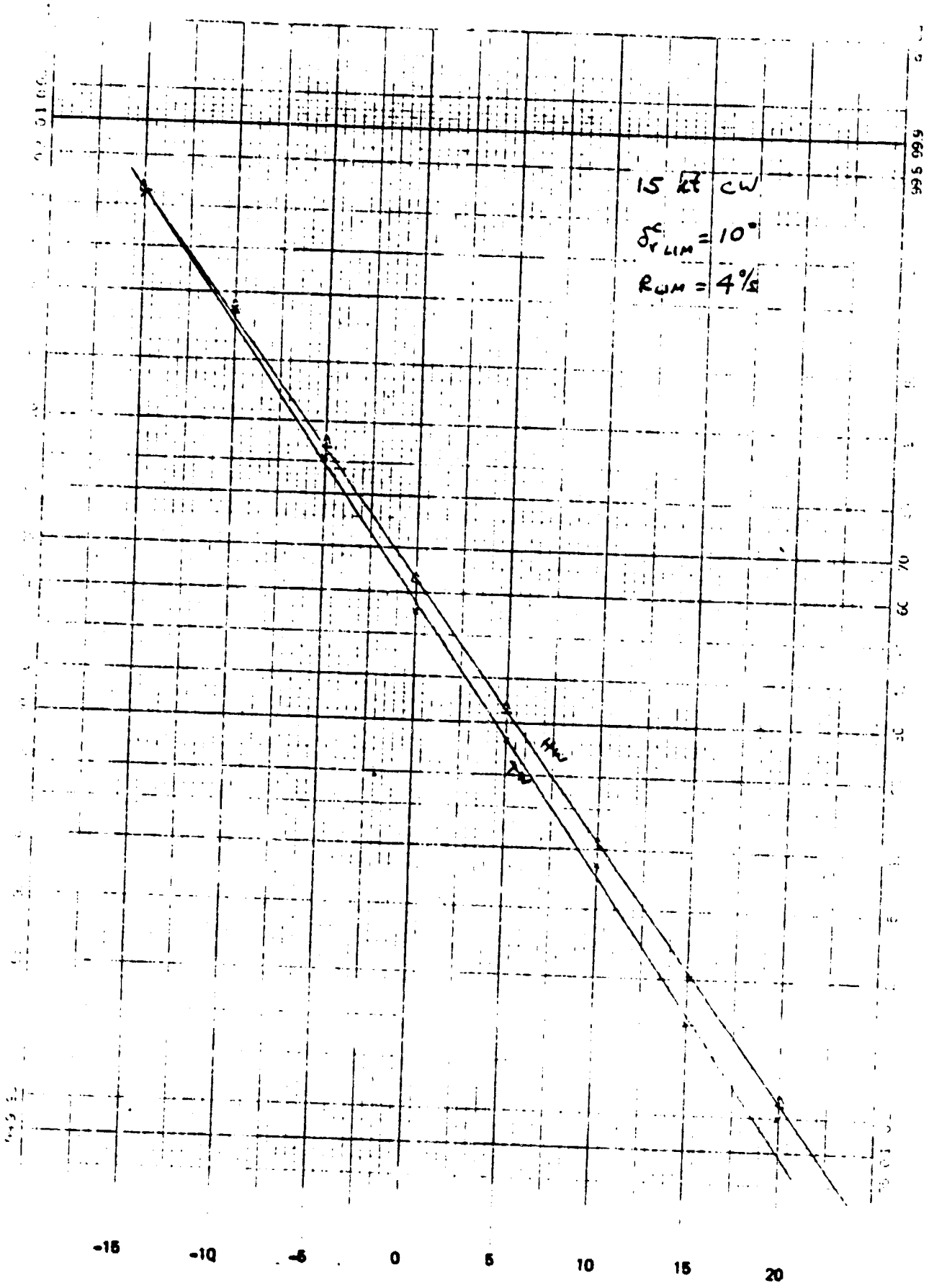

Figure C-44. Nominal Configuration Headwind Variation Y_{100}

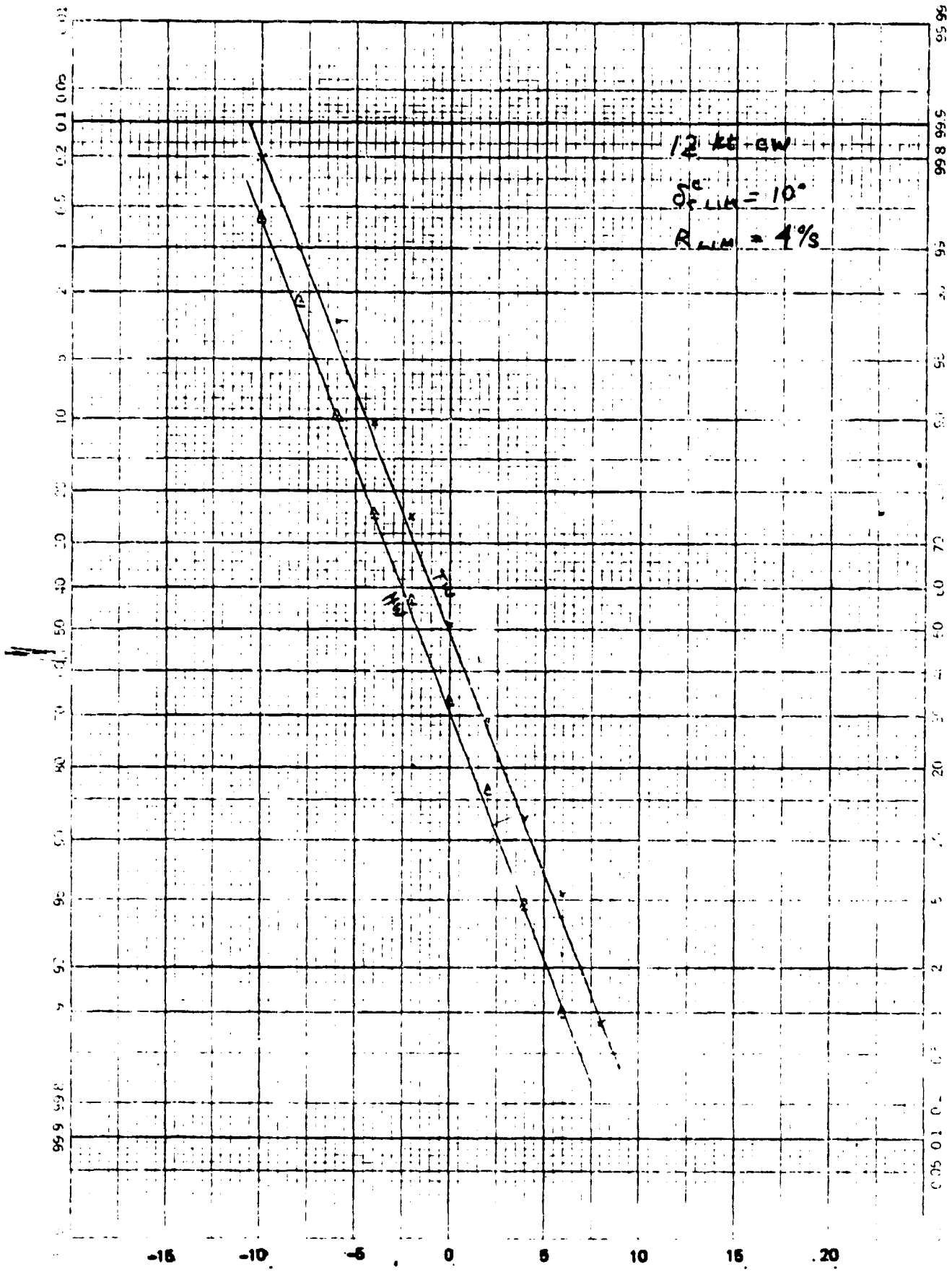

Figure C-45. Nominal Configuration Headwind Variation Y_{TD}

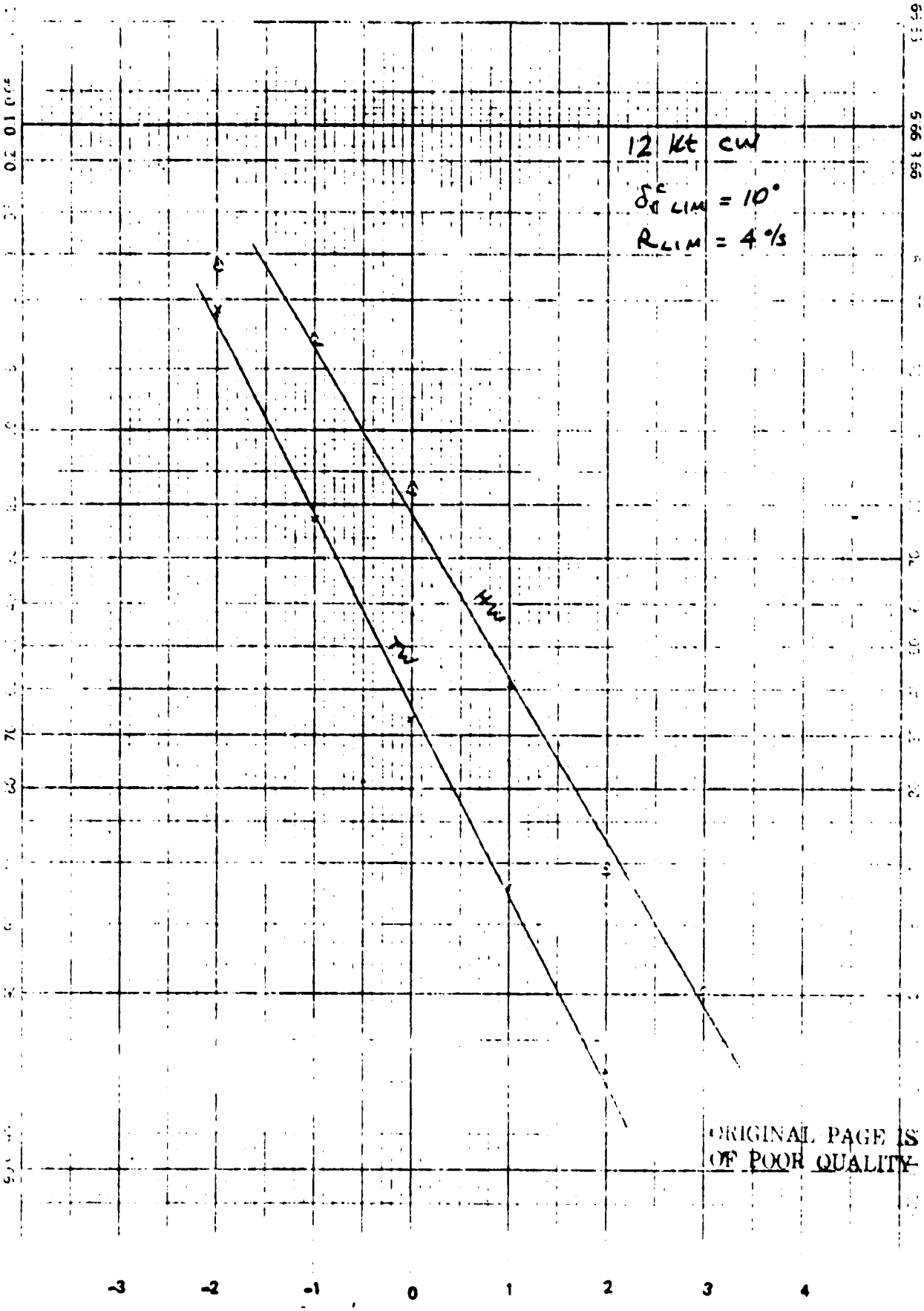

Figure C-46. Nominal Configuration Headwind Variation

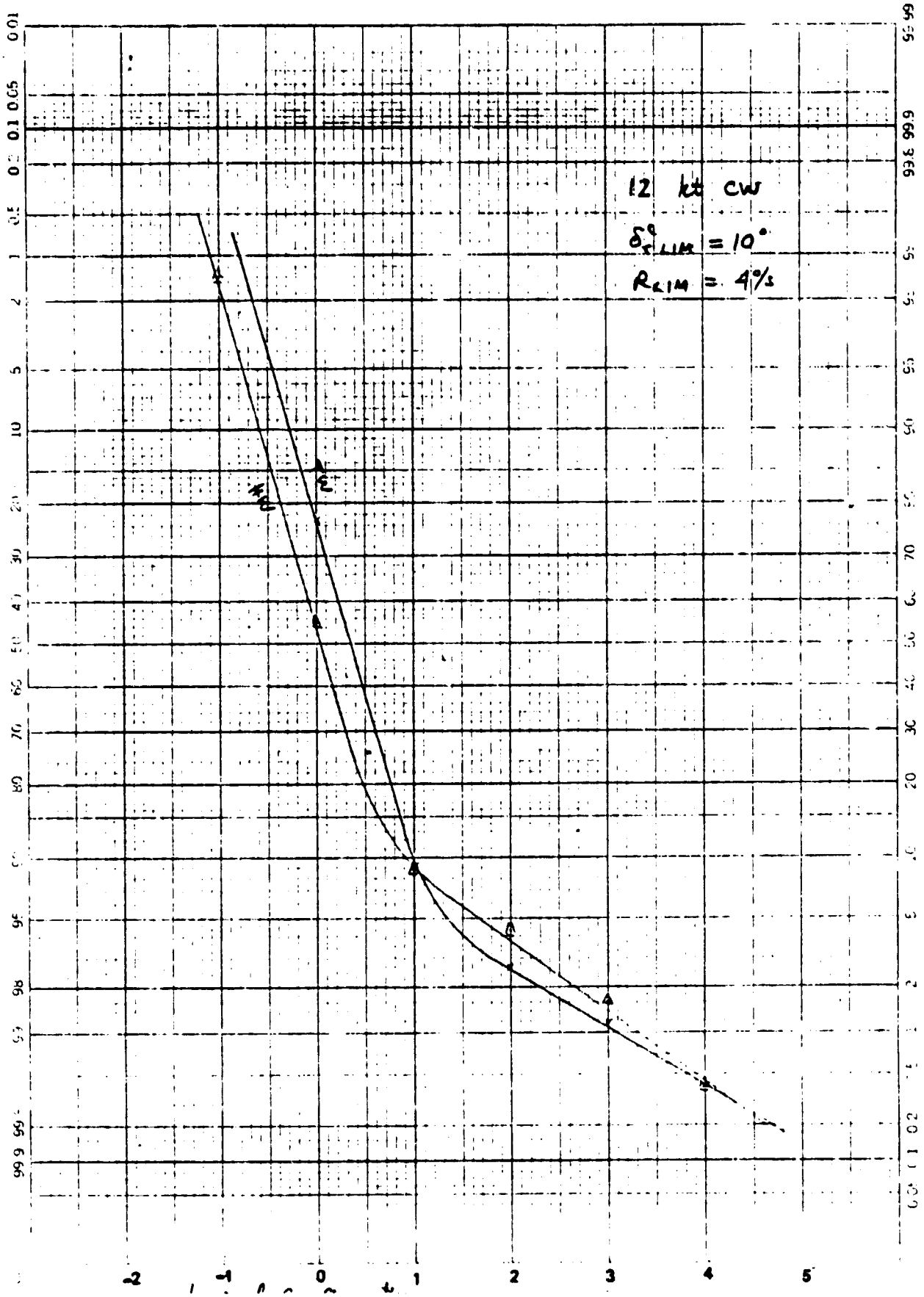

Figure C-47. Nominal Configuration Headwind Variation Ψ_{TD}

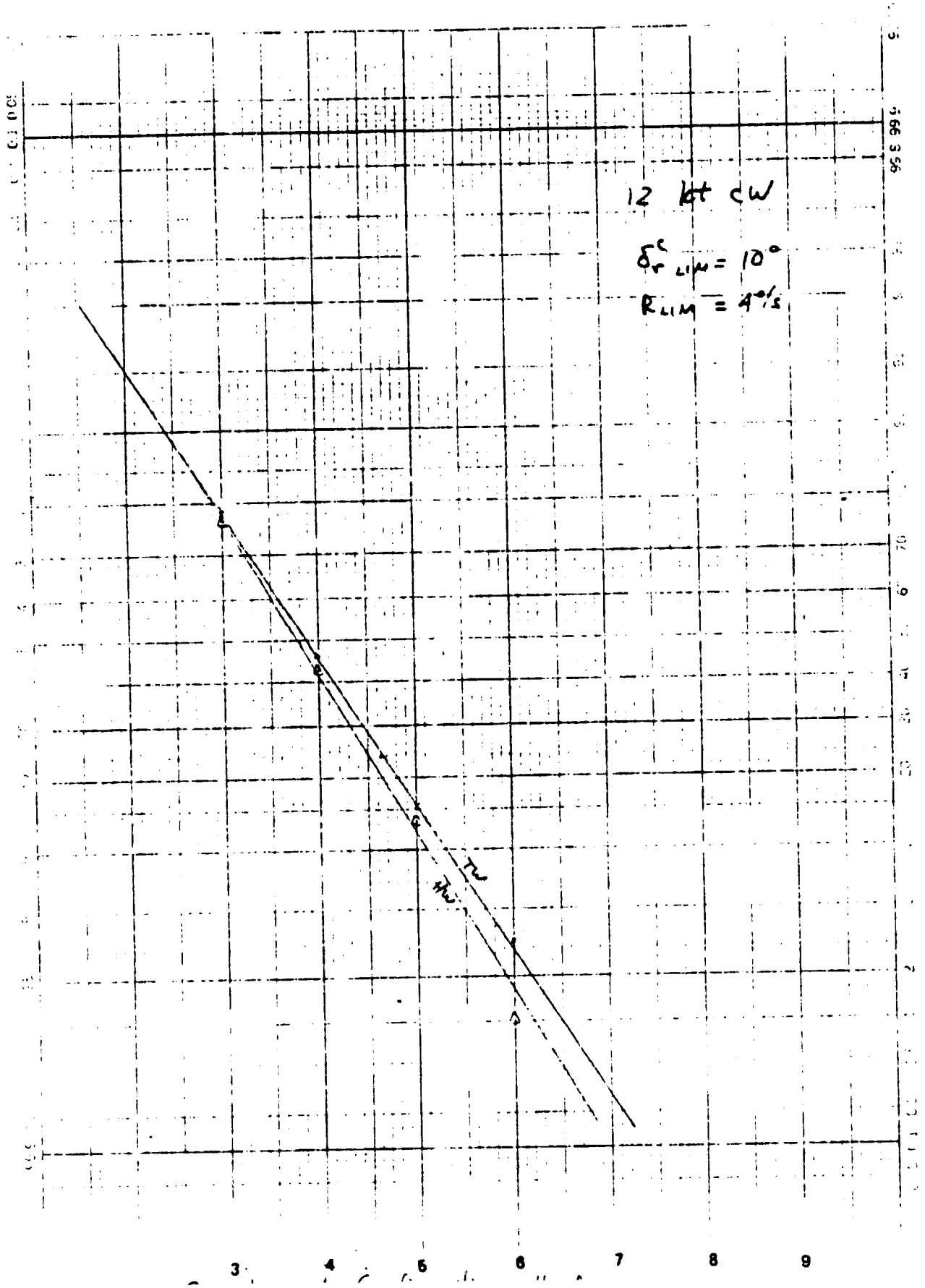

Figure C-48. Nominal Configuration Headwind Variation ♦TD

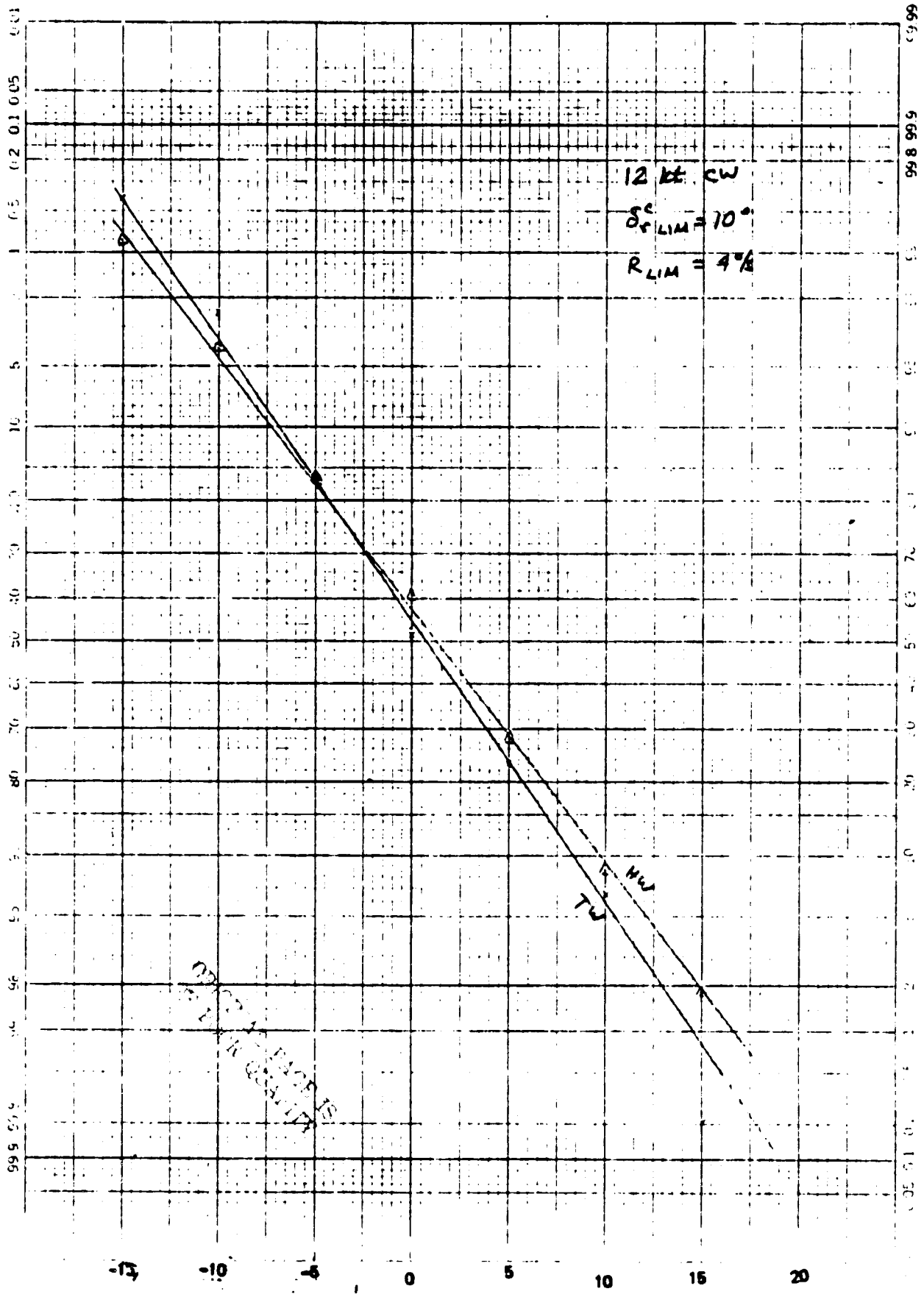

Figure C-49. Nominal Configuration Headwind Variation Y_{100}

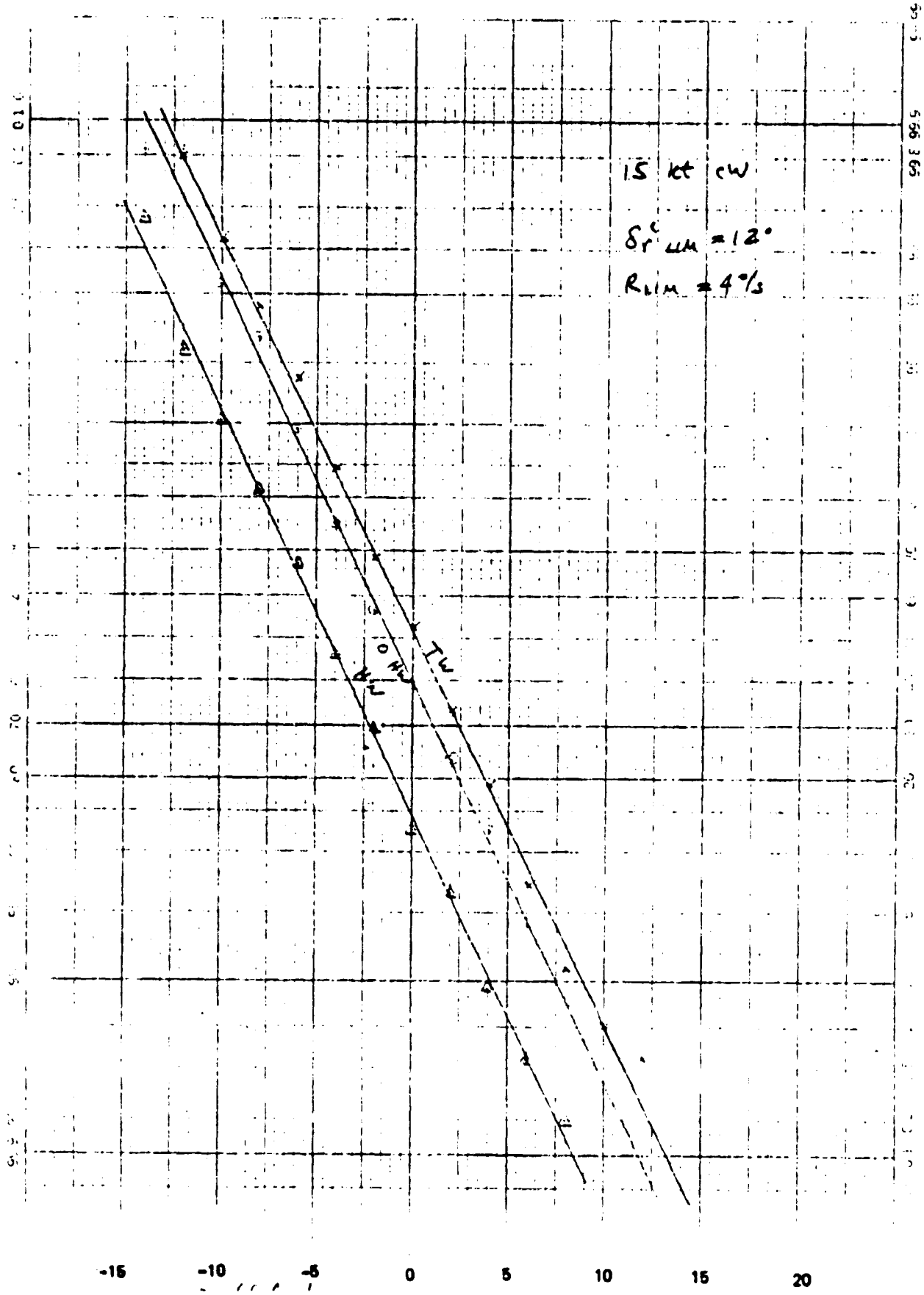

Figure C-50. Doubled Ky, Headwind Variation Y_{TD}

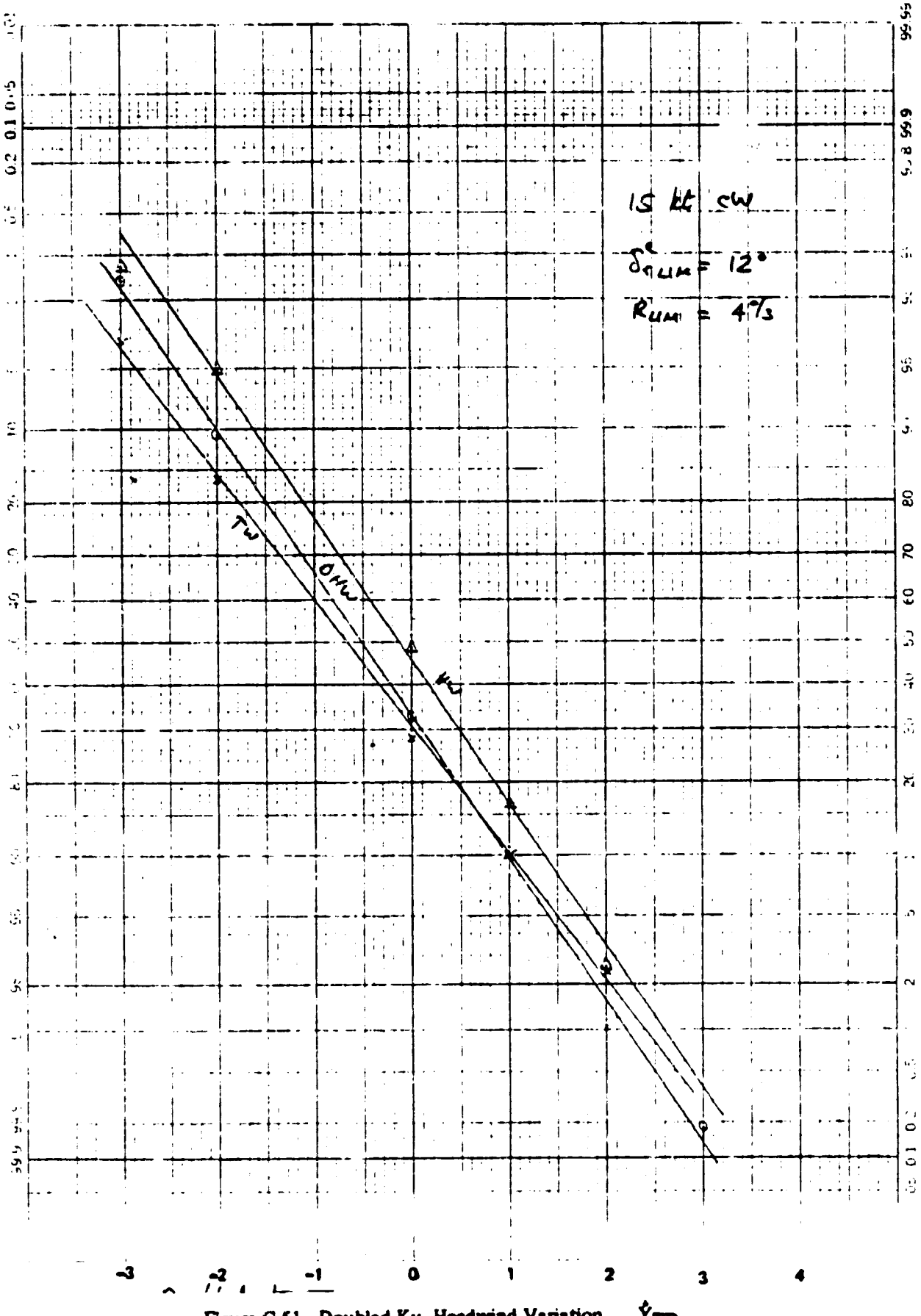

Figure C-51. Doubled Ky, Headwind Variation Y_{TD}

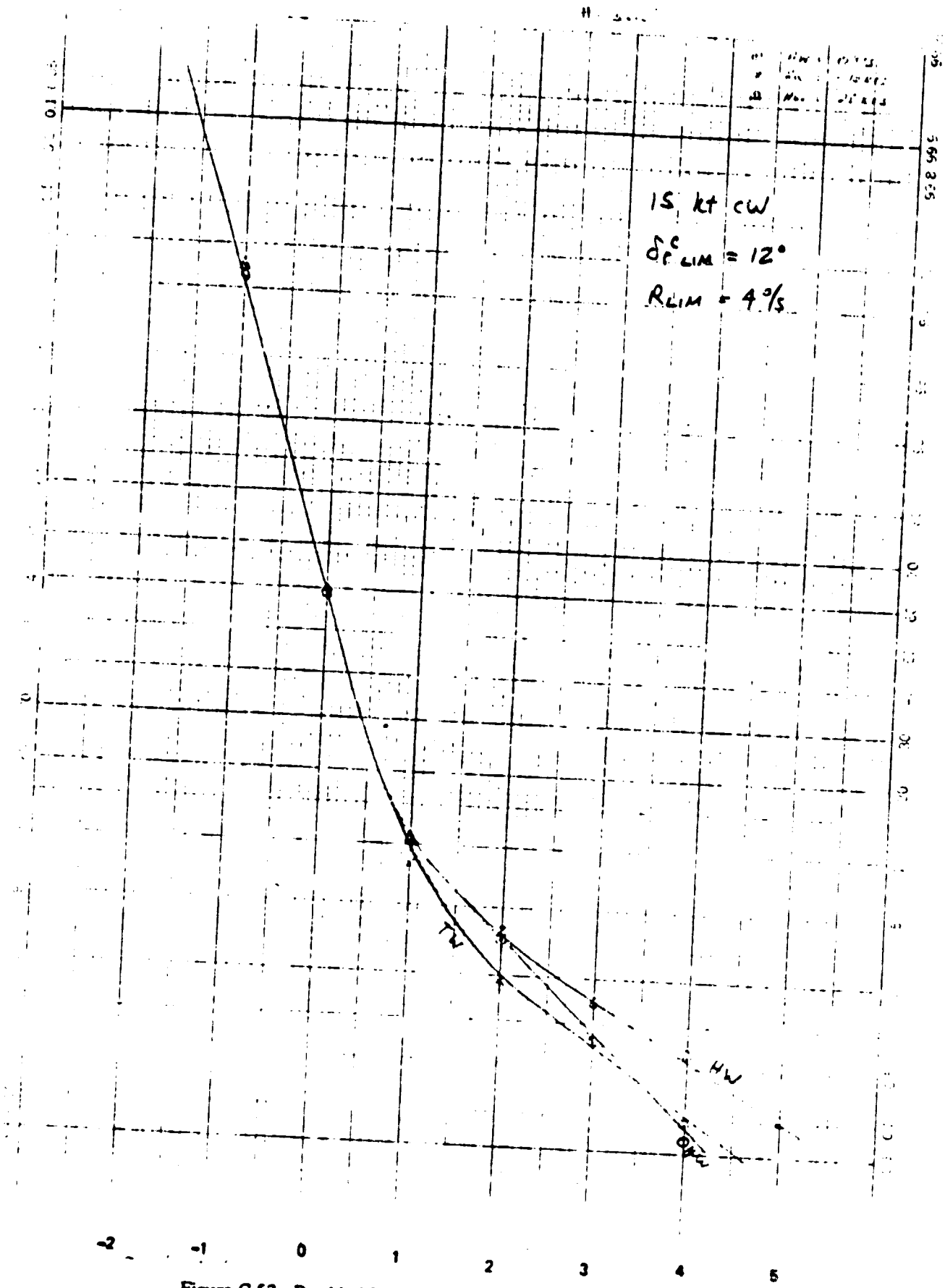

Figure C-52. Doubled Ky, Headwind Variation

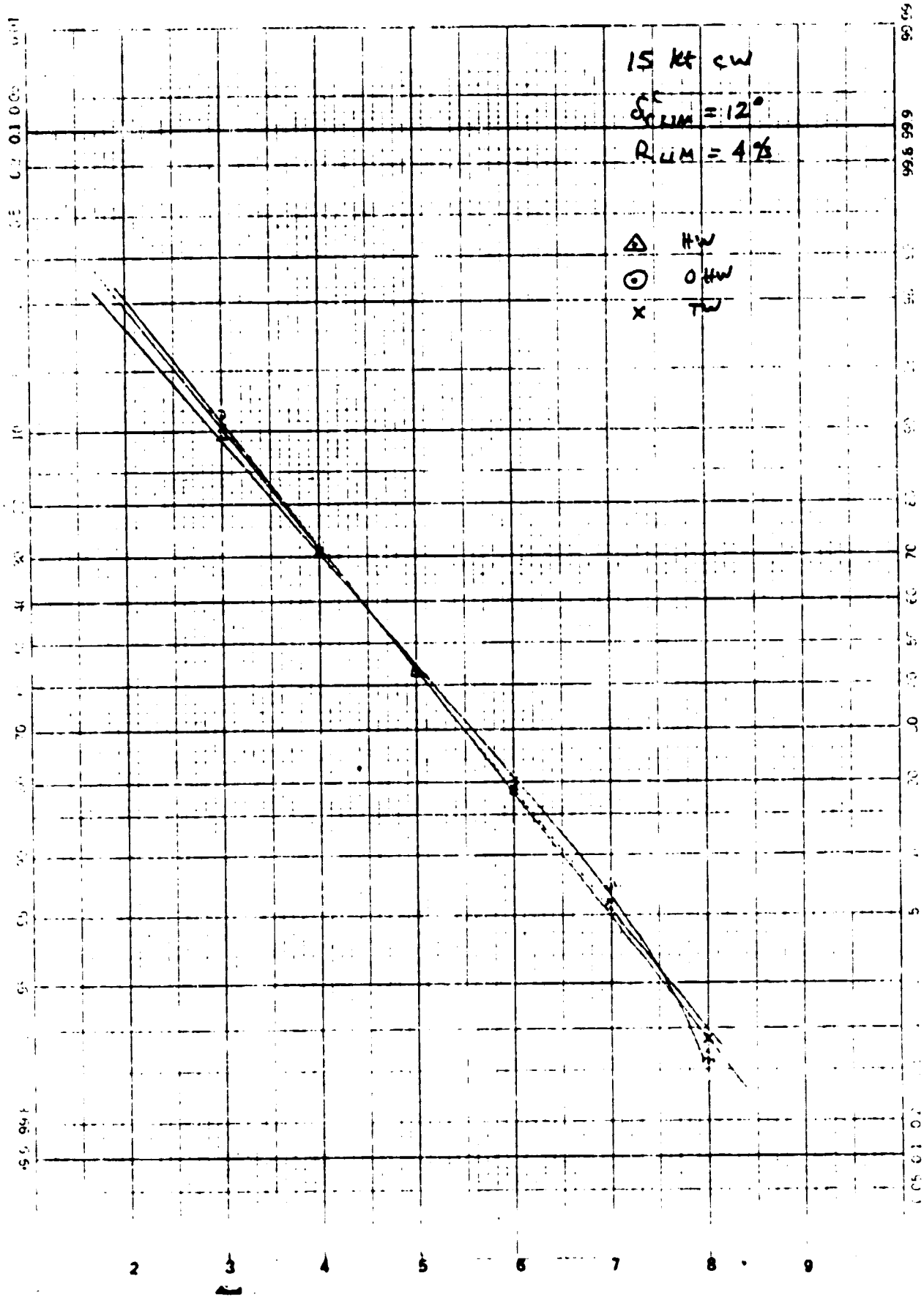

Figure C-53. Doubled Ky, Headwind Variation

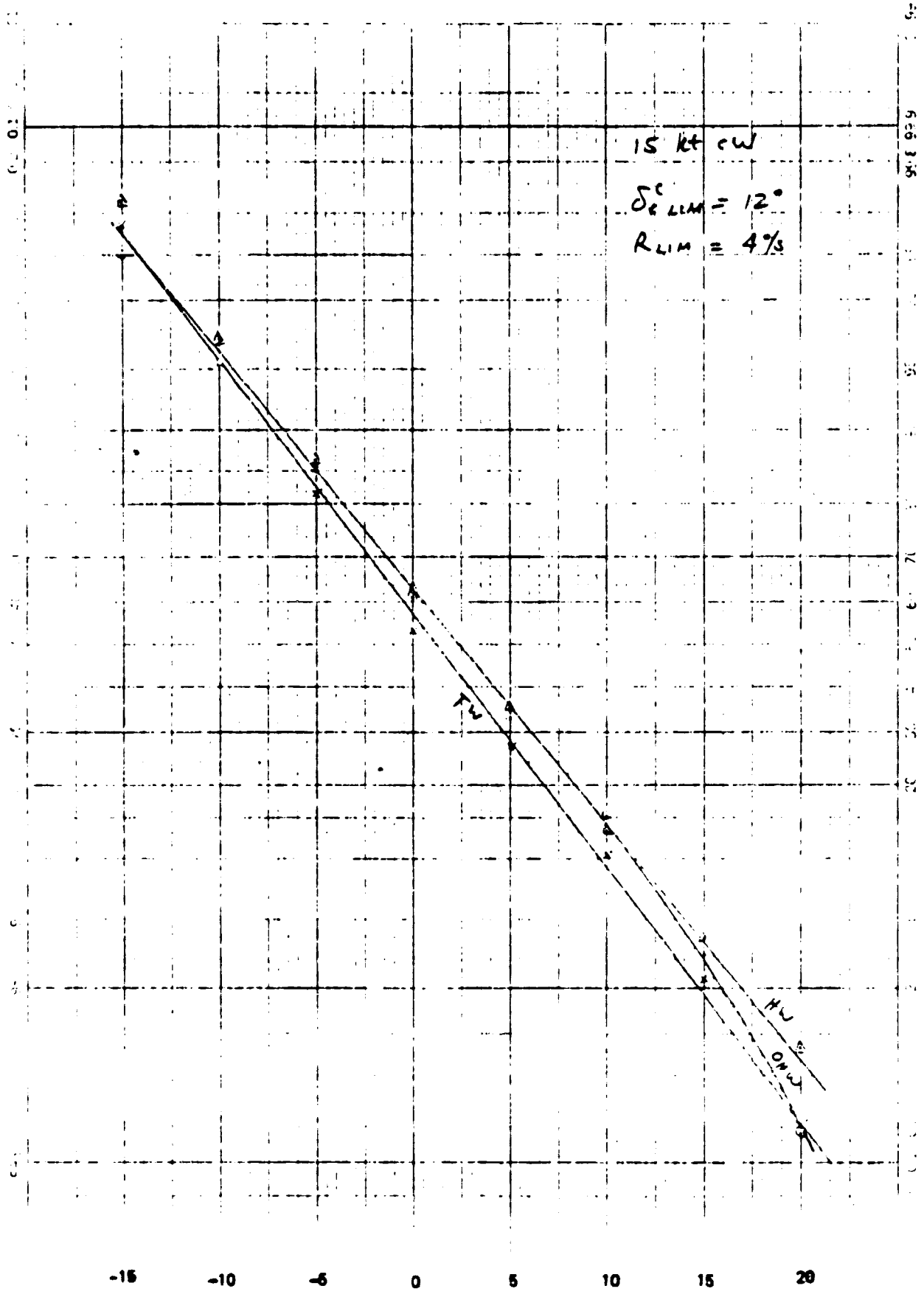

Figure C-54. Double k_y, Headwind Variation, Y_{100}

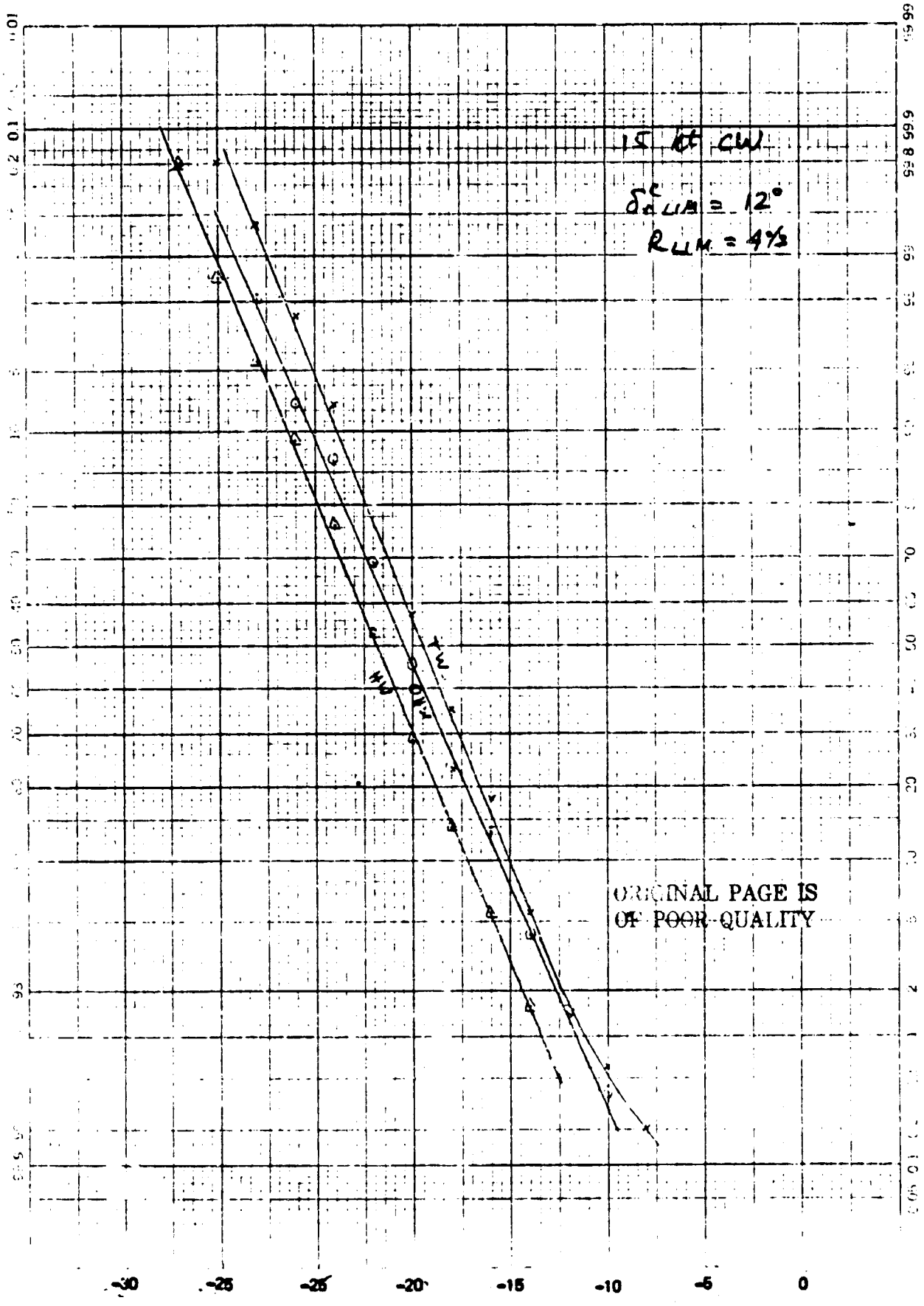

Figure C-55. No Crossfeeds, Y_{TD}

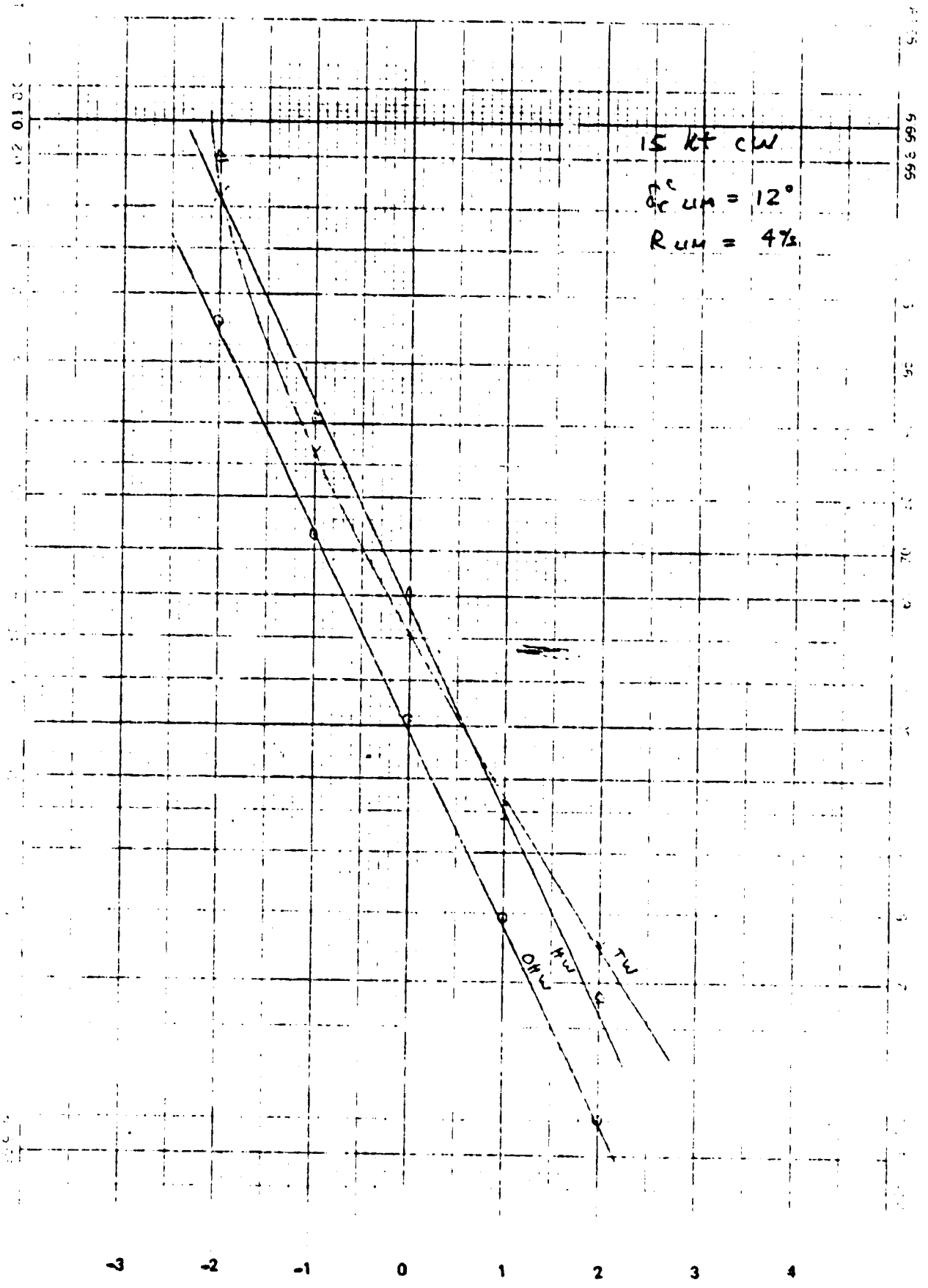

Figure C-56. No Crossfeeds, $\dot{Y}_{TD}$

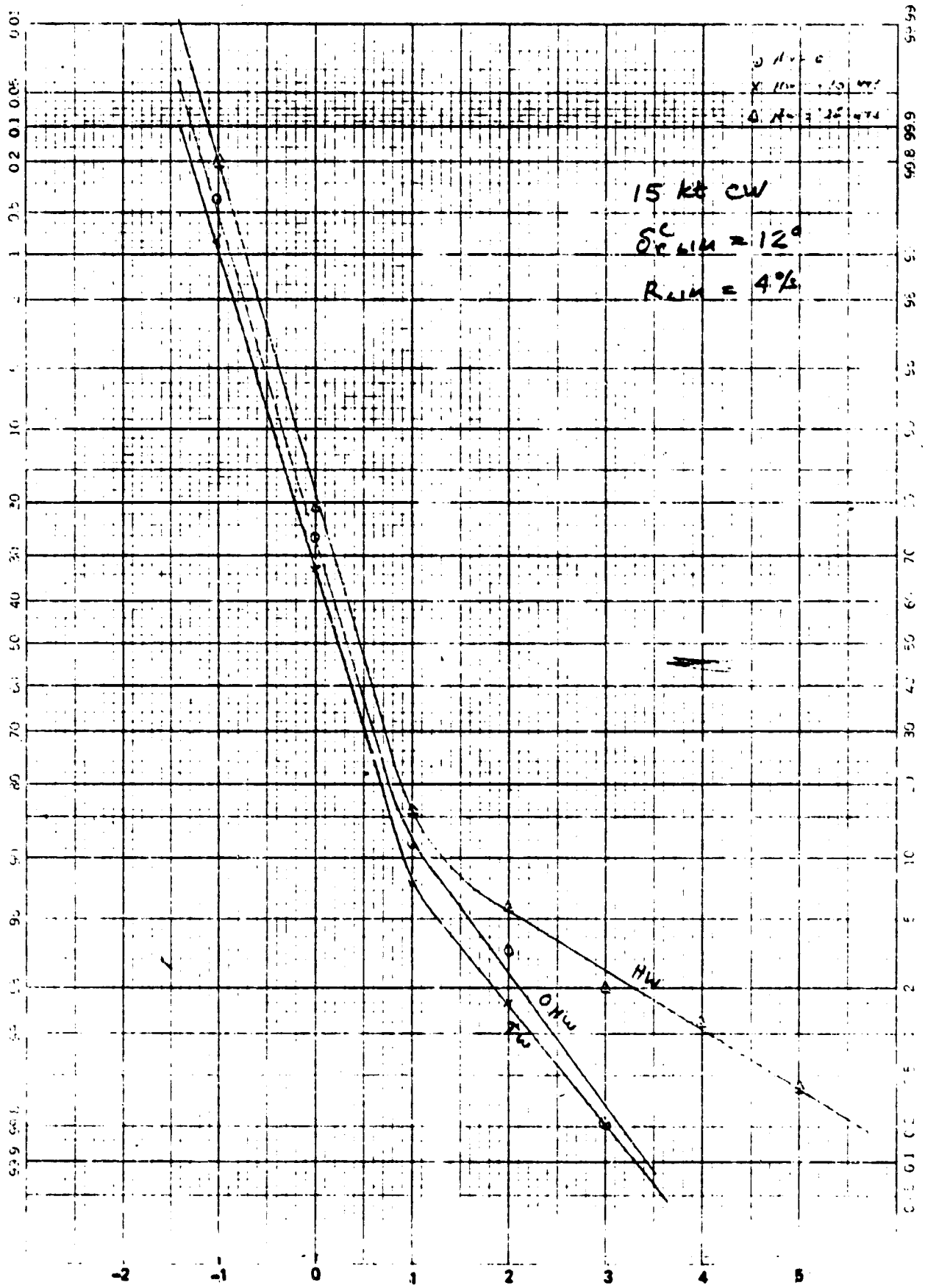

Figure C-57. No Crossfeeds, ψ_{TD}

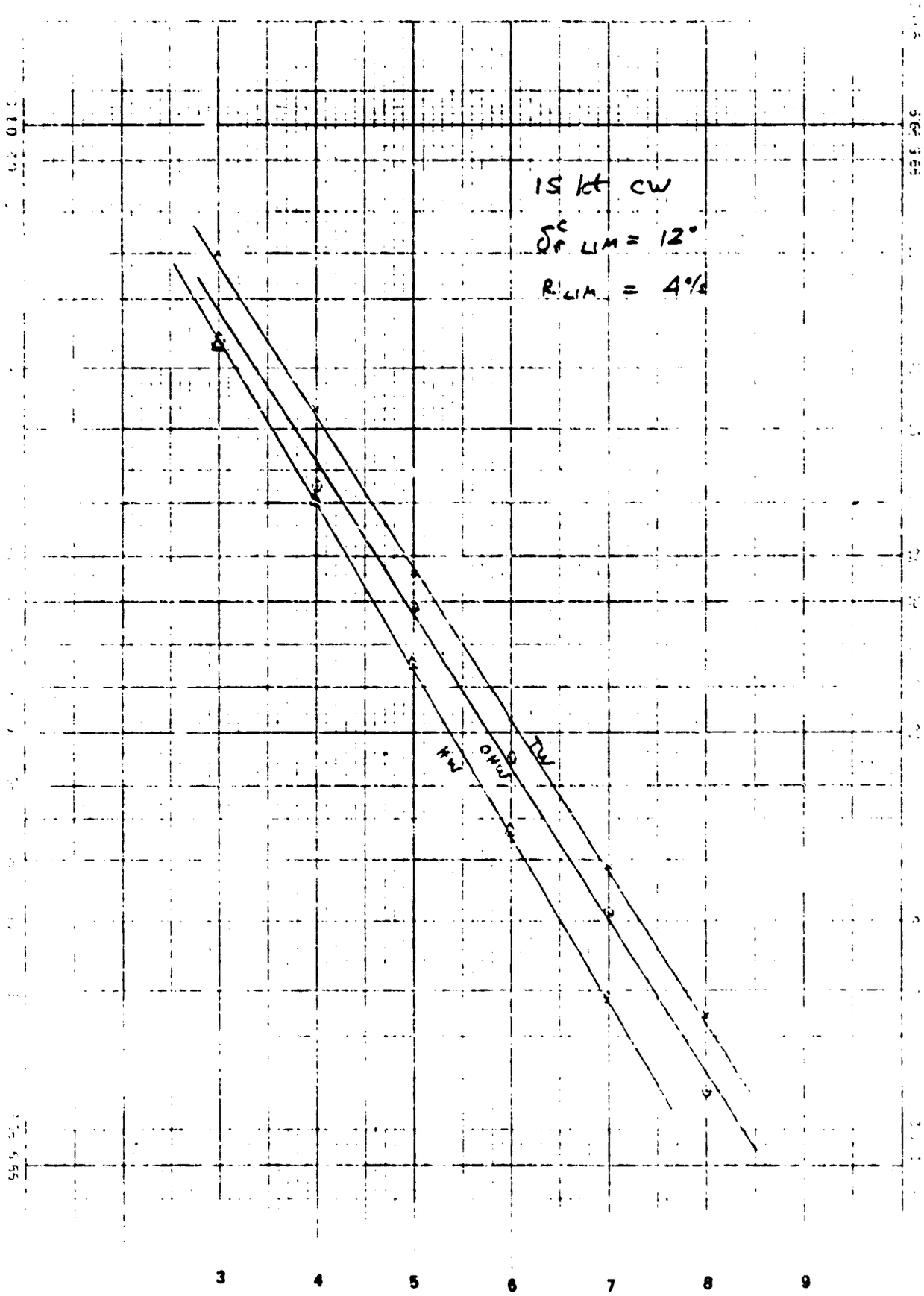

Figure C-58. No Crossfeeds, ϕ_{TD}

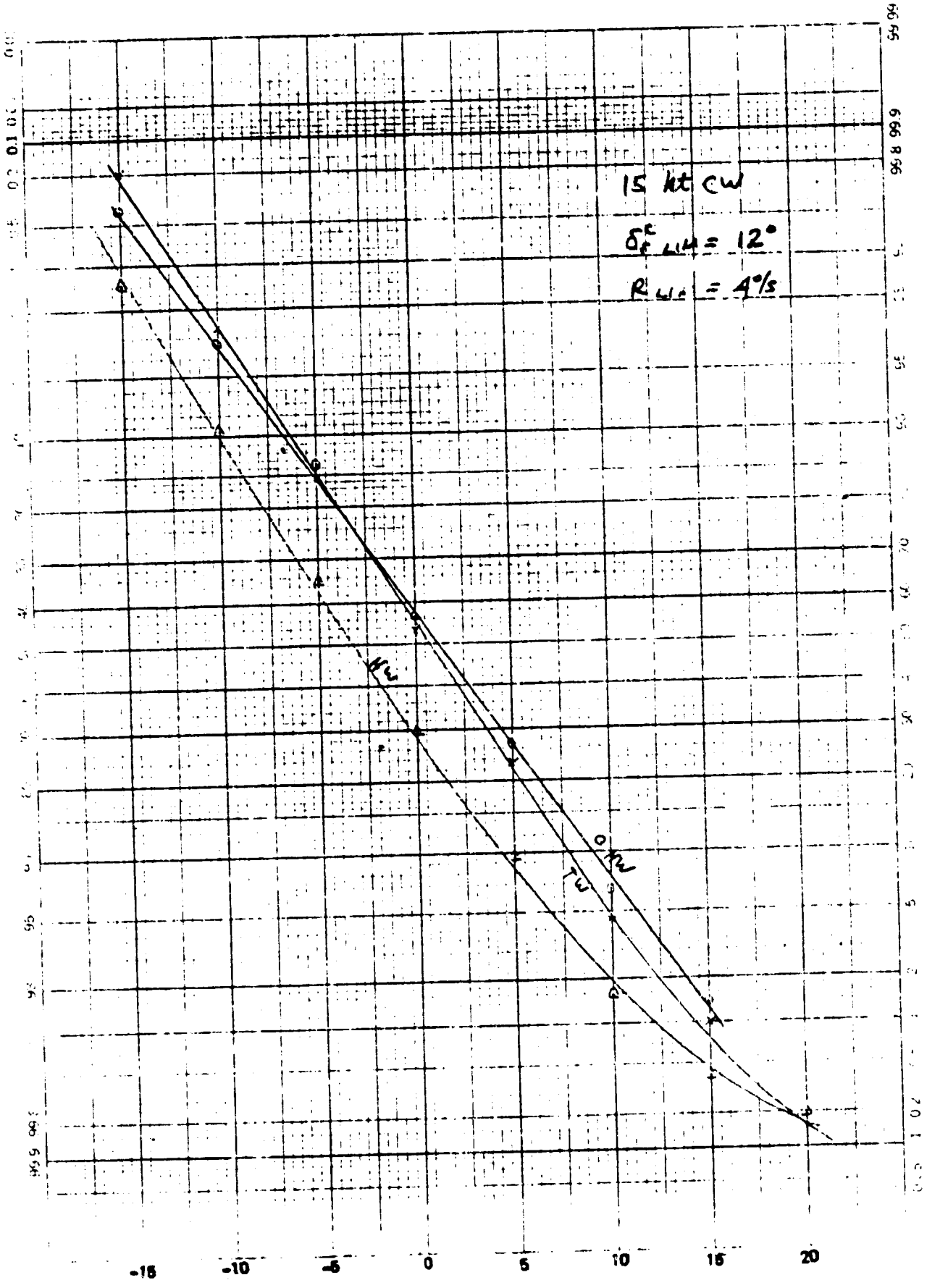

Figure C-59. No Crossfeeds, Y_{100}

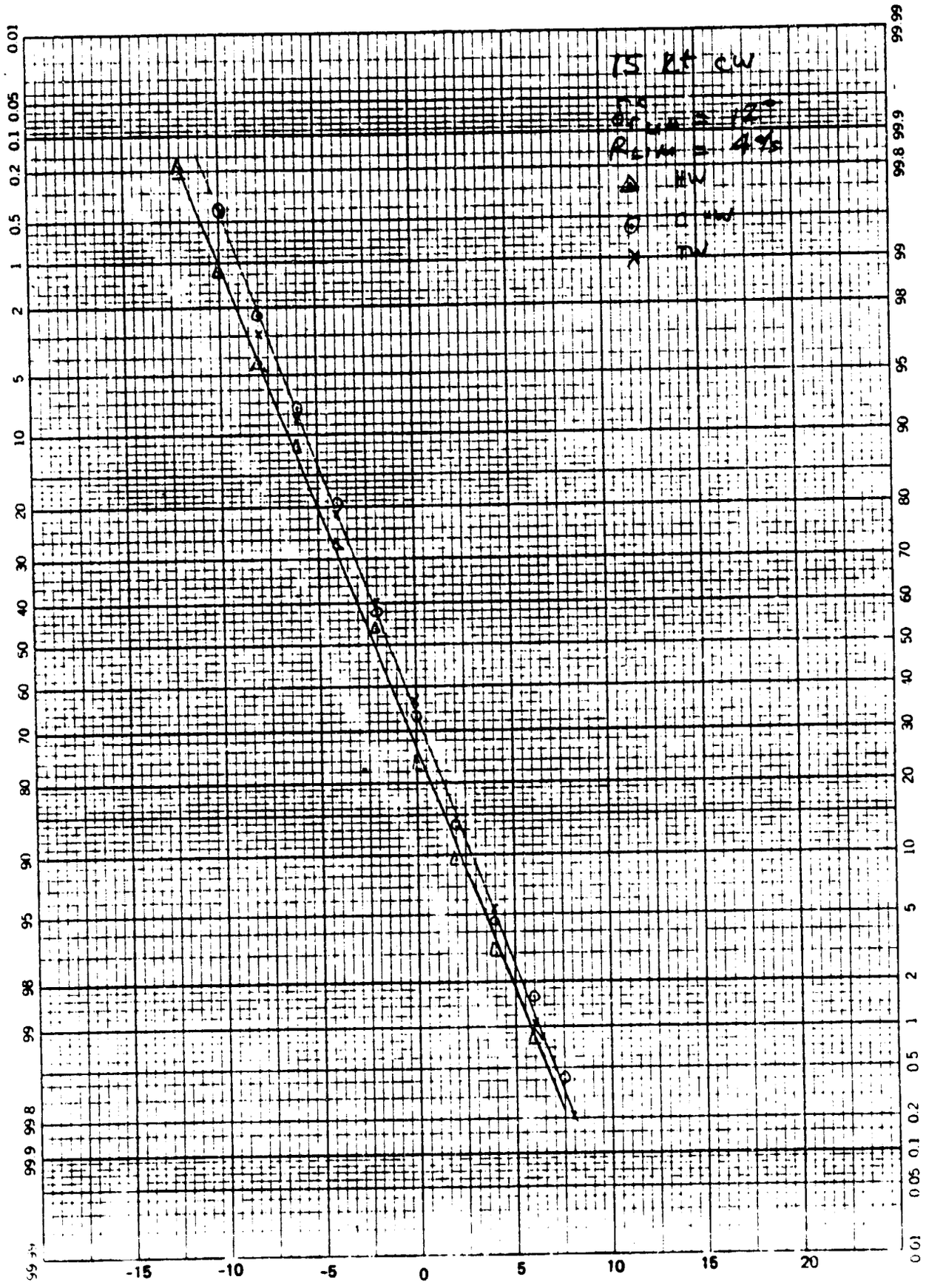

Figure C-60. Nose Located Antenna, Y_{TD}

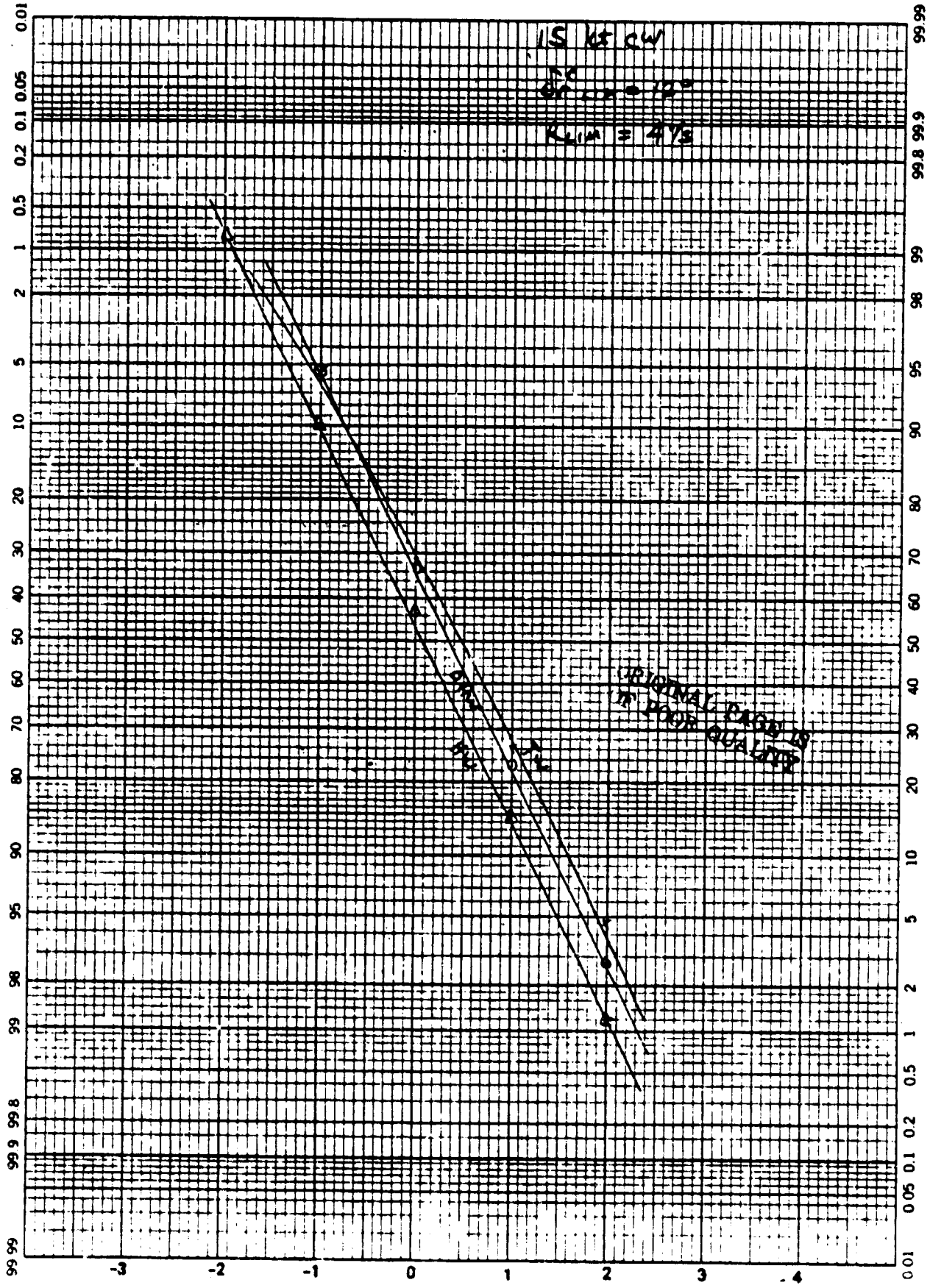

Figure C-61. Nose Located Antenna, $\dot{Y}_{TD}$

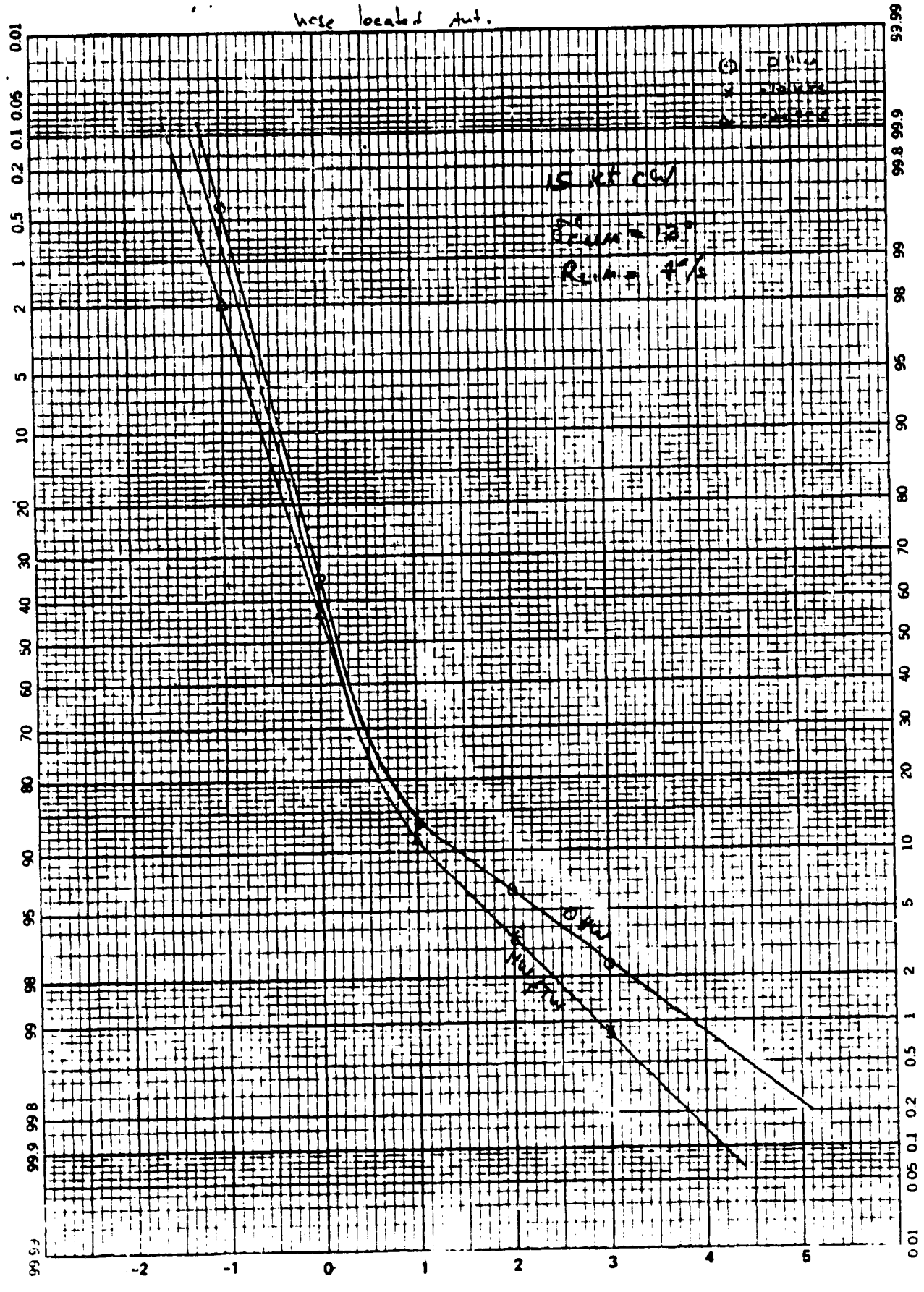

Figure C-62. Nose Located Antenna, ψTD

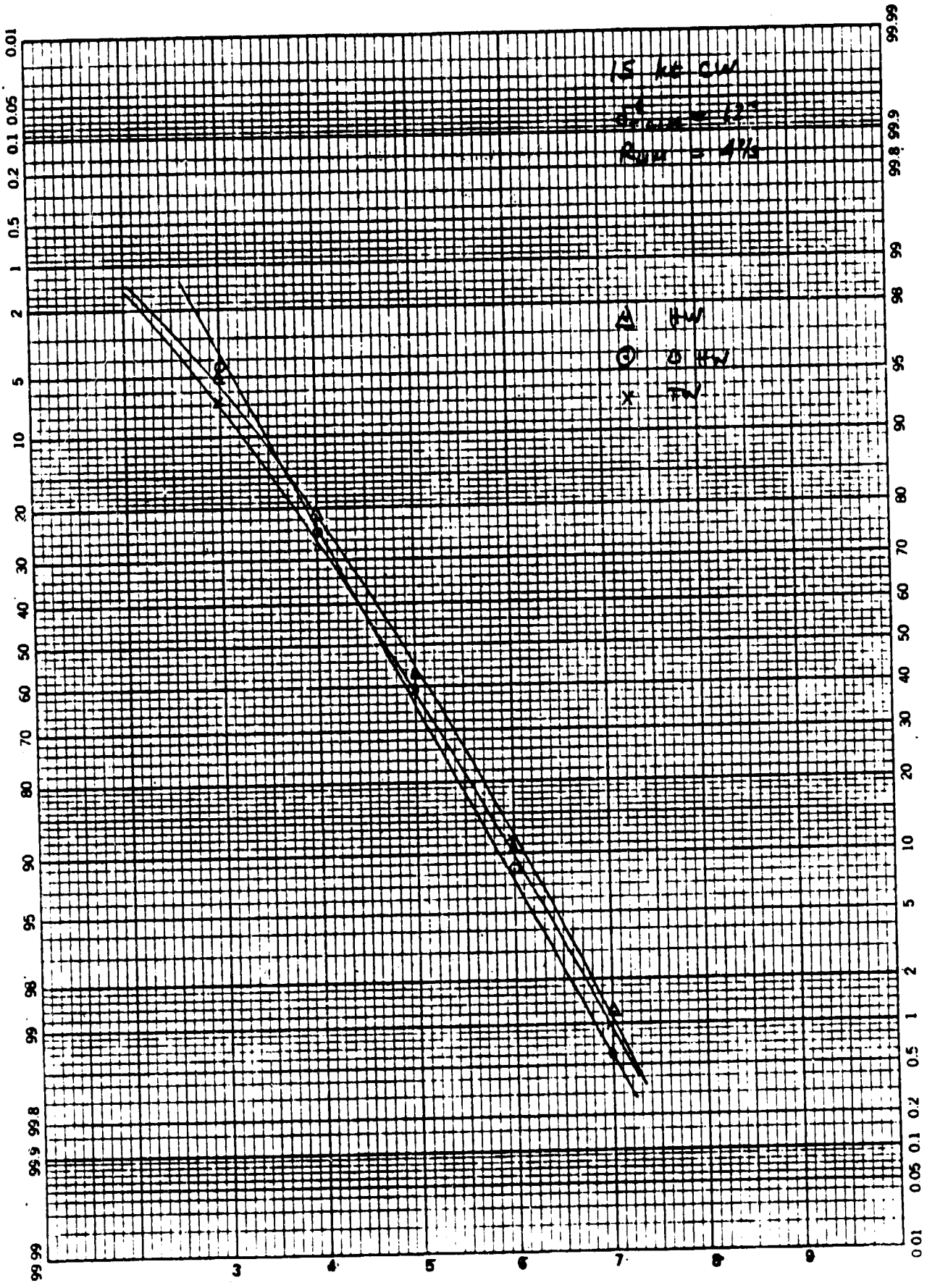

Figure C-63. Nose Located Antenna, ΦTD

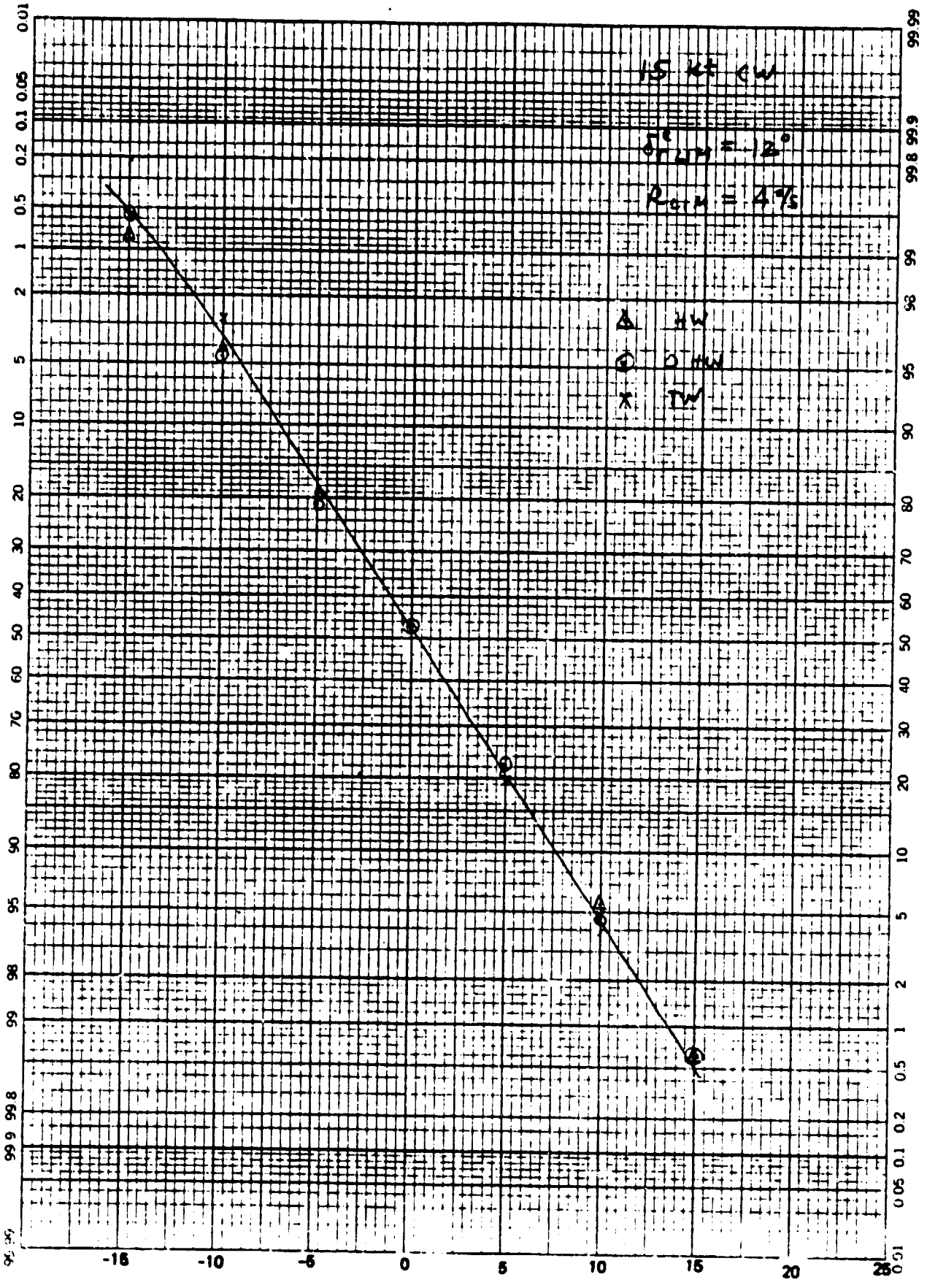

Figure C-64. Nose Located Antenna, Y_{100}

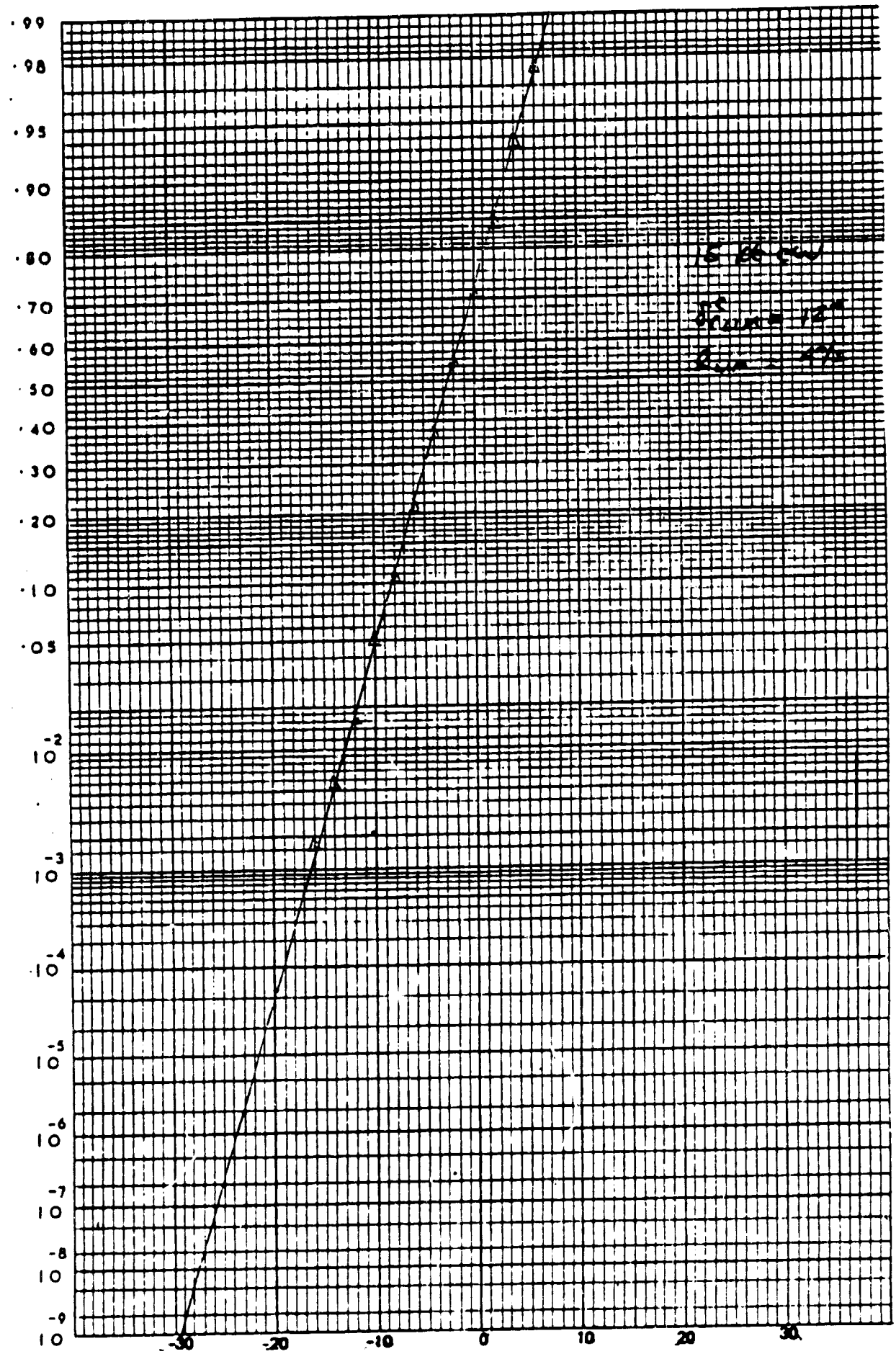

Figure C-65. MODILS Discretization, Y_{TD}

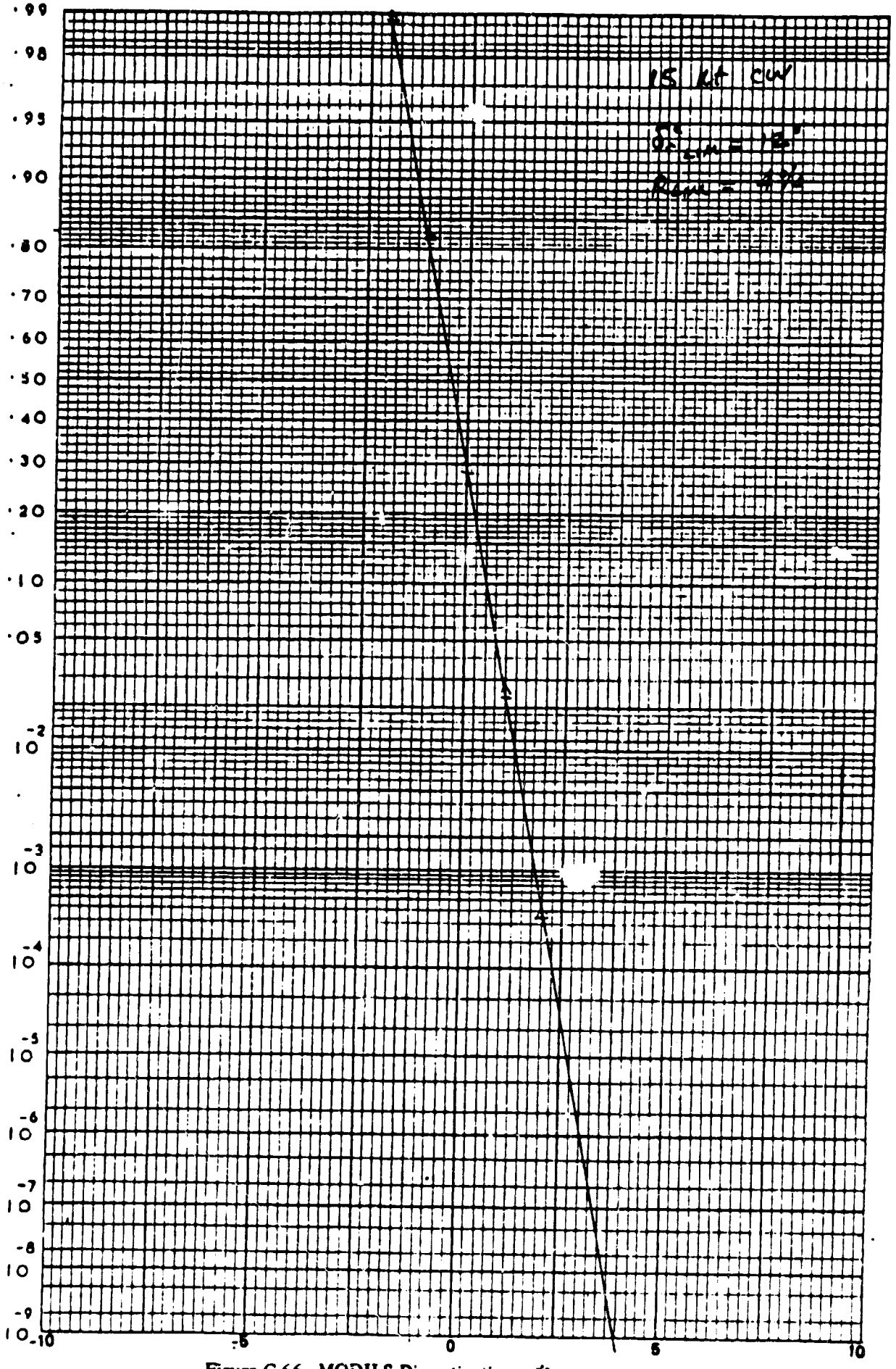

Figure C-66. MODILS Discretization, $\dot{Y}_{TD}$

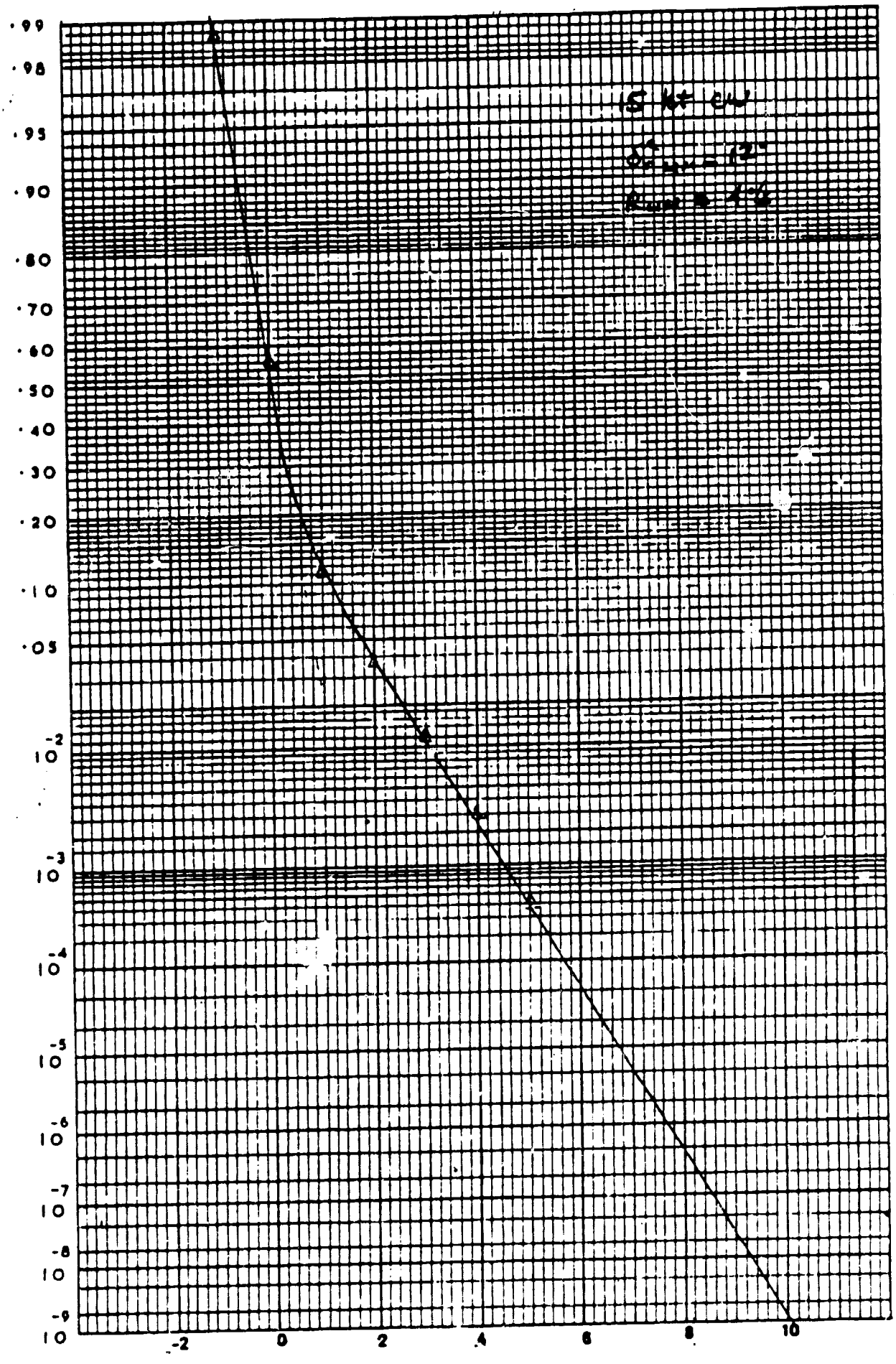

Figure C-67. MODILS Discretization, ψ_{TD}

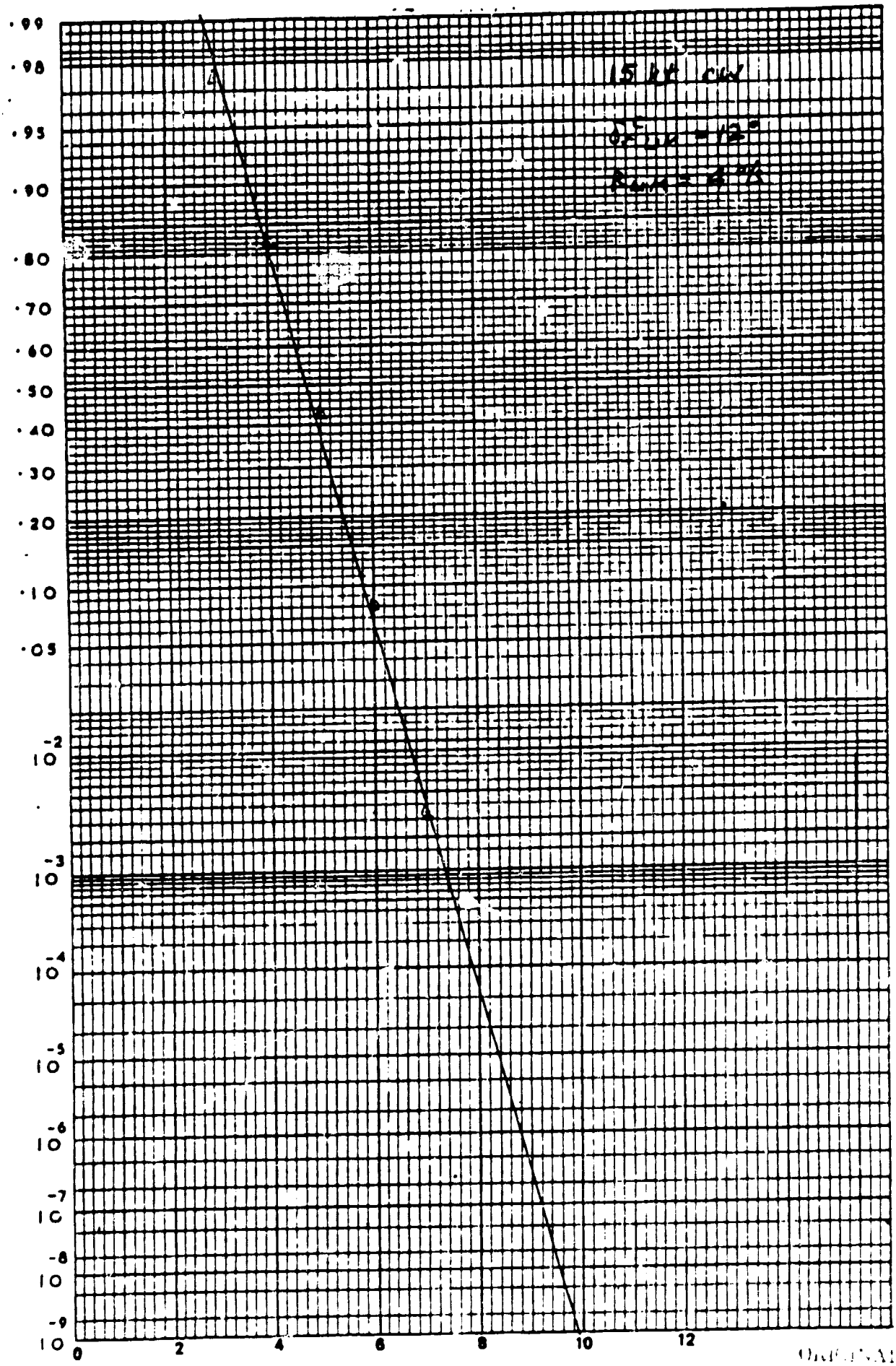

Figure C-68. MODILS Discretization, ϕ_{TD}

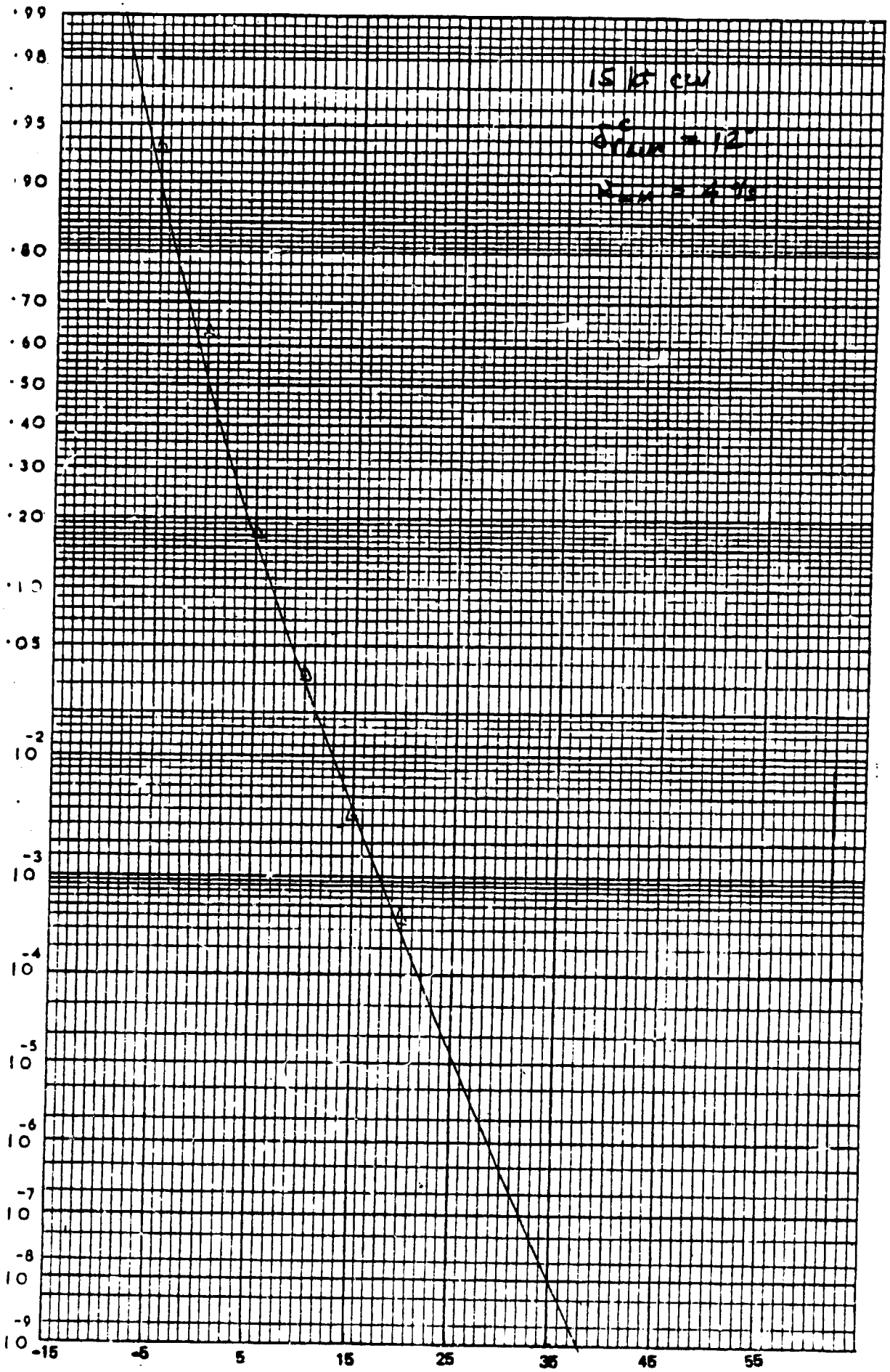

Figure C-69. MODILS Discretization Y_{100}

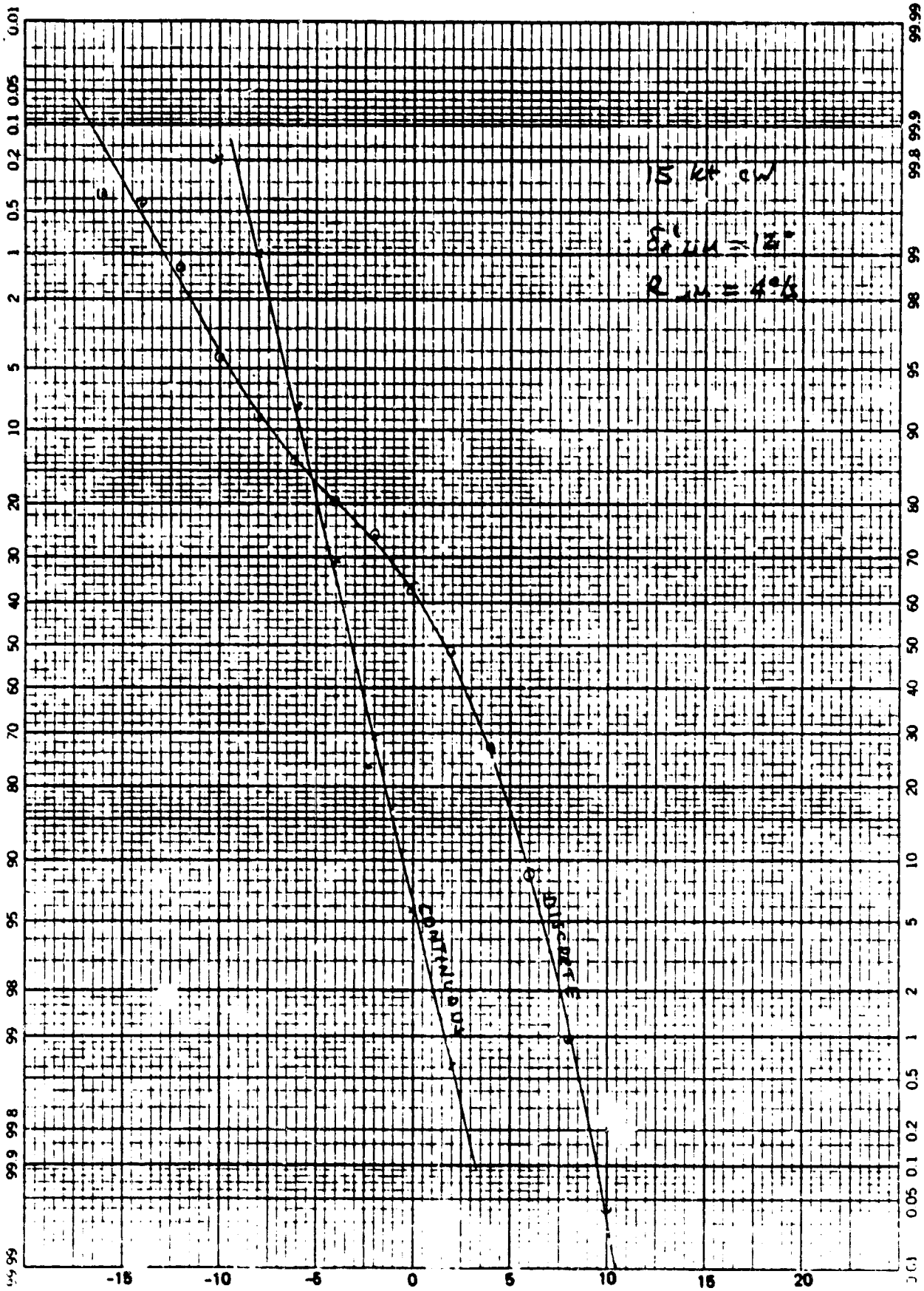

Figure C-70. MODILS Discretization without Beam Noise, Y_{TD}

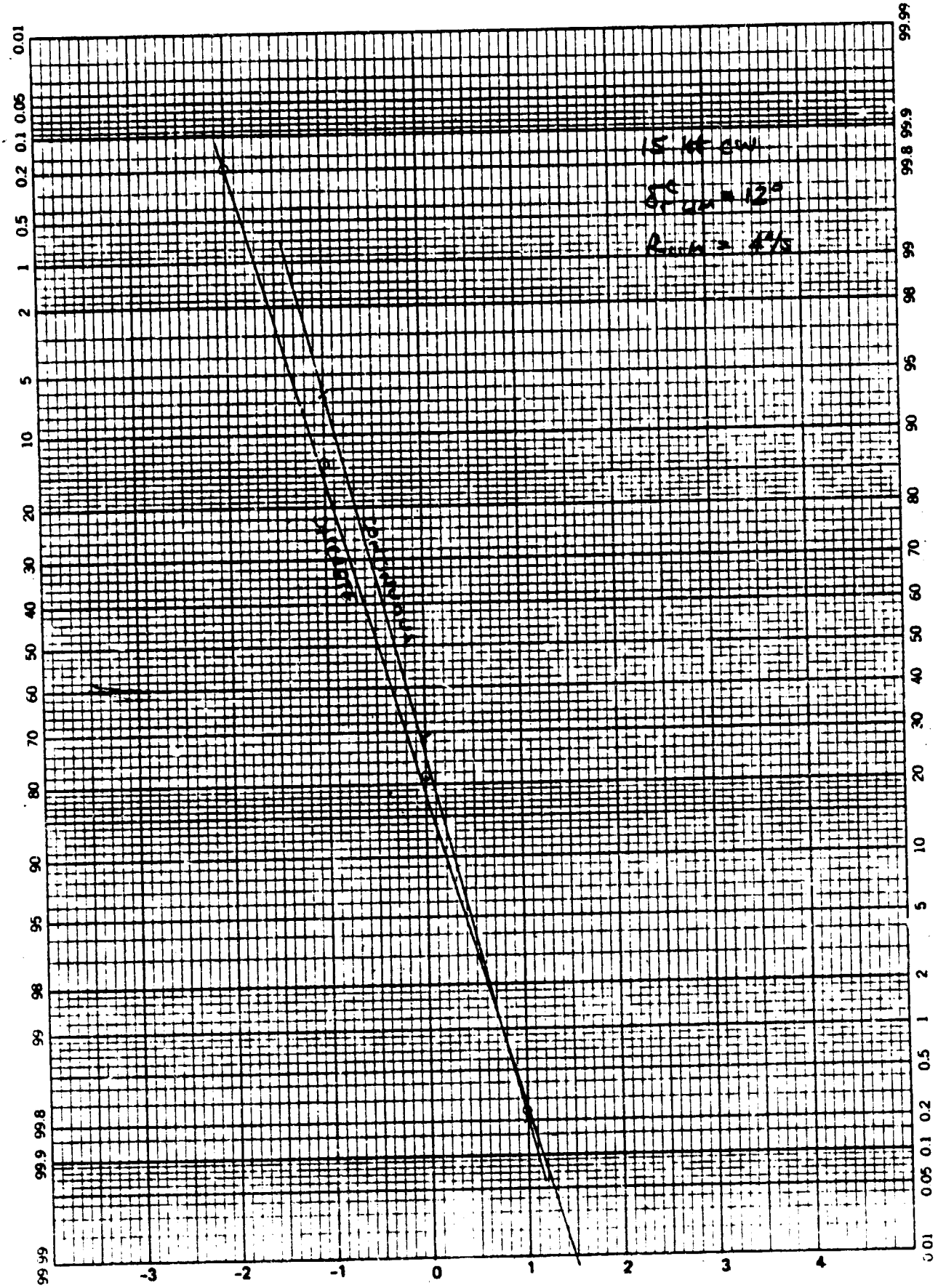

Figure C-71. MODILS Discretization without Beam Noise, $\dot{\gamma}_{TD}$

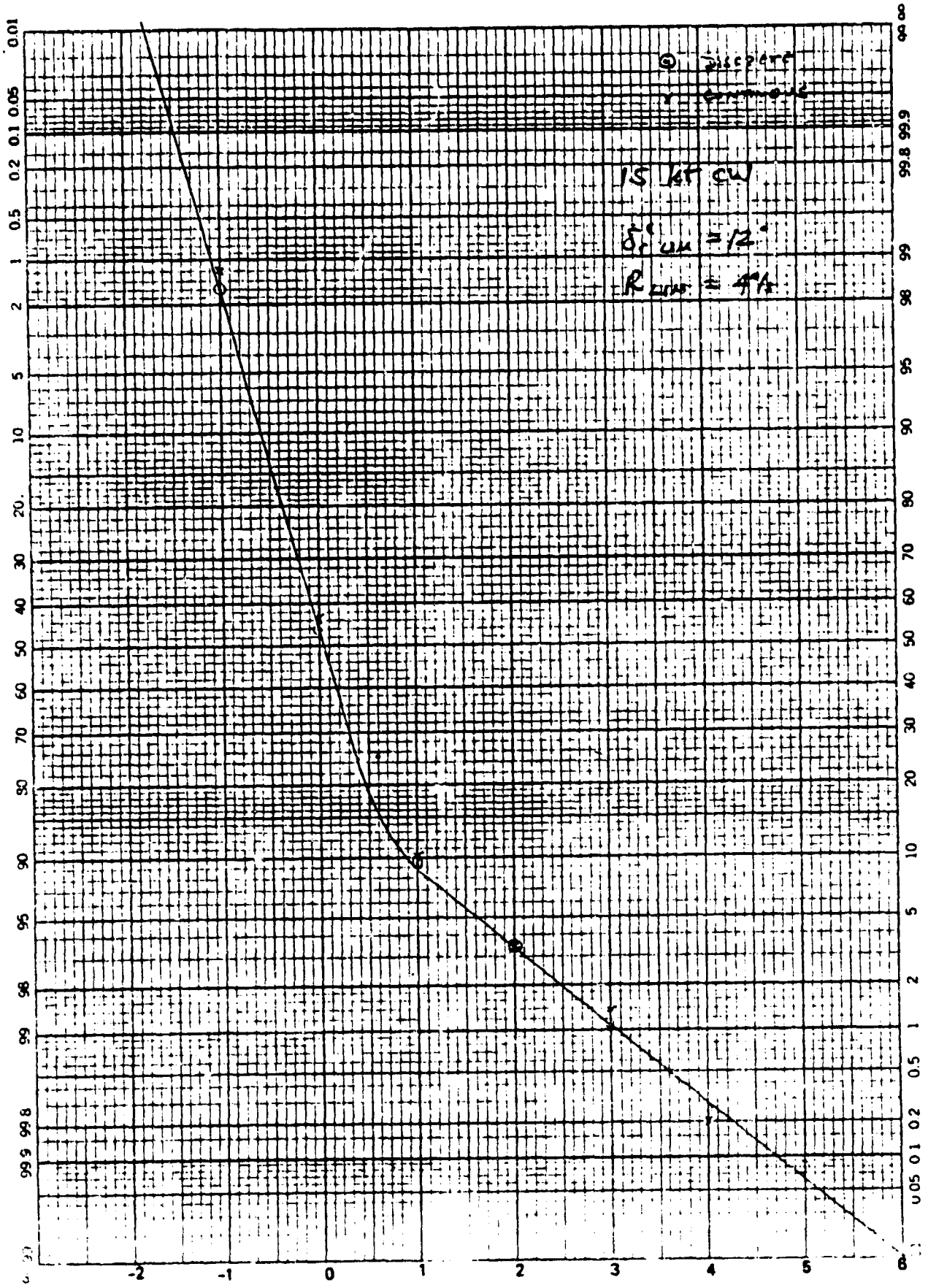

Figure C-72. MODILS Discretization without Beam Noise, Ψ_{TD}

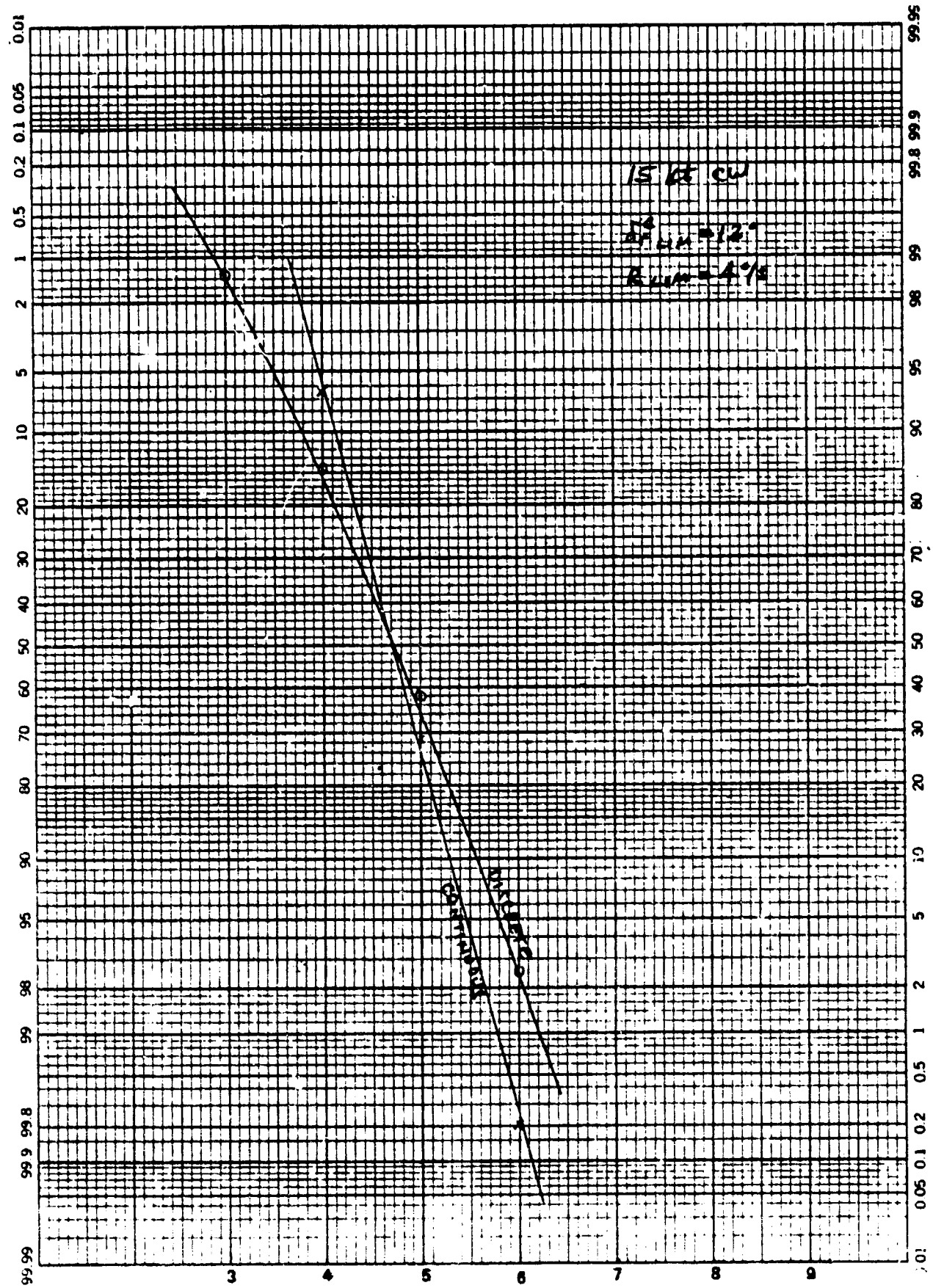

Figure C-73. MODILS Discretization without Beam Noise. ϕ_{TD}

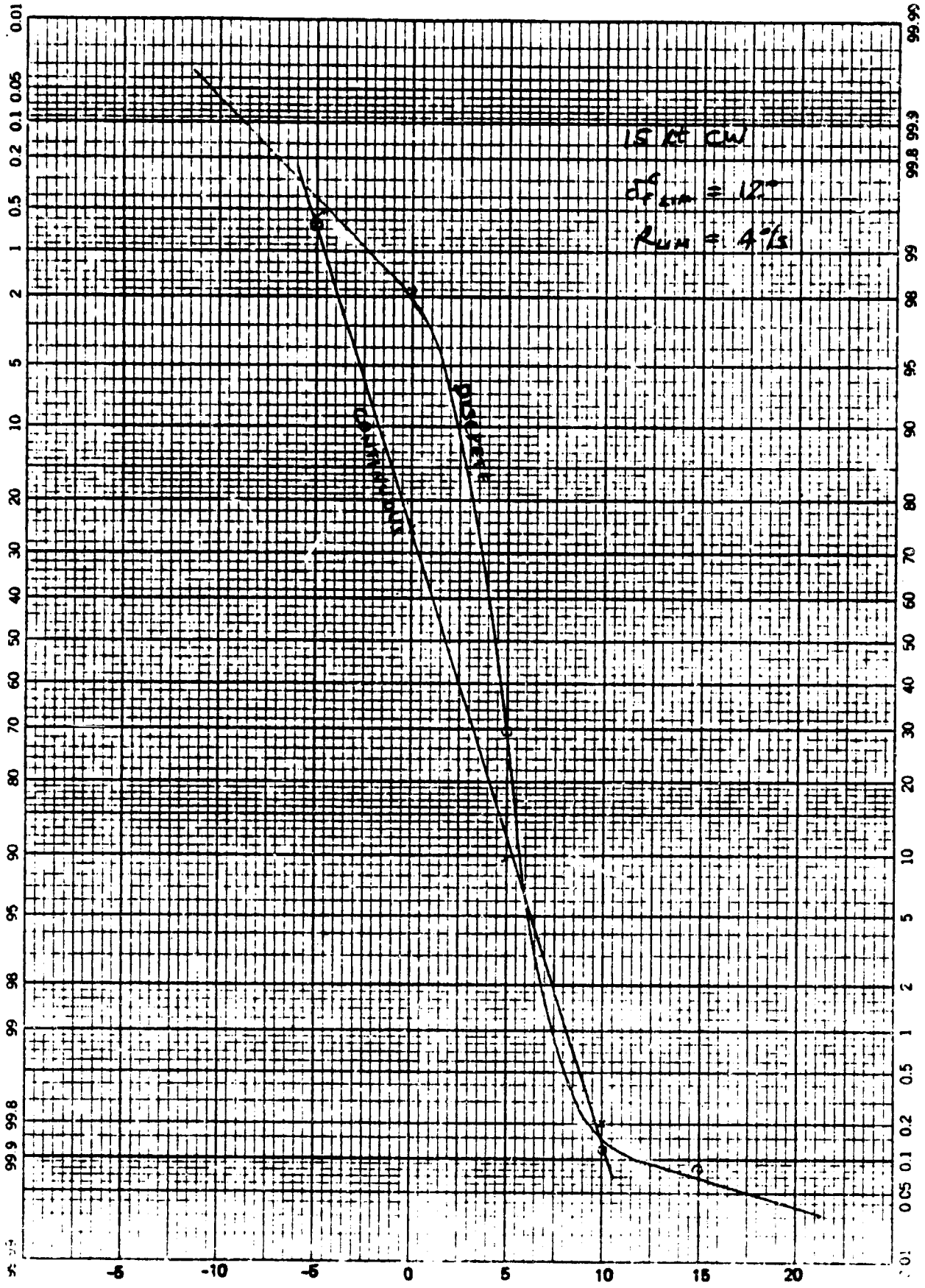

Figure C-74. MODILS Discretization without Beam Noise, Y_{100}

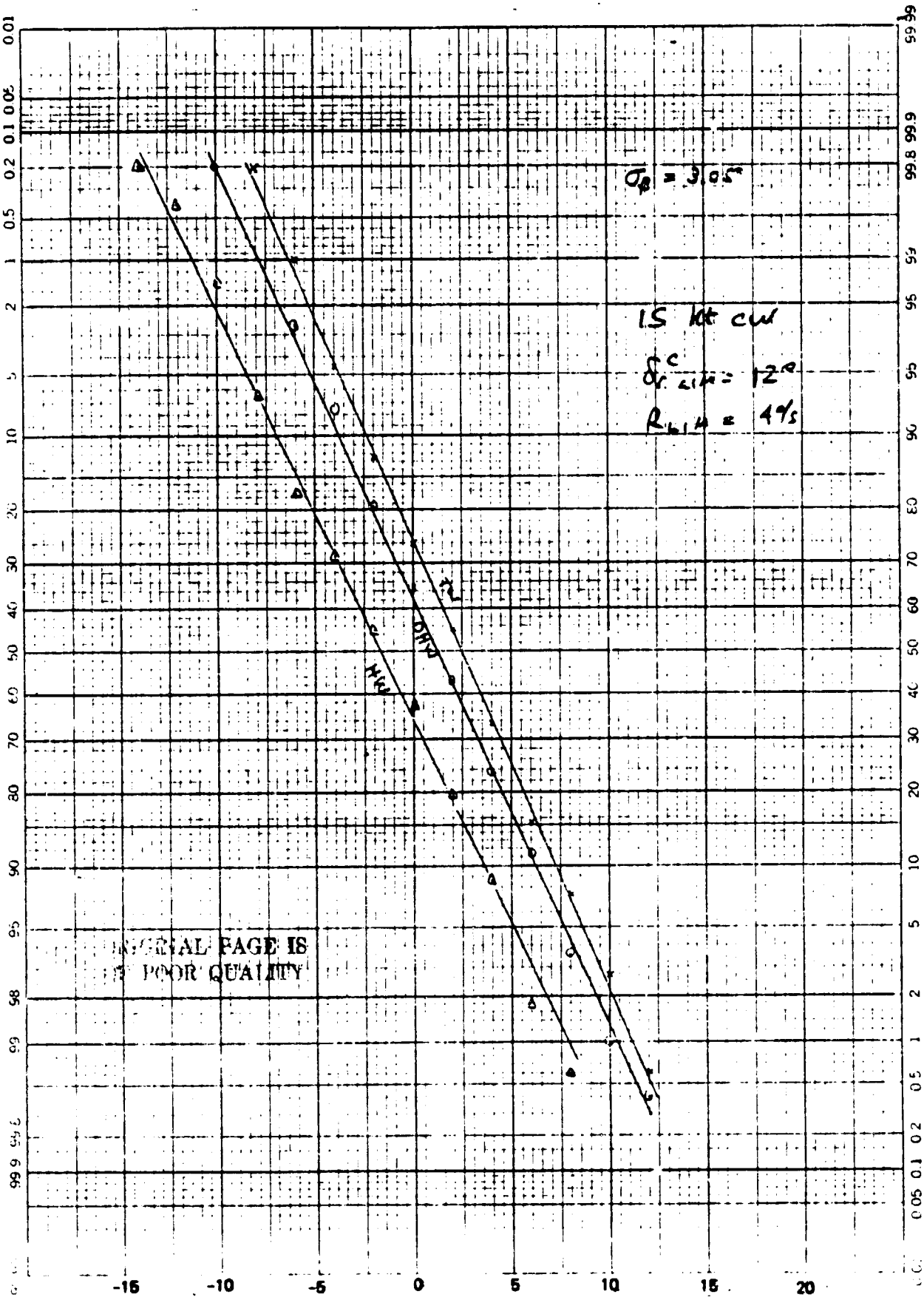

Figure C-75. Increased β_G, Y_{TD}

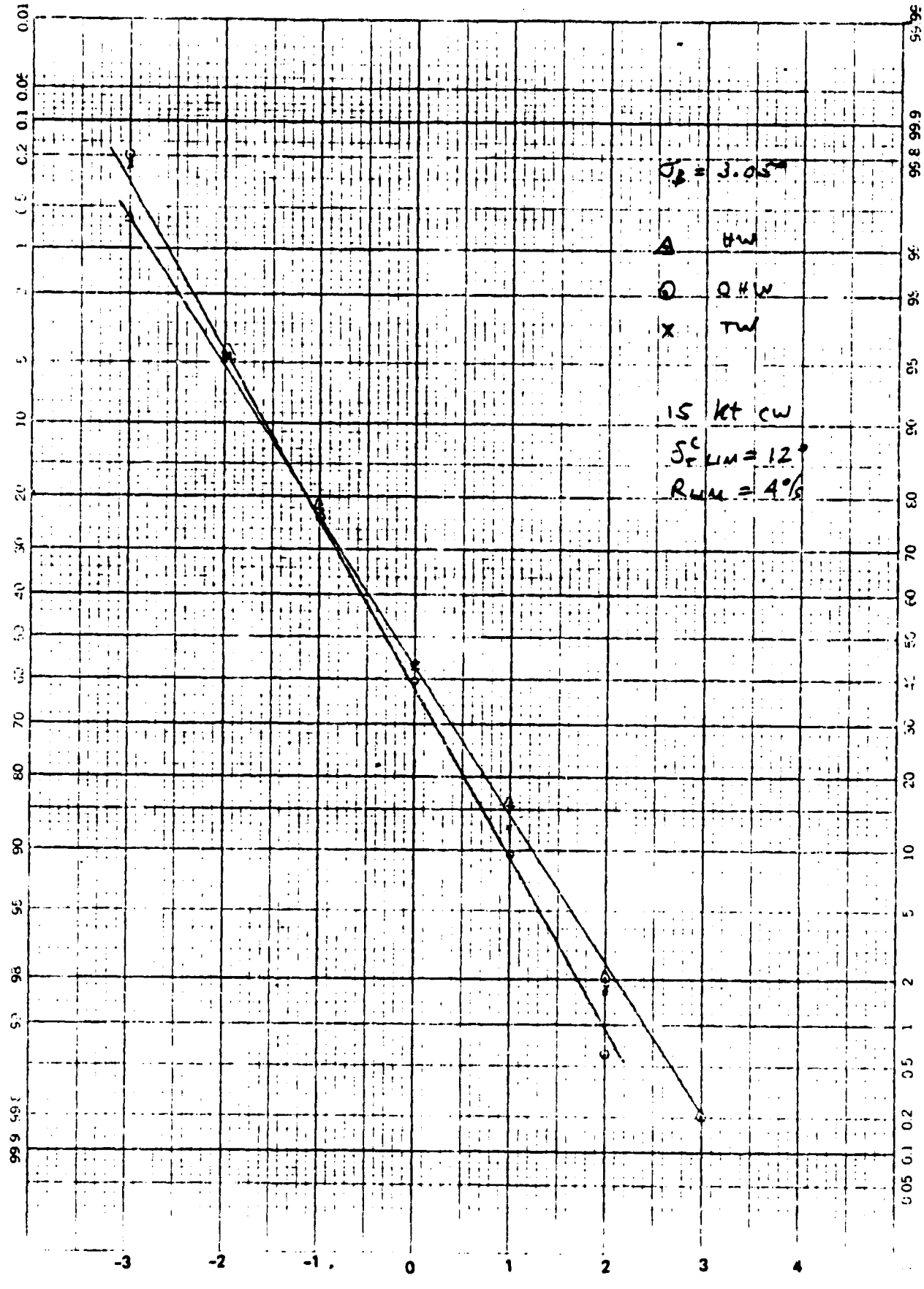

Figure C-76. Increased β_G, $\dot{Y}_{TD}$

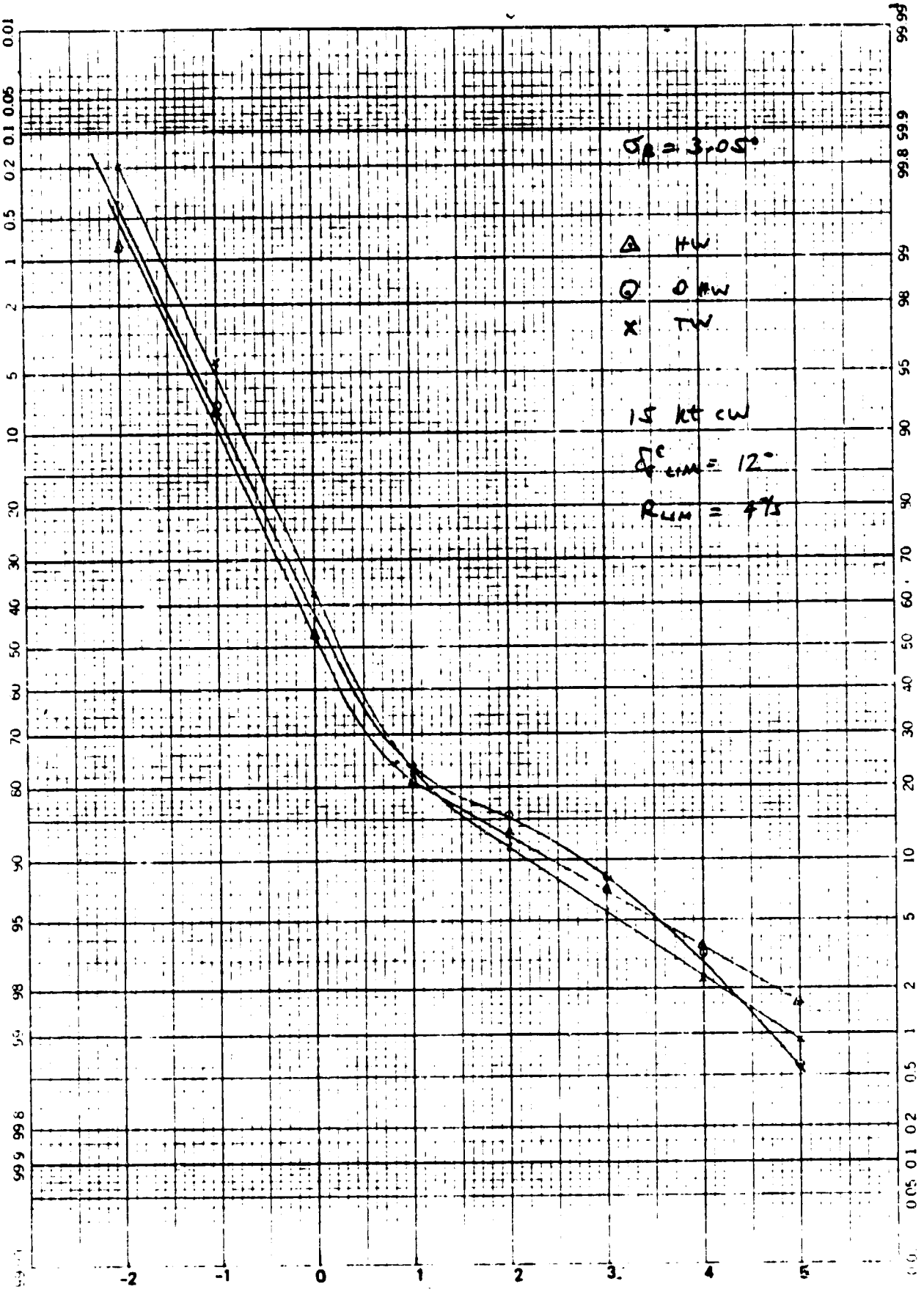

Figure C-77. Increased β_G, ψ_{TD}

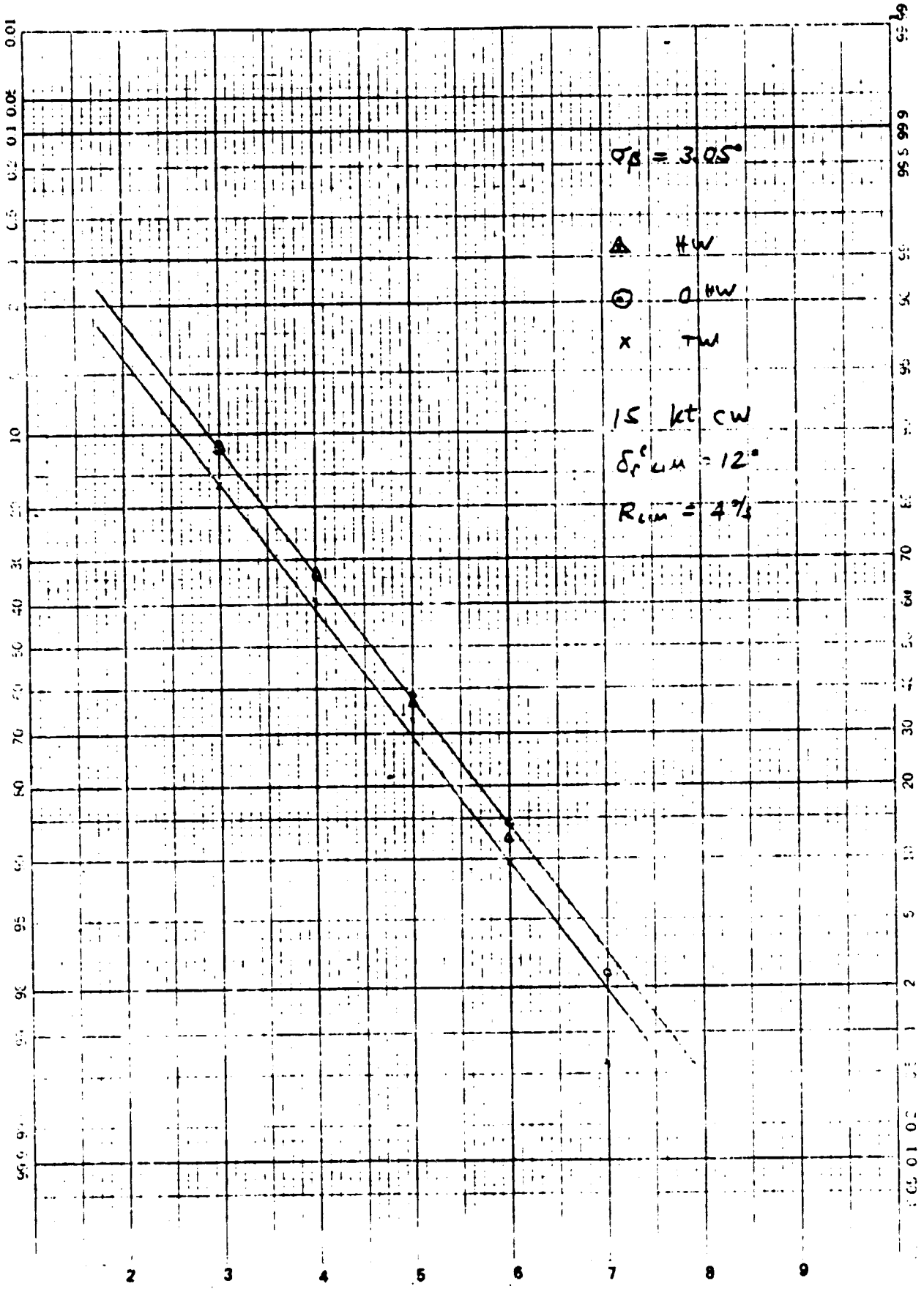

Figure C-78. Increased β_G, ϕ_{TD}

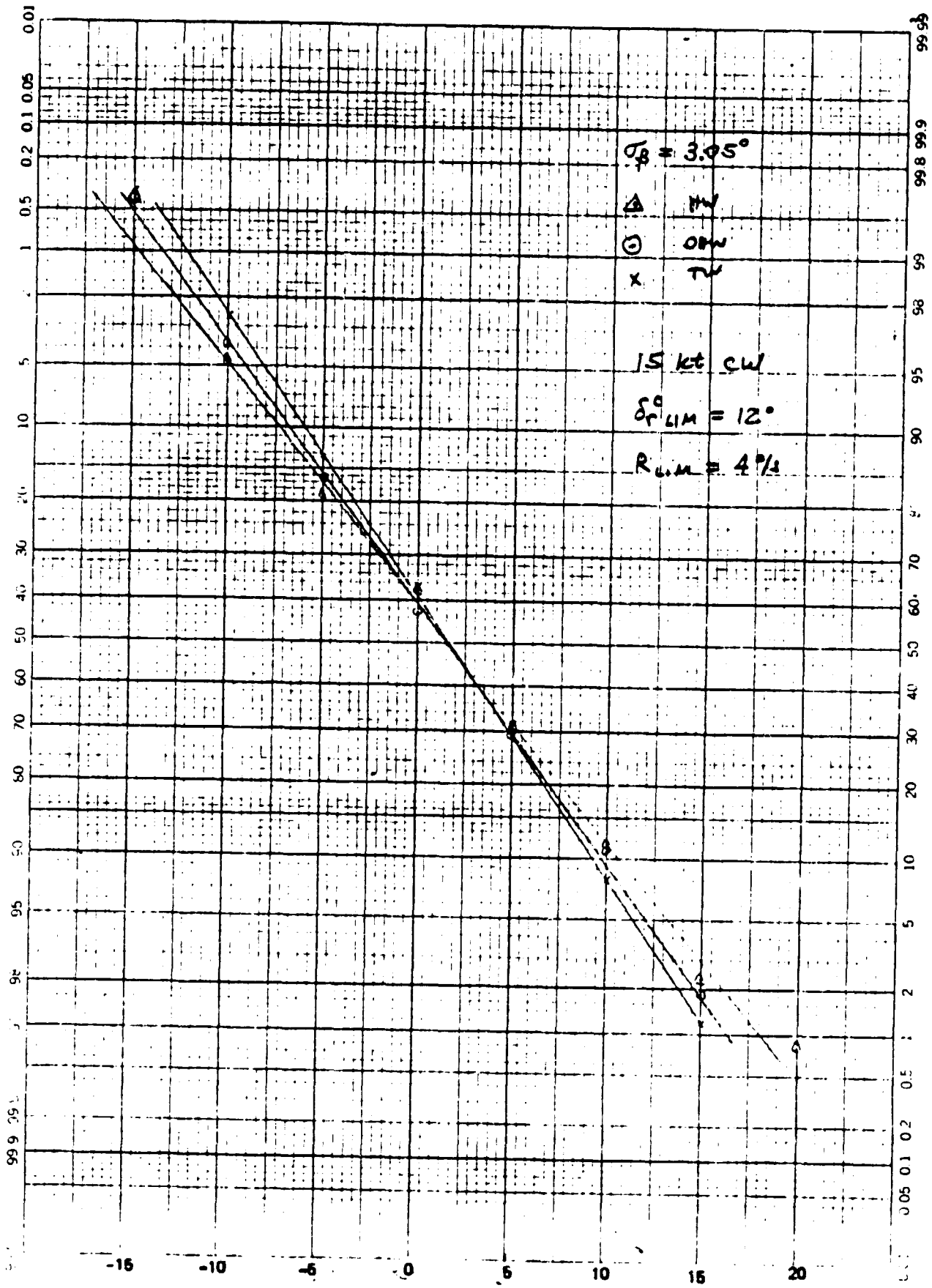

Figure C-79. Increased β_G, Y_{100}